NASA TECHNICAL TRANSLATION NASA TT F-15,666

AUTOMATIC PLANETARY STATIONS

V. V. Andreyanov, V. V. Artamonov, I. T. Atmanov, V. I. Berezin, V. M. Zhukin, V. S. Troshin and V. B. Cherenkov

Translation of "Avtomaticheskiye Planetnyye Stantsii," Moscow, Nauka Press, 1973, 280 pages

NATIONAL AERONAUTICS AND SPACE ADMINISTRATION
WASHINGTON, D. C. 20546 JUNE 1974

STANDARD TITLE PAGE

1. Report No. NASA TT F-15,666	2. Government Accession No.	3. Recipient's Catalog No.
4. Title and Subtitle AUTOMATIC PLANETARY STATIONS		5. Report Date June 1974
		6. Performing Organization Code
7. Author(s) Andreyanov, V. V., Artamonov, V. V., Atmanov, I. T., Berezin, V. I., Zhukin, V. M., Troshin, V. S. and Cherenkov, V. B.		8. Performing Organization Report No.
		10. Work Unit No.
9. Performing Organization Name and Address Leo Kanner Associates P. O. Box 5187 Redwood City, California 94036		11. Contract or Grant No. NASw-2481
		13. Type of Report and Period Covered Translation
12. Sponsoring Agency Name and Address NASA, Code KSS-1 Washington, D. C. 20546		14. Sponsoring Agency Code

15. Supplementary Notes Translation of "Avtomaticheskiye Planetnyye Stantsii," Moscow, Nauka Press, 1973, 280 pages.

16. Abstract This book is dedicated to problems of space research by means of automatic stations landed on the surfaces of planets. Examples are presented of scientific and technical tasks performed by such stations. Problems concerning method of delivery of stations to the planetary surface, peculiarities of their design, and transmission of information back to Earth are studied. Conditions of assurance of long operating life are studied: power supplies, maintenance of the necessary thermal mode and protection from external factors.

These problems are studied in greatest detail as they concern automatic lunar stations.

This book should be of interest for specialists working in the area of space technology. 166 figures, 23 tables, 106 references.

17. Key Words (Selected by Author(s))	18. Distribution Statement
	Unclassified. Unlimited.

19. Security Classif. (of this report)	20. Security Classif. (of this page)	21. No. of Pages	22. Price
None	None	384	

TABLE OF CONTENTS

Foreword 1
Introduction 3
PART 1. PROSPECTS FOR SCIENTIFIC RESEARCH BY MEANS OF AUTOMATIC PLANETARY STATIONS 9
Chapter 1. The Study of the Moon and the Planets 11
1.1. Study of Seismic Activity 11
1.2. Refinement of Shape and Laws of Motion of the Moon 11
1.3. Experiments on the Detection of an Ionosphere 12
1.4. Determination of Electrical and Acoustical Characteristics of the Moon 13
1.5. Determination of the Heat-Physical Characteristics of the Soil and Measurement of Heat Fluxes 14
Chapter 2. Astrophysical Studies 15
2.1. Observations of the Earth 15
2.2. Observations of the Sun 16
2.3. Detection and Study of Small Bodies in Space 17
Chapter 3. Scientific-Technical and Technological Tasks of Planetary Stations 19
3.1. Navigation and Communications 19
3.2. Testing of Materials and Mechanisms 20
3.3. The Search for Natural Resources for the Operation of Planetary Stations 21
3.4. Testing of Conditions for Life and Search for Life Forms 22
Chapter 4. Brief Information on the Conditions on Surfaces of the Planets 24
4.1. General Characteristics 24
4.2. Thermal and Optical Characteristics 25
4.3. Conditions of Radio Communications and Orientation 26
4.4. Comparison of Conditions on the Surfaces of the Planets 28
PART 2. PROVISION OF THE REQUIRED THERMAL MODE OF AUTOMATIC PLANETARY STATIONS 31
Chapter 5. Basic Information on Radiant Heat Exchange of Bodies 38
5.1. Characteristics of Radiation 38
5.2. Definition of the Concepts of Natural, Incident, Effective and Resulting Radiation of Bodies 42
5.3. Basic Regularities of Natural Radiation of Absolutely Black and Grey Bodies 43
5.4. Radiant Heat Exchange of Two Bodies Arbitrarily Placed in Space. Irradiance Factor 47
5.5. Properties of Radiation Fluxes 51
5.6. Radiant Heat Exchange of Two Flat Bodies Separated by Screens 55
Chapter 6. Static Calculation of the Thermal Mode of Automatic Planetary Stations 69
6.1. Production of Basic Equations Defining the Thermal State of a Spacecraft 69
6.2. Method of Calculation of Heat-Physical Characteristics of the Thermal Mode Support System 79

6.3. Definition of the Concepts of Passive and Active Thermal Mode Support Systems 86
6.4. Determination of Power of Active Thermal Mode Support System 89
Chapter 7. Basic Elements of Thermal Mode Support Systems 93
7.1. Screen-Vacuum Thermal Insulation 93
7.2. Heat-Regulating Coatings 96
7.3. Thermal Batteries 105
7.4. Evaporators 116
7.5. Radiation Heat Exchangers 121
Chapter 8. Heat Conductors 128
8.1. Liquid and Gas Heat Conductors 128
8.2. Vapor Heat Conductors 135
8.3. Radiant Heat Conductors 141
8.4. Selection of Optimal Thickness of Heat Conductor Insulation 143
Chapter 9. Dynamic Thermal Calculation of Automatic Planetary Stations 153
9.1. Summary and Effective Heat Capacity of Spacecraft 153
9.2. Experimental Determination of the Effective and Summary Heat Capacities and Penetrating Heat Flux 155
9.3. Examples of Dynamic Thermal Calculation of a Spacecraft 158
Chapter 10. Method of Terrestrial Thermal Testing of Automatic Planetary Stations 164
10.1. Methodology of Determination of Permissible Error of Imitation of Heat-Physical Properties of the Surrounding Space Medium 168
10.2. Permissible Pressure of Residual Gas in Vacuum Chambers 169
10.3. Permissible Error in Degree of Blackness of Surrounding Space Medium Radiation Imitator 171
10.4. Permissible Error in Surrounding Space Medium Radiation Imitator 175
10.5. Permissible Error in Irradiance Factor of Outer Surface of Spacecraft with Surrounding Space Medium Radiation Imitator 178
10.6. Permissible Errors in Value, Spectral Composition and Homogeneity of Radiant Flux Imitating Solar Radiation 181
10.7. Permissible Angle of Divergence of Radiant Flux Imitating Solar Radiation 183
10.8. Space Vacuum Imitators 188
10.9. Free Space Radiation Imitators 192
10.10. Devices Imitating the Radiation of the Surface of a Celestial Body 193
10.11. Solar Radiation Imitators 202
10.12. Duration of Theraml Testing $\tau_{\Delta T_a}$ 211

PART 3. DESIGN OF AUTOMATIC PLANETARY STATIONS AND METHODS OF THEIR DELIVERY TO THE SURFACES OF THE PLANETS 218
Chapter 11. Requirements for the Structure 220
11.1. Weight and Dimensions 220
11.2. Reliability 221
11.3. Operation in a Vacuum 221
11.4. Operations Under Conditions of Radiation and Meteor Impact 226
11.5. The Effects of Linear and Vibration Acceleration 230
11.6. Special Requirements Placed on the Structure of a Planetary Station 231
Chapter 12. Delivery of Automatic Planetary Stations to the Surfaces of the Planets 232
12.1. Methods of Delivery of Stations 232
12.2. Descent to a Planet with an Atmosphere and Requirements on Structure 237
12.3. Absorption of Shock Upon Landing of the Station 239
12.4. Orientation of Station on Surface 244
12.5. Movement of the Station over the Surface 248
12.6. Separation of Equipment 248
12.7. Materials 254
12.8. Testing of Structures 257
Chapter 13. Design of Radio Electronic Equipment of Automatic Planetary Stations 260
13.1. Placement of Radio Electronic Equipment and Some Problems of its Design 260
13.2. Electromagnetic Compatibility of Electronic Apparatus 266
13.3. Influence of Ionizing Radiation on the Operation of Electronic Equipment 271
13.4. Mechanical Effects of Electronic Apparatus 278
13.5. The Thermal Mode of Electronic Apparatus 285
Chapter 14. The Communications System of an Automatic Planetary Station 298
14.1. Characteristics of Information Sources 298
14.2. Selection of a Coding Method 303
14.3. Rate of Interrogation of Sensors and Number of Quantization Levels of Analog Signal 312
14.4. Storate and Reproduction of Information 322
14.5. Effectiveness of the Communications System 324
14.6. Radio Link Parameters 343
Chapter 15. Peculiarities of the Apparatus of Automatic Planetary Stations 350
Chapter 16. Power Supply Systems 359
16.1. Chemical Sources of Current 359
16.2. Photoelectric Solar Energy Converters 362
16.3. Thermoelectric Generators 365
16.4. Fuel Cells (Electrochemical Generators) 372
16.5. Thermal Emission Converters 378

FOREWORD

This book represents one of the first attempts to study the basic prerequisites used in the planning of automatic space stations, particularly automatic planetary stations (APS) for long-term studies. These prerequisites include determination of the scientific and technical goals of the APS, analysis and selection of technical decisions and recommendations for realization of these purposes. This is a difficult and complex task; therefore, the authors have succeeded in analyzing only examples of APS tasks, the design, methods and devices used to maintain the temperature mode in stations, power supply systems, various versions of APS design and methods of their delivery to the planets, as well as some of the problems of collection and transmission of information. /3*

The examples are mainly taken from lunar space stations. Methods and means of maintaining the temperature mode of the stations are presented in greatest detail in the book.

The introduction and Part 1 were written by V. V. Andreyanov. Part 2 was written by V. B. Cherenkov (Chapters 5, 6, 9, 10, §8.3 and §7.4 were written together with Yu. M. Lukoyanov), I. T. Atmanov (Chapters 7, 8) and V. V. Artamonov (§7.5 and the Appendix). The second part contains materials graciously provided by A. T. Ulubekov (§7.1 and §8.4). The third part was produced by V. S. Troshin (Chapters 11, 12) and V. M. Zhukin (Chapter 13). Part 4 was written by V. I. Berezin (Chapters 14, 15) and V. V. Artamonov (Chapter 16). The idea of creating the book belongs to V. V. Andreyanov.

The introduction makes an attempt to discuss the expediency of the creation not only of complex, but also of specialized automatic stations for scientific research. Part 1 presents examples of the scientific and technical tasks of such stations for the case of study of the moon or for experiments performed from its surface. In Part 2, problems of the thermal balance of the station, planning and testing of systems for maintenance of the thermal mode are studied in detail.

Part 3 studies the design requirements for automatic planetary stations and versions of their delivery to the surfaces of planets. Part 4 discusses individual problems in the important overall task of collection and transmission of information produced by a station over radio transmission lines to Earth, and also presents a review and comparison of power supplies for stations with long operating lives. /4

*Numbers in the margin indicate pagination in the foreign text.

The authors acknowledge that the work is not intirely free of shortcomings, and that the overall content of the book is not divided among its sections in the optimal manner.

However, a long process of improvement of the material presented in books on space subjects, and the considerable time required to publish a book present the danger that the events whose development the book is to aid may outrun it.

The authors hope that this monograph will be useful not only for students and scientific workers, but also for planners of spacecraft, particularly those making their first steps in this direction.

All constructive advice will be gratefully accepted.

The Authors

INTRODUCTION

Achievements in the area of space science and technology /5
have given researchers the welcome ability to send their devices away from the Earth -- aboard spacecraft and to the surfaces of other planets. This ability allows the conduct not only of direct, maximally reliable, studies of these planets, but also systematic observation and study "from afar" of our Earth, other objects in the universe and their interactions. This can solve a number of scientific and practical problems, the solution of which would be impossible under terrestrial conditions.

The ability of man to work fruitfully on other planets has not yet been sufficiently studied, but even if all necessary conditions could be provided, it is hardly justified to perform long-term investigations on the surfaces of the planets with the direct participation of man. Even on this old Earth, where there are very few places not yet visited by man, scientists and researchers attempt to use all sorts of automatic probes, stations and instruments for their studies, collecting the necessary information and transmitting them to convenient information collection points. This method is most suitable in difficultly accessible regions of the Earth's surface, its atmosphere and beneath the surface.

There is no doubt that studies performed on or from the surfaces of the other planets should also be performed primarily by automatic laboratory stations, while the planets themselves will for some time yet remain for us "difficulty accessible regions."

For these reasons, the authors of the present book have considered it useful for a broad range of readers -- scientists, engineers, students and simply those interested in space -- to study the range of tasks which can be performed by APS, to study the possibility of maintaining the required thermal mode and other problems of achievement of long operating lives for stations on the surfaces of the planets, to describe possible designs of such stations, methods of their "unloading" onto the planets, problems of collection and transmission of information from APS to Earth, as well as methods of controlling their operation.

This book studies these problems in detail as applicable to a lunar automatic laboratory capsule[1], presents the necessary calculations, figures and examples. Versions of the tasks and peculiarities of stations for studies of the surface of Mars and

[1]Here and subsequently, to the detriment of terminological strictness, but to the benefit of brevity, we will take the term "planet" to include the moon.

Venus are significantly less fully covered. This is explained not only by the fact that the authors are less familiar with these problems, but also by the fact that the moon, with almost no atmosphere, is in many cases a convenient point of observation, while the Earth-moon distance allows comparatively simple equipment to be used to exchange the necessary information. /6

At present [illegible] of a number of [illegible] on the surfaces [illegible]

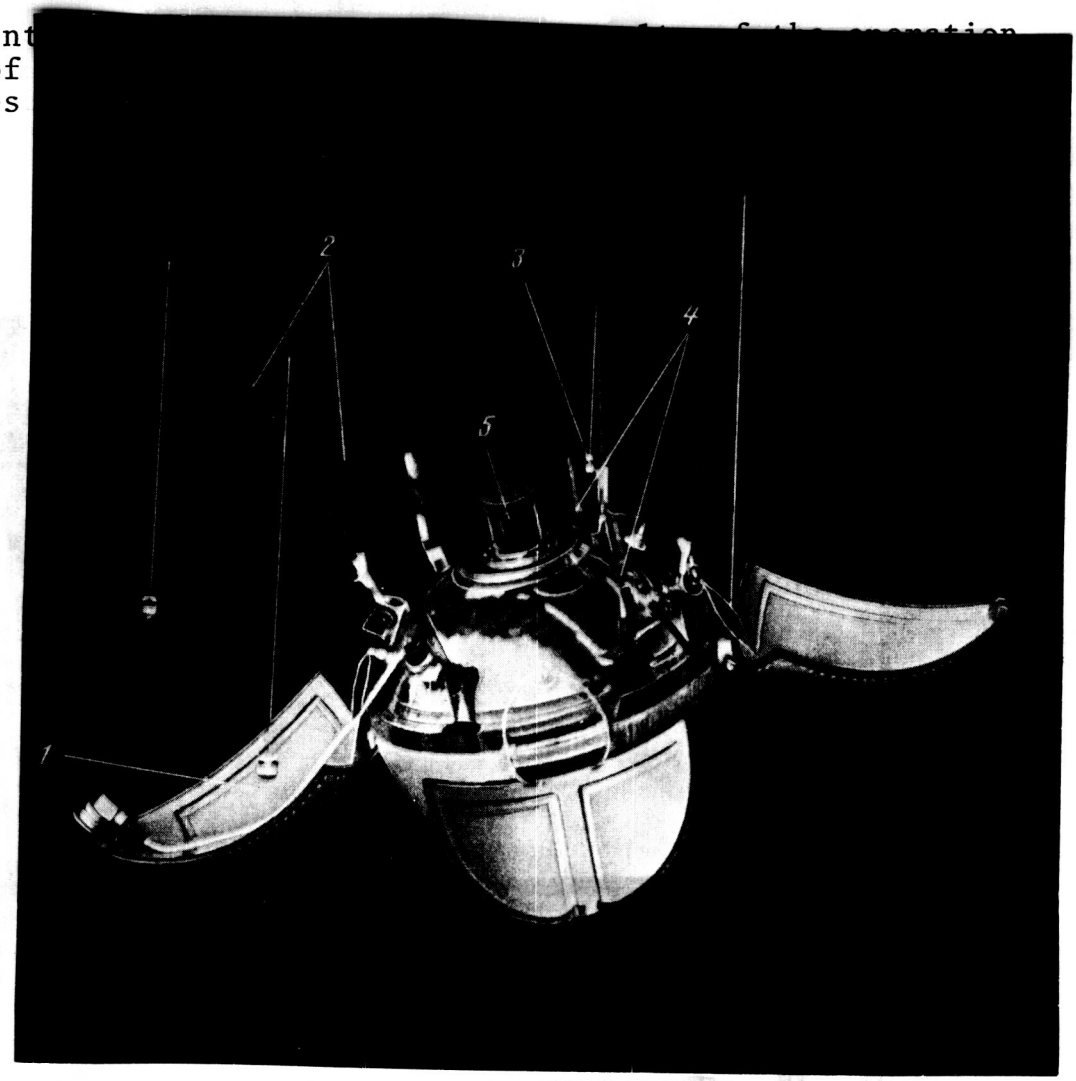

Figure 1. Automatic Lunar Stations
Luna-9 (this page); Luna-13 (next page)

/7

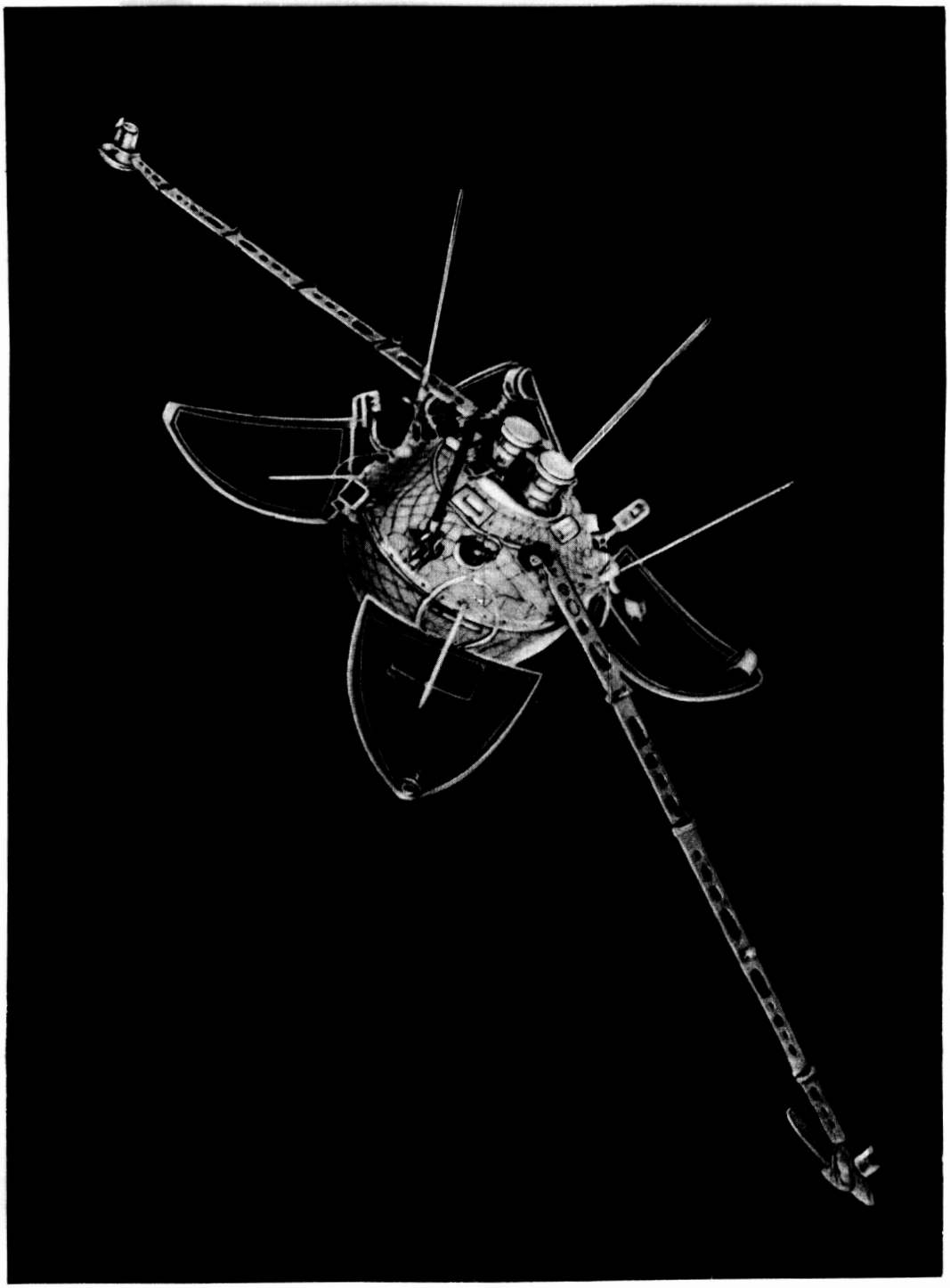

In 1966, the Soviet stations Luna-9 and Luna-13 were delivered to the surface of the moon and performed a number of experiments; in 1966-1967, American stations of the Surveyor series were sent to the moon.

The specialized automatic stations include, for example, the apparatus for seismic studies left on the moon by the American

astronauts in 1969, as well as the soil collection device of Luna-16, which shuttled from the Earth to the moon and back in 1970. /8

The Soviet mobile automatic stations Lunokhod-1 and Lunokhod-2, delivered to the surface of the moon in 1970 and 1972, occupy a special position. These stations prove the possibility of performing studies not only at one point on the surface, but over significant areas.

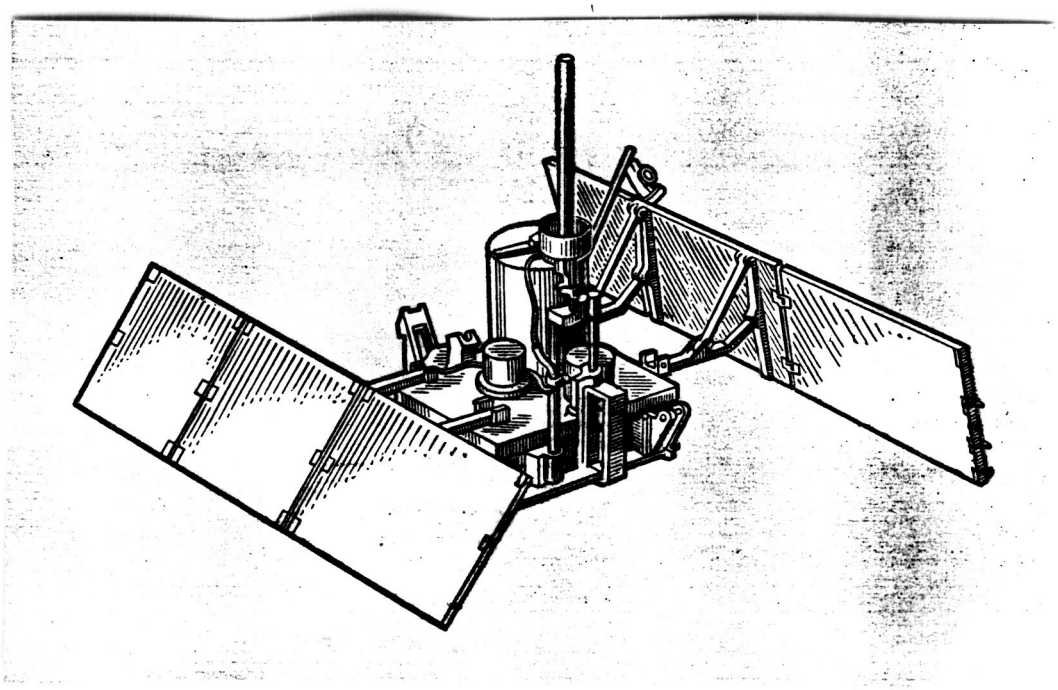

Figure 2. Overall View of Lunar Seismograph

Furthermore, the mobile station opened the way to performance of studies in regions far from the landing point, including on the far side of the moon.

As concerns the planets in the solar system, it seems that we have come closest to studies on the surface of Venus. Several Soviet stations have traveled through the atmosphere of Venus and performed measurements: Venera-4 in 1967, Venera-5 and Venera-6 in 1969 and Venera-7 in 1970. In 1972, Venera-8 landed on the surface of Venus and operated there for about 50 minutes.

Simultaneously with the studies of Venus, automatic stations are being sent to study Mars -- a more remote but less inaccessible planet [4]. Late in 1971, the Soviet automatic station Mars-2 became an artificial satellite of the planet Mars. As it approached Mars, the station released a capsule, which landed a package on the surface, carrying the national emblem of the Soviet Union. The descent module of Mars-3 made the first soft

landing on the surface of Mars. In 1973, four automatic stations were sent to Mars: Mars-4, Mars-5, Mars-6 and Mars-7, which should advance our knowledge of this planet. /9

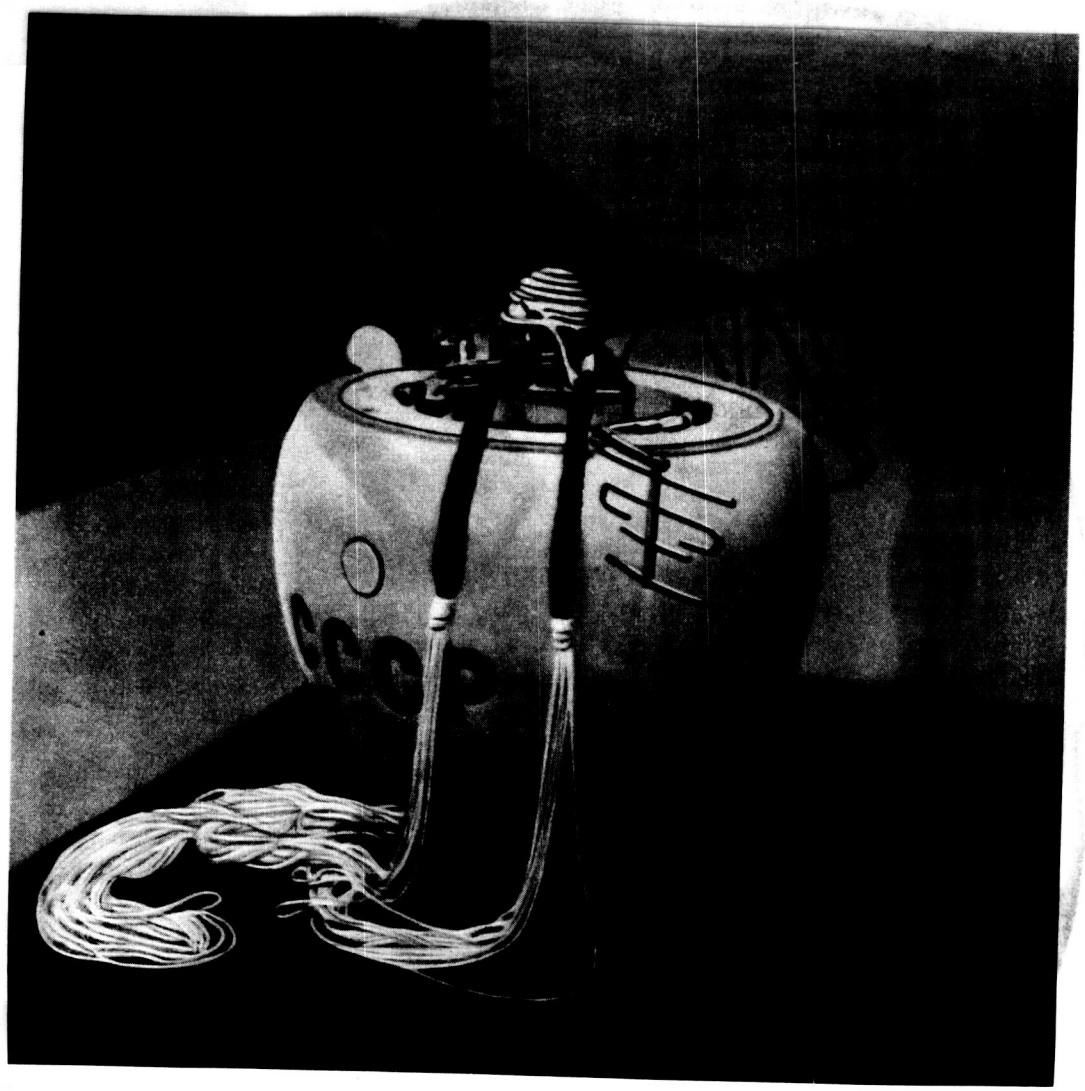

Figure 3. Overall View of the Venera-4 Automatic Station

The Luna, Surveyor and Venera spacecraft mentioned carried a complex variety of scientific apparatus, devices maintaining the effeciency of the instruments (landing systems, temperature control systems, power supply and protection systems), and communications systems. Figures 1, 2 and 3 show some of these stations: Luna-9, Luna-13, Venera-4 and the American lunar seismograph. The weight of the Luna-9 capsule was about 100 kg, of the Surveyor-7 capsule -- 280 kg, of Venera-4 -- 383 kg, a significant fraction of the weight consisting of systems designed to maintain efficiency and communications of the research apparatus for which the spacecraft are created. Due to this forced situation, it is /10

rather rare that a spacecraft can be created for any one scientific experiment, no matter how unique. However, the most precise space experiments will doubtless require the creation of specialized automatic space laboratories.

In the performance of space studies, there are too many unknowns, since it is difficult or impossible to reproduce some of the experimental conditions on Earth.

When precise measurements are performed, a difficult problem of apparatus compatibility arises; this is particularly true of combined automatic stations, where it is particularly difficult to eliminate harmful mutual influences of the many devices carried. Actually, it is impossible to make reliable studies of the distribution of magnetic fields if the station itself carries magnetic materials. It is difficult to measure the electromagnetic radiation of space sources if the apparatus on board the station can create interference, which remains unnoticed under terrestrial conditions in the general background of noise. It is difficult to determine whether the rocks of a planet are radioactive if the station, for example, carries an isotope or nuclear power supply. Determination of the composition of a thin atmosphere on a planet under study is problematical if the materials which coat the station can sublimate and create their own microatmosphere. It is not by chance that precise measurements on Earth are performed using nonmagnetic ships, anechoic or shielded test chambers and other special equipment. It is thus possible that simple, specialized spacecraft designed for one or a very few scientific tasks may become common in the near future. The time is coming when space station laboratories will be delivered to the surfaces of the planet for extended operation, frequently along with the delivery of other equipment or expeditions; this will be an event as ordinary for man as the launching of weather balloons or the placement on instrumented sensors in the ice, on the oceans and mountains of our Earth.

PART 1

PROSPECTS FOR SCIENTIFIC RESEARCH BY MEANS OF AUTOMATIC PLANETARY STATIONS

Planetary stations, equipped with the necessary apparatus, /11
are promising means for the performance of various scientific and technical tasks. First of all, such stations can be expediently used for automatic study of phenomena characteristics of the planets themselves to which the stations are sent, i.e., for the study of the planets. In addition to planetary studies, these stations can be used to study external processes and phenomena inaccessible for study or distorted when observed from the Earth.

Planetary stations, particularly those with long service lives, can perform a number of service functions, for example can act as beacons for space navigation systems. Stations with long service lives represent a unique opportunity for the detection of slow or rare processes (biological, seismic, etc.).

Automatic stations can serve as a basis for the testing of materials, mechanisms and organisms under the conditions of other planets.

Scientific research can be performed both using an individual planetary station, and using combined planetary and Earth stations or several planetary stations, or planetary and space stations. The simultaneous use of several stations allows the range of experiments to be significantly expanded, studies to be performed at different points on the surface or in space, and interferometric methods of measurement to be used.

Methods of research using planetary stations can sometimes be conveniently classified into passive and active. Passive methods are based on measurement of the parameters of natural phenomena using receptors. Active methods are most frequently based on measurement of changes in the parameters of an artificially excited process, for example radio radiation, under the influence of the phenomenon being studied. Active methods of investigationare of the greatest promise when two or more interacting stations are used.

Let us study in more detail the range of tasks of automatic stations in the case of their placement on the moon (Figure 4). As was noted in the introduction, the moon is a very convenient range for space studies: first of all, it has almost no atmosphere or magnetic field; secondly, the "moderate" distance between the moon and the Earth allows information to be exchanged using comparatively simple apparatus.

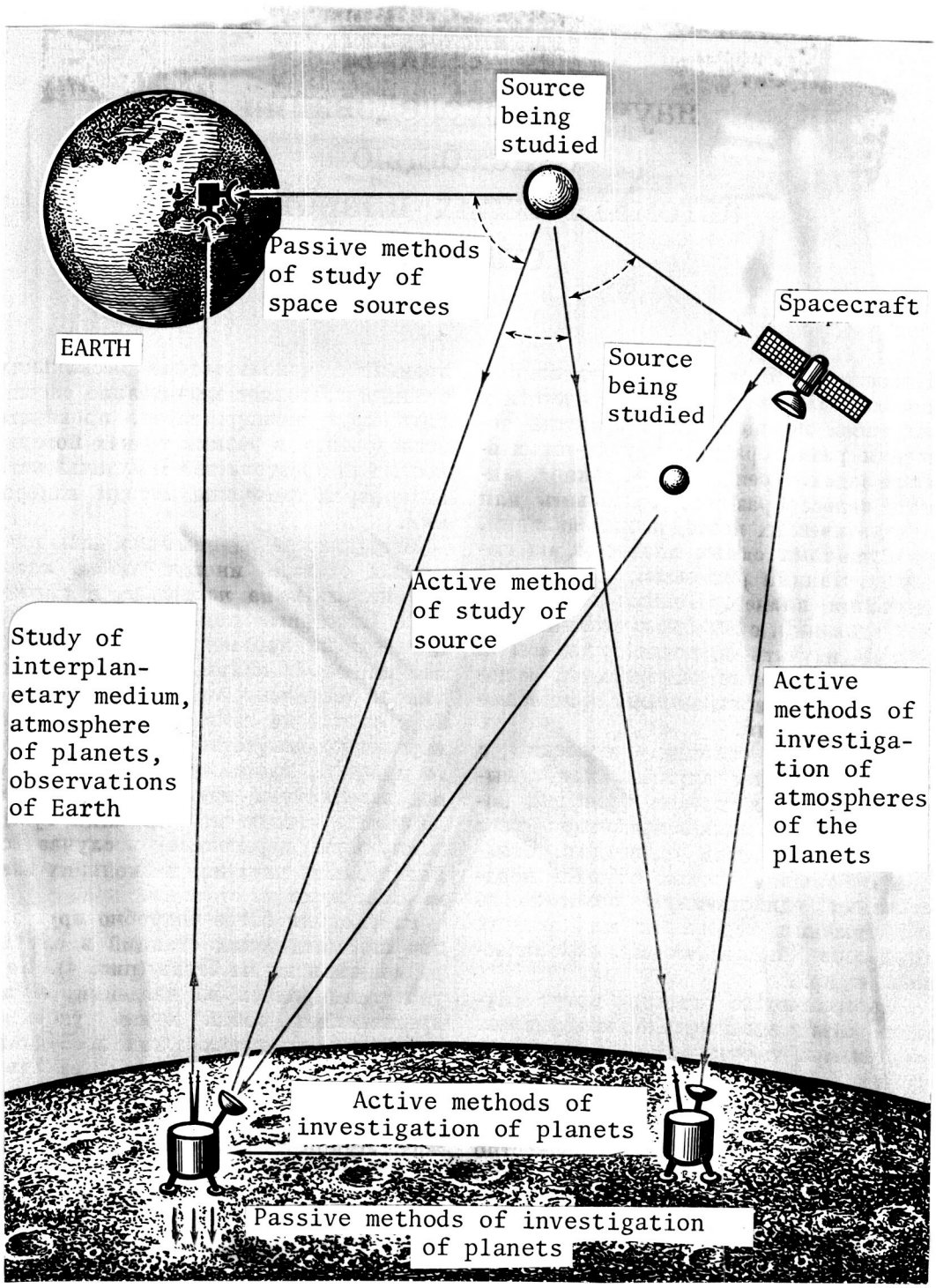

Figure 4. Diagrams of the Participation of Planetary Stations in Space Studies

CHAPTER 1

THE STUDY OF THE MOON AND THE PLANETS

In spite of the great volume of investigations performed by Soviet lunar spacecraft, as well as the American spacecraft, many phenomena remain unclear, requiring further experiments. /13

1.1. Study of Seismic Activity

These studies have been conducted by direct methods, by placement of seismographs on the surface of the moon. In order to determine the intensity and frequency of moonquakes, extended observations are necessary, i.e., the lunar station must have a long service life. Of particular interest is the placement of several such stations at different points on the moon simultaneously. This allows us to establish, for example, how seismic activity is distributed over the individual regions of the moon, what is the interrelationship between moonquakes and meteor showers and other phenomena. Seismic activity is one of the criteria used to establish the age and internal structure of a planet. Such stations can be used to record meteor falls, the impacts of jettisonned stages of booster rockets and other collisions. In many cases, active methods of seismic investigation are useful, when the excitation (impact or explosion) is artificially caused. In this case, at least two stations are necessary, and the passive station should contain a seismograph plus, of course, a system of data transmission, a power supply system and a system to maintain the thermal mode required.

1.2. Refinement of Shape and Laws of Motion of the Moon

Terrestrial astronomical observations established long ago the phenomenon of "rocking" (libration) of the moon as it moves around the Earth and rotates. It was established that the libration is caused by the force of gravity of the Earth which tends to "turn" the long axis of the moon in the direction of the center of the Earth. Therefore, lunar objects observed from the Earth shift relative to the edge of the disc of the moon, making it difficult to establish the precise shape of the moon and the laws of libration. The problem can be solved by placing several (three or four) radio or optical benchmarks as close as possible to the edges of the disc of the moon (Figure 5).

Laser reflectors can be used as optical benchmarks. In this case, the lunar stations must protect the reflectors from

temperature changes and meteorites. This type of station can function with no consumption of electric power. The presence of such benchmarks will help to "tie in" objects to the map of the moon [5].

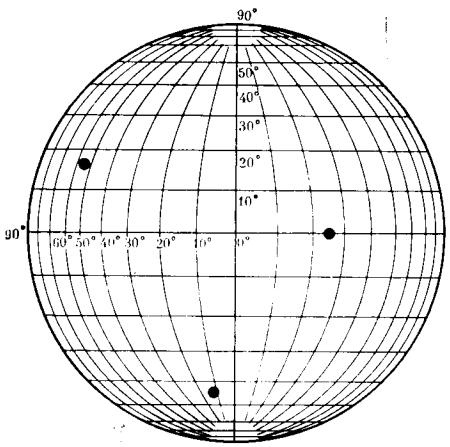

Figure 5. One Version of Placement of Stations for Refinement of the Laws of Libration of the Moon

The American astronauts placed a laser reflector on the surface of the moon, although it is located near the center of the disc of the moon, at the point where the Apollo spacecraft landed. /14

Other, French reflectors were carried on board the Lunokhod-1 and Lunokhod-2 spacecraft, which were placed on the surface of the moon by Soviet automatic stations.

1.3. Experiments on the Detection of an Ionosphere

The moon has no atmosphere. However, the interaction of the solar wind with the surface of the moon, secondary effects in the continuous meteorite bombardment, and, finally, the comparatively close location of the gassy Earth might create a thin, probably irregular medium over the surface of the moon, containing, in particular, charged particles. In other words, we cannot eliminate the possibility of the existence of a lunar ionosphere. It has now been established that the concentration of electrons in such an ionosphere could hardly exceed 10^3-10^4 per cubic centimeter. Nevertheless, without determining the presence or absence of an ionosphere, we cannot trust the results of measurements of electrical parameters of the moon, nor can we properly plan lunar radio communication lines for stations created.

Automatic lunar stations, equipped with the necessary instruments, might solve the problem of detection of the ionosphere and determination of its characteristics in the area where the station is located. This would require the performance of measurements considering the influence of the sun, i.e., measurements should be performed during various phases of the moon and possible variations in the ionosphere determined (for example, due to the emission of gasses from the surface), i.e., measurements should be performed on various points on the surface. The performance of measurements would require long-term existence of stations.

The resulting method of study of the ionosphere has been tested under the conditions present on Earth, Venus and Mars. It is the method of radio translumination by two or more coherent oscillations at different frequencies from a spacecraft. In studying the lunar ionosphere, this method can also be used, except that the receivers (or transmitters) of these oscillations should be located not on the Earth, but rather on a lunar station. Thus, the experiment requires at least two interacting stations -- a planetary station and a space station (for example, a satellite of the moon). In this case, measurements would not be hindered by the powerful, unstable background created by the Earth's ionosphere.

1.4. Determination of Electrical and Acoustical Characteristics of the Moon

/15

Detailed investigation of lunar samples on Earth has not allowed us to draw conclusions concerning the integral characteristics of the lunar material, particularly deeply bedded material, under natural conditions.

By electrical characteristics, we mean the conductivity σ, dielectric permeability ε and magnetic permeability μ; acoustical characteristics refer to the velocity of propagation of sound and the sonic conductivity. In addition to the great significance of these parameters for the performance of applied tasks, for example communications tasks, this information is necessary for the structure and physical-chemical composition of the surface and deeper strata of the moon.

Indirect methods of measurement of electrical parameters, based on terrestrial radio astronomy and radar observations, have yielded the averaged values $\sigma = 10^{-3}$-10^{-6} $ohm^{-1}.m^{-1}$ and $\varepsilon = 2$-5 at radio frequencies in the meter and shorter wave bands, accessible for terrestrial observation. These quantities correspond to the external conditions of soil, since deeper measurements require longer-wave oscillations. As concerns magnetic permeability, which may change through the volume of a planet, and acoustical characteristics, they can be measured most reliably by direct contact with the soil, i.e., using planetary stations. The performance of direct electrical and acoustical measurements requires at least two stations -- the exciter and receiving stations.

The frequency and indirectly the depth dependence of electrical parameters of the moon should be measured in the frequency band from 0 to a few megaHertz, since it is in this band of frequencies that measurements cannot be easily performed from the Earth or from spacecraft. Measurements in direct current and at low frequencies require direct, good contact between the instruments and the lunar soil. The low conductivity of the soil makes measurement over long distances difficult, since it is technically

difficult to excite intensive electrical and magnetic fields. Probably, stations for these measurements cannot be placed further than a few hundreds of meters apart. For measurements at low radio frequencies, on the other hand, in order to avoid the influence of the direct wave the stations must be placed over the horizon from each other, i.e., at distances of 2 to 20 km.

No significant magnetic field has been detected with the moon. However, it is quite possible that there are ferromagnetic materials in the depths of the moon, which could be detected only by the study of the internal structure of the moon. Furthermore, magnetic measurements performed simultaneously at several widely separated points on the lunar surface could yield information on the interaction of the interplanetary magnetic field with the moon. These experiments require that the lunar station be magnetically clean, i.e., contain no magnetic materials capable of distorting the weak magnetic fields. Obviously, such a station should be a small, nonmagnetic capsule, far from the large mass of the rocket landing platform [6].

1.5. Determination of the Heat Physical Characteristics of the Soil and Measurement of Heat Fluxes

The study of the radio thermal radiation of the moon with terrestrial equipment has allowed us to determine the mean values of the temperature of the surface and surface layers of the soil, as well as its rate of change with various degrees of solar illumination. The approximate values of heat conductivity [about 10^{-4} cal/(cm·sec·deg)] and heat capacity [approximately 0.2 cal/(g·deg)] of this layer have been calculated.

The heat physical parameters of individual specimens of lunar soil have been measured under laboratory conditions. We refer here to the specimens returned by the American astronauts. However, the parameters of specimens of soil isolated from their surroundings may differ from those exhibited under lunar conditions. Direct measurements of heat physical characteristics have significantly specified the properties of the soil in the areas of the stations, allowing reliable temperature dependences with soil depth, with time and at various points on the surface to be measured [7]. /16

One important task is the measure of the intensity of heat fluxes from the center of the moon. In addition to information on the moon, these measurements will yield factual data for the solution of applied problems, for example the constructin of systems for maintenance of the thermal mode of the stations themselves. Stations for "thermal" studies should be equipped with heat probes, thermometers and heat flux measuring equipment. The stations should have long service life to allow measurement of diurnal and longer variations in thermal processes.

CHAPTER 2

ASTROPHYSICAL STUDIES

The placement of astronomical instruments and measuring devices on the surface of the moon will immeasurably broaden the frequency window available to researchers. On the Earth, this window is restricted by the atmosphere to narrow slits in the optical band (from about 2000 A to 2 μ) and the radio band (from about 1 cm to 30 m). The absence of an atmosphere eliminates the blurring and winking of images of objects observed, allowing the accuracy and resolution of angular measurements to be improved [8]. Less bright sources will be accessible for observation, since the absorption and glowing atmospheric background are eliminated. /17

The absence of an atmosphere and of the magnetic barrier allows interplanetary electromagnetic and corpuscular streams which either do not reach the Earth or are distorted in terrestrial observations, to be detected and studied. However, these and other prospects are largely true of observations from spacecraft, particularly Earth satellites.

2.1. Observations of the Earth

Observations of the Earth and its cloud cover by means of Earth satellites yield valuable information for meteorological, geodetic, research and other purposes. However, at each moment in time a satellite "sees" only a small section of the surface; for example, from an altitude of 200 km, only 3% of one hemisphere of the Earth is visible. Near-Earth phenomena are not visible and it is quite impossible to study the Earth globally as a planet against the background of external, primarily solar, phenomena. Observations "from afar" will allow detailed studies of the cloud, gas and dust surroundings of the Earth and interactions with the sun.

A lunar station "sees" almost half of the Earth simultaneously, and the direction to the Earth remains approximately constant. This fact allows comparatively simple automatic equipment to be used to orient instruments in the direction of the Earth. The angular size of the Earth observed from the moon is about 2°, the libration of the moon causes variations in the direction toward the Earth by approximately ±5° more. Thus, an immobile (non-tracking) lunar instrument must have an angle of view of at least 12°. A tracking or scanning instrument can be created with a resolving capacity of a few angular seconds.

Automation of studies can be performed in two directions. First of all, by production of optical, thermal, radio and other

images and their transmission over communication lines to the Earth. Secondly, by direct performance of measurements of individual parameters of the processes studied, with subsequent transmission of the results of these measurements.

For example, it is possible to photograph the Earth in the desired spectral range at the desired time interval, then transmit the photographs to the Earth slowly over a narrow-band communication channel. Study of the photographs on the Earth is then used to extract the necessary information. Measurement of the dimensions of dust particles in near-Earth space, for example, should be performed by spectral analysis of the light scattered by these particles. /18

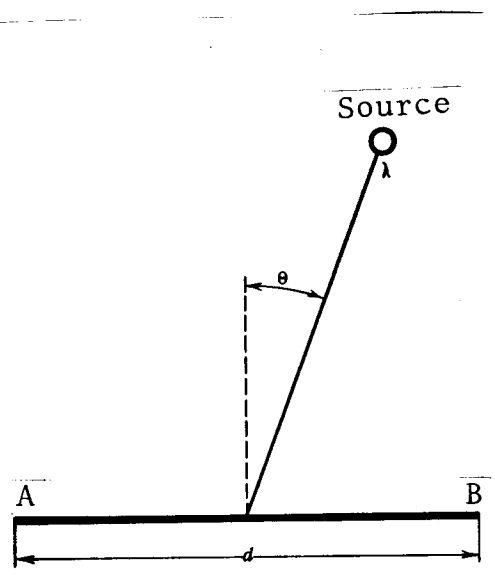

Figure 6. Diagram of an Interferometer

An automatic lunar station is particularly suitable for the recording of comparatively rare processes on Earth or in near-Earth space. In this case, the apparatus is left in the standby mode, and the communication channel is loaded only if the process desired is recorded. The results of the observation of Earth by means of lunar stations will be determined to a great extent by the capabilities for transmission of information to Earth. It is possible that large volumes of data may be delivered to the Earth by astronauts traveling to the moon to pick it up [9].

2.2. Observations of the Sun

The sun determines the most important phenomena occurring both on Earth and throughout the solar system; therefore, the study of processes on the sun and their influence on other phenomena is one of the central scientific and practical tasks.

On Earth, special solar observation services are organized, satellites are launched to make observations of the sun and predict solar phenomena, solar probes are launched -- spacecraft designed to fly around the sun, as close as possible to it.

Automatic lunar stations can also make a significant contribution to the study of our star. Lunar stations, for example can

be used to study the conversion, the "intergrowth" of the solar corona into the interplanetary medium, to study the sun as it is eclipsed by the Earth, to record solar flares in frequency ranges and intensities inaccessible to terrestrial observation, and to study individual areas on the sun.

Observations from the moon can also see stars at angles close to the sun and therefore provide a practical test of some aspects of the theory of relativity, according to which the light of a star should be bent by the field of gravity of the sun as it passes. The duration of such an experiment would be determined only by the time required for the sun to "drift" out of the area of the sky observed.

The prospects for determination of the radiation patterns of solar activity centers and establishment of the relationship between processes in various areas of the sun by simultaneous observation from a lunar station and from on board one or more spacecraft are also quite promising. These measurement can be performed in any radiation band, promising great success in the prediction of the development of processes on the sun, which significantly influence phenomena on Earth. /19

The equipment on a lunar station for observation of the sun should include astrophysical instruments and devices to orient them toward the sun and stars.

2.3. Detection and Study of Small Bodies in Space

In recent years, radio astronomers have discovered a number of stellar radio sources (pulsars and quasars) of very small dimensions. These discoveries have been largely a result of the use of large terrestrial radio telescopes. In order to increase angular resolution, interferometers are used, stations with two receiving antennas in each of two planes. The resolving capacity $\Delta\theta$ of an interferometer is determined by the accuracy of measurement of the phase difference $\Delta\phi$ (or propagation time) of the radiation of a source received by the different antennas, while the phase difference itself depends on the ratio of the base length d (Figure 6) of the interferometer to the length of the wave being studied λ:

$$\Delta\theta = \Delta\phi\frac{\lambda}{2\pi d}\cos\theta.$$

With terrestrial measurements, two limitations are present. First of all, the base length cannot be greater than the diameter of the Earth, which, for example, where λ = 20 cm limits $\Delta\theta$ to a value on the order of 10^{-3}-10^{-4} angular seconds. Secondly, the

frequency of the radiation studied is actually limited due to the influence of the atmosphere to the upper end of the radio band.

The placement of astrophysical stations on the moon can significantly decrease both of these limitations. For example, an interferometer could be constructed with a base consisting of the distance from the Earth to the moon, the length of which would be over 30 times the maximum possible terrestrial base. True, in this case the lunar station would have to be equipped with a large antenna in order to increase its sensitivity to the level of the radiation received, which involves significant technical difficulties.

Small lunar stations can act successfully as interferometers in the millimeter, submillimeter and shorter wave bands of the electromagnetic radiation spectrum. In this case, the radiation receivers can be of moderate size, the base length from a few tens or hundreds of meters to several tens of kilometers. Such an interferometer, consisting of two or three lunar stations, would have one very significant advantage over an interferometer consisting of several spacecraft in flight (for example satellites), in that the problem of maintaining a stable base length would be solved. For space stations, stability of base length requires the use of special devices for precision measurement of the parameters of motion of the stations and devices for correction of this motion.

Automatic lunar stations for interferometric measurement should have identical systems for reading of directions and devices for spatial orientation of the observation instruments. The electronic equipment of the stations must be synchronized for processing of the signals received.

CHAPTER 3

SCIENTIFIC-TECHNICAL AND TECHNOLOGICAL TASKS OF PLANETARY STATIONS

The success of the performance of scientific research by planetary stations depends primarily on the reliability of all systems of the stations: provision of the proper thermal mode, power supply, communications with the Earth, orientation of the instruments of the station. The process of delivery of the station to the planet itself is also important. Solution of these problems requires that specific studies and tests be performed under the conditions of the planets, and that automatic support stations be created. /20

3.1. Navigation and Communications

The provision of planetary research bases consisting of several long-lived automatic stations, requires that rockets be sent to predetermined regions on the planet. Piloted spacecraft must also land in strictly selected areas. On the Earth, this navigational problem is primarily solved using a system of radio beacons, especially airfield guide beacons.

A similar function could be performed by a comparatively simple planetary station, the main requirement of which would be a long service life. For a landing on the moon, such a radio or light beacon would be used together with the stars, and astronauts would also utilize visual observation. On Venus, covered with clouds, a radio beacon "tied in" to its coordinates by means of terrestrial and space stations, might be the only reliable benchmark for navigational measurements. In addition to the problems of flight and landing of spacecraft onto the surface of the planet, such a beacon station would also be needed for navigation over the surface. Such systems are under development for the moon and are in planning for Mars.

An unusual atmospheric composition or the absence of any atmosphere at all, the lack of a magnetic field of a planet or an anomalous field, require a completely new approach to the problem of communications and navigation. Even for the moon, the problem of communications over the horizon between stations has not been solved. Many versions have been suggested: relay through a terrestrial station or through a lunar satellite, or over a train of lunar UHF relay stations placed by astronauts, or communication by wires.

There is no doubt of the possibility of relay through an Earth station, although this method is unusable for studies of the far side of the moon, which can be performed most safely by automatic equipment. One promising method, particularly for narrow-band systems, is radio communication by means of comparatively long wavelengths, which can propagate around obstacles [10].

If there are several research stations on a planet, it may be undesirable or impossible to maintain direct radio communications between each station and the Earth. The results of measurements or observations of these stations might be slowly transmitted over the narrow-band communication channels mentioned above to a service station for collection of information. This station would be equipped with long-range communications equipment, including an antenna directed toward the Earth, and would transmit, at regularly scheduled times or on command, all of the information accumulated. Thus, the composition of apparatus carried by research stations is determined basically by the scientific instruments, while the composition of the service station would be determined by the equipment required to collect information and maintain communications with the Earth. /21

3.2. Testing of Materials and Mechanisms

The development of principles and practical creation of primary support systems for planetary stations require that the characteristics and properties of the structural materials, coatings, lubricants, mechanisms and all sorts of sensing elements of scientific devices, electronic units, etc. be tested in a situation corresponding to exposure to the conditions of space. Parts 2 and 3 of this book present certain factual and calculated data on the effects of the space medium.

Today, tests conducted on the Earth can successfully imitate many of the conditions of space: vacuum, temperature mode, mechanical loads during powered flight, and partially solar and cosmic radiation. It is significantly more difficult to reproduce the corpuscular streams, forces of gravity, compositions of atmospheres and, most importantly, the entire complex of conditions on another planet simultaneously.

When the American astronauts arrived on the moon and found the Surveyor spacecraft sent there years earlier, they were surprised by the external appearance of the station, which had been "sunburned," changed in color as a result of the summary effect of conditions on the moon, including collisions with meteorites, causing erosion of the structural materials of the station. All of this indicates the need to perform a number of tests of materials, mechanisms, elements under actual planetary conditions. This is particularly important for reliable planning of long-lived

automatic stations and, in the final analysis, for reliability of studied performed using these stations.

Automatic planetary stations can also be used as a basis for these tests. It would seem convenient to create not only large, complex stations, but also small, specialized stations for the performance of one or a few combined tests. In this case, the design and composition of the station could be selected so as not to interfere with the experiment to be performed.

The tests needed under planetary conditions, for example, include:

-- the study of the changes in characteristics of absorption and reflection of various materials and coatings;

-- study of changes in the effectiveness of solar batteries and other power supplies and methods of their stabilization;

-- study of moving (rotating) mechanisms;

-- study of the strength, elasticity, insulation and other properties of materials;

-- testing of the tightness of seal of closed elements and instruments;

-- study of inflated, stressed, hardening and other structures;

-- testing of devices for storage and pumping of gasses and liquids;

-- testing of the properties of optical, semiconductor, magnetic and other elements.

3.3. The Search for Natural Resources for the Operation of Planetary Stations /22

In analyzing problems of automatic stations for the study of the planets, we have not discussed investigation of the chemical and physical composition and properties of planetary rock, although production of this information is a fundamental scientific problem. The fact is that physical and chemical analysis of rock, as well as analysis of the atmosphere of the planets, is an inseparable part of any planetary investigation, and frequently should be performed even by means of short-lived stations. However, the duration of the conduct of analysis and the time necessary to transmit information to Earth require that automatic planetary stations be planned to have long service lives.

Automatic stations are equipped with mass spectrometers, gas chromatographs, neutron analysis instruments and other microlaboratories for the performance of physical and chemical studies; the stations are equipped with sample collectors, drills and probes.

In addition to their purely scientific significance, such experiments are necessary to determine the capabilities for the use of planetary resources for the operation of the systems of the stations. For example, in this book in our analysis of power supply sources for stations it will be shown that the most effective are the so-called fuel elements, the operation of which requires fuel (for example, hydrogen or carbon monoxide) and an oxidizer (such as oxygen). Naturally, for a long period of operation of a station it is impossible to deliver the required quantity of these substances from Earth. They must be sought on the planet and we must learn to extract them in the required form.

Thus, planetary stations of the future will contain equipment for the processing and use of local resources.

3.4. Testing of Conditions for Life and Search for Life Forms

These problems are closely interrelated, although they may have quite different significance. For example, testing of conditions for life is necessary for preparation for the activity of astronauts on the planets. The testing agents might be organisms delivered from the Earth. It is important to search for water, and test methods of growing of plants. However, the planet itself might be dead.

In the case of search for extraterrestrial life, stations must perform a complex of biological investigations, complicated by the need to automate the performance of the complex analyses and processes of life stimulation.

At the present time, the criteria of life most frequently used are one or a combination of the following conditions: signs of metabolism, indications of growth and proper chemical composition.

The required apparatus is also being developed. For example, an American plan [11] for an automatic biological laboratory, an overall view of which is shown in Figure 7, calls for the inclusion of chambers with nutrient media for microorgansims, sampling mechanisms, growth analyzers, a chromatograph, a spectral analyzer and other devices.

It is hard to imagine that specimens of the natural formations of other planets could be brought back to Earth for utilitarian purposes. They are needed today only for scientific research. However, the use of the atmosphere, terrain relief and comparatively shallow formations for life support of planetary stations does seem desirable.

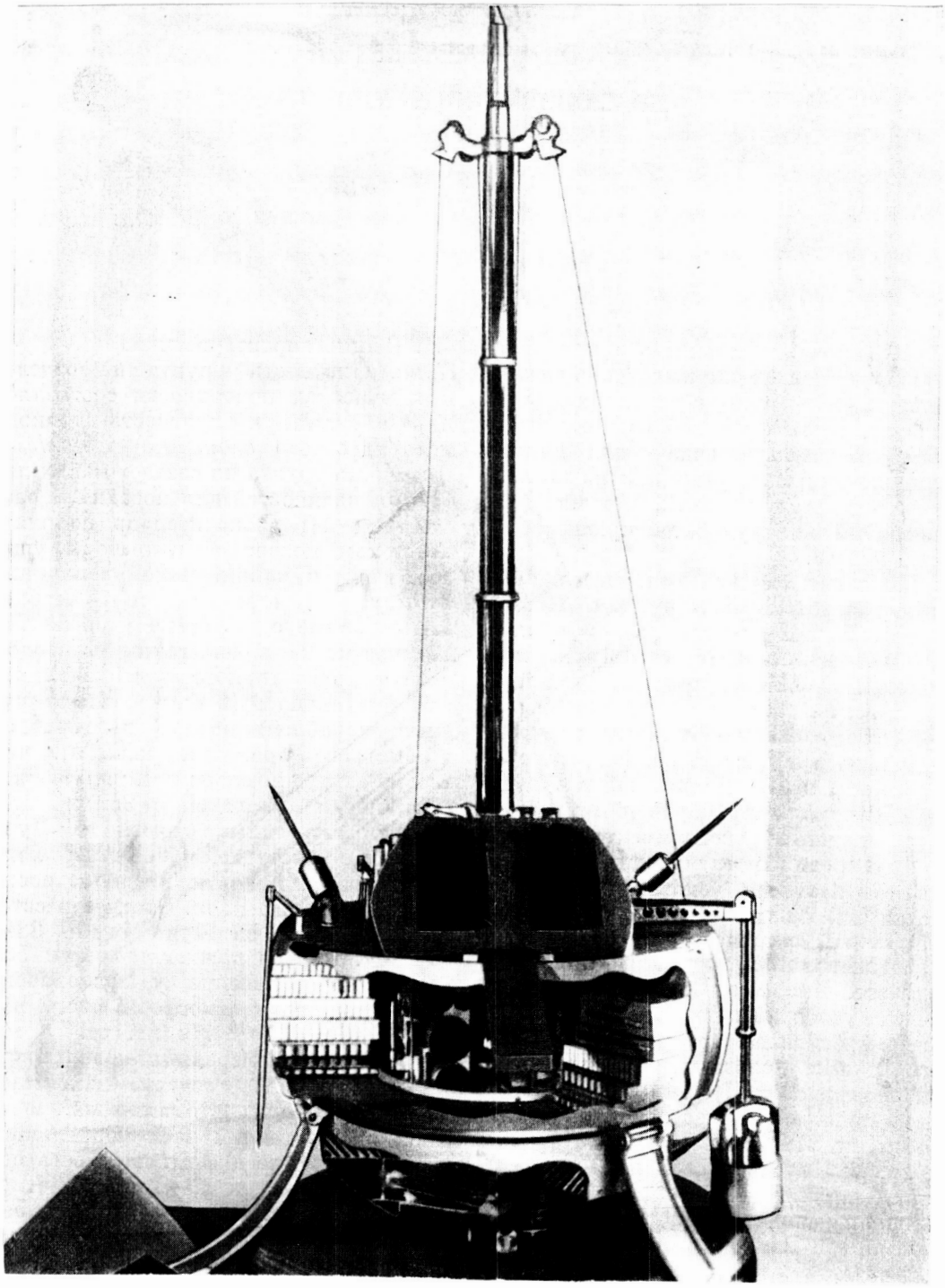

Figure 7. An American Automatic Station for Biological Studies on Mars (Planned)

CHAPTER 4

BRIEF INFORMATION ON THE CONDITIONS ON SURFACES OF THE PLANETS

The planning of stations and devices designed for the performance of research work under the conditions of other planets differs significantly from the similar tasks for terrestrial and near-Earth stations, both due to the unusual nature of these conditions and sometimes due to the great difficulties in adapting to them. /24

Extraterrestrial conditions are considered in the development of APS designs, in particular in calculations of strength, areas of contact with the surface, meteorite protection, in selection and planning of systems for maintenance of the desired thermal mode of the station, in selection and design of radio communication lines and orientation devices, and in the development of methods and instruments for the performance of scientific experiments.

The difficulties of planning are multiplied by the fact that conditions on the surface of the planets differ significantly from conditions in space, which must be encountered during the flight to the planets. Furthermore, even if we know the planetary conditions, it is frequently a problem to imitate them under terrestrial laboratory conditions. Whereas the conditions on the surface of the moon have been tested to a great extent by direct observation, conditions on the surface of, for example, Mars and Venus have been determined to date only under a number of assumptions. Let us briefly study the information available on conditions on the planets.

4.1. General Characteristics

Moon. The density of the soil in some areas of the surface is 2-3.5 g/cm^3, while the density of the thin surface layer is 0.8-1.6 g/cm^3. The strength of the soil creates no problems for landing and placement of APS. The surface relief is considerably more unfavorable: craters, gorges, rocks and stones of various sizes. Since the landing of APS requires smooth, even surface sectors, the search for such areas requires real-time television or visual (in the case of manned spacecraft) observation of the surface and rapid decision making, which is very difficult when landing devices are controlled from Earth.

The acceleration of the force of gravity on the moon averages 1.62 m/sec^2, although significant heterogeneities of the

gravitational field are observed. The main distance from the Earth to the moon is about $384 \cdot 10^3$ km. The period of rotation around the axis is 27.3 days. The pressure at the surface, due to the absence of an atmosphere, is almost zero: 10^{-12}-10^{-13} mm hg.

Mars. Direct measurements on the surface have never been performed. Calculations, measurements from Earth and from automatic interplanetary spacecraft and comparisons yield the following figures: density of surface layer 1-2 g/cm^3, atmospheric pressure at surface 5-15 mbar, nature of surface reminiscent of the moon.

The mean value of acceleration of the force of gravity on the surface is 3.72 m/sec^2. The period of rotation about Mars' axis is about 24.5 hours. Strong winds are sometimes present (with speeds up to some tens of meters per second), causing dust storms. This factor must be considered in calculating the stability of Martian APS. The minimum distance from the Earth to Mars (in opposition) is from 55.7 to 101.2 million km. However, the length of a radio communications line must be calculated for less favorable conditions, at about 250-300 million km. /25

Venus. In spite of the intensive studies of Venus conducted by means of spacecraft and terrestrial equipment, we still have no reliable information concerning its surface and the individual characteristics of the atmosphere. The atmospheric pressure at the surface of Venus is about 100 atm. This is the first difficult encountered in the development of APS for operation on the surface of Venus. The density of the surface layer is not reliably known, the mean density is about 5 g/cm^3. Winds are possible with speeds of up to tens of meters per second. The acceleration of the force of gravity at the equator is about 8.8 m/sec^2. The distance between the Earth and Venus varies from 38 to 61 million km. The period of rotation of Venus about its axis is 243 days, and the direction of rotation is opposite to that of the Earth.

4.2. Thermal and Optical Characteristics

Moon. The temperature of the surface at the equator varies from +(120-130)° C in the daytime to -150° C at night. At other latitudes, these fluctuations are less. Due to the low heat conductivity of surface rocks, fluctuations in the temperature decrease sharply with depth. The maximum flux of solare energy on the surface of the moon reaches approximately 0.14 w/cm^2. The reflectivity of the lunar surface (albedo) based on the lunar disc visible from the Earth averages 0.07, although it reaches 0.4 at the edges of some craters. The coefficient of thermal radiation of the lunar surface apparently is 0.96-0.99. Thus, the temperature conditions place rigid demands on planned lunar APS, while the optical conditions favor the development of astronomical studies on the moon.

Mars. The surface temperature varies seasonally and during the course of the day, fluctuating from -100 to +20° C at the equator. The solar constant is about 0.06 w/cm^2. The mean value of the albedo of Mars is 0.15.

Venus. The temperature of the surface of Venus by extrapolation of data, may reach 500-600°. In the polar areas, the temperature is lower -- about 300° C. The dense atmosphere, with phase composition not reliably known, may absorb light significantly; therefore, the conditions of illumination at the surface are also unknown[1]. This uncertainty hinders the performance of such tasks as production of photographic images of the surface, calculation of the effectiveness of solar batteries for electric power supply of apparatus, selection of methods of orientation of APS instruments, etc. Knowledge of the mean albedo of the planet (about 0.76) indicates little of the characteristics of reflection of the solid surface.

The thermal balance of the planet and the nature of the high temperatures require further clarification. This information is necessary for the planning of APS, particularly for proper selection of a system for maintenance of the thermal mode of the station. The solar constant near Venus is about 0.27 w/cm^2.

4.3. Conditions of Radio Communications and Orientation /26

The conditions of radio communications are determined primarily by the presence or absence of an ionosphere, the electrical characteristics of the soil (dielectric constant and conductivity), absorption in the atmosphere and the nature of the relief of the planet. We are interested both in radio communications conditions between the APS and Earth, and between several APS located on the surface.

Moon. Radio communications between APS on the visible side of the moon and the Earth are limited only by the Earth's atmosphere. Therefore, APS-Earth radio lines operate quite successfully in the meter, decimeter and centimeter wave bands. Communications are also possible in shorter wave bands, for which there is a transparency window in the Earth's atmosphere.

The possibilities of radio communications between two or mor APS on the surface of the moon are limited by the following factors. First of all, due to the practical absence of an

[1]The Venera-8 APS measured the temperature and illumination on the surface. The expected value of temperature was confirmed. It was established that sunlight, although weakened, does reach the surface of Venus.

ionosphere, ionospheric scatter cannot be used for shortwave communications as is the case on Earth. Secondly, the small radius of the moon (great curvature) significantly reduces the range of line-of-sight communications which can be used for UHF and SHF radio devices, in comparison to the Earth. Therefore, as was noted in an earlier chapter, it is possible in principle to use the following methods of radio communications on the moon over long distances: relay through specially constructed UHF relay stations, the use of long waves, capable of bending around obstacles, relay through an Earth station (if the APS to be connected are visible from the Earth) and, finally, artificial lunar satellites. Apparently, relay through an Earth station and long wave communications are the most realistic alternatives.

Orientation of APS instruments on the moon can be most simply performed by the use of the stars and astrosensors. Thus, the problems of radio communications and orientation on the moon are primarily technical in nature although, for example, the electrical parameters of the moon require some clarification.

Mars. Experiments involving radio occultation performed using APS have established that there is a Martian ionosphere with a maximum electron concentration of about 10^5 per cubic centimeter at an altitude of 130 km on the day side. Therefore, in contrast to lunar conditions, it is possible in principle to achieve radio communications by short wave between remote points on Mars, at least in the daytime. Other methods are also possible.

Communications with Earth can be maintained by well-tested methods: directly in the SHF and even UHF bands or by relay through an artificial Mars satellite equipped with the necessary apparatus. The primary task is concentration of the signals transmitted in the direction toward the Earth.

The main method of orientation is stellar, although difficulties related to ambiguous determination of the required direction due to interfering reference points (stars) make it desirable to perform orientation toward the Earth using radio direction finding on the radiation of the terrestrial transmitter.

Venus. In planning a system for radio communications through the atmosphere of Venus, one must consider the following factors [4, 10]. Due to the high density of the atmosphere, strong absorption and scattering of radio waves are observed, particularly in the centimeter and shorter wave bands. Calculations have shown that with a pressure at the surface of 80-100 atm a content of 97% carbon dioxide and 0.1% water vapor, the total vertical attenuation for a 10 cm wave would be less than 1 db, for a 1 cm wave -- over 40 db. Furthermore, an ionosphere has been recorded around Venus with a maximum electron concen- /27

concentration of 10^4-10^5 per cubic centimeter, placing a bottom limit on the wavelength band suitable for communications with the Earth.

Thus, communications between Venusian APS and Earth are most reliable in the decimeter wave band. As concerns communications on the surface of Venus, we do not as yet have sufficiently reliable data to make a judgment, although we cannot exclude the possibility of communications by reflection from the ionized layers of the atmosphere and line-of-sight UHF communications.

The orientation of APS on the surface of Venus will probably be performed by artificial radiation of Earth stations or the natural radio emissions of other space sources on the decimeter or somewhat longer wave bands, until we have reliable information on the visibility of stars from the surface of Venus.

4.4. Comparison of Conditions on the Surfaces of the Planets

The conditions on the planets discussed above, which have significant influence on the planning and operation of APS, are presented for comparison in Table 1; here also are presented data for the Earth.

TABLE 1

Planet	Atmospheric Pressure at Surface, atm	Acceleration of Force of Gravity, m/sec^2	Extreme Surface Temperatures, °C	Solar Constant, w/cm^2	Albedo	Maximum Electron Concentration, Electrons/cm^3
Earth	1.0	9.8	-70-+50	0.14	0.35	Up to 10^6
Moon	10^{-12}-10^{-13}	1.62	-150-+130	0.14	0.07	10-10^3 (Expected)
Mars	(5-15)·10^{-3}	3.72	-100-+20	0.06	0.15	Up to 10^5 Day
Venus	About 100	8.8	About +500	0.27	0.76	10^4-10^5 Day

Note. The albedo of Earth and Venus are given as mean values considering cloud cover.

In comparison with terrestrial conditions, the most difficult conditions of survival, orientation and communications are those on Venus. However, these conditions require further refinement and confirmation.

The moon is dangerous for APS primarily due to the very great changes in temperature (up to 280° C on the equator) and the lack of atmospheric protection from meteorites and radiation. However, conditions here are most favorable for celestial orientation of instruments and communications with the Earth, from the visible side of the moon.

If APS are placed on Mars, a problem arises in the planning of a compact system for communications with Earth, due to the great communications range, although in principle radio communications links can be produced today with ranges of up to a billion kilometers. The rarefied atmosphere of Mars requires that we be particularly careful in evaluating the possibility of electrical breakdown in open electronic apparatus.

The different values of atmospheric density of the planets, accelerations of the force of gravity and densities of the soil require that different methods of delivery of APS to the surface of the planets be used. Although several delivery methods have been tested in practice, automatic placement of several stations /28
over the surface of the planet is a new, little-tested task. Thus, the principles of design and construction of APS, methods of delivery and communications with them must be selected for each specific planet. Some possible solutions of these problems are studied in subsequent chapters in this book.

REFERENCES

1. "Astronautics," Sovetskaya Entsiklopediya [Soviet Encyclopedia], Moscow, 1970.
2. Jaffe, L. D., "Results of Recent Studies of the Moon by Manned and Unmanned Spacecraft," Trudy XIII Kongressa KOSPAR, 1971, No. 1.
3. Andreyanov, V. V., "The Day is Coming," Pravda, 29 September 1970.
4. Konashenok, V. N., K. Ya. Kondrat'yev, Novoye o Venere i Marse [What's New on Venus and Mars], Moscow, Gidrometeoizdat Press, 1970.
5. Kokurin, Yu. L., V. F. Lobanov, "The Possibility of Studying the Physical Libration of the Moon by the Method of Optical Location," Kosmicheskiye Issledovaniya, 1968, Vol. 6, No. 2.
6. Andreyanov, V. V., "Automata in Space," Pravda, 23 May 1969.
7. Krotikov, V. D., V. S. Troitskiy, "The Thermal Conductivity of Moon Rocks According to Precision Measurements of Radio Emissions of the Moon," Astron. Zh., 1963, Vol. 40, No. 1.
8. Moroz, V. I., Fizika Planet. [Physics of the Planets], Moscow, Nauka Press, 1967.
9. Kulikov, K. A., Pervyye Kosmonavty na Lune [The First Astronauts on the Moon], Moscow, Nauka Press, 1965.
10. Kolosov, M. A., N. A. Armand, O. I. Yakovlev, Rasporstraneniye Radiovoln pri Kosmicheskoy Svyazi [Propagation of Radio Waves in Space Flight], Moscow, Svyaz' Press, 1968.
11. Spaceflight, 1967, No. 7.

PART 2

PROVISION OF THE REQUIRED THERMAL MODE OF AUTOMATIC PLANETARY STATIONS

Any program of study of space, based on the use of automatic spacecraft (and not even automatic devices alone) can be successfully performed only if all elements of the spacecraft operate properly. /29

One of the most important conditions required for fulfillment of this requirement is maintenance of the thermal state of each component element of the spacecraft within strictly defined limits throughout the entire time of its existence (flight). Failure to observe this condition causes deterioration of the operation of any element and its failure.

One quantitative measure for evaluation of the thermal state of a spacecraft is the temperature of its elements (FIgure 8), the spatial distribution of which throughout the entire volume of the spacecraft forms its temperature field. In this book, by the temperature of the spacecraft T_a we shall mean the average temperature of the spacecraft as a whole or of its individual elements.

The change in the temperature field with time is called the thermal mode of the spacecraft, and maintenance of the temperature within limits between the minimum permissible ($T_{a\ min}$) and the maximum permissible ($T_{a\ max}$) throughout the entire time of the flight is called provision of the required thermal mode of the spacecraft.

In analyzing the thermal state of a spacecraft, its flight trajectory is divided into several stages:

stage SE -- flight of the spacecraft in orbit around the Earth, when it is a satellite of Earth;

stage EP -- flight of the spacecraft from orbit around the Earth to orbit around another planet;

stage SP -- flight of the spacecraft in orbit around another planet, when it is a satellite of the planet;

stage P -- time spent by the spacecraft on the surface of another planet.

For example, when a spacecraft flies to the moon or Mars, these stages can be represented as follows: SE -- EL -- SL -- L and SE -- EM -- SM -- M.

The stages of flight between the surface of the Earth or a planet and orbits around them usually have little influence on the

mode of the spacecraft (except for boosters) and therefore will not be studied here.

Usually a spacecraft in flight is subjected to the thermal effects of the surrounding medium, corresponding to each flight stage, while the temperature of its elements is determined by the relationship between the thermal energy applied to it and carried away from it. Heat transfer away from a spacecraft is achieved by means of the thermal radiation of its outer surface and by heat conductivity at points of contact with the surrounding medium. Heat transfer to the spacecraft from the surrounding medium occurs by the same mechanisms as does heat liberation from the spacecraft.

The difference between the applied heat (Q_k) and liberated heat (Q_ε) is called the heat exchange of the spacecraft with the surrounding medium (Q); we will refer to this difference also as the penetrating heat flux (Q_π). /30

The penetrating heat flux Q_π is considered positive if more heat is applied than is liberated ($Q_k > Q_\varepsilon$), and negative if more heat is liberated than applied ($Q_k < Q_\varepsilon$).

Heating (or cooling) of spacecraft may also result from liberation (or absorption) of thermal energy within the spacecraft, referred to as internal heat liberation (Q_T). For example, heat is liberated as instruments operate and is absorbed as fluids evaporate in the evaporator and are exhausted in vapor form outside the spacecraft.

The internal heat liberation Q_T is considered positive if it causes an increase in temperature T_a, or negative if it decreases this temperature.

In our analysis of the thermal state of a spacecraft, we cannot follow the temperature of all points of its temperature field; for this reason, several of the most characteristic points are selected, at which the expected rate of change of the temperature is greatest in comparison to all others, and where a shift in temperature outside the permissible limits would cause a disruption of normal operation of the spacecraft.

If at the initial moment in time, the temperature at any point in the spacecraft was T_{a0}, it may subsequently change in flight approximately as shown in Figure 9.

Temperature T_a and its rate of change $dT_a/d\tau$ depend on the value of internal heat liberation Q_T, penetrating heat flux Q_π

and the thermal inertia of the spacecraft, usually characterized by the effective heat capacity C_{eff}, i.e., the quantity of thermal energy necessary to change the temperature of the spacecraft by 1°.

If we know Q_T, Q_π and C_{eff}, we can determine the change in the temperature of the spacecraft with the passage of time by using the following thermal balance equation:

$$C_{eff} \frac{dT_a}{d\tau} - Q_T - Q_\pi = 0. \qquad (2.1)$$

As a rule the penetrating heat flux Q_π and internal heat liberation Q_T depend on temperature T_a and flight time τ:

$$Q_\pi = f_\pi(T_a, \tau), \qquad (2.2)$$

$$Q_T = f_T(T_a, \tau). \qquad (2.3)$$

Substituting (2.2) and (2.3) into (2.1), we produce the thermal balance equation:

$$C_{eff} \frac{dT_a}{d\tau} - f_\pi(T_a, \tau) - f_T(T_a, \tau) = 0. \qquad (2.4)$$

If after solution of this equation for temperature T_a we find that it remains unchanged with the passage of time ($dT_a/d\tau = 0$), we refer to the thermal state of the spacecraft as stable; if temperature T_a changes with the passage of time ($dT_a/d\tau \neq 0$), it is unstable.

As was noted above, the change in the thermal state of the spacecraft with time is called its thermal mode; naturally, both stable and unstable thermal modes are possible.

For a stable thermal mode, equation (2.4) becomes

$$f_\pi(T_a) + f_T(T_a) = 0. \qquad (2.5)$$

In order to determine the temperature of the spacecraft in flight, we must know the heat-physical characteristics of the spacecraft, the surrounding space medium and the characteristics of the thermal coupling between them.

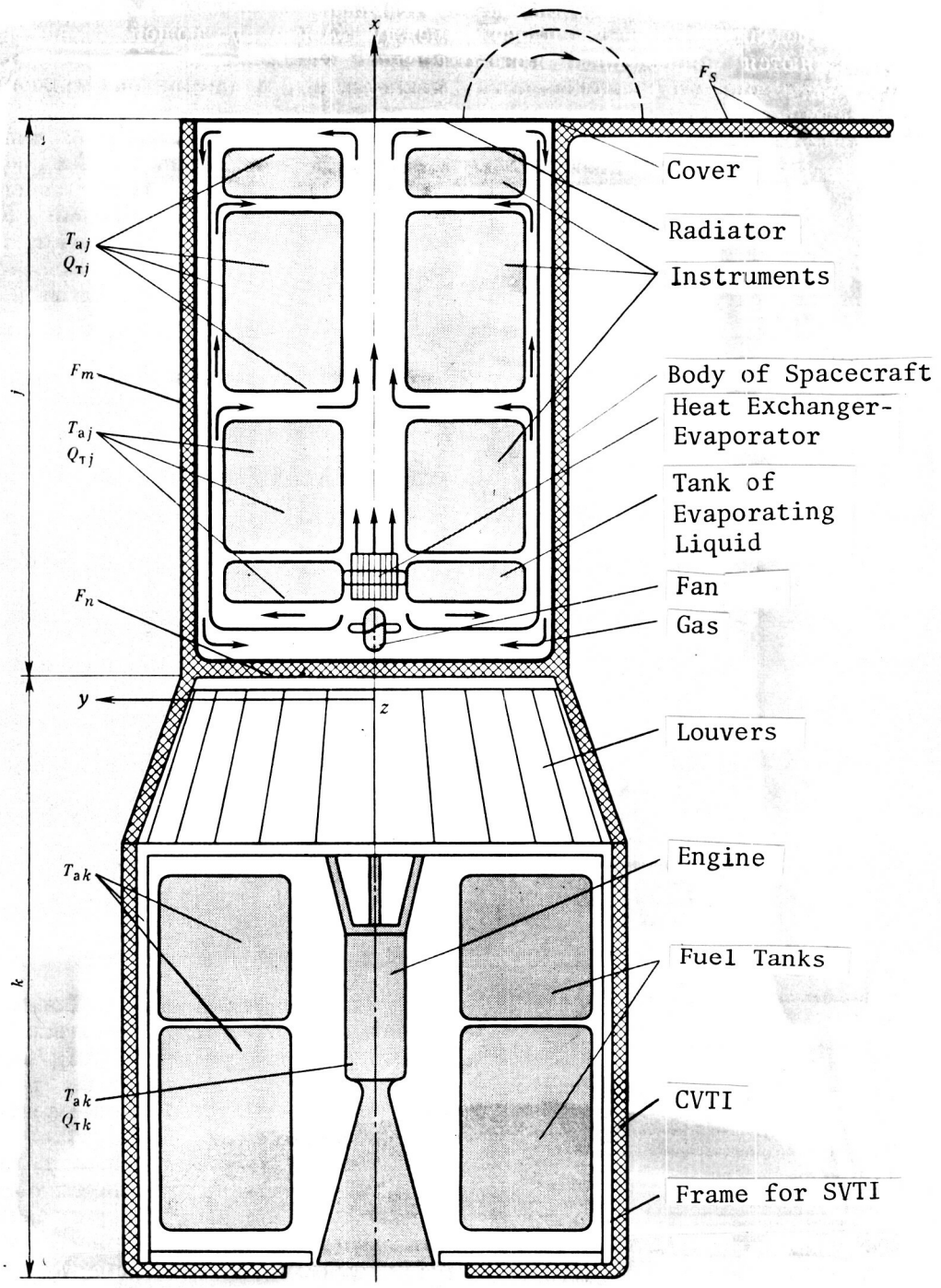

Figure 8. Thermal Model of a Spacecraft. j, k, Parts of Spacecraft; F_S, Surface of Spacecraft Illuminated by Direct Solar Radiation; T, Temperature of Spacecraft, Q, Heat Liberation; F_m, Side Surface of Spacecraft; F_n, Surface of Spacecraft Not Illuminated by the Sun

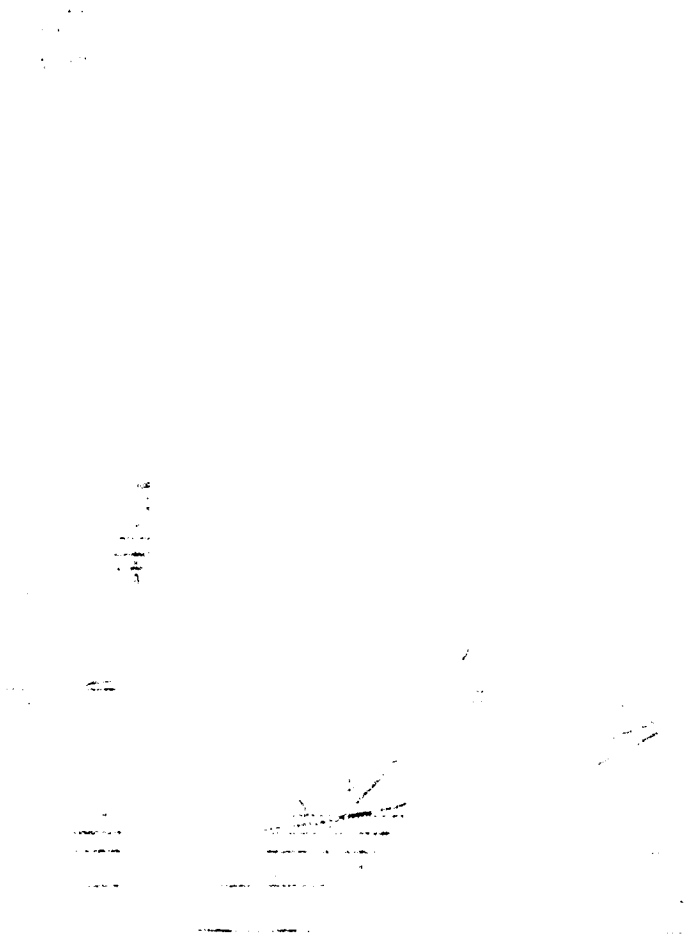

The heat-physical characteristics of the spacecraft, which determine its thermal mode, are the adjusted radiation factor of its heat insulation ε_{aa}, the degree of blackness ε_a and the solar radiation absorption factor A_a of the outer surface of the spacecraft, internal heat liberation Q_T and effective heat capacity $C_{eff\ a}$. /32

The heat-physical characteristics of the surrounding medium are its temperature T_k, degree of blackness ε_k, solar radiation absorption factor A_k, heat conductivity λ_k, heat capacity C_k and specific gravity γ_k.

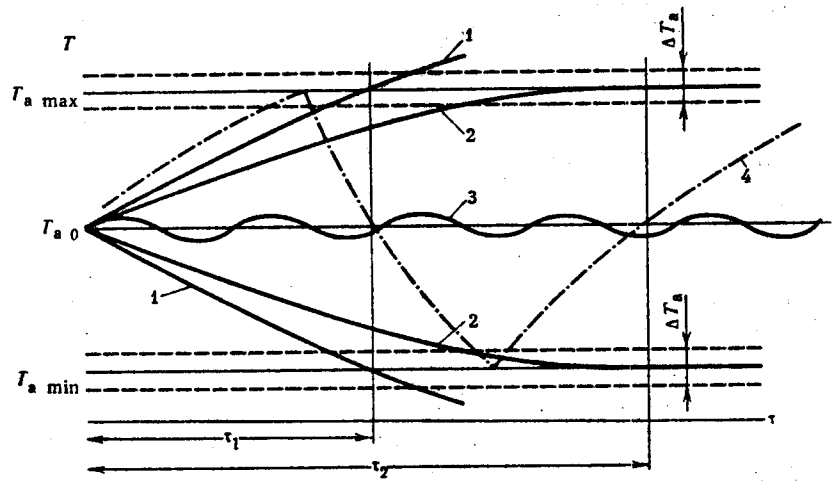

Figure 9. Possible Cases of Change in Temperature of Spacecraft in Flight. 1, After time $\tau = \tau_1$, temperature goes beyond fixed limit $T_{a\ max}$ or $T_{a\ min}$; 2, After moment $\tau = \tau_2$, temperature remains constant; 3, Temperature is constant from $\tau = 0$; 4, Temperature varies periodically from $T_{a\ max}$ to $T_{a\ min}$.

The characteristics of the thermal couple between the spacecraft and the surrounding medium are the radiation factor ϕ_{ak} and the contact heat conductivity λ_{ak}.

Usually, the values of certain heat-physical characteristics of the spacecraft are known in advance. Determination of the values of the heat-physical characteristics of the spacecraft which

provide for maintenance of its temperature within fixed limits throughout the flight is called thermal design of the spacecraft. Thermal design based on a stable thermal mode [equation (2.5)] is called static thermal design, while design based on an unstable thermal mode [equation (2.4)] is called dynamic thermal design. Initially, as a rule, static thermal design is performed, followed, if necessary by refinement of the values of heat-physical characteristics of the spacecraft produced by dynamic thermal design; in many cases, only static thermal design is required. /33

The system of spacecraft elements used to maintain its heat-physical characteristics at their required values in various stages of flight is called the thermal mode support system (TMSS); this system may be passive (PTMSS) or active (ATMSS, frequently called TRS -- the thermal regulation system).

TMSS include, for example, such elements as the heat insulation of the spacecraft, coatings on the outer surfaces of the spacecraft (used to provide the required values of optical coefficients ε_a and A_a), cooling radiators, heating radiators, heat liberation sources, heat accumulators and evaporators.

The thermal couple between these elements of the TMSS and the elements of the spacecraft, frequently located at some distance from each other, is achieved by means of TMSS elements called heat conductors, which are divided into liquid, gas, vapor, radiation, metal and electrical heat conductors.

The elements of the TMSS also include temperature sensors and actuating mechanisms which, depending on the temperature of the structural elements of the spacecraft, apply or liberate the required quantities of thermal energy.

The optimal TMSS, in other words the TMSS superior to all other types, is that which maintains the temperature of the spacecraft within fixed limits, has maximum reliability and minimum weight; the technical possibility of creation of such a system depends primarily on proper selection of its type (PTMSS or ATMSS) and on the weight and reliability of its component elements.

The group of methods used to determine the values of heat-physical characteristics of spacecraft required to maintain the temperature of its elements within fixed limits in all stages of flight and selection of the actual equipment to be used to create the optimal TMSS is called the methodology of the thermal mode of the spacecraft TMSS.

The necessary information and approach to composition of the methodology of the spacecraft TMSS thermal mode are presented in Chapters 5, 6 and 9, while a description of some TMSS elements is presented in Chapters 7 and 8.

As a result of possible inaccuracies of the thermal design of spacecraft and differences in the values of true heat-physical characteristics of the spacecraft from calculated characteristics, a final conclusion of its thermal mode and the efficiency of the TMSS in flight can be drawn only after ground thermal testing of the spacecraft is performed.

The necessary information and approach to composition of a methodology for ground thermal testing of spacecraft are presented in Chapter 10.

CHAPTER 5

BASIC INFORMATION ON RADIANT HEAT EXCHANGE OF BODIES

Radiant heat exchange refers to the process of exchange of thermal energy between bodies by means of thermal radiation of the surfaces of these bodies. /34

The radiation results from processes within the atoms on the surface of a body, causing its thermal energy to be converted into electromagnetic wave energy, i.e., radiant energy. When it strikes the surface of another body, this radiant energy may be partially or completely converted to the thermal energy of the body.

The process of radiation follows certain rules, and radiant energy has a number of characteristics which must be known in calculating the thermal state of a spacecraft, since the most important type of heat exchange between spacecraft and the surrounding space medium is radiant heat exchange (with the exception of cases when the spacecraft is located in the dense atmosphere of the planets) [1-14].

5.1. Characteristics of Radiation

Monochromatic radiation is radiation in a range of wavelengths between λ and $\lambda + d\lambda$.

The total or integral radiation is radiation in the entire range of wavelengths from $\lambda = 0$ to $\lambda = \infty$.

The radiant flux E_F is the total quantity of radiant energy radiated by the surface of a body F in all directions per unit time (FIgure 10):

$$E_F = Q/\tau \ [w; \ kcal/hr]. \qquad (2.6)$$

The surface radiation density E is the total quantity of radiant energy radiated by a unit surface of a body in a unit time:

$$E = \frac{dE_F}{dF} \ [w/m^2; \ kcal/(m^2 \cdot hr)]. \qquad (2.7)$$

The spectral radiation density E_λ is that portion of the surface radiation density related to a selected wavelength interval $d\lambda$:

$$E_\lambda = \frac{dE}{d_\lambda} \left[w/m^3;\ kcal/(m^3 \cdot hr)\right]. \qquad (2.8)$$

The angular radiation density E_ϕ is the total quantity of radiation density per unit solid angle radiated in a fixed direction by a unit of surface

$$E_\phi = \frac{dE_{dF,\ d\omega}}{dF d\omega}$$

$$\left[w/(m^2 \cdot ster);\ kcal/(m^2 \cdot hr \cdot ster)\right]. \qquad (2.9)$$

Intensity of radiation J_ϕ -- the total quantity of radiant energy per unit of solid angle radiated in a given direction by the surface over a unit of its projection on a plane perpendicular to the direction of the radiation:

$$J_\phi = \frac{dE_{dF,\ d\omega}}{dF \cos\phi\ d\omega} = \frac{E_\phi}{\cos\phi}$$

$$\left[w/(m^2 \cdot ster);\ kcal/(m^2 \cdot hr \cdot ster)\right]. \qquad (2.10)$$

The spectral intensity of radiation -- that portion of the intensity radiation related to a selected wavelength interval $d\lambda$: /35

$$J_{\phi\lambda} = \frac{dJ_\phi}{d\lambda} \left[w/m^3 \cdot ster);\ kcal/(m^3 \cdot hr \cdot ster)\right]. \qquad (2.11)$$

Figure 11 shows the change in the intensity of radiation J_ϕ and an angular radiation density E_ϕ of an absolutely black body.

We can see from the figure that the intensity of radiation J_ϕ is identical in all directions, while the angular radiation density E_ϕ changes from the maximum $E_\phi = E_{\phi 0}$ (where $\phi = 0$) to the minimum $E_\phi = 0$ (where $\phi = 90°$).

Diffuse radiation is radiation for which the intensity of radiation J_ϕ is identical in all directions. For diffuse radiation, the surface radiation density E can be expressed through the intensity of radiation if we integrate the angular density of

radiation E_ϕ within the limits of a hemisphere:

$$E = \iint\limits_{\omega=2\pi} E_\varphi d\omega = J_\varphi \iint\limits_{\omega=2\pi} \cos\varphi \, d\omega.$$

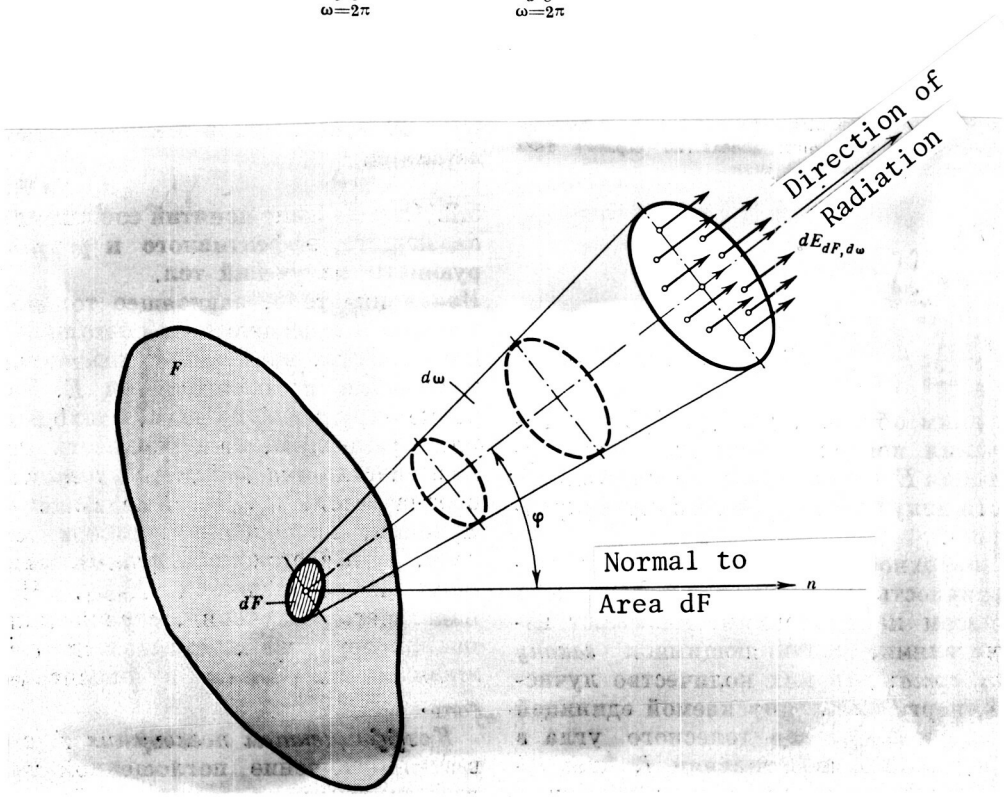

Figure 10. Determination of the Angular Density of Radiation E_ϕ of an Elementary Area dF in Direction ℓ

In order to perform this integration, we express the elementary solid angle $d\omega$ through elementary angles of latitude ϕ and longitude θ in spherical coordinates (Figure 12).

As we know, the elementary solid angle $d\omega$ is defined by the formula

$$d\omega = dF/R^2,$$

where dF is an elementary area, cut out by solid angle $d\omega$ on the surface of a sphere of radius R. We can see from Figure 12 that $dF = Rd\phi R \sin\phi \, d\theta$. Consequently,

$$d\omega = \sin\phi \, d\phi \, d\theta.$$

Then

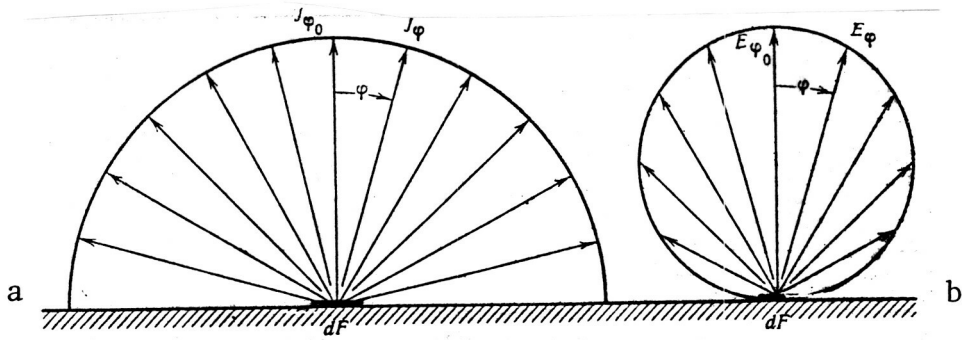

Figure 11. Distribution of Intensity (a) and Angular Density (b) of Radiation of an Absolutely Black Body as a Function of Direction

Thus, for diffuse radiation, the surface radiation density E is π times greater than the radiation intensity J_ϕ in any direction.

The surfaces of bodies for which radiation intensity J_ϕ is identical in all directions are called radiators which follow the Lambert law: for these radiators, the quantity of radiant energy E_ϕ emitted by a unit area in a unit solid angle in direction ℓ is proportional to the cosine of angle ϕ between this direction and the perpendicular to the area n, as follows from (2.10), i.e.,

$$E_\phi = E \cos \phi = \frac{E}{\pi} \cos \phi.$$

For many bodies, the intensity of radiation J_ϕ changes as a function of radiation direction. Figure 13 shows the change in the value of J_ϕ for certain materials as a function of angle ϕ.

We can see from the figure that the value of J_ϕ for metals is significantly higher where ϕ = 60-80° than in the perpendicular direction.

5.2. Definition of the Concepts of Natural, Incident, Effective and Resulting Radiation of Bodies

The radiation of a body which depends only on the thermal and physical states of its surface is called its natural radiation and represented by E. The radiation of the surrounding medium, striking or "falling" on the surface of the body is called the incident radiation and is represented by E_{inc}. That portion of the incident radiation absorbed by the surface of a body is called the absorbed radiation and is represented by E_{abd}. That portion of the incident radiation reflected from the surface of the body is called the reflected radiation and is represented by E_{rfd}.

Absorption factor A refers to the ratio of radiant energy absorbed by the body to the incident energy:

$$A = E_{abd}/E_{inc}. \tag{2.12}$$

Reflection factor R refers to the ratio of reflected energy to incident energy:

$$R = E_{rfd}/E_{inc}. \tag{2.13}$$

The sum of natural radiation E and reflected radiation E_{rfd} is called the effective radiation of the body:

$$E_{eff} = E + E_{rfd}. \tag{2.14}$$

The resulting radiation E_{res} refers to the difference between absorbed radiation E_{abd} and natural radiation E: /37

$$E_{res} = E_{abd} - E. \tag{2.15}$$

The resulting radiation will also be referred to in this book as the heat exchange of the spacecraft with the surrounding medium (Q) or the penetrating radiation (Q_p).

The resulting radiation can also be defined as the difference between the fluxes of incident and effective radiation:

$$E_{res} = E_{inc} - E_{eff}. \tag{2.16}$$

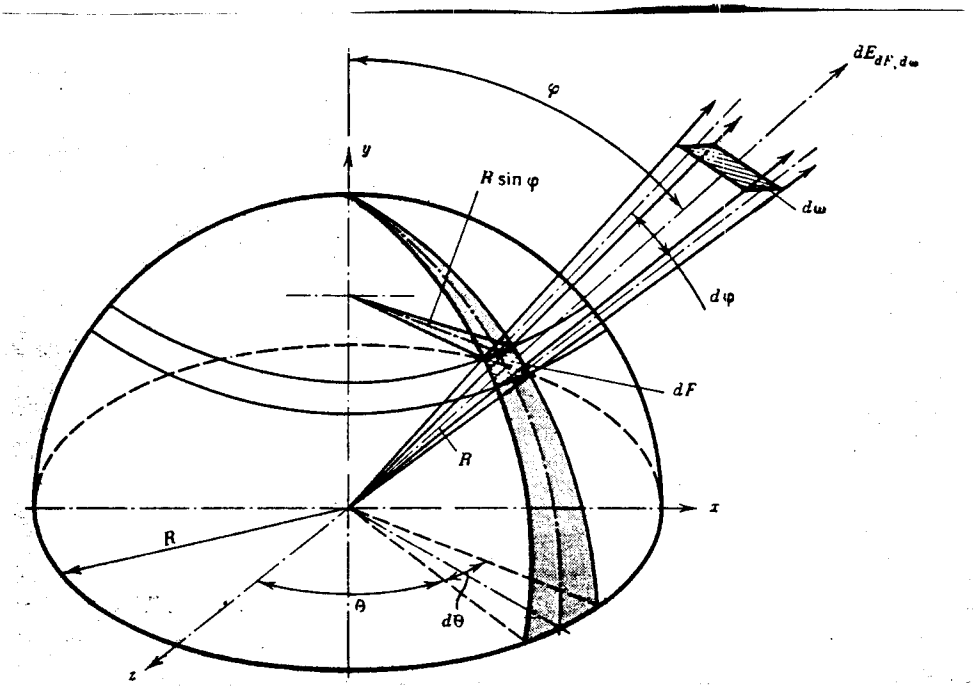

Figure 12. Determination of the Relationship Between Surface Radiation Density and Intensity of Radiation

Utilizing formulas (2.12), (2.15) and (2.16), the expression for effective heat radiation can be written as

$$E_{eff} = \frac{E}{A} + Q\left(\frac{1}{A} - 1\right). \qquad (2.17)$$

This formula, suggested by G. L. Polyak [13], relates the effective radiation of a body to its resulting radiation and significantly simplifies the production of calculation equations and analysis of the radiant heat exchange between bodies.

5.3. Basic Regularities of Natural Radiation of Absolutely Black and Grey Bodies

Determination of the value of natural radiation of bodies is based on the use of Planck's law, giving the value of the spectral density of radiation E_λ of an absolutely black body as a function of wavelength of electromagnetic radiation λ and temperature of the body T:

(2.18)

where $C_1 = 3.74 \cdot 10^{-16}$ w·m^2 = $3.21 \cdot 10^{-16}$ kcal·m^2/hr, $C_2 = 1.4387 \cdot 10^{-2}$ m·K. Here, an absolutely black body is generally taken to mean a body which fully absorbs all incident radiation (regardless of wavelength λ). /38

The change in the value of E_λ as a function of λ for various values of T is shown in Figure 14. The surface radiation density E can be found by integrating equation (2.18) within limits $0 \leq \lambda \leq \infty$, producing the Stefan-Boltzmann law

$$E = C_0 (T/100)^4, \qquad (2.19)$$

where $C_0 = 5.67$ w/(m^2·K^4) = 4. cal/m^2·hr·K^4) = $5.73 \cdot 10^3$ erg/(cm^2·sec·K^4) -- the Stefan-Boltzmann constant.

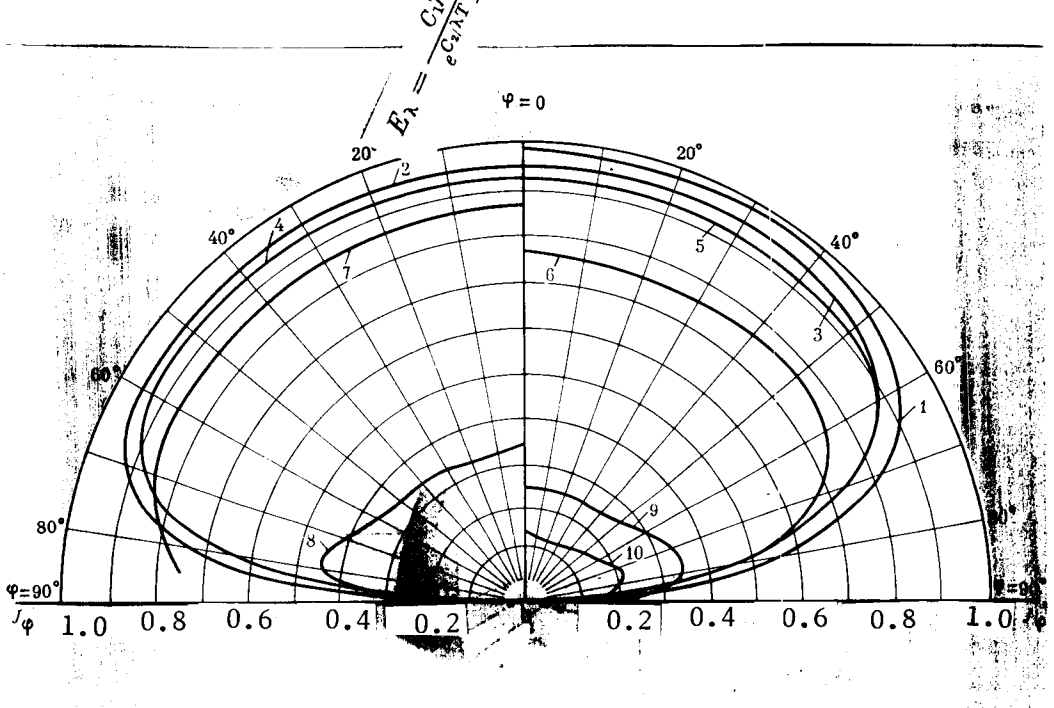

Figure 13. Intensity of Radiation of Certain Materials as a Function of Radiation Direction: 1, Wet ice; 2, Wood; 3, Glass; 4, Paper; 5, Clay; 6, Oxidized copper; 7, Rough corundum; 8, Bismuth; 9, Aluminum bronze; 10, Dull iron

The Stefan-Boltzmann law shows that the total radiated energy of an absolutely black body depends only on its absolute temperature.

If the derivative of Planck's law with respect to λ is set equal to 0, the expression produced

$$\lambda_{max} T = B, \qquad (2.20)$$

where $B = 2.896 \cdot 10^3$ $\mu \cdot K$, is called the Wien displacement law, which shows that as temperature increases, the maximum of the spectral density of radiation of an absolutely black body is displaced in the direction of shorter wavelengths.

The quantity of thermal energy corresponding to wavelengths $\lambda < \lambda_{max}$, amounts to 25% of the total energy, while 75% is found in the area of wavelengths $\lambda > \lambda_{max}$. The quantity of thermal energy radiated by the surface of a body with temperature T in the area of wavelengths less than any given wavelength λ ($\lambda \neq \lambda_{max}$) can be determined from the graph presented in Figure 15, after first calculating constant $B = \lambda T$ [9]. /39

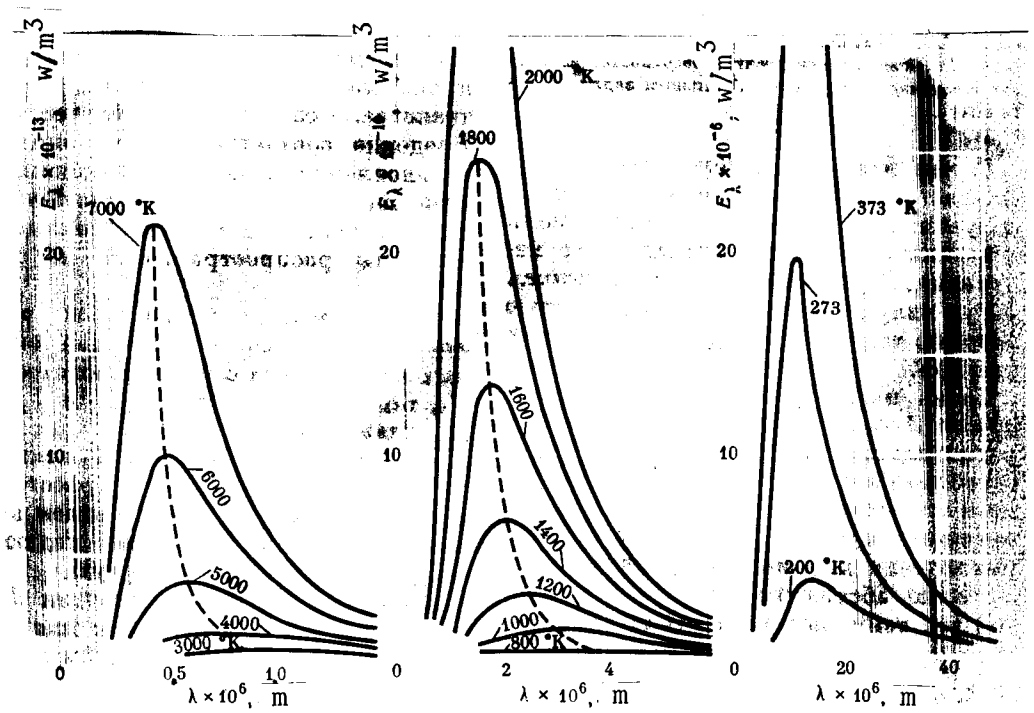

Figure 14. Spectral Density of Radiation of an Absolutely Black Body as a Function of Wavelength λ and Temperature of the Body T

For example, let us determine the quantity of thermal energy from a source of radiation with a temperature of 1000 K for the wavelength areas shorter and longer than 2 μ. In this case, $B = 2 \cdot 1000 = 2000$ $\mu \cdot K$. Using the graph, we find that only 7% of

the radiation of the body is to be found in the area of wavelengths shorter than 2 μ and, consequently, 93% falls in the a area of wavelengths longer than 2 μ. We can also determine that portion of the thermal energy, for example, in the wavelength interval between 8 and 14 μ, radiated by a heavenly body with a temperature of 300 K. In this case, $B_1 = 8 \cdot 300 = 2400$ and $B_2 = 14 \cdot 300 = 4200$. We see from the graph that 37% of the total energy of radiation of the celestial body falls in the wavelength range between 8 and 14 μ.

All of this is true of an absolutely black body, which actually does not exist; the spectral and total natural thermal radiations of actual bodies differ from the radiation of an absolutely black body for any given temperature, and are always less than it.

For practical solution of problems of radiant heat exchange, we generally utilize the ratio of natural radiation of a body for a fixed wavelength λ, temperature T and direction φ to the corresponding radiation of an absolutely black body

$$\varepsilon_{\lambda,\ T,\ \phi} = \frac{E_{\lambda,\ T,\ \phi}}{E_{(\lambda,\ T,\ \phi)_{bb}}}. \qquad (2.21)$$

The quantity $\varepsilon_{\lambda,\ T,\ \phi}$ is called the degree of blackness (or radiation factor) of a nonblack body, and is always less than 1; depending on the form of this relationship, all bodies are divided into grey bodies and bodies with selective radiation.

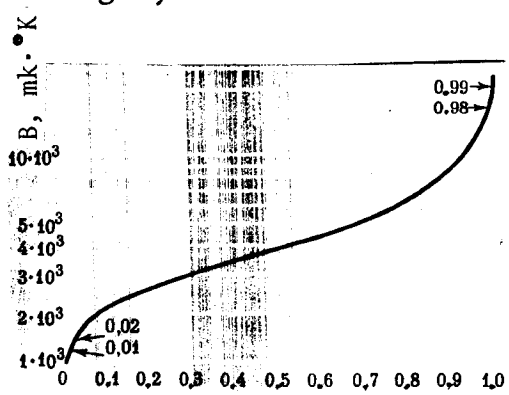

Figure 15. Use of Wien's Law to Determine the Portion of the Total Energy of Radiation of the Surface of a Body Corresponding to Wavelengths Less than a Fixed Value of λ

/40

A grey body refers to a body which absorbs the same portion of incident radiation throughout the entire interval of wavelengths λ regardless of the direction of the radiation. Bodies with selective radiation can radiate and absorb radiant energy only in certain areas of the spectrum.

The relationship between absorption factor A and natural radiation E is established by Kirchhoff's law, according to the ratio of natural radiation E to absorption factor A for a body is independent of the material of the body and equal to the natural radiation of an

absolutely black body at the same temperature. Under conditions of temperature equillibrium, Kirchhoff's rule is correct both for monochromatic and for integral radiation, i.e.,

$$\frac{E_\lambda}{A_\lambda} = \frac{E}{A} = E_{bb} \tag{2.22}$$

Determining the value of E using formula (2.21) and substituting into (2.22), we produce

$$\varepsilon = A. \tag{2.23}$$

Thus, for any grey body with temperature T, absorption factor A in relationship to the radiation of an absolutely black body is equal to the radiation factor ε of this body at the same temperature.

If one surface absorbs n times more energy than another, the radiation of the first surface will also be n times greater than the radiation of the second. If we know the radiation factor ε of a grey body, we can calculate the natural radiation of the body using the Stefan-Boltzmann rule:

$$E = \varepsilon C_0 \left(\frac{T}{100}\right)^4. \tag{2.24}$$

5.4. Radiant Heat Exchange of Two Bodies Arbitrarily Placed in Space. Irradiance Factor

The required concepts are usually introduced and basic regularities established first for black bodies, after which the results produced are extended to grey bodies.

suppose there are two convex black bodies with surfaces F_1 and F_2, arbitrarily placed in space, with temperatures T_1 and T_2 held constant (Figure 16). Let us set off on the surfaces of the bodies elementary areas dF_1 and dF_2, the distance between which is r, and calculate the quantity of radiant energy from one area incident on the other.

The quantity of radiant energy dE_{2-1} which strikes area dF_1 from area dF_2 is determined by the equation

while the quantity of radiant energy E_{1-2}, striking area dF_2 from area dF_1, is determined by the equation

$$dE_{1-2} = \frac{C_0}{\pi} \left(\frac{T_1}{100}\right)^4 dF_1 \cos \phi_1 \cdot d\omega_1.$$

The values of the elementary solid angles $d\omega_1$ and $d\omega_2$ are:

$$d\omega_1 = \frac{dF_2 \cos \varphi_2}{r^2}, \quad d\omega_2 = \frac{dF_1 \cos \varphi_1}{r^2}.$$

Substituting the values of $d\omega_1$ and $d\omega_2$ into the formulas for dF_{2-1} and dE_{1-2}, we produce /41

$$dE_{2-1} = C_0 \left(\frac{T_2}{100}\right)^4 \frac{\cos \varphi_2 \cos \varphi_1}{\pi r^2} dF_2 dF_1,$$

$$dE_{1-2} = C_0 \left(\frac{T_1}{100}\right)^4 \frac{\cos \varphi_1 \cos \varphi_2}{\pi r^2} dF_1 dF_2. \qquad (2.25)$$

The factors

$$dF_2 \frac{\cos \varphi_2 \cos \varphi_1}{\pi r^2} dF_1 = dH_{2-1}$$

and

$$dF_1 \frac{\cos \varphi_1 \cos \varphi_2}{\pi r^2} dF_2 = dH_{1-2} \qquad (2.26)$$

are called the elementary **mutual area** of radiant heat exchange between elementary areas dF_1 **and** dF_2, while the dimensionless portions of these factors

$$\frac{\cos \varphi_2 \cos \varphi_1}{\pi r^2} dF_1 = \varphi_{dF_2 - dF_1}$$

and

$$\frac{\cos \varphi_1 \cos \varphi_2}{\pi r^2} dF_2 = \varphi_{dF_1 - dF_2}, \qquad (2.27)$$

showing that portion of the natural radiation of elementary area dF_1 or dF_2 which strikes the elementary area dF_1 or dF_2, is called the elementary irradiance factor or elementary angular factor of these surfaces.

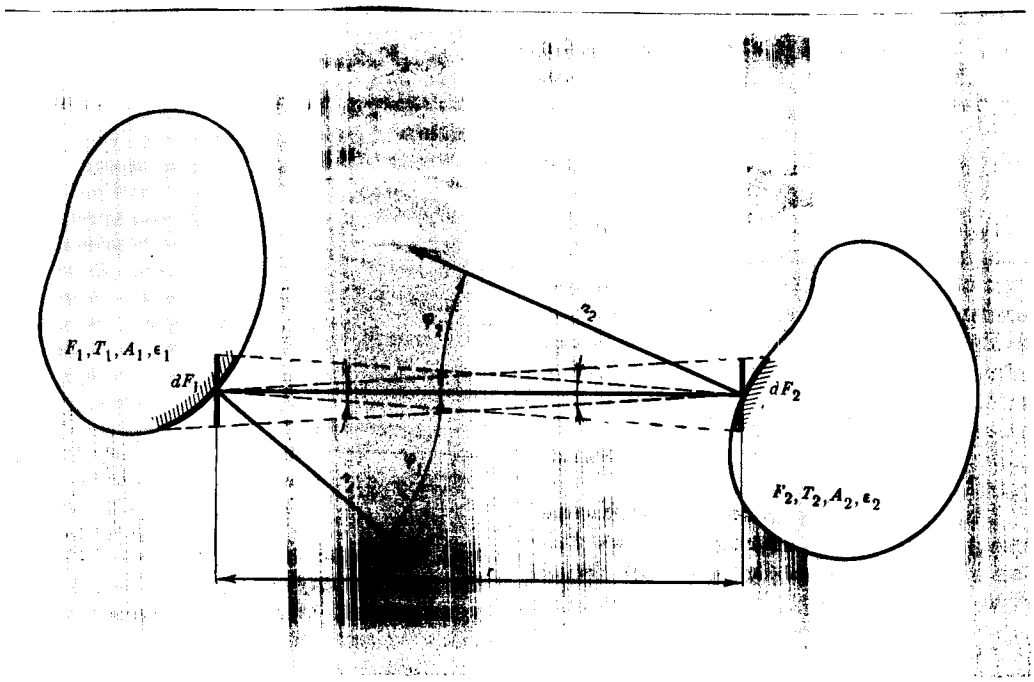

Figure 16. Determination of Irradiance Factor of Two Bodies Located Arbitrarily in Space

The total quantity of radiant energy striking surface F_1 or F_2 from surface F_2 or F_1 can be found by integrating equations (2.25):

$$E_{2-1} = C_0 \left(\frac{T_2}{100}\right)^4 \int_{F_2} dF_2 \int_{F_1} \frac{\cos \varphi_2 \cos \varphi_1}{\pi r^2} dF_1$$

and

$$E_{1-2} = C_0 \left(\frac{T_1}{100}\right)^4 \int_{F_1} dF_1 \int_{F_2} \frac{\cos \varphi_1 \cos \varphi_2}{\pi r^2} dF_2.$$

In these equations, the factors /42

$$\int_{F_2} dF_2 \int_{F_1} \frac{\cos \varphi_2 \cos \varphi_1}{\pi r^2} dF_1 = H_{2-1} \qquad (2.28)$$

and

are called the mutual area of irradiance (the area of radiant heat exchange between surfaces F_1 and F_2).

If the mutual areas of radiant heat exchange H_{2-1} and H_{1-2} are known, we can determine the mean irradiance factors or the mean angular factors ϕ_{2-1} and ϕ_{1-2} by using the formulas

$$\varphi_{2-1} = \frac{H_{2-1}}{F_2}, \quad \varphi_{1-2} = \frac{H_{1-2}}{F_1}. \tag{2.29}$$

The areas of mutual irradiance and the mean irradiance factors for bodies of various shapes and various mutual placements are presented in the appendix. Using them, we can determine the quantity of radiant energy striking elements of the outer surface of a spacecraft from the surface of a celestial body and the heat exchange between these elements.

The radiant heat exchange between two absolutely black bodies can be determined by the formulas

$$\begin{aligned}
&Q_{2-1} = E_{2-1} - E_{1-2} = \\
&= \varphi_{2-1} F_2 C_0 \left[\left(\frac{T_2}{100}\right)^4 - \left(\frac{T_1}{100}\right)^4\right] = \\
&= H_{2-1} C_0 \left[\left(\frac{T_2}{100}\right)^4 - \left(\frac{T_1}{100}\right)^4\right], \\
&Q_{1-2} = E_{1-2} - E_{2-1} = \\
&= \varphi_{1-2} F_1 C_0 \left[\left(\frac{T_1}{100}\right)^4 - \left(\frac{T_2}{100}\right)^4\right] = \\
&= H_{1-2} C_0 \left[\left(\frac{T_1}{100}\right)^4 - \left(\frac{T_2}{100}\right)^4\right].
\end{aligned} \tag{2.30}$$

The problem of the radiant heat exchange of grey bodies can be solved approximately (but with accuracy sufficient for most cases) by using the concept of effective radiation of bodies defined by formula (2.17). The approximate nature of this metod follows from the assumption that the heat flux sent by one body to another

$$\int_{F_1} dF_1 \int_{F_2} \frac{\cos\varphi_1 \cos\varphi_2}{\pi r^2} dF_2 = H_{1-2}$$

is distributed over the surface of the latter and reflected from it evenly. For example, the radiant heat exchange between convex grey bodies can be represented as

$$Q_{2-1} = -Q_{1-2} = \phi_{2-1}F_2E_{eff2} - \phi_{1-2}F_1E_{eff1}. \quad (2.31)$$

Using formula (2.17), we can write

$$E_{eff1} = \frac{F_1E_1}{A_1} + (\frac{1}{A_1} - 1)Q_{2-1},$$

$$E_{eff2} = \frac{F_2E_2}{A_2} + (\frac{1}{A_2} - 1)Q_{1-2}.$$

Then, substituting the expressions for E_{eff1} and E_{eff2} into (2.31), we produce

$$Q_{2-1} = -Q_{1-2} = \frac{\varphi_{2-1}F_2\frac{E_2}{A_2} - \varphi_{1-2}F_1\frac{E_1}{A_1}}{1 + \varphi_{1-2}\left(\frac{1}{A_1} - 1\right) + \varphi_{2-1}\left(\frac{1}{A_2} - 1\right)}. \quad (2.32)$$

5.5. Properties of Radiation Fluxes

In many cases, the solution of some specific problem on radiant heat exchange can be significantly simplified by using a number of properties of the irradiance factors and mutual areas. Let us note the most important of these.

The property of mutuality. If two bodies are in mutual radiant heat exchange, their mutual areas of radiant heat exchange are equal, and the irradiance factor of 1 can be expressed through the irradiance factor of the other. Actually, formulas (2.28) and (2.29) indicate that

$$H_{1-2} = H_{2-1} = H, \ \varphi_{1-2}F_1 = \varphi_{2-1}F_2. \quad (2.33)$$

Consequently, if we know the irradiance factor ϕ_{2-1} of surface F_1 by surface F_2, irradiance factor ϕ_{1-2} of surface F_2 by surface F_1 can be determined by the formula

$$\varphi_{1-2} = \varphi_{2-1}\frac{F_2}{F_1}. \quad (2.34)$$

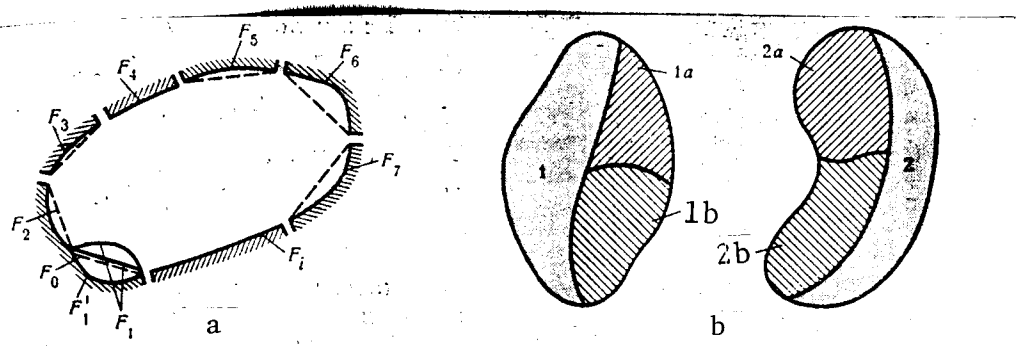

Figure 17. Determination of Properties of Irradiance Factors and Mutual Areas

First property of closure. For closed system of bodies, the sum of the irradiance factors of any body with no concavities to all other bodies is equal to 1, while the summary area of mutual irradiance is equal to the area of the outer surface of this body (Figure 17a).

Actually, irradiance factor ϕ_{1-i} from body 1 to any other body i is nothing more than that portion E_{i-1} of radiant flux E_1 which strikes body i:

$$\varphi_{1-i} = \frac{E_{1-i}}{E_1}.$$

Consequently,

$$\sum_{i=1}^{n} \varphi_{1-i} = \sum_{i=1}^{n} \frac{H_{1-i}}{F_1} = \sum_{i=1}^{n} \frac{E_{1-i}}{E_1}$$
$$(i = 1, 2, 3, \ldots, n).$$

Since

$$\sum_{i=1}^{n} E_{1-i} = E_1, \text{ then}$$

$$\sum_{i=1}^{n} \varphi_{1-i} = 1, \quad \sum_{i=1}^{n} H_{1-i} = F_1. \qquad (2.35) \qquad (2.35)$$

Second property of closure. For a closed system of bodies, the sum of the irradiance factors from any body with a concave surface to all other bodies is less than 1 by the value of the irradiance factor from this surface to itself, while the summary mutual area of irradiance is less than the area of the surface of this body by the value of the mutual irradiance area of this

surface with itself (Figure 17a).

Actually, the heat flux from body 1' to all i other bodies

Consequently,

$$\sum_{i=1}^{n} \varphi_{1-i} = 1 - \varphi_{1-1},$$
$$\sum_{i=1}^{n} H_{1-i} = F_1' - H_{1-1}. \tag{2.36}$$

Property of distribution. The mutual area of irradiance with radiant heat exchange of one body with another, both of which consist of several parts, is equal to the sum of the mutual irradiance areas between the parts of these bodies (Figure 17b).

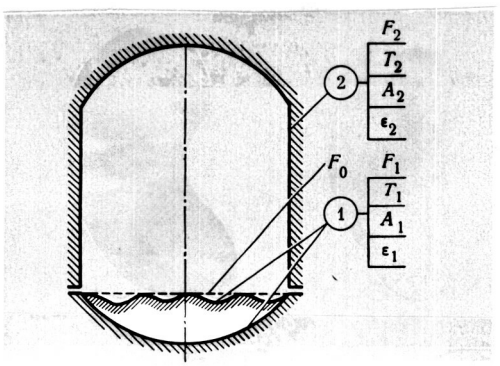

Figure 18. Heat Exchange Between Two Concave Surfaces

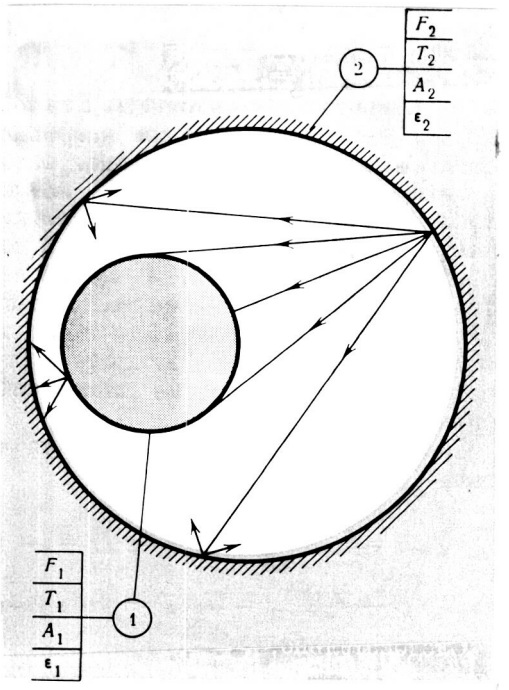

Figure 19. Heat Exchange Between Two Bodies One of Which is Located in a Cavity of the Other

/44

Actually, the radiant flux from body 1 to body 2 consists of the radiant fluxes between the individual parts of bodies 1 and 2.

For example, if body 1 consists of parts 1a and 1b, while body 2 consists of parts 2a and 2b, the radiant flux from body 1 to body 2 will be

$$E_1H_{1-2} = E_1H_{1a-2a} + E_1H_{1a-2b} + E_1H_{1b-2a} + E_1H_{1b-2b}.$$

Consequently,

$$H_{1-2} = H_{1a-2a} + H_{1a-2b} + H_{1b-2a} + H_{1b-2b}.$$

As our first example of the use of these properties of the irradiance factors and mutual areas, let us determine the heat exchange between concave surfaces F_1 and F_2, forming a closed system (Figure 18).

Based on the second property of closure, $\phi_{1-2} = 1 - \phi_{1-1}$; based on the first property of closure and the property of mutuality

$$\varphi_{1-1} = 1 - \varphi_{1-0} = 1 - F_0/F_1,$$

where ϕ_{1-0} is the irradiance factor of supplementary surface F_0, with no concavities, by surface F_1. Consequently, $\phi_{1-2} = F_0/F_1$.

Using the expression produced for ϕ_{1-2} and the property of mutuality, the heat exchange between surfaces F_1 and F_2 can be determined from equation (2.32), which in this case becomes

$$Q_{2-1} = -Q_{1-2} = \frac{F_0\left(\frac{E_2}{A_2} - \frac{E_1}{A_1}\right)}{1 + \frac{F_0}{F_1}\left(\frac{1}{A_1} - 1\right) + \frac{F_0}{F_2}\left(\frac{1}{A_2} - 1\right)}. \quad (2.38)$$

As our second example of the use of the properties of radiant fluxes, let us study the case of heat exchange between two bodies, one of which (concave body 1) is located in a cavity in the other (2) (Figure 19).

Using the property of mutuality and the first property of closure, the heat exchange between bodies 1 and 2 can be defined by equation (2.32), which in this case becomes /45

$$Q_{2-1} = -Q_{1-2} = \frac{F_1\left(\frac{E_2}{A_2} - \frac{E_1}{A_1}\right)}{\frac{1}{A_1} + \frac{F_1}{F_2}\left(\frac{1}{A_2} - 1\right)}. \qquad (2.39)$$

5.6. Radiant Heat Exchange of Two Flat Bodies Separated by Screens

For two plane-parallel bodies (Figure 20), the distance between which is slight in comparison to the height and width of the bodies ($F_1 = F_2$), equation (2.39), defining the radiant heat exchange between the two bodies, becomes

$$Q_{2-1} = -Q_{1-2} = \frac{F_1\left(\frac{E_2}{A_2} - \frac{E_1}{A_1}\right)}{\frac{1}{A_1} + \frac{1}{A_2} - 1}.$$

In this formula, the denominator can be looked upon as the sum of the two resistances to the transfer of radiant energy [1]:

$$\left(\frac{1}{A_1} - \frac{1}{2}\right) + \left(\frac{1}{A_2} - \frac{1}{2}\right).$$

Here, resistance ($1/A_1$ - $1/2$) corresponds to the transfer of radiant energy from the first body to the medium between the bodies, while resistance ($1/A_2$ - $1/2$) corresponds to the resistance to the transfer of radiant energy from the medium to the second body.

If we place N thin sheet screens between bodies 1 and 2, and the thermal resistance of the material of the screens is slight, then

$$Q_{2-1} = -Q_{1-2} = F_1\left(\frac{E_2}{A_2} - \frac{E_1}{A_1}\right) \times \left[\left(\frac{1}{A_1} - \frac{1}{2}\right) + \left(\frac{1}{A'_S} - \frac{1}{2}\right) + \left(\frac{1}{A''_S} - \frac{1}{2}\right) + \ldots \left(\frac{1}{A_2} - \frac{1}{2}\right)\right]^{-1}, \qquad (2.40)$$

where A'_s, A''_s are the absorption factors of the surfaces of the screens.

If the absorption factors of the screens and surfaces of the bodies are identical and equal to A_s, then formula (2.40) becomes

$$Q_{2-1} = -Q_{1-2} = \frac{F_1\left(\frac{E_1}{A_s} - \frac{E_2}{A_s}\right)}{2(N+1)\left(\frac{1}{A_s} - \frac{1}{2}\right)}. \tag{2.41}$$

If the temperatures of the screens and surfaces of the bodies are sufficiently close to each other, absorption factor A_s is equal to radiation factor ε_s. Introducing the symbol

$$\varepsilon_c = \left[\left(\frac{1}{\varepsilon_1} - \frac{1}{2}\right) + \left(\frac{1}{\varepsilon'_s} - \frac{1}{2}\right) + \left(\frac{1}{\varepsilon''_s} - \frac{1}{2}\right) + \ldots + \left(\frac{1}{\varepsilon_2} - \frac{1}{2}\right)\right]^{-1} \tag{2.42}$$

or

$$\varepsilon_c = \left[2(N+1)\left(\frac{1}{\varepsilon_s} - \frac{1}{2}\right)\right]^{-1},$$

formula (2.40) or (2.41) can be written as

$$Q_{2-1} = -Q_{1-2} = -\varepsilon_{c\,1-2} F_1 C_0 \left[\left(\frac{T_2}{100}\right)^4 - \left(\frac{T_1}{100}\right)^4\right]. \tag{2.43}$$

Quantity ε_c is called the corrected degree of blackness or corrected radiation factor of the surfaces of bodies 1 and 2.

It follows from formula (2.41) that when one screen is present, the radiant heat transfer is cut in half; when there are two screens, it is reduced by a factor of 3, etc. Particularly effective is the use of screens with low values of ε_s. Thus, if $\varepsilon_s = 0.05$, while $\varepsilon_1 = \varepsilon_2 = 0.8$, radiant heat transfer is decreased

by 27 times when one screen is used. This fact is presently widely used in space technology for the creation of so-called screen-vacuum thermal insulation (SVTI), consisting of a set of screens with very low degree of blackness ε_s. /46

The heat-physical characteristics of SVTI will be studied in detail in Chapter 7; here we shall discuss only the problem of calculation of the heat flux which passes through it.

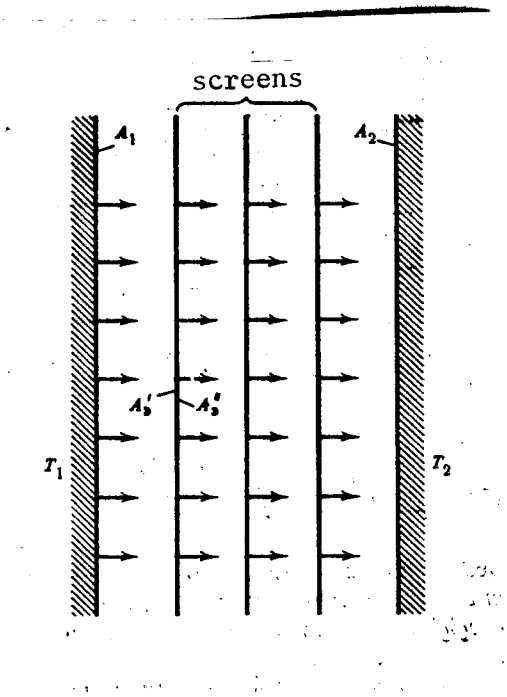

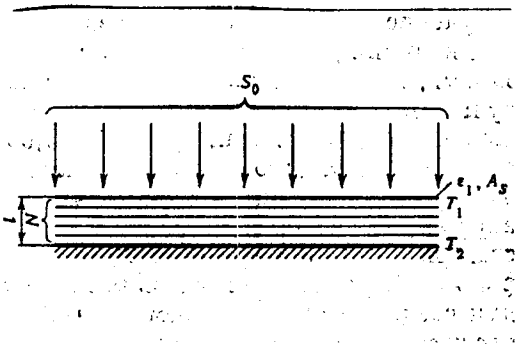

Figure 20. Heat Exchange Between Two Flat Bodies Separated by Screens ($T_1 > T_2$)

Figure 21. Determination of Heat Flux Through SVTI

The heat insulating properties of SVTI, by analogy with ordinary heat insulating materials, are characterized by the conductivity factor λ (or thermal resistance R), which greatly complicates calculation and analysis of the thermal state of a spacecraft during flight or during surface thermal testing.

Actually, if we need, for example, to determine temperature T_1 of the outer surface of the insulation of a spacecraft illuminated by the sun (Figure 21), the thermal balance equation necessary for solution of this problem is

$$S_0 A_S - \frac{\lambda}{l}(T_1 - T_2) - \varepsilon_1 C_0 \left(\frac{T_1}{100}\right)^4 = 0, \qquad (2.44)$$

where A_S, ε_1 are the absorption factor of solar radiation and the degree of blackness of the outer surface of the insulation respectively; l is the thickness of the insulation.

Temperature T_1 can be determined from this equation either graphically or by the method of successive approximations, and it is necessary either to consider the very strong dependence of λ on temperature (which still further complicates calculations) or to assume the value of λ constant, which causes significant calculation errors.

However, it has been experimentally established that the process of transmission of heat through SVTI is basically radiant, and that its value can be determined by equation (2.43) if the value of the corrected radiation factor ε_c in this equation is determined experimentally. This can be done by using data on the heat conductivity of the SVTI as a function of packing density n (n is the number of screens per unit length) and temperature of the screens (Figure 22 [14]) as follows.

On the one hand, the heat flux through SVTI can be determined by the formula /47

$$Q_{1-2} = \lambda \frac{F_1}{l}(T_1 - T_2) = \\ = \lambda \frac{n}{N} F_1 (T_1 - T_2), \tag{2.45}$$

where N is the number of screens;

on the other hand by formula (2.43), after first putting it in the form

$$Q_{1-2} = \frac{\varepsilon_{c_1} C_0 F_1}{100}\left(\frac{T_1}{100} + \frac{T_2}{100}\right)\left[\left(\frac{T_1}{100}\right)^2 + \right. \\ \left. + \left(\frac{T_2}{100}\right)^2\right](T_1 - T_2). \tag{2.46}$$

Setting the right portion of (2.45) and (2.46) equal, we produce

$$\varepsilon_{c_1} = \lambda \frac{n}{N} \frac{100}{C_0 f(T_1, T_2)}, \tag{2.47}$$

Where

$$f(T_1, T_2) = \left(\frac{T_1}{100} + \frac{T_2}{100}\right)\left[\left(\frac{T_1}{100}\right)^2 + \left(\frac{T_2}{100}\right)^2\right].$$

Figure 22 shows that the dependence of λ on $f(T_1, T_2)$ is linear:

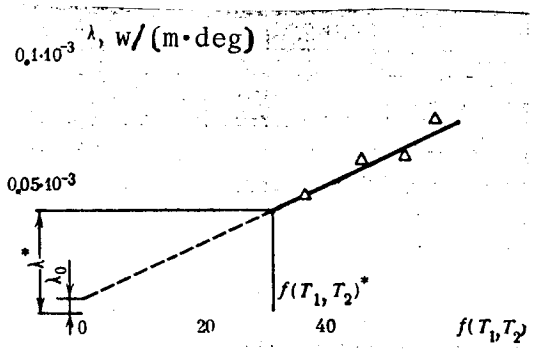

Figure 22. Heat Conductivity Factor λ of SVTI of Aluminum Foil with Glass-Wool Interlayers as a Function of Temperature of Outer Layers of SVTI T_1, T_2 with Packing Density n = 15

$$\lambda = kf(T_1, T_2) + \lambda_0 \approx kf(T_1, T_2), \quad (2.48)$$

where

$$k = \frac{\lambda^* - \lambda_0}{f^*(T_1, T_2)}.$$

With the optimal values of n = 20-25 cm^{-1} and values of $f(T_1, T_2)$ obtained in practice, $\lambda_0 << \lambda$.

Substituting (2.48) into (2.45) and setting the right parts of equations (2.45) and (2.48) equal, we produce

$$\varepsilon_c \approx k \frac{n}{N} \frac{100}{C_0}, \quad (2.49)$$

i.e., with sufficient accuracy we can consider ε_c to be independent of temperature. This allows us to write the thermal balance equation (2.44) as

$$S_0 A_S - \varepsilon_c C_0 \left[\left(\frac{T_1}{100}\right)^4 - \left(\frac{T_2}{100}\right)^4\right] - \varepsilon_1 C_0 \left(\frac{T_1}{100}\right)^4 = 0,$$

from which it is easy to produce the analytic expression for T_1 which we need.

Therefore, it is desirable to use experimental studies of the heat-physical characteristics of the SVTI, in addition to the usual calculated heat conductivity factor λ, to determine the adjusted radiation factor of the thermal insulation ε_c, so as to avoid the calculations involved in the conversion from the heat conductivity factor of the SVTI λ to the corrected radiation factor ε_c.

Mutual Placement and Shape of Surfaces	Diagram	Irradiance Factors and Areas of Mutual Irradiance
Two parallel planes, dimensions of which are significantly greater than distance between	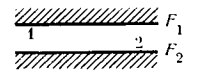	$\varphi_{1-2} = \varphi_{2-1} = 1$ $H_{1-2} = H_{2-1} = F_1 = F_2$
One body with no concave sections located within another	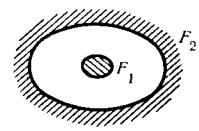	$\varphi_{1-2} = 1, \quad \varphi_{2-1} = \frac{F_1}{F_2}$ $H_{1-2} = H_{2-1} = F$
Two surfaces form a closed system, one surface has no concave portions	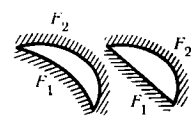	$\varphi_{1-2} = 1, \quad \varphi_{2-1} = \frac{F_1}{F_2}$ $H_{1-2} = H_{2-1} = F_1$
Two equal rectangles, located in parallel planes	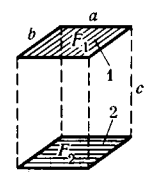	$\varphi_{1-2} = \frac{2}{\pi xy}\left[\frac{1}{2}\ln\frac{(1+x^2)(1+y^2)}{1+x^2+y^2} + y\sqrt{1+x^2}\,\operatorname{arc-tan}\frac{y}{\sqrt{1+x^2}} + x\sqrt{1+y^2}\,\operatorname{arc-tan}\frac{x}{\sqrt{1+y^2}} - y\,\operatorname{arc-tan} y - x\,\operatorname{arc-tan} x\right]$, $x = \frac{b}{c}, \quad y = \frac{a}{c}$
Two rectangles with a common edge	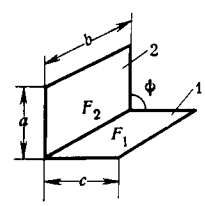	$\varphi_{1-2} = \frac{1}{\pi x}\left[x\,\operatorname{arc-tan}\frac{1}{x} + y\,\operatorname{arc-tan}\frac{1}{y} - \sqrt{x^2+y^2}\,\operatorname{arc-tan}\frac{1}{\sqrt{x^2+y^2}} + \frac{1}{4}\ln\frac{(1+x^2)(1+y^2)}{1+x^2+y^2} + \frac{x^2}{4}\ln\frac{x^2(1+x^2+y^2)}{(1+x^2)(x^2+y^2)} + \frac{y^2}{4}\ln\frac{y^2(1+x^2+y^2)}{(1+y^2)(x^2+y^2)}\right]$ $x = \frac{c}{b}, \quad y = \frac{a}{b}$

Mutual Placement and Shape of Surfaces	Diagram	Irradiance Factors and Areas of Mutual Irradiance
Two parallel circular plates with centers on a common perpendicular	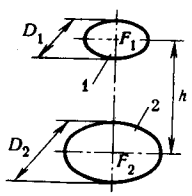	$\varphi_{1-2} = \left[\sqrt{\frac{1}{4}(x+1)^2 + y^2} - \sqrt{\frac{1}{4}(x-1)^2 + y^2}\right]^2$ $x = \frac{D_2}{D_1}, \quad y = \frac{h}{D_1}$
Two infinitely long planes intersecting at an angle	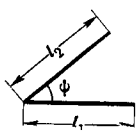	$\varphi_{1-2} = \left[1 + \frac{l_2}{l_1} - \sqrt{\left(\frac{l_2}{l_1}\sin\psi\right)^2 + \left(1 - \frac{l_2}{l_1}\cos\psi\right)^2}\right]$
Two infinitely long planes located in parallel planes one opposite the other	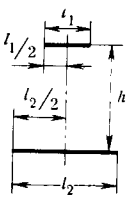	$\varphi_{1-2} = \sqrt{\frac{1}{4}\left(\frac{l_2}{l_1}+1\right) + \left(\frac{h}{l_1}\right)^2} - \sqrt{\frac{1}{4}\left(\frac{l_2}{l_1}-1\right)^2 + \left(\frac{h}{l_1}\right)^2}$
Two parallel infinitely long cylinders	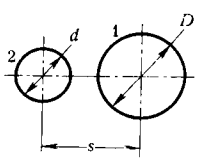	$\varphi_{1-2} = \frac{1}{\pi}\left[\frac{1+y}{2}\arcsin\frac{1+y}{2x} - \frac{y-1}{2}\arcsin\frac{y-1}{2x} + \sqrt{x^2 - \left(\frac{1+y}{2}\right)^2} - \sqrt{x^2 - \left(\frac{y-1}{2}\right)^2}\right]$ $x = \frac{s}{D}, \quad y = \frac{d}{D}, \quad \frac{F_1}{F_2} = \frac{D}{d}$ where y = 1 $\varphi_{1-2} = \frac{1}{\pi}\left(\arcsin\frac{1}{x} + \sqrt{x^2-1} - x\right)$
A convex body located between two parallel planes (dimensions of body small in comparison to dimensions of planes)	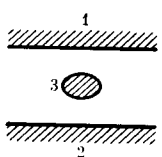	$\varphi_{1-2} = \varphi_{2-1} = 1$ $\varphi_{2-3} = \varphi_{1-3} = 0$ $\varphi_{3-1} = \varphi_{3-2} = \frac{1}{2}$ $H_{1-2} = F_1 - F_2$ $H_{1-3} = H_{3-1} = H_{2-3} = H_{3-2} = \frac{1}{2}F_3$

Mutual Placement and Shape of Surfaces	Diagram	Irradiance Factors and Areas of Mutual Irradiance
Elementary area and arbitrary circular plate, plane of which is parallel to plane of area	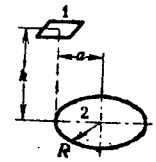	$\varphi_{1-2}=\frac{1}{2}\left[1-\frac{h^2+a^2-R^2}{\sqrt{(h^2+a^2+R^2)-4a^2R^2}}\right]$
Elementary area and arbitrary circular plate, plane of which is perpendicular to plane of the area	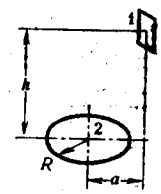	$\varphi_{1-2}=\frac{h}{2a}\left[\frac{h^2+a^2+R^2}{\sqrt{(h^2+a^2+R^2)-4a^2R^2}}-1\right]$
Elementary area and rectangle, plane of which is parallel to plane of area, with one point of rectangle located on a perpendicular to the center of the area	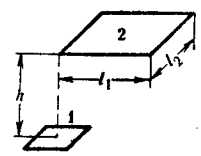	$\varphi_{1-2}=\frac{1}{2\pi}\left(\frac{l_1}{\sqrt{h^2+l_1^2}}\operatorname{arc-tan}\frac{l_1}{\sqrt{h^2+l_1^2}}+\right.$ $\left.+\frac{l_2}{\sqrt{h^2+l_2^2}}\operatorname{arc-tan}\frac{l_1}{\sqrt{h^2+l_1^2}}\right)$
Elementary area and rectangle, plane of which is parallel to the plane of the area	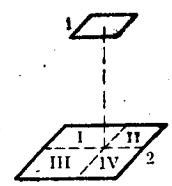	$\varphi_{1-2}=\varphi_{1-\mathrm{I}}+\varphi_{1-\mathrm{II}}+\varphi_{1-\mathrm{III}}+\varphi_{1-\mathrm{IV}}$
Unlimited plane and row of pipes located in a parallel plane	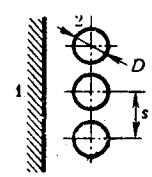	$\varphi_{1-2}=1-\sqrt{1-\frac{D}{s}}$

Mutual Placement of Shape of Surfaces	Diagram	Irradiance Factors and Areas of Mutual Irradiance
Two parallel half cylinders of identical diameter and a tangent plane	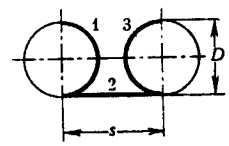	$\varphi_{1-2}=\frac{1}{2}-\frac{1}{\pi}\left(\arcsin\frac{1}{x}+\sqrt{x^2-1}-x\right)$ $\varphi_{1-3}=\frac{2}{\pi}\left(\arcsin\frac{1}{x}+\sqrt{x^2-1}-x\right)$ $x=\frac{s}{D}$
Two infinitely long cylinders of identical diameter and a cross piece between them	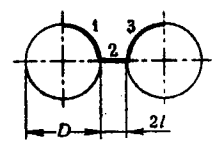	$\varphi_{1-2}=\frac{2x}{\pi}\left(1-\frac{1}{x}+\frac{1}{2x}\operatorname{arc-tan}\sqrt{4x(1+x)}\right)$ $\varphi_{1-3}=1-\frac{2}{\pi}-2\varphi_{1-2}$ $x=\frac{2l}{D}$
Infinitely long cylinder and rectangular plate	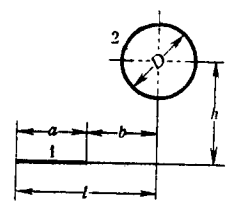	$\varphi_{1-2}=\frac{D}{2a}\left(\operatorname{arc-tan}\frac{l}{h}-\operatorname{arc-tan}\frac{b}{h}\right)$
Infinitely long elementary plate and surface forming a plane-parallel system	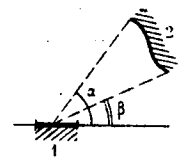	$\varphi_{1-2}=\frac{1}{2}(\cos\beta-\cos\alpha)$
Infinitely long elementary plate and plane forming a plane-parallel system	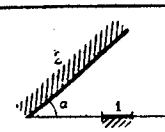	$\varphi_{1-2}=\frac{1}{2}(1+2\cos\alpha)$
Elementary area and rectangular located in perpendicular planes	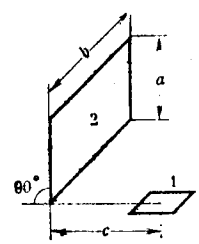	$\varphi_{1-2}=\frac{1}{2\pi}\left(\arcsin\frac{1}{\sqrt{1+y^2}}-\right.$ $\left.-\frac{y}{\sqrt{x^2+y^2}}\arcsin\frac{1}{\sqrt{1+x^2+y^2}}\right)$

Mutual Placement of Shape of Surfaces	Diagram	Irradiance Factors and Areas of Mutual Irradiance
Three nonconcave surfaces forming a closed system of infinite length	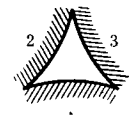	$\varphi_{1-2} = \frac{1}{2}\left(1 + \frac{F_2}{F_1} - \frac{F_3}{F_1}\right)$ $\varphi_{2-1} = \frac{1}{2}\left(1 + \frac{F_1}{F_2} - \frac{F_3}{F_2}\right)$ $\varphi_{1-3} = \frac{1}{2}\left(1 + \frac{F_3}{F_1} - \frac{F_2}{F_1}\right)$ $\varphi_{2-3} = \frac{1}{2}\left(1 + \frac{F_3}{F_2} - \frac{F_1}{F_2}\right)$ и т. д. $H_{1-2} = \frac{1}{2}(F_1 + F_2 - F_3)$
Infinitely small sphere and rectangular plate (perpendicular to plane drawn from one point passes through center of sphere)	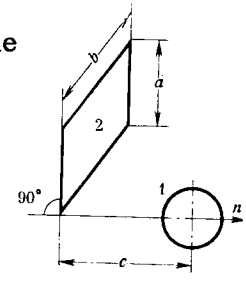	$\varphi_{1-2} = \frac{1}{4\pi} \arctan \frac{xy}{\sqrt{1 + x^2 + y^2}}$ $x = \frac{b}{c}, \quad y = \frac{a}{c}$
Portion of surface of a sphere limited by two parallel planes and an infinite plane a)	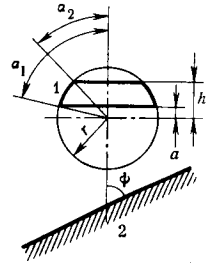	$\varphi_{1-2} = \frac{1}{2}\left[1 - \frac{\sin\psi}{2}(\cos\alpha_1 + \cos\alpha_2)\right]$ $H = 2\pi r h \varphi_{1-2}$ $\varphi_{1-2} = \frac{1}{2}\left(1 - \frac{\delta}{2r}\sin\psi\right)$ $\delta = h + 2a$
	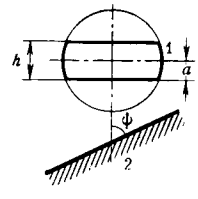	$\varphi_{1-2} = \frac{1}{2}$

Mutual Placement of Shape of Surfaces	Diagram	Irradiance Factors and Areas of Mutual Irradiance
b)	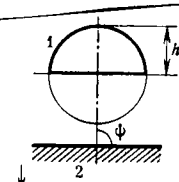	$\varphi_{1-2} = \frac{1}{4}$
c)	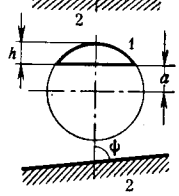	$\varphi_{1-2} = \frac{1}{2}\left(1 - \frac{2r-h}{2r}\sin\psi\right)$ where $\psi = \frac{\pi}{2}$ $\varphi_{1-2} = \frac{h}{2r}$
d)	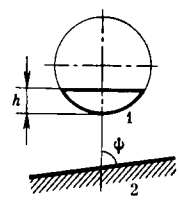	$\varphi_{1-2} = \frac{1}{2}\left(1 + \frac{2r-h}{2r}\sin\psi\right)$ where $\psi = \frac{\pi}{2}$ $\varphi_{1-2} = 1 - \frac{h}{4r}$
Elementary area and sphere	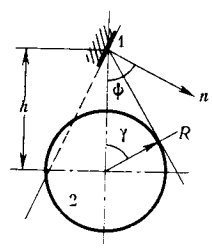	$\varphi_{1-2} = \frac{\cos^2\gamma\cos\psi}{\pi}\left(\pi - \arccos\frac{\operatorname{tg}\gamma}{\operatorname{tg}\psi}\right) + \frac{1}{\pi}\arcsin\frac{\sqrt{\cos^2\gamma - \cos^2\psi}}{\sin\psi} - \frac{\sin\gamma}{\pi}\sqrt{\cos^2\gamma - \cos^2\psi}$ $\cos\gamma = \frac{R}{h}$
a) Plane of elementary area does not intersect sphere	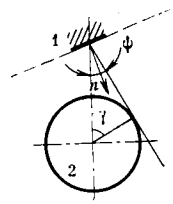	$\varphi_{1-2} = \cos^2\gamma\cos\psi$

Mutual Placement of Shape of Surfaces	Diagram	Irradiance Factors and Areas of Mutual Irradiance
b) Plane of elementary area passes through center of sphere $\psi = \frac{\pi}{2}$	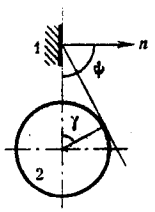	$\varphi_{1-2} = \frac{1}{\pi}[\arcsin(\cos\gamma) - \sin\gamma\cos\gamma]$
Sphere and circular plate, plane of which does not intersect sphere (normal from center of plate passes through center of sphere)	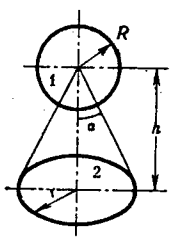	$\varphi_{1-2} = \frac{1-\cos\alpha}{2}$ or $\varphi_{1-2} = \frac{1}{2}\left(1 - \frac{h}{\sqrt{h^2+r^2}}\right)$ $H_{1-2} = 4\pi R^2 \varphi_{1-2}$
Sphere and arbitrary figure inscribed in solid angle with central angle 2α (under the condition that the tangential plane at any point of the inscribed figure does not intersect the sphere)	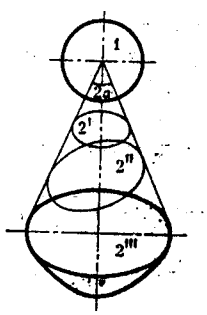	$\varphi_{1-2} = \frac{1-\cos\alpha}{2}$
Sphere and arbitrary surface, tangential plane at any point of which does not intersect the sphere (Ω is the solid angle)	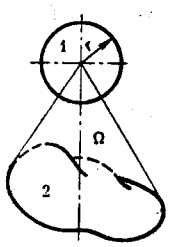	$\varphi_{1-2} = \frac{\Omega}{4\pi}$ $H_{1-2} = 4\pi r^2 \varphi_{1-2}$

Mutual Placement of Shape of Surfaces	Diagram	Irradiance Factors and Areas of Mutual Irradiance
Sphere and flat elliptical plate (perpendicular from center of plate passes through center of sphere)	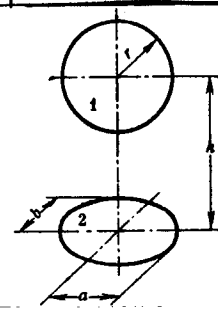	$\varphi_{1-2}=\frac{ab}{\pi h\sqrt{a^2+h^2}}\int_0^1\frac{\sqrt{1-t^2}}{\left(1+\frac{b^2}{h^2}t^2\right)}\times$ $\times\frac{1}{\sqrt{1-\frac{a^2-b^2}{a^2+h^2}t^2}}dt$
Sphere and portion of a ring, plane of which passes through the center of the sphere	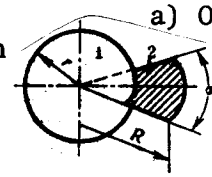	a) One side of ring $\varphi'_{1-2}=\frac{\alpha}{8\pi^2}\left[(k^2-1)\ \text{arc-tan}\frac{1}{k}+\frac{\pi}{2}-k\right]$ $k=\sqrt{\frac{R^2}{r^2}-1}$ b) Both sides of ring $\varphi_{1-2}=2\varphi'_{1-2}$
Sphere and portion of a ring, plane of which intersects sphere at some distance from center (one side of ring analyzed)	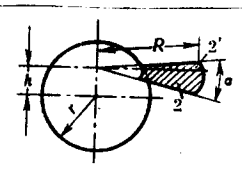	a) If greater portion of sphere visible from side of ring $\varphi_{1-2}=\frac{(1+x)^2}{8}-\frac{xy}{2\pi\sqrt{1+x^2y^2}}\times$ $\times[\pi-\arccos(x\sqrt{1-y^2(1-x^2)}\,]-$ $-\frac{1}{2\pi}\arcsin(y\sqrt{1-x^2})+$ $+\frac{\arcsin(y\sqrt{1-x^2})-y\sqrt{1-x^2}\sqrt{1-y^2(1-x^2)}}{4\pi y^2}$ $x=\frac{h}{r},\quad y=\frac{r}{R}$ b) If smaller portion of sphere visible from side of ring $\varphi_{1-2'}=\frac{(1-x)^2}{8}+$ $+\frac{xy}{2\pi+\sqrt{1+x^2y^2}}\arccos\left[x\sqrt{1-y^2(1-x^2)}-\right.$ $\left.-\frac{1}{2\pi}\arcsin(y\sqrt{1-x^2})\right]+$ $+\frac{\arcsin(y\sqrt{1-x^2})-y\sqrt{1-x^2}\sqrt{1-y^2(1-x^2)}}{4\pi y^2}$

Mutual Placement of Shape of Surfaces	Diagram	Irradiance Factors and Areas of Mutual Irradiance
a) Plane tangent on sphere ($x \to 1$) b) Plane intersects sphere through center ($x \to 0$) в) $y = \frac{r}{R} \to \infty$ г) $x = -1$	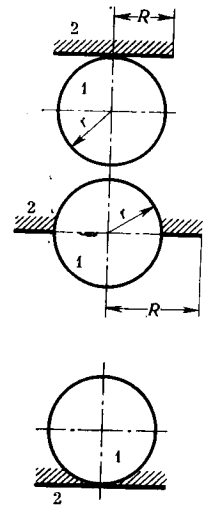	а) $\varphi_{1-2} = \frac{1}{2}\left(1 - \frac{r}{\sqrt{R^2 + r^2}}\right)$ б) $\varphi_{1-2} = \frac{1}{8} - \frac{1}{2\pi}\arcsin\frac{r}{R} + \frac{\arcsin\frac{r}{R} - \frac{r}{R}\sqrt{1-\left(\frac{r}{R}\right)^2}}{4\pi\left(\frac{r}{R}\right)^2}$ в) $\varphi_{1-2} = \frac{(1+x)^2}{8}$ г) $\varphi_{1-2} = 0$
Cylinder and ring at its base (axis of cylinder perpendicular to plane of ring and passes through its center)	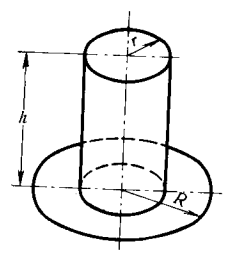	$\varphi_{1-2} = \frac{1}{\pi}\left[\operatorname{arc-tan}\frac{\sqrt{1-x^2}}{y} + \frac{y}{4x}\arccos x - \frac{\sqrt{y^2+(1+x)^2}\,\sqrt{y^2+(1-x)^2}}{2xy} \times \operatorname{arc-tan}\sqrt{\frac{y^2+(1+x)^2}{y^2+(1-x)^2}\,\frac{(1-x)}{(1+x)}} + \frac{1-x^2}{2xy}\operatorname{arc-tan}\sqrt{\frac{1+x}{1-x}}\right]$ $x = \frac{r}{R}, \quad y = \frac{h}{R}$
Two bands on the inside of a cylinder	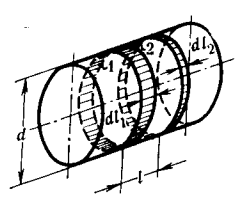	$d\varphi_{1-2} = \left\{1 - \frac{l}{d}\,\frac{2\,(l/d)^2+3}{2\,[(l/d)^2+1]^{3/2}}\right\} d\left(\frac{l}{d}\right).$

CHAPTER 6

STATIC CALCULATION OF THE THERMAL MODE OF AUTOMATIC PLANETARY STATIONS

6.1. Production of Basic Equations Defining the Thermal State of a Spacecraft /57

The first step in static calculation of the thermal mode of a spacecraft is production of the following initial data: dependence of heat liberation of devices Q_T on time; geometric dimensions, weights and heat capacities of individual elements and of the spacecraft as a whole; heat physical characteristics of the surrounding medium during each stage of flight and characteristics of thermal coupline with this medium.

The next stage is composition of a thermal model (or plan) of the spacecraft, simpler than the actual structure; only in this case will calculation of the necessary heat-physical characteristics be practically possible. Like an actual spacecraft, the thermal model should have surfaces:

--illuminated by the direct radiation of the sun (F_S);

--illuminated periodically due to changes in orientation of the spacecraft relative to the sun (F_m);

--constantly in shade (F_n);

--with various irradiance factors with the surface of the celestial body (see Figure 8).

Each of these surfaces can consist of several sections having various types of heat insulation and various optical factors A_S and ε.

Frequently, the thermal model of a spacecraft can be divided into a number of parts, the thermal coupling between which is slight, while the temperature of each part is determined by internal heat liberation Q_T and penetrating heat flux Q_p. The influence of heat exchange between individual parts of the spacecraft on the temperature of each part is usually determined by dynamic calculation of the thermal mode of the spacecraft.

The necessary heat-physical characteristics of any part and, consequently, of the spacecraft as a whole, can be determined if we find the dependence of penetrating heat flux Q_p on temperature T_a, the heat-physical characteristics of the spacecraft, the surrounding medium and the characteristics of the thermal coupling between them.

It follows from the definition of the concept of penetrating heat flux Q_p that it can be determined for the ith sector from the following equation

$$Q_{p_i} = (A_i S_i + A_i E_{\text{inc } S_i} + \varepsilon_i E_{\text{inc } \varepsilon_i}) F_i - E_{\varepsilon_i} F_i, \quad (2.50)$$

where E_{ε_i} is the natural thermal radiation of the outer surface of the ith section; S_i is the direct solar radiation striking the ith section; $E_{\text{inc } S_i}$ is the solar radiation reflected from the surface of a celestial body (or chamber) and striking the ith sector; $E_{\text{inc } \varepsilon_i}$ is the thermal radiation of the surface of a celestial body (or chamber) striking the ith section; A_i, ε_i and F_i are the absorption factor for direct and reflected solar radiation, the degree of blackness and the area of the ith sector respectively. /58

Expression (2.50) can be written in a different form if we use the concepts of natural and resulting "solar" (E_{S_i}, Q_{S_i}) and "thermal" (E_{ε_i}, Q_{ε_i}) radiation of the ith section of the spacecraft surface [see formula (2.15)]:

$$Q_{S_i} = A_i E_{\text{inc } S_i} F_i - E_{S_i} F_i,$$

$$Q_{\varepsilon_i} = A_i E_{\text{inc } \varepsilon_i} F_i - E_{\varepsilon_i} F_i, \quad (2.51)$$

where E_{ε_i} is determined by formula (2.24), while E_{S_i} is determined by formula

$$E_{S_i} = (1 - A_i) S_i. \quad (2.52)$$

By analogy with E_{ε_i}, heat flux E_{S_i} can be called the natural "solar" radiation.

After determining the expressions for $E_{\text{inc } S_i}$ and $E_{\text{inc } \varepsilon_i}$

from (2.51) and substituting them into (2.50), we produce

$$Q_{p_i} = \dots \quad (2.53)$$

The resulting radiations Q_{S_i} and Q_{ε_i} can be determined through the effective radiation of the ith section $E_{\text{eff } i}$ and the surrounding medium $E_{\text{eff } k}$ [see formula (2.16)]:

$$Q_{\varepsilon_i} = \dots$$
$$Q_{S_i} = \dots \quad (2.54)$$

In turn, $E_{\text{eff } i}$ and $E_{\text{eff } k}$ can be found from formula (2.17):

$$E_{\text{eff}\varepsilon_i} F_i = \frac{E_{\varepsilon_i} F_i}{\varepsilon_i} + \left(\frac{1}{\varepsilon_i} - 1\right) Q_{\varepsilon_i},$$
$$E_{\text{eff}S_i} F_i = \frac{E_{Si} F_i}{A_i} + \left(\frac{1}{A_i} - 1\right) Q_{S_i},$$
$$E_{\text{eff}\varepsilon_K} F_K = \frac{E_{\varepsilon_K} F_K}{\varepsilon_K} + \left(\frac{1}{\varepsilon_K} - 1\right) Q_{\varepsilon_K},$$
$$E_{\text{eff}S_K} F_K = \frac{E_{S_K} F_K}{A_K} + \left(\frac{1}{A_K} - 1\right) Q_{S_K}. \quad (2.55)$$

The expression for the penetrating heat flux Q_{p_i} will be sought for the most complex case -- when the spacecraft is in a vacuum chamber. In this case, in order to simplify the problem, we assume that the radiation of any ith section of the outer surface of the spacecraft is distributed evenly over the entire inner surface of the vacuum chamber. In order to reduce the volume of computation, we shall limit ourselves to producing the expressions for Q_{S_i}, and determine the expression for Q_{ε_i} by analogy.

For the surrounding medium forming a closed system and the stable thermal mode of the spacecraft, we can write

$$Q_{S_к} = -\sum_{i=1}^{n} Q_{S_i} = -Q_{S_i} - \sum_{i=1}^{n-1} Q_{S_i}. \tag{2.56}$$

Substituting (2.56) into the fourth formula of (2.55), we produce

$$E_{\text{eff}\ S_к F_к} = \frac{E_{S_к F_к}}{A_к} - \left(\frac{1}{A_к} - 1\right) Q_{S_i} - \left(\frac{1}{A_к} - 1\right) \sum_{i=1}^{n-1} Q_{S_i}. \tag{2.57}$$

Substituting the second expression of (2.55) and expression (2.57) into the second equation of (2.54), we produce

$$Q_{S_i}\left[\frac{1}{A_i} + \left(\frac{1}{A_к} - 1\right)\varphi_{кi}\right] = \varphi_{кi}\frac{E_{S_к F_к}}{A_к} - \frac{E_{S_i F_i}}{A_i} - \varphi_{кi}\left(\frac{1}{A_к} - 1\right)\sum_{i=1}^{n-1} Q_{S_i}. \tag{2.58}$$

Similarly

$$Q_{\varepsilon_i}\left[\frac{1}{\varepsilon_i} + \left(\frac{1}{\varepsilon_к} - 1\right)\varphi_{кi}\right] = \varphi_{кi}\frac{E_{\varepsilon_к F_к}}{\varepsilon_к} - \frac{E_{\varepsilon_i F_i}}{\varepsilon_i} - \varphi_{кi}\left(\frac{1}{A_к} - 1\right)\sum_{i=1}^{n-1} Q_{\varepsilon_i}. \tag{2.59}$$

The natural "solar" radiation E_{S_i} is determined from formula (2.52), while the natural "thermal" radiation E_{ε_i} is determined from formula (2.24), in which the temperature of the outer surface (represented subsequently as T_i) is not yet known. To determine this temperature, we use equation (2.43), which we write as

$$Q_{n_i} = \varepsilon_{C.ai} C_0 F_i \left[\left(\frac{T_i}{100}\right)^4 - \left(\frac{T_a}{100}\right)^4\right] = \varepsilon_{C.ai}\left(\frac{E_{\varepsilon_i} F_i}{\varepsilon_i} - \frac{E_{\varepsilon_a} F_i}{\varepsilon_a}\right), \quad (2.60)$$

where T_a, ε_a are the temperature and degree of blackness of the outer surface of the body of the spacecraft; T_i, ε_i are the temperature and degree of blackness of the outer layer of the SVTI.

Setting the right parts of equations (2.53) and (2.60) equal, we find

$$\frac{E_{\varepsilon_i} F_i}{\varepsilon_i} = \frac{E_{\varepsilon_a} F_i}{\varepsilon_a} - \left(\frac{Q_{S_i}}{\varepsilon_{C.ai}} + \frac{Q_{\varepsilon_i}}{\varepsilon_{C.ai}} - \frac{S_i F_i}{\varepsilon_{C.ai}}\right).$$

Substituting the expression produced into (2.59), we produce

$$Q_{\varepsilon_i}\left[\frac{1}{\varepsilon_к} + \left(\frac{1}{\varepsilon_к} - 1\right)\varphi_{кi} + \frac{1}{\varepsilon_{C.ai}}\right] = \frac{E_{\varepsilon_к} F_к}{\varepsilon_к}\varphi_{кi} - \frac{E_{\varepsilon_a} F_i}{\varepsilon_a} - \frac{S_i F_i}{\varepsilon_{C.ai}} - \varphi_{кi}\left(\frac{1}{\varepsilon_к} - 1\right)\sum_{i=1}^{n-1} Q_{\varepsilon_i} - \frac{Q_{S_i}}{\varepsilon_{C.ai}}. \quad (2.61)$$

The unknowns in equations (2.58) and (2.61) are Q_{S_i} and Q_{ε_i}, which can be determined by composing n equations for Q_{S_i} and n equations for Q_{ε_i}.

Substituting the expressions produced for Q_{S_i} and Q_{ε_i} into formula (2.53), which determines the penetrating thermal flex Q_{p_i} through the ith section of the outer surface of the spacecraft, we produce

$$Q_{p_i} = \left(1 - \frac{\varepsilon_{C\,i}}{\Phi_\varepsilon \varepsilon_{C\,.\,ai}}\right)\left[\left(1 - \frac{1 - A_i}{\Phi_S}\right)F_i S_i + \right.$$
$$\left. + \varphi_{K\,i}\frac{1 - A_K}{\Phi_S A_K} F_K S_K A_i\right] -$$
$$- \frac{\varepsilon_{C\,i}}{\Phi_\varepsilon}\left[C_0 F_i \left(\frac{T_a}{100}\right)^4 - \varphi_{K\,i} F_K C_0 \left(\frac{T_K}{100}\right)^4\right], \qquad (2.62)$$

where

$$\varepsilon_{C\,i} = \frac{1}{\frac{1}{\varepsilon_i} + \frac{1}{\varepsilon_{C\,.\,ai}}}, \qquad (2.63)$$

$$\Phi_\varepsilon = 1 + \left(\frac{1}{\varepsilon_K} - 1\right)\sum_{i=1}^{n} \varepsilon_{C\,i}\varphi_{K\,i}, \qquad (2.64)$$

$$\Phi_S = 1 + \left(\frac{1}{A_K} - 1\right)\sum_{i=1}^{n} A_i \varphi_{K\,i}. \qquad (2.65)$$

The problem of static calculation of the thermal mode of the spacecraft consists in that, in accordance to the heat balance equation (2.1), equation $\sum_{i=1}^{n} Q_{p_i} = -Q_T$ must be fulfilled. Then equation (2.62) becomes

$$Q_T = -\sum_{i=1}^{n} Q_{p_i} =$$
$$= \frac{1}{\Phi_\varepsilon} C_0 \left(\frac{T_a}{100}\right)^4 \sum_{i=1}^{n} F_i \varepsilon_{C\,i} -$$
$$- \frac{1}{\Phi_\varepsilon} C_0 \left(\frac{T_K}{100}\right)^4 \sum_{i=1}^{n} F_K \varepsilon_{C\,i}\varphi_{K\,i} -$$
$$- \sum_{i=1}^{n}\left(1 - \frac{\varepsilon_{C\,i}}{\Phi_\varepsilon \varepsilon_{C\,.\,ai}}\right)\left[\left(1 - \frac{1 - A_i}{\Phi_S}\right) \times \right.$$
$$\left. \times F_i S_i + F_K \varphi_{K\,i}\frac{1 - A_K}{\Phi_S A_K} S_K A_i\right]. \qquad (2.66)$$

Replacing the product $\phi_{ki}F_k$ in this last equation with $\phi_{ik}F_i$ (based on the property of mutuality of radiant fluxes) and

solving it for T_a, we produce /60

$$C_0\left(\frac{T_a}{100}\right)^4 \sum_{i=1}^{n} F_i \varepsilon_{C\,i} = Q_T \Phi_\varepsilon + \\ + C_0\left(\frac{T_K}{100}\right)^4 \sum_{i=1}^{n} F_i \varepsilon_{C\,i} \varphi_{i\,K} + \\ + S_0 \sum_{i=1}^{n} F_i \varepsilon_{C\,i}\left(\frac{\Phi_\varepsilon}{\varepsilon_{C\,i}} - \frac{1}{\varepsilon_{C\cdot a i}}\right) S_{sK}\,, \tag{2.67}$$

where

$$S_{sK} = \left[\left(1 - \frac{1 - A_i}{\Phi_S}\right)\frac{S_i}{S_0} + \\ + \frac{S_K}{S_0}\frac{A_i}{\Phi_S}\frac{1 - A_K}{A_K}\varphi_{iK}\right].$$

Equation (2.66) yields the summary value of heat flux $\sum_{i=1}^{n} Q_{P_i}$, penetrating through the outer surface of any part or the entire spacecraft with fixed mean temperature T_a, while equation (2.67) gives us the mean temperature T_a with fixed internal heat liberation Q_T as a function of the heat-physical and geometric characteristics of the spacecraft (ε_i, $\varepsilon_{C\,ai}$, A_i, F_i), surrounding medium (ε_k, A_k, S_i, S_k, T_k, F_k) and the characteristics of the thermal couple between them (ϕ_{ik}).

We shall present below examples of the use of equation (2.67) for calculation of the thermal state of a spacecraft and development of a method for thermal testing to be performed on Earth. Let us now study the physical sense of the terms included in this equation, and give this equation the form most convenient for solution of both problems.

1. Using the property of mutuality of radiant fluxes, expressions (2.64) and (2.65) can be written as

$$\Phi_S = 1 + \frac{1}{F_к}\left(\frac{1}{A_к} - 1\right)\sum_{i=1}^{n} \varphi_{iк} F_i A_i, \tag{2.68}$$

(2.69)

Since always $0 \leq \phi_{ik} \leq 1$, $A_i \leq 1$, $\varepsilon_{c\,i} < 1$, then

$$\sum_{i=1}^{n} \varphi_{iк} F_i A_i < \sum_{i=1}^{n} F_i$$

and

$$\sum_{i=1}^{n} \varphi_{iк} F_i \varepsilon_{c\,i} < \sum_{i=1}^{n} F_i.$$

For spacecraft on the surface of a planet or flying above one, F_k is nothing other than the "surrounding" surface, and always

$$F_к \gg \sum_{i=1}^{n} F_i.$$

Consequently,

$$\frac{1}{F_к}\frac{1-A_к}{A_к}\sum_{i=1}^{n} \varphi_{iк} F_i A_i \leqslant$$
$$\leqslant \frac{F_i}{F_к}\frac{1-A_к}{A_к} \ll 1 \text{ and } \Phi_S \approx 1,$$
$$\frac{1}{F_к}\frac{1-\varepsilon_к}{\varepsilon_к}\sum_{i=1}^{n} \varphi_{iк} F_i \varepsilon_{c\,i} \leqslant \frac{F_i}{F_к}\frac{1-\varepsilon_к}{\varepsilon_к} \ll 1$$

and

$$\Phi_\varepsilon \approx 1.$$

Thus, substituting $\Phi_\varepsilon = 1$ and $\Phi_S = 1$ into (2.67) and considering expression (2.63), we produce

$$C_0\left(\frac{T_a}{100}\right)^4\sum_{i=1}^{n}F_i\varepsilon_{Ci}=$$

$$=Q_T+C_0\left(\frac{T_K}{100}\right)^4\sum_{i=1}^{n}F_i\varepsilon_{Ci}\varphi_{iK}+$$

$$+\sum_{i=1}^{n}\frac{A_i}{\varepsilon_i}F_i\varepsilon_{Ci}\left[S_i+S_K\varphi_{iK}\frac{1-A_K}{A_K}\right]. \qquad (2.70)$$

With fixed internal heat liberation, heat-physical characteristics of the spacecraft, surrounding medium and characteristics of the thermal couple between them, equation (2.70) can be used to determine the temperature of the spacecraft on the surface of a planet, in orbit about one or in free space. This same equation can also be used to select the necessary heat-physical characteristics of the TMSS of the spacecraft, for which it can be given a more convenient form by dividing all of its terms by $C_0\ (T_a/100)^4$ and introducing the following symbols: /61

$$\Phi_\varepsilon=1+\frac{1}{F_K}\left(\frac{1}{\varepsilon_K}-1\right)\sum_{i=1}^{n}\varphi_{iK}F_{i\varepsilon_{Ci}}-A_K\varphi_{iK}=q_{iS},$$

$$\frac{\alpha_i}{C_0(T_a/100)^4}$$

$$F_i\varepsilon_{Ci}=F_{Ci}, \qquad (2.71)$$

$$Q_T/[C_0(T_a/100)^4]=F_T\ [м^2].$$

Then (2.70) becomes

$$\sum_{i=1}^{n}F_{Ci}=F_T+\sum_{i=1}^{n}F_{Ci}(q_{i_K}+q_{i_S})\ \ [m^2]. \qquad (2.72)$$

Equation (2.72) can also be written as

$$\sum_{i=1}^{n}F_{Ci}q_i=F_T\ \ [m^2], \qquad (2.73)$$

where

$$q_i=(1-q_{i_K}-q_{i_S}). \qquad (2.74)$$

In the following we will say: $F_{c\,i}$ is the corrected area of the ith section; F_T is the relative internal heat liberation. We note that $\sum_{i=1}^{n} F_{c\,i} q_i$ is the relative penetrating heat flux, taken with the reverse sign.

Analysis of equation (2.73) shows that with fixed internal heat liberation Q_T and temperature T_a (i.e., with fixed relative internal heat liberation F_T), the necessary heat-physical characteristics of the TMSS (A_i, ε_i, $\varepsilon_{c\,i}$ and F_i) can be determined from the condition of equality of the sums of relative penetrating heat flux $\sum_{i=1}^{n} F_{c\,i} q_i$ through each ith section to the relative internal heat liberation F_T.

The value of F_T, with the dimensionality of square meters, shows the surface area necessary at temperature T_a and degree of blackness equal to 1 to "clear" the internal heat liberation Q_T if it is positive (for example, when the instruments are operating), or the surface area at temperature T_a and degree of blackness equal to 1 equivalent to internal heat liberation Q_T if it is negative (for example, when an evaporator is operating).

It should be noted that if it is necessary to consider heat exchange between individual parts or elements of the spacecraft for which thermal balance equations have been written in the form of (2.70) or (2.73), the value of this heat exchange with the corresponding sign should be included in the internal heat liberation Q_T. An example of the use of equation (2.73) for determination of the necessary heat-physical characteristics of the spacecraft TMSS is presented in § 6.2.

2. Analysis of the third term of equation (2.66) indicates that the quantity $\varepsilon_{c\,i}/\Phi_\varepsilon \varepsilon_{c\,ai}$ shows what portion of the direct solar radiation and solar radiation reflected from the surface of the chamber or a celestial body and absorbed by the outer surface of the spacecraft is "cleared" without passing through the insulation. Consequently, the factor $[1 - (\varepsilon_{c\,i}/\Phi_\varepsilon \varepsilon_{c\,ai})]$ is the "effective absorption factor" for direct and reflected solar radiation for a spacecraft beneath heat insulation.

The value $(1 - A_i)/\Phi_S$ is the "effective reflection factor", while factor $(1 - \frac{1-A_i}{\Phi_S})$ is the "effective absorption factor" for /62

direct solar radiation of the outer surface of the ith section of the spacecraft, considering the effect of multiple reflection between the surface of the ith sector and the surface of the surrounding media. The less the absorption factor for solar radiation of the surrounding medium A_k, the greater the value of Φ_S [see (2.65)] and, consequently, the greater the effective absorption factor of the surrounding surface.

When the spacecraft is in a vacuum chamber, conditions $\Phi_S \simeq 1$ and $\Phi_\varepsilon \simeq 1$ are not fulfilled, and in determining temperature T_a it is necessary to use equation (2.67), which can be conveniently written as

$$C_0\left(\frac{T_a}{100}\right)^4 \sum_{i=1}^{n} F_i \varepsilon_{Ci} = \Phi_\varepsilon Q_T + C_0\left(\frac{T_K}{100}\right)^4 \times$$
$$\times \sum_{i=1}^{n} F_i \varepsilon_{Ci} \varphi_{iK} + S_0 \sum_{i=1}^{n} F_i \varepsilon_{Ci} \times$$
$$\times \left(\frac{\Phi_\varepsilon}{\varepsilon_{Ci}} - \overline{\varepsilon_{Ci}}\right) S_{SK}. \qquad (2.75)$$

6.2. Method of Calculation of Heat-Physical Characteristics of the Thermal Mode Support System

As an example of the application of the thermal state equation (2.73), let us use it to determine the necessary heat-physical characteristics of the TMSS of one part of a spacecraft (for example, that marked with index j in Figure 8), for a spacecraft designed to fly to the moon and spend considerable time on its surface, based on the requirement that the temperature of this portion of the spacecraft should stay between $T_{a\ min} = 0°$ C and $T_{a\ max} = +40°$ C during all flight stages.

Suppose during the EME stages (flight from Earth to moon and back) the spacecraft spins around its x axis, which stays oriented toward the sun at all times; in stage Ld (lunar day) the sun is at the zenith, the temperature of the surface of the moon is near its maximum (396 A); in stage Ln (lunar night) the temperature of the surface is at its minimum (about 100 K).

We shall perform our thermal calculation in the following sequence.

1. We divide the outer surface of the spacecraft into a number of surfaces:

-- surface F_S, including sections from i = 1 to i = S,

illuminated by the direct radiation of the sun;

-- surface F_m, including sections from i = S + 1 to i = m, not illuminated by the sun or illuminated periodically due to inaccurate orientation of the x axis toward the sun and the rotation of the spacecraft around this axis;

-- surface F_n, including sections from i = m + 1 to i = n, the penetrating flux through which may be either negligible in comparison to the heat flux through surfaces F_S and F_m (with fully closed louvers) or comparable to it (with fully open louvers).

2. We assume that each ith section within the limits of one surface F_S, F_m and F_n has identical mean values of corrected radiation factors $\varepsilon_{c\,i}$, optical factors A_i, ε_i and irradiance factors with the surrounding medium ϕ_{ik}. Then, equation (2.73) can be written as follows:

$$\varepsilon_{c\,S} q_S \sum_{i=1}^{S} F_i + \varepsilon_{c\,m} q_m \sum_{i=S+1}^{m} F_i + \varepsilon_{c\,n} q_n \sum_{i=m+1}^{n} F_i = F_T$$

or

$$F_{c\,S} q_S + F_{c\,m} q_m + F_{c\,n} q_n = F_T.$$

The task of further calculation is determination of the mean corrected radiation factors $\varepsilon_{c\,S}$, $\varepsilon_{c\,m}$ and $\varepsilon_{c\,n}$, included in the corresponding corrected areas $F_{c\,S}$, $F_{c\,m}$ and $F_{c\,n}$, as well as the mean ratios of optical factors A_S/ε_S, A_m/ε_m and A_n/ε_n, included in the second equation of (2.71). /63

3. Let us write the last equation for each of the flight stages: for the Earth-moon-Earth stage:

$$F_{c\,S} q_S^{EME} + F_{c\,m} q_m^{EME} + F_{c\,n}^{EME} 2_n^{EME} = F_T^{EME}, \qquad (2.76)$$

for the Ld stage

$$F_{c\,S}q_S^{Ld} + F_{c\,m}q_m^{Ld} + F_{c\,n}^{Ld}q_n^{Ld} = F_T^{Ld}, \qquad (2.77)$$

for the Ln stage

$$F_{c\,S}q_S^{Ln} + F_{c\,m}q_m^{Ln} + F_{c\,n}^{Ln}q_n^{Ln} = F_T^{Ln}. \qquad (2.78)$$

We can see from the first and second equations of (2.71) and equation (2.74) that when the spacecraft is on the moon at night (stage Ln), $q_S^{Ln} = q_m^{Ln} = q_n^{Ln} \simeq 1$. These second equations show that q_S^{Ld} and q_S^{EME} are always less than $q_S^{Ln} \simeq 1$; q_m^{Ld} and q_m^{EME} are less than $q_m^{Ln} \simeq 1$; q_n^{Ld} and q_n^{EME} are less than $q_n^{Ln} \simeq 1$, i.e., the left parts of equations (2.76) and (2.77) are essentially less than the left part of equation (2.78). Consequently, with unchanged corrected areas $F_{c\,S}$, $F_{c\,m}$ and $F_{c\,n}$ during flight, permissible relative heat liberations F_T^{Ld} and F_T^{EME} will always be essentially less than the required relative heat liberation F_T^{Ln} at night.

Since heating power should be minimal, the corrected areas $F_{c\,S}$, $F_{c\,m}$ and $F_{c\,n}$ should also be minimal, and if the internal heat liberation is selected equal to the necessary heat liberation at night and is identical in all flight stages, then with unchanged corrected areas $F_{c\,S}$, $F_{c\,m}$ and $F_{c\,n}$, the temperature of the spacecraft during stages EME and Ld will be significantly greater than the maximum permissible $T_{a\,max}$.

Therefore, it is necessary first to determine the heat-physical characteristics of the spacecraft for the stages EME and Ld with the same relative internal heat liberation F_T but with different spacecraft temperatures ($T_a = T_{a\,min}$ during stage EME and $T_a = T_{a\,max}$ during stage Ld), then use fromula (2.78) and the fourth formula of (2.71) to determine the required heat liberation Q_T^{Ln} at night. If it is found that it is significantly higher than the heat liberation Q_T during stages EME and Ld, it is necessary either to artificially increase the heat liberation of the instruments at night Q_T^{Ln}, or to use a special heater.

Using equations (2.76) and (2.77), we produce

$$F_{c\,S} = (F_T^{EME} + q_n^{Ld}\frac{q_m^{EME}}{q_m^{Ld}}F_{c\,n}^{Ld} -$$

$$- \frac{q_m^{EME}}{q_m^{Ld}}F_T^{Ld} - q_n^{EME}F_{c\,n}^{EME}\ x$$

$$x\ (q_S^{EME} - q_S^{Ld}\frac{q_m^{EME}}{q_m^{Ld}})^{-1},$$

$$F_{c\,m} = [F_T^{Ld} + (F_{c\,n}^{EME}q_n^{EME} - F_T^{EME})q_S^{Ld}/q_S^{EME}]\ x$$

$$x\ (q_m^{Ld} - q_m^{EME}\frac{q_S^{Ld}}{q_S^{EME}})^{-1}. \qquad (2.79)$$

4. Let us construct a supplementary graph of the dependence of the corrected areas $F_{c\,S}$ and $F_{c\,m}$ on relative internal heat liberation F_T for various values of factor ratio A_S/ε_S and corrected area $F_{c\,n}$. We will analyze the change in relative internal heat liberation F_T within limits of 0 to 0.5, and select the range of change of ratio A_S/ε_S on the basis of the following considerations.

Since the spacecraft temperature should not exceed +40° C during the hottest time on the moon (at noon) when, in addition to the solar radiation, the thermal radiation of the moon is at its maximum, the ratios A_S/ε_S and A_m/ε_m, obviously, must be the minimum possible. If white paint is used on the outside of the spacecraft, these ratios can be reduced to 0.2-0.25 (see § 7.2). Therefore, further calculations must be performed for the following case: /64

$$A_S/\varepsilon_S = A_m/\varepsilon_m = 0.2;\ 0.25 \text{ and } 0.3.$$

The results of calculation are presented in Figure 23. Calculation was performed for a cylindrical spacecraft with F_S = = 1 m^2, F_n = 5 m^2, F_n = 1 m^2; for these surfaces ϕ_{Sk} = 0, ϕ_{mk} = = 0.5, ϕ_{mk} = 0 (louvers closed on the surface of the moon). During the EME flight stage, $F_{c\,n}$ = 0, 0.01 and 0.1, during stages

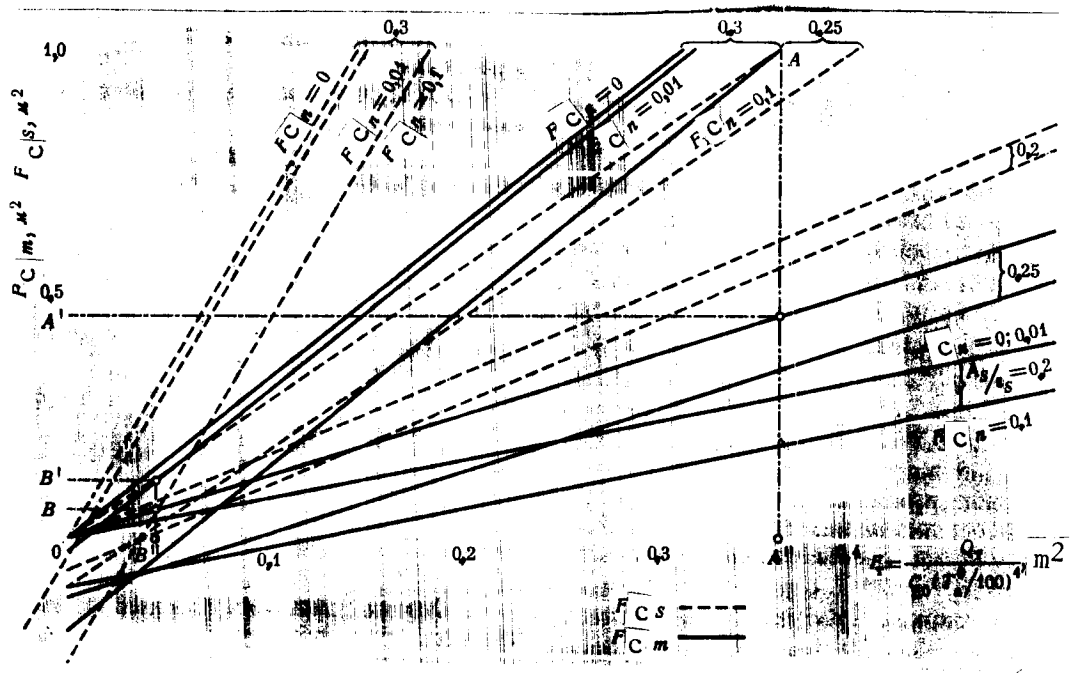

Figure 23. Corrected Areas $F_{c\,S}$ and $F_{c\,m}$ and Corrected Radiation Factors $\varepsilon_{c\,S}$ and $\varepsilon_{c\,m}$ as Functions of Corrected Area of Internal Heat Liberation F_T for Various Values of A_i/ε_i and $F_{c\,n}$

Ld and Ln, $F_{c\,n} = 0$. The solar radiation absorption factor by the surface of the moon $A_L = 0.93$, while $A_m/\varepsilon_m = A_S/\varepsilon_S$. During stages EME and Ln, temperature $T_a = T_{a\,min} = 0°$ C, during stage Ld $T_a = T_{a\,max} = +40°$ C.

5. Using the graphs of Figure 23, we can determine various versions of heat-physical characteristics of the TMSS as functions of the purpose of the spacecraft.

If the maximum possible elimination of heat is required as the spacecraft is resting on the surface of the moon, area $F_{c\,S}$ must be maximal, and with fixed F_S the factor $\varepsilon_{c\,S}$ should also be maximal. Since the maximum possible value of $\varepsilon_{c\,S}$ is approximately 1 [see formula (2.63)], corresonding to a surface without heat insulation (usually called a cooling radiator), by using the graphs of Figure 23 (see AA' and AA"), we find (where $A_S/\varepsilon_S = 0.25$) /65

$$F_{c\,m} = 0.45\ m^2,\ F_T = 0.36\ m^2.$$

Consequently,

$$\varepsilon_{c\ m} = 0.09,$$

$$Q_T^{EME} = F_T C_0 (T_a^{EME}/100)^4 = 98 \text{ kcal/hr} =$$

$$= 115 \text{ w},$$

$$Q_T^{Ld} = F_T C_0 (T_a^{Ld}/100)^4 = 166 \text{ kcal/hr} =$$

$$= 200 \text{ w}.$$

Substituting the values of $F_{c\ S}$ and $F_{c\ m}$ which we have found into (2.78), we produce the required heat liberation at night

$$Q_T^{Ln} = F_T^{Ln} C_0 (T_T^{Ln}/100)^4 =$$

$$= (F_{c\ S} + F_{c\ m}) C_0 (T_a^{Ln}/100)^4 =$$

$$= 400 \text{ kcal/hr} = 460 \text{ w}.$$

Thus, the TMSS of the spacecraft, providing a heat elimination capacity of about 200 w when the spacecraft is resting on the surface of the moon a lunar noon, should have the following heat-physical characteristics (first version of TMSS):

$$F_{c\ S} \simeq 1 \text{ m}^2 \ (\varepsilon_{c\ S} \simeq 1), \ F_{c\ m} =$$

$$= 0.45 \text{ m}^2 \ (\varepsilon_{c\ m} = 0.09), \ F_{c\ n} \leq 0.01,$$

$$A_S/\varepsilon_S = A_m/\varepsilon_m = 0.25, \ Q_T^{EME} = 115 \text{ w},$$

$$Q_T^{Ld} = 200 \text{ w}, \ Q_T^{Ln} = 460 \text{ w}.$$

In this case, the temperature of the spacecraft during stage EME will be 273 K, during stage Ld 313 K and, in order to maintain the temperature of the spacecraft during stage Ln at 273 K, internal neat liberation (heating) with a power of 460 w is required.

Provision of this level of heating for the entire lunar night (about 15 Earth days) is a difficult task due to the limited power reserves available on board the spacecraft. Therefore, let us determine the heat-physical characteristics of a spacecraft TMSS requiring the minimum possible heating value at night and at the same time providing sufficient heat elimination at lunar noon.

Given the minimum practical possible corrected radiation factor $\varepsilon_{c\ m}$ of surface F_m (for example, $\varepsilon_{c\ m} = 0.01$), we can use the graphs of Figure 23 to find (see BB' and BB")

$$F_{c\ S} = 0.11\ m^2,\ F_T = 0.04\ m^2.$$

Consequently,

$$Q_T^{EME} = F_T C_0 (T_a^{EME}/100)^4 = 11\ kcal/hr =$$
$$= 12.6\ w,$$

$$Q_T^{Ld} = F_T C_0 (T_a^{Ld}/100)^4 = 18.6\ kcal/hr =$$
$$= 21.5\ w.$$

Substituting the value of $F_{c\ S}$ and the given $F_{c\ m}$ into formula (2.78), we produce the required internal heat liberation at night

$$Q_T^{Ln} = F_T^{Ln} C_0 (T_a^{Ln}/100)^4 =$$
$$= (F_{c\ S} + F_{c\ m}) C_0 (T_a^{Ln}/100)^4 = 50\ w.$$

Thus, the TMSS of a spacecraft providing for a heat elimination level of 21.5 w with the spacecraft on the surface of the moon at lunar noon should have the following heat physical characteristics (second TMSS version):

$$F_{c\ S} = 0.11\ m^2\ (\varepsilon_{c\ S} = 0.11),$$
$$F_{c\ m} = 0.05\ m^2\ (\varepsilon_{c\ m} = 0.01),$$
$$F_{c\ n} \leq 0.01,\ A_S/\varepsilon_S = A_m/\varepsilon_m = 0.25,$$
$$Q_T^{Ld} = 21.5\ w,\ Q_T^{EME} = 12.5\ w,$$
$$Q_T^{Ln} = 50\ w.$$

We can see from these examples that even with good heat insulation and minimum heat liberation at lunar noon (only 21.5 w), at nighttime a heating power of 50 w is required, and the problem of maintaining the thermal state of the spacecraft is reduced primarily either to provision of sources of thermal energy (chemical, electrical, isotopic, etc.), which is not always possible, or to the need for a change in heat-physical characteristics of the spacecraft TMSS upon transition from one flight stage to another, to allow minimum heating. /66

This last method of providing the required thermal state of a spacecraft is studied in the next section.

6. After determining the mean summary values of corrected areas $F_{c\,S}$, $F_{c\,m}$ and $F_{c\,n}$ and the ratios of optical factors A_S/ε_S, A_m/ε_m, A_n/ε_n for the surfaces F_S, F_m, F_n, let us find the corrected areas $F_{c\,i}$ and the ratio of factors A_i/ε_i for each ith section of these surfaces, where for sections without heat insulation (corresponding to so-called heat leaks), the corrected areas are equal to the outer surface areas of these sections. These calculations are related to the design of specific spacecraft and therefore are not presented in this work.

6.3. Definition of the Concepts of Passive and Active Thermal Mode Support Systems

With known heat-physical characteristics of the spacecraft TMSS, surrounding medium and characteristics of the thermocouple between them, the temperature of the spacecraft is determined by the formula

$$T_a = T_a^* \sqrt[4]{\frac{F_T^* + \sum_{i=1}^{n} F_{Ci}(q_{iK}^* + q_{iS}^*)}{\sum_{i=1}^{n} F_{Ci}}}, \qquad (2.80)$$

which can be produced from (2.72). The quantities $Q_{i_k}^*$ and $q_{i_S}^*$ and F_T^* included in this formula are defined by the corresponding formulas of (2.72), with the replacement of temperature T_a by arbitrary temperature T_a^* (for example, $T_a^* = T_{a\,min}$).

The results of calculation of temperature T_a for the thermal model of the spacecraft which we studied as an example (first

version of TMSS) for stages EME and Ld, depending on the corrected area of internal heat liberation, are shown in Figure 24. We can see from this figure that were F_T = 0.36 m^2 and A_S/ε_S = = 0.25, temperature T_a during stage EME will not be below 0° C, and during stage Ld will not be above +40° C. However, due to possible random deviations in heat-physical characteristics of the TMSS, surrounding medium and in heat exchange conditions between them from the calculated values, the temperature of the spacecraft in flight may go beyond the design limits $T_{a\ max}$ and $T_{a\ min}$.

/67

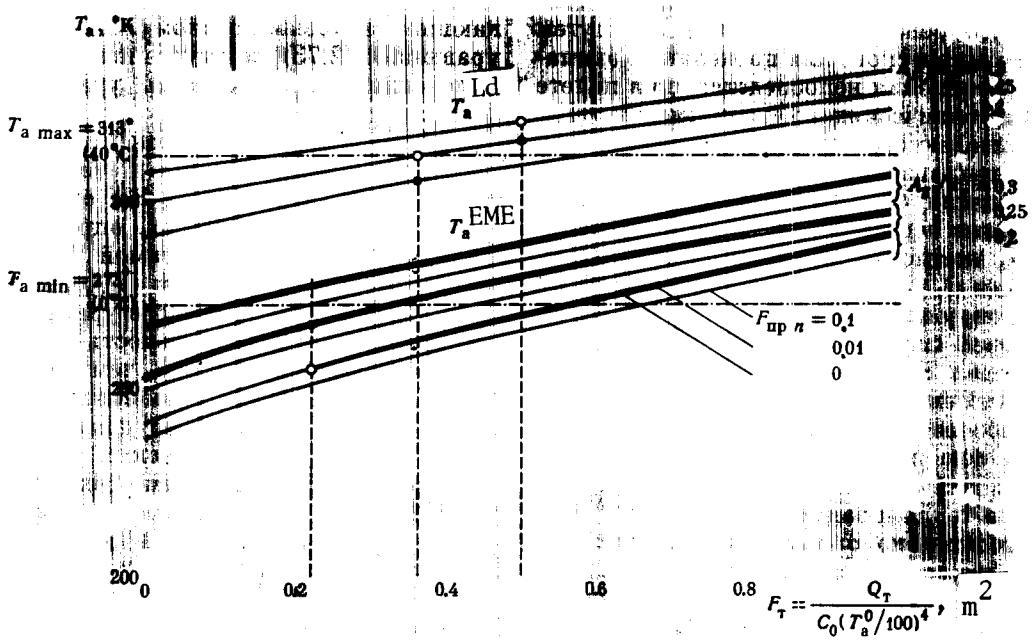

Figure 24. Spacecraft Temperature as a Function of Corrected Area of Internal Heat Liberation F_T During Flight Stage Between Earth and Moon (T_a^{EME}) and on Surface of Moon at Lunar Noon (T_a^{Ld})

Thus, an increase in the value of corrected heat liberation F_T and in ratio A_S/ε_S, for example to F_T = 0.5 m^2 and A_S/ε_S = = 0.3, leads to an increase in the temperature of the spacecraft on the surface of the moon to +50° C, while for the spacecraft during stage EME a decrease in the values of F_T and A_S/ε_S, for example to F_T = 0.22 m^2 and A_S/ε_S = 0.2, leads to a drop in the temperature to -18° C (Figure 24). To decrease the probability that the temperature will be outside the fixed limits due to random deviations in heat-physical characteristics of the spacecraft, the surrounding medium and the heat exchange

conditions between them, calculations are performed "with a reserve," for which in place of the permissible $T_{a\ max}$ = +40° C and $T_{a\ min}$ = 0° C we take $T_{a\ max}$ = 30-35° C and $T_{a\ min}$ = 5-10° C.

However, we may find that when this approach is taken either the weight of the TMSS becomes impermissibly great, or it becomes impossible to maintain the required temperature. For example, if we set ourselves the goal of maintaining T_a = +30° C and F_T = 0.36 m^2 at lunar noon, we would see that this is impossible, since even with A_S/ε_S = 0.2 we produce T_a = +35° C (Figure 24). Obviously, the reliability of maintenance of spacecraft temperature within fixed limits will become higher if the heat-physical characteristics of the TMSS and conditions of heat exchange with the surrounding medium could be changed automatically or by the crew depending on the temperature of the spacecraft during flight. For example, if the danger arises of exceeding the maximum permissible temperature of the spacecraft, the corrected areas through which heat is eliminated must be increased (opening of louvers, covers over cooling radiators, switching on evaporators, etc.) and vice versa.

The need to change the heat-physical characteristics of the TMSS is also frequently dictated by the fact that without this type of change, it is impossible in principle to maintain the temperature within fixed limits for all spacecraft flight stages. We can see this by turning once more to the calculations related to the first version of the thermal model of the spacecraft, in which we determine that upon transition to flight stage Ln, an internal heat liberation of 460 w is necessary, significantly exceeding the maximum permissible heat liberation at lunar noon (200 w).

We can see from these examples that there are two main methods of providing the required thermal mode of a spacecraft, differing from each other in the ability to change the heat-physical characteristics of the TMSS during the flight. In principle, it is true, there is yet another method: transformation of the heat-physical characteristics of the surrounding medium on the scale of the entire celestial body or just in the area directly surrounding the spacecraft. However, this method will not be studied in this work.

The system for maintaining the thermal mode (state) of the spacecraft by selection of its heat-physical characteristics (corrected radiation factor ε_c, thermal insulation, solar radiation absorption factor A_S and degree of blackness ε of the outer surface, power of internal heat liberation Q_T) and the orientation of the spacecraft relative to its surroundings, without making /68

changes with the passage of time, is called a passive thermal mode support system (PTMSS).

The system of maintaining the required thermal mode (state) of a spacecraft by automatic or crew-controlled changes of the heat-physical characteristics of the spacecraft (corrected radiation factor ε_c of heat insulation, solar radiation absorption factor A_s and degree of blackness ε of outer surface, power of internal heat liberation Q_T) and its orientation relative to its surroundings is called an active thermal mode support system (ATMSS).

A passive system in many cases is simpler, lighter and more reliable, since it contains but a few elements: heat insulation, coverings, sources of heat and assigned orientation of the spacecraft relative to its environment. An active system is usually, but not always, more complex, heavier and less reliable, since it includes additional elements such as temperature sensors and signal amplifiers, moving actuating mechanisms, switchable pumps, heaters, evaporators, etc. For this reason, the use of ATMSS is justified only when the thermal mode cannot be maintained by a PTMSS during certain stages of the flight, so that we are forced to utilize ATMSS as supplementary devices.

6.4. Determination of Power of Active Thermal Mode Support System

Analysis of equations (2.70) and (2.72) indicates that the purpose of passive and active thermal mode support systems is to maintain equality between the thermal energy lost by the spacecraft, which depends on temperature T_a (left-portion of equation), the sum of thermal energy received by the spacecraft from the surrounding medium and by means of internal heat liberation (right portion of equations) or, in other words, the maintenance of equality between penetrating thermal radiation [left portion of equation (2.73)] and internal heat liberation [right portion of equation (2.73)].

PTMSS allow internal heat liberation and thermal fluxes received by the spacecraft from the environment to change within limits determined by the maximum permissible ($T_{a\ max}$) and minimum permissible ($T_{a\ min}$) spacecraft temperatures [left portion of equation (2.70)]. The less the difference between these temperatures, i.e., the less the permissible range of change of temperature T_a, the less the permissible deviations in heat-physical characteristics of the spacecraft, the environment and characteristics of the thermal couple between them from the design values.

If thermal calculation indicates that during some stage of flight the maintenance of the spacecraft temperature within the required limits by means of PTMSS alone is impossible, the heat-physical characteristics of the spacecraft must be changed during this stage, i.e., ATMSS must be used.

The degree of this change can be defined quantitatively by equation (2.72), which can be written in the following form for the case of utilization of ATMSS:

$$\sum_{i=1}^{n} F_{c\,i} = F_T + \sum_{i=1}^{n} F_{c\,i}(q_{ik} + q_{iS}) + F_a, \qquad (2.81)$$

where F_a is the relative internal heat liberation of the ATMSS, m^2. /69

Consequently,

$$F_a = \sum_{i=1}^{n} F_{c\,i} - \left[\sum_{i=1}^{n} F_{c\,i}(q_{iк} + q_{iS}) + F_T\right], \qquad (2.82)$$

or

$$F_a = \sum_{i=1}^{n} F_{c\,i}(1 - q_{iк} - q_{iS}) - F_T, \qquad (2.83)$$

or

$$F_a = \sum_{i=1}^{n} F_{c\,i} q_i - F_T. \qquad (2.84)$$

The power Q_a of an ATMSS refers to the required quantity of thermal energy per unit time necessary to maintain the permissible thermal state (temperature) of the spacecraft in case of a change in heat-physical characteristics of the spacecraft PTMSS, environment and characteristics of the thermalcouple between them which would otherwise shift the thermal state (temperature) of the spacecraft beyond the permissible limits. Using the fourth equation of (2.71) and equation (2.84), we produce

$$Q_a = F_a C_0 (T_a/100)^4. \qquad (2.85)$$

As an example of the application of equation (2.84), Figure 25 shows the dependence of the required corrected area of internal heat liberation of the ATMSS on ratio A_S/ε_S for the first version of the thermal spacecraft model which we studied (see § 6.2), for the conditions of lunar noon

We can see from Figure 25 that as the ratio A_S/ε_S varies from the design value of 0.25 to a value of 0.3, we have

$$\begin{gathered}(T_{\text{к}} = 396^\circ\ \text{K},\ T_a^{\text{Ld}} = +40^\circ\ \text{C}).\\ F_a = -0.1\ \text{m}^2,\\ Q_a = F_a C_0 (T_a/100)^4 = -47\ \text{w},\end{gathered} \tag{2.86}$$

i.e., at spacecraft temperature T_a = +40° C, the power of the ATMSS must be at least -47 w in order to prevent heating of the spacecraft to above the maximum permissible temperature T_a = = +40° C.

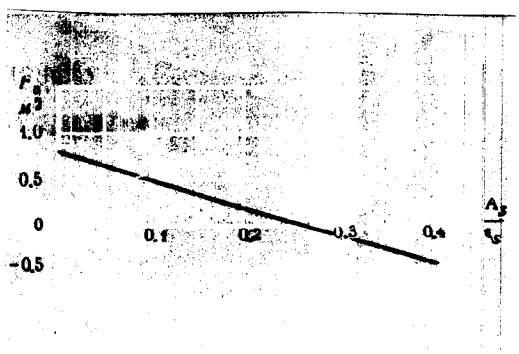

Figure 25. Required Corrected Area F_a of Internal Heat Liberation of ATMSS as a Function of Ratio A_S/ε_S

Active internal heat liberation Q_a (positive or negative) can be achieved by various means: therefore, the most important and interesting task of thermal design is the selection of an ATMSS plan which provides the required power of internal heat liberation with the minimum weight.

Thus, active heat elimination with a power Q_a = -47 w as in our example can be achived by several means:

-- by the use of phase conversions of substances (for example, evaporation of liquid within the spacecraft, with ejection of vapors into the vacuum);

-- installation of a screen above the cooling radiator (surface F_S) to protect it from the direct radiation of the sun;

-- provision of the possibility of eliminating heat into the soil of the celestial body;

-- creation of a microclimate around the spacecraft, decreasing the ratio A_S/ε_S of the surface of the celestial body (for example, by means of a thin layer of small white particles);

-- increasing the heat insulation of the side surface of the spacecraft (by decreasing corrected area $F_{c\ m}$).

CHAPTER 7

BASIC ELEMENTS OF THERMAL MODE SUPPORT SYSTEMS

7.1. Screen-Vacuum Thermal Insulation

In Chapter 6, we presented a method for calculation of the /70
thermal resistance of screen-vacuum thermal insulation (SVTI), which is widely used in spacecraft. The materials of which the screens and interlayers of SVTI are made may vary widely. For example, with an SVTI working temperature of up to 150° C, polyethylene terephthalate film (coated with aluminum, silver or gold) is usually used, while at temperatures of up to 450° C -- aluminum foil is used (with glass fiber interlayers). At temperatures over 450° C, the screens may be made of foil consisting of copper, nickel or steel with quartz fiber as interlayers between the screens. However, no matter what the texture of the SVTI, there are several common regularities determining its optimal thickness in each individual case.

In this section, we will briefly study the qualitative aspects of some of the general problems involved in the selection of the proper thickness of spacecraft SVTI. Quantitative calculation of the required number of layers (thickness) of the SVTI can be performed only on the basis of specific flight conditions and designs of specific spacecraft.

Packing density of SVTI layers. In planning spacecraft, one generally attempts to achieve the greatest possible effectiveness per unit weight of the design; for example, in the case of SVTI, one strives for maximum thermal resistance with a fixed number of screens. Since the radiated heat flux is inversely proportional to the quantity n + 1 (where n is the number of screens or layers of the SVTI), one should analyze quite carefully the question of the influence of the heat conductivity of the material of the screens and interlayers as a function of the number of layers per unit thickness of the SVTI.

As the packing density of SVTI layers increases, the component of the heat flux resulting from heat conductivity increases, so that optimal effectivenss of the SVTI is achieved at a certain packing density of the screens; rather detailed theoretical and experimental material on this problem has been presented in [14, 15]. This dependence differs for different textures and working temperatures of the SVTI, and therefore the extreme of heat conductivity occurs at various values of layer packing density, but the nature of the change of SVTI effectiveness in these cases is similar.

Figure 26 shows the heat conductivity factor of SVTI as a function of packing density of its layers, where $\bar{\lambda} = \lambda/\lambda_{min}$. We find that the minimum effective heat conductivity of SVTI is most frequently observed with free layup of screens (without compression), corresponding to about 10-30 layers per cm of thickness (depending on the material and conditions of use of the SVTI). The lower the degree of blackness of the surfaces of the screens, the less the heat conductivity. /71

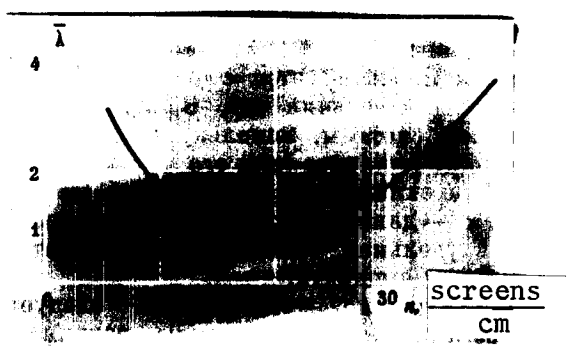

Figure 26. Dependence of SVTI Heat Conductivity on Layer Packing Density

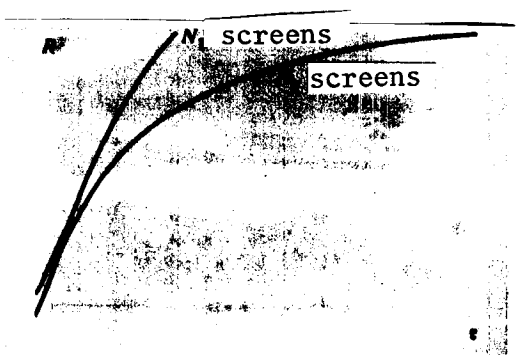

Figure 27. SVTI Thermal Resistance as a Function of Time Spent by Spacecraft in Deep Vacuum for Various Numbers of SVTI Layers ($N_1 < N_2$)

In what follows, we will assume that the packing density of the SVTI layers is near optimal, and that the question of the required thickness of the SVTI can be reduced to the question of the effective number of screens.

Selection of SVTI thickness for unstable flight section. As we know, the thermal resistance of SVTI depends significantly on the gas pressure between the screens [14]. Therefore, the launch section of the flight from Earth and the next hours (and even days) which the spacecraft spends in space requires particularly careful attention, due to the extended period of reduction of pressure between SVTI screens.

The pressure in the outer layers of the SVTI during this time approaches the pressure of the surrounding environment more rapidly than that between the inner layers, since the hydraulic resistance of the path to the vacuum of outer space is greater for the inner layers.

This process is also retarded by the fact that the material of the screens, inserts and the outer walls of the spacecraft (to which the SVTI is applied) "gasses" continually, adding new gas molecules to the SVTI. The residual gas pressure in the inner SVTI layers is always greater than in the outer layers,

and this difference increases with increasing thickness (i.e., number of layers) of the SVTI.

According to what we have said, SVTI with a smaller number of layers increases its effectiveness relatively more quickly than SVTI with a larger number of layers; the thermal resistance of SVTI reaches a value near its maximum when the residual gas pressure drops below 10^{-3} mm hg. This fact is illustrated by the graph of Figure 27.

Analysis of this graph indicates that for certain short flight durations, it is more expedient (at least as concerns weight) to use SVTI with relatively few screens.

Stable characteristics of SVTI. During a long flight in free space, when a rather low and approximately constant pressure is established between the screens of the SVTI, the thermal resistance of the SVTI will depend only on its temperature.

Selection of the required number of SVTI layers is determined by a number of factors. Usually, SVTI is used to prevent /72
significant heating or great thermal losses in the outer surfaces of the spacecraft and decrease unregulated heat exchange with the surrounding media. However, there are other sources of heat gain or loss. They include, for example, equipment, various devices and apparatus on the outer parts of the spacecraft which cannot be fully covered by SVTI due to their required operating conditions, and other sources.

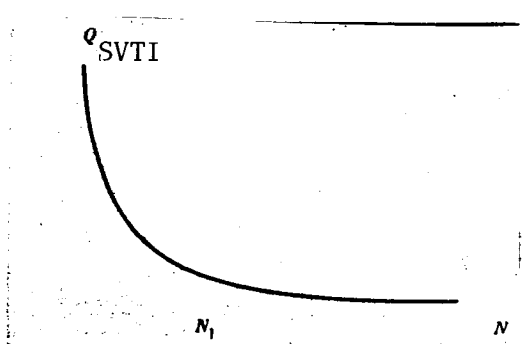

Figure 28. Heat Flux Through SVTI as a Function of the Number of Layers

For definition and simplicity of discussions, let us assume that the spacecraft continually loses the following quantity of heat into the surrounding space

$$\Delta Q = Q_{SVTI} + Q_{ee} + Q_{app} \quad [\text{kcal/hr}], \qquad (2.87)$$

where Q_{SVTI} is the heat loss through the SVTI; Q_{ee} is the heat loss through external equipment; Q_{app} is the mean quantity of heat introduced to the inside of the spacecraft as a result of functioning of its apparatus.

If an active thermal regulation system is used, its heat productivity should generally exceed ΔQ kcal/hr; in particular, with a rather extended discrete change in the value of ΔQ (when the thermal inertia is comparatively slight), the thermal regulation system is planned considering the extreme values of ΔQ. In the case of a passive system using the thermal capacity of the apparatus (or a portion of it), the permissible cooling $\Delta t = \Delta Q\tau/cG$ [degrees], where τ is the duration of the flight; c is the mean specific heat capacity of the apparatus; G is the weight of the apparatus.

Naturally, one should always attempt to decrease the value of Q_{SVTI}, so that the active thermal regulation system can be less cumbersome. To decrease Q_{SVTI}, one must increase the thermal resistance of the SVTI, i.e., the number of screens. But where is the intelligent limit in this case?

Let us look at Figure 28, showing the nature of change of thermal flux through SVTI as a function of the number of layers. We can see from the figure that when the number of SVTI layers exceeds a certain value N_1 (in most cases near the most effective value), the effectiveness of the SVTI increases only slightly. Consequently, increasing the number of SVTI layers above N_1 is rarely expedient [the function $Q_{SVTI} = f(N)$ should be established experimentally].

If it is determined that the heat flux Q_{SVTI} must be less than that produced with N_1 screens, it is sometimes expedient to take measures to increase the heating of the spacecraft, rather than increasing the number of SVTI screens or increasing the heat productivity of the active thermal regulation system.

One method of such heating (radiant heat transfer) is studied in Chapter 8. In many cases, the use of radiant heat transfer is more favorable (as concerns weight and reliability) than further complication of the active thermal regulation system or the use of more than N_1 SVTI screens. One should consider in this case that the weight of 10 screens of polyethylene terephthalate film with an area of 1 m^2 each is 0.2-0.3 kg, while an equivalent area of metal foil screen weighs about 1 kg. /73

7.2. Heat-Regulating Coatings

In order to clarify the principle of operation of heat regulating coatings in relationship to solar radiation, let us study the spectrum of solar radiation (Figure 29). We can see from thegraphs that the greatest energy contribution is made by

that portion of the spectrum in the range of wavelength of 0.2 to 1.0 μ.

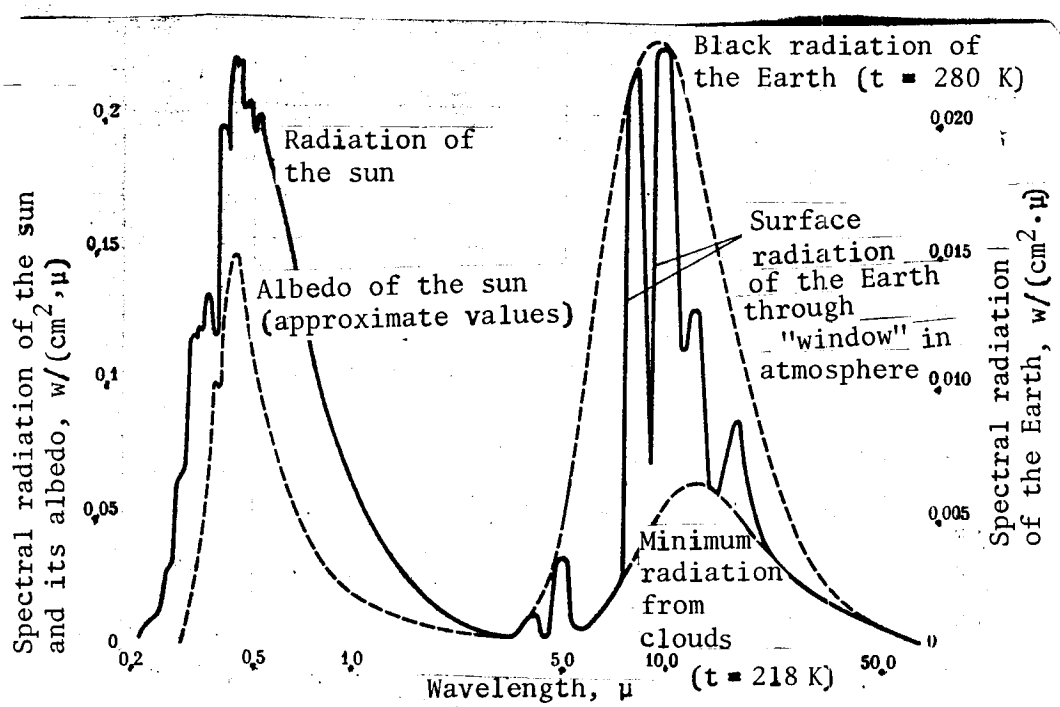

Figure 29. Spectral Distribution of Energy of the Sun and Earth

This same figure shows the spectral radiation of the Earth. The heat absorbed by the Earth is equal to the total solar flux minus the albedo of the Earth. The absorbed energy is reradiated at long wavelengths in the infrared band.

Similarly, the surface of a spacecraft absorbs the solar flux and reradiates the absorbed energy in the infrared spectrum. Figure 30 shows curves characterizing the absorption of solar energy and the change in the quantity of heat radiated by a spherical spacecraft at 280 K.

In the example presented, the quantity of heat radiated by an absolutely black radiator at 280 K is equal to the quantity of heat absorbed by the black coating of a spherical spacecraft. When a white organic coating is used in place of a black coating, the absorption of solar radiation is significantly less, while the radiating capacity is near the radiating capacity of an absolutely black body.

This factor causes a reduction in the surface temperature of the spacecraft. The reduction in temperature will continue until the energy radiated by the spacecraft is comparable to the solar flux absorbed. With a coating of polished aluminum or /74

gold, the absorbed solar flux will fall within limits of 0.2-0.3, and the radiating capacity will be very low (0.03-0.05).

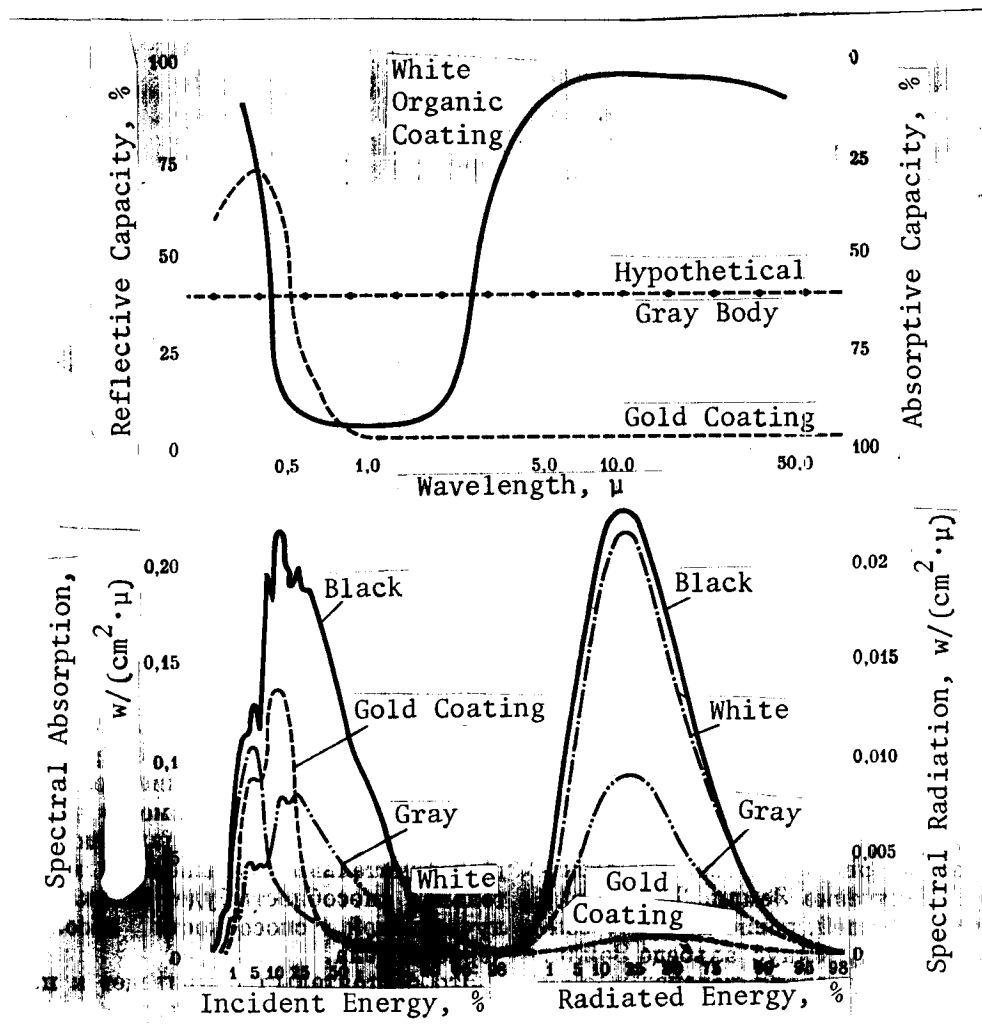

Figure 30. Absorptive and Reflective Capacities of Spacecraft Surface Coatings

The temperature of spacecraft surface illuminated by the sun will be rather high, some 500-600 K. When a gray body is used, the absorption and radiation factors will be equal. With identical reduction of absorption and radiation factors, the surface temperature remains constant. The properties of most coatings used for temperature control differ significantly from the properties of a gray body. Coatings which approximate gray bodies include black paint ($A_S \simeq \varepsilon \simeq 0.9$) and paints pigmented with aluminum ($A_S \simeq \varepsilon \simeq 0.4$). /75

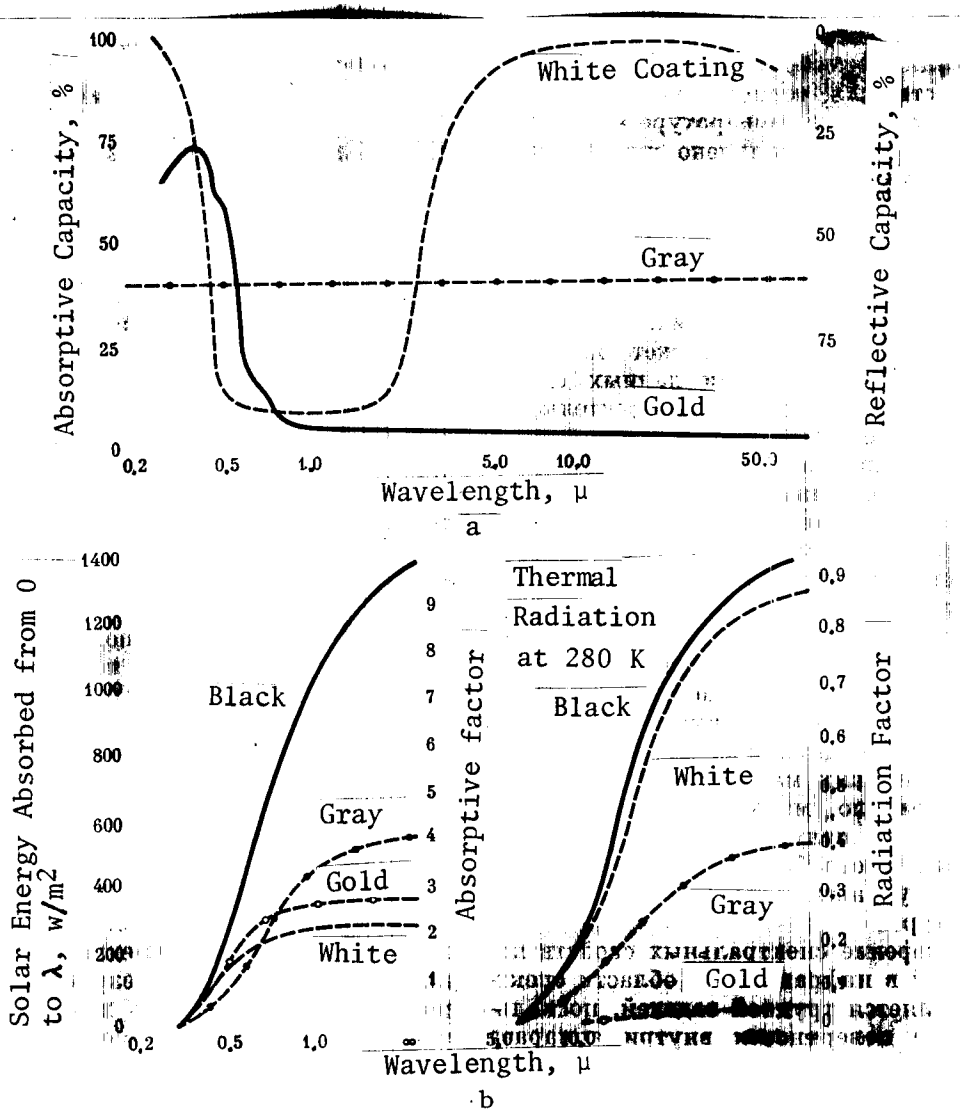

Figure 31. Spectral (a) and Integral (b) Absorptive and Radiative Capacities of Coatings

Figures 29 and 30 show curves which illustrate the principle of temperature regulation by the use of the radiating properties of coatings. However, these graphs do not allow us to determine the full integral radiative or absorptive capacity of a surface in a form convenient for analysis. Therefore, Figure 31 presents graphs characterizing the spectral and integral absorptive and radiative properties of coatings. In the case of solar radiation, 94% of the energy corresponds to the area with wavelengths less than 2 μ; therefore, the absorption curve has a bend at 2 μ, and the energy absorbed at longer wavelengths determines the value of A_s. Similarly, the radiated energy, as we can see from the graph, is concentrated in wavelengths of 5 to 50 μ. /76

For most purposes, the values of A_s and ε are not graphically defined. There are detailed tables of solar radiation over the Earth's atmosphere, so that the necessary values of A_s can be obtained rather quickly.

The radiation factor of a coating can be determined from the data on spectral absorption by calculation of the full absorptive capacity for black body radiation at the same source temperature. This can be achieved by drawing the curve for a black body following Planck's law. Radiation with logarithmic dependence immediately characterizes the spectral intensity.

The approximate value of radiative capacity can be calculated on the basis of data on spectral absorption and the relative distribution of energy.

If the curve of spectral absorption approximates that of a gray body, the calculated radiative capacity is independent of temperature. For most actual coatings, the absorptive capacity depends on wavelength and temperature. For metallic materials, for example, absorption increases at shorter wavelengths and higher temperatures. The absorptive capacity of dielectric materials is generally less than that predicted, while the radiative capacity is generally much greater and has a tendency to decrease with increasing temperature.

Measurement of the spectral properties of coatings in the infrared area of the spectrum is a difficult task, since all surfaces within the spacecraft radiate or reflect energy at the same wavelengths. Thus, the radiative capacity is usually measured directly, using a black surface for comparison. The radiative capacity can also be calculated from the rate of cooling of small specimens suspended in a vacuum chamber with cold walls.

Materials for temperature regulating coatings. In order for a radiator to emit the planned heat flux, its surface must have certain radiative capacity characteristics. Generally, a surface with high radiative capacity in the infrared area is desirable. If the surface is exposed to the sun, in order for the temperature of the surface to be moderate, it must have low radiative (high reflective) capacity in the shortwave portion of the solar spectrum. Heat-absorptive surfaces must have low radiative capacity in the infrared area of the spectrum and high absorptive capacity in the shortwave portion of the solar spectrum.

Usually, materials (such as steel and aluminum) which can be used for the structure of the radiator and surface of the spacecraft do not have the required radiative and absorptive characteristics. They are produced using various surface coatings. The materials of the coatings can be classified according to the ratio of their absorptive capacity in the shortwave area

of the solar spectrum to their radiative capacity in the long-wave area. The differences in these ratios are not the result of chance. They result from the electron, vibrational and rotary interactions of the atoms within the molecules of the coatings. These conversions are determined by the chemical composition and structure of the surface. /77

Metal coatings. Figure 32 shows the characteristics of metals which can be used as coatings. The distinghishing feature of all metallic coatings is a reduction in longwave absorption energy. This means that the A_S/ε ratio is always

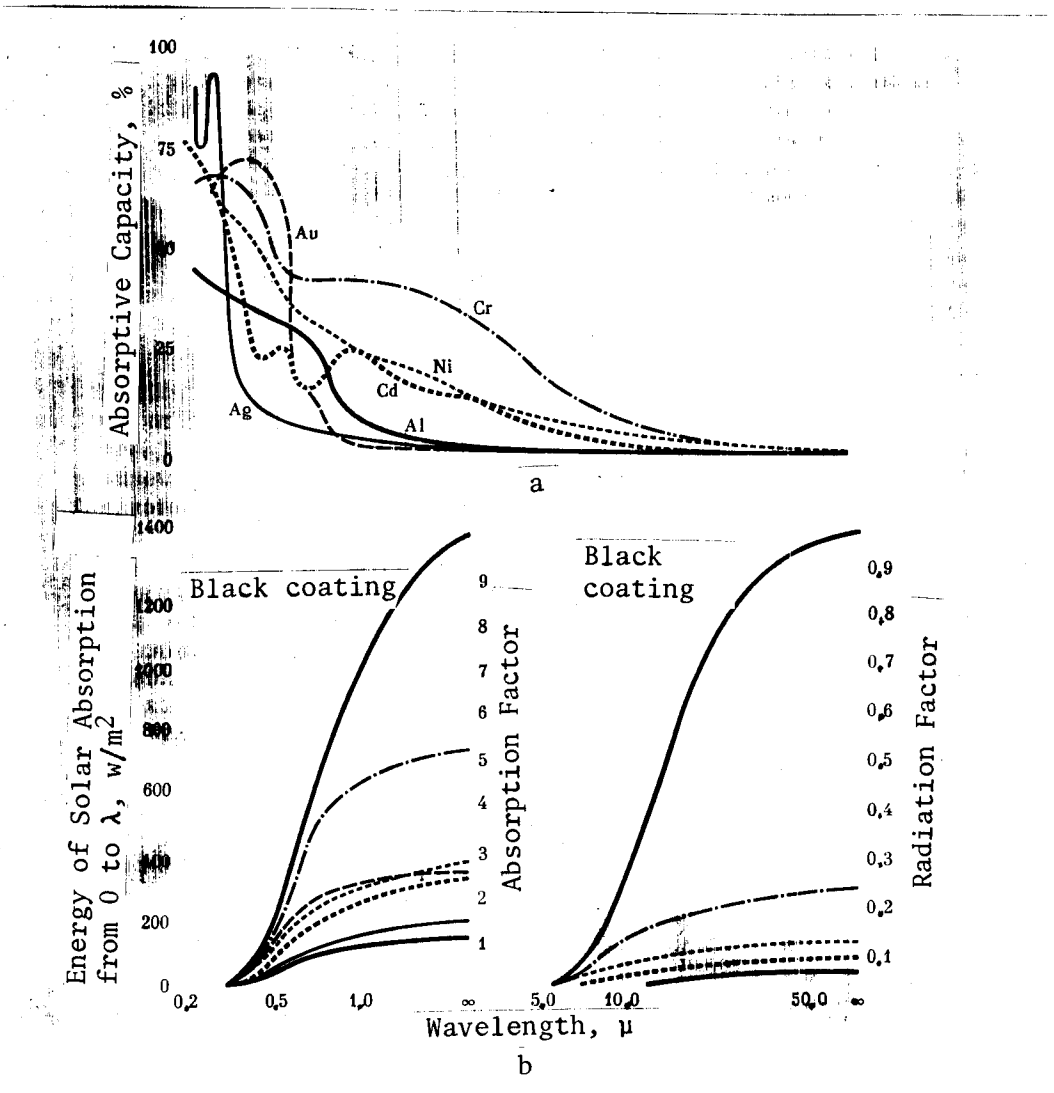

Figure 32. Spectral (a) and Integral (b) Characteristics of Metal Coatings

greater than 1, in some cases much greater than 1. The highest value of A_S/ε ratio is exhibited by such highly conductive

coatings as gold, silver and aluminum, since their radiative capacity is very low. A surface made of such coatings, turned toward the sun, has an equillibrium temperature of 200 to 400 ° C or higher. A similar phenomenon is observed under terrestrial conditions, in spite of the softening effect in the atmosphere. /78 The unpainted aluminum skin of an aircraft or galvanized iron roof of a building becomes quite hot if exposed to the noonday sun. However, this same metal, if it is anodized or painted, may have a lower temperature, i.e., these coatings increase the radiative capacity of the surface without significantly increasing its absorptive capacity. Sharp differences in the absorptive and radiative capacities of a metal can be achieved by the level of surface smoothness, crystalline structure of the metal and degree of surface oxidation. In some cases, the value of the A_S/ε ratio can be decreased by increasing the roughness of the surface.

Ceramic coatings and coatings of metal oxides. Ceramic coatings on a base (substrate) are created either by melting of the ceramic on the surface of the substrate, or by heating the metal base until an oxide coating is formed. The oxidation may be natural or may be accelerated by thermal or chemical effects. Anodized metals form an oxide film under normal conditions. Passive metals (aluminum, stainless steel) can be oxidized by chemical, electrical or thermal methods, and inorganic coatings are applied to the metal surface.

When sunlight passes through a ceramic surface film, it is partially absorbed, and partially reflected by the substrate. The thermal properties of the coatings in this case are combined with the thermal properties of the substrates. When metal oxide coatings are partially transparent, the thickness of the film may be very significant for regulation of the radiative capacity. This is illustrated by Figure 33. Coatings of silicon monoxide are transparent films with unilateral absorption in the infrared area. Changing the film thickness can be used to regulate the radiative capacity without changing the absorptive capacity A_S in the solar spectrum.

Glass coatings are most frequently used on aluminum mirrors, and the optical properties of this combination are similar to the properties of anodized aluminum. In comparing the absorption of glass with the absorption of an aluminum mirror, we should recall that the light reflected by the metal surface passes through the glass once more before leaving.

Another variety of ceramic coating is the light-scattering reflection surface. Wherever the absorptive capacity is low, reflection by scattered light may be quite effective; for example, freshly prepared magnesium oxide has a reflective capacity of 97 to 99% in the area of the visible spectrum. For flame deposited aluminum or zirconium $A_S/\varepsilon \approx 0.2\text{-}0.25$. This value of

absorptive capacity is explained by the fact that the particles of aluminum or zirconium are softened by the flame and adhere to the surface of the metal, scattering light. At the wavelengths absorbed by the metal oxide, there is a tendency toward increased absorptive capacity. If the metal oxide absorbs in the infrared area, a coating prepared by deposition with a flame will have a higher radiative capacity than a smooth coating with the same level of oxidation. Thus, the radiative capacity for flame-sprayed aluminum is usually 0.8-0.85, whereas the capacity for a smooth coating is 0.6.

/79

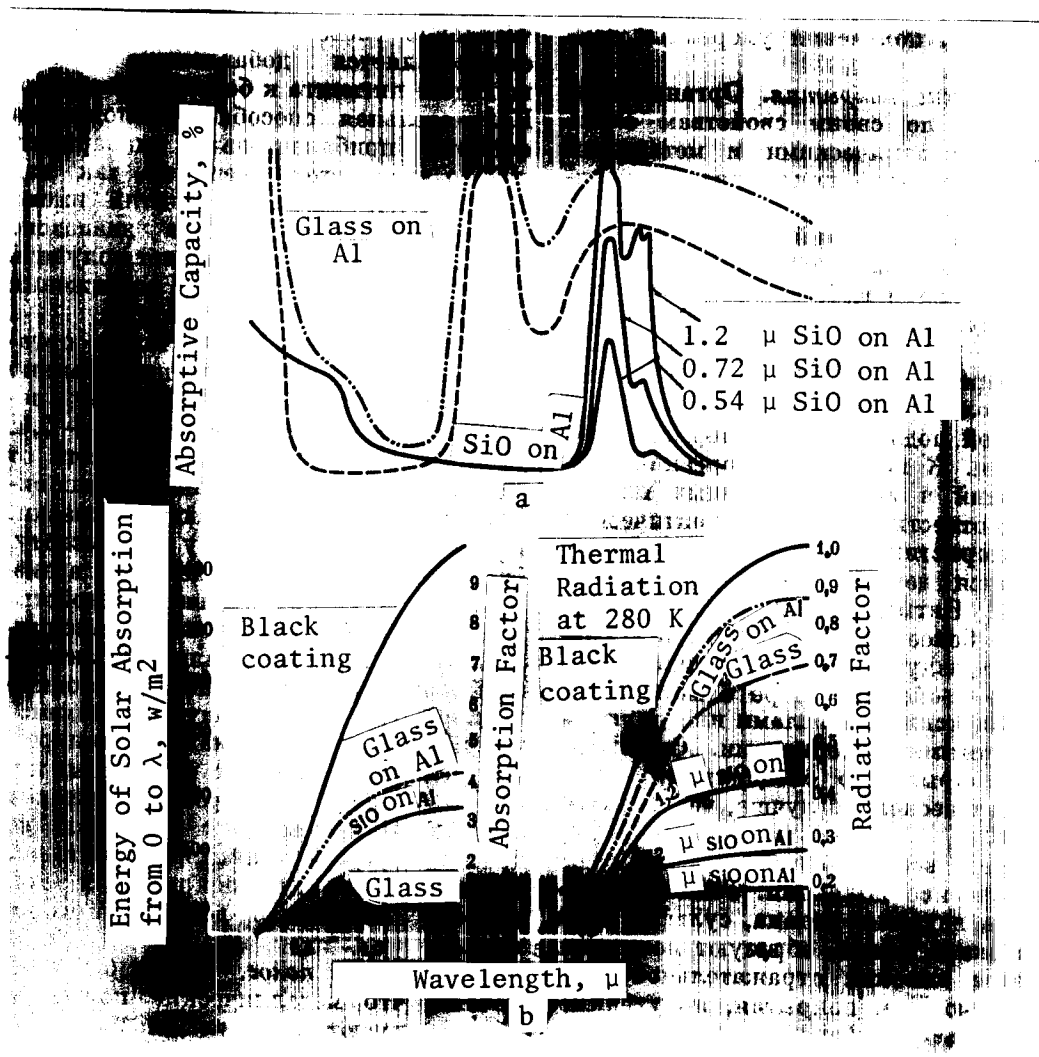

Figure 33. Spectral (a) and Integral (b) Characteristics of Ceramic Coatings

White porcelain enamel reflects light similarly. The effectiveness of enamel for reflection of light is determined by the difference in indices of refraction of the scattering

oxide and glass (if both phases are transparent). Both phases of porcelain enamel absorb energy in the infrared area. The curve of the absorptive capacity of porcelain enamel is similar to the curve of the absorptive capacity of white paint. Aluminum and zirconium have the same properties when applied with a flame. The shortwave reflection of a coating is decreased by metal oxide impurities, which characteristically have high absorptive capacity. These include chromium and cobalt oxide. Thus, ceramic coatings yield lower values of A_s/ε ratio when white enamel or a white flame-sprayed coating is used. /80

Metal oxide and ceramic coatings have high radiative capacity if the coating is not too thin. When desired, the shortwave absorptive capacity can be increased by the addition of an absorbing oxide in the form of a film. Ceramic and metal oxide coatings have values of $A_s/\varepsilon \approx 0.2$. The combination of ceramic and metal coatings can be used to produce moderate temperatures.

Organic coatings. Organic coatings are quite similar in their properties to ceramic and metal oxide coatings. Transparent organic coatings can be used to produce rather high transparency for short waves and very high radiative capacity for long waves.

Transparent varnishes can be effectively used with a reflective metallic substrate for temperature control. The shortcomings of organic coatings in the form of transparent films include changes in their optical characteristics when the coating is subjeeted to solar radiation. Pigmented organic coatings are more stable to the effects of sunlight and provide the required properties in combination with metals, metal oxides or other pigmented materials. Organic coatings with special pigments are somewhat better than ceramic coatings.

White organic coatings are most frequently used. Such pigments as titanium dioxide, zinc sulfide and zinc oxide form coatings with higher reflective capacity than coatings produced using porcelain enamels. Coatings of white paints pigmented with titanium dioxide rutile have $A_s/\varepsilon = 0.15\text{-}0.18$. In many cases, the whiteness of the coating is lost, so that in practice white paints with a blue shade are usually used. The blue tone causes an increase in energy absorption in the near-infrared area, increasing the A_s/ε ratio to 0.25 and higher.

In some cases it is desirable to increase the absorption of solar energy in order to increase the stability of the radiative capacity of the coating. This is achieved by addition of absorbing pigment to the white coating. The radiative capacity of the coating remains approximately constant with this mixing, since the component parts of the two coatings have significant absorption in the band from 5 to 25 μ. This allows the desired mean temperature to be achieved by a comparatively simple method.

Organic coatings pigmented with aluminum are also widely used. These coatings have $A_S/\varepsilon \simeq 1$ where $A_S = 0.3\text{-}0.4$. The precise value of A_S will depend on the quality of the pigmented aluminum and the properties of the covering paint. Paint containing water or acid will change its properties with time, i.e., will age. The thermal properties of improperly applied paint differ greatly and are of no practical value. Properly compounded aluminum paint yields the necessary combination of properties for each specific case. Brushed-on coatings result in variation of optical properties from coating to coating in comparison to sprayed coatings. The stability of these coatings to solar radiation is rather good.

The use of strips. It was noted above that metal coatings usually have high values of A_S/ε ratio and, consequently, high equillibrium temperature on their surfaces. Organic and ceramic /81
coatings can be used to produce cold surfaces. An optimally combined coating includes both metal and dielectric components. The values of A_S and ε of such a coating are determined as fol-

$$A_S = A_m X_m + A_c (1 - X_m), \tag{2.88}$$

(2.89)

where the subscripts m and c relate to the base metal (or metal coating) and covering strips respectively, while X_m is that portion of the surface covered by metal.

Using these equations and the equations for determination of the equillibrium temperature, we can calculate the surface area occupied by the various components required to produce the desired temperature.

7.3. Thermal Batteries

Thermal batteries, used to provide the required thermal mode of a spacecraft, are most expedient when the spacecraft falls under the influence of cyclically changing external heat fluxes. These conditions occur either during the shadow portion of an orbit around any planet in the solar system, or on the surfaces of the planets and their satellites. The batteries accumulate thermal energy during the sunlit section and liberate it when the spacecraft is in the shadow of the planet. Thus, thermal batteries, by absorbing heat, protect the instrument compartments of the spacecraft from overheating, then by liberating the heat, protect the spacecraft from overcooling, thus supporting operation of the equipment within the required

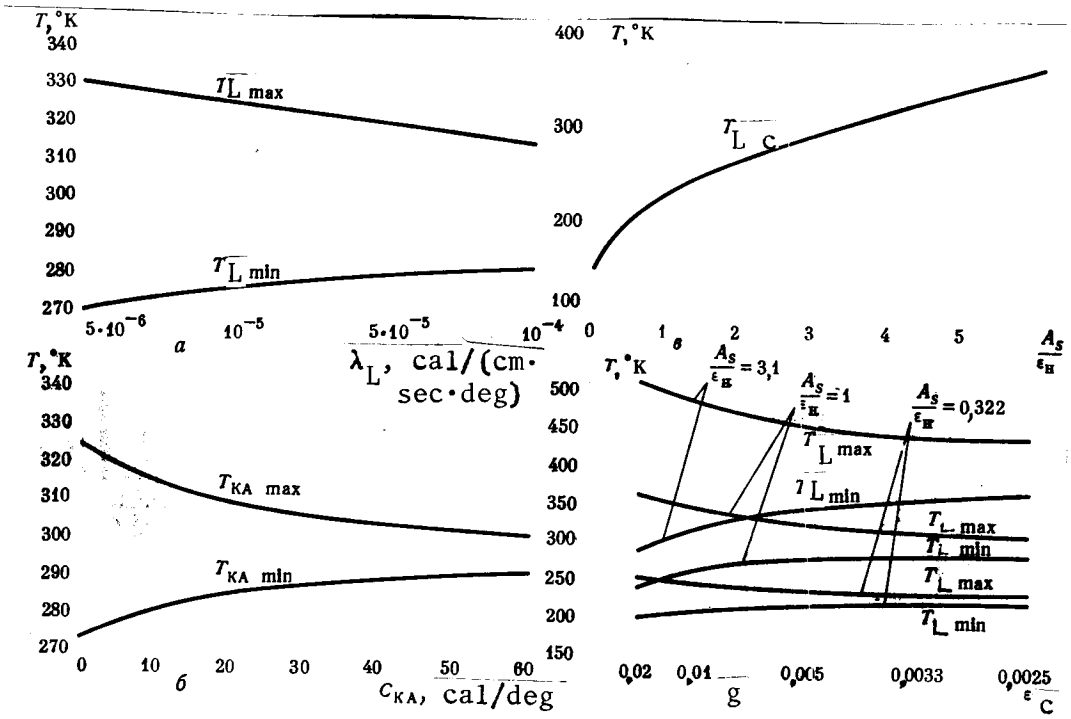

Figure 34. Temperature of Lunar Surface and Spacecraft Covered with Thermal Insulation as Function of Heat-Physical Parameters of Lunar Soil and Spacecraft: a, $A_S = 0.93$, $\varepsilon_H = 0.93$, $\varepsilon_c = 0.005$, $C_L = 0.2$ cal/(g·deg), $\rho_L = 1.5$ g/cm^3, $C_{KA} = 0$; b, $\varepsilon_c = 0.005$, $\lambda_L = 10^{-5}$ cal/(cm·sec·deg), $C_L = 0.2$ cal/(g·deg), $\rho_L = 1.5$ g/cm^3, $C_{KA} = 0$; c, $\lambda_L = 10^{-5}$ cal/(cm·sec·deg), $C_L = 0.2$ cal/(g·deg), $\rho_L = 1.5$ g/cm^3, $C_{KA} = 0$; d, $\lambda_L = 10^{-5}$ cal/(cm·sec·deg), $C_L = 0.2$ cal/(g·deg), $\rho_L = 1.5$ g/cm^3

lunar surface and the thermal insulation. The insulation cover is designed to decrease the external heat fluxes passing through the surface of the lunar soil, thus decreasing the fluctuations of temperature both of the lunar surface and of the object during the course of the lunar day. The object and lunar soil beneath the heat insulating cover in this case make up a single heat accumulating system. /83

The change in temperature of the object and of the section of the lunar surface covered by the thermal insulation during the course of the lunar day will be determined basically by the A_S/ε_H ratio on the outer surface of the thermal insulation, the corrected degree of blackness of the SVTI-type thermal insulation ε_c, the heat-physical characteristics of the lunar soil, the heat-physical characteristics of the object and the power of the

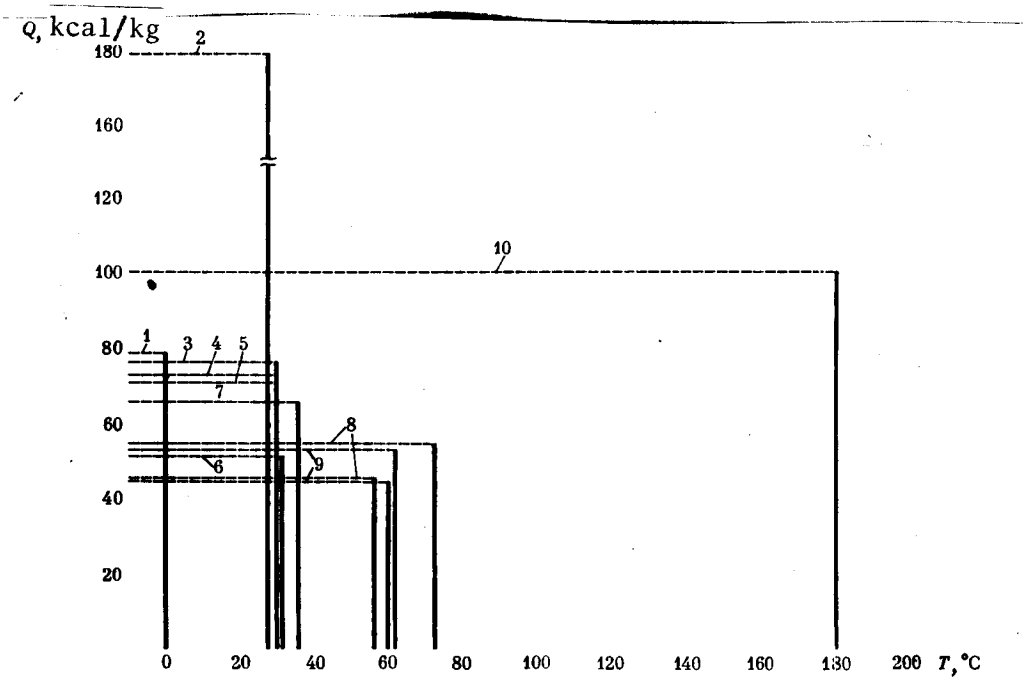

Figure 35. Values of Latent Heat of Melting and Melting Points of Various Compounds: 1, Water H_2O; 2, Phosphonium Chloride PH_4Cl; 3, Nitrogen Pentoxide Na_2O_5 [sic -- tr.]; 4, Type 86 Coolant; 5, Lithium Nitrate $LiNo_3 \cdot 3H_2O$; 6, Sodium Sulfate $Na_2SO_4 \cdot 12H_2O$; 7, Sodium Hydrophosphate $Na_2HPO_4 \cdot 12H_2O$; 8, Tristeary1 $(C_{13}H_{35}COC) \cdot C_3H_5$; 9, Argaric Acis $C_{17}H_{34}O_2$; 10, Lithium

thermal source located within the object. Figure 34 shows several dependences of the temperature of the lunar surface and an object covered with thermal insulation on these parameters.

Heat of melting. The latent heat of melting is determined by the quantity of heat which must be expended per unit weight of a solid substance in order to convert it from the solid state to the liquid state at constant temperature. For most substances, melting occurs at a certain temperature which, generally, is little dependent on pressure. The change in volume upon melting of most substances is insignificant.

Figure 35 shows values of the heat of phase conversion Q and the temperature of the phase conversion for various compounds which may be of practical interest. As we know, lithium hydride /84 has the greatest advantage as concerns latent heat of melting

and low dissociation pressure (27 mm hg) and therefore melts practically without noticeable loss. One shortcoming of lithium hydride is its high melting point, generally beyond the limits of the operating temperature of equipment.

Another substance with comparatively high latent heat of melting is water. Although its heat of melting is much lower than that of lithium hydride, it has the advantage that it melts at a temperature within the operating range of temperatures of equipment.

Thermochemical reactions. The liberation or absorption of heat may occur in various types of chemical reactions, including combustion, dissolution, hydration, polymerization, etc. Table 2 presents examples of chemical reactions and their relative characteristics for normal conditions.

TABLE 2

Chemical Reaction	$-\Delta H$ [kcal/kg] at 293 K
$Li_{(s)} + 0{,}5H_{2(g)} \rightarrow LiH_{(s)}$	2720
$Mg_{(s)} + H_{2(g)} \rightarrow MgH_{2(s)}$	710
$NO_{(g)} + 0{,}5\ Cl_{2(g)} \rightarrow NOCl_{(g)}$	293
$H_{2(g)} + 0{,}5\ O_{2(g)} \rightarrow H_2O$	3200
$CO_{(g)} + 0{,}5_{2(g)} \rightarrow CO_{2(g)}$	1530
$Na_2SO_{4(s)} + 10H_2O \rightarrow Na_2SO_4 \cdot 10H_2O_{(s)}$	172
$CO_{(g)} + H_2O_{(l)} \rightarrow CO_{2(s)} + H_{2(g)}$	211
$nCH_{2(l)} + 1{,}5\ nO_{2(g)} \rightarrow nCO_{2(g)} + nH_2O_{(l)}$	2430
$LiNO_3 + 3H_2O \rightarrow LiNO_3 \cdot 3H_2O$	70

We can see from the table that the reactions for lithium and hydrogen, hydrogen and oxygen have the maximum energy per unit weight. Many other reactions, particularly the reactions between compounds of boron and fluorine, may yield still higher energies, but they are irreversible and the process of regeneration is difficult.

Most oxidation-reduction reactions which liberate a significant quantity of heat occur at high temperatures (this is also true of polymerization). As concerns hydration, there are a number of substances for which this reaction occurs at low temperatures -- for example sodium sulfate forms its decahydrate at about 25° C, and a water molecule splits off of lithium nitrate in a chemical reaction at about 30° C. This type of reaction can be used in lunar apparatus thermal energy accumulators.

The use of thermal batteries. In order to select the optimal spacecraft temperature regulation system with a thermal battery, one must know the requirements placed on the apparatus, including the power, mode of load, duration of operation, supplementary systems, as well as environmental conditions. The thermal battery may be designed to absorb heat during operation of the apparatus and absorption of solar energy, which then can be used during the time the spacecraft is in the shaded section of its orbit or on the night side of the planet.

The sources of heat liberation determine the permissible overload and minimum radiating surface. The operating temperatures of the radiator may change over broad limits depending on its application. Regenerative thermal batteries can be used in the closed Brighton cycle of in the Stirling cycle. The purpose of the spacecraft must be known in order to match it to the proper thermal battery.

A thermal battery system as an element in an active temperature control system. The optimal use of a thermal battery will be achieved when it serves as the source of heat as the spacecraft passes through a shaded section of its trajectory or /85
the night side of a planet, and also in case of significant short-term heat loads. The necessary thermal energy is determined by the following prarameters: thermal efficiency of the cycle, required power of spacecraft temperature regulation system, planned service life in orbit or on the surface of the planet, and reliability.

The efficiency and power capacity determine the size and weight of the thermal battery. The time of functioning of the spacecraft is quite significant in the selection of an electrochemical or thermal energy source, since the service life of chemical batteries is quite limited and depends to a great extent on the load. The selection between these types of power sources is determined to a greater extent by requirements for reliability than by requirements for weight.

Spacecraft which must operate over an extended time require thermal power sources in the temperature control system. The installation of a thermal battery in the temperature control system can be performed in two versions, as is shown by Figure 36. In the series-connection version (Figure 36a), the solar or internal energy is transmitted to the thermal battery, then to the working fluid. Temperature T_a in the battery is always higher than temperature T_ℓ of the working fluid.

The version with parallel connection of heat exchanger and thermal battery (Figure 36b) works by transmitting the heat to the working fluid, then from it to the thermal battery. The temperature of the working fluid in this case is always higher than the temperature in the thermal battery. When there

are no external or internal heat sources, energy is transmitted from the thermal battery to the working fouid, and its temperature drops according to the heat exchange conditions.

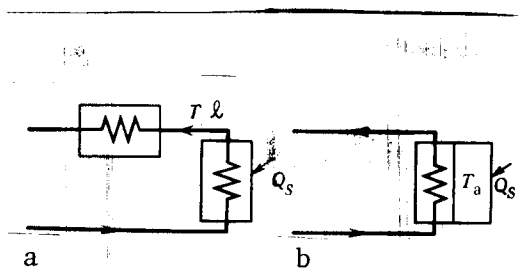

Figure 36. Versions of Installation of Thermal Batteries

Parallel connection of a thermal battery allows a more constant working fluid temperature to be achieved. Series connection of the battery allows the thermal battery to be placed separate from the heat exchanger and external energy absorber, which may be important for the temperature control system if solar energy is used. For example, if the heat exchanger-absorber together with its reflector must be turned in the direction of the sun, then it is expedient to keep the weight of the heat exchanger to a minimum in order to decrease the required rotation torque. The weight of the thermal battery should be determined considering the weight of the material which accumulates the heat and the weight of the surrounding envelope. The weight of the envelope and heat exchanger significantly reduces the specific heat capacity, particularly if the overall capacity is low.

An increase in the intensity of thermal energy transfer, determined by a change in power consumption, decreases the specific thermal capacity, which is particularly significant in the area of low values of total capacity. This results from an increase in the ratio of weight of heat transfer surface to total system weight. A significant improvement in the weight relationship can be achieved by optimal solution of heat transfer problems. For example, the use of finned tubes on the /86
side exposed to the working substance of the thermal battery can increase the temperature and result in a reduction of weight in comparison to the weight produced for unfinned tubes. In the area of high heat capacities, the thermal efficiency becomes predominant.

The temperature limitations resulting from the operating conditions of equipment or devices should be carefully defined. If considerations are based on the fact that conditions must be maintained in the spacecraft so as to allow normal operation of equipment, the heat accumulation system must absorb heat beginning at a certain fixed temperature and liberat it at lower temperatures.

Design of a thermal battery utilizing the process of melting of the working fluid. A number of problems relating to

heat transfer are involved in the design of thermal batteries intended to operate on spacecraft. The main problem is that of finding a relationship of thermal resistances of each element of the heat accumulating system such that the required rate of accumulation and discharge can be achieved. In studying thermal resistances related to the melting process, in addition to the ordinary thermal resistances resulting from conductivity, resistance of the liquid film to radiation, one must also consider the equivalent mean resistance of the accumulating medium. For certain points of the medium as it melts, thermal energy is applied or liberated through a variable thickness of material. In the general case, the thermal resistance of an energy accumulator will be a certain nonlinear function of temperature and quantities dependent on the configuration of the installation. This function must be determined numerically in each specific case.

In all cases for each phase a parabolic temperature profile is used. Suppose X = S(t) defines the position of the melting line. For convenience, the melting point will be taken as 0, so that

$$T[S(t), t] = 0. \tag{2.90}$$

The thermal balance at the melting boundary gives us

$$\lambda_2 \frac{\partial T_2}{\partial X} - \lambda_1 \frac{\partial T_1}{\partial X} = \pm \rho_2 r \frac{dS}{dt}, \quad X = S(t), \tag{2.91}$$

where r is the latent heat of melting; the "plus" sign is used upon freezing, the "minus" sign upon melting of the substance.

From the standpoint of mathematical description, equation (2.91) means that the difference between the quantity of heat reaching the melting boundary and the quantity of heat departing from this boundary is equal to the heat of melting absorbed or liberated.

In order to simplify the solution, let us assume that the temperature changes in only one of the phases. Sometimes, this simplification corresponds quite fully to the physical aspect of the problem, but cases also occur in which this assumption is a simplification of the actual phenomenon [16].

Let us first study the frequently encountered case of melting of the working substance in a thermal battery as the temperature of its surface changes. According to the assumptions made, we assume that the working substance is at the

melting point. Then equation (2.91) is simplified:

(2.92)

where $A_1 = \rho r/\lambda$ (subscripts in equation omitted since there is only one phase). The conditions of the surface are determined by the expression $T(0, t) = T_S$. Integrating the expression $a\frac{\partial^2 T}{\partial X^2} = \frac{\partial T}{\partial t}$ $(X > 0, t > 0)$ from $X = 0$ to $X = S$ and using equation (2.91), we produce the following integral thermal balance /87

$$\overline{\frac{d\theta}{dt}} = -a\left[A_1\frac{dS}{dt} + \overline{\frac{\partial T}{\partial X}(0, t)}\right], \tag{2.93}$$

where

$$\overline{\theta = \int_0^{S(t)} T dX.} \tag{2.94}$$

Suppose T is a second power polynomial for X. The equations $T(0, t) = T_S$ and (2.90) are the two boundary conditions for determination of the arbitrary constants. The third boundary condition is equation (2.92). However, this equation is inconvenient in the form as written, since if it is used the coefficients of the polynomial will include dS/dt. The expression for θ also includes dS/dt, and the thermal balance integral in this case yields a second order differential equation for S(t) whereas there is only one boundary condition available for S(t), namely $S(0) = 0$.

In order to avoid the difficulty which arises, let us represent equation (2.90) in another form. Differentiating it with respect to t, we produce

$$\overline{\frac{\partial T}{\partial X}\frac{dS}{dt} + \frac{\partial T}{\partial t} = 0.} \tag{2.95}$$

Excluding dS/dt from equations (2.92) and (2.95), we produce

$$\overline{\left(\frac{\partial T}{\partial X}\right)^2 = A_1\frac{\partial T}{\partial t}.} \tag{2.96}$$

The presence of the partial derivative with respect to time makes this equation unusable for determination of coefficients of the polynomial, since in this case the coefficients would have to be found from the differential equation, not from an algebraic equation. Therefore, using expression $T(0, t) = T_S$ and equation (2.96), let us exclude $\partial T/dt$. As a result, the third condition is written as

$$\left(\frac{\partial T}{\partial X}\right)^2 = aA_1 \frac{\partial^2 T}{\partial X^2}, \quad X = S(t). \tag{2.97}$$

After writing the third boundary condition in this form, the nonlinearity of the problem becomes obvious.

Suppose the expression for temperature T is

$$T = g(X - S) + b(X - S)^2. \tag{2.98}$$

The values of g and b are determined from the expressions

$$g = \frac{A_1 \alpha}{S}[1 - (1 + \mu)^{1/2}], \tag{2.99}$$

$$b = \frac{gS + T_S}{S^2}, \tag{2.100}$$

where g is an arbitrary parameter; b is a parameter;

$$\mu = \frac{2T_S}{A_1 \alpha}. \tag{2.101}$$

Substituting (2.98) into equations (2.93) and (2.94), we produce the following differential equation for S:

$$S\frac{dS}{dt} = \frac{6\alpha[1 - (1 + \mu)^{1/2} + \mu]}{5 + \mu + (1 + \mu)^{1/2}}. \tag{2.102}$$

The initial condition S(0) = 0 yields

$$S = \lambda\sqrt{t}, \tag{2.103}$$

where

$$\frac{K}{2\sqrt{\alpha}} = \sqrt{3}\left[\frac{1-(1+\mu)^{1/2}+\mu}{5+(1+\mu)^{1/2}+\mu}\right]^{1/2}. \qquad (2.104)$$

Karslou and Yeger [17] present the precise solution in the form of (2.103). A comparison of the expressions determined by equation (2.104) with the true expression $K/(2\sqrt{\alpha})$ as a function of μ is presented in [12], where it is shown that the error is about 7.8% with the maximum value $\mu = 2.8$. For lower values of μ, the error is correspondingly less.

Let us now study the case of melting of the working substance of a thermal battery with fixed heat flux on its surface. This problem is similar to the preceding problem, except now in place of condition $T(0, t) = T_S$ on the surface we fix the condition

$$\lambda\frac{\partial T}{\partial X} = -F(t), \quad X=0, \quad t>0. \qquad (2.105)$$

The thermal balance integral becomes /88

$$\frac{d}{dt}(\theta+\alpha A_1 S) = \frac{\alpha F(t)}{\lambda}, \qquad (2.106)$$

where the value of θ is determined by expression (2.94). Integrating and using the initial condition $S(0) = 0$, we produce

$$\theta+\alpha A_1 S = \frac{\alpha}{\lambda_0}\int_0^t F(t_1)\,dt_1. \qquad (2.107)$$

Let us assume once again that polynomial T has parabolic form. With the boundary conditions, we have equations (2.105), (2.90) and (2.97) for determination of the coefficients of the polynomial. After performing elementary conversions, we produce the following relationship between time and position of the melting boundary:

$$\tau = \frac{\sigma}{6}[\sigma+5+(1+4\sigma)^{1/2}], \qquad (2.108)$$

where

$$\tau = \frac{F(t)}{a\lambda^2 A_1^2}\int_0^t F(t_1)\,dt_1, \qquad (2.109)$$

$$\sigma = \frac{F(t)\,S}{\alpha A_1 \lambda}. \qquad (2.110)$$

The precise solution for F = const was given by Evans et al. [16] in the form of a Taylor series of functions $\sigma(\tau)$. Expressing relationship (2.108) in the same form, we can show that the coefficients of the first four terms of the series coincide, while the error in the fifth coefficient is about 4%.

The dependence of surface temperature on time is determined by parametric equation (2.108), as well as equation

$$\frac{T(0, t)}{A_1 \alpha} = -\frac{1}{4} + \frac{1}{4}(1 + 4\sigma)^{1/2} + \frac{\sigma}{2}. \qquad (2.111)$$

In addition to the use of thermal batteries in active temperature control systems, they can be widely used in passive temperature control systems as well. One of the primary advantages of a passive system with thermal battery is the absence of moving parts, which helps to increase reliability. The main task in such thermal regulation systems is to minimize the distance between elements where heat transfer is achieved by heat conductivity, which in turn allows the temperature gradient between sources of energy and the thermal battery to be reduced.

7.4. Evaporators

In spacecraft thermal mode support systems, the excess heat liberated within the object is usually transferred outward by radiation into the surrounding space by means of an external radiator. However, in some cases for spacecraft with long operating lives and significant heat liberation, it may be more suitable to absorb the excess heat by means of the phase conversion of substances from the liquid or solid state to the gaseous state with subsequent exhausting of the gas into space.

The devices in which a working fluid is converted to the gaseous state are called evaporators. If the working fluid is in the solid state, such an evaporator is called a sublimator [18].

The working fluids for evaporators should be those with maximum heat of evaporation, although the working temperature of the evaporator should not be below the freezing point of the substance being evaporated. In developing evaporator designs for spacecraft, one must keep in mind that these devices will be used under conditions of vacuum and weightlessness.

In order to explain how a mixture of liquid and vapor in a vacuum acts, the following experiment was undertaken. A mixture of steam (70-80% by weight) and water was fed into a glass tube 8 mm in diameter and 300 mm long. It was found that /89
the presence of unevaporated water resulted in the formation of ice crystals at the outlet from the tube, which after some time completely blocked the flow of the steam-water mixture. A similar picture was also produced in the case when the outlet from the pipe was metallic.

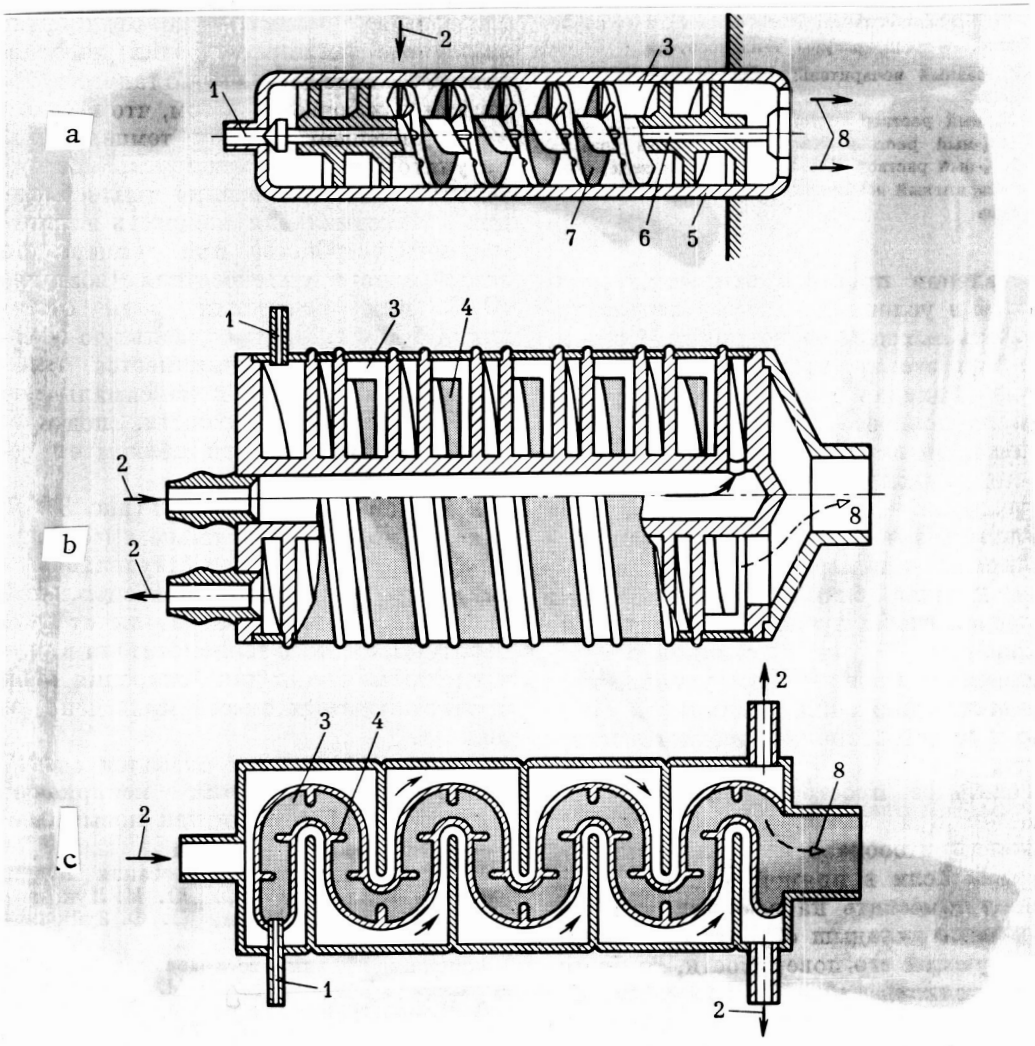

Figure 37. Pipes of Evaporators: a, With Spiral Vapor Channel and Bimetallic Regulator; b, With Spiral Vapor Channel and Coolant; c, With Labyrinth Vapor Channel and Coolant; 1, Inlet of Fluid to be Evaporated; 2, Coolant Channel; 3, Vapor Channel; 4, Walls; 5, Duralumin Body; 6, Invar Rod; 7, Spiral Insert; 8, Vapor

Based on these experiments, the following conclusions was drawn: during evaporation of fluids under a vacuum, a vapor- /90

liquid mixture cannot be allowed to leave the evaporator, since this might cause freezing of the output aperture and interruption of the process of evaporation. Consequently, the primary requirement which must be satisfied by an evaporating device is complete evaporation of the liquid within the device. In order to achieve this condition in the evaporator, its design must be such that the gas phase is separated from the liquid phase, with a simultaneous significant reduction in the rate of motion of the liquid evaporated in the direction of the output aperture.

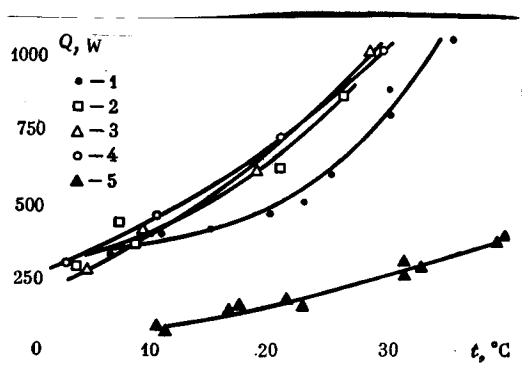

Figure 38. Power Capacity of Various Types of Evaporators as Functions of Coolant Temperature, Spiral Evaporator: 1, Water; 2, 5% Solution of Ethyl Alcohol in Water; 3, 10% Solution of Ethyl Alcohol in Water; 4, 20% Solution of Ethyl Alcohol in Water; Labyrinth Evaporator: 5, Water

This problem is solved most simply by making the evaporator channel in a spiral or labyrinth shape. If a spiral insert with depressions on its surfaces is placed in a straight evaporator channel, the centrifugal force which acts on the vapor-liquid mixture as it moves through the channel causes the liquid to be separated from the vapor and pressed against the walls of the channel (which is particularly important when evaporators are used under conditions of weightlessness) while the depressions in the walls of the channel reduce its speed significantly and increase the quantity of evaporated liquid.

In one such evaporator[1], an invar rod was placed at the center of the insert (Figure 37a) and covered the input aperture for the evaporated liquid when the body reached a certain temperature (due to the difference in coefficients of linear expansion of these materials). The primary advantage of this type of evaporator is that a single unit combines the temperature sensor, fluid feed regulator, evaporating channel and external heat exchanger. The maximum power capacity of the evaporation device with a temperature of the gaseous coolant (air) of 40° C and evaporation of water was 100 w. The maximum capacity of an evaporator refers to its capacity at the maximum flow rate of the working fluid fed to the evaporator for which it is totally evaporated.

[1]Experimental studies performed by V. B. Cherenkov, Yu. M. Lukoyanov, V. A. Korolev, L. F. Zuykov and N. N. Zabelina.

In another type of evaporator (Figure 37b), the coolant channel is also spiral in spate (double thread)[1]. The dependence of maximum capacity Q of this evaporator on temperature of the liquid coolant is presented in Figure 8 for the case when water and alcohol-water mixtures are used for evaporation.

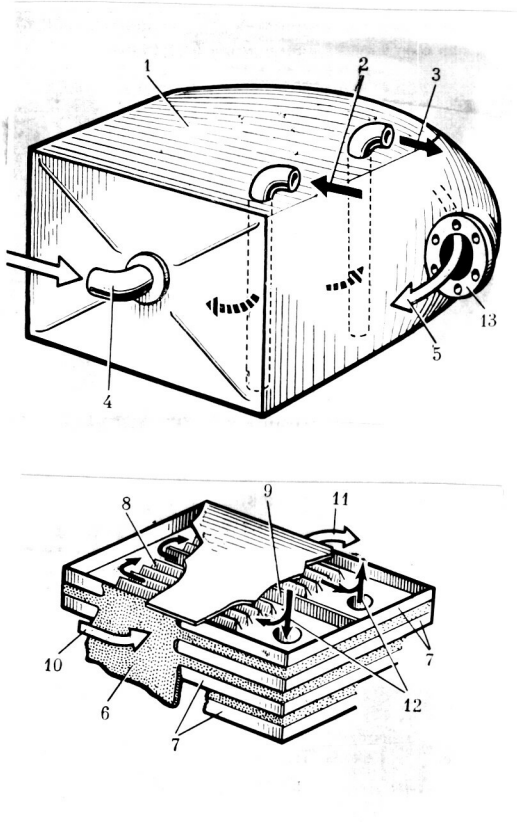

Figure 39. Apollo-8 Evaporator. 1, Chamber; 2, Coolant Inlet; 3, Coolant Outlet; 4, Water Inlet; 5, Steam Outlet; 6, Wick; 7, Plates; 8, Ribs; 9, Wall; 10, Water; 11, Steam; 12, Coolant; 13 Additional Pipe

One particularly effective method is that of decreasing the flow of the fluid being evaporated by using a so-called labyrinth channel, as diagrammed in Figure 37c. For an evaporator with this type of fluid trap, the dependence of power capacity on coolant temperature is shown in Figure 38. The weight of the labyrinth evaporator is several times less than the weight of an evaporator with a spiral channel. /91

Space technology also utilizes other methods of evaporation, in which the working fluid is distributed over the surface of evaporation by means of materials with a capillary structure (wicks). One example of a device which uses this principle is the evaporator carried by the Apollo-8 spacecraft (Figure 39) [19].

The evaporator consists of steel chamber 1; within it is a packet of plates 7, the surfaces of which carry ribs to intensify heat exchange. All of the plates are interconnected, and a liquid coolant is pumped through them. Wick 6 is packed between the plates. The liquid evaporated (water) is fed to the wick and is then evenly distributed over the surfaces of all plates by capillary action, where its evaporation occurs. The pressure in the evaporator necessary for evaporation of the liquid without its freezing is regulated by an automatic valve, the setting of which

[1]Experimental studies performed by V. B. Cherenkov, Yu. M. Lukoyanov, V. Ye. Zakatin with the help of O. V. Surguchev, V. I. Nesynov, Yu. B. Kulikov, Yu. M. Prokhorov and others.

is determined by the indications of a humidimeter in the wick. The steam formed passes through a special additional pipe 13 into the surrounding medium (space). The pipe is used for further evaporation of the liquid, in case a certain quantity of the liquid does not evaporate completely in the main chamber.

One other very important aspect of the operation of an evaporator in a vacuum is the possibility of condensation of vapor on the surfaces around the output aperture of the evaporator, resulting in a change in the characteristic A_s and ε of these surfaces (which is significant for the surfaces of spacecraft optical instruments).

The answer to the question of the possibility of condensation of liquid vapor in a vacuum can be produced by determination of the parameters of the exhausting stream of liquid vapor (concentration, velocity and temperature) in a given region of the spacecraft and determination of the condition under which condensation is possible. We present below the results of measurement of the condensation temperatures of liquid vapors on the surfaces of solids in a vacuum as a function of the flux of vapor particles n [(particles/m^2.sec)]. /92

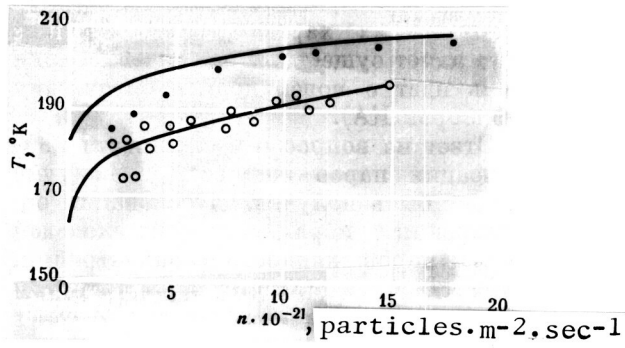

Figure 40. Condensation Point of Vapors of Water (Dots) and Ethyl Alcohol (Circles)

An evaporator was placed in a vacuum chamber with a pressure of 10^{-5} mm hg, and the liquid vapor leaving the evaporator condensed on the surface of a specimen, the temperature of which was varied from -100 to +50° C. The apperance of condensate and the corresponding value of flux was determined using a specially developed method. The measurements were used to determine the dependence of temperature T at which condensation begins on the incident flux of water and ethyl alcohol vapors (Figure 40).

These same dependences were theoretically calculated. Actually, the temperature at which condensation begins corresponds to the moment when the rate of evaporation is equal to the rate of condensation, i.e.

(2.112)

where α is the condensation factor; p_s is the saturated liquid vapor pressure at temperature T; R is the gas constant for vapors of the condensing substance.

The experimental data agreed well with the calculated dependence where $\alpha = 1$.

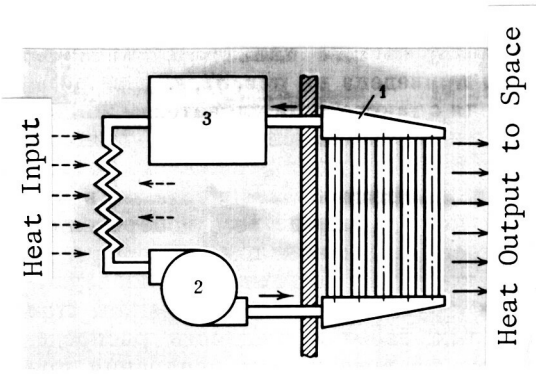

Figure 41. Diagram of Heat Liberation Into Space Using Heat Exchanger Radiators

7.5. Radiation Heat Exchangers

One of the main requirements of normal functioning of scientific and service apparatus on an APS over a long period of time under unfavorable external conditions is the assurance of the required thermal mode within the spacecraft. It may be found that due to the significant heat liberation of the equipment within the station or external heat fluxes caused by the "hot" surface of the planet and penetrating into the spacecraft, the temperature within the station increase unacceptably. If the passive thermal regulation system (thermal regulation screens, SVTI, etc.) cannot maintain the necessary thermal mode, a system of forced ejection of excess heat using radiation heat exchangers may be utilized. It should be noted that the use of these radiators on small automatic planetary stations is quite undesirable, since they require additional weight and, which is particularly important, additional power consumption. A schematic diagram of the ejection of heat into space using radiation heat exchangers (radiators) is presented in Figure 41 (1, radiator; 2, pump; 3, coolant reservoir). /93

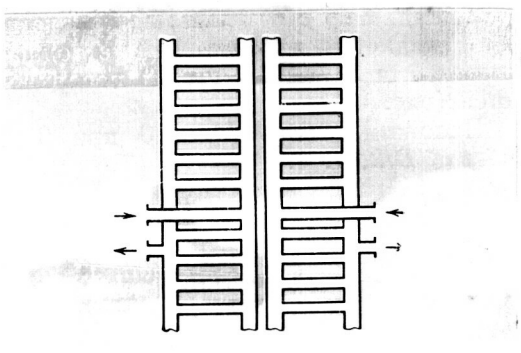

Figure 42. Sectional Radiator

Obviously, the main task in the planning of such thermal regulation system is the creation of an effective radiator design, allowing the maximum quantity of heat to be ejected with minimum size and mass.

We know that in terms of specific heat transfer per square meter, the most effective is a flat surface which radiates on both sides. However, structural considerations and particularly meteorite safety considerations require that the surface occupied by the coolant be reduced.

The use of highly heat conductive parts connecting coolant channels can reduce the danger of meteorite damage to the radiator and its total weight.

Provision of reliable meteorite protection is particularly important for stations with long planned service lives on the surfaces of planets with very thin atmospheres or no atmosphere at all. In this case, meteorite protection can be provided either by installation of light protective shields to reduce the kinetic energy of falling meteorites or by sectioning of the radiator. This latter method is most attractive, since shield protection causes a significant reduction in the quantity of heat emitted by the radiator. A possible design of a sectional radiator is shown in Figure 42.

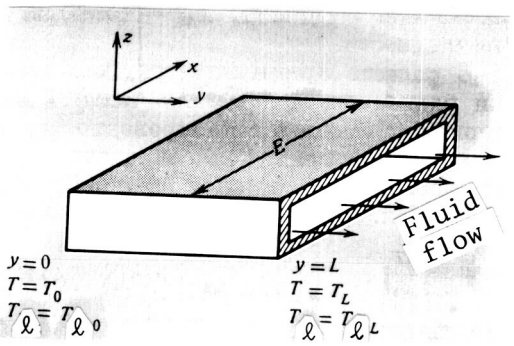

Figure 43. Flat Radiator

It should be noted that thermal design of radiation heat exchangers and determination of their structural parameters are rather complex. There are various methods of calculation of radiators, differing only in their premises. We presente below one method of design of a spacecraft radiator [14].

1. A flat radiator with parallel walls and radiation from one or both surfaces (Figure 43).

Since the cooled fluid washes the entire surface of the radiator, $\partial T/\partial x = 0$, where T is the temperature of the surface of the radiator.

In the stable mode, the following thermal balance equation obtains:

$$-\sigma\varepsilon T^4 E dy = \omega c_\ell dT_\ell, \qquad (2.113)$$

where σ is the Stefan-Boltzmann constant; ε is the radiative capacity factor of the radiator surface; E is the dimension of the radiator perpendicular to the direction of fluid flow; ω is the fluid flow rate by weight; c_ℓ is the sepcific heat capacity of the liquid, T_ℓ is the temperature of the liquid. /94

In the calculation, it is assumed that the walls of the radiator are made of a thin material with high heat conductivity and that the heat transfer coefficient of the boundary layer of liquid next to the wall is also high. Then

(2.114)

Considering equation (2.114) and integrating (2.113) over the length of the radiator, we produce

(2.115)

where L is the dimension of the radiator in the direction of fluid flow.

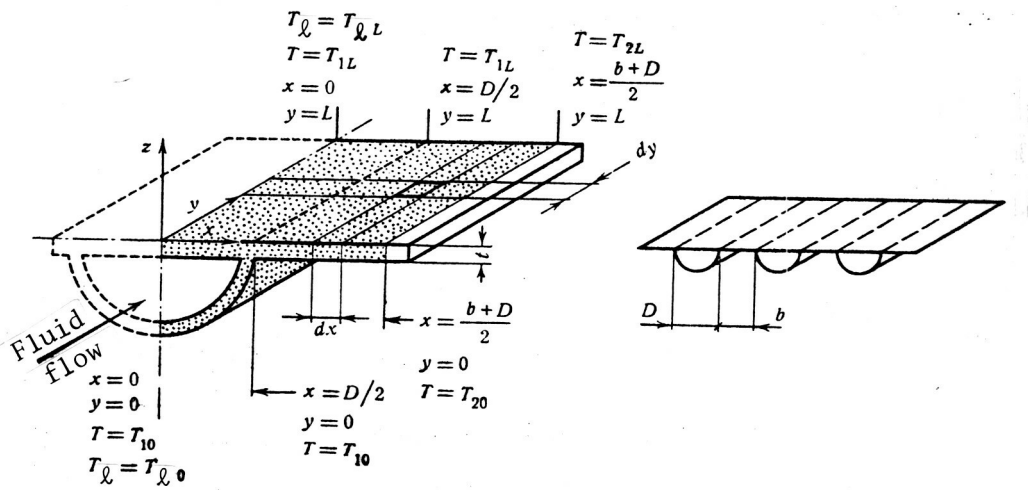

Figure 44. Heat Exchanger with Radiation from One Flat Surface and One Convex Surface

The total quantity of heat dissipated is

$$Q = \omega c_\ell (T_{\ell 0} - T_{\ell L}). \tag{2.116}$$

2. A radiator with separate channels for the liquid and radiation from one flat and one convex surface (Figure 44).

Let us assume that $\partial T/\partial x = 0$ where $0 \leq x \leq D/2$, i.e.

$$T = f(y) = T_{iy} \text{ and } T = f(x, y) = T_{xy}$$

where $\frac{D}{2} \leq x \leq \frac{b + D}{2}$. Then, for the shaded area of the radiator, we obtain the following stable mode:

(2.117)

where η is the thermal effectiveness of the section not covered by the channel.

Consideration eq (2.114) and integrating (2.117) over the length of the rac

$$\frac{\omega}{2} c_{\ell} dT_{\ell} = -\sigma\varepsilon \left(T_{1y}^4 \frac{D}{2} + \eta T_{1y}^4 \frac{b}{2} \right) dy, \qquad (2.118)$$

$$L(D + \bar{\eta}b) -$$

where $\bar{\eta}$ is the mean value of η.

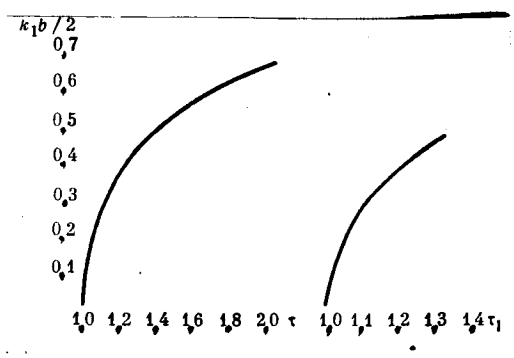

Figure 45. Parameter $k_1 b/2$ as a Function of τ and τ_1

Quantity A_1 is found from equation (2.15), the value of parameter η -- from the expression /95

$$\eta = \frac{\int_{D/2}^{(b+D)/2} T_{xy}^4 \, dx}{T_{1y}^4 b/2}. \qquad (2.119)$$

Considering that in element t dx dy, the main direction of heat conductivity coincides with the direction of the axis, we produce under conditions of stable thermal equillibrium

$$\frac{d^2T}{dx^2} = \frac{\sigma\varepsilon}{kt} T^4, \qquad (2.120)$$

where t is the wall thickness; k is the heat conductivity of the wall.

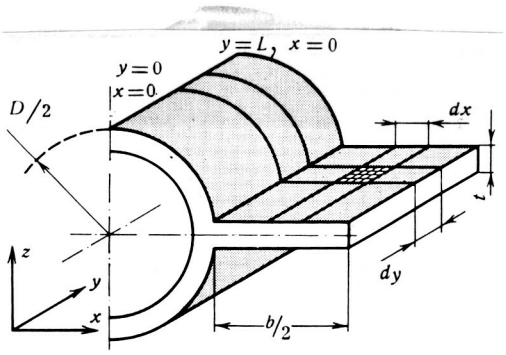

Figure 46. Radiator with Two Radiating Surfaces

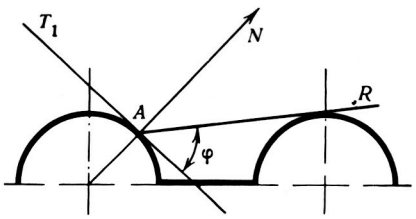

Figure 47. Determination of Field of Vision of a Radiator Tube

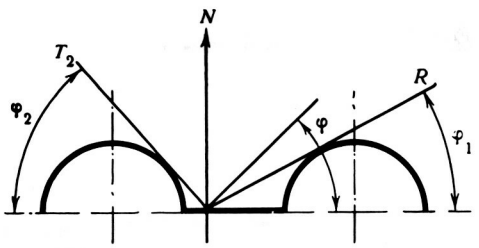

Figure 48. Determination of Field of Vision of a Radiator Flat Surface

Let us integrate equation (2.120) under the boundary conditions x = (b + D)/2, T = T_{2y} and $\partial T/\partial x = 0$ and substitute the expression produced for dx into equation (2.119)

$$\eta b = \frac{1}{T_{1m}^4}\sqrt{1{,}6\,\frac{kt}{\sigma\varepsilon}(T_{1m}^5 - T_{2m}^5)}, \qquad (2.121)$$

where

$$T_{1m} = \left(\frac{T_{10}^4 + T_{1L}^4}{2}\right)^{1/4}. \qquad (2.122)$$

From equation (2.120) following integration within limits of x = (b + D)/2 to x = D/2 and from T = T_{2y} to T = T_{1y}, we produce the following expression

$$k_1\frac{b}{2} = \int_0^{\tau_1}\frac{d\tau}{\tau^5 - 1}, \qquad (2.123)$$

where

$$\tau = \frac{T}{T_{2y}},\quad \tau_1 = \frac{T_{1y}}{T_{2y}},\quad k_1 = \sqrt{0{,}4\,\frac{\sigma\varepsilon}{kt}T_{2y}^3}.$$

The dependence of $k_1 b/2$ on τ and τ_1 is presented in Figure 45. /96

Fixing T_{1y} and T_{2y}, we can use the known k, t and ε to find b/2. Then we use equations (2.118), (2.121) and (2.123) to calculate the parameters of the radiator. Performing calculations for several values of T_{2y}, we find the radiator of minimum weight.

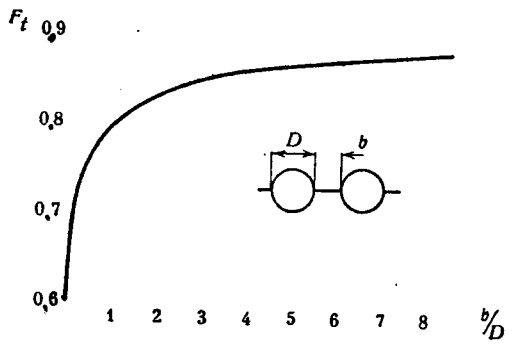

Figure 49. Field of Vision of a Radiator Tube as a Function of Ratio b/D

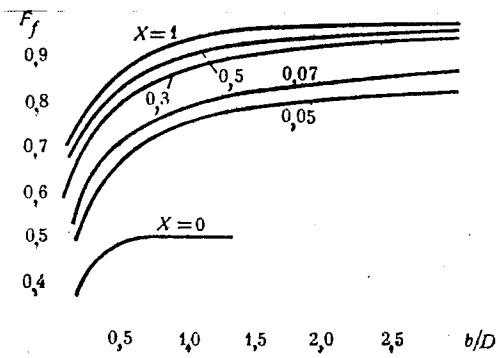

Figure 50. Field of Vision of a Radiator Flat Area as a Function of b/D Ratio; X = [x - (D/2)]/(b/2)

3. A radiator with two radiation surfaces (Figure 46).

We assume that over the channel surface $T = T_{1y}$, while over the surface of a flat section $T = T_{xy}$. For this case we have

$$\frac{\omega}{2} c_\ell dT_\ell = -\sigma\varepsilon\left[F_t T_{1y}^4\left(\frac{\pi D}{2} - t\right) + \int_{D/2}^{(b+D)/2} F_f T_{xy} dx\right] dy. \tag{2.124}$$

Integrating equation (2.124), we produce

$$L\left[(\pi D - 2t) F_t + \bar{\eta} b\right] = A_1, \tag{2.125}$$

$$\eta = \frac{\int_{D/2}^{(b+D)/2} F_f T_{xm}^4 dx}{T_{1m}^4 b/2}. \tag{2.126}$$

The coefficients F_t and F_f define the field of vision of the radiator at points on its cylindrical and flat sections respectively (Figure 47 and 48, where A is the point on the surface of the radiator; N is a perpendicular to the surface; T_1, T_2 and R are tangents to the cylindrical surfaces).

Coefficients F_t and F_f are defined as follows:

(2.127)

$$F_f = \frac{1}{\pi}\left[k(\varphi_1)\cos\varphi_1 + k(\varphi_2)\cos\varphi_2\right]. \tag{2.128}$$

The values of parameters F_t and F_f can be taken from graphs presented in Figures 49 and 50.

To determine $\overline{\eta}$, we separate the element t dx ty. It can be shown that the thermal balance equation for the case of radiation from both surfaces indiates that

(2.129)

The boundary conditions for equation (2.129) are: where $x = D/2$, $T = T_{1m}$ (known), where $x = (b + D)/2$, $T = T_{2m}$ (a quantity which must be ass

$$\frac{d^2T}{\partial T}\,(S, t) = A_1 \frac{dS}{dt},$$

culation.

CHAPTER 8

HEAT CONDUCTORS

Heat exchange between spacecraft elements can be achieved by three heat transfer mechanisms. Heat may be transmitted by one or a combination of two or three heat transfer mechanisms, by conduction, convection (free or forced) and radiation. In order to achieve heat transfer between spacecraft elements, heat conductors must be available, over which the process of heat transfer occurs. The heat conductors used in spacecraft to provide the proper thermal mode can be divided into the following five groups: heat conductors using the heat conductivity of metal, plus liquid, gas, vapor and radiant types. /97

The transfer of heat through metal heat conductors is low in comparison to the other types. This can be illustrated by the following example. In order to transmit 100 kcal of heat from one elements in a spacecraft to another located 1 m away and maintain a temperature difference of 10° between these elements, even when copper is used, a copper bar 20 cm in diameter weighing 255 kg is necessary. Obviously, the use of metal heat conductors for heat transfer between spacecraft elements, even with moderate heat liberation intensity in the elements, is not promising, and therefore in this chapter we will not discuss the use of heat conductors of this type. It should only be noted that they can be used in instruments with short distances between heat sources and heat sinks, when their weight will have no significant influence on the weight of the overall device. Heat transfer by conduction from heat sources should be combined with other mechanisms of heat transfer.

Liquid, gas and vapor heat conductors are most commonly used for the transfer of heat in spacecraft temperature regulation systems. The heat transmitting capacity of heat conductors is determined by the rate of motion of the heat transfer medium, its heat-physical parameters, hydraulic characteristics of the material, as well as the heat transfer coefficients at the ends of the heat conductor. Movement of the working medium may be either by free convection or by forced convection.

8.1. Liquid and Gas Heat Conductors

Heat conductors can be differentiated according to the type of heat transfer medium, used to transmit the heat from one section of a spacecraft to another. The type of heat transfer medium used in a heat conductor goes far to determine its

effectiveness. Therefore, the selection of a heat transfer medium (depending on the purposes for which the heat conductor is intended in the thermal regulation system) must meet requirements determined by the intensity of heat exchange (for liquid or gaseous heat transfer media), absence of corrosive action, nonflammability and thermal stability. The most important aspect is proper determination of the conditions for comparison of various heat transfer media [6]. /98

For example, the following expression can be used in the selection of a heat transfer medium for a heat conductor radiator to determine the surface area of the tubular radiator F_x to produce a change in heat transfer medium within the radiator from T_{in} to T_{out} [18]:

$$F_x = \frac{Q}{3\varepsilon\sigma T_{in}^4} \frac{(T_{in}/T_{out})^3 - 1}{1 - \frac{T_{out}}{T_{in}}} \qquad (2.130)$$

Obviously, the primary requirements for selection of a heat transfer medium for a heat conductor of a given cross section will be: 1) pumping of the required flow rate of heat transfer medium with a given pump power N; 2) transfer of the required quantity of heat Q; 3) maintenance of the required levels of temperature T and pressure p in the heat conductor.

The expediency of a given type of heat transfer medium is determined by the provision of the transfer of the necessary quantity of heat α in the spacecraft area being cooled or heated.

Gas heat transfer medium. The requirements established above for a heat conductor can be expressed by the following relationships.

1. The rate at which the heat transfer medium is pumped ω, from the expression for pumping power consumption

$$N = G\frac{\Delta p}{\rho}\frac{1}{\eta_н} = \rho F\omega\frac{\Delta p}{\rho\eta_н} = \frac{1}{\eta_н}\Delta p\omega F \qquad (2.131)$$

Substituting into this equation

$$\frac{\partial T}{\partial X}(S, t) = A_1\frac{dS}{dt},$$

$$\frac{d^2T}{dx^2} = \frac{2\alpha\varepsilon}{kt}F_f T_{xy}^4.$$

where Δp is the pressure loss, $\xi = 0.3164/Re^{0.25}$ is the coefficient of friction, $Re = \rho\omega d/\mu$ is the Reynolds number, $\rho = p/RT$ is the gas constant equation, we produce, after simplifications

$$N = \text{const}\,\frac{\mu^{0,25}}{Re^{0,75}}\,\omega^{2,75} \qquad (2.132)$$

or, in comparing two heat transfer media

$$\bar{\omega} = \frac{\bar{R}^{0,27}}{\bar{\mu}^{0,09}}. \qquad (2.133)$$

2. The difference in temperatures for the heat transfer medium ΔT, from the equation for the quantity of heat

$$Q = GC_p(T_{in} - T_{out}) = GC_p\Delta T, \qquad (2.134)$$

where

$$\Delta p = \xi\frac{L}{d}\frac{\rho\omega^2}{2}, \quad \frac{p}{T}\omega,$$

or

$$Q = \text{const}\,\frac{C_p}{R}\,\omega\Delta T,$$

and considering relationship (2.133)

$$\Delta\bar{T} = \frac{\bar{R}^{0,73}}{C_p}\,\bar{\mu}^{0,09}.$$

3. The temperature head Θ or the area of heat exchange surface F_{TO}, from the heat transfer equation

$$Q = \alpha\Theta F_{TO}, \qquad (2.135)$$

$$\bar{\Theta}\bar{F}_{TO} = \frac{1}{\bar{\alpha}}. \qquad (2.136)$$

Since as gasses flow the Nusselt number

$$Nu = 0.018\ Re^{0.8},$$

while the heat transfer coefficient

$$\alpha = Nu\ \frac{\lambda}{d} = const\ \lambda\left(\frac{\omega}{R\mu}\right)^{0.8},$$

then

$$\overline{\alpha} = \overline{Nu}\ \overline{\lambda}$$

or /99

$$\overline{\alpha} = \frac{\overline{\lambda}}{\overline{Re}^{0.58}\ \overline{\mu}^{0.72}} \qquad (2.137)$$

Using relationships (2.131)-(2.137), if we know the properties of heat transfer media it is easy to compare them.

Table 3, as an example, shows the results of calculation for one interesting problem: a low temperature heat conductor with cooling at a temperature $t \approx 20°$ C at pressure $p \approx 1 \cdot 10^5$ n/m^2. Here also we show the relative values of radiator areas produced with a temperature difference at the input $T = 50°$ (from 320 to 270 K) and with a very slight mean temperature head at the input Θ, equal to 10°.

TABLE 3

Heat Transfer Medium	R, m/deg	$C_p \cdot 10^3$ j/(kg·deg)	$\lambda \cdot 10^3$ w/(m·deg)	$\mu \cdot 10^7$ kg/(sec·m^2)	$\overline{\omega}$	Δ	$\overline{\alpha}$	$\overline{\Theta}$	$\overline{F}$
Air	29.3	1.01	25.2	1.85	1.00	1.00	1.00	1.00	1.00
Nitrogen	30.1	1.03	25.0	1.80	1.01	1.01	0.98	1.02	1.00
Helium	212.0	5.21	150.0	2.10	1.69	0.83	1.78	0.57	0.93
Carbon monoxide	30.3	1.04	24.4	1.80	1.02	0.98	0.97	1.04	1.00
Hydrogen	420.0	14.30	180.0	0.90	2.17	0.47	2.56	0.39	0.80
Ammonia	2.04	2.04	23.50	1.04	1.20	0.69	1.04	0.96	0.87

TABLE 4

Heat Transfer Medium	$C_p \cdot 10^{-3}$ j/(kg·deg)	λ, w/(m·deg)	$\rho \cdot 10^{-3}$ kg/m^3	$\mu \cdot 10^5$ kg/(sec·m^2)	$\overline{\rho}$ ($\overline{G}_{wt}$)	$\overline{\omega}$	$\Delta\overline{T}$	$\overline{\alpha}$	$\overline{\Theta}$	$\overline{F}_x$
Water	4,20	0,70	1,00	0,29	1,00	1,00	1,00	1,000	1,00	1,00
Dowtherm	1,90	0,12	1,00	1,03	1,00	1,10	2,00	0,165	6,10	1,25
Mercury	0,14	11,60	13,40	1,23	13,40	0,63	3,60	5,000	0,20	1,77
NA-K eutectic	0,96	24,00	0,85	0,48	0,85	1,06	4,80	8,500	1,18	2,15
Pb-Bi eutectic	0,15	9,00	10,50	1,80	10,50	0,66	4,10	4,000	0,25	1,94

Table 3 indicates that hydrogen is the best heat transfer medium, since it provides the greatest effectiveness of heat exchange of all gasses.

Liquid heat transfer medium. From the standpoint of the molecular structure of a liquid, the processes occurring in liquids involving the movement of particles from one volume to another (particularly collective mass and heat transfer) are similar to the processes in gasses. Consequently, the thermokinetic dependences for liquid heat transfer media are basically the same as for gasses. However, such processes as viscous flow are characteristics for liquids, and from this standpoint we must expect certain specific peculiarities in liquid heat transfer media.

With forced motion of the heat transfer medium, the process of heat exchange is described by the criterial equation

$$\overline{\mathrm{Nu}} = f\left(X, \mathrm{Re}, \mathrm{Pr}, \frac{\gamma_{st}}{\gamma_T}, \frac{C_{st}}{C_T}, \frac{\lambda_{st}}{\lambda_T}, \frac{\mu_{st}}{\mu_T}\right), \qquad (2.138)$$

where X is the geometric simplex.

Determination of the specific form of (2.138) is quite difficult. Therefore, the dependence of physical constants on temperature in the criterial equations is considered by two methods. In the first case, the identical influence of temperature on physical quantities is assumed, causing the additional relationship /100

$$\frac{\gamma_T C_T \nu_T \lambda_{ST}}{\gamma_{ST} C_{ST} \nu_{ST} \lambda_T} = \frac{\mathrm{Pr}_T}{\mathrm{Pr}_{ST}} \qquad (2.139)$$

to be included in the criterial equation. This method of considering the temperature dependence of physical quantities in criterial equations was introduced by N. A. Mikheyev [6]. In the second case, the only influence on heat exchange considered is that of the simplex μ_{ST}/μ_T.

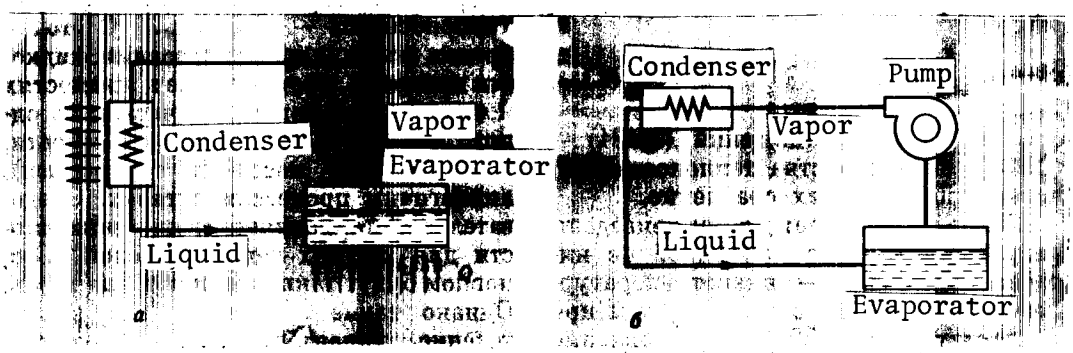

Figure 51. Diagrams of Condensate Return: a, Under the Influence of Gravity; b, By Pump

Thus, solution of the problem of heat exchange using liquid heat transfer media with forced motion is sought in the form

$$\overline{Nu} = f\left(X, Re, Pr, \frac{Pr_T}{Pr_{st}}\right) \qquad (2.140)$$

or

$$\overline{Nu} = \phi\left(X, Re, Pr, \frac{\mu_{st}}{\mu_T}\right).$$

For metal drop liquids, the following relationship obtains:

$$\overline{Nu} = 0.021 Re^{0.8} Pr^{0.43}. \qquad (2.141)$$

The equation for the expenditure of power in pumping (2.131) can be used to find an expression for the speed of the liquid (here, in contrast to gasses, relationship $\rho = p/RT$ is eliminated)

$$\overline{\omega} = \frac{1}{\overline{\rho}^{0.27}\overline{\mu}^{0.09}}. \qquad (2.142)$$

From the equation for the quantity of heat (2.134) we find

$$\Delta T = \frac{\overline{\mu}^{0.09}}{\overline{C}_p \overline{\rho}^{0.73}}. \qquad (2.143)$$

The heat exchange coefficient $\overline{\alpha}$ in equation (2.136) for a liquid is written by using the Nusselt criterion

$$\overline{\alpha} = \overline{Nu}\,\overline{\lambda}. \qquad (2.144)$$

The equation for the weight content of heat transfer medium in the system (in relative quantities $\overline{G}_{wt} = \overline{\rho}$) is added to equations (2.141)-(2.144). The relationship $\overline{G}_{wt} = \overline{\rho}$ for liquids, in contrast to gasses, may be very significant in evaluating the weight balance.

Equations (2.141)-(2.144) allow us to perform all necessary estimates. Let us first study the comparison of low-temperature heat transfer media. For example, as the initial heat transfer medium let us take water at t = 100° c and Re = 6000; we assume ΔT = 50° (from 373 to 323 K).

Table 4 presents the results of calculation.

Table 5 yields the comparison $\Delta\overline{T}$ and $\overline{\rho}$ for water and air at t ≈ 30° C, ΔT = 50°, T_{in} = 333 K, T_{out} = 283 K.

Using Table 5, we can establish that the limitation of pumping rate (i.e., limitation on pumping power) results in a significant gain if a system with a gas heat transfer medium (even at high pressures) is replaced by a system with a liquid. However, this replacement is frequently impossible due to purely operational considerations. Therefore, the comparison of gas heat transfer media with liquid media is still sensible.

The calculation data presented in the tables for specific temperatures are rather general, since a change in the temperature of the heat transfer medium causes only a quantitative change, without altering the qualitative aspects.

Let us now go over to determination of an efficient flow rate of the heat transfer medium in a heat conductor. The heat transmitted Q is related to the flow rate of the heat transfer medium and the temperature drop by the relationship $Q = GC_p\Delta T$.

TABLE 5

Heat Transfer Medium	$\Delta\overline{T}$	$\overline{\rho}(\overline{G}_{wt})$
Water	1	1
Air at $p = 1 \cdot 10^5$ n/m^2	500	0.001
Air at $p = 1 \cdot 10^7$ n/m^2	20	0.1

An increase in coolant flow rate with a decrease in ΔT causes equallization of the temperatures in the cooling device which, as a rule, is desirable. In a geometrically defined heat conductor, the energy expenditure in pumping of the heat transfer medium (pump power) can be defined as

$$N = G\frac{\Delta p}{\rho}\frac{1}{\eta_H} \approx G\omega^2 \approx \omega^3 \approx G^3,$$

i.e., increases as the cube of flow rate.

8.2. Vapor Heat Conductors

Vapor heat conductors connect the volume where the liquid evaporates with a volume where it is condensed. The condensate may return over the same line through which the vapor moves, or may have its own line. The vapor moves through a pipe under the influence of the pressure difference formed as a result of constant evaporation of the fluid at one end and its condensation at the other end of the vapor line. The motive force in the final analysis is the difference in temperatures between the heat source and the heat sink. In order to return the condensate to the evaporator, it is necessary to apply work to move it. This work may be supplied by the force of gravity (Figure 51a), mechanical pumps (Figure 51b) or capillary forces (Figure 52).

One example of the use of the force of gravity is the heating system in buildings, when a boiler acts as the evaporator, the condenser consists of the radiators installed in the rooms heated, and the condensate returns to the boiler due to the action of the force of gravity.

The use of mechanical pumps to move the liquid from the condenser to the evaporator is most common. This method allows significantly more heat to be transmitted from the evaporator to the condenser than does the method using the force of gravity.

Capillary forces also can be used to return the condensate to the evaporator. Vapor heat conductors in which the liquid returns under the influence of capillary forces have come to be called heat pipes.

The use of capillary forces to return the condensate is most convenient in the temperature regulation systems of orbital spacecraft, where there are no gravity forces and high operating reliability is required. /102

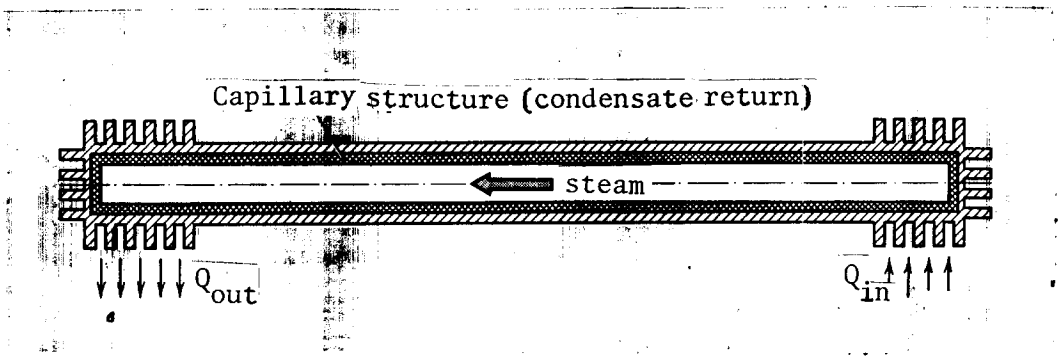

Figure 52. Condensate Return Under the Influence of Capillary Forces

Operating principle of the heat pipe. The heat transmitting device called a heat pipe in the simplest case consists of a sealed pipe, within which is a capillary structure which contains the working fluid. Except when the vapor is moving rapidly through the pipe, its pressure is almost identical over its entire length. Since for a given pressure the vapor can be at equillibrium with the liquid only at a definite temperature, the temperature along the entire surface of the wet capillary body (wick) is also almost identical. The method of heat transmission consists in the use of the latent heat of evaporation of the working fluid in the area where the heat is applied.

In contrast to systems in which the condensate is returned to the evaporation sector by means of a pump, the heat pipe uses a special capillary system for this purpose, which returns the condensate by forces of surface tension. Therefore, the heat pipe can operate under weightless conditions and even (within certain limits) under accelerations directed opposite to the directionof flow of the condensate.

The wick. The capillary structure should provide for return of the condensate to the evaporator in order that the rate of condensation in the pipe can be equal to the rate of evaporation. Failure to observe this condition may cause drying of the evaporator and cessation of the operation of the heat pipe. The capillary structure under terrestrial conditions must lift the working fluid against the action of the force of gravity with minimal internal resistance of its motion.

These requirements are essentially contradictory, since the small pore diameters necessary to lift the liquid to the required

height simultaneously create high internal resistance.

In this case, the most suitable solution is the use of bundles of parallel capillary tubes or fibers, in which this contradiction is minimal. In space, there are no forces of gravity, so that the wetting liquid reaches all of the surfaces accessible to it. It fills all pores, cracks, channels and narrow passages, minimizing its total free surface. For example, a millimeter passage between two metal sheets quickly "sucks up" any suitable liquid. This design can be considered in a certain sense a capillary structure with low resistance for weightless conditions. If it is necessary to provide for evaporation of the liquid from the surface of the capillary structure or condensation onto the surface, the metal sheets should be replaced by a fine metal honeycomb structure or other permeable material. /103

The simplest method of manufacture of the wick is to place a thin metal screen (several dozen apertures per running centimeter) in one or more layers on the inner surface of the heat pipe, and cold press it into place.

The advantages of this type of wick consist in its simplicity of manufacture and the fact that metal screens can be made of many materials. Unfortunately, the diameter of the capillaries through which the condensate reaches the evaporator in this type of screen cannot be determined with sufficient accuracy; furthermore, the diameter of the capillaries depends on the degree of compression of the layers of the screen against each other. Special springs are used to mount the wick, pressing the layers of screen against the wall of the pipe.

The system of capillaries for carrying the condensate can be created directly on the inner surface of the pipe in the form of axial rectangular channels 0.2-0.4 mm wide and approximately 0.5 mm deep (Figure 53). Capillaries in the longitudinal direction can be connected by circular passages in order to improve evenness of heat transfer from the surface of the pipe. Composite wicks have been used, in which the systems of longitudinal capillaries on the inner surface of the pipe are covered with one or more layers of thin metal screen.

Selection of a working fluid. In selecting the working fluid, one must consider many factors, the most important of which are as follows:

-- high heat of evaporation, in order to achieve the maximum heat transfer with the minimum fluid flow rate;

-- high heat conductivity to reduce the temperature drop through the thickness of the layer of liquid in the evaporator, which reduces the probability of local boiling on the wall of the pipe;

-- low viscosity of the liquid and of the vapor in order to reduce the resistance to motion of the heat transfer medium;

-- high surface tension for effective action of the capillary system;
-- good wettability of the wick material;
-- suitable boiling point, corresponding to the range of working temperatures selected.

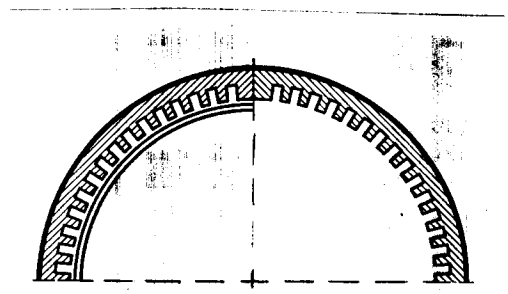

Figure 53. Capillary System in Cross Section

Ethyl and methyl alcohol, as well as mixtures of these two components, are most suitable for temperature control in space, since they satisfy these requirements better than other liquids.

Operating conditions of heat pipes. The basic condition of normal operation of a heat pipe is that the sum of losses of pressure in the liquid due to forces of viscous friction and gravity, and also in the vapor due to forces of viscous friction and inertia, must not exceed the capillary pressure. These losses of pressure in the liquid and the vapor should be calculated for sectors located between the points of maximum and minimum curvature of the meniscus of the working fluid. The curvature of the meniscus is maximum at the beginning of the evaporation section. The minimum value of radius of curvature of the meniscus $\rho = R_k \sec \theta$, where R_k is the radius of the capillary and θ is the contact wetting angle. /104

The minimum curvature of the liquid meniscus ($\rho \to \infty$) is located in the zone of condensation, but its precise placement depends on the operating mode of the heat pipe.

With low heat fluxes, the meniscus is located in the end of the section of condensation, i.e., at the end of the insulated zone. The liquid-vapor division boundary in the condensation zone may be on the surface of the wick, or if there is an excess of liquid -- outside the wick. Therefore, the maximum radius of curvature may become equal to the radius of the vapor channel.

At the point of maximum curvature of the meniscus, the pressure difference between the liquid and the vapor is at its maximum and is equal to $\frac{2\sigma}{p} = 2\sigma \cos \frac{\theta}{R_k}$, where σ is the surface tension. At the point of minimum curvature of the meniscus ($\rho \to \infty$), the vapor and liquid pressures are practically equal. If the pipe "works" against the action of the force of gravity with angle of inclination Φ, the maximum rise height of the liquid, determined by the minimum radius of curvature of the meniscus, is

equal to

$$Z_{max} \sin \Phi = 2\sigma \cos \frac{\theta}{\rho_{\ell} g R_k}$$

where ρ_{ℓ} is the density of the liquid; g is the acceleration of the force of gravity.

The heat pipe operating conditions formulated can be written as

$$\Delta p_{v(inert + f)} + \Delta p_{\ell(f)} + \Delta p_{\ell(grav)} \leq$$

$$\leq 2 \frac{\sigma}{R_k \sec \theta}.$$

In the case of laminar flow of the vapor, it is recommended that the losses of its pressure in the evaporator Δp_{ev} and insulated section Δp_{ins} be calculated using the relationship

$$\Delta p_{v.ev} + \Delta p_{v.ins} + (4\mu_v \frac{\overline{V}}{R_v^2}) \times [\ell_{ev}(1 + FRe) +$$

$$+ 2\ell_{ins}],$$

where

$$F = \frac{7}{9} - \frac{8a_p}{27} + \frac{23}{405}a_0^2;$$

a_0 is the correction for the velocity profile at the beginning of the zone of condensation ($0 \leq a_0 \leq 0.665$); μ_v is the viscosity of the vapor; R_v is the radius of a vapor channel.

A more convenient formula for calculation in the case of low Re numbers and long heat pipes is written as

$$\Delta p_v = \frac{1}{2}p_v V_v^2 [\frac{16}{Re} \frac{2\ell_{ev} + 4\ell_{ins}}{2R_v} + \frac{28}{9} -$$

$$- \frac{0.69\ \mathrm{Re}}{29\ \frac{\ell_{ev}}{2R_v} + \mathrm{Re}} \exp\left(- \frac{30\ell_{ins}}{\mathrm{Re}R_v}\right)],$$

where

$$\mathrm{Re} = \frac{dQ}{dZ}\frac{1}{2\pi\nu_v\rho_v r} \quad \text{or} \quad \mathrm{Rd} = \frac{2Q}{\pi R_v \nu_v \rho_v r};$$

Q is the quantity of heat carried along the heat pipe; r is the heat of evaporation.

The mean velocity of the vapor $\overline{V}$ is calculated by the formula

$$\overline{V} = \frac{\dot{Q}}{\pi\rho_p r R_p^2}.$$

In the case of high Re numbers and short pipes with a cosinusoidal velocity profile, the formula

$$\Delta p_p = \frac{1}{2}\rho_p \overline{V}^2\left(\frac{2\xi l}{R}_p + \frac{\pi^2}{4}\right)$$

is suggested, where coefficient of friction ξ, on the assumption that a smooth transition to turbulent flow occurs, is calculated by the formula /105

$$\xi = \frac{2\pi^2}{\mathrm{Re}} + \frac{0{,}03}{R_p^{0,2}}$$

(the coefficient 0.03 was produced experimentally).

With very low Re numbers and long pipes, the inertial term can be ignored, and then

$$\Delta p_p = \frac{16 l \rho_p \overline{V}^2}{\mathrm{Re} p_p}.$$

Where Re >> 1 for laminar flow one can use the dependence

$$\Delta p_p = (1 - 4\pi^{-2}) \frac{\dot{Q}}{8\rho_p R_p^4 r^2}.$$

The losses of vapor pressure in the evaporator can be estimated using theformula

$$\Delta p_p = \frac{\dot{Q}^2}{8\rho_p R_p^4 r^2}.$$

For conditions of weightlessness or horizontal placement of the pipe, the following relationship obtains:

$$\Delta p_p + \Delta p_\ell \leqslant 2\sigma \cos\frac{\theta}{R_к}.$$

8.3. Radiant Heat Conductors

A radiant heat conductor (RHC) refers to a device in which heat is transmitted from a warmer body to a cooler body by repeated reradiation of the radiant energy of the bodies within a hollow closed surface connecting the bodies (the thermal resistance may be rather great). A metal heat conductor (MHC) refers to a device in which heat is transmitted by heat conductivity through metal. Diagrams of RHC and MHC are presented in Figure 54.

Direct radiant heat exchange between surfaces 1 and 2 (ignoring rereflection) is determined by the following formula, produced from (2.23) by using (2.33):

$$Q_{1-2} = \frac{F_1\left[\left(\frac{T_1}{100}\right)^4 - \left(\frac{T_2}{100}\right)^4\right]}{\left(\frac{1}{\varepsilon_1} - 1\right) + \frac{F_1}{F_2}\left(\frac{1}{\varepsilon_2} - 1\right) + \frac{1}{\varphi_{1-2}}},$$

(2.145)

where ϕ_{1-2} is the irradiance factor of surface 1 with surface 2.

If we assume $\varepsilon_1 = \varepsilon_2 \approx 1$, then

$$Q_{1-2} = C_0 \varphi_{1-2} \left[\left(\frac{T_1}{100} \right)^4 - \left(\frac{T_2}{100} \right)^4 \right] F_1.$$

(2.146)

The radiant heat exchange between two bodies connected by a hollow closed surface with good reflection of thermal radiation is determined by the formula [3]

(2.147)

where ϕ^0_{1-2} is the irradiance factor of surface 1 with surface 2, considering the influence of the hollow closed surface which connects them on the radiant heat exchange between them.

The hollow connecting surface may be made of several layers of SVTI stretched over a light frame of a solid material or may be formed by the surfaces of certain elements of the spacecraft.

The dependennce of the ratio $Q^0_{1-2}/Q_{1-2} = \phi^0_{1-2}/\phi_{1-2}$ on the ratio L/a for three shapes of RHC cross sections is presented in Figure 54. We can see from the graphs that where L/a greater than 1, heat exchange by means of RHC is significantly higher than heat exchange between bodies not connected by the RHC. For example, for a cylindrical RHC where $L/a \geq 10$, the ratio Q^0_{1-2}/Q_{1-2} is approximately 40.

Let us compare the transmission of heat by means of RHC with the transmission of heat through MHC, which is determined by the equation /106

$$Q^{\lambda}_{1-2} = \frac{F_{MHC} \lambda_{MHC}}{L} (T_1 - T_2).$$

If the cross-sectional area of the RHC is equal to F_{RHC}, the ratio of heat fluxes transmitted through RHC and MHC will be

$$\frac{Q^0_{1-2}}{Q^{\lambda}_{1-2}} = \phi^0_{1-2} \frac{C_0}{\lambda_{MHC}} \frac{F_{RHC}}{F_{MHC}} f(T_1, T_2) L,$$

where $f(T_1, T_2)$ is determined by the formula which follows (2.47).

number of works [1, 2, 6], in which the existence of an extreme value of outside diameter of the pipe defining the minimal thermal resistance with fixed heat transfer factors and heat conductivity of the insulation has been noted. However, these works do not consider radiant heat exchange between the outer surface of the heat conductor and the surrounding medium, or the change in temperature of the surfaces of the heat conductor, heat transfer and heat conductivity factors upon variation of the outside diameter and thickness of the thermal insulation. /107

Let us study the stable process of heat exchange of a heat conductor with the surrounding medium, ignoring the influence of the thermal resistance of the metal portion of the heat conductor and considering radiant heat exchange.

Let us introduce the following symbols (Figure 56):

T_1 -- temperature of liquid in pipe;

T_2 -- temperature of surrounding gas medium;

T_3 -- temperature of bodies (walls) surrounding medium;

T_{w1} -- temperature of inner surface of pipe;

T_{w2} -- temperature of outer surface of pipe;

α_1 -- heat transfer factor from liquid in pipe to its inner surface;

α_2 -- heat transfer factor from surrounding medium to outer surface of pipe;

$\delta_{ins} = 0.5\ (d_2 - d_2)$ -- thickness of thermal insulation;

ε_c -- corrected degree of blackness of outer surface;

λ -- heat conductivity factor of thermal insulation.

Heat exchange of liquid (gas) in heat conductor with surrounding medium, ignoring radiant heat exchange with constant α_1, α_2 and λ. Let us analyze the equation

$$Q = \frac{T_1 - T_2}{R} \text{ [kcal/(m·hr)]}, \qquad (2.148)$$

defining the heat flux from the heat conductor to the surrounding medium; here

$$R = R_1 + R_2 + R_3 = \frac{1}{\alpha_1 \pi d_1} + \frac{\ln (d_2/d_1)}{2\pi\lambda} + \frac{1}{\alpha_2 \pi d_2} \text{ [m·hr·°C/kcal]}.$$

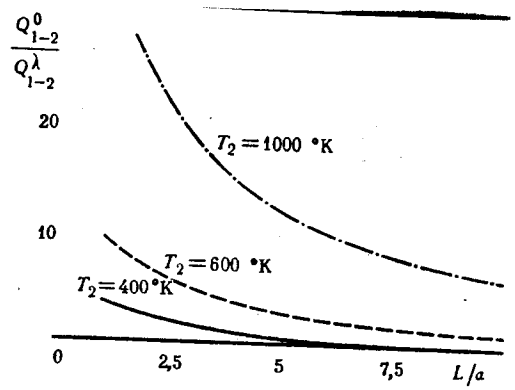

Figure 55. Ratio $Q^0_{1-2}/Q^\lambda_{1-2}$ as a Function of L/a with Various Values of Temperature T_2: L = 1 m; T_1 = 300 K; F_{RHC}/F_{MHC} = 1; λ_{MHC} = 100 kcal/(m·hr·K)

With fixed T_1 and T_2, the value of Q is determined by the value of R, but with increasing δ_{ins}, the value of R increases due to the component $\ln(d_2/d_1)/2\pi\lambda$, but decreases due to the component $1/\alpha_2\pi d_2$. As we know, quantity Q reaches its extreme value at

$$d_{2e} = 2\lambda/\alpha_2. \qquad (2.149)$$

If $d_1 < 2\lambda/\alpha_2$, the presence of thermal insulation increases heat losses in comparison to a heat conductor without thermal insulation. This conclusion (since point d_{2e} corresponds to Q_{max}) can be extended to a certain area $d_2 > d_{2e}$ (Figure 57), up to the value $d_2 = d_2'$, at which point the heat losses are the same as for an uninsulated heat conductor; therefore, the heat conductivity factor of the thermal insulation λ should be selected so that the inequality $2\lambda/\alpha_2 < d_1$ is observed.

Formula (2.149) was produced on the assumption of constancy /108 of α_2 and λ; it was assumed that d_{2e} is independent of d_1. It will be shown below that in the general case the value of d_{2e} depends, in particular, on the thickness of the insulation (through T_{w2} and d_2) and, consequently, on d_1 as well.

In conclusion, we should comment on the quantities α_1, α_2 and λ. In the first approximation, it will be sufficient to assume $T_{w2} = 0.5\ (T_1 + T_2)$, $T_{w1} = T_1$, $d_2 = 2d_1$; the value of λ should be selected experimentally with $T = 0.5\ (T_{w1} + T_{w2})$; the values of α_1 and α_2 can be calculated by formulas presented in [6], the heat flux -- by equation (2.148).

After determination of d_{2e} by formula (2.149), we must calculate α_2 where $d_2 = d_{2e}$ and find the new value of d_{2e}. Influence of temperature of surface of heat conductor and thickness of thermal insulation on α_1, α_2 and λ (and correspondingly on Q, d_{2e}). As we know, α_2 depends on the outside diameter of the pipe d_2,

the temperature on its outer surface T_{w2}, the temperature of the surrounding medium T_2 and the heat-physical parameters of the medium; the value of λ depends on the material and mean temperature of the insulation T_{av}. Thus, for correct (within the limits of slight influence of radiant heat exchange) determination of d_{2e} during determination of α_2 and λ, one must know the temperature of the surfaces T_{w1} and T_{w2}.

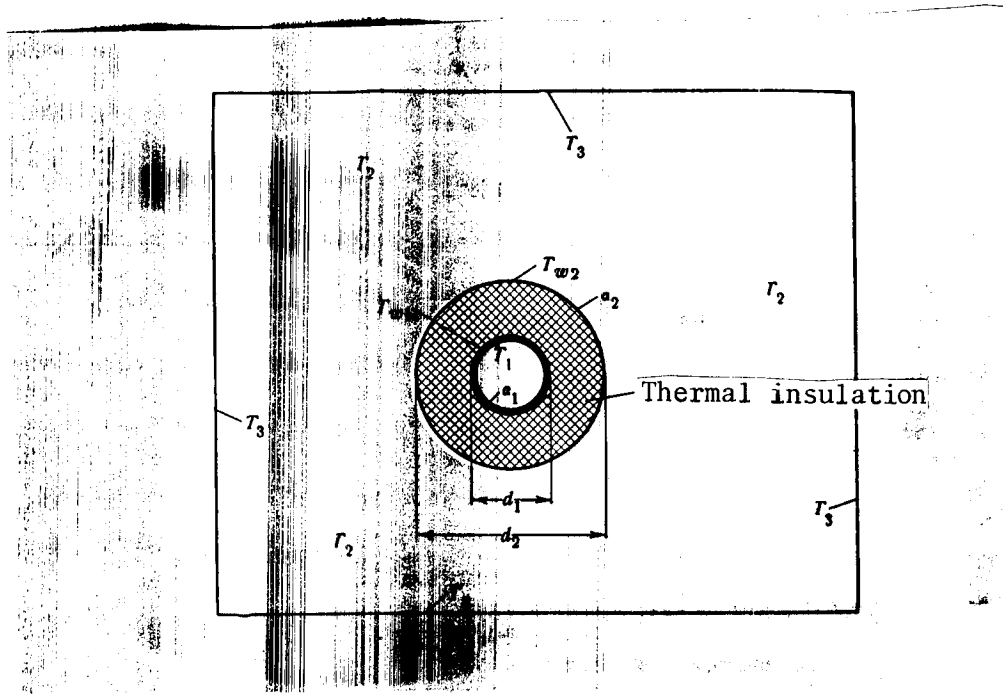

Figure 56. The Problem of the Stationary Process of Heat Exchange Between a Heat Conductor and its Environment

Studies can be conveniently performed in the following sequence. Assuming in the first approximation $T_{w1} = T_1$, $T_{w2} = 0.5 (T_1 + T_2)$, the mean temperature of the insulation $T_{av} = 0.5 (T_{w1} + T_{w2})$, we can find the preliminary values of α_1, α_2 and λ for $d_2 = d_1$; $1.1\, d_1$;...; $3d_1$.

The precise values of α_1, α_2 and λ are produced after calculation T_{w1} and T_{w2} by the relationships /109

$$\overline{T_{w1} = \frac{T_1 + K_1 T_2}{1 + K_1}} \quad \text{and} \quad \overline{T_{w2} = \frac{T_1 + K_2 T_2}{1 + K_2}}, \qquad (2.150)$$

where

$$K_1 = \alpha_1 d_1 \left(\frac{1}{\alpha_2 d_2} + \frac{\ln (d_2/d_1)}{2\lambda} \right),$$

$$K_2 = \alpha_2 d_2 \left(\frac{1}{\alpha_1 d_1} + \frac{\ln (d_2/d_1)}{2\lambda} \right),$$

which are produced by simple algebraic conversions from the relationships of the thermal balance equations.

For final calculation of Q (and determination of d_{2e}), as experience has shown, one or two more approximations must be made. The value of d_{2e} is found from the graphic dependence of Q on d_2.

The extent to which a change in temperature T_{w2} and diameter d_2, determining the value of α_2 with a change in thickness of the thermal insulation, can influence d_{2e} can be seen from the following example.

Using the method presented, the value of Q was calculated for various values of $d_2 \geq d_1$, considering the corresponding change in T_{w1}, T_{w2}, α_2, λ (α_1 = const) under the following conditions: T_1 = 400 K; T_2 = 250 K; α_{av} = 0.2 kcal/(m^2·hr·°C); d_1 = 0.03 m; α_1 = 100 kcal/(m^2·hr·°C). The results of calculations are presented in Figure 58, from which it follows that during calculation of Q and d_{2e}, the value of α_2 cannot be assumed constant: as d_2 changes from 0.03 to 0.09 m, the value of T_{w2} changes from 387 to 307 K, that of α_2 from 9.15 to 5.94 kcal/(m^2·hr·°C).

Thus, the decrease in the value of α_2 with increasing d_2 and the change in T_{w2} cause a continuous reduction in Q, although with a mean value of α_2 = 7 kcal/(m^2·hr·°C) (ignoring the change in T_{w2}), the value of Q has its maximum at d_{2e} = 0.4/7 = 0.057 m. Consequently, since α_2 and λ depend on d_2 (since T_{w2} changes), the formula $d_{2e} = 2\lambda/\alpha_2$ can be used only for very approximate calculations.

Heat exchange of a liquid (gas) in a heat conductor with the surrounding medium, considering thermal insulation. The radiant heat exchange of the outer surface of a heat conductor with the

surrounding medium has a very significant influence of T_{w2}, and consequently on α_2, Q, d_{2e}, particularly with high temperature differences $T_3 - T_2$ and $T_3 - T_1$.

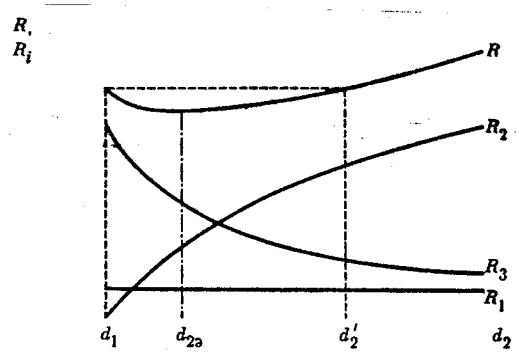

Figure 57. Thermal Resistance of a Pipe as a Function of Its Diameter, Parameters of Thermal Insulation and Heat-Physical Properties of the Medium

We will consider that the values of T_1, T_2, T_3, λ, α_1 are constant, and arbitrarily assume that $T_1 < T_2$, $T_1 < T_3$ (the case where $T_1 > T_2$, T_3 does not change the essence of the following discussion). In the first approximation, let us assume values of λ and α_1 with $T_{w1} = T_1$ and $T_{w2} = 0.5 (T_1 + T_2)$. If the heat conductor is placed in a vacuum, the formulas presented below are simplified: one should assume $\alpha_2 = 0$ and $T_2 = 0$ in them. Let us assume preliminarily that $T_3 = T_2$, $\alpha_2 = \text{const}$.

The heat flux from the surrounding medium to the outer surface of the heat conductor and from this surface into the heat conductor can be determined by the following equations:

$$Q = Q_{RAD} + Q_{CONV}$$

$$Q = \frac{T_{w2} - T_1}{\frac{\ln (d_2/d_1)}{2\pi\lambda} + \frac{1}{\alpha_1 \pi d_1}}, \qquad (2.151)$$

/110

where

$$Q_{RAD} = \alpha_л \pi d_2 (T_2 - T_{w2}) \qquad (2.152)$$

is the radiant heat flux:

$$Q_{CONV} = \alpha_2 \pi d_2 (T_2 - T_{w2}) \qquad (2.153)$$

is the convective heat flux;

$$\alpha_\ell = \frac{4{,}9\varepsilon_C}{100}\left[\left(\frac{T_2}{100}\right)^2 + \left(\frac{T_{w2}}{100}\right)^2\right] \times \left(\frac{T_2}{100} + \frac{T_{w2}}{100}\right).$$

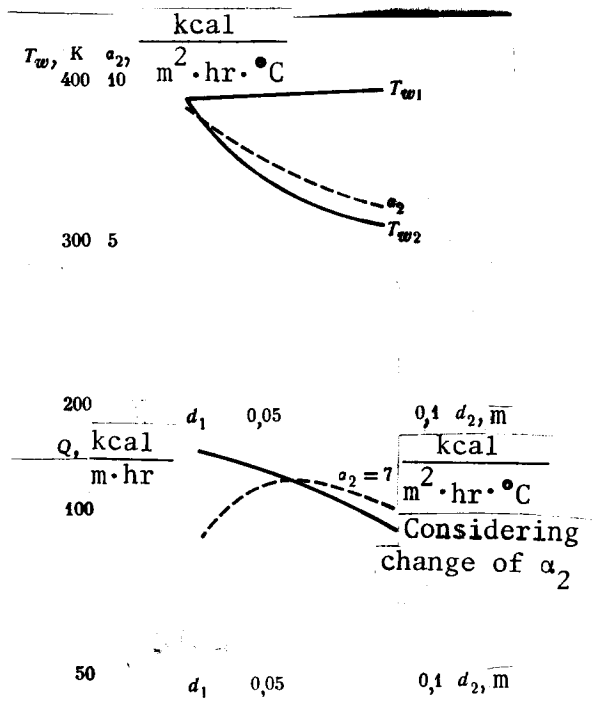

Figure 58. T_w and α_2 as Functions of d_2 and Change in Q with Increasing Thickness of Insulation on the Assumption of Constancy of T_{w1}, T_{w2}, α_2 and Considering their Variability

On the other hand, $Q = (T_2 - T_1)/R$, so that

Representing $\partial\alpha_\ell/\partial d_2 = \alpha'_\ell$, we have

$$\frac{\partial R}{\partial d_2} = \frac{1}{2\pi\lambda d_2} - \frac{1}{(\alpha_2 + \alpha_\ell)\pi d_2^2} - \frac{\alpha'_\ell}{(\alpha_2 + \alpha_\ell)^2 \pi d_2}.$$

The extreme value of d_{2e} is determined from the condition $\partial R/\partial d_2 = 0$,

$$\frac{1}{2\lambda} - \frac{1}{(\alpha_2 + \alpha_\ell) d_2} - \frac{\alpha'_\ell}{(\alpha_2 + \alpha_\ell)^2} = 0$$

(Here the trivial root $d_{2e} = 0$ is discarded):

$$d_{2e} = \frac{2\lambda(\alpha_2 + \alpha_\ell)}{(\alpha_2 + \alpha_\ell)^2 - \alpha'_\ell} \cdot \frac{1}{(\alpha_2 + \alpha_\ell)\pi d_2}. \quad (2.154)$$

In the particular case when $T_{w2} = \text{const}$ (for example, with great thickness of heat insulation), $R = \frac{1}{\alpha_1 \pi d_1} + \frac{\ln(d_2/d_1)}{2\pi\lambda}$, $d_{2e} = 2\lambda/(\alpha_2 + \alpha_\ell)$ and $\alpha'_\ell = 0$, i.e., the influence of radiant heat exchange causes a reduction in the extreme value of d_{2e} (due to the additional component α_ℓ).

Since in the general case (for example with fixed d_1) α_ℓ is a function of temperature T_{w2}, which depends on d_2, for α'_ℓ (even where $T_3 = T_2$) a cumbersome analytic expression is produced,

containing T_{w2}, d_1, d_2, α_1, α_2, λ, T_1, T_2 and ε_c. Consequently, the values of d_{2e} could be produced for various combinations of fixed values of T_{w2}, d_1,... However, the values of T_{w2} and α_2 are related to λ, d_1, d_2, α_1, ε_c, T_1 and T_2 and cannot be arbitrarily assigned.

The use of formulas (2.154) to determine the extreme values of d_{2e} is quite complex, although it is convenient for qualitative analysis. Therefore, let us find the dependence of Q on d_2 (and therefore on Q_{max}, d_{2e}) in the general case, when $T_3 \neq T_2$. Let us define the values of T_{w2} and Q with variation of d_2 from d_1 to $d_1 + 2\delta_{ins}$, where $\delta_{ins} \leq d_1$; here, with increasing δ_{ins} the values of T_{w2} vary from close to T_1 to close to T_2 or T_3.

In our calculation, we first use the average values of α_2 with $d_2 = 2d_1$, $T_{w2} = 0.5\ (T_1 + T_2)$ and λ with $T_{ins} = 0.5\ (T_1 + T_{w2})$; we determine the dependence of T_{w2} on d_1, d_2, α_2, λ, ε_c, T_1, T_2, T_3 in the range $d_1 \leq d_2 \leq 3d_1$ for several values of λ. Then, using equation (2.151), we calculate and construct function Q with respect to d_2 (parameter λ), analysis of which can be used to determine the extreme value of d_2 and the expedient values of λ and δ_{ins} (assuming that α_1, d_1, ε_c, T_1, T_2, T_3 are fixed). After selection of λ and d_2 in the first approximation, we similarly refine the final values of α_2, T_{w2} and Q. /111

The most difficult problem is analytic determination of T_{w2}; therefore, it can be done conveniently using a supplementary graph as follows. T_{w2} is found by simultaneous solution of equations (2.150)-(2.153): /112

$$\frac{T_{w2} - T_1}{\frac{1}{\alpha_1 \pi d_1} + \frac{\ln (d_2/d_1)}{2\pi\lambda}} =$$
$$= 4{,}9\varepsilon_c \pi d_2 \left[\left(\frac{T_3}{100}\right)^4 - \left(\frac{T_{w2}}{100}\right)^4\right] +$$
$$+ \alpha_2 \pi d_2 (T_2 - T_{w2}).$$

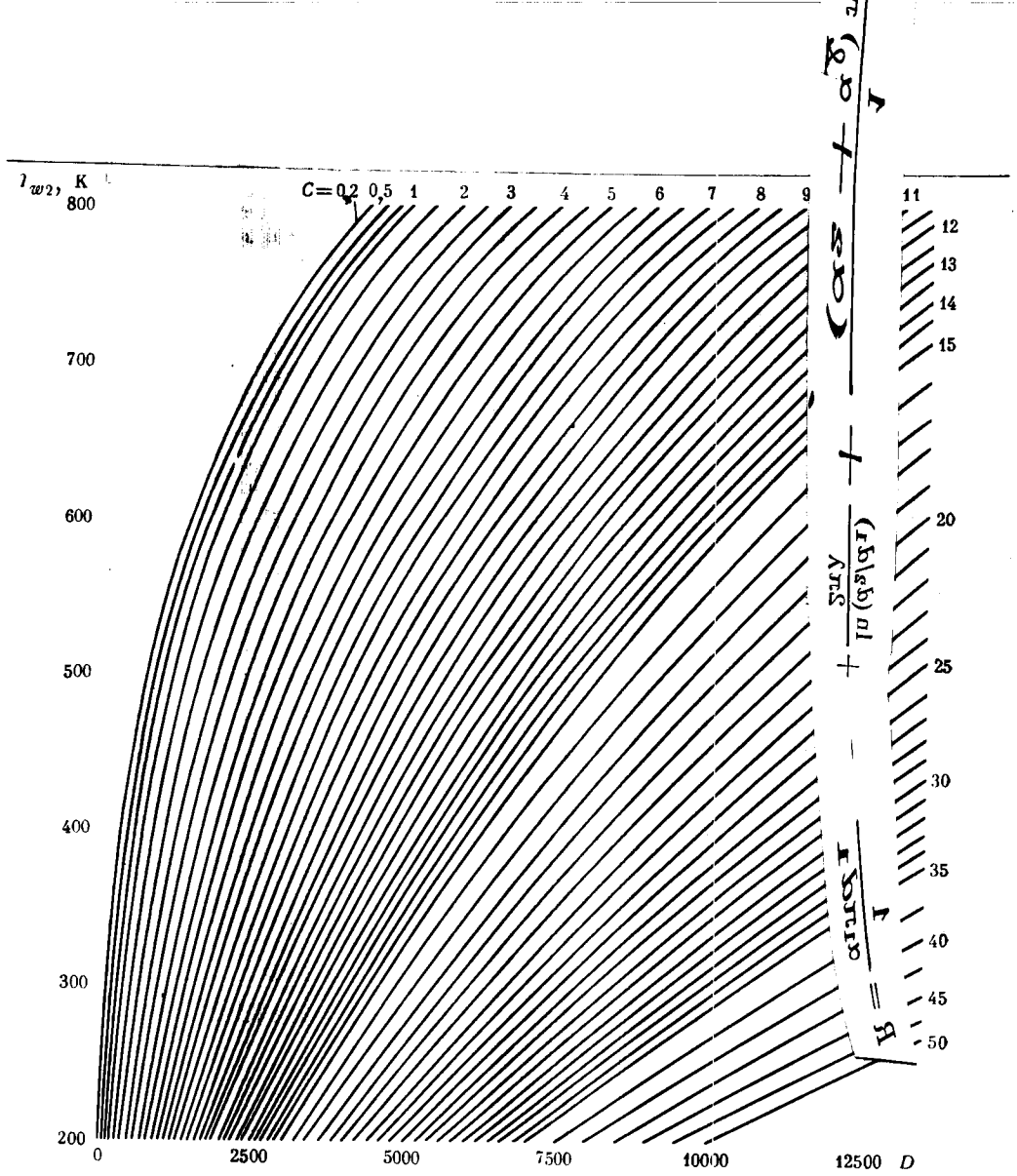

Figure 59. Graphs for Determination of T_{w2} with Fixed Parameters of Heat Conductor, Thermal Insulation and Surrounding Medium

As a result of simple conversions we produce

$$\left(\frac{T_{w2}}{100}\right)^4 + CT_{w2} = D, \tag{2.155}$$

where

$$C = \frac{\alpha_2 + B}{4{,}9\varepsilon_C},$$

$$D = \left(\frac{T_3}{100}\right)^4 + \frac{\alpha_2 T_2 + BT_1}{4{,}9\varepsilon_C},$$

Assigning various values of T_{w2}, C and calculating D in the range which we require, we produced graphs for determination of T_{w2}.

Figure 59 presents graphs allowing with fixed values of d_1, α_1, T_1, T_2, T_3, ε_c, α_2, d_2, λ the determination of T_{w2} with an accuracy of 2°. More precise determination of T_{w2} (with an error of 1°) can be performed using equation (2.155) by the method of multiple selection. Naturally, all of the calculations presented here are applicable in particular to the case when $T_3 = T_2$.

In conclusion to this section, we should note that comparative calculations of Q and d_{2e} with various values of d_1, α_1, T_1, T_2, T_3, ε_c and λ have shown the significant influence of radiant heat exchange on the thermal mode of a liquid heat conductor. In particular, we can note a significant change in the extreme value of d_{2e} in comparison to its value calculated without considering radiant heat exchange. Furthermore, in certain cases (for example with high values of λ), the use of thermal insulation of pipes leads to an increase in heat exchange with the surrounding medium; to decrease it, one should select insulation with low heat conductivity. In other cases (for example, when $Q_{RAD} \gg Q_{CONV}$) heat flux to the liquid can be reduced not by using thermal insulation, but rather by creation of low values of ε_c on the outer surface of the conductor. And, finally, for the most typical cases in the selection of effective thicknesses of thermal insulation, one must perform preliminary analysis of the dependence of effectiveness of thermal insulation on its thickness considering the corresponding heat-physical parameters (by the method presented in this section).

$$B = \frac{2\alpha_1\lambda}{(d_2/d_1)\left[\alpha_1 d_1 + \ln(d_2/d_1) + 2\lambda\right]}.$$

CHAPTER 9

DYNAMIC THERMAL CALCULATION OF AUTOMATIC PLANETARY STATIONS

9.1. Summary and Effective Heat Capacity of Spacecraft

/113

The thermal mode of a spacecraft, i.e., the change of its thermal state with time, is determined, as we can see from the thermal balance equation (2.1), by the internal heat liberation Q_T, the penetrating heat flux Q_p and the thermal inertia of the spacecraft, characterized by its heat capacity C. This heat capacity, a heat-physical characteristic of the spacecraft, frequently and to a significant extent determines both the type of the TMSS (what kind it should be, passive or active, and of what elements it should consist), as well as its power. Two types of spacecraft heat capacity are distinguished -- summary and effective.

The summary heat capacity C_Σ is determined by the formula

$$C_\Sigma = \sum_{j=1}^{n} C_j G_j, \tag{2.156}$$

where C_j and G_j are the specific heat capacity and weight respectively of each element in the structure of the jth portion of the spacecraft (see Figure 8); n is the number of elements in the structure of the jth portion of the spacecraft.

If the summary heat capacity C_Σ, the internal heat liberation Q_T and the penetrating heat flux Q_p are known, the change in temperature T_a in time $\Delta\tau$ can be determined by the formula

$$\Delta T_a = \frac{Q_T + Q_p}{C_\Sigma}\Delta\tau.$$

This equation shows that the greater the summary heat capacity C_Σ, the greater the thermal inertia of the spacecraft, i.e., the less the change in its temperature in time $\Delta\tau$ with the same values of internal heat liberation Q_T and penetrating flux Q_p.

Of course, it would be good to have a value of spacecraft heat capacity such that as the internal heat liberation and penetrating heat flux changed periodically, temperature T_a would

remain within its fixed limits (see Figure 9, curve 4), since otherwise additional measures must be taken (for example, the use of evaporators for cooling), resulting in an increase in the rate of the spacecraft. Unfortunately, the heat capacity of spacecraft cannot be above the summary capacity, the maximum possible, and even this can be achieved only if the design of the elements of the sapcecraft and the thermal couplings between them have infinite heat conductivity which, obviously, is impossible in practice. The heat capacity of the spacecraft may be near the summary heat capacity, if the heat liberation in each of the elements of the structure is so slight that even at the actual heat conductivity an even temperature field is achieved over the entire volume of the spacecraft.

However, for most spacecraft internal heat liberation is rather great. This means that if heat liberation occurs in any element of the spacecraft, due to the finite rate of heat propagation the temperature of this element changes first, and then, after a certain temperature field within the spacecraft is developed, the temperature of the remaining elements also changes. /114

As we have already stated, in the analysis of the thermal mode of spacecraft, several points of its temperature field which are most characteristic as concerns danger of overheating or overcooling are usually selected, for example the temperature of the body of the radio transmitter, chemical batteries, gas, fuel, etc. The temperature at these points defines the thermal mode of the spacecraft and is therefore called the determining temperature.

Obviously, a change in the determining temperature in the area of heat liberation will always be greater than at other points in the temperature field. Then, if we know the heat liberation $Q_T + Q_p$, the time of heat liberation $\Delta\tau$ and the measured actual (effective) change in determining temperature ΔT_{eff}, we can calculate the heat capacity of the spacecraft, which will differ from the summary capacity.

The heat capacity determined on the basis of actual measurement in time $\Delta\tau$ of the determining temperature with fixed internal heat liberation (Q_T) and penetrating heat flux (Q_p) is called the effective heat capacity:

$$C_{eff} = \frac{(Q_p + Q_T)\,\Delta\tau}{\Delta T_{eff}}. \qquad (2.157)$$

Since $\Delta T_{eff} > \Delta T_a$, the effective heat capacity is always greater than the summary heat capacity, and this difference will

be greater with a given heat liberation, the poorer the organization of process of heat exchange both in the heat liberating element itself, and between all remaining elements of the structure of the spacecraft.

The degree of perfection of the mutual heat exchange of the spacecraft elements can be characterized quantitatively by the ratio of effective heat capacity to summary heat capacity:

The value of this ratio η_{eff} is called the effectiveness of internal heat exchange.

One method frequently used at present for achievement of high values of η_{eff} is placement of heat liberating instruments and other spacecraft elements whose temperature should lie within fixed limits in one sealed container filled with gas. Equalization of temperature in this case is achieved by gradient heat exchange between them and the heat conductivity of the gas, and also (and primarily) by means of forced convection of this gas, created by a special fan (see Figure 8). If the heat liberating and other elements of the spacecraft are not placed in a sealed container, but rather outside the frame covered with the SVTI, high values of η_{eff} can be achieved by other types of heat conductors, as described in Chapter 8.

9.2. Experimental Determination of the Effective and Summary Heat Capacities and Penetrating Heat Flux

In order to calculate the thermal mode of a spacecraft and determine the effectiveness of internal heat exchange, we must know the effective and summary heat capacities of the spacecraft. The summary heat capacity C_Σ can be approximately determined using formula (2.156); the effective heat capacity C_{eff} will always be less than the summary heat capacity, by an extent which depends on the effectiveness of internal heat exchange. The value of C_{eff} is difficult to calculate in advance; it is usually based on available experimental data taken from earlier spacecraft, with a certain reserve.

The value of C_{eff} can be determined precisely by experimentation. If constant heat liberation first at level Q_T', then at /115

Q_T'' is achieved within a spacecraft within a vacuum chamber (by turning on instruments of a special heater imitating the heat liberation of these instruments), then after a certain time interval τ_0 (Figure 60), the rate of change of temperature of a spacecraft element for which the effective heat capacity is determined can be considered constant within a sufficiently short time interval $\Delta\tau$. Then, the thermal balance equation (2.1) for the first and second cases of heat liberation will become

$$C_{eff}\Delta T' - (Q_p + Q_T')\Delta\tau' = 0,$$
$$C_{eff}\Delta T_a'' - (Q_p + Q_T'')\Delta\tau'' = 0, \qquad (2.158)$$

where the penetrating heat flux Q_p is also an unknown quantity.

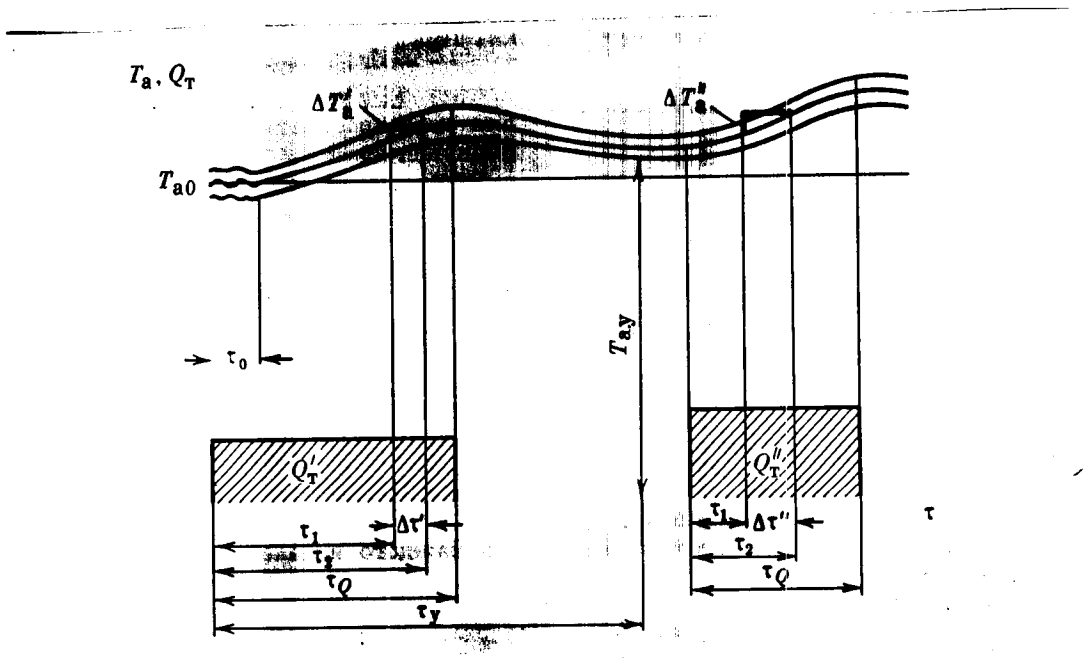

Figure 60. Experimental Determination of Effective Heat Capacity C_{eff} and Penetrating Heat Flux Q_p

In performing this experiment, one must attempt to see that Q_T' and Q_T'' do not differ too much from each other, while the initial and final temperatures with heat liberation Q_T' and Q_T'' are approximately equal.

dependences are needed not only to refine the calculations of the thermal mode, but also to perform measures for refinement of TMSS after terrestrial thermal testing and measures related to maintenance of the fixed thermal mode of the spacecraft in case emergency situations arise during the flight.

9.3. Examples of Dynamic Thermal Calculation of a Spacecraft

Example 1. Let us study the method of calculation for a simple spacecraft (Figure 61) moving in orbit around a celestial body. We assume that during the flight, temperature T_1 of the apparatus should change from the minimum permissible (T_{min}) to the maximum permissible (T_{max}); when T_{max} is reached, the fan is turned on and the spacecraft is cooled to T_{min} (heat ejected by radiation of the body-radiator), after which the fan is turned off and the process of changing temperature is repeated.

After selection of a calculation plan, we compose an equation for the thermal balance for each of the elements of the spacecraft, in this case for the equipment 1, inner thermal insulation 2 and radiator body 3:

$$\Delta T_1 C_{eff} G_1 = [Q_t - \alpha_{g1} F_1 \Delta T_{eff1} - \alpha_1 F_1 (T_1 - T_2) - \alpha_\lambda F_\lambda (T_1 - T_3)]\Delta\tau,$$

$$\Delta T_2 C_{eff} G_2 = [\alpha_1 F_1 (T_1 - T_2) - \alpha_2 F_2 (T_2 - T_3)]\Delta\tau,$$

$$\Delta T_3 C_{eff} G_3 = [Q_p + \alpha_{g2} F_2 \Delta T_{eff2} + \alpha_2 F_2 (T_2 - T_3) + \alpha_\lambda F_\lambda (T_1 - T_3)]\Delta\tau,$$

(2.162)

where ΔT_1, ΔT_2, ΔT_3 are the temperature increments for elements 1, 2 and 3 respectively in time $\Delta\tau$; α_{g1} and α_{g2} are the heat transfer factors as the gas moves in the spaces between elements 1 and 2, 2 and 3 respectively; α_1 and α_2 are the "heat transfer" factors due to radiation and heat conductivity of the gas between elements 1 and 2, 2 and 3 respectively; α_λ is the "heat transfer" factor due to heat conductivity through the attachment points of equipment 1 to body-radiator 3; ΔT_{eff1}, ΔT_{eff2} are the effective mean logarithmic temperature drops between equipment 1 and the gas, between the gas and body-radiator 3 respectively; Q_p is the

/117

penetrating heat flux through the outer surface of the spacecraft, which depends on time, orbital parameters and optical factors of the outer surface, the values of which are usually selected in advance in static thermal calculation (see Chapter 6).

The external heat fluxes striking the outer surface of the spacecraft and included in the penetrating heat flux Q_p can be determined according to [8-10] or using the formulas presented in the appendix to Chapter 5. The effective temperature drops are determined by the formulas [6]

$$\Delta T_{eff1} = \frac{T_{g1} - T_{g2}}{\ln\frac{T_{g1} - T_1}{T_{g2} - T_1}}, \quad \Delta T_{eff2} = \frac{T_{gf} - T_{g1}}{\ln\frac{T_{gf} - T_3}{T_{g1} - T_3}}, \tag{2.163}$$

where T_{g1}, T_{g2} are the gas temperatures before and after passing through the equipment respectively; T_{gf} is the gas temperature after the fan (see Figure 61).

On the other hand, ΔT_{eff1} and ΔT_{eff2} can be determined from the equations

$$\begin{aligned} F_1\alpha_{g1}\Delta T_{eff1}\Delta\tau &= C_p G_g (T_{g2} - T_{g1})\Delta\tau, \\ F_2\alpha_{g2}\Delta T_{eff2}\Delta\tau &= C_p G_g (T_{gf} - T_{g1})\Delta\tau, \end{aligned} \tag{2.164}$$

where C_p and G_g are the heat capacity and flow rate of the gas respectively.

Assuming that the temperature of elements 1, 2 and 3 in time $\Delta\tau$ does not change, we can use equations (2.163) and (2.164) to produce the following formulas for determination of the gas temperatures T_{g1}, T_{g2} and T_{gf} in the kth interval of time $\Delta\tau$:

$$T_{g1}=\frac{T_3(1-A)+T_1e^{-B}(1-e^{-B})+\frac{Q_f}{a}e^{-A}}{1-e^{-(A+B)}},$$

$$T_{g2}=\frac{T_1(1-e^{-B})+T_3e^{-B}(1-e^{-A})+\frac{Q_f}{a}e^{-(A+B)}}{1-e^{-(B+A)}},$$

(2.165)

where Q_f is the heat liberation of the fan;

$$A=\frac{\alpha_{g_2}F_2}{C_pG_g},\quad B=\frac{\alpha_{g_1}F_1}{C_pG_g};\quad a=C_pG_g.$$

The temperature of the ith element of the spacecraft (i = 1, 2, 3) for the (k + 1)th interval of time $\Delta\tau$ is calculated by the fromula

$$T_{i(k+1)}=T_{ik}+\Delta T_{ik},$$

where

$$\Delta T_{1k}=\{[Q_\tau-C_pG_g(T_{g_2}-T_{g_1})-$$
$$-\alpha_\lambda F_\lambda(T_1-T_3)-\alpha_1F_1(T_1-T_2)]\Delta\tau\}\times$$
$$\times(C_{eff_1}G_1)^{-1},$$
$$\Delta T_{2k}=\frac{\alpha_1F_1(T_1-T_2)-\alpha_2F_2(T_2-T_3)}{C_{eff_2}G_2}\Delta\tau,$$
$$\Delta T_{3k}=\{[Q_\pi+C_pG_g(T_{gf}-T_{g_1})+$$
$$+\alpha_\lambda F_\lambda(T_1-T_3)+\alpha_2F_2(T_2-T_3)]\Delta\tau\}\times$$
$$\times(C_{eff_3}G_3)^{-1}.$$

In the calculation, it was assumed that when the fan was turned on $\alpha_1 \simeq \alpha_2 \simeq 0$, while when it is off $G_g = 0$. The results of calculation are presented in Figure 61.

If the thermal model of the spacecraft is divided into a larger number of elements than in the example in question, then

the corresponding number of thermal balance equations must be composed. For example, to calculate the thermal mode of the landing unit of the Apollo spacecraft, some 135 equations were composed, the solution of which for the temperature of each element was performed by computer [20]. /118

Example 2. Let us study the possibility of maintaining the temperature of a spacecraft on the surface of the moon within fixed limits by use of a PTMSS based on the heat-physical properties of the lunar soil (heat capacity C_L, heat conductivity λ_L, specific gravity γ_L) and SVTI covering the surface of the lunar soil and the spacecraft on it.

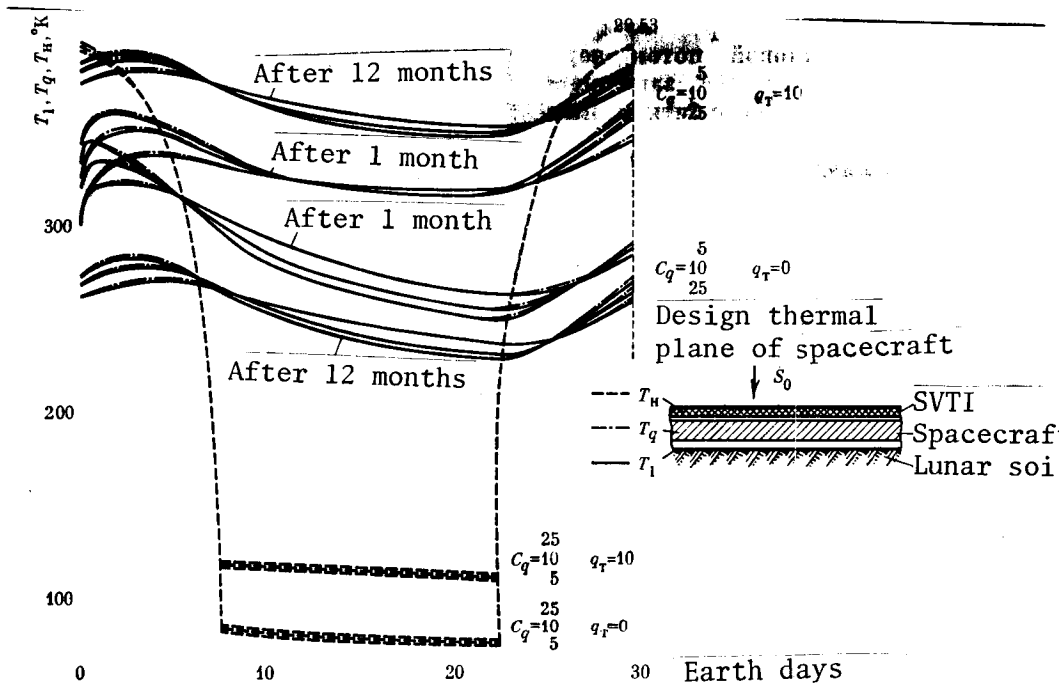

Figure 62. Thermal Mode of Spacecraft on Surface of Moon

Internal heat liberation Q_T and the effective heat capacity C_{eff} of the spacecraft, per unit surface area, limited by the contour of projection of the spacecraft on the surface of the moon, can be represented by q_T and c_q respectively. Considering the assumptions made, the calculated thermal plan of the spacecraft will be as shown in Figure 62.

The spacecraft temperature T_q in the (k + 1)th time interval is determined by the equation

$$T_{gf} = \frac{T_1(1-e^{-B}) + T_{3e}}$$

$$T_{q(k+1)} = T_{qk} + \Delta T_{qk},$$
$$\Delta T_{qk} = \frac{q_T^k + q_{Hq}^k + q_{Lq}^k}{c_q} \Delta\tau.$$

Here q_T^k, q_{Hq}^k and q_{Lq}^k are the internal heat liberation and thermal fluxes to the spacecraft from the SVTI and surface of the moon respectively:

$$q_{Lq}^k = C_0 \varepsilon_{cLq} \left[\left(\frac{T_{1k}}{100} \right)^4 - \left(\frac{T_{qk}}{100} \right)^4 \right],$$
$$q_{Hq}^k = C_0 \varepsilon_{c.Hq} \left[\left(\frac{T_{Hk}}{100} \right)^4 - \left(\frac{T_{qk}}{100} \right)^4 \right],$$

where T_{ik}, T_{qk}, T_{Hk}, ε_{cLq} and ε_{cHq} are the temperatures of the surface of the moon, spacecraft, outer surface of the SVTI (in the kth time interval) and corrected radiant heat exchange factors between them respectively; /119

$$\left(\frac{T_{Hk}}{100} \right)^4 = \frac{\frac{A_{SH}}{\varepsilon_H} \frac{S}{C_0} + \frac{\varepsilon_{C.Hq}}{\varepsilon_H} \left(\frac{T_{qk}}{100} \right)^4}{1 + \frac{\varepsilon_{C.Hq}}{\varepsilon_H}};$$
$$T_{1(k+1)} = \frac{T_{1k} + \left(\frac{\partial T_1}{\partial x} \right)_k \Delta x + (p-2) T_{1k} + T_{2k}}{p};$$

A_{SH} and ε_H are the solar radiation absorption factor and degree of blackness of the outer surface of the SVTI;

$$S = S_0 \cos 360^\circ \frac{k\Delta\tau}{t};$$
$$p = \frac{\gamma_L C_L \Delta x^2}{\lambda_L \Delta\tau};$$
$$\left(\frac{\partial T_1}{\partial x} \right)_k = \frac{C_0 \varepsilon_{cLq} \left[\left(\frac{T_{qk}}{100} \right)^4 - \left(\frac{T_{1k}}{100} \right)^4 \right]}{\lambda_L};$$

t = 29.53 Earth days (synodic month); Δ_x is the thickness of one

layer of lunar soil, produced by division of the total calculated depth into n layers (the calculated depth of lunar soil is taken from the condition of absence of practically noticeable fluctuations in temperature at this depth during the lunar day).

The temperature of the nth layer during the kth time interval is determined by the formula

The values of Δx and $\Delta\tau$ are selected so that $p \geq 2$.

The thermal mode of the spacecraft (i.e., the change in temperature T_q), as well as temperature T_1 of the surface of the moon beneath the spacecraft, temperature T_H of the outer surface of the SVTI (one month and 12 months after landing of the spacecraft) for one particular case of combination of heat-physical characteristics ($A_{SH} = 0.93$, $\varepsilon_H = 0.93$, $\varepsilon_{cHq} = 0.01$, $\varepsilon_{cLq} \approx 1.0$, $C_q = 5$, 10 and 25 kcal/(m^2·deg), $q_T = 0$ and 10 w) and lunar soil ($\lambda_L = 2.52 \cdot 10^{-2}$ kcal/(m^2·ch·° C), $\gamma_L = 800$ kg/m^3, $C_L = 0.2$ kcal/(kg·deg)) are presented in Figure 62.

Analysis of this figure shows that the fluctuations in temperature T_1 of the surface of the moon and, consequently, in spacecraft temperature T_q, covered by several layers of SVTI, are reduced significantly in comparison to the changes in the temperature of the surface of the moon not covered by SVTI. The results produced show that selection of proper values of corrected radiation factor of the SVTI ε_{cHq} and ratio A_{SH}/ε_H on its outer surface can assure a spacecraft temperature $T_q = 20 \pm 10°$ C throughout the entire lunar month using PTMSS alone[1].

[1]Calculations performed together with N. A. Spiridonova with the help of I. T. Atmanov.

CHAPTER 10

METHOD OF TERRESTRIAL THERMAL TESTING OF AUTOMATIC PLANETARY STATIONS

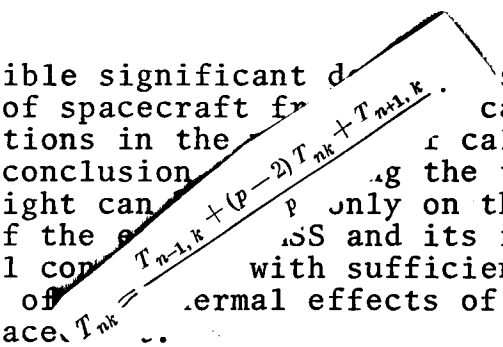

Due to possible significant d[illegible]s in actual heat-physical /120
characteristics of spacecraft f[illegible] calculated characteristics
and the imperfections in the [illegible]r calculation of thermal
states, a final conclusion [illegible]g the thermal state of a
spacecraft in flight can [illegible]p only on the basis of testing of
the efficiency of the [illegible]SS and its individual elements
under terrestrial co[illegible] with sufficiently precise reproduc-
tion (imitation) of [illegible]ermal effects of the surrounding space
medium on the space[illegible].

Terrestrial thermal testing can be conducted only after an answer is obtained to the following three main questions:

-- What is "sufficient" accuracy (or, in other words, "permissible" error) in the imitation of the thermal effects of the surrounding space medium on the spacecraft?

-- What technical devices can be used to imitate the thermal effects of the surrounding space medium on the spacecraft?

-- What must be the minimum duration of thermal testing for each spacecraft flight stage?

The combination of methods of determination and selection of the necessary accuracy of imitation of the thermal effects of the surrounding space medium on a spacecraft, technical devices for its achievement and duration of thermal testing is called the methodology of terrestrial thermal testing of the spacecraft.

If the methodology of terrestrial thermal testing is not developed, there is always the danger of selecting either an unjustifiably high accuracy of imitation and unjustifiably long duration of testing, which may lead the entire problem of thermal testing into a blind alley due to technical and economic difficulties, or of selecting a too-rough imitation and production of false data on the thermal state of the spacecraft in flight.

Thermal testing of the entire spacecraft, in which the composition of devices and program of their heat liberation correspond to those to be encountered in flight, is called complete testing; the purpose of these tests is to determine the thermal state of the spacecraft throughout the entire time of its flight.

Thermal testing of individual elements of the spacecraft (including the active TMSS) is called independent testing; the

purpose of these tests is experimental determination of the heat-physical characteristics of these elements.

Tests can be performed either with the spacecraft actually to be flown ("flight," "actual") or a similar spacecraft ("thermal model," "duplicate"), in which some of the "flight" heat liberating devices may be replaced by "thermal models," the heat capacity, geometric dimensions and program of heat liberation of which correspond to the "flight" instruments.

In addition to ground test, flying thermal tests may be conducted, most frequently independent, in order to test the efficiency of individual TMSS elements (for example evaporators, heat conductors, etc.) under conditions of weightlessness and space vacuum. /121

The thermal mode of the spacecraft during terrestrial testing will be similar to the flight mode only if the heat-physical characteristics of the surrounding medium and heat exchange conditions (i.e., irradiance factors) of the spacecraft with this medium are similar to those which will be encountered during the flight.

Let us note the most important heat-physical characteristics of the surrounding space medium.

1. Intensity S_0 [w/m^2], spectral composition and nonparallelness (angle of divergence) of direct solar radiation.

2. Intensity S_k [w/m^2], spectral composition and angular distribution of solar radiation reflected from the surface of a celestial body.

3. Intensity E_k [w/m^2], spectral composition and angular distribution of natural thermal radiation of the surface of a celestial body.

4. Optical factors A and ε of the surface of the celestial body and of space.

5. Heat conductivity λ_k [$w/(m \cdot deg)$], heat capacity C_k [$j/(kg \cdot deg)$] and specific gravity γ_k [kg/m^3] of the soil of the celestial body on which the spacecraft will be located.

Precise imitation of these heat-physical characteristics of the surrounding medium and spacecraft irradiance factors with this medium is sometimes impossible under terrestrial conditions due to technical and economic difficulties, and in other cases is simply unnecessary. One must provide sufficiently accurate

imitation, meaning imitation with the "permissible" error, causing no significant difference in the temperature of the spacecraft during tests and during flight. Therefore, the most important task and the first step in terrestrial thermal testing is determination of the permissible error of imitation of these heat-physical characteristics of the surrounding medium and the irradiance factors of the spacecraft with this medium.

The next, second step in terrestrial thermal testing is selection of the necessary technical devices to perform the imitation with sufficient accuracy. The solution of this problem is somewhat complicated by the fact that the heat-physical characteristics and irradiance factors change during the course of time not only as a result of transition from one flight stage to another, but also due to changes in the orientation of the spacecraft relative to the surrounding medium during each of these stages.

Imitation of changing spacecraft irradiance factors with the surrounding medium with the passage of time requires either that the spacecraft be rotated relative to nonmoving radiation imitators (first method) or that the radiation imitators rotate relative to the nonmoving spacecraft (second method). A third method is also possible: rotation of the nonmoving spacecraft is imitated by successive connection and disconnection of special nonmoving heat flux imitators located within the vacuum chamber and surrounding the spacecraft.

The first method can be used only for small spacecraft, but even in this case significant technical difficulties arise, which are practically unsurmountable for large spacecraft.

The best solution to this problem is the second method, although this requires that thermal radiation imitators be used, the design of which is so simple that they can be placed within the vacuum chamber and moved relative to the spacecraft. In § 10.11 of this chapter, it is demonstrated that the most acceptable solar radiation imitator for this purpose is an imitator with straightening grids, using a xenon arc lamp (XAL) with reflectors as the light source; the use of solar radiation imitators made according to the "classical" plan (radiation source outside the vacuum chamber) is practically impossible. /122

After the necessary accuracy of imitation of the heat-physical properties of the surrounding medium and irradiance factors of the spacecraft have been determined, technical equipment for imitation with permissible error has been selected, the third step must be taken: the question of the duration of testing for each flight stage must be answered.

The maximum test time for any flight stage of the spacecraft can be considered the time required for the elements of the

spacecraft to reach stable temperatures; the performance of longer testing is simply senseless from the thermal standpoint in many cases (unless the task of determination of the degree of change of the heat-physical characteristics of the spacecraft with time is also set).

It may sometimes be necessary to perform thermal testing in extremely short periods of time -- in a time not only shorter than the flying time, but even insufficient for the temperature of the structural elements of the spacecraft to take on its stable value. In this case, a conclusion concerning the thermal load of the spacecraft can be drawn if the heat-physical characteristics of the spacecraft (such as effective heat capacity C_{eff}, rate of change of temperature $dP_a/d\tau$ in various flight stages, summary corrected radiation factor ε_{ca} or thermal resistance of the spacecraft thermal insulation R_a, etc.) can be determined, then, using the dependences produced experimentally, the thermal mode of the spacecraft for the entire time of the flight can be constructed by extrapolation.

Complete thermal tests are the final stage in large volume terrestrial thermal testing of individual TMSS elements, i.e., independent tests. For example, for radiators and evaporators -- testing to determine the heat rejection capability, effective heat capacity of the structure and efficiency for various temperatures and flow rates of coolant passing through these elements; for thermal insulation -- testing to determine the corrected radiation factor (thermal resistance) as a function of temperature on the outer and inner surfaces, etc. If the thermal characteristics produced differ from the calculated characteristics, either these elements are further refined or the calculation of the thermal mode of the spacecraft is made more accurate.

Usually independent thermal testing is used to determine the heat-physical characteristics of ATMSS, combined thermal testing being used for PTMSS. However, cases may arise when, due to unavailability of test equipment (for example, imitators and vacuum chambers of sufficient size), combined thermal testing is impossible. In this case, independent thermal testing of the elements of PTMSS is required (for example, to determine the thermal resistance of individual sections of the body of the spacecraft with thermal insulation, solar battery panels, etc.).

As in the case of combined thermal testing, during independent testing of PTMSS elements it is also necessary to imitate heat exchange with the surrounding medium, but this is easier due to the significantly smaller dimensions of the elements tested in comparison with the dimensions of the entire spacecraft.

The data produced in independent thermal testing of ATMSS and PTMSS can be used to refine the calculation of the thermal state of the spacecraft, which will now be determined much more precisely than in the calculations before testing, and in some cases this calculation can be used as a basis for final conclusions concerning the thermal mode of the spacecraft in flight without performance of complex and expensive combined ground thermal testing. /123

This chapter presents some examples of solution of these problems, which arise in the development of a methodology for terrestrial independent and combined thermal testing of spacecraft.

10.1. Methodology of Determination of Permissible Error of Imitation of Heat-Physical Properties of the Surrounding Space Medium

The permissible error of imitation of heat-physical properties of the surrounding space medium can be determined on the basis of analysis of the influence of deviations of the heat-physical properties imitated from the flight properties on the temperature of the spacecraft as a whole or its individual parts, as defined by equation (2.75).

If a reasonable value of permissible relative (δT_a^0) or absolute (ΔT_a^0) error in spacecraft temperature T_a^0 is assigned (in the following, temperature T_a^0 will refer to the temperature of the spacecraft as a whole or of its individual elements), the permissible absolute error in [illegible] of equation (2.75) will be determined:

$$C_0\left(\frac{T_a^0}{100}\right)^4\left[(1+\delta T_a{}^0)^4-1\right]\sum_{i=1}^{n}F_i\varepsilon_{ci}=$$

$$=C_0\left(\frac{T_a^0}{100}\right)^4\left[\left(1+\frac{\Delta T_a{}^0}{T_a{}^0}\right)^4-1\right]\sum_{i=1}^{n}F_i\varepsilon_{ci}=$$

$$=C_0\left(\frac{T_a^k}{100}\right)^4\sum_{i=1}^{n}F_i\varepsilon_{ci}-C_0\left(\frac{T_a^0}{100}\right)^4\sum_{i=1}^{n}F_i\varepsilon_{ci}, \qquad (2.166)$$

where the superscript "0" relates to the conditions of the spacecraft in flight, the superscript "k" -- in a vacuum chamber during testing.

The permissible error or permissible absolute value of any heat-physical characteristic of the surrounding space medium included in the right portion of equation (2.75) can be determined if equation (2.75) is written twice -- considering the changes in the characteristic in comparison to its value in flight and without changes, these equations are substituted into expression (2.166), then the equation produced is solved for the permissible absolute value or permissible error of the heat-physical characteristic of interest to us.

Since a "reasonable" value of permissible error δT_a^0 in the spacecraft temperature in terrestrial thermal testing may be interpreted variously, all subsequent calculations are performed for a permissible relative error $\delta T_a^0 = 0.005$, 0.01, 0.02, 0.03 and 0.05. In any case, however, there is no reason to require accuracy of imitation exceeding the accuracy of recording of spacecraft temperature during testing or flight (2-3° C).

10.2. Permissible Pressure of Residual Gas in Vacuum Chambers

During the flight stages between Earth and the celestial body to which a spacecraft flies and as a satellite of another celestial body, and also on the surface of some celestial bodies (for example, the moon), the spacecraft will be located in a gas medium with extremely low pressure (10^{-12}-10^{-14} torr), so that in these flight stages the surrounding gas medium has practically no influence on its thermal state.

Imitation of the heat exchange of the spacecraft with the surrounding space gas medium during terrestrial thermal testing is achieved by placing the spacecraft in a sealed vessel (a so-called vacuum chamber) and evacuating the gas from this chamber using special vacuum pumps to a sufficiently low pressure. Evacuation to the pressure of the gas medium of space (or, as is said, to the point of a space vacuum) is an extremely difficult technical task (particularly for large chambers) and is simply unnecessary from the standpoint of the methodology of terrestrial thermal testing. /124

The maximum permissible pressure p_k in the vacuum chamber can be estimated as follows. The quantity of thermal energy Q_{mi} carried away from the surface F_i by the molecules of the residual gas, the free path length of which is greater than the dimensions of the vacuum chamber, can be determined by the following formula, produced from the expressions for Q_{mi} presented in [21] and [22]:

$$Q_{mi} = \frac{1{,}44 \cdot 10^4}{\sqrt{A}} p_K (\sqrt{T_{iH}} - \sqrt{T_K}) F_i \quad [W],$$

where A is the atomic w[illegible]of the molecules of residual gas (A_{N_2} = 28, A_{H_2} = 2); T_{iH} the temperature of the outer surface of the insulation of the spacecraft, K; T_k is the temperature of the inner surface of the vacuum chamber, K; p_k is the maximum permissible pressure in the vacuum chamber, torr.

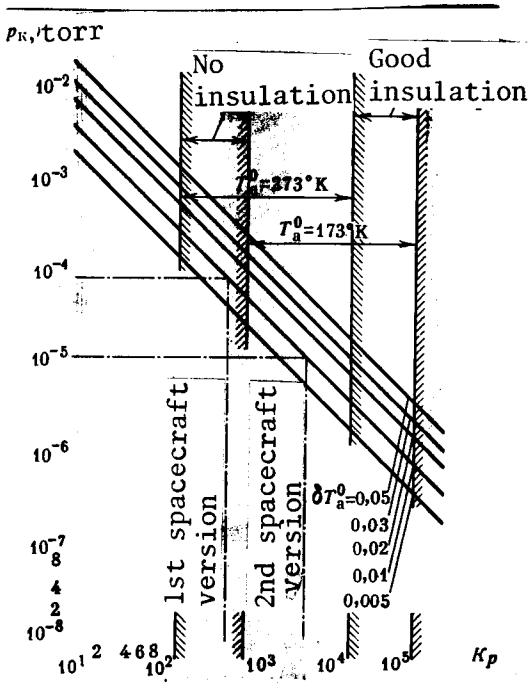

Figure 63. Permissible Pressure p_k of Residual Gas (N_2) in Vacuum Chamber as a Function of Factor K_p for Various Values of Permissible error δT_a^0

With no external heat flux, when $T_k \approx 0$, the maximum heat exchange between surface F_1 and the chamber, temperature T_{iH} will be

$$T_{iH} = T_a^0 (\varepsilon_{ci}/\varepsilon_{iH})^{1/4}.$$

Since residual gas conductivity heat loss must be limited by the left portion of (2.166), we should have:

$$\frac{1{,}44 \cdot 10^4}{\sqrt{A}} p_K \sqrt{T_a^0} \sum_{i=1}^{n} (\varepsilon_{ci}/\varepsilon_{Hi})^{1/8} \leqslant$$

$$\leqslant [(1 + \delta T_a^0)^4 - 1] C_0 \left(\frac{T_a^0}{100}\right)^4 \sum_{i=1}^{n} F_i \varepsilon_{ci}.$$

From this relationship, we can produce a formula determing the maximum permissible pressure p_k in the vacuum chamber, for which the error of temperature of the spacecraft during testing will not exceed the permissible error δT_a^0:

$$p_K \leqslant \frac{(1 + \delta T_a^0)^4 - 1}{K_p} \approx \frac{4\delta T_a^0}{K_p}, \qquad (2.167)$$

/125

(since $\delta T_a^0 << 1$), where

(2.168)

If we must determine the permissible pressure in the vacuum chamber designed for the performance of thermal testing of any spacecraft, we should select a spacecraft thermal model placing the highest requirements on the vacuum. Analysis of formulas (2.167) and (2.168) shows that this case corresponds to a well-insulated ($\varepsilon_{ci} \leq 0.01$; $\varepsilon_{iH} = 0.1$) and cold ($T_a^0 = 173$ K) spacecraft, i.e., the maximum possible coefficient $K_{pmax} = 5.3 \cdot 10^4$ (for residual gas N_2).

In order to produce the minimum value of coefficient K_{pmin}, we must take noninsulated elements of the spacecraft ($\varepsilon_{ci} = \varepsilon_{iH} \simeq 1$), with a maximum possible temperature, which can be taken as 273 K, since if there are spacecraft elements heated to a higher temperature there are always others with temperatures with 273 to 313 K. Using formula (2.168), we calculate $K_{pmin} = 7.2 \cdot 10^2$.

The results of calculation of the permissible pressure p_k of residual gas in a vacuum chamber for terrestrial thermal testing as a function of the practically possible range of change of coefficient K_p for various values of permissible relative error δT_a^0 of determination of spacecraft temperature during the tests are presented in Figure 63.

Assuming $\delta T_a^0 = 0.01$, we see that the permissible pressure in a universal vacuum chamber designed for testing of all spacecraft should be not over $6 \cdot 10^{-5}$ torr; on the other hand, there is no sense in evacuating it to a pressure of $7.5 \cdot 10^{-7}$ torr.

The pressure in a vacuum chamber designed for testing of a specific spacecraft may be higher than the pressure in the universal chamber. For example, for thermal models of spacecraft of the first and second versions which we studied earlier as examples (see § 6.2) for $\delta T_a^0 = 0.01$, $T_a^0 = 273$ K we produce: $K_{p1} = 4.5 \cdot 10^2$, $p_{k1} = 9 \cdot 10^{-5}$ torr; $K_{p2} = 3.0 \cdot 10^3$, $p_{k2} = 1.3 \cdot 10^{-5}$ torr.

10.3. Permissible Error in Degree of Blackness of Surrounding Space Medium Radiation Imitator

The degree of blackness of free space ε_0 is equal to 1, since the thermal radiation of the surface of the spacecraft and solar radiation reflected from it do not return to the spacecraft. During terrestrial thermal testing, the degree of blackness ε_k of the radiation imitator imitating free space is always less than 1, so that a portion of the radiation is reflected from the

imitator and strikes the surface of the spacecraft again. Therefore, the temperature of the spacecraft during tests will always be higher than the temperature during an actual space flight.

The temperature of the spacecraft during testing will differ from the temperature during flight also if the degree of blackness of the device imitating the radiation of the surface of a celestial body ε_k differs from the degree of blackness of this surface ε_0.

The permissible value of the degree of blackness ε_k of surrounding medium radiation imitators can be found using equations (2.166) and (2.75) on the assumption that all the heat-physical characteristics of the spacecraft and surrounding medium in flight and under terrestrial conditions are identical with the exception of ε_0. In this case we will have

$$C_0\left(\frac{T_a^0}{100}\right)^4 [(1+\delta T_a^0)^4 - 1] \sum_{i=1}^{n} F_i \varepsilon_{ci} = (\Phi_\varepsilon^к - \Phi_\varepsilon^0)\left(q_т + S_0 \sum_{i=1}^{n} F_i S_{iк}\right). \quad (2.169)$$

Since /126

$$\Phi_\varepsilon^0 = 1 + \frac{1}{F_к}\left(\frac{1}{\varepsilon_0} - 1\right) \sum_{i=1}^{n} F_i \varepsilon_{ci} \varphi_{iк},$$

$$\Phi_\varepsilon^к = 1 + \frac{1}{F_к}\left(\frac{1}{\varepsilon_к} - 1\right) \sum_{i=1}^{n} F_i \varepsilon_{ci} \varphi_{iк},$$

then relationship (2.169) becomes

$$C_0\left(\frac{T_a^0}{100}\right)^4 [(1+\delta T_a^0)^4 - 1] \sum_{i=1}^{n} F_i \varepsilon_{ci} = \frac{1}{F_к}\left(\frac{1}{\varepsilon_к} - \frac{1}{\varepsilon_0}\right)\left(q_т + S_0 \sum_{i=1}^{n} F_i S_{iк}\right) \times \times \sum_{i=1}^{n} F_i \varepsilon_{ci} \varphi_{iк}.$$

From this

$$\frac{1}{\varepsilon_к} - \frac{1}{\varepsilon_0} = \frac{C_0 (T_a^0/100)^4 [(1+\delta T_a^0)^4 - 1]}{\left(q_т + \sum_{i=1}^{n} F_i S_{iк}\right) / F_к} \frac{\sum_{i=1}^{n} F_i \varepsilon_{ci}}{\sum_{i=1}^{n} F_i \varepsilon_{ci} \varphi_{iк}}.$$

Introducing the symbol

$$K_\varepsilon = \frac{\left(q_т + \sum_{i=1}^{n} F_i S_{iк}\right)}{F_к C_0 (T_a^0/100)^4} \frac{\sum_{i=1}^{n} F_i \varphi_{iк} \varepsilon_{ci}}{\sum_{i=1}^{n} F_i \varepsilon_{ci}}, \qquad (2.170)$$

we produce

$$\frac{1}{\varepsilon_к} - \frac{1}{\varepsilon_0} = \frac{(1+\delta T_a^0)^4 - 1}{K_\varepsilon}. \qquad (2.171)$$

Consequently, the permissible degree of blackness of the device imitating the surrounding space medium will be defined by the formula

$$\varepsilon_к = \frac{1}{\frac{1}{\varepsilon_0} + \frac{(1+\delta T_a^0)^4 - 1}{K_\varepsilon}}. \qquad (2.172)$$

Figure 64 shows the dependence of permissible difference $(1/\varepsilon_k) - (1/\varepsilon_0)$ from coefficient K_ε for various values ofpermissible relative error δT_a^0 of the temperature of the spacecraft during the tests. The limits of change of coefficient K_ε are selected from $K_\varepsilon = 0$ to $K_\varepsilon = 1$, since analysis of formulas (2.170) and (2.75) shows that $K_{\varepsilon max} = 1$, while $K_{\varepsilon min} \approx 0$. Practically always $0 < K_\varepsilon < 1$, where with increasing dimensions of the vacuum chamber and decreasing dimensions of the spacecraft, coefficient

K_ε, as we can see from formula (2.170), decreases.

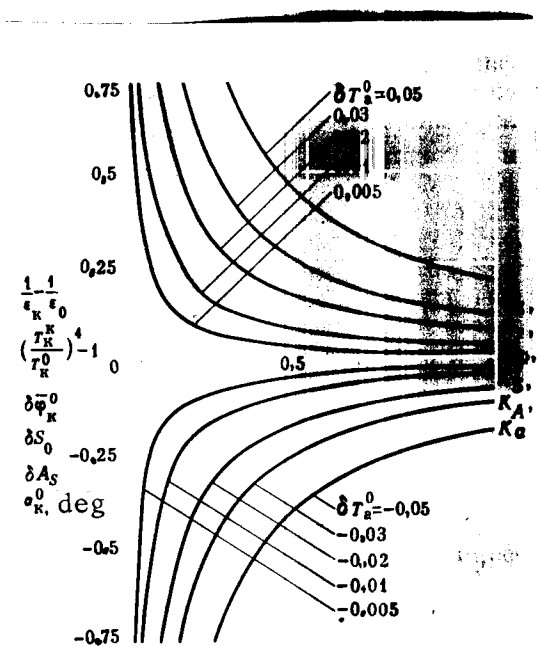

Figure 64. Generalized Graph of Permissible Deviations in Heat-Physical Characteristics of Surrounding Space Medium as a Function of Thermal Parameters K

If we must determine the permissible degree of blackness of the surrounding space medium radiation imitator designed for testing of all spacecraft (i.e., for univeral vacuum chambers), we must select a spacecraft thermal model placing the most rigid requirements on imitation accuracy. /127

Analysis of formula (2.171) shows that this requirement is fulfilled where $K_\varepsilon = 1$. In this case, equation (2.171) becomes:

$$\frac{1}{\varepsilon_K}-\frac{1}{\varepsilon_0}=(1+\delta T_a^0)^4-1=\left(1+\frac{\Delta T_a^0}{T_a^0}\right)^4-1. \quad (2.173)$$

The results of calculation of the permissible difference $(1/\varepsilon_k) - (1/\varepsilon_0)$ for surrounding space medium radiation imitators of universal vacuum chambers as a function of relative (δT_a^0) and absolute (ΔT_a^0) permissible errors for various spacecraft temperatures T_a^0 for K = 1 are presented in Figure 65.

Figure 66 shows the results of calculation of the minimum permissible degree of blackness ε_k of the free space radiation imitator ($\varepsilon_0 = 1$, solid lines) and for the surface of the moon ($\varepsilon_0 \approx 0.93$, dotted lines) as functions of coefficient K_ε for various values of permissible relative error δT_a^0 during testing, while Figure 67 shows these same figures as functions of relative (δT_a^0) and absolute (ΔT_a^0) permissible errors for a universal vacuum chamber designed for testing of all spacecraft.

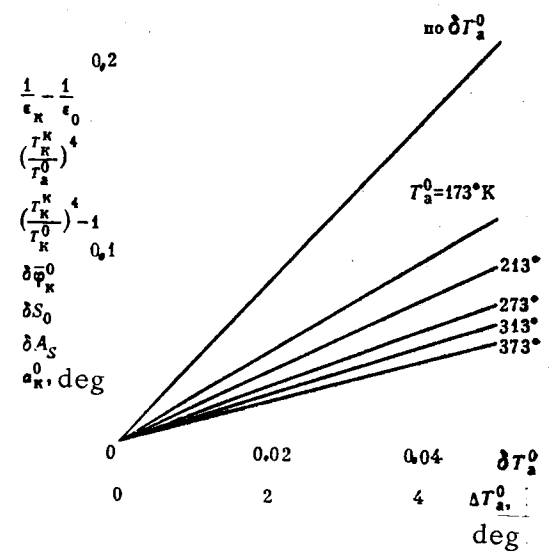

Figure 65. Generalized Graph of Permissible Deviations of Heat-Physical Characteristics of the Surrounding Space Medium as Functions of Permissible Spacecraft Temperature Errors for K = 1

10.4. Permissible Error in Surrounding Space Medium Radiation Imitator

Using equations (2.166) and (2.75) and assuming that all heat-physical characteristics of the spacecraft and the surrounding medium are the same in flight and during terrestrial testing, with the exception of the temperature of the surrounding medium T_k^0, we can produce the following equation

$$C_0\left(\frac{T_a^0}{100}\right)^4[(1+\delta T_a^0)-1]\sum_{i=1}^{n}F_i\varepsilon_{ci} = C_0\left[\left(\frac{T_K^K}{100}\right)^4-\left(\frac{T_K^0}{100}\right)^4\right]\sum_{i=1}^{n}F_i\varepsilon_{ci}\varphi_{iK}. \quad (2.174)$$

Temperature T_k^k can be expressed as a function of relative (δT_k^0) and absolute (ΔT_k^0) errors by the formula

$$T_K^K = T_K^0(1+\delta T_a^0) = T_K^0(1+\Delta T_K^0/T_K^0).$$

Substituting this formula into (2.174) and solving the equation produced for δT_k^0 or ΔT_k^0, we will have

$$\delta T_K^0 = \left[1+\frac{(1+\delta T_a^0)^4-1}{K_T}\right]^{1/4}-1,$$
$$\Delta T_K^0 = \left[1+\frac{(1+\delta T_a^0)^4-1}{K_T}\right]^{1/4}T_K^0 - T_K^0. \quad (2.175)$$

where

$$K_T = \left(\frac{T_к^0}{T_a^0}\right)^4 \frac{\sum_{i=1}^{n} F_i \varepsilon_{ci} \varphi_{iк}}{\sum_{i=1}^{n} F_i \varepsilon_{ci}}. \qquad (2.176)$$

For the free space radiation imitator $\phi_{ik} = 1$, $T_k^0 = 0$; therefore, the permissible absolute error ΔT_k^0 must be calculated by the formula

$$\Delta T_к^0 = T_к^к = T_a^0 [(1 + \delta T_a^0)^4 - 1]^{1/4}, \qquad (2.177)$$

which is produced by substitution of expression (2.176) into the second formula of (2.175).

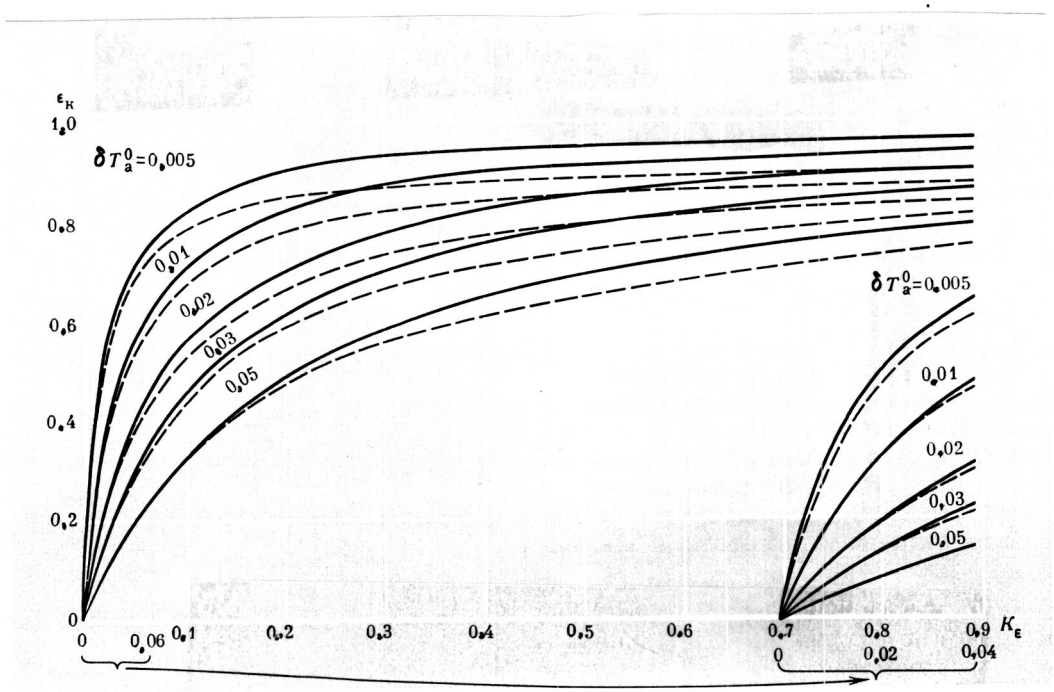

Figure 66. Minimum Permissible Degree of Blackness ε_k of Free Space Radiation Imitator (Solid Lines) and Surface of Moon (Dotted Lines) as a Function of K_ε for Various Values of Permissible Relative Error δT_a^0

Since $\delta T_k^0 = T_k^k/T_k^0 - 1$, by using the first formula of (2.175), we can produce the relationship

(2.178)

the right portion of which is similar to the right portion of equation (2.171). Furthermore, from formula (2.177) for a free space imitator we have the relationship

$$\left(\frac{T_{\text{к}}^{\text{к}}}{T_{\text{a}}^0}\right)^4 = (1+\delta T_{\text{a}}^0)^4 - 1 = \left(1+\frac{\Delta T_{\text{a}}^0}{T_{\text{a}}^0}\right)^4 - 1 \approx 4\delta T_{\text{a}}^0, \tag{2.179}$$

the right portion of which coincides to the right portion of (2.173).

The maximum value of coefficient K_t is equal to 1, which follows from the conditions of fulfillment of the thermal balance of the spacecraft [see equation (2.75) and formula (2.176)].

If in planning the imitator the heat-physical characteristics of the spacecraft are unknown, the permissible errors in its temperature must be determined from the condition of the possibility of testing of any spacecraft, including those placing the most rigid requirements on imitation accuracy; analysis of formula (2.175) shows that this requirement corresponds to the thermal model of a spacecraft for which the maximum value coefficient $K_t = 1$ is obtained. In this case, formulas (2.175) and (2.178) become as follows

/129

$$\delta T_{\text{к}}^0 = \delta T_{\text{a}}^0 = \frac{\Delta T_{\text{a}}^0}{T_{\text{a}}^0} \tag{2.180}$$

and

(2.181)

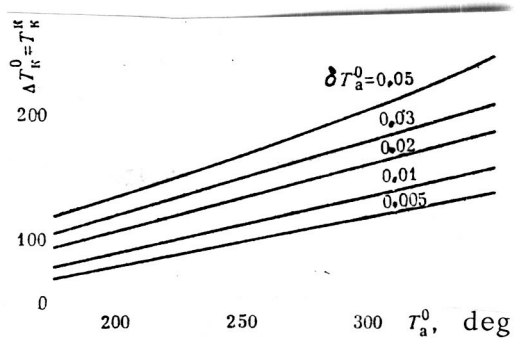

Figure 68. Permissible Absolute Error ΔT_k^0 of Temperature of Free Space Radiation Imitator as a Function of Temperature of Spacecraft T_a^0 for Various Values of Permissible Relative Error δT_a^0

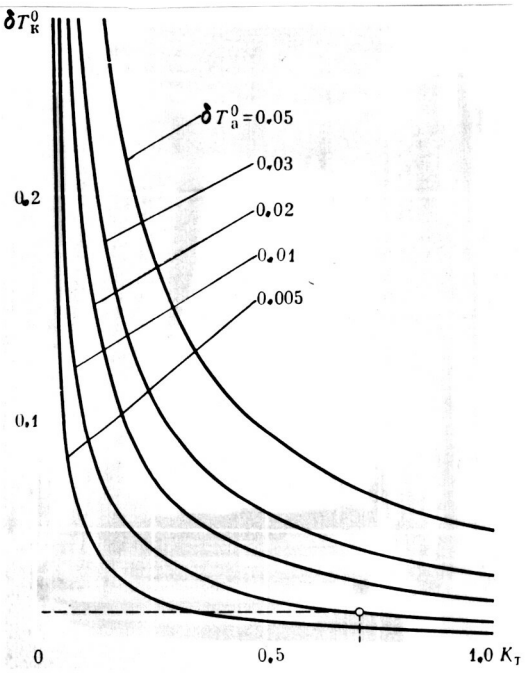

Figure 69. Permissible Relative Error δT_k^0 of Temperature of Celestial Body Surface Radiation Imitator as a Function of Coefficient K_T for Various Values of Permissible Relative Error δT_a^0

of equation (2.166), we can produce the following formula for determination of the permissible error in the mean irradiance factor of the outer surface of a spacecraft with a device imitating the radiation of the surface of a celestial body:

(2.182)

where

(2.183)

The results of calculation /131 of the permissible relative error $\delta\bar{\phi}_k^0$ using formula (2.182) as a function of coefficient K_ϕ for various values of permissible relative error δT_a^0 of spacecraft temperature during testing are presented in Figure 64.

If during the selection of an imitator plan, the heat-physical characteristics of the spacecraft are unknown, the problem of determination of the permissible errors in spacecraft irradiance factor with the planned imitator can be solved if we calculate them for a thermal model of the spacecraft

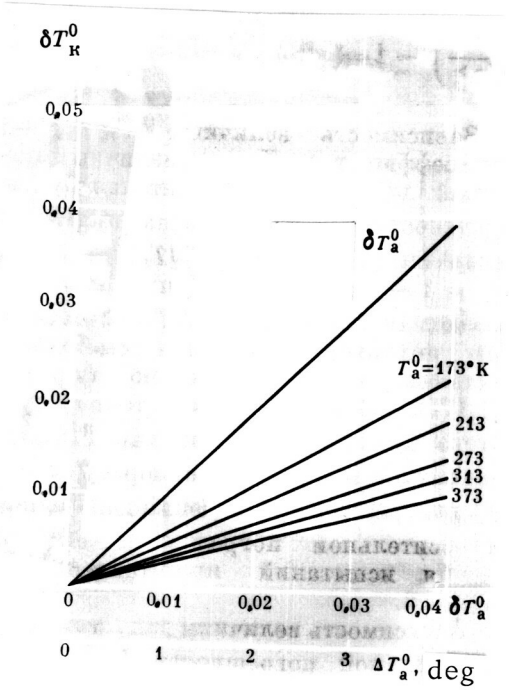

Figure 70. Permissible Relative Error δT_k^0 of Temperature of Celestial Body Surface Radiation Imitator of Universal Vacuum Chambers as a Function of Relative (δT_a^0) and Absolute (ΔT_a^0) Permissible Errors for Various Values of Spacecraft Temperature T_a^0

of the spacecraft; in this case and heat exchange conditions with the surrounding medium requiring the most precise imitation. As formula (2.182) shows, this requirement is fulfilled if coefficient K_ϕ reaches its maximum value, equal to 1. Figure 65 shows the results of calculation of permissible relative error $\delta\bar{\phi}_k^0$ for $K_\phi = 1$ as a function of permissible errors in spacecraft temperature δT_a^0 and ΔT_a^0 for various values of temperature T_a^0.

As we can see from expression (2.183) for coefficient K_ϕ, its value depends on the irradiance factors ϕ_{ik}^0 of each ith sector of the outer surface of the spacecraft; if the angle between normals to these surfaces and the normal to the surface of the celestial body is represented by β_i, then

The dependence of permissible relative error $\delta\bar{\phi}_{ik}^0$ on angle β_i can be easily produced for a surface determining the thermal mode

(2.184)

The results of calculation of $\delta\phi_{ik}^0$ as a function of angle β_i for various values of permissible relative error δT_a^0 of spacecraft temperature during testing at T_k^0 = 396 K and T_a^0 = 273 K are presented in Figure 71.

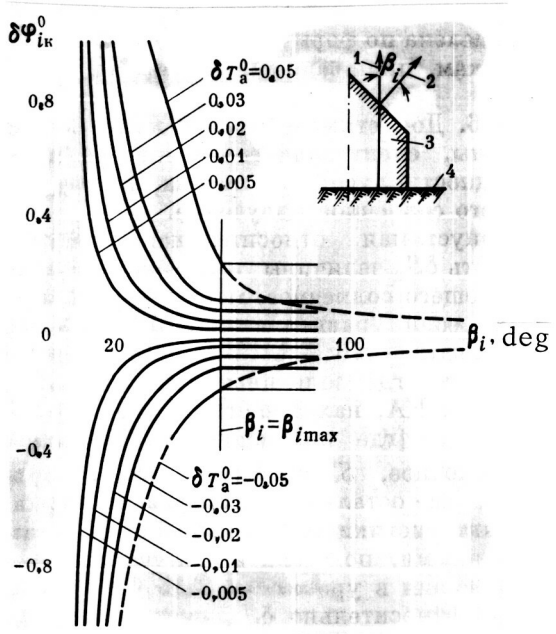

Figure 71. Permissible Relative Error in Irradiance Factor $\delta\phi^0_{ik}$ of Spacecraft as a Function of Angle β_i for Various Values of Permissible Relative Error δT^0_a: 1, Perpendicular to Surface of Celestial Body; 2, Perpendicular to Spacecraft Surface; 3, Spacecraft; 4, Celestial Body

Coefficient K_ϕ, determined by formula (2.184), depends on angle β_i right up to its value of β_{imax}, which can be produced from the equation

$$\cos\beta_{i\max} = 1 - 2\left(\frac{T^0_a}{T^0_к}\right)^4.$$

Where $\beta_i > \beta_{imax}$, coefficient $K_\phi = 1$; therefore, the permissible relative error $\delta\phi^0_{ik}$ where $\beta_i > \beta_{imax}$ remains constant and can be taken as the limiting value for the fixed value of error δT^0_a.

Examples of the use of the results produced will be presented in § 10.10. Here we note one interesting peculiarity: the value of $\delta\phi^0_{ik} = -1$ shows that the imitation of the radiation of the surface of the celestial body is not required; here, the error in spacecraft temperature during testing will not exceed the permissible value δT^0_a. /132

If the heat-physical characteristics of the spacecraft are known (i.e., coefficient K_ϕ is known), the permissible imitation error of the mean irradiance factor may be easily determined by formula (2.182) or the graphs presented in Figure 64.

10.6. Permissible Errors in Value, Spectral Composition and Homogeneity of Radiant Flux Imitating Solar Radiation

The permissible relative error δS_0 in the quantity of radiation imitating solar radiation can be found if equation (2.75) is written twice -- for a spacecraft in flight (where solar radiation is S_0) and for the spacecraft in the vacuum chamber [where the radiation imitating the solar radiation $S^k_0 = S_0(1 + \delta S_0)$],

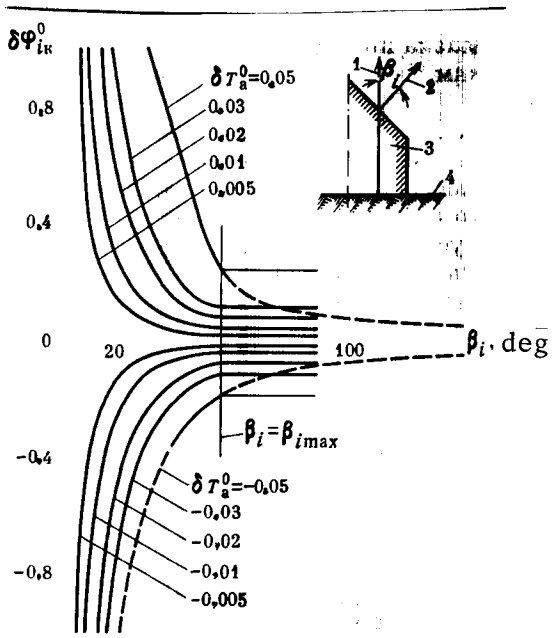

Figure 71. Permissible Relative Error in Irradiance Factor $\delta\phi^0_{ik}$ of Spacecraft as a Function of Angle β_i for Various Values of Permissible Relative Error δT^0_a: 1, Perpendicular to Surface of Celestial Body; 2, Perpendicular to Spacecraft Surface; 3, Spacecraft; 4, Celestial Body

Coefficient K_ϕ, determined by formula (2.184), depends on angle β_i right up to its value of β_{imax}, which can be produced from the equation

$$\cos\beta_{i\max} = 1 - 2\left(\frac{T^0_a}{T^0_k}\right)^4.$$

Where $\beta_i > \beta_{imax}$, coefficient $K_\phi = 1$; therefore, the permissible relative error $\delta\phi^0_{ik}$ where $\beta_i > \beta_{imax}$ remains constant and can be taken as the limiting value for the fixed value of error δT^0_a.

Examples of the use of the results produced will be presented in § 10.10. Here we note one interesting peculiarity: the value of $\delta\phi^0_{ik} = -1$ shows that the imitation of the radiation of the surface of the celestial body is not required; here, the error in spacecraft temperature during testing will not exceed the permissible value δT^0_a. /132

If the heat-physical characteristics of the spacecraft are known (i.e., coefficient K_ϕ is known), the permissible imitation error of the mean irradiance factor may be easily determined by formula (2.182) or the graphs presented in Figure 64.

10.6. Permissible Errors in Value, Spectral Composition and Homogeneity of Radiant Flux Imitating Solar Radiation

The permissible relative error δS_0 in the quantity of radiation imitating solar radiation can be found if equation (2.75) is written twice -- for a spacecraft in flight (where solar radiation is S_0) and for the spacecraft in the vacuum chamber [where the radiation imitating the solar radiation $S^k_0 = S_0(1 + \delta S_0)$],

taking all remaining heat-physical characteristics of the surrounding medium unchanged, the expressions produced are substituted into equation (2.166) and it is solved for δS_0, considering the permissible relative error in spacecraft temperature δT_a^0 fixed. Then

$$\delta S_0 = \frac{(1+\delta T_a^0)^4 - 1}{K_S} = \frac{(1+\Delta T_a^0/T_a^0)^4 - 1}{K_S} \approx \frac{4\delta T_a^0}{K_S}, \tag{2.185}$$

where

$$K_S = \frac{S_0 \sum_{i=1}^{n} F_i \varepsilon_{ci} S_{sk} [(\Phi_\varepsilon/\varepsilon_{ci}) - (1/\varepsilon_{c.ai})]}{C_0 (T_a^0/100)^4 \sum_{i=1}^{n} F_i \varepsilon_{ci}}. \tag{2.186}$$

The results of calculation of the permissible relative error δS_0 by formula (2.185) is a function of coefficient K_S for various values of permissible relative error δT_a^0 of spacecraft temperature during testing are presented in Figure 64.

If the heat-physical characteristics of the spacecraft are unknown, error δS_0 in the radiation of an imitator designed for testing of any spacecraft including cases when the most rigid requirements are placed on accuracy of imitation, should not be greater than values for which the error in temperature of such a spacecraft exceeds the maximum permissible error. Analysis of formula (2.185) and the graphs presented in Figure 64 shows that this limiting case corresponds to the maximum possible value $K_S = 1$. Figure 65 presents the results of calculation of the permissible relative error δS_0 for $K_S = 1$ as a function of permissible errors in spacecraft temperature δT_a^0 and ΔT_a^0 for various values of temperature T_a^0. For any other spacecraft, the permissible value of δS_0 is produced by dividing the values of δS_0 presented in Figure 65 by coefficient K_S, corresponding to the given specific spacecraft (usually $K_S < 1$).

angle α_S, the question arises of the possibility of using such fluxes for terrestrial thermal testing of spacecraft.

In order to answer this question, we must determine the permissible angle of divergence of the radiation flux α_k, i.e., the angle at which the relative error in spacecraft temperature during testing will not exceed the permissible value δT_a^0. With this purpose in mind, we write equation (2.75) twice -- for a spacecraft in flight and for a spacecraft in a vacuum chamber where the angle of divergence of the radiation flux α_k differs from angle of divergence α_S, while all other heat-physical characteristics of the spacecraft, surrounding medium and irradiance factors between them correspond to flight conditions. Substituting these relationships into (2.166), we will produce

$$C_0\left(\frac{T_a^0}{100}\right)^4 [(1+\delta T_a^0)^4 - 1] \sum_{i=1}^{n} F_i \varepsilon_{ci} = S_0 \sum_{i=1}^{n} F_i \varepsilon_{ci}\left(\frac{S_i^K}{S_0} - \frac{S_i^0}{S_0}\right)\left(\frac{\Phi_\varepsilon}{\varepsilon_{ci}} - \frac{1}{\varepsilon_{ci}}\right). \quad (2.189)$$

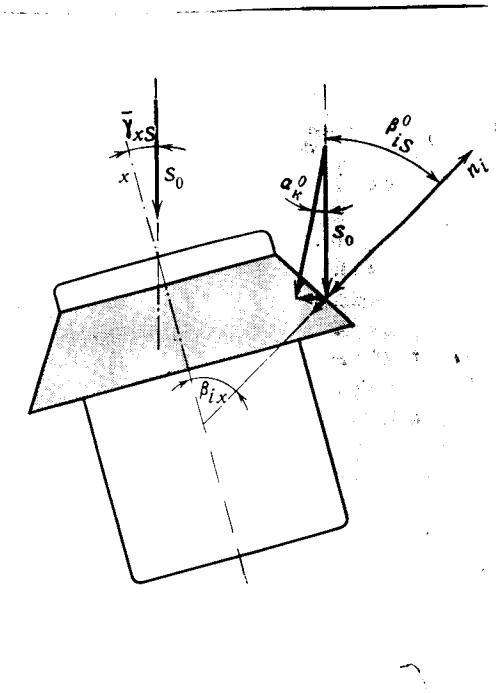

Figure 72. Determination of Permissible Angle α_k of Divergence of Radiant Flux Imitating Solar Radiation

The difference $(S_i^K/S_0) - (S_i^0/S_0)$ included in this equation can be defined as follows (see Figure 72):

$$\frac{S_i^K}{S_0} - \frac{S_i^0}{S_0} = (\cos\beta_{iS}^K - \cos\beta_{iS}^0) + (\sin\beta_{iS}^K \operatorname{tg}\alpha_K - \sin\beta_{iS}^0 \operatorname{tg}\alpha_S), \quad (2.190)$$

where β_{iS}^0 is the angle between normal n_i to the ith surface and the direction to the sun S_0. /134

Due to the practical unavoidance of a mismatch in the construction axes of the spacecraft (x, y, z)

and its main axes of inertia, the value of angle β_{iS}^{0} is not constant in flight even if the spacecraft spins arouns some one of its axes, precisely oriented in space at the moment the spin was started (for example, relative to the x axis, see Figure 72).

Due to this, angle β_{iS}^{0} can be conveniently represented as:

$$\bar{\beta}_{iS}^{0} = \beta_{ix} + \bar{\gamma}_{xS},$$

where β_{ix} is the angle between normal n_i and the x axis of the spacecraft; $\bar{\gamma}_{xS}$ is the mean (over the period of oscillations of the spacecraft) value of the angle between the x axis and the direction to the sun, characterizing the inaccuracy of orientation of the spacecraft in space.

If expression (2.190) is substituted into equation (2.189) and the equation produced is solved for tan α_k (keeping in mind that tan $\alpha_S \approx 0$), we can produce the following formula for determination of the permissible angle of divergence α_k of the radiant flux:

$$\alpha_K = \arctan\left[\frac{(1+\delta T_a^{0\,4}-1}{K_\alpha} + K_\gamma\right], \tag{2.191}$$

where

$$K_\alpha = \frac{\sum_{i=1}^{n} F_i \varepsilon_{ci}\left(1-\frac{1-A_i}{\Phi_S}\right)\left(\frac{\Phi_\varepsilon}{\varepsilon_{ci}}-\frac{1}{\varepsilon_{C.ai}}\right)}{C_0 (T_a^0/100)^4 \sum_{i=1}^{n} F_i \varepsilon_{ci}}, \tag{2.192}$$

$$K_\gamma = \left[\sum_{i=1}^{n} F_i \varepsilon_{ci}\left(1-\frac{1-A_i}{\Phi_S}\right)\left(\frac{\Phi_\varepsilon}{\varepsilon_{ci}}-\frac{1}{\varepsilon_{C.ai}}\right)\times \right.$$
$$\times(\cos\beta_{iS}^{K}-\cos\beta_{iS}^{0})\Big]\Big[\sum_{i=1}^{n} F_i \varepsilon_{ci}\left(1-\frac{1-A_i}{\Phi_S}\right)\times$$
$$\left.\times\left(\frac{\Phi_\varepsilon}{\varepsilon_{ci}}-\frac{1}{\varepsilon_{C.ai}}\right)\sin\beta_{iS}^{K}\right]^{-1}. \tag{2.193}$$

If the change in position of the spacecraft in space relative to the surrounding space medium were precisely imitated during testing, including its oscillations relative to the x, y, z axes and the change in direction to the sun, permissible angle α_k of divergence of the radiant flux would be determined only by the value of coefficient K_a and the permissible relative error δT_a^0, since in this case $\beta_{iS}^k = \beta_{iS}^0$ and $K_\gamma = 0$. However, most spacecraft are presently placed immobily in vacuum chambers, with no imitation of the oscillations about the axes of inertia, and one of the structural axes, for example the x axis, which is to be oriented toward the sun in flight, is oriented as accurately as possible with the direction of the radiant flux imitating solar radiation. Therefore, it can be considered that during testing $\bar{\gamma}_{xS} = \gamma_{xS}^0 = 0$, while in flight $\bar{\gamma}_{xS} = \gamma_{xS}^0$; consequently, $\beta_{iS}^k = \beta_{ix}$, and

$$(\cos\beta_{iS}^{\kappa} - \cos\beta_{iS}^0) = \\ = \sin\beta_{ix}\sin\bar{\gamma}_{xS}^0 - \cos\beta_{ix}(1 - \cos\bar{\gamma}_{xS}^0).$$

Since the second term in the last equation is slight in comparison with the first term right up to angles $\beta_{ix} = \bar{\gamma}_{xS}^0$, formula (2.191) becomes

$$\alpha_{\kappa} = \frac{\text{arc-}}{\tan}\left[\frac{(1+\delta T_a^0)^4 - 1}{K_\alpha} + \sin\bar{\gamma}_{xS}^0\right].$$

For angles α_k and $\bar{\gamma}_{xS}^0$ of not over 10°, the last formula for α_k can be finally written in following form:

$$\alpha_{\kappa} = \alpha_{\kappa}^0 + \bar{\gamma}_{xS}^0, \qquad (2.194)$$

where

$$\alpha_{\kappa}^0 = \frac{(1+\delta T_a^0)^4 - 1}{K_\alpha} \approx \frac{4\delta T_a^0}{K_\alpha}. \qquad (2.195)$$

The results of calculation of the permissible angle of divergence α_k^0 (in radians) of the radiant flux imitating solar radiation as a function of coefficient K_α for various values of /135

permissible relative error δT_a^0 of spacecraft temperature during testing are shown in Figure 64.

The value of angle $\bar{\gamma}_{xS}^0$ depends on the accuracy of the system of stabilization of the spacecraft in space, the correspondence between the intertial axes and the structural axes x, y and z about which "twisting" occurs and, obviously, can reach several degrees.

If the planned imitator is designed for testing of all spacecraft, the heat-physical characteristics of which are unknown, selection of a permissible angle of divergence α_k^0 must be based on the value $K_\alpha = 1$. Results of calculation of the limiting value of α_k^0 as a function of permissible errors δT_a^0 and ΔT_a^0 for various values of temperature T_a^0 are presented in Figure 65.

It is interesting to produce the dependence of the value of α_k^0 on the angle between the direction toward the sun and the perpendicular to the ith sector of the outer surface of the spacecraft. This can be easily done for surfaces defining the thermal state of the spacecraft. We have

$$K_\alpha = K_\alpha^\beta / \sin\beta_{iS}^0, \tag{2.196}$$

where

$$K_\alpha^\beta = \frac{\left(\dots - \frac{1 - A_i}{\dots}\right)(\Phi_e/\varepsilon_{ci} - 1/\varepsilon_{C.ai})}{C_0 (T_a^0/100)^4}. \tag{2.197}$$

Coefficient K_α, defined from this formula, depends on angle β_{iS}^0 right after the value $(\beta_{iS}^0)_{max}$, which can be produced from the equation

$$\sin(\beta_{iS})_{max} = \frac{1}{K_\alpha^\beta},$$

since coefficient K_α cannot 1.

With $\beta^0_{iS} < (\beta^0_{iS})_{max}$, coefficient $K_\alpha = 1$. Therefore, the permissible angle of divergence α_k with $\beta^0_{iS} > (\beta^0_{iS})_{max}$ remains constant and equal to the minimum value of α_{kmin} corresponding to the value $\beta^0_{iS} = (\beta^0_{iS})_{max}$.

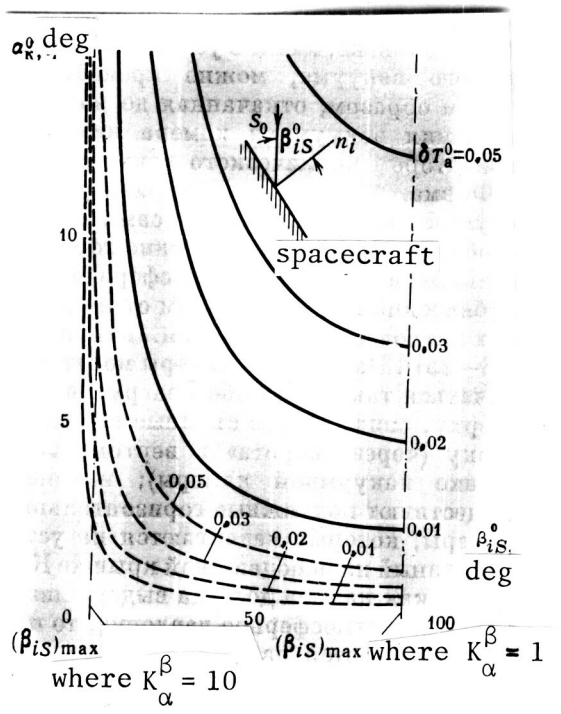

Figure 73. Permissible Angle α^0_k of Divergence of Radiant Flux Imitating Solar Radiation as a Function of Angle β^0_{iS} for Various Values of Permissible Relative Error δT^0_a as Coefficient K^β_α (Solid Lines: $K^\beta_\alpha = 1$, Dotted Lines: $K^\beta_\alpha = 10$)

The results of calculation of α^0_k is a function of angle β^0_{iS} for various values of permissible relative error δT^0_a and coefficient K^β_α are presented in Figure 73.

If the heat-physical characteristics of the spacecraft are known, i.e., factor K_α is known, the permissible angle of divergence of the radiant flux α^0_k upon imitation of a given specific spacecraft can be easily determined by formula (2.191) or the graphs presented in Figure 64. /136

10.8. Space Vacuum Imitators

Imitation of the heat exchange of the spacecraft with the surrounding space gas medium during terrestrial thermal testing is achieved by placing the spacecraft in a vacuum chamber, the pressure of which is so slight that the influence of heat exchange of the spacecraft with the residual gas on its thermal state can be ignored, as is the case in the vacuum of space. Thus, the vacuum chamber, evacuated to a low pressure, imitates the vacuum of space.

The shape, placement and dimensions of vacuum chambers may vary widely: cylindrical horizontal and vertical, spherical, cubic, etc., with volumes of a few liters to 100,000 m^3 (for example, see [23-25]). Vacuum chambers may also differ in the method of insertion of the spacecraft: through the top, through the bottom (through removable covers), from the side (through "gates" in the vertical wall of the vacuum chamber); finally, there are mobile horizontal chambers, which are placed around a

spacecraft installed on a nonmoving cover.

Since the chamber must withstand the outside atmospheric pressure, it is made of strong metals, the properties of which must satisfy a number of requirements. The most important of these is the gas liberation rate of the chamber material at low pressures (on the order of 10^{-2} torr), which must be minimal.

The most suitable material for vacuum chambers is stainless steel: its gas liberation rate after 10 hours evacuation is on the order of $1 \cdot 10^{-8}$ torr$\cdot$sec$^{-1}\cdot$scm^{-2} (for anodized aluminum, $1 \cdot 10^{-7}$ torr$\cdot$sec$^{-1}\cdot$cm^{-2}); it does not oxidize upon exposure to the atmosphere and has lower permeability than ordinary steel, is easily polished and worked. Chambers are welded in a protective gas medium (helium or argon), decreasing leakage of gas from the atmosphere into the vacuum chamber through welded seams.

In addition to gas liberation, gas also flows in through the seals of various elements of the vacuum chamber (flanges, covers, electric leads, etc.); therefore, special seals must be used which assure minimum leakage.

Usually, two types of seals are used -- organic and metallic. For small vacuum chambers, requiring vacuums of lower than 10^{-8} torr, metal seals must be used, since they have low gas liberation rate and withstand high temperatures (about 450° C), to which the chamber must be heated in order to increase the outgassing rate of its internal surface during the initial period of evacuation. Metal seals are made of aluminum, copper, silver and gold. The primary shortcomings of these seals are their unsuitability for repeated (or at least multiple repeated) use, and the need to use tremendous numbers of bolts to compress large covers and flanges. Therefore, organic and polymer materials are most frequently used; the initial gas liberation rates of some of these materials are presented in Table 6.

TABLE 6

Sealing Material	Gas Liberation Rate, Torr$\cdot$sec$^{-1}\cdot$cm^{-2}
Silicone rubber	$7 \cdot 10^{-6}$
Nylon	$2.6 \cdot 10^{-6}$
Natural rubber	$1.2 \cdot 10^{-6}$
Teflon	$2 \cdot 10^{-7}$

The seals usually have O-shaped cross section and are placed /137
ina slot in one flange, most frequently the nonmoving flange; two concentric seals are used for large flanges, and the space between them is evacuated to a pressure on the order of 10^{-2} torr by a vacuum pump separate from the main pump system.

Achievement of pressures of 10^{-5}-10^{-6} torr requires a number of different types of vacuum pumps, since none can produce evacuation to a pressure of 10^{-6} torr alone.

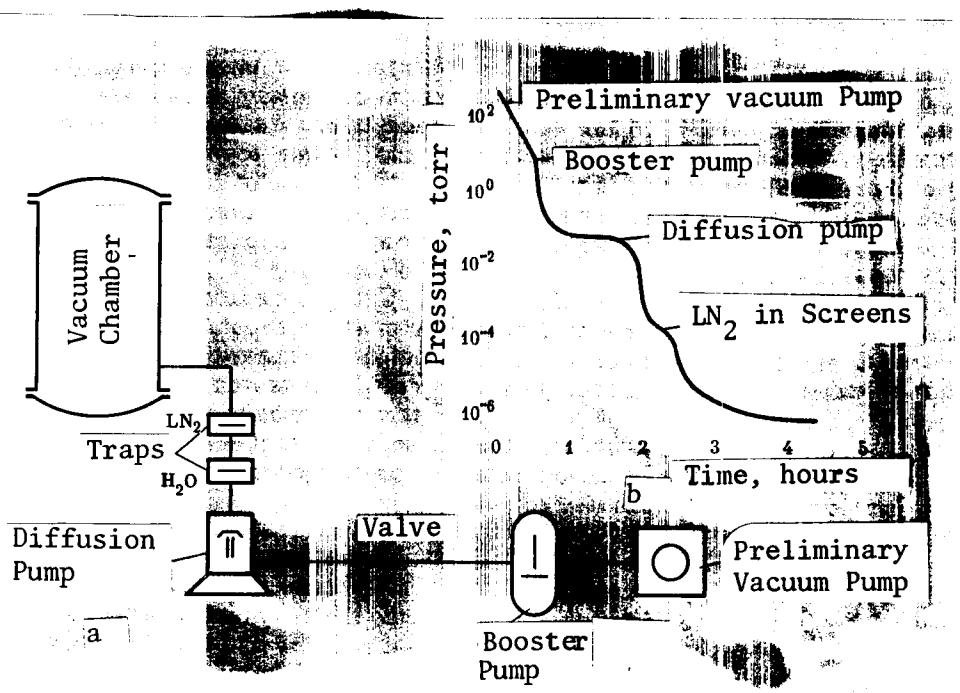

Figure 74. Diagram of Vacuum System and Typical Evacuation Rate Curve of the System

Figure 74a shows a diagram of a vacuum system consisting of a preliminary vacuum pump, booster pump and diffusion pump. The first pump reduces the pressure to 10^{-2} torr, the second to 10^{-3} torr, andthe last (which is turned on after a pressure of 10^{-2} torr is reached) reduced the pressure to 10^{-5}-10^{-6} torr and lower.

A typical evacuation rate curve of such a vacuum system is shown in Figure 74b. The limits of working pressures of some of the pumps used at the present time are presented in Table 7.

In addition to the working pressure limits, another important characteristic of vacuum pumps is their productivity, usually expressed as the volume of gas evacuated per unit time (ℓ/sec) at a defined pressure.

The productivity of diffusion pumps lies between a very few and 100,000 ℓ/sec (corresponding to output aperture diameters of

25 to 1300 mm). The main shortcoming of these pumps is that as they operate, a portion of the oil (about 0.03 $mg \cdot cm^{-2} \cdot sec^{-1}$) enters the vacuum chamber and is precipitated on various surfaces. To eliminate this, traps are installed before the intake of the vacuum pump (Figure 74a), cooled with water or liquid nitrogen, and the oil vapor precipitates on the surface of the trap, without entering the vacuum chamber, condenses and flows back into the pump; however, this reduces the productivity of the pump by about 60%. /138

TABLE 7

Type of Pump	Pressure (torr)
	10^{1} 10^{0} 10^{-1} 10^{-2} 10^{-3} 10^{-4} 10^{-5} 10^{-6} 10^{-7} 10^{-8}
Mechanical (preliminary vacuum)	
Booster	
Diffusion	
Molecular	
Sublimation (titanium)	
Ion	
Freezing (cryopumps)	

Molecular pumps do not share this shortcoming of diffusion pumps, but are rarely used due to their low productivity.

The operating principle of sublimation (titanium) pumps consists in the capability of titanium precipitated (after evaporation) onto a cold surface, to form chemical compounds with H_2, O_2, N_2 and CO_2. A productivity of about 20,000 ℓ/sec is easily produced in chambers of medium size. The shortcoming of this type of pump is the inability of titanium to absorb the noble gasses.

Ion pumps [25] evacuate all gasses and are most frequently used in combination with sublimation pumps. Ion pumps have productivities of around 5,000 ℓ/sec and are usually used in chambers of medium size.

If any surface within the vacuum chamber has a low temperature, many gasses will condense (freeze) on the surface: at a temperature of 20 K (cooling by liquid hydrogen) all gasses with the exception of Ne, He and H_2 freeze, while at 4 K (cooled by liquid helium) all of the noble gasses freeze, even hydrogen.

Using these pumps (sometimes called cryopumps) productivities on the order of 10^6 ℓ/sec can be achieved.

It should be noted that the free space imitator, consisting

of screens cooled with liquid nitrogen (LN_2) is actually a cryopump for CO_2 and H_2O. More detailed descriptions of pumps and their characteristics are presented in [26 and 27].

10.9. Free Space Radiation Imitators

The radiation of free space corresponds to the radiation of an absolutely black body ($\varepsilon_0 = 1$) at $T_k \approx 4$ K, i.e., the thermal radiation of the surface of the spacecraft and the solar radiation reflected from it do not return to it. In order to imitate these conditions of heat exchange, screens consisting of a number of panels usually made of aluminum or stainless steel and cooled to a very low temperature are placed between the spacecraft and the internal surface of the vacuum chamber. Typical diagrams of such imitators are shown in Figure 75.

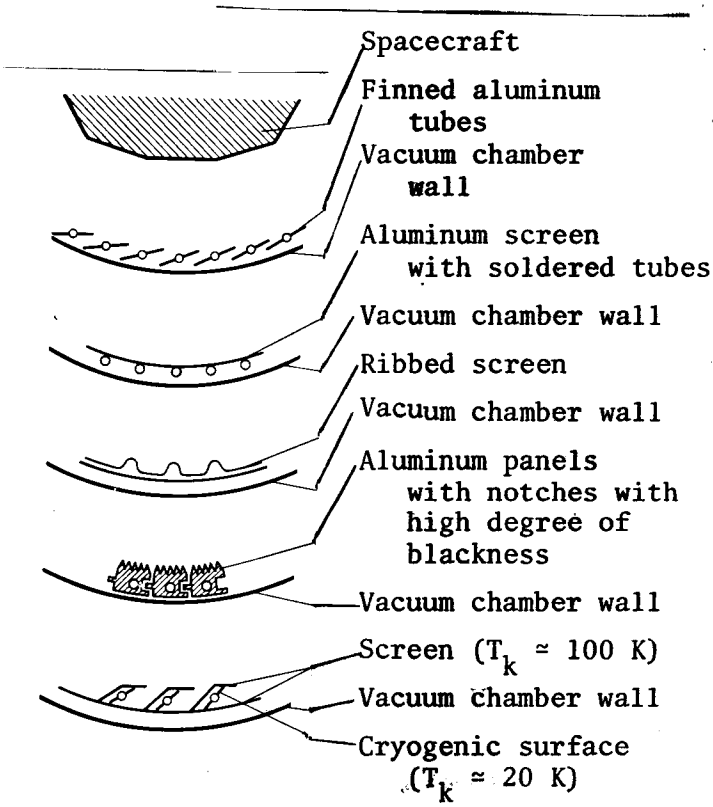

Figure 75. Diagrams of Free Space Radiation Imitators

The surface of the screens turned toward the chamber wall should be polished (in order to produce low radiation factors), while the surface turned toward the spacecraft should have a high degree of blackness ε_k to decrease the reflection of the radiation which strikes it. This is achieved by anodizing (for aluminum) or painting; the achieved values of $\varepsilon_k = 0.9$-0.95. Further increases in degree of blackness ε_k are possible only by creation of multiple reflection and absorption of the radiation striking the screens. Sometimes a number of uncooled screens with surface degree of blackness $\varepsilon_k = 0.1$ are placed between the cooled screens and the walls of the vacuum chamber in order to decrease heat exchange between them.

Screen panels are usually cooled by the evaporation of liquid nitrogen (LN_2). There are two main systems of panel cooling: open and closed. In the open system (Figure 76a), the

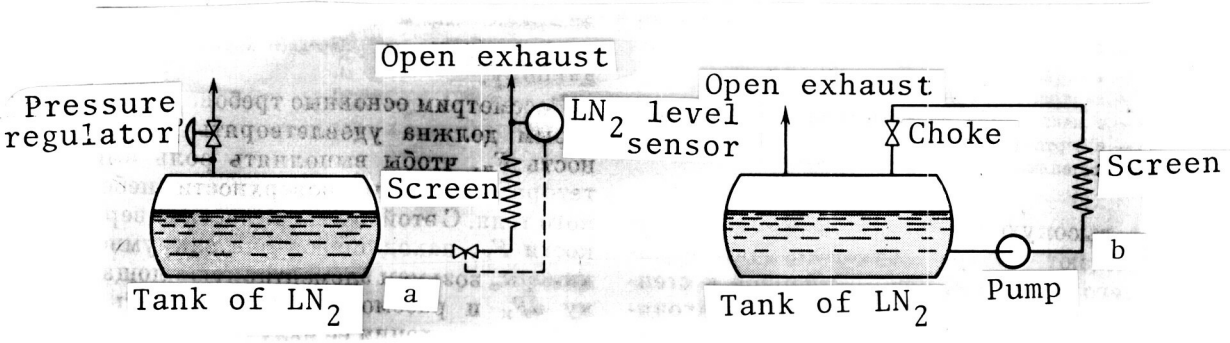

Figure 76. Open (a) and Closed (b) Systems of of Cooling Screen Panels

panels are cooled by the heat of evaporation of liquid nitrogen LN_2 (47.5 kcal/kg) fed to them under the influence of the pressure difference between the LN_2 tank and the atmosphere.

One shortcoming of the open system is the possibility of local overheating due to thr formation of gas bubbles. These systems are used only for small chambers (up to 2 m diameter).

In the closed system (Figure 76b), the panels are cooled by heating of LN_2 (not over 10° C). The LN_2 is pumped through the panels and the pressure in the system (on the order of 5 atm) is maintained by a pump. After passing through the choke, a portion of the LN_2 (4-5%) is evaporated, carrying away the heat produced in the panels; the recooled liquid nitrogen LN_2 is returned to the tank, the evaporated nitrogen is exhausted to the atmosphere. Usually the ratio of LN_2 evaporated to LN_2 recirculated for medium-sized chamber (2-5 m diameter) is 1:25. /140

In order to decrease heat losses, particular attention must be given to mounting points and points of connection of pipes with the vacuum chamber. For this purpose, thin-wall pipes of stainless steel, with low heat conductivity, high strength and high surface smoothness, are placed within another pipe of larger diameter, connected to the wall of the vacuum chamber, and the gas in the space between them is evacuated by the main vacuum system or a separate pump to a pressure of 10^{-2}-10^{-3} torr.

10.10. Devices Imitating the Radiation of the Surface of a Celestial Body

During terrestrial thermal testing of spacecraft, the radiation of the surface F_k of a celestial body must be reproduced (Figure 77). This is achieved by the radiation of surface F_i,

placed within the vacuum chamber. This radiation must agree quite closely in magnitude, direction and spectral composition with the actual radiation being imitated.

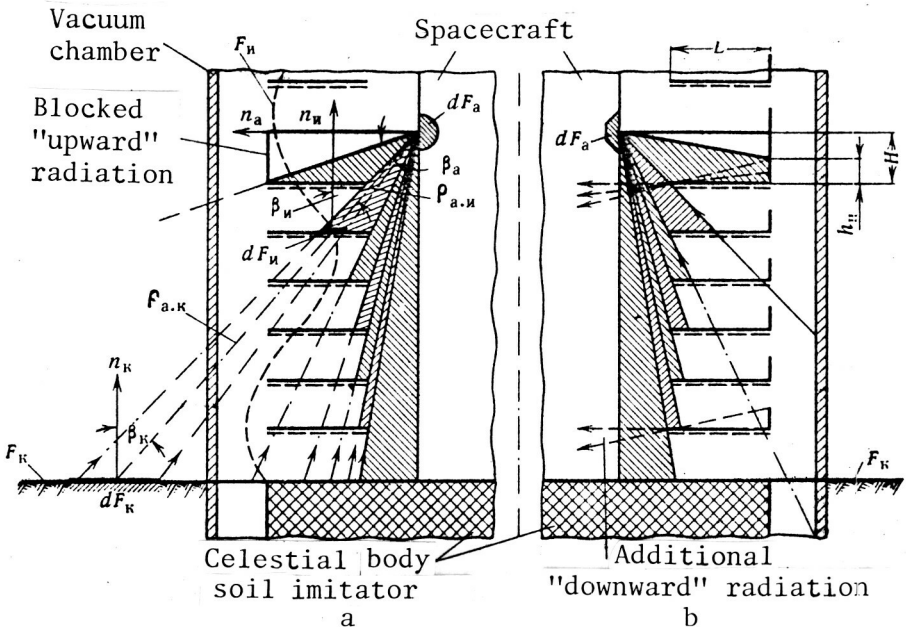

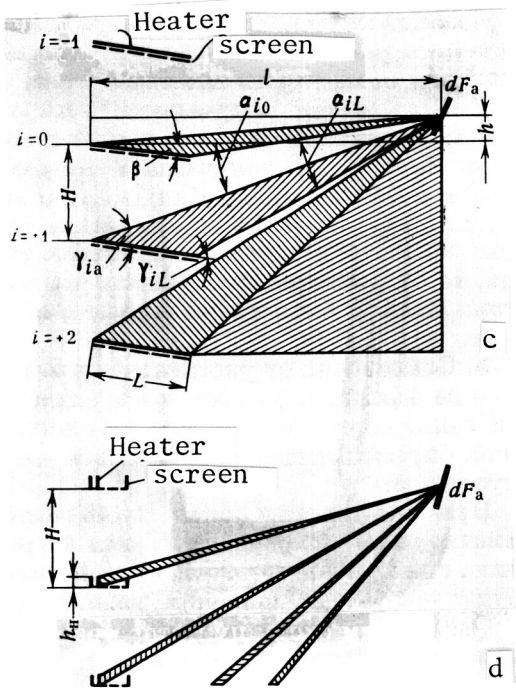

Figure 77. Diagrams of Celestial Bodies Surface Radiation Imitators: a, With Horizontal Heaters; b, With Corner Heaters; c, With Inclined Heaters; d, With Vertical High Temperature Heaters

Let us study the primary requirements which must be satisfied by surface F_1 in order to act as an imitator of the radiation of the surface of a celestial body. For this purpose, let us select a portion of surface F_k located outside the vacuum chamber and take an elementary area dF_k and study the possibility and conditions of imitation of its radiation.

The solid angle within which area dF_k is enclosed, if it is observed from area dF_a selected on the surface of the spacecraft, which is defined by the formula /141

(see § 5.3)

$$d\omega^{k}_{dF_a} = \frac{dF_k \cos \beta_k}{\rho^2_{ak}},$$

passing through surface F_i, cuts out elementary area dF_i on this surface. The solid angle over which this area will be visible from element dF_a is determined by the similar formula

$$d\omega^{i}_{dF_a} = \frac{dF_i \cos \beta_i}{\rho^2_{ai}},$$

In these formulas, ρ_{ak}, ρ_{ik} represent the distances between area dF_a and areas dF_k and dF_i respectively; β_k and β_i are the angles between perpendiculars to areas dF_k and dF_i and the direction to area dF_a respectively.

Obviously, $d\omega^{k}_{dF_a} = d\omega^{i}_{dF_a}$. Using this equation, let us find the size of area dF_i, imitating the radiation of area dF_k within the same solid angle:

$$dF_i = dF_k \left(\frac{\rho_{ai}}{\rho_{ak}}\right)^2 \frac{\cos \beta_k}{\cos \beta_i}.$$

The elementary heat fluxes transmitted by areas dF_k and dF_i to area dF_a are defined by the following equations (see § 5.4)

$$dE_{к.a} = \frac{C_0}{\pi} \varepsilon_к \left(\frac{T_к}{100}\right)^4 dF_к \cos \beta_к d\omega^{a}_{dF_к},$$

$$dE_{ia} = \frac{C_0}{\pi} \varepsilon_i \left(\frac{T_и}{100}\right)^4 dF_i \cos \beta_i d\omega^{a}_{dF_i},$$

where $d\omega^{a}_{dF_a}$ and $d\omega^{a}_{dF_i}$ are the solid angles defined by the formulas

$$d\omega^{a}_{dF_к} = \frac{dF_a \cos \beta_a}{\rho^2_{a.к}}, \quad d\omega^{a}_{dF_i} = \frac{dF_a \cos \beta_i}{\rho^2_{ai}}.$$

From the condition of compatibility of radiant fluxes (see § 5.5) it follows that $dE_{ka} = dE_{ia}$; using this equation, we can produce the following expression for [illegible] perature of area dF_i:

$$\left(\frac{T_i}{100}\right)^4 = \frac{\varepsilon_к}{\varepsilon_i}\left(\frac{T_к}{100}\right)^4 \frac{dF_к}{dF_i}\frac{\cos\beta_к}{\cos\beta_i}\frac{\rho_{ai}^2}{\rho_{ak}^2}. \qquad (2.199)$$

Substituting (2.198) into (2.199), we produce

$$\left(\frac{T_i}{100}\right)^4 = \frac{\varepsilon_к}{\varepsilon_i}\left(\frac{T_к}{100}\right)^4.$$

Analysis of the permissible error in the degree of blackness of the imitator of the surrounding space medium (see § 10.3) indicates that $\varepsilon_i \simeq \varepsilon_k$.

We then finally produce

$$T_i \simeq T_k. \qquad (2.200)$$

We can see from expression (2.198) that the radiation of surface element dF_k of a celestial body located at distance ρ_{ak} from the spacecraft, which distance significantly exceeds the diameter of the vacuum chamber, can be replaced by the radiation of a surface element dF_i located within the vacuum chamber at distance ρ_{ai} from the spacecraft, the area of which is $(\rho_{ak}/\rho_{ai})^2$ times less than the actual area dF_k. /142

It is possible in principle to imitate the radiation of an elements of surface dF_k by an element of surface dF_i, the area of which is significantly less than that required by formula (2.198), but in this case the temperature of the element of surface dF_i must be significantly higher than the temperature of the surface of the celestial body.

However, the difference in spectral composition of the radiation produced in this case from the actual radiation as a result of the displacement of the maximum on the spectral radiation curve in the direction of shorter wavelengths (see § 5.3) and the greater unevenness of radiation resulting from the need to separate the individual radiating elements from each other by

some considerable distance may cause impermissibly great errors in spacecraft temperature produced in the tests.

In order for surface element dF_i to radiate in the same (and only the same) directions as an element of the actual surface, it is necessary that angles β_k and β_i between the perpendiculars to areas dF_k and dF_i and the fixed directions be equal, i.e., if area dF_k is horizontal, area dF_i which imitates its radiation must also be horizontal.

In principle, the radiation of the horizontal surface in a given direction can be imitated by a vertical surface; however, in this case radiation appears which is absent under the actual conditions, and special design measures must be taken to eliminate it. The permissible degree of deviation of the position of area dF_i from the position of area dF_k must be defined on the basis of the condition of the permissible influence of additional radiation, absent under actual conditions, on the spacecraft temperature (see below).

Obviously, the radiation of the entire surface F_k of the celestial body can be replaced by radiation of surface F_i, also located within the vacuum chamber around the spacecraft.

It follows then that the device imitating the radiation of the surrounding space medium must satisfy the following basic requirements.

1. The temperature and degree of blackness of the radiating surface of the imitator must be equal to the temperature and degree of blackness of the surface of the celestial body.

2. The position of the radiating surface of the imitator must correspond to the position of the radiating surface of the celestial body. For example, if we must imitate the radiation of a horizontal surface, the radiating surface of the imitator must also be horizontal.

3. Deviations from these requirements should not lead to errors in spacecraft temperature during the time of the testing exceeding the maximum permissible error.

If these requirements are fulfilled, the imitating radiation will correspond in direction, spectral composition and magnitude to the actual radiation.

Let us study a diagram of a device designed to imitate the radiation of the surrounding space medium which satisfies these requirements.

Imitation of the radiation of the entire surface of a celestial body can be achieved by a set of horizontal strips located at a certain distance from each other (see Figure 77a), each of which consists of two parts, separated by thermal insulation: an upper part, heated to the temperature of the surface T_k (heater) and a lower part, which has the temperature and degree of blackness of the free space imitator (screen).

Due to the finite dimensions of each heater (width L), the radiation of the sections of the surface of the celestial body most distant from the spacecraft will not be imitated (unshaded areas on Figures 77a, b). This deficiency in heat flux can be made up by two methods. /143

The first method (see Figure 77b, c) consists in that the heater is either made in two parts, a horizontal (main) part of width L and a vertical (supplementary) part of height h_H, or the horizontal heater is rotated downward by angle β, determined by the formula $\tan \beta = h_H/L$. (obviously, the radiation of the inclined surface is equal to the radiation of a corner heater). In both these cases, the radiation of more distant sections of the surface of the celestial body is imitated without increasing dimensions (width L). The second method consists in that the temperature of the horizontal heaters is increased to a quantity not exceeding the permissible temperature.

Let us study these two methods in more detail.

The irradiance factor of the vertical surface dF_a, the height of which is equal to the distance between the horizontal plates, with an imitator of this type can be determined by the formula

$$\varphi_{ak} = \frac{1}{2}\left[1 + \sqrt{\left(\frac{h_H}{H}\right)^2 + \left(\frac{L}{H}\right)^2} - \sqrt{\left(1 - \frac{h_H}{H}\right)^2 + \left(\frac{L}{H}\right)^2}\right] \quad (2.201)$$

The results of calculation of φ_{ak} using this formula are presented in Figure 78a, from which we can see that where $h_H/H = 0.5$, irradiance factor $\varphi_{ak} = 0.5$, i.e., for the given surface dF_a an imitator of this type absolutely precisely imitates the radiation of the real infinite surface (for example, the surface of the moon) both as to magnitude and as to spectral composition of the radiation.

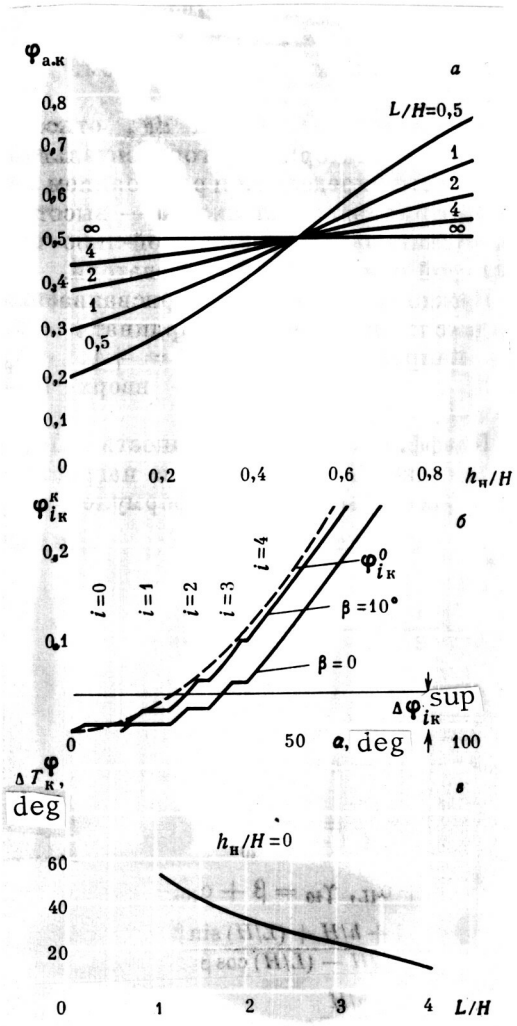

Figure 78. Irradiance Factor ϕ_{ak} of Vertical Surface of Height H of Imitator with Corner Heaters (a), Irradiance Factor $\phi^{к}_{ik}$ of Imitator Plate with Inclined Heaters (b) and Dependence of $\Delta T^{\phi}_{к}$ on L/H Ratio (c)

However, a vertical heater (or an inclined horizontal heater) will also produce "downward" radiation (see Figure 77b, c), leading to errors $\Delta\phi_{ak}$ for the surface, /144 the angle between perpendicular n_a to which and perpendicular n_k to the surface of the celestial body is not equal to 90°. Therefore, permissible height h_H of the supplementary vertical heater must be selected from the condition of production of error $\Delta\phi_{ak}$ not over the permissible value with any angle of inclination of the surface dF_a.

With this purpose in mind, let us determine the irradiance factor of plate dF_a with a device imitating the radiation of the surface of a celestial body as a function of the angle of its inclination to the horizon α, angle of rotation of horizontal heaters β, their width L and the distance between them H (see Figure 77c).

The position of plate dF_a relative to the imitator in the horizontal plane is determined by distance ℓ, a in the vertical plane -- height h read from any initial axis of rotation of the heater.

Each heater is assigned subscript i: at the coordinate origin i = 0, in the direction downward i = +1, +2, +2,..., in the direction upward i = -1, -2, -3,...

The irradiance factor $\Delta\phi_{ik}$ of plate dF_a with each of the heaters is calculated by the formula

(2.202)

where

$$\varphi_{iL} = \frac{1}{2}(1 - \cos\gamma_{iL}) = \frac{1}{2}\left(1 - \frac{1}{\sqrt{1 + \operatorname{tg}^2\gamma_{iL}}}\right),$$

$$\varphi_{i0} = \frac{1}{2}(1 - \cos\gamma_{i0}) = \frac{1}{2}\left(1 - \frac{1}{\sqrt{1 + \operatorname{tg}^2\gamma_{i0}}}\right),$$

$$\gamma_{iL} = \beta + \alpha_{iL},\ \gamma_{i0} = \beta + \alpha_{i0},$$

$$\tan\alpha_{iL} = \frac{i + h/H + (L/H)\sin\beta}{l/H - (L/H)\cos\beta},$$

$$\tan\alpha_{i0} = \frac{i + h/H}{l/H}.$$

The summary irradiance factor ϕ_{ik}^{k} of plate dF_a with the heaters of the imitator is determined by the formula

$$\varphi_{iK}^{K} = \sum_{i=0}^{+\infty} \Delta\varphi_{iK}. \qquad (2.203)$$

As an example, Figure 78b shows the results of calculation of ϕ_{ik}^{k} as a function of angle of inclination α of plate dF_a for angles of inclination of heaters $\beta = 0$ and $\beta = 10°$ where $L/h = 1$, $\ell/L = 5$ and $h/H = 0$ (see Figure 77c). Here also for comparison is the curve of irradiance factor ϕ_{ik}^{0} of plate dF_a with the actual surface of the celestial body (dotted line).

The design of the imitator is selected properly if the error in irradiance factor $\Delta\phi_{ik}^{0} = \phi_{ik}^{0} - \phi_{ik}^{k}$ does not exceed the permissible value calculated by formula (2.182); for the defining surface of the spacecraft it becomes

$$\delta\varphi_{iK}^{0} = \frac{\Delta\varphi_{iK}^{0}}{\varphi_{iK}^{0}} = \frac{1 + \delta T_a^0)^4 - 1}{(T_K^0/T_a^0)^4\varphi_{ik}^0}. \qquad (2.204)$$

Since the maximum value of ratio $T_k^0/T_a^0 = 1$, with permissible relative error in the temperature of the spacecraft during testing

$\delta T_a^0 = 0.01$, the permissible absolute error in irradiance factor $\Delta\phi_{ik}^0 = 0.04$.

Analysis of the graphs presented in Figure 78d shows that with an angle of inclination of the heaters of the imitator $\beta \simeq 10°$ (or, which amounts to the same thing, with a ratio $h_H/L = 0.2$), the error in the irradiance factor of any surface of the spacecraft with the imitator and, consequently, the error of the mean irradiance factor of the spacecraft, will not exceed the permissible value $\Delta\phi_{ik}^{per} = 0.04$.

With the second method of "making up" the shortage of radiation from the most distant sectors of the surface of the celestial body, the required increase in the temperature of the horizontal heaters ($\beta = 0$) by ΔT_k^ϕ is determined by the expression /145

$$\Delta T_к^\varphi = T_к^к - T_к^0 = [(\varphi_{iк}^0/\varphi_{iк}^к)^{1/4} - 1]\, T_к^0. \qquad (2.205)$$

The dependence of ΔT_k^ϕ on the L/H ratio is shown in Figure 78c (where $T_k^0 = 396$ K).

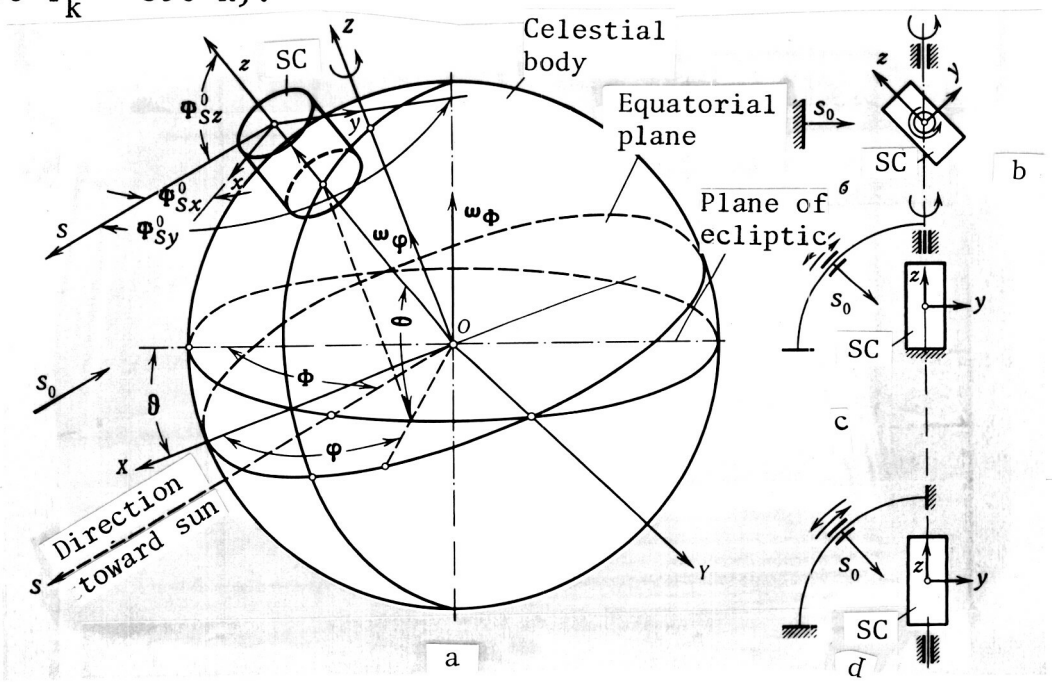

Figure 79. Orientation of Spacecraft Relative to Solar Radiation: a, On Surface of Celestial Body; b, In Vacuum Chamber (Imitator Immobile, Spacecraft Rotates Relative to Two Axes); c, In Vacuum Chamber (Spacecraft Immobile, Imitator Rotates Relative to Two Axes); d, In Vacuum (Imitator Rotates Relative to Horizontal Axis, Spacecraft Relative to Vertical Axis)

The increase in the temperature of the horizontal heaters by ΔT_k^{ϕ} disrupts the requirement of equation (2.200) and somewhat changes the spectral composition of the radiation of the imitator in comparison to the actual surface. However, based on the displacement law of Wien and the dependence of absorption factor on wavelength of incident radiation for coatings used in space technology, it can be shown that an increase in the temperature of the heaters of 50 to 60° C in comparison to the temperature of the surface of a celestial body causes practically no change in the spectral composition of the radiation, while the absence of radiation striking inclined surfaces near horizontal can be permissible if the spacecraft is placed at a distance of (2-3) L from the section of the imitator (where $L/H \approx 1$).

Based on similar calculations, we can show that imitators with vertical heaters alone with H/h_H = 10-30 (see Figure 77d), as well as various infrared bulbs located at some distance from each other, cannot be used to imitate the thermal radiation of a celestial body, since due to their high temperature, defined by equation (2.199), the spectral composition of their radiation differs so greatly from the spectral composition of the radiation of an actual surface that the error in spacecraft temperature may reach dozens of degrees. For example, for a white coating at a temperature T_k^0 = 396 K and T_k^k = 800-1000 K, the heat flux absorbed by the surface of the spacecraft in the tests will be 40 to 50% less than the flux absorbed by the surface of the spacecraft resting on the surface of the moon at lunar noon, so that the spacecraft, although its temperature was permissible in testing, might be overheated under actual conditions. A description of certain other plans for celestial body surface radiation imitation is presented in [28-31]. /146

10.11. Solar Radiation Imitators

Any type of solar radiation imitator must rather precisely reproduce the intensity, angle of divergence and spectral composition of true solar radiation, since errors in these heat-physical characteristics at any point over the cross section of the flux imitating the solar radiation should not exceed the permissible values defined in § 10.6 and 10.7.

Orientation of the spacecraft relative to the radiation imitating solar radiation. In selecting any given plan for an imitator, one must keep in mind that the orientation of the spacecraft during various stages of flight relative to the direction of the radiation imitating the solar radiation and the thermal radiation of a celestial body must be reproduced with good accuracy. For certain spacecraft, designed to operate on the surface of a celestial body, the orientation relative to the direction of radiation must be reproduced while retaining the

actual direction of the force of gravity relative to the spacecraft. Therefore, it is necessary first of all to select a plan for solar radiation imitators allowing the required orientation of the spacecraft relative to the sources of radiation, and then to select from among possible plans those in which the erros in heat-physical characteristics of the radiation which they create are within the permissible limits.

Let us study the change in orientation of the spacecraft relative to the direction of solar radiation S_0 as it rests on the surface of a celestial body moving in orbit around the sun at angular velocity ω_Φ and rotating with angular velocity ω_ϕ (Figure 79a). The rectangular system of coordinates XYZ rotates together with the celestial body. The coordinate origin of this system O coincides with the center of the celestial body, the Z axis with its axis of rotation, and the Y axis with the line of intersection of the equatorial plane with the plane of the ecliptic, the angle between which is equal to ϑ. The direction to the sun is fixed by angle Φ in the plane of the ecliptic.

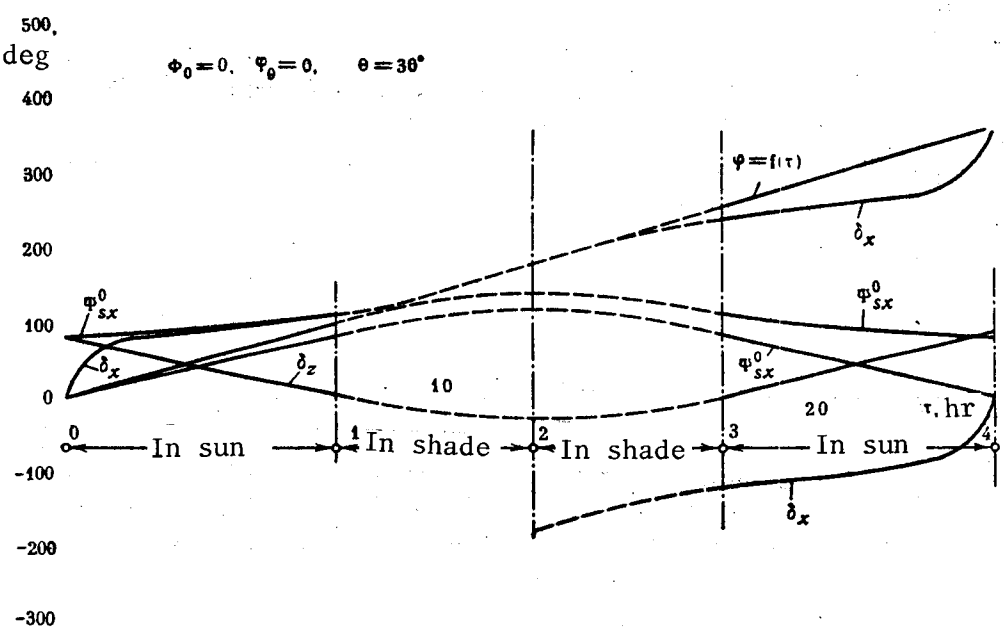

Figure 80a. Change in Angles of Rotation of "Moving Sun" and Spacecraft

The position of the spacecraft on the surface of the celestial body is determined by latitude θ and longitude ϕ, while its orientation relative to this surface is fixed by the rigidly coupled coordinate system xyz, the z axis of which is aimed in the direction opposite to the direction of the force of gravity,

while the x axis is aimed along a tangent to the meridian, the y axis -- in the direction of rotation of the celestial body.

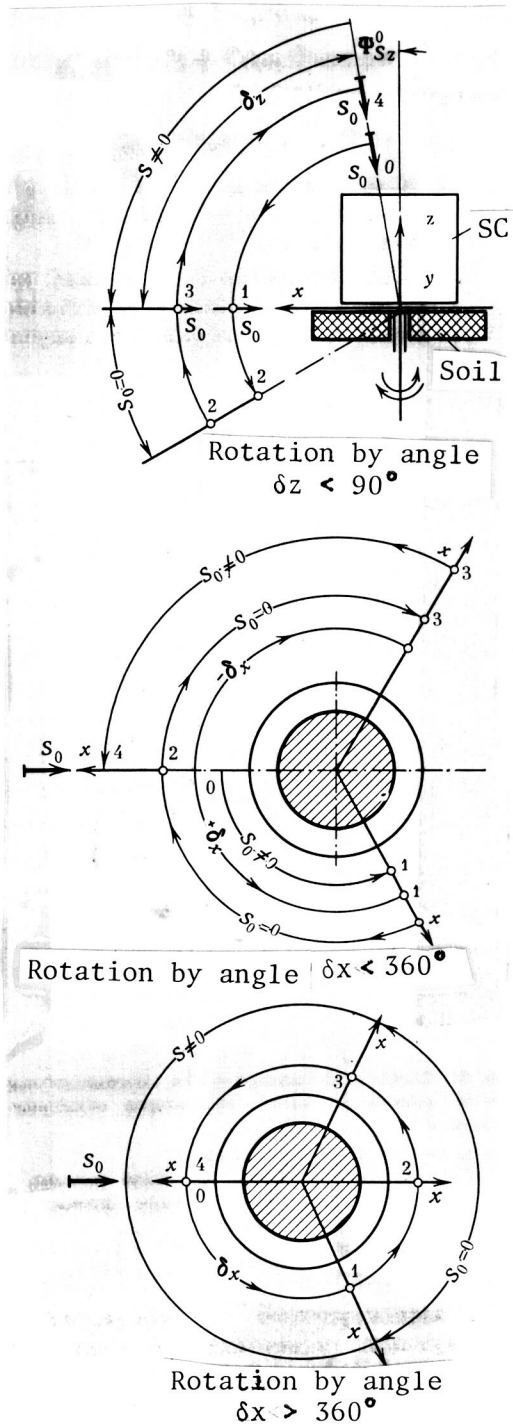

Figure 80b. Plan of Rotation of Spacecraft

We can see from Figure 79a that angles ψ^0 between the direction toward the sun S and the axes x, y, z are defined by the equations

$$\cos\psi^0_{Sx} = -\cos\theta\cos\Phi\sin\vartheta + \\ + \sin\theta\cos\varphi\cos\Phi\cos\vartheta + \sin\theta\sin\varphi\sin\Phi, \quad (2.206)$$

$$\cos\psi^0_{Sy} = -\sin\varphi\cos\Phi\cos\vartheta + \\ + \cos\varphi\sin\Phi, \quad (2.207)$$

$$\cos\psi^0_{Sz} = \sin\theta\cos\Phi\sin\vartheta + \\ + \cos\theta\cos\varphi\cos\Phi\cos\vartheta + \sin\theta\sin\varphi\sin\Phi. \quad (2.208)$$

/148

Here

$$\Phi = \omega_\Phi\tau + \Phi_0, \quad \varphi = \omega_\varphi\tau + \varphi_0,$$

where Φ_0 and ϕ_0 are the values of angles Φ and ϕ at the moment of touchdown, τ is the time which has passed since touchdown.

If the spacecraft is located in a vacuum chamber, its orientation relative to the radiation imitating the solar radiation, corresponding to the orientation in an actual flight, can be achieved by rotation of the spacecraft at a certain angular rate around two axes (see Figure 79b).

The opposite approach can also be taken: with the spacecraft stationary, the solar radiation imitator can be rotated simultaneously about axes x and z at the

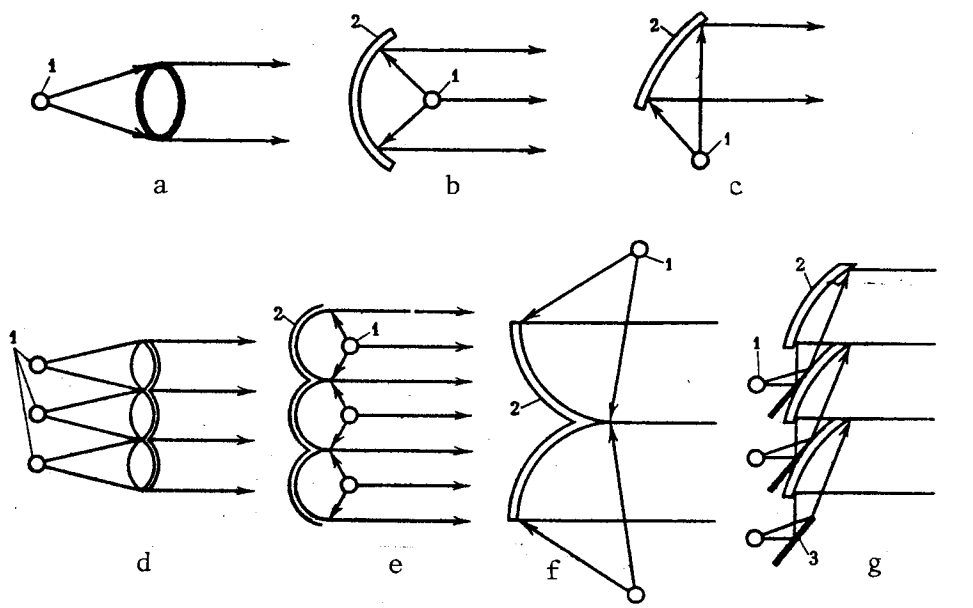

Figure 81. Diagrams of Individual (a-c) and Multiple Modular (d-g) Optical Systems of Solar Radiation Imitators: a, d, Refractive Systems; b, e, Axisymmetrical Reflecting Systems; c, f, g, Asymmetrical Reflecting Systems; 1, Lamp; 2, Reflectors; 3, Mirror

same angular rates as in the preceding case (see Figure 79c).

Since simultaneous1 rotation of the spacecraft or radiation imitator about two axes is a difficult technical problem (or simply impermissible if, for example, the spacecraft carries an astronaut), a simpler approach can be taken: the spacecraft is rotated around only its vertical axis, corresonding to the direction of the force of gravity, and the solar radiation imitator is rotated relative to its horizontal axis (see Figure 79d). In this case, we maintain the proper orientation of the spacecraft relative to the direction of solar radiation, direction of the radiation of the surface of the celestial body and direction of the force of gravity corresponding to actual operating conditions /149 of the spacecraft at any latitude on the surface of the celestial body at any moment in time.

The angle of rotation ("elevation above the horizon") of the "moving sun" at any moment in time from the horizontal plane is defined by the formula

(2.209)

and does not exceed 90°, while the angle of rotation of the spacecraft relative to its vertical axis for the same moment in time is determined by the formula

and may be greater than 390° (if the spacecraft rotates by more than 360°) or less than 360° (if the spacecraft is returned to its initial position during the time interval when it would be shaded by the celestial body).

Figure 80a shows changes in angles ψ^0_{Sz}, δ_z, ψ^0_{Sx} and δ_x for the case when the spacecraft is on the surface of Mars at latitude $\theta = 30°$ with various versions of rotation of the spacecraft relative to the vertical axis when it is in a vacuum chamber (Figure 80b).

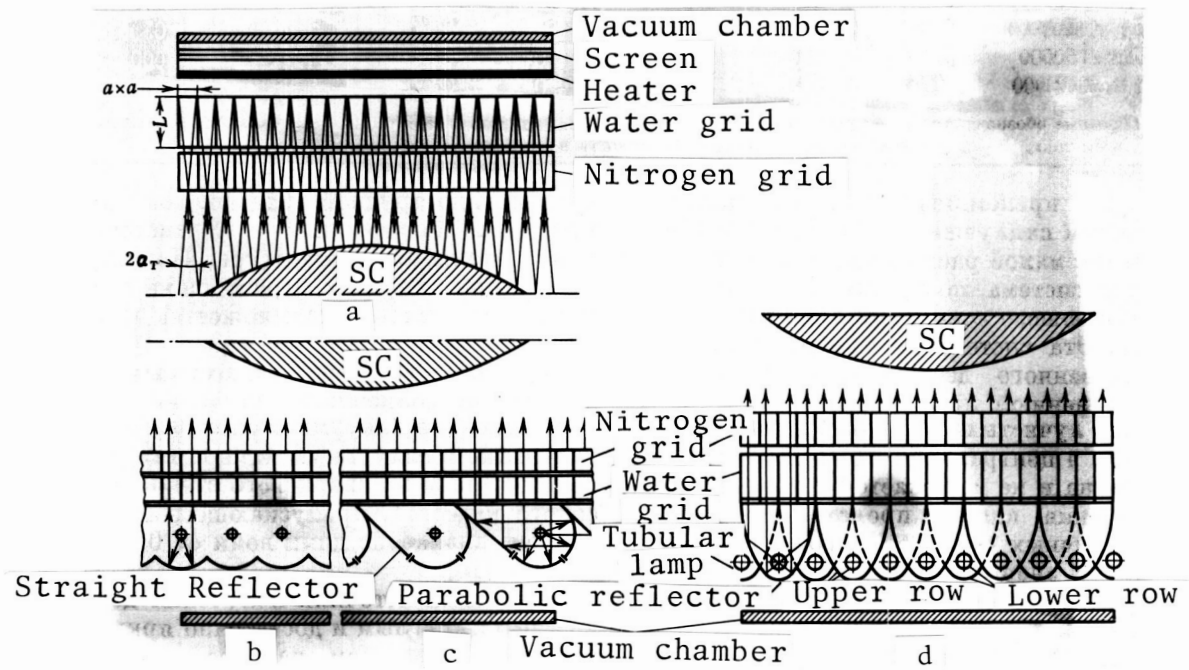

Figure 82. Diagrams of Solar Radiation Imitators Based on the Use of Straightening Grids: a, Source of Radiation Heated Metal Surface; b, c, d, Source of Radiation Tubular Xenon Arc Lamp

Obviously, such a system of orientation of a spacecraft relative to the imitated solar radiation is acceptable only for spacecraft arbitrarily placed in space and flying in orbit around a celestial body or in free space.

Optical diagrams of solar radiation imitators. Several diagrams of the optical systems of "classical" solar radiation imitators are presented in Figure 81 [32].

Of the refracting and reflecting systems, the best, from the point of view of production of slight divergence of flux, is a system based on a reflecting asymmetrical paraboloid. This system requires no high quality quartz, which is in short supply (in contrast to the refracting system) for the creation of radiant fluxes of large cross section, and the central portion of the flux is not shaded and not distorted by the source of radiation, as occurs in axisymmetrical system; furthermore, the thermal energy reflected or radiated by the surface of the spacecraft does not return to it. /150

For small spacecraft, one reflector is sufficient; however, even in this case the system is cumbersome and insufficiently effective. For larger spacecraft, these shortcomings increase significantly; the best solution is a combination of several small imitators [33, 34].

In combined systems, neighboring reflecting mirrors should be placed so as to prevent shading or superimposition of light fluxes and formation of unevenness at the point where the mirrors join, which is a very difficult task, since the entire system must be maintained at a constant temperature. Therefore, in some cases the reflecting mirrors are made up of a set of many small mirrors.

The radiation sources of the "classical" solar radiation imitators are located outside the vacuum chamber, and their radiation is admitted to the vacuum chamber through windows of high quality quartz glass, which transmits radiation in the wavelength range from 0.2 to 1.1 μ [10].

An ideal radiation source should be circular and rather bright, so that with an angular dimension equal to that of the sun it could imitate the distribution of brightness and spectral composition of the sun, approximately corresponding to the radiation of an absolutely black body at 6000 K [36].

Two point sources of radiation are currently known: the carbon arc and the xenon lamp (one variety of the latter is the mercury-xenon lamp), the radiation spectrum of which differ slightly from that of the sun. In order to produce a spectrum near that of the sun, the radiation of these lamps must be filtered, reducing their power output by approximately 20% [37, 38].

TABLE 8

Type of Lamp	Power, w	Operating Voltage, v	Ignition Voltage, v	Current Through Lamp, a	Light Flux, lm	Luminous Intensity, candles
DKsTB2000	$2 \cdot 10^3$	60±5	195	31 + 2	$37 \cdot 10^3$	$34 \cdot 10^2$
DKsT2000	$2 \cdot 10^3$	40	50	52 max	$33 \cdot 10^3$	$3 \cdot 10^3$
DKsT5000	$5 \cdot 10^3$	110	100	48 max	$88 \cdot 10^3$	$8 \cdot 10^3$
DKsT10000	10^4	220	200	46±4	$22 \cdot 10^4$	$2 \cdot 10^4$
DKsT20000	$2 \cdot 10^4$	380	360	56±4	$6 \cdot 10^5$	$56 \cdot 10^3$
DKsTP6000	$6 \cdot 10^3$	110	100	55	$13 \cdot 10^4$	$12 \cdot 10^3$
DKsTV6000	$6 \cdot 10^3$	220	200	30±5	$2 \cdot 10^5$	$18 \cdot 10^3$
DKsTV15000	$15 \cdot 10^3$	220	200	68±5	$55 \cdot 10^4$	$5 \cdot 10^4$
DKsTV50000	$5 \cdot 10^4$	380	360	132±8	$2 \cdot 10^6$	$19 \cdot 10^4$
DKsT50000	$5 \cdot 10^4$	380	370	140±10	$1.8 \cdot 10^6$	$1.8 \cdot 10^5$
DKsT100000	10^5	380	370	270±20	$3.0 \cdot 10^6$	$3.01 \cdot 10^5$

Explanation of Type Numbers: D = Arc, Ks = Xenon, T = Tubular, B = Capacitive ballast, P = dc, V = Water cooled (numbers indicate power in watts)

Recently, a number of plans have been suggested for solar radiation imitators which differ significantly from those described above (in simplicity and small size), which can be placed with a vacuum chamber.

The simplest of these plans[1] (Figure 82a) consists of a heater and two straightening grids, with which the diffused radiation of the surface is formed into a sufficiently parallel flux with an angle of divergence of about 5° with geometric dimensions of the grating L/a = 3-4. Since the temperature of the heater is not great, the radiation flux produced is in the infrared; the necessary quantity of radiation is determined by the ratio

$$Q = A_i S_0 / \varepsilon_i, \qquad (2.210)$$

where S_0, A_i, ε_i represent the flux of incident solar radiation, its absorption factor and the degree of blackness of the ith sector of the outer surface of the spacecraft respectively.

The effeciency (ratio of radiation energy after the grids to energy applied to the heater) is rather high, several percent.

[1]Suggested by V. B. Cherenkov, A. T. Ulubekov and I. Kh. Shteyngardt.

TABLE 8 (Cont'd)

Dimensional Brilliance, sb	Dimensions of Luminous Object		Dimensions of Lamp		Pressure in Cold Lamp, mm hg
	d, mm	ℓ, mm	D, mm	L, mm	
95	18	170	22	370	210±3
90	24	140±3	28	352^{+4}_{-5}	75^{+10}
85	22	430±3	25	642^{+4}_{-6}	60^{+15}
100	21	950±3	35	1260_{-10}	80^{+10}
160	21	1680±3	35	1990_{-10}	75^{+9}
125	21	450±1	27	720	75±5
1050	7	250±1	25	475±2	350±10
3550	7	200±1	36	460±4	340±5
3050	12	520±2	60	932±5	220
600	38	2100	42	2600	60
100	70	2500	80	3100	110

/151

One grid (that closest to the heater) is cooled with water, while the other, that turned toward the spacecraft is cooled with liquid nitrogen and acts as a free space imitator.

The use of the infrared solar radiation imitator yields good results when the outer surface of the spacecraft consists of homogeneous sectors of rather large area (about 1 m^2), and when the optical characteristics of these sectors A_i and ε_i are known.

Other plans have also been suggested for solar radiation imitators using straightening grids. In these plans, the source of radiation is a series of xenon arc tube lamp (DKsT) with parabolic cylindrical reflectors, the line of focuses of each of which coincides with the axis of the lamp[1] (Figure 82b, c, d). The characteristics of DKsT lamps produced by Soviet industry are presented in Table 8.

The lamps used in these plans are powered by an ordinary ac line, but the lamps are "lit" by feeding a series of ignition pulses several seconds in length from a special 10-20 kv igniter to the lamp. Table 8 also presents the geometric characteristics of the lamps: D, d are the diameters of the bulb and of the glowing object; L, ℓ are the lengths of the lamp and the glowing object respectively.

In the systems suggested, the directed radiant flux is formed in a plane perpendicular to the axes of the lamp, by means

[1]Suggested by V. B. Cherenkov, Yu. M. Lukoyanov, Yu. V. Krestov, V. V. Kupchenko, L. I. Skotnikov, A. V. Godin et al.

of the reflectors, and in a plane passing through the axis of the lamp and the line of focuses of the reflector by means of the straightening grid. /152

To produce radiation in the imitator similar in spectral composition to solar radiation, the surface of the reflector turned toward the lamp must have the minimum possible value of A_s with a rather high value of ε, and in order to carry away the heat absorbed by the reflector, it must be cooled by water.

Experimental studies of such systems have shown that DKsT lamps can operate in a vacuum at near-maximum modes for long enough to perform the full cycle of thermal testing of a spacecraft, and their power can be smoothly varied by several times during the course of the testing without significantly changing the spectral composition of the radiation at the output of the straightening grids.

It has also been experimentally determined that with a spectral composition of the exiting radiation similar to solar radiation, an angle of divergence of 3-5° and unevenness through the cross section of the radiation flux of approximately 5-10%, the efficiency of such imitators reaches 8-12%.

An imitator of this type is rather simple in design, small in size, requires no scarse materials or complex equipment for its manufacture, and the electric lamps are powered by a 380 v or 220 v ac line.

Analysis of possible optical plans of solar radiation imitators indicates that the "classical" systems can be used to create only nonmoving imitators, and the spacecraft should be oriented relative to the radiation flux by rotating the spacecraft relative to two mutually perpendicular axes (see Figure 79b). Imitation of rotation of the spacecraft by division of the radiant flux into two components (use of two nonmoving imitators placed at an angle of 90° to each other, and alteration of the value of each component according to the rule $S_1 = S_0 \cos \delta_z$, $S_2 = S_0 \sin \delta_z$, where δ_z is the angle of "elevation" of the sun over the horizon of the celestial body) leads to unacceptable errors in the temperature of the external elements of the spacecraft and cannot be seriously considered.

Rotation of the spacecraft relative to two mutually perpendicular axes is practically possible only for small spacecraft; a typical plan for such rotation in a vacuum chamber with a nonmoving solar radiation imitator is shown in Figure 83a. For large spacecraft, rotation is generally limited to rotation around one axis. Rotation around the second axis causes complex technical problems, disrupts the actual direction of the force of

gravity relative to the spacecraft, which is particularly important for manned spacecraft carrying astronauts, and makes it necessary to rotate the devices imitating the heat-physical characteristics of the soil and the radiation of the surface of the celestial body along with the spacecraft.

Use of the new optical systems with straightening grids and DKsT lamps with reflectors not only allows the creation of small, simple, reliable and highly effective nonmoving solar radiation imitators, but also opens the way to creation of basically new systems for imitation of the thermal effects of the surrounding space medium by using moving solar radiation imitators placed within the vacuum chamber and rotation of the spacecraft around only one (for example the vertical) axis.

Figure 83b shows a vacuum chamber with a "moving sun," rotated around the horizontal axis by angle δ_z, a nonmoving device imitating the heat-physical properties of the soil and the radiation of the surface of the celestial body and a spacecraft which rotates only around its vertical axis. Such an imitation system allows orientation of the spacecraft relative to the direction of radiation from the sun, the surface of the celestial body and the direction of the force of gravity corresponding to the actual conditions of use of the spacecraft at any latitude on the celestial body at any moment in time. /153

10.12. Duration of Thermal Testing $\tau_{\Delta T_a}$

After writing the thermal balance equation (2.1) as

$$C_{\text{eff}} \frac{dT_a}{d\tau} = Q_T + Q_K - Q_e = \\ = (Q_T + Q_K) - C_0 \left(\frac{T_a}{100}\right)^4 \sum_{i=1}^{n} F_i \varepsilon_{ci},$$

where the sum $(Q_R + Q_k)$ is equal to the right portion of equation (2.75), and solving it, we can produce the following relations

$$\alpha\tau = \ln \frac{1 - f^{1/4}}{T_a/T_{a0} - f^{1/4}} + \ln \frac{T_a/T_{a0} + f^{1/4}}{1 + f^{1/4}} + \\ + 2\left(\operatorname{arc-tan} \frac{T_a}{T_{a0}} \frac{1}{f^{1/4}} - \operatorname{arc-tan} \frac{1}{f^{1/4}}\right). \quad (2.211)$$

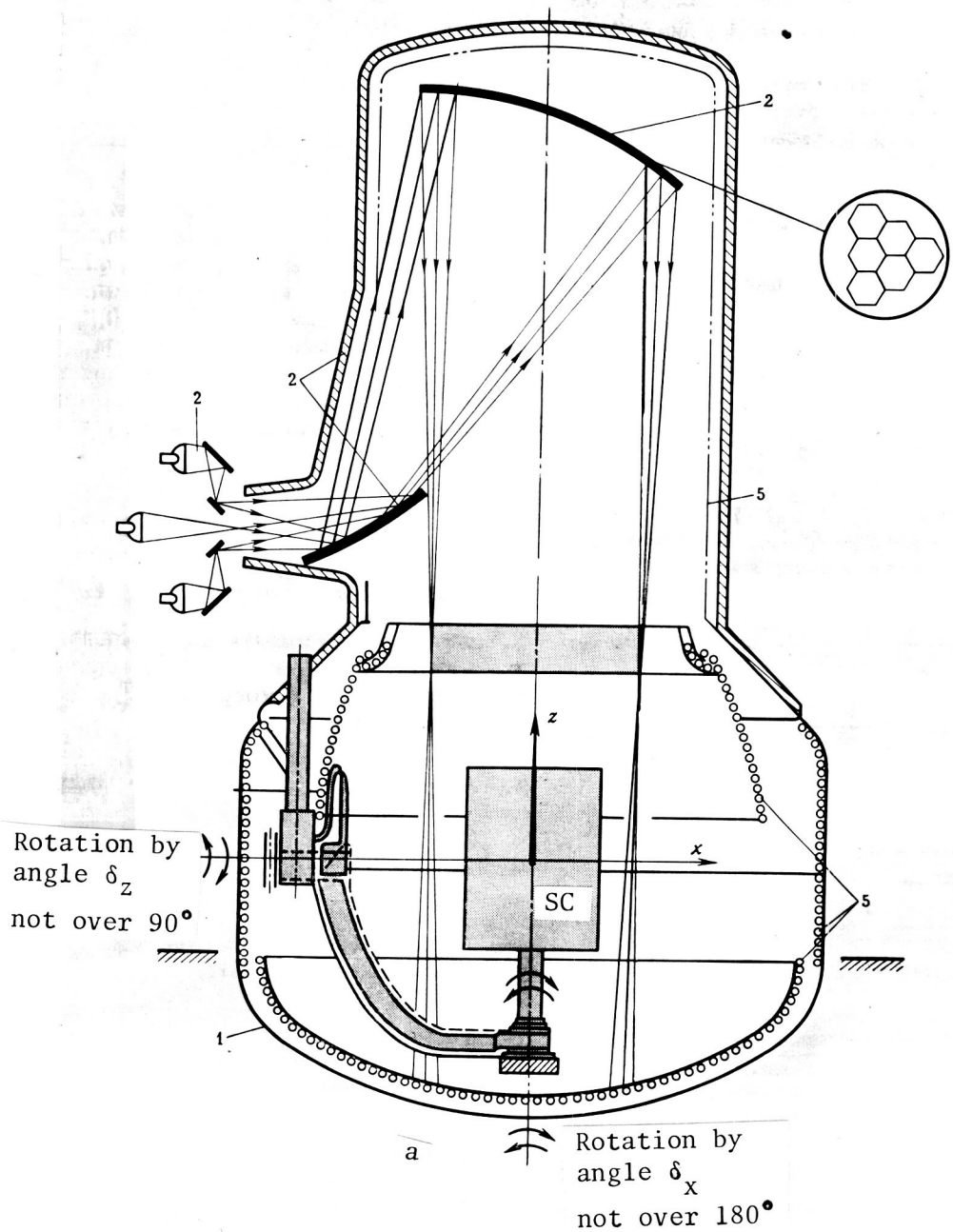

Figure 82. Vacuum Chamber with Solar Radiation Imitator: a, Nonmoving Sun; b, Moving Sun; 1, Vacuum Chamber; 2, Solar Radiation Imitator; 3, Celestial Body Soil Imitator; 4, Celestial Body Surface Radiation Imitator; 5, Nitrogen Screen

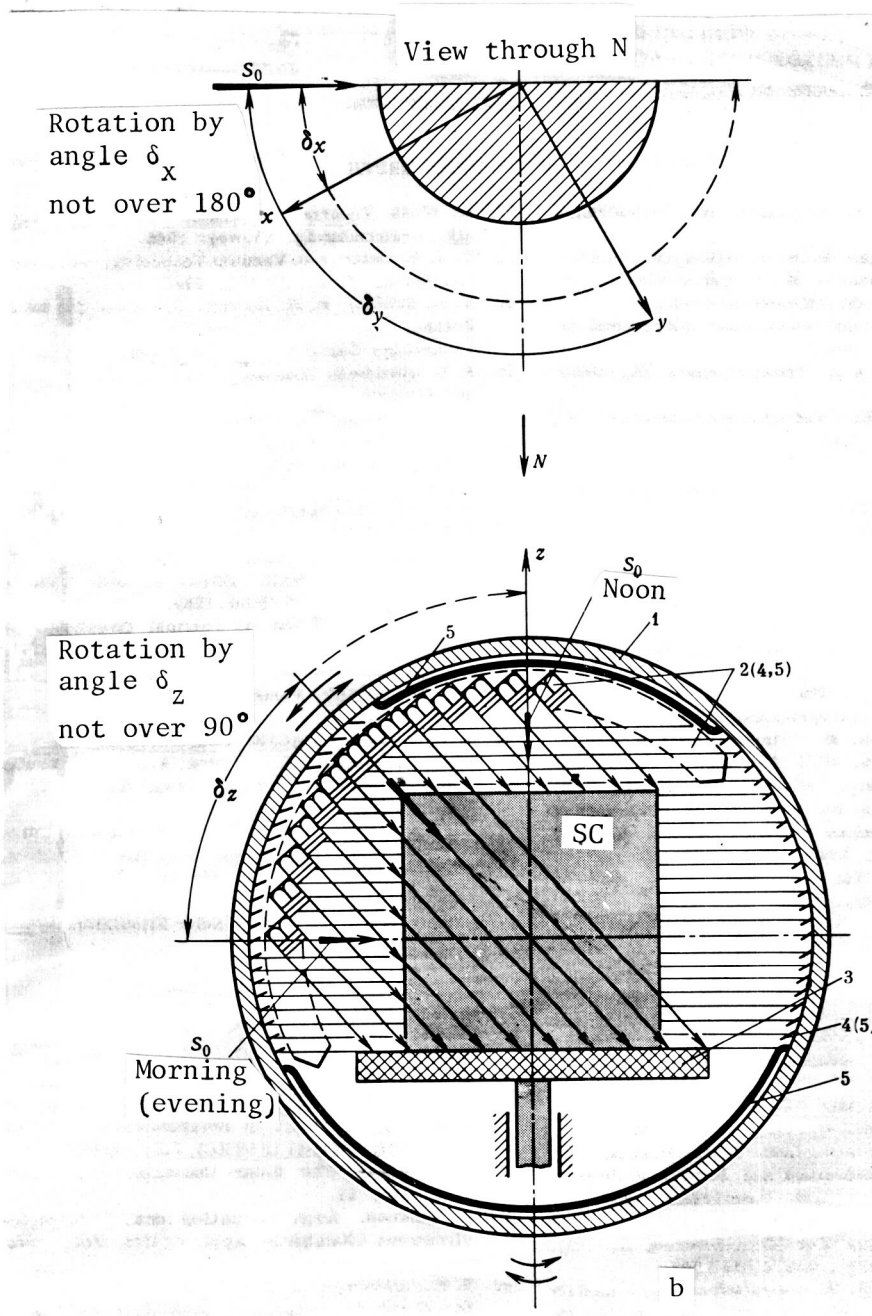
View through N
S_0
Rotation by angle δ_x not over 180°
δ_x
x
δ_y
y
N
z
S_0
Noon
1
5
2(4,5)
Rotation by angle δ_z not over 90°
δ_z
SC
3
4(5)
5
S_0
Morning
(evening)
b

Here

$$\alpha = \frac{4(Q_T + Q_K)}{C_{eff} T_{a0} f^{1/4}};$$

$$f = \frac{Q + Q_K}{C_0 (T_{a0}/100)^4 \sum_{i=1}^{n} F_i \varepsilon_{Ci}} = \left(\frac{T_{a.y}}{T_{a0}}\right)^4;$$

T_{a0} and T_{ay} are the initial and stable temperatures of the spacecraft respectively.

Obviously, thermal testing of the spacecraft should be continued until it reaches a temperature similar to T_{ay} and equal to $T_{ay} \pm \Delta T_a$, where ΔT_a is the permissible error of spacecraft temperature during the tests. In this case, equation (2.211) becomes

$$\alpha\tau_{\Delta T_a} = \ln \frac{1 - f^{1/4}}{\pm \Delta T_a / T_{a0}} + \ln \frac{\pm \Delta T_a / T_{a0} + 2f^{1/4}}{1 + f^{1/4}} + 2\left[\operatorname{arc-tan}\left(1 \pm \frac{\Delta T_a / T_{a0}}{f^{1/4}}\right) - \operatorname{arc-tan} \frac{1}{f^{1/4}}\right]. \qquad (2.212)$$

The α and f included in this equation can be taken from thermal design of the spacecraft or determined as follows. For the case of a change in spacecraft temperature within the range of $\pm$ 50° C ($0.8 < f^{1/4} < 1.2$), the sum of the second and third terms of equation (2.211) will not exceed 10% of the first term. Therefore, equation (2.211) can be written as

From this

$$T_a = T_{a0} + (T_a / T_{a0})(1 - e^{-\alpha\tau}). \qquad (2.213)$$

$$\alpha\tau \approx \ln \frac{1 - f^{1/4}}{T_a / T_{a0} - f^{1/4}}.$$

Taking the values of the corresponding temperatures T_{a0}, T_{a1} and T_{a2} from experiments for moments in time $\tau_0 = 0$, τ_1 and $\tau_2 = 2\tau_1$, we produce

$$\alpha = -\frac{1}{\tau_1} \ln \frac{T_{a2} - T_{a1}}{T_{a1} - T_{a0}}, \tag{2.214}$$

$$T_{a.y} = \frac{T_{a0}T_{a2} - (T_{a1})^2}{T_{a0} + T_{a2} - 2T_{a1}}. \tag{2.215}$$

Knowing α and T_{ay}, it is now not difficult to calculate the value of f, and then $\tau_{\Delta T_a}$.

Practical utilization of equations (2.212)-(2.215) shows that /156
they can be applied not only for determination of the duration of thermal testing $\tau_{\Delta T_a}$, but also for the conduct of reduced tests (for $\tau < \tau_{\Delta T_a}$) and prediction of the temperature of the spacecraft in flight.

REFERENCES FOR PART 2

1. Sorin, S. N., Teploperedacha [Heat Transfer], Moscow, Stroizdat Press, 1952.
2. Kutateladze, S. S., V. M. Borshchanskiy, Spravochnik po Teploperedache [Handbook on Heat Transfer], Moscow, Gosenergoizdat Press, 1959.
3. Yakob, M., Voprosy Teploperedachi [Problems of Heat Transfer], Moscow, Foreign Literature Press, 1960.
4. Blokh, A. G., Osnovy Teploobmena Izlucheniyem [Principles of Radiant Heat Transfer], Moscow, Gosenergoizdat Press, 1962.
5. Isachenko, V. P. et al., Teploperedacha [Heat Transfer], Moscow, Energiya Press, 1969.
6. Mikheyev, N. A., Kratkiy Kurs Teploperedachi [A Short Course in Heat Transfer], Moscow, Gosenergoizdat Press, 1960.
7. Klyuchnikov, A. D., G. P. Ivantsov, Teploperedacha Izlucheniyem v Ognetekhnicheskikh Ustanovkakh [Radiant Heat Transfer in Pyrotechnical Installations], Moscow, Energiya Press, 1970.
8. Avduyevskiy, V. S., et al., Osnovy Teploperedachi v Aviatsionnoy i Raketnoy Tekhnike [Principles of Heat Transfer in Aviation and Rocket Technolgy], Chapter VIII, Moscow, Oboronizdat Press, 1960.
9. Van Vliet, R. M., Passive Temperature Control in the Space Environment, N. Y.-Longon, 1965.
10. Clossen, E. H., et al., Generating the Thermal Environment of a Spacecraft in the Laboratory, ESRO TN-72, Feb. 1969.
11. Makkey, D. B., Konstruirovaniye Kosmicheskikh Silovykh Ustanovok [Design of Space Power Plants], Moscow, Mashinostroyeniye Press, 1966.
12. Favorskiy, O. N., Ya. S. Kadaner, Voprosy Teploobmena v Kosmose [Problems of Heat Exchange in Space], Moscow, Vysshaya Shkola Press, 1967.
13. Polyak, G. L., "Analysis of Radiant Heat Exchange Between Diffuse Surfaces by the Saldo Method," ZhTF, 1935, No. 5.
14. Kaganer, M. G., Teplovaya Izolyatsiya v Tekhnike Nizkikh Temperatur [Thermal Insulation in Low-Temperature Technology], Moscow, Mashinostroyeniye-Press, 1966.
15. Mikhal'chenko, R. S., A. G. Gershin, et al., "Experimental Study of Heat Conductivity of Layered-Vacuum Insulation," IFZ, 1967, No. 4.
16. Problemy Teploobmena [Problems of Heat Exchange, Collection of Translations], Moscow, Atomizdat Press, 1967.
17. Karslou, Kh. S., D. K. Yeger, Teploprovodnost' Tverdykh Tel. [Heat Conductivity of Solids], Moscow, Nauka Press, 1964.
18. Balakhonova, V. I., et al., "Study of the Process of Evaporation of a Fluid from a Porous Metal Under Vacuum Conditions," IFZ, 1968, Vol. 14, No. 1.
19. Samonski, F. H., I. M. Ross, Environmental Control System for Command and Service Modules of Apollo Program-System Description and Discussion of Problem Areas, National Aeronautical and Space Engineering and Manufacturing Meeting, Los Angeles, Calif., Oct. 6-10, 1969.

20. Renman, R. E., A. R. Mendelsohn, "Lunar Module Thermal Control and Life Support Systems for Apollo Applications," SAE Preprints, 1969, N. 625.
21. Deshman, S., Nauchnyye Osnovy Vakuumnoy Tekhniki [Scientific Principles of Vacuum Technology], Moscow, Foreign Literature Press, 1950.
22. Wutz, M., Theorie und Praxis der Vakuumtechnik, Braunschweig, Vieweg Press, 1965.
23. Santeler, D. J., Vacuum Technology and Space Simulation, NASA SP-105, 1966.
24. Schutz, H. A., E. H. Classen, "Facilities for Heat Balance Tests of Satellites in the Euroepean Space Technology Center," Vacuum Technik, 1967, 16.
25. Choumoff, P. S., "Les Techniques du Vide en Recherche Spatiale," Trans. Third Internat. -- Vacuum Congr., Stuttgart, 1965, 1.
26. Korolev, B. I., Osnovy Vakuumnoy Tekhniki [Pricniples of Vacuum Technology], Moscow, Gosenergoizdat Press, 1957.
27. Danilin, B. S., V. Ye. Minaichev, Osnovy Konstruirovaniya Vakuumnykh Sistem [Principles of the Design of Vacuum Systems], Moscow, Energiya Press, 1971.
28. Doenecke, J., "Imperfections in the Simulation of the Thermal Environment of a Spacecraft," Lecture given at the Sixth ESRO Summer School, 1968, in ESRO SP-41, February 1969.
29. Wutz, M., "Simulation of Thermal Conditions of a Satellite and Their Experimental Realization," 1 Congr. Internat. des Techniques du Vide en Recherche Spatiale, Paris, 1964 -- Z. Angew. Phys., 1964, XVII.
30. Simons, J. C., Adequate Consideartions for Lunar Environmental Simulation, AIAA/JES/ASTM, Space Simulation Conference., Houston, Texas, September 1966.
31. Wood, R. D., J. N. Wilkinson, Thermal Simulation of the Lunar Surface, AIAA/JES/ASTM, Space Simulation Conference., Houston, Texas, Sepbember 1966.
32. Mann, A. E., M. Dubey, "Solar Simulators," Space/Aeronaut., 1962, Vol. 37, No. 3.
33. Le Vantine, A., R. P. Kipkis., "Solar Simulation in Space Environment," J. Spacecraft and Rockets, Jan/Feb. 1964, 1.
34. Doenecke, J., "The Conversion of Measured Heat Fluxes into Average Radian Incident on Curved Shapes," ESRO TN-26 (ESTEC), May 1968.
35. Taussaint, M., "Determination of the Simulated Solar Flux Incident on Spacecraft in Text Chamber," ESRO TN-11 (ESTEC), July, 1967.
36. Jonson, F. S., "The Solar Constant," J. Meteorol., 1959, 11.
37. Liebman, R., "Solar Simulation for a 3-m Space Environment Chamber," Appl. Optics, February 1968, Vol. 7, No. 2.
38. Latvala, E. K., R. C. Birkebak, "Simulation of the Space Solar-Thermal Conditions in Ground Test Facilities," Proc. 16 Internat. Astronaut Congr., Athens, 1965, 3. Supporting Equipment, Paris, Gauther-Villars, 1968.

PART 3

DESIGN OF AUTOMATIC PLANETARY STATIONS AND METHODS OF THEIR DELIVERY TO THE SURFACES OF THE PLANETS

The design of a spacecraft is determined by its purpose, /157
operating conditions and flight plan, as well as the possibility of placement on a booster rocket. Automatic planetary stations, as one variety of spacecraft, are designed to perform scientific studies on the surfaces of the planets. They must operate under conditions of space and in the atmosphere of the planets, must be equipped with devices and systems to deliver the station to its working location, to allow functioning on the surface of the planet and to transmit scientific information back to Earth. We study below some of the requirements placed on the design of such apparatus, and possible design solutions and plans for stations assuring that they will be able to perform the tasks set before them.

APS generally consist of the following main parts: the engine, orientation system with reserves of working fluid and orientation motors, systems for navigation, control and stabilization, electric power supply system, radio telemetry system, temperature control system, on-board cable network, scientific apparatus and structure.

Stations which do not participate in the flight to the planet or descent to its surface usually include only an electric power supply system, radio telemetry system, temperature control system, on-board cable network and scientific apparatus.

In this book, when we speak of the structure of the APS, we will be referring to its load-bearing elements (body, frame), designed to carry the systems, instruments and aggregates of the station, as well as various mechanical devices, individual mechanisms and elements of attachment.

The mutual placement and connection together of systems, instruments, aggregates and mechanisms on the load-bearing elements will be referred to as the arrangement of the APS. The shape of the APS depends on the arrangement and structure selected.

The placement of systems and mechanisms on the station is performed to assure their normal functioning and to meet the requirements of minimum structural weight.

Thus, the basic factors defining the arrangement and structure of the APS are:

-- the requirement for minimum weight and dimension;

-- the operating conditions of the station;
-- the requirements placed on the structure by all systems of the station;
-- the method of delivery of the APS to the surface of the planet and the location of performance of experiments.

Furthermore, one must consider:
-- simplicity of manufacture;
-- convenience of operation;
-- cost.

CHAPTER 11

REQUIREMENTS FOR THE STRUCTURE

The structure of an APS, as of any other spacecraft, should /158
have minimum weight and size, should be reliable, should operate under conditions of the space medium, characterized by high vacuum, radiation and meteorite danger, should withstand linear and vibrational acceleration during powered phases of flight. Furthermore, the structure should be easy to manufacture and use [1].

11.1. Weight and Dimensions

A spacecraft is placed in its flight trajectory toward a planet using a booster rocket which has a certain power reserve. The most important requirements placed on a planetary spacecraft and its structure are minimum weight and size. The following means are available to reduce the weight of a spacecraft:

-- reduction of the weight of its elements;
-- use of high energy fuel for trajectory correction and braking upon landing;
-- separation of the systems and equipment servicing the spacecraft during its flight trajectory into individual compartments which are ejected before braking of the station;
-- creation of an arrangement of the system such as to minimize the length of cables between units.

In the analysis of systems for descent of the station onto the surface of the planet, depending on the characteristics of the atmosphere, in each specific case one must find the optimal descent plan considering the expenditures of weight for aerodynamic braking (thermal protection, load-bearing structure, parachute system), for braking with the rocket engine (fuel, engine, control system) and for absorption of the shock upon touchdown (design of landing devices, energy damper).

Weight reduction of the structure of the station itself is achieved by:

-- proper selection of the load-bearing structural system;
-- proper determination of the strength reserve;
-- use of light, strong material;
-- reduction in dimension;
-- application of progressive technology.

The dimensions of the station can be reduced by selection of a compact arrangement plan, application of folding structural elements (folding antennas, solar batteries, etc.).

One important requirement placed on the arrangement of the system is provision of the required mass symmetry (position of center of mass) relative to the longitudinal axis of the engine. The eccentricity is determined by the permissible perturbation of the control system.

11.2. Reliability

Reliability of any structure is evaluated as the probability of its failure-free operation for a certain fixed period of time. The reliability of an APS structure is particularly important, /159
since its is impossible to replace or repair its elements during operation.

High reliability is achieved by a combination of measured performed during planning, manufacture and experimental testing, as well as during operation of the station. Reliability is increased by: strict consideration of the actual conditions; improvement of the quality of production; precise testing in all stages of manufacture; testing of structures under conditions near actual usage conditions; reduction in the number of parts of the structure and duplication of the most important mechanical systems of the spacecraft (duplication achieves the maximum effect when the duplicating mechanisms operate according to different systems).

11.3. Operation in a Vacuum

Space, as we know, is characterized by extremely low pressures and densities of matter.

At an altitude of 10,000 km over the surface of the Earth, the pressure reaches about 10^{-13} mm hg, and changes very little thereafter (Figure 84). With this great rarefaction, the heat conductivity of gas is practically absent, evaporation (and sublimation) rates of materials increase sharply, the mechanical properties of materials change, the consumption of lubricants increases, the danger of cold molecular welding (cohesion) appears, and the friction and wear of friction couples increase.

The temperature fields of the structural elements in space are characterized by high gradients, since the equalization of temperature resulting from convective heat exchange and the heat conductivity of the surrounding atmosphere is absent. Heat is applied to structural elements in space by the radiation of the sun, the Earth and the planets, and also be heat liberation of operating instruments; heat is carried away only by radiation into space.

The overall heat balance is determined basically by the quantity of heat which the structure receives from the sun and the working instruments, and the quantity of heat radiated by the structure into space.

The temperature difference between the illuminated and shaded sides is determined by the thermal resistance of the structure and may reach several tens of degrees.

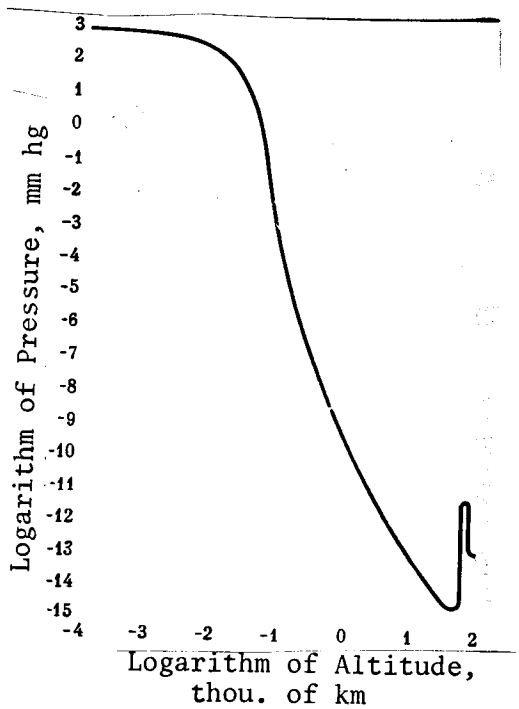

Figure 84. Dependence of Atmospheric Pressure on Altitude

The presence of high temperature gradients leads to thermal stresses and deformations of structures, as well as seizing of rotating couples as a result of uneven expansion or contraction (under the influence of temperature) of the inner and outer parts. Equalization of the temperature of elements of the structure can be achieved by the use of screen-vacuum thermal insulation, which covers almost the entire struture with the exception fo surfaces which must be open (radiation, optical and other surfaces). /160

The rate of evaporation (sublimation) of inorganic substances from the surface of a body in a vacuum

$$W = \frac{p}{17{,}14}\sqrt{\frac{M}{T}} \quad [g/(cm^2 \cdot sec)], \qquad (3.1)$$

where p is the saturated vapor pressure at temperature T, mm hg; M is the molecular weight; T is the temperature, K.

The dependence of the vapor pressure of various metals on temperature is shown in Figure 85 [2]. If the vapor pressure is greater than the pressure of the medium, sublimation of the material will occur at a rate determined by equation (3.1).

The equation for determination of the rate of reduction in the thickness of a wall of a material is

$$[cm \cdot yr^{-1}], \qquad (3.2)$$

where ρ is the density of the material, $g \cdot cm^{-3}$.

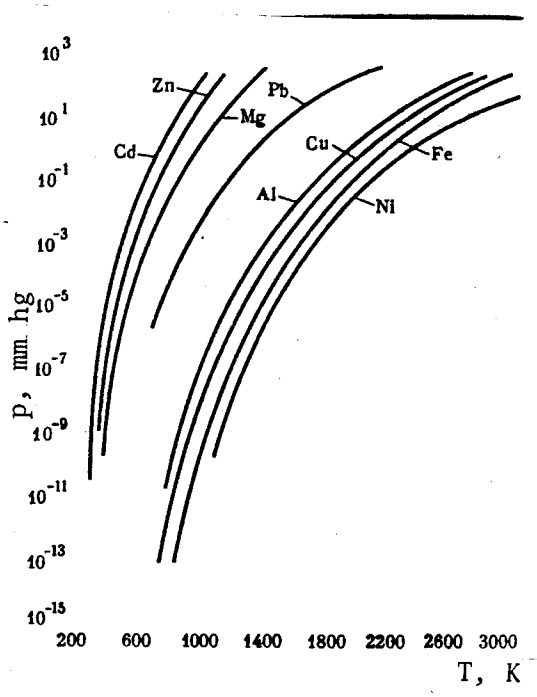

Figure 85. Metal Vapor Pressure as a Function of Temperature

Figure 86 shows the rate of evaporation of various metals as a function of temperature [2]. The graphs show that the evaporation of metals usually used in structures is insignificant up to 100-150° C. Most plastics also have low rates of evaporation. However, it should be noted that the rate of evaporation of plastics depends not only on the type of plastic, but also on its manufacturing technology (the presence of small impurities in the plastic). Plastics with high content of plasticizer should not be used. The evaporation of volatile plasticizers makes the material very brittle.

The evaporation of metal alloys occurs unevenly over the surface. Alloys are not homogeneous in structure, but rather consists of grains. The evaporation is most intensive along grain boundaries, where disordered placement of atoms and large numbers of crystalline defects are present. The uneven evaporation of metals and alloys causes microscopic roughness of the surface and changes its optical characteristics, disrupting the thermal mode of the structure.

Another undesirable factor resulting from the influence of the vacuum is the precipitation of evaporated metal and organic dies on the coolest parts of the structure, particularly on dielectric and optical parts, resulting in changes of resistivity and deterioration of optical properties. To avoid the contamination of optical parts, practically non-evaporating paints must be used, or care must be taken to see that the optical systems have higher temperatures than the surrounding structures. /161

The sublimation of metals can be significantly reduced by creating protective coatings (oxide, phosphate) on their surfaces, having higher stability in a vacuum than the base metals. Vacuum has no significant influence on the mechanical properties of metals.

One of the most important problems involved in the operation of mechanisms under deep vacuum conditions is friction and lubrication. With long exposure to deep vacuum, the surface of a metal looses its adsorbed gasses and oxide films, which form a

$$S = 1{,}85 \cdot 10^6 \frac{p}{\rho}\sqrt{\frac{M}{T}}$$

unique lubricating layer under terrestrial conditions. Many of the liquid and solid lubricants ordinarily used under terrestrial conditions are unsuitable for use in a vacuum, since they have high vapor pressure and evaporate rapidly. The loss of lubrication and absence of secondary substances on the friction surfaces lead to an increase in the coefficient of friction and may cause partial or complete cold welding at points of contact due to the diffusion of molecules of one metal into the other. Cold welding depends on the contacting materials, contact time, applied force and temperature. As the contact time, compressive force and temperature increase, cohesion increases. Graphite lubricant is unsuitable for use in a vacuum, since without its adsorbed water film it is converted from a lubricating material to an abrasive material.

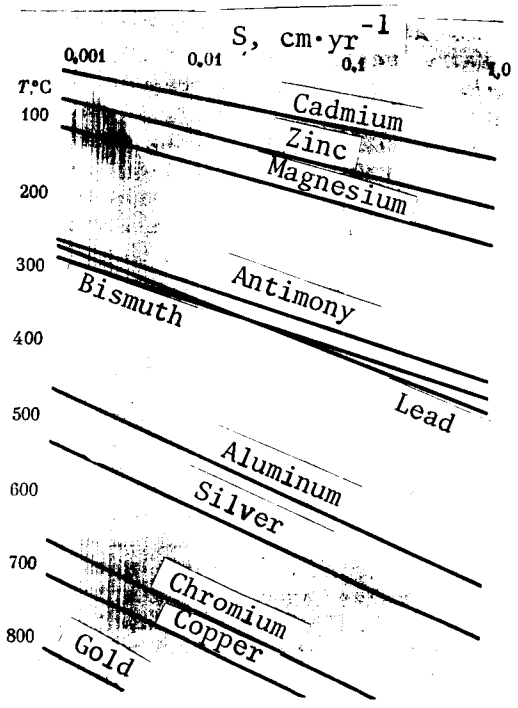

Figure 86. Rate of Evaporation of Metals as a Function of Temperature

The increased friction and cohesion in a vacuum result in rapid wear of friction couples and increased loads on drive units. A number of methods have been suggested to eliminate the harmful influence of vacuum on the operation of mechanisms, based both on design solutions and on the use of solid coatings or lubricants with low vapor pressure and proper selection of the materials of friction couples.

One radical design method is the installation of mechanisms in a sealed body. Movement of parts and units installed outside the automatic station can be performed using drive units with sealed output shafts at low rotation speeds. One shortcoming of this method is the increased wear of the seal and the increased friction torque on the shaft. Drive units with magnetic clutches or wave-type and magnetic reducers are frequently used, in which the engine and high-speed portion of the reducer are located in a sealed body, while rotation is transmitted to the low speed shaft through a sealed wall.

Figure 87 shows a drive unit with a wave-type reducer, designed for operation in space [3]. The shaft of the electric motor carries a wave generator consisting of an oval cam with intermediate rolling bodies (balls). A flexible link of complex shape is used to decrease the stress in the area of greatest /162

deformation. The central portion of the flexible link has external teeth, which mesh with the teeth of the rigit link. This link consists of two twisted half rings. The area within the flexible link is sealed and isolated from the surrounding space. Rotation of the wave generator causes motion of a deformation wave of the flexible link around its circumference. As the wave generator turns, the flexible link remains stationary, the rigid link rotates in the same direction. The transfer number of this type of drive

$$i = \frac{Z_r}{Z_r - Z_f},$$

where Z_r and Z_f are the number of teeth of the rigid and flexible links respectively.

/163

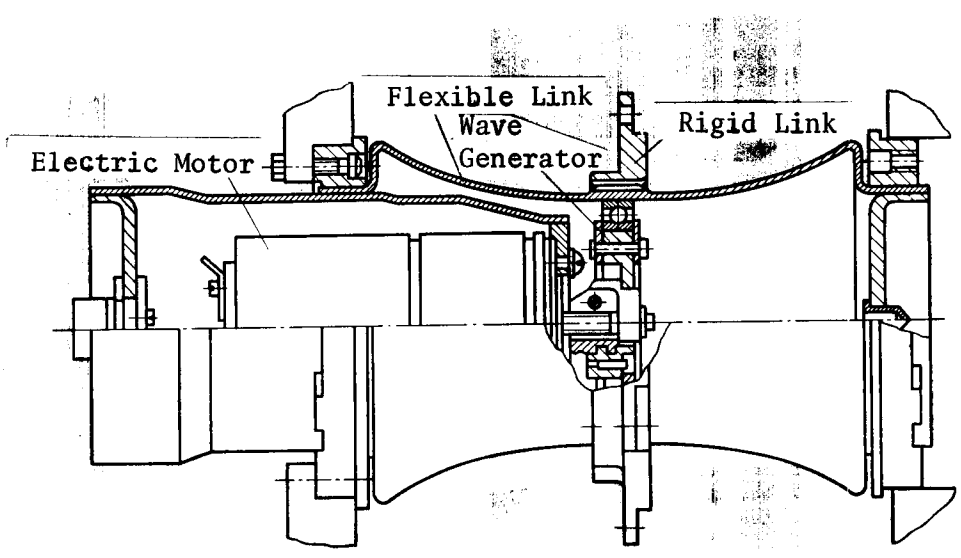

Figure 87. Drive with Wave-Type Reducer

The difference in the number of teeth $Z_r - Z_f$ is selected equal to the number of deformation waves n. The number of deformation waves of the flexible link may be any desired, beginning at n = 1, but it is more expedient to use n = 2, 3 or 4. With symmetrical cams and $n \geq 2$, the reaction of the flexible link is closed in the body of the cam and not transmitted to the supports. Problems of the theory, design and construction of wave-type transmission links are studied in detail in [3].

For mechanisms working in a vacuum it is recommended that contactless electric motors and measurement sensors be used, as well as rolling-surface bearings in place of friction bearings.

One interesting method is the use of dynamic sealing, consisting in that the mechanism is placed in a body, within which there is a gas-liberating substance which compensates for the leakage of gas from the body through the gap between the body and the output shaft. A labyrinth type seal is placed on the output shaft to increase the leak resistance. Selection of the gas liberating substance can provide a pressure in the body of between 1 and 10^{-4} mm hg. With this pressure level within the body, a practically nonevaporating lubricant can be selected. The difficulty in selecting a suitable gas-liberating substance must be considered a shortcoming of this method. One apparently expedient type of drive for use in space is a wave-type reducer in which the low speed portion is sealed by the dynamic principle.

Proper selection of the materials of friction couples is important for reduction of friction and elimination of vacuum welding. Good results have been achieved by use of metals in couple with nonmetallic materials. This type of combination assures nonweldability of the contacting couple under high loads. Under dry friction conditions, these couples are self-lubricating. As a metal part moves over teflon, the coefficient of friction is 0.04. One shortcoming of teflon is its low radiation resistance.

Metal friction couples operating in a vacuum are covered by a thin layer of soft metals (silver, gold, cobalt, etc.) which acts as a solid lubricant. One shortcoming of this method is the rapid wear of these coatings. The most effective lubricating material in a vacuum is molybdenum disulfide MoS_2. It is used as a solid coating for metal parts, and also as a component element of vacuum greases, based on organosilicon resins. Some metal friction surfaces should be covered with oxide or phosphate films and lubricated with vacuum lubricants.

11.4. Operations Under Conditions of Radiation and Meteor Impact

A station in space is exposed to electromagnetic radiation consisting of radio waves, infrared radiation, visible light, ultraviolet radiation, x-rays and gamma rays. Within the solar system, the primary source of electromagnetic radiation is the sun. In addition to electromagnetic radiation, a station in space is also acted upon by corpuscular radiation, consisting of protons, electrons, alpha particles and nuclei. The sources of corpuscular radiation are the cosmic rays, the sun (solar wind, flares), and the radiation belts of the Earth.

Flares on the sun generate intensive streams of high energy particles. These streams consist of protons, alpha particles and nuclei. Flares are also accompanied by sharp increases in shortwave electromagnetic radiation from the sun. The radiation belts of the Earth consist of high energy protons and electrons.

Shortwave electromagnetic radiation -- ultraviolet, x-rays and gamma rays, as well as corpuscular radiation with sufficient energy, have a damaging influence on materials. Radiation damage is manifested as ionization of substances, displacement of atoms in the crystalline lattice and erosion of surfaces. For metals and semiconductors, the main type of damage is displacement of atoms, for organic compounds (plastics, lubricants) it is ionization of substances, for glass -- both of these types of damage.

The most sensitive to cosmic radiation are radiation surfaces, optical parts, semiconductor devices and the photocells of solar batteries. Ultraviolet and corpuscular radiation cause changes in the optical factors of coatings. The absorptive capacity (coefficient A_S) of inorganic and organic white coatings on radiators is increased, while the radiative capacity (factor ε) remains practically unchanged. For certain coatings, coefficient A_S increases by 2 or 3 times. This results in serious disruption of the thermal mode. Ceramic white heat regulating coatings are more resistant to bombardment than white organic coatings. /164

Irradiation decreases the transparency of the glass in portholes and optical instruments. Darkening of glass can be minimized by addition of cerium oxide to the glass, and also be the use of quartz glass with low content of impurities.

The current of solar batteries drops under the influence of radiation bombardment. For example, as a satellite flies through the radiation belts, solar batteries consisting of silicon photocells with p-n junction fail completely in two to three weeks. To increase the service life of solar batteries, optically transparent coatings are used and photocells with p-n junctions are replaced by photocells with n-p junctions, which are more resistant to irradiation.

Cosmic radiation has no significant influence on the strength characteristics of the metals. Bombardment increases the strength of a metal, decreases its plasticity and viscosity. Organic compounds (plastics, oils, etc.) are less resistant to bombardment than metals. Some of these loose their strength and become porous and brittle. /165

The damage to materials and semiconductors depends on the absorbed integral radiation dose, measured in rads (1 rad = 100 $erg \cdot g^{-1}$). With doses below the permissible levels, damage does not occur. Figure 88 shows the comparative radiation sensitivity of certain materials and elements of electronic circuits [4].

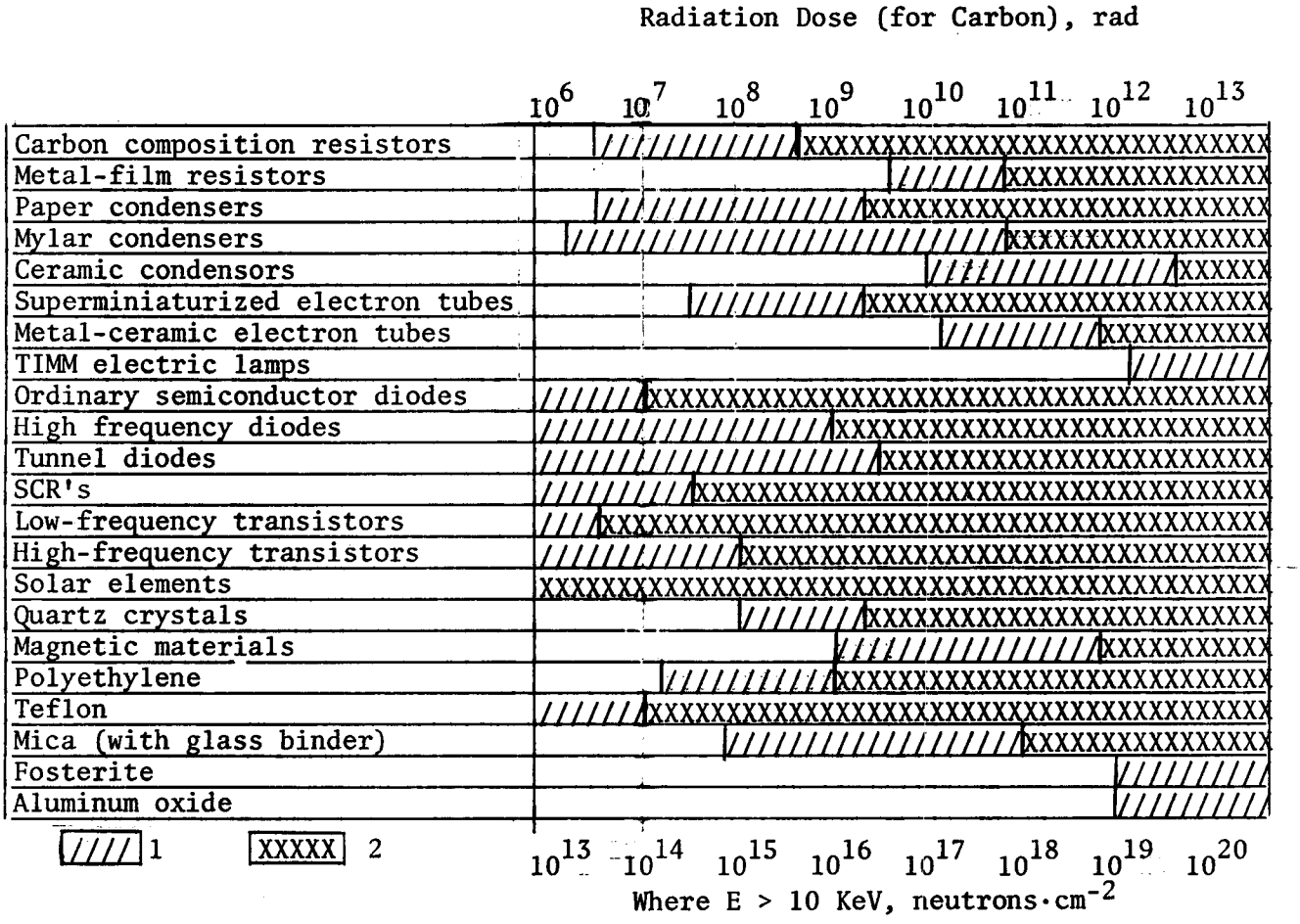

Figure 88. Comparative Sensitivity to Radiation of Certain Materials and Elements in Electronic Circuits. 1, Some Deterioration of Characteristics; 2, Total Failure

The dose of cosmic rays during the period of maximum solar activity is about 5 rad per year, in the internal portion of the radiation belts around the Earth -- 6 rad per hour, while the dose during powerful solar flares, which average 180 minutes in duration, may reach $2 \cdot 10^3$-$3 \cdot 10^4$ rad. As a station flies to a planet, it passes through the radiation belts of the Earth during the initial sector of its trajectory in approximately 4 hours, so that the dose received by the structure and apparatus of the station in this time is slight. For planetary stations, the most dangerous source of radiation is the solar flares.

In space, hard meteorite particles also impinge on the structure of the station.

The maximum velocity of these particles at a distance of 1 a.u. from the sun is 42 km/sec. The speed of collision of meteorite particles with a spacecraft is equal to the vector

difference of the heliocentric velocities of the spacecraft and the particles. The effect of a meteorite particle on the structure depends on the mass of the particle and the collision velocity. The effects of particles with masses of less than 10^{-7} g consists mainly in erosion of optical surfaces, solar batteries and reflecting surfaces. Meteorite particles with masses of over 10^{-7} g can penetrate thin-wall envelopes.

Calculations have shown that the total loss of matter as a result of meteorite erosion at great distances from the Earth amounts to less than 1 A per year, near the Earth at an altitude of a few hundred kilometers it amounts to about 200 A per year. The dependence of the probable frequency of penetration of aluminum and iron spacecraft walls on sheet thickness is presented in Figure 89 [5]. These dependences were produced by calculation on the basis of known data on meteorite fluxes and analysis of the mechanism of penetration on the assumption that the thickness of a penetrated sheet is 1-1/2 times the depth of the crater in a semiinfinite mass of the material.

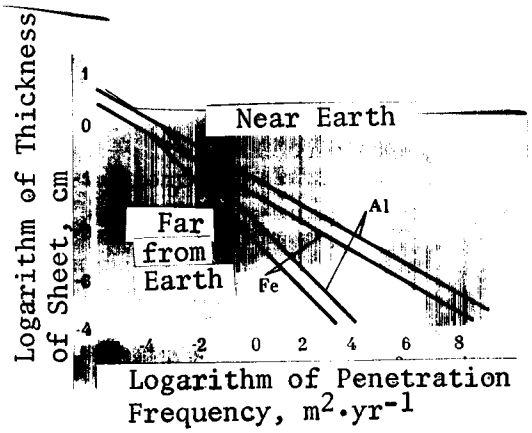

Figure 89. Probable Frequency of Penetration of Aluminum and Iron Spacecraft Walls as a Function of Sheet Thickness

One method of protection from meteorite particles flying at supersonic speeds is the use of a two-wall structure. In this case, a thin meteorite shield is placed around the main envelope. The purpose of the shield is to break up meteorite particles into tiny fragments. To assure sufficiently wide separation of the fragments, the shield should be placed at some distance from the basic envelope. The minimum mass m capable of penetrating a double wall of this type is [6]

$$m = 1{,}44 C_2 (\xi/C_2)_a m_2 S^2/V, \qquad m_1/\rho d > 1,$$

$$m = \left[\frac{1{,}44\,(\pi/6)^{1/3} C_2 (\xi/C_2)_a m_1 m_2 S^2}{\rho^{2/3} V}\right]^{3/4}, \qquad m_1/\rho d < 1.$$

/166

Here $C_2 = \sqrt{\frac{E_2}{\rho_2}\frac{1-\mu}{(1+\mu)(1-2\mu)}}$ is the velocity of propagation of sound in the material of the wall [7]; E_2 is the modulus of elasticity of the material of the rear wall; ρ_2 is the density of the material of the rear wall; μ is Poisson's coefficient; $\xi/C_2)_a$ is

the permissible ratio of velocities for the material of the rear wall, dependent on the relative elongation δ at rupture and ratio E_2/σ_y, where σ_y is the yield point [for aluminum and magnesium alloys, we can accept $(\xi/C_2)_a$ = 0.075-0.09, for titanium alloys $\simeq$ 0.09]; m_1, m_2 are the masses of a unit area of the front and rear walls respectively; S is the distance between the front and rear walls; V is the perpendicular component of impact velocity of the meteorite; ρ is the density of the meteorite; d is the diameter of the meteorite.

Assuming that the number of meteorites striking the spacecraft follows Poisson's distribution, we can determine the probability of impact of n particles having a mass of no less than m grams:

$$p_n = \frac{(ANt)^n}{n!} e^{-ANt},$$

where p_n is the probability of impact of n meteorites; A is the area bombarded by meteorites; $N = 10^{-14.33} m^{-1.34}$ is the mean number of meteorites of mass m grams or more in the area of the Earth encountered by one m^2 of surface in one second [8]; t is the time interval.

In conclusion, we note that the material of meteorites in the space around the sun has not been sufficiently studied; therefore, reliable estimation of meteorite danger is quite difficult. The question of the combined influence of vacuum, temperature, radiation and meteorite impact on materials and elements of electronic circuits has not been sufficiently studied.

11.5. The Effects of Linear and Vibration Acceleration

During the powered sector, linear longitudinal and lateral acceleration and vibration loads act on the planetary station. The linear g loads on the rockets used to boost spacecraft are not great (along the longitudinal axis of the rocket $n \leq 6$, in the lateral direction $n \leq 3$). A more serious danger is represented by vibration loads, which are complex in nature and act throughout the powered flight sector. They can be characterized by their frequency and amplitude and depend on the rigidity of the booster rocket. The frequency usually lies between 5 and 3000 Hz at n = = 5-11.5, with the g loads increasing with increasing frequency.

Vibration loads have no preferential direction; therefore, when a structure is tested for vibration, its strength must be checked in three mutually perpendicular directions. In order for a structure to be vibration resistant, one must attempt to make it a closed structure, with no long cantilevers. If there are

movable masses in the structure held down by wire retainers, the strength of the retainers must be determined by vibration testing.

11.6. Special Requirements Placed on the Structure of a Planetary Station

The structure of a planetary station must meet a number of requirements to assure the working capability of the station under the conditions present on the surface of the planet and also related to delivery of the station to the surface. The most important of these are: protection of the station during descent through the planet's atmosphere, absorption of the impact upon landing, orientation of the station on the surface, movement over the surface and deployment of systems and apparatus.

CHAPTER 12

DELIVERY OF AUTOMATIC PLANETARY STATIONS TO THE SURFACES OF THE PLANETS

12.1. Methods of Delivery of Stations /167

Two methods of delivery of a station to the surface of a planet are possible. The first method is that the station is an independent apparatus or included as a part of an apparatus designed to fly near the planet studied. In this case, it is equipped to fly and descend to the planet. In the second method of delivery, the station is a part of a base spacecraft which flies to and lands on the surface of the planet.

Let us study some possible plans for delivery of a station using the first method. The descent to the planet may be performed from a collision trajectory or from orbit around the planet. The collision trajectory should pass through the visible disc of the planet at some distance from its center. Intersection of the trajectory and the planet in the required region is assured by a course correction utilizing the correcting engine and the orientation and control systems. If the station is a part of a spacecraft designed to fly past the planet, it must be separated from the spacecraft at some distance from the planet and, utilizing its own correcting engine, shifted to a trajectory which will strike the planet.

Descent from orbit around the planet requires greater energy expenditure. However, descent to the planet from an intermediate orbit has the advantage that the possibility of selection of the landing point is expanded and when a landing is made on a planet with an atmosphere the acceleration and thermal loads on the station are decreased due to the reduced angle of entry into the atmosphere (see § 12.2). Deceleration of a station descending to a planet with no atmosphere is achieved by means of the rocket engines.

As an example, let us study a plan for landing a station on the moon. For a descent to the moon from a collision trajectory, at some distance from the surface of the moon the station is oriented so that its longitudinal axis, along which the retrorockets are placed, coincides with the velocity vector. The oriented descent of the spacecraft to the surface begins at this moment. In order to reduce weight, deceleration is usually performed in two stages. The primary deceleration is performed by a high-thrust braking engine. It is turned on by a signal from the altimeter, and turned off by a signal from an integrator when the

assigned velocity is reached. After its operation is over, the braking engine is jettisonned. Before the braking engine is turned off, low-thrust vernier engines are started up, and are used for the final speed reduction. The vernier engines can also be used as control engines during operation of the braking engine. During /168
the final stage of descent, from an altitude of 2-5 km, the vernier engines are controlled by a Dopper velocity-measuring device and a radar altimeter. At about 4 m above the surface, the vernier engines are switched off, when the vertical velocity is not over 1.5 m/sec, the lateral velocity not over 2 m/sec. From this altitude, the station drops freely to the surface. At the moment when the vernier engines are turned off, the station is oriented so that its longitudinal axis coincides with a perpendicular to the surface of the moon. The change in orientation of the station during the period of free fall is slight, since the perturbations upon shutdown of the vernier engines are slight. The speed of impact with the surface of the moon is not over 4.5 m/sec. The impact is absorbed by means of shock absorbing devices on the landing supports.

For a descent from an intermediate orbit, the station must be placed in a descent trajectory. This is done by orienting the braking engine approximately along the velocity vector and at the required point, which is determined to assure a landing in the region selected, a braking burn is performed. The plan of deceleration and landing of the station is similar to that studied above for a descent from a collision trajectory.

In the second method of delivery, the APS is landed on the surface of the planet as a part of the base apparatus, then delivered to its working location by various means.

If the base spacecraft is manned, the automatic station might be carried out onto the surface by an astronaut. If the base spacecraft is an automatic apparatus, the task of delivery of the station to its operating point is most simply solved by including transport equipment to carry cargo over the surface as a part of the base spacecraft. Placement of the station on the transport equipment and its unloading onto the surface at the required point can be performed by a special manipulator. In both cases (placement of the station on the surface by astronauts or by a manipulator), the structure of the station is simple and no special requirements are placed on it as concerns absorption or shock and orientation on the surface (see § 12.3 and 12.4).

If the station is equipped with its own means of transport, it can travel under its own power to its operating location. In this case, the station drives out of the base spacecraft along guides or is removed by a manipulator. However, travel of the station to a region several kilometers distant under its own power over broken terrain is a very difficult problem due to the

great expenditures of energy, complex requirements placed on transportation equipment and the movement control system. Obviously, small stations should not be given the task of moving to their region of operation under their own power.

Delivery of a station over a distance of a few meters of even a few dozens of meters from the base spacecraft can be achieved by ejection of the station by means of pyrotechnical devices.

Figure 90 shows a diagram of ejection of a station.

/169

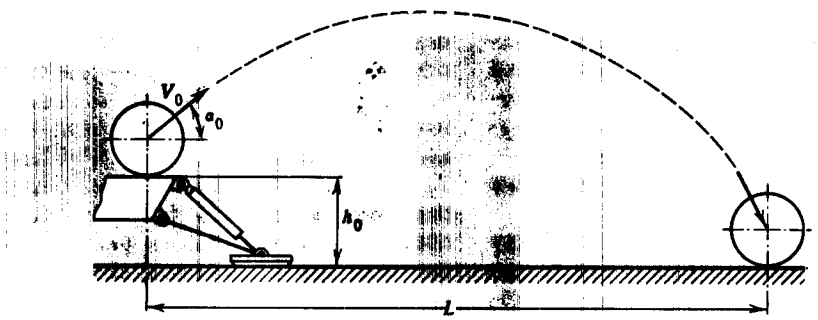

Figure 90. Diagram of Ejection of Station

The distance L which the station is thrown on a planet with no atmosphere or with a rarefied atmosphere whose influence can be ignored is determined by the formula

$$L = V_0 \cos \alpha_0 t, \tag{3.3}$$

where V_0 is the initial velocity of the station, α_0 is the ejection angle; t is the flight time of the station to impact with the surface.

Expressing time t through the initial velocity V_0, ejection angle α_0, height of placement of the station over the surface h_0 and acceleration of the force of gravity on the surface of the planet g_p, we convert formula (3.3) to

$$L = \frac{V_0 \cos \alpha_0}{g_p}\left(V_0 \sin \alpha_0 + \sqrt{V_0^2 \sin^2 \alpha_0 + 2 g_p h_0}\right). \tag{3.4}$$

If $h_0 = 0$, then

$$L = \frac{2V_0^2 \cos \alpha_0 \sin \alpha_0}{g_p}. \qquad (3.5)$$

Figure 91 shows the ejection range L on the moon as a function of angle α_0 for various values of ejection velocity, where $h_0 = 1$ m. We can see from the graph that in order to throw a station 40 m, it must be ejected from the base spacecraft at 8 m/sec. The collision velocity with the surface will be 8.4 m/sec. Reliable surrounding shock absorption is required to protect the station, since perturbations upon ejection (eccentricity of force, variation in forces of pushers, variation in force of separation of plugs) make it impossible to determine the point of contact between station and surface.

In regions of the planet which are difficult to cross, the station might be ejected from the base spacecraft before it lands on the surface. To eject the station, the base spacecraft must drop to the required altitude then, after ejecting the station, continue to the assigned region for a landing. The possibilities for such a maneuver are limited by the fuel reserves available. In some cases, it might be desirable to deliver a platform carrying several stations, ejected at a low altitude over the surface, in which case the platform itself might not even have landing equipment.

The surface impact velocity of a station ejected from altitude h is determined by the formula

$$V_{imp} = \sqrt{V_v^2 + V_\ell^2 + V_0^2 + 2g_p h}, \qquad (3.6)$$

where V_v and V_ℓ are the vertical and lateral velocities of the spacecraft at the ejection point; V_0 is the velocity of separation of the station from the base spacecraft.

This method of delivery produces a high impact velocity. For example, on the moon where h = 50 m and $V_v = V_\ell = V_0 = 1$ m/sec, velocity $V_{imp} \approx 12.8$ m/sec.

When a station is ejected from a base spacecraft, one should note the perturbation of the base spacecraft. This perturbation is manifested as an angular velocity and angular deviation relative to the axes passing through the center of mass of the apparatus, due to the eccentricity of the force applied upon separation of

the station. The perturbations received by the spacecraft should be compensated by forces applied by the control system.

Figure 92 shows a plan of velocities upon separation of a station from a base spacecraft. The compensating force from the control thrusters is not considered, since its influence on the angular velocity and angular deviation of the station is slight in comparison to the perturbing forces during the time of separation (a flat picture of separation is analyzed, and it is assumed that all forces lie in a single plane or in parallel planes). /170

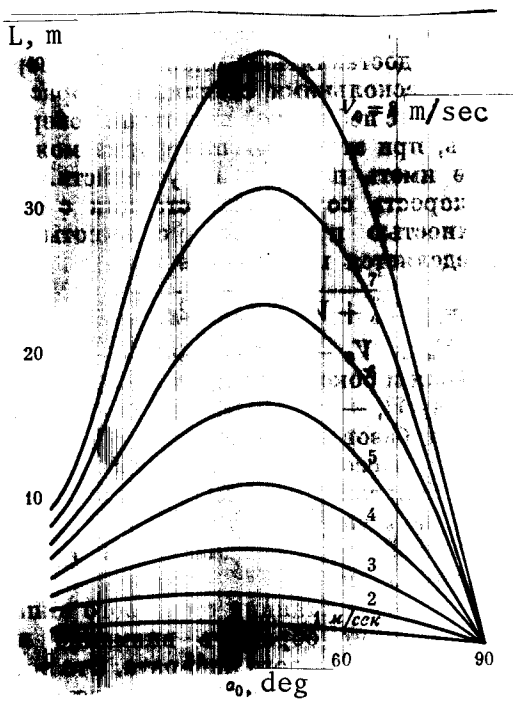

Figure 91. Ejection Range L on the Moon as a Function of Angle α_0 for Various Values of Ejection Velocity Where h_0 = 1 m

In order to determine the relationships between velocities arising upon separation, let us write the equation for the momentum of the base spacecraft-station system relative to the center of mass of the system and the equation for the work performed upon separation:

$$J_2\omega_2 - m_2V_2\varepsilon_2 - m_1V_1\varepsilon_1 = 0,$$
$$A = \frac{m_1V_1^2}{2} + \frac{m_2V_2^2}{2} + \frac{J_2\omega_2^2}{2}, \qquad (3.7)$$

where J_2 is the moment of inertia of the base spacecraft relative to an axis passing through its center of mass perpendicular to the plane of the drawing; ω_2 is the angular velocity of the base spacecraft relative to the same axis; m_1 and m_2 are the masses of the station and the base spacecraft respectively; V_1 and V_2 are the linear velocities of the station and base spacecraft after separation; A is the work performed upon separation of the station; ε_1 and ε_2 are the arms of application of the forces.

The work performed upon separation, the moment of inertia, the masses of the bodies separated and the arms of application of the impulses upon separation are generally known. Thus, we have two equations with three unknowns V_1, V_2 and ω_2.

For approximate determination of the angular velocity, we can assume $V_2 = 0$. This assumption is possible if the mass of the station is significantly less than the mass of the base spacecraft. For precise determination of angular velocity ω_2, we can utilize numerical integration. The perturbation of the base spacecraft can be decreased upon separation by changing arms ε_1 and ε_2, and when there are two stations to be separated from the base spacecraft -- by symmetrical and simultaneous separation.

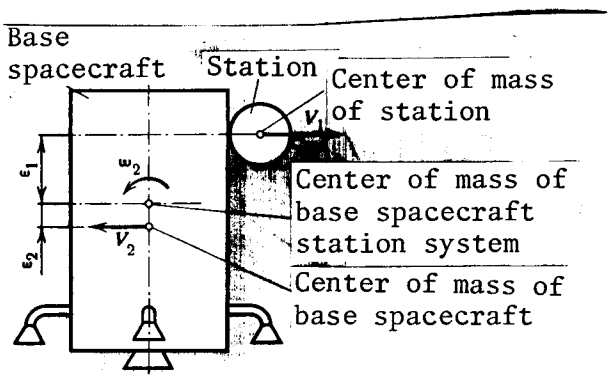

Figure 92. Diagram of Velocities Upon Separation of a Station from a Base Spacecraft

12.2. Descent to a Planet with an Atmosphere and Requirements on Structure

The most economical (from the standpoint of weight requirement) method of braking of a station landing on a planet with a sufficiently dense atmosphere is aerodynamic braking. The velocity of the spacecraft is decreased by braking in the atmosphere of the planet to a speed at which it becomes possible to use a parachute or glider system. The landing speed with a parachute system is 8-10 m/sec. For planets with a thin atmosphere, for example for Mars, it may be necessary to use a braking rocket motor in place of a parachute during the last stage.

As it moves through the atmosphere, a station is subjected to significant accelerations and heating of the surface. The acceleration of the station

$$n = -\frac{R}{mg},$$

where $R = \sqrt{Q^2 + Y^2 + Z^2}$ is the total aerodynamic drag; m is the mass of the station; g is the acceleration of the force of gravity on the surface of the Earth; Q, Y, Z are the drag, lift and lateral force respectively. The "minus" sign shows that the aerodynamic drag force is directed opposite to the velocity.

If only frontal drag acts on the station, and the lift and lateral forces are equal to 0, the descent is called ballistic. If $Y \neq 0$ and $Z \neq 0$, the descent is called gliding.

If we accept an exponential rate of change of the density of the atmosphere for a ballistic descent, the maximum acceleration can be approximately estimated by the formula

(3.8)

where ν is the coefficient of distribution of density by altitude ($\rho = \rho_0 e^{-\nu h}$); θ_{en} is the angle of entry of the station into the atmosphere (angle between velocity vector and horizontal plane drawn at the point of entry); V_{en} is the velocity of the station at the point of entry (at the point of intersection of the descent trajectory with the upper boundary of the atmopshere); e is the base of the natural logarithms; ρ_0 is the density of the atmosphere at the surface (for the Earth, $\rho_0 = 1.393$ kg$\cdot$m^{-3}; $\nu = 1/7170$ m^{-1}).

The maximum value of acceleration is reached at velocity $V = 0.605\ V_{en}$. The maximum acceleration should not exceed the permissible acceleration for the structure, instruments and mechanisms of the station. The range of permissible accelerations for various space structures and instruments is quite broad. Some instruments can withstand accelerations of hundreds of g's.

The energy dissipated as the station descends through the atmosphere is converted to heat. In order to protect the structure from overheating, special heat protection is used. The most important parameter which can be varied to reduce acceleration and heating is the entry angle. During descent from orbit around a planet, this angle is determined by the initial orbit, the position of the point of descent, the thrust vector and time of operation of the braking engine. The entry angle used during descent from orbit is between 1 and 10°, since this angle determines the range of descent. For descent from an intersecting trajectory, in order to assure a low entry angle the spacecraft must enter a narrow corridor at the edge of the planet, requiring a high order of accuracy of course correction, and bringing up the possibility that the station may land on the far side of the planet from Earth.

When this type of entry is used, the entry velocity is always higher than the escape velocity for the planet and depends on the trajectory selected and the mass of the planet. For the moon, the entry velocity is 2.55-3.3 km/sec, depending on the trajectory selected, for Venus it is 11-12.5 km/sec, for Mars 6-8.2 km/sec. Descent from a circular orbit involves an entry velocity somewhat lower than orbital velocity. Table 9 shows the values of orbital and escape velocities for several planets and the moon. /172

$$n_{max} = -\frac{1}{2}\frac{v \sin \theta_{BX}}{eg} V_{en}^2,$$

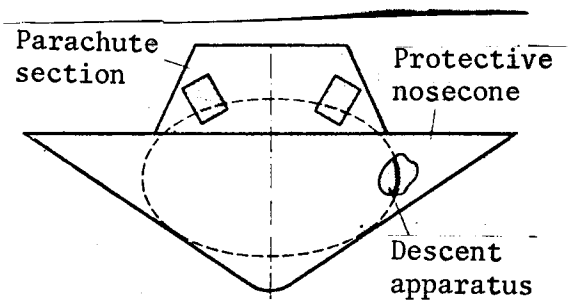

Figure 93. Spacecraft for Descent to Mars

The drag of a spacecraft upon descent is given by the formula

$$Q = c_x \frac{\rho V^2}{2} S,$$

where c_x is the aerodynamic factor; ρ is the density of the atmosphere; V is the velocity of the station; S is the middle cross-sectional area of the station. The greater the density of the planet's atmosphere, the less cross-sectional area required to achieve the required braking.

TABLE 9

Planet	Orbital Velocity (Circular), km/sec	Escape Velocity, km/sec
Mercury	2.94	4.17
Venus	7.23	10.78
Earth	7.91	11.19
Mars	3.6	5.09
Moon	1.68	2.33

A station designed to descend through the atmopshere of Venus has a compact spherical or cylindrical shape with a spherical base. Descent through the atmopshere of Mars requires an increased cross section. The cross section is increased by increasing the width of the nose cone (Figure 93 [9]) or by opening braking flaps, which is more convenient in many cases, since the structure is then compact when folded and easy to place within the nose section of a booster rocket.

12.3. Absorption of Shock Upon Landing of the Station

At the moment of landing on the surface, the station may have both vertical and horizontal velocity components, the values of which may be from a few meters per second to a few dozens of meters per second, depending on the method of delivery of the station to its operating site.

Shock absorbing devices are used to protect the instruments and structure from damage upon impact. The shock absorbing device is designed to absorb the kinetic energy of the station by the crushing of special structural elements, the compression and

exhausting of gas or the flow of liquid.

Shock absorbing devices must be reliable, light and small.

If the station performs an oriented landing on the surface, the shock absorbing device is usually placed on its supporting legs. Figure 94 shows an example of the placement of the shock absorbing device on a support. Upon impact with the surface, the energy absorbing disc, which is less strong that the cylindrical energy absorber, first ruptures, after which the piston crushes the energy absorbing material in the cylindrical support. The energy absorbing disc is used to assure more even loading of the support.

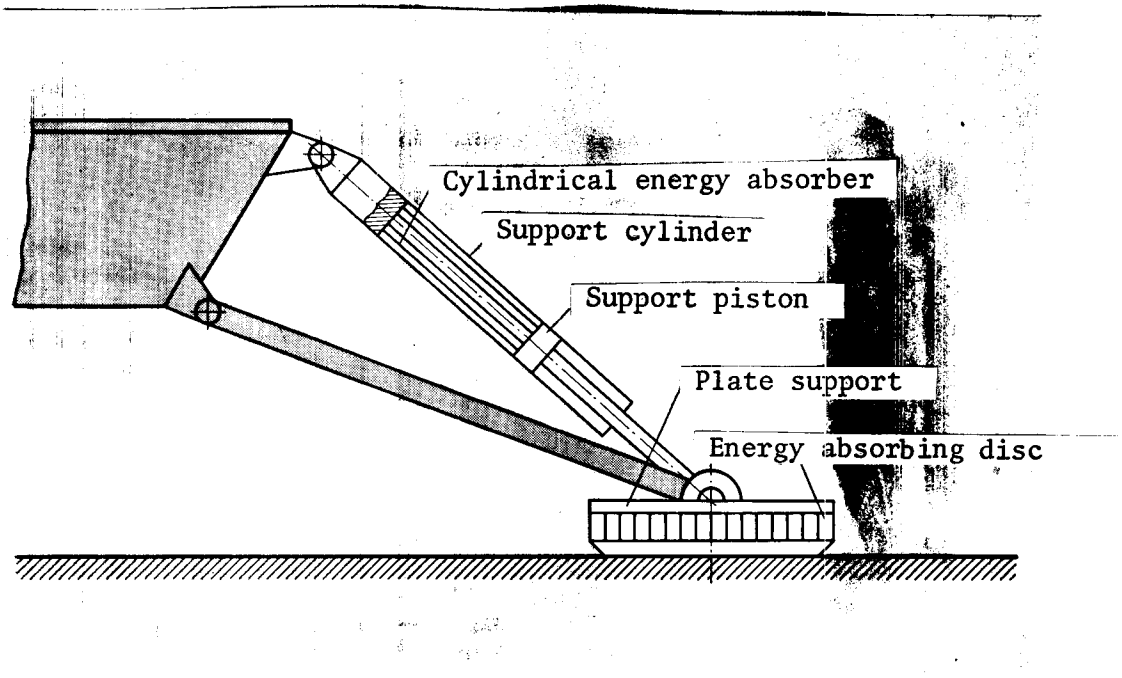

Figure 94. Example Diagram of Placement of Shock Absorbing Device on Support

The crushable elements used are honeycomb structures of aluminum or titanium alloy (Figure 95), plastic foam or balsa wood. The design of this type of shock absorbing device is simple, /173 it is light and insensitive to changes in velocity. The honeycomb elements should be preliminary compressed in order to pass the initial peak of rupture load before placement in the shock absorber. The specific rupture σ_{rup} (kg/cm^2) of honeycomb shock absorbers depends on the material used, foil thickness and cell dimensions.

Other shock absorbing devices used include:
a) metal cutting supports, in which cutting blades move along

a rod, cutting longitudinal channels; a smooth increase in force is achieved by decreasing the cutting depth at the beginning of the stroke; one shortcoming of this type of support is the difficulty of regulation of the blades;

b) rupturing tubes or calibrated bars; these devices absorb energy well, are light and independent of impact velocity; development of the design, however, requires a large number of tests;

c) pneumatic balloons; these are convenient and compact shock absorbers; they can be made of rubber envelopes surrounded with capron fabric or of rubber-treated fabric; holes are made in the balloons and covered with diaphragms; upon impact with the surface, the gas pressure within the balloon increases until the diaphragm ruptures and the gas flows outward; the advantages of this type of shock absorber include ease of storage, ease of opening and high absorption of energy;

d) shock absorbing supports with pneumatic cylinders, filled with liquid or with friction devices; the pneumatic cylinders /174
contain a compressed gas, and upon impact with the surface a diaphragm covering the exhaust apertures ruptures, the shock being absorbed as the gas flows outward; in supports filled with liquid, the energy is absorbed as the liquid flows through the apertures between the piston and cylinder; in supports with friction devices shock is absorbed by the effect of the forces of friction.

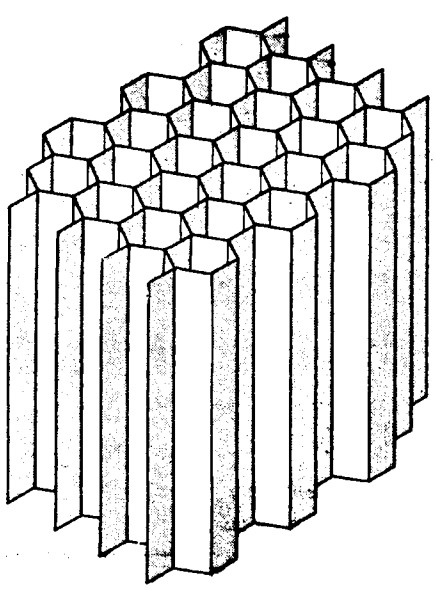

Figure 95. Honeycomb Energy Absorber

If the station cannot be oriented before landing and, consequently, may strike the surface on any side, a surrounding shock absorber must be used to protect it. In order to reduce the weight of such a shock absorber, the station must have the minimum possible surface area and no projecting parts. The best shape to satisfy this requirement is a sphere. The instruments in such a station must be arranged very compactly.

Figure 96 shows a diagram of a station with a spherical shock absorber. After landing, the shock absorber is discarded. The advantage of a spherical shock absorber is that with this type of protection, there is no problem of tipping of the station upon landing. The landing can be performed at high lateral velocities, or when there are large irregularities on the surface. Balsa wood, plastic foam or pneumatic balloons can be used as spherical shock absorbers.

The kinetic energy of the station at the moment of contact with the surface

$$E = \frac{mV^2}{2},$$

where m is the mass of the station; V is the velocity of the station at the moment of contact with the surface.

The change in potential energy of the station during the time of deceleration

$$\Pi = G_p \Delta H_{max},$$

where G_p is the weight of the stationon the planet; ΔH_{max} is the maximum travel of the shock absorber.

In our case

$$\Delta H_{max} = r - H_{min},$$

where r is the external radius of the shock absorber; H_{min} is the distance from the center of gravity of the station to the surface at the end of deceleration.

For a direct fall to the surface, assuming that the surface is absolutely hard and the structure of the station is absolutely rigid, all of the energy of the station is absorbed by compression of the shock absorber. The dependence of the force of compression of the shock absorber on its travel is shown in Figure 97. The dotted line shows the work expended in compression. It can be determined by the formula

$$A = kR_{max}\Delta H_{max},$$

where k is the filling factor of the diagram, equal to the ratio of the area limited by curve $R = f(\Delta H)$, the ΔH axis and the line $\Delta H = \Delta H_{max}$, to the area limited by the axes R, ΔH and the lines $\Delta H = \Delta H_{max}$ and $R = R_{max}$; R_{max} is the maximum force of compression of the shock absorber. Coefficient k depends on the change in contact area and the change in specific rupture load upon compression. /175

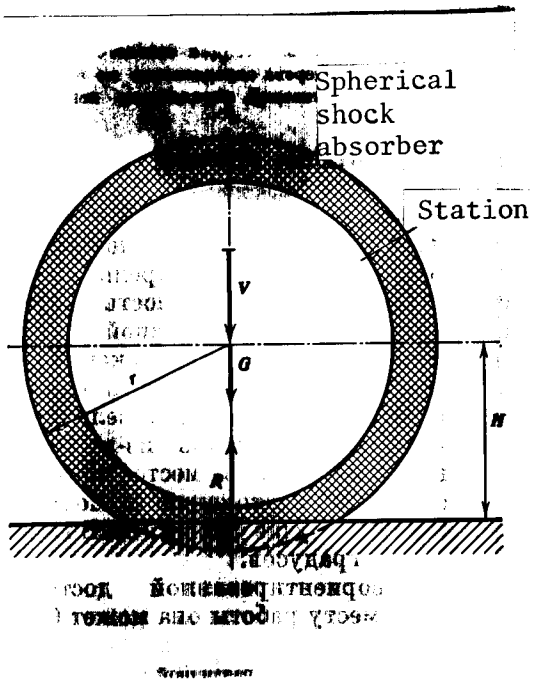

Figure 96. Schematic Drawing of Station with Spherical Shock Absorber

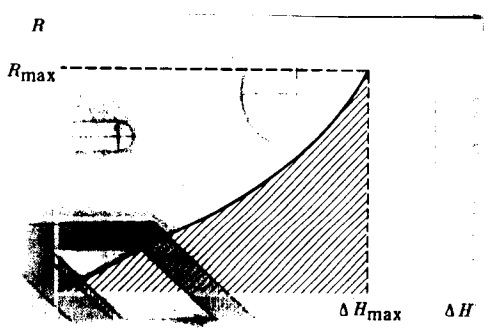

Figure 97. Force of Compression of Shock Absorber as a Function of its Travel

Setting the energy of the station equal to the work of the shock absorbing device, we can find an expression for the maximum compressive force

(3.9)

The value of R_{max} is limited by the maximum acceleration permissible upon landing

$$n_{max} = \frac{R_{max}}{G},$$

where G is the weight of the station on Earth.

Considering the expression for R_{max}, we can write

$$n_{max} = \frac{v^2}{2kg\Delta H_{max}} + \frac{g_p}{kg}, \qquad (3.10)$$

where g_p is the acceleration of the force of gravity on the planet; g is the acceleration of the force of gravity on Earth.

We can see from this formula that the acceleration is less, the greater the value of coefficient k and the greater the travel of the shock absorber ΔH_{max}.

In cylindrical supports, depending on the shock absorbing material used, coefficient k can be near unity, since the area of the piston compressing the shock absorbing material is constant and the specific rupture load changes little.

In planning a shock absorbing device, one must know the effectiveness of each material in compression, which is evaluated by the factor K. Effectiveness factor K for each material, in contrast to filling factor k, is determined with a constant contact area.

Figure 98 shows the effectiveness of various shock absorbing materials in comparison to an ideal shock absorber [8].

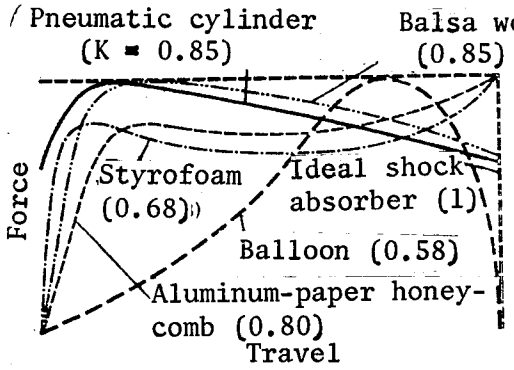

Figure 98. Effectiveness of Various Shock Absorbing Materials (Effectiveness for Honeycomb Filler and Balsa Wood Determined for Load Applied Parallel to Cell Axes)

/176

12.4. Orientation of Station on Surface

After an oriented landing, an APS retains its vertical position by means of supports which prevent it from tipping. The accuracy of the vertical position on a level surface with no large stones or depressions will be determined by the inclination of the surface and the variations in compression of the shock absorbers due to heterogeneity of the soil at the landing point. The deviation from vertical in this case may be a few degrees.

With nonoriented delivery of the station to its working location it may be arbitrarily located on the surface. In order to deploy the solar batteries, extend antennas and equipment sensors, the station must first be oriented relative to the surface in the required direction.

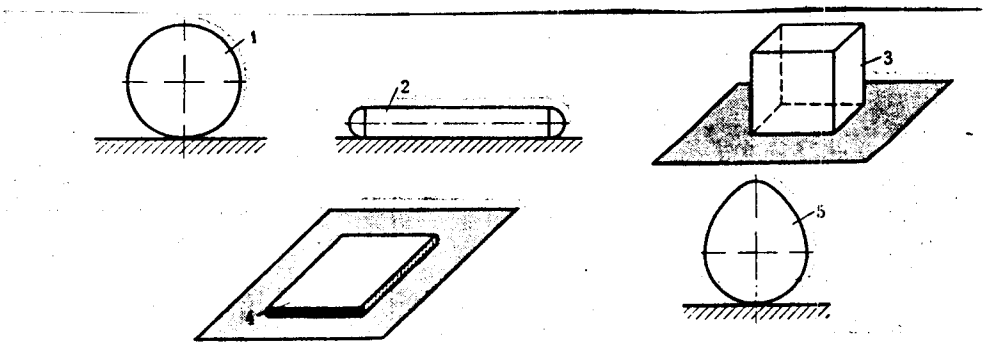

Figure 99. Stability of Bodies of Various Geometric Shapes on a Horizontal Plane

Orientation relative to a vertical line on a smooth, hard surface can be achieved by selection of the geometric shape of the station and corresponding placement of the center of gravity. Let us study the stability of bodies of various geometric shapes on a horizontal plane (Figure 99). Spherical body 1 with its center of gravity at the center of the sphere has no preferential direction of orientation -- any position is stable. This equilibrium is called indifferent. Cylindrical body 2 has a

preferential stable position: its longitudinal axis always tends to occupy a horizontal position. Relative to this axis, any position of the cylinder is stable. Cube 3 has six stable positions, flat body 4 has 2, while ovoid body 5 has one stable position. No matter what side of such a body strikes the surface, on a smooth, hard surface restoring moment M_B produced by its weight acts on this body, tending to rotate it to its stable position (Figure 100):

$$M_B = G\ell,$$

where G is the weight of the body; ℓ is the arm of application of the force.

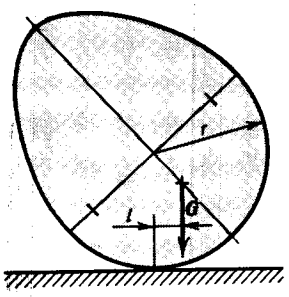

Figure 100. Restoring Moment Acting on an Ovoid Body

In its stable position, the restoring moment is equal to 0, since the line of application of the force produced by the weight passes through the supporting point. The orientation achieved by selection of the geometric shape of the station and the position of its center of gravity is called passive. One shortcoming of passive orientation is its dependence on surface quality. If there are depressions on the surface comparable to the dimensions of the station or if the friction is too high, orientation will not be achieved. Figure 101a shows an ovoid body which has encountered a depression on the surface. In this case, there is no restoring moment, since the line of application of the force produced by the weight passes between the supporting points. The orientation of such a body will fail for the same reason on soft soil (Figure 101b). It should be noted that passive orientation is aided by the initial angular perturbations of the station which it receives after separation or during shock absorption. /177

Another method of orientation of a station is orientation by means of mechanical devices; we will call this active orientation. Figure 102 shows a system for raising of a station by means of supporting bars. In the initial position, the bars are located along the body of the station and are held in place by an explosive retainer. After the retainer is removed, the drive system (electric or spring) rotates the bars around axis O_1. With its end resting against the surface of the planet, the bar rotates the station relative to point O. The restoring moment relative to point O is determined by the formula

$$M_B = N_2 \ell_1 - G\ell_3, \qquad (3.11)$$

where N_2 is the reaction of the support; G is the weight of the station; ℓ_1 and ℓ_3 are the arms of the forces.

The reaction of the support N_2 can be found from the condition of equillibrium of the support (R_1 and R_2 are the reactions at the hinge; the moment of friction in the hinge is ignored);

$$N_2\ell_2 + F_2\ell_4 = M_p,$$

where $F_2 = N_2 f$ is the force of friction; f is the coefficient of friction; ℓ_2 and ℓ_4 are the arms of the forces; M_p is the moment produced by the drive. From this /178

$$N_2 = \frac{M_p}{\ell_2 + f\ell_4}.$$

Substituting the value N_2 into (3.11), we produce

$$M_B = \frac{M_p \ell_1}{\ell_2 + f\ell_4} - G\ell_3. \qquad (3.12)$$

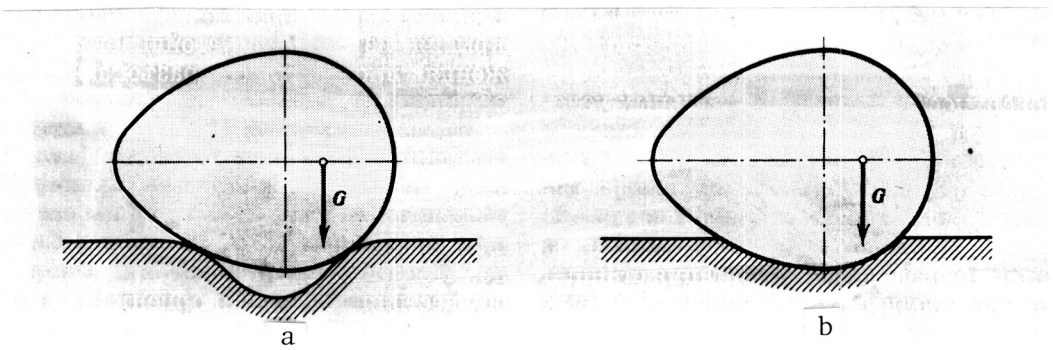

Figure 101. An Ovoid Body on Uneven (a) and Soft (b) Surfaces

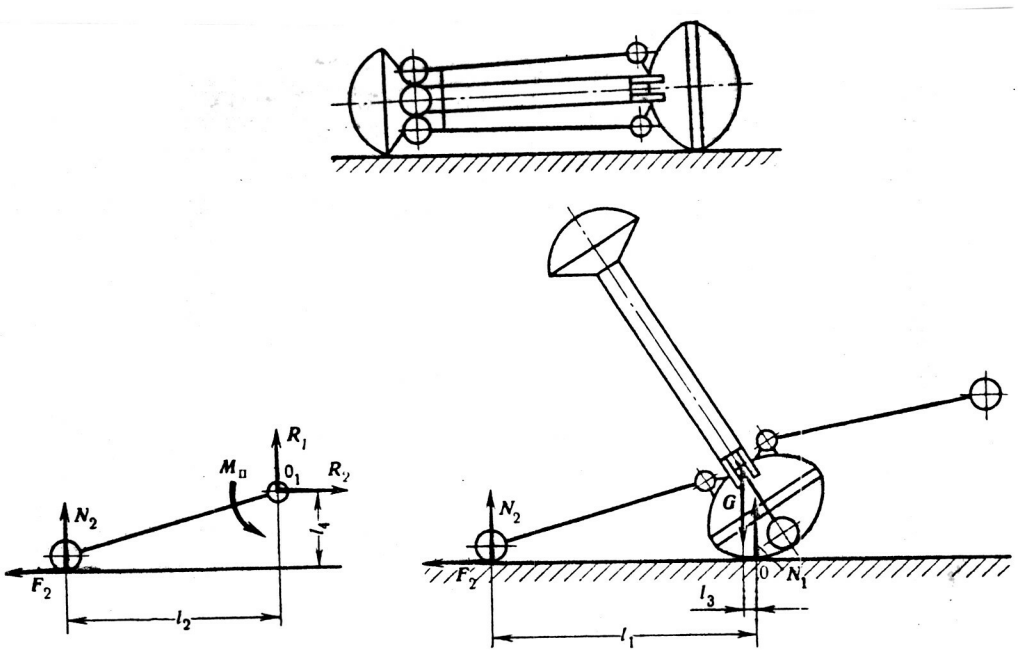

Figure 102. Diagram of Raising of Station Using Supporting Bars

We have studied passive and active methods of orientation of a station on the surface of a planet. Under actual conditions, it is convenient to use both methods together, since in this case the selection of the shape and position of the center of gravity provides for one stable position on the surface, after which the station is oriented vertically by means of active orientation devices. Combined utilization of passive and active methods of orientation is schematically diagrammed in Figure 103.

/179

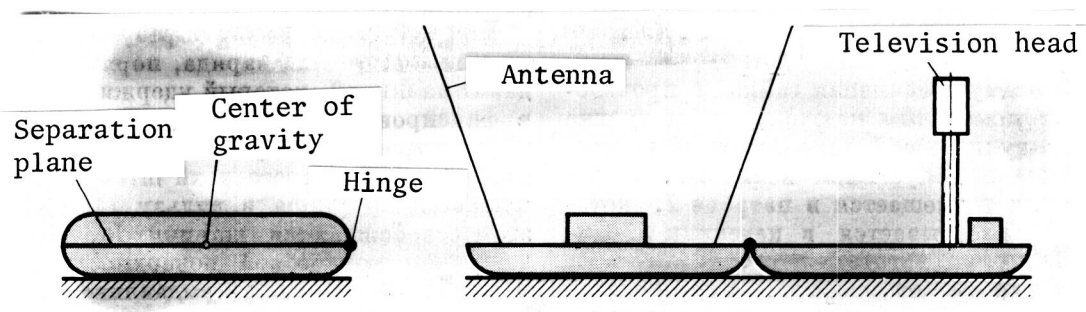

Figure 103. Diagram of Use of Combined Methods of Orientation of a Station

The station is made in two parts, hinged to each other. In its assembled form, it has the shape of a disc, which has two stable positions. After the station occupies one of its stable positions on the surface, it is opened by its drive system and

takes up its operating position. It is characteristic for this station that its separation plane is always turned away from the surface after it opens from either of its stable positions.

Sometimes, certain individual elements of the station (for example antennas or scientific instruments) must be precisely oriented relative to the vertical and subsequently aimed to the Earth or the sun. Following rough orientation of the station, precise orientation of these elements relative to the body of the station is performed by drive motors. The motors are controlled by either a pendulum or optical-television position sensor.

12.5. Movement of the Station over the Surface

The APS may be assigned the task of moving over the surface in order to place scientific equipment at some distance from the base spacecraft, or in order to collect information concerning a significant area of the surface. An important problem then arises -- the selection of a means of movement. Various wheeled, tracked and walking devices have been suggested for movement over the surface of the moon. A brief review of several designs of these devices was presented in [10]. The means of motion should provide good traversing ability (the ability to travel on slopes, cross fissures, rock falls, loose and weak soil), stability of the station as slopes are crossed, minimum consumption of electric power, good speed and maneuverability; its should also be light and small.

12.6. Separation Equipment

In addition to its mechanical connections, the station is also connected to the base spacecraft by electrical and high frequency lines, necessary for the functioning of the station during the flight trajectory and on the surface of the planet until it separates from the base spacecraft. When the station is separated, these connections are broken and the station is given the required separation velocity. Various energy storage devices capable of separation at the required moment in time can be used to break the connections and give the station the required separation energy. Pyrotechnical devices and spring mechanisms have been used for this purpose in space technology. Pyrotechnical devices are reliable in operation, have high specific power, are compact, have the necessary operating speed, can be easily switched on and are convenient to use.

Explosive bolts or clamps are used to attach the station to the base spacecraft. An explosive bolt consists of a hollow body with a hexagonal head for a wrench at one end and a threaded cylinder at the other. An explosive charge and cap are placed inside the body. The bold explodes when an electric current is

passed through the filament in the cap. The bolt explodes at the point where the two bolted parts are joined.

Explosive clamps have various designs. One sample is shown in Figure 104. The explosive clamp connects parts 8 and 9. /180
The clamp is tightened by nut 6, using a torque wrench, so that the friction between shaft 7 and balls 10 is no higher than the maximum permissible level. The explosive charge is carried in cartridge 1, screwed into breech 2. Explosive cartridges are made with various charges. The weight of the charge is selected as a function of the required clamp opening force. The charge is ignited when current passes through the ignition cap.

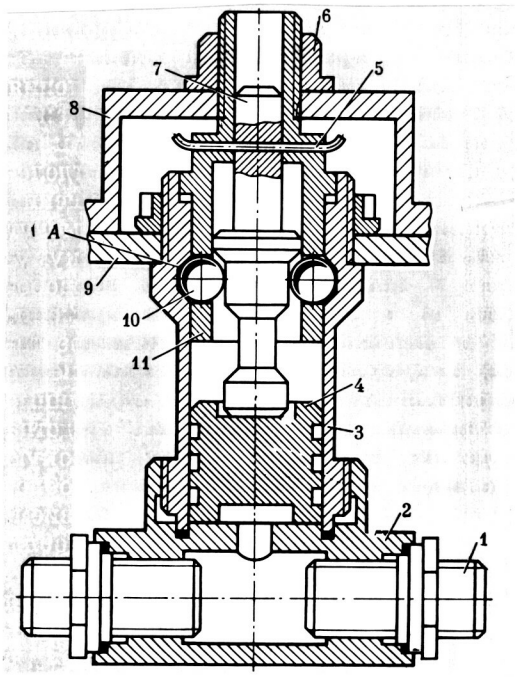

Figure 104. Pyrotechnical Clamp. 1, Explosive Charge; 2, Breech; 3, Tube; 4, Piston; 5, Pin; 6, Nut; 7, Shaft; 8 and 9, Parts Connected; 10, Ball; 11, Bushing

For greater reliability, it is recommended that two explosive charges be placed one opposite the other.

The gasses formed when the charge ignites push piston 4 against shaft 7, which is held in its position by pin 5 and the force of friction between shaft 7 and balls 10. After the pin breaks, the shaft moves downward to the stop in bushing 11, freeing balls 10. Conical surface A in tube 3 presses the balls inward, releasing the clamp.

Spring pushers and explosive pushers are used to impart the separation velocity. Figure 105 shows the design of an explosive pusher. When cartridges 5 burst, the powder gasses push against piston 3. When a certain pressure is reached, pin 2 breaks and piston 3 begins to move, accelerating the mass to be thrown.

Let us determine the work performed by an explosive pusher. Burning of the powder composition in an explosive pusher occurs very rapidly, in a few thousandths of a second. Therefore, for simplicity of calculation, we can assume that the piston does not move during the time of burning of the powder, so that the burning occurs in a constant volume. Then, the maximum pressure behing the piston can be determined by the formula

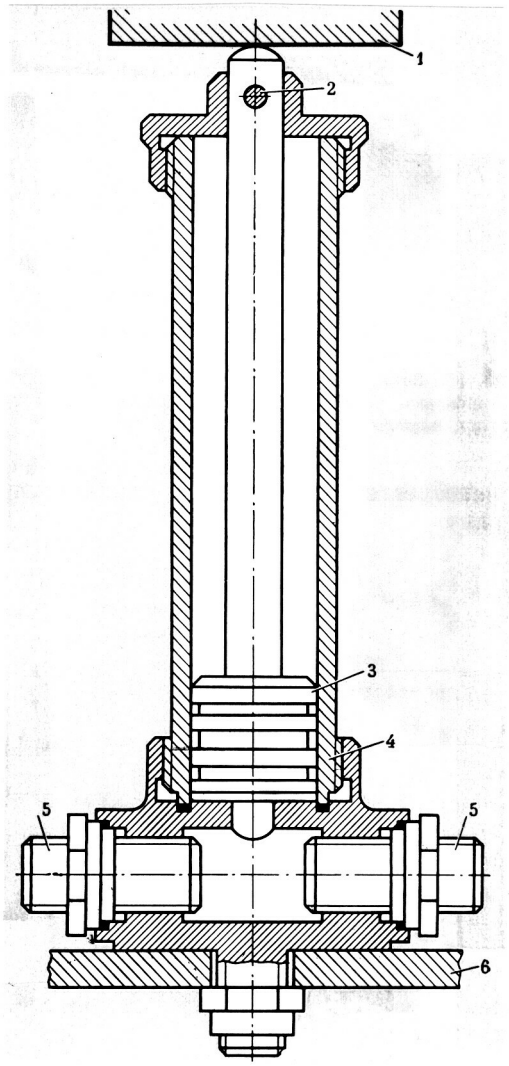

Figure 105. Explosive Pusher. 1, Mass to be Thrown; 2, Pin; 3, Piston; 4, Tube; 5, Explosive Cartridge; 6, Base Spacecraft

$$p_{max} = \frac{f\Delta}{1 - \alpha\Delta}, \qquad (3.13)$$

where p_{max} is the maximum pressure behind the piston, $kg \cdot cm^{-2}$; f is the force of the power (work which can be performed by 1 kg of powder), $kg \cdot cm \cdot kg^{-1}$; $\Delta = \omega/W_0$ is the charge density, $kg.cm^{-3}$; ω is the weight of the powder charge, kg; W_0 is the initial volume of the chamber behind the piston, cm^3; α is the covolume of the gas (the volume occupied by 1 kg of gas at full compression), $cm^3 \cdot kg^{-1}$.

However, this formula is not used for explosive cartridges. For these cartridges, the maximum pressure and volume of the space in which the pressure is developed are given as functions of the explosive charge. Ignoring thermal losses and considering the low charge density used in explosive pushers, we can determine the maximum pressure behind the piston by the formula

$$p_{max} = p_{max\ b} \frac{W_b}{W_0}, \qquad (3.14)$$

where $p_{max\ b}$ is the maximum pressure developed in the bomb; W_b is the volume of the bomb.

As the piston moves through the tube, the gas expands. The pressure behind the piston is then determined by the adiabatic equation

$$p(v - \alpha)^k = p_{max}(v_0 - \alpha)^k,$$

from which

$$p = p_{\max}\left(\frac{v_0 - \alpha}{v - \alpha}\right)^k, \qquad (3.15)$$

where $v_0 = W_0/\omega$ is the specific initial gas volume; $v = (W_0 + S\ell)/\omega$ is the current specific gas volume; k = 1.25 is the adiabatic index; S is the area of the piston; ℓ is the stroke of the piston.

Let us introduce the symbol

$$l_1 = \frac{W_0 - \alpha\omega}{S}, \qquad (3.16)$$

where ℓ_1 is the corrected chamber length, cm.

We can express the specific free gas volume v - α through the corrected chamber length and piston stroke:

$$v - \alpha = \frac{W_0 + Sl}{\omega} - \alpha = \frac{S}{\omega}(l_1 + l). \qquad (3.17)$$

Substituting expressions (3.16) and (3.17) into equation (3.15), we produce the dependence of pressure behind the pressure on piston stroke:

$$p = p_{\max}\left(\frac{l_1}{l_1 + l}\right)^k. \qquad (3.18)$$

Figure 106 shows a curve of the change in force acting on the piston as a function of piston stroke.

The work performed by an explosive pusher is shown by the shaded area (we ignore the aftereffect of the gas) and is numerically equal to the integral /182

$$A = \int_0^l p_{\max} S\left(\frac{l_1}{l_1 + l}\right)^k dl =$$
$$= -\frac{p_{\max} S l_1^k}{(k-1)(l_1 + l)^{k-1}}\Bigg|_0^l =$$
$$= \frac{p_{\max} S l_1}{k-1}\left[1 - \left(\frac{l_1}{l_1 + l}\right)^{k-1}\right]. \qquad (3.19)$$

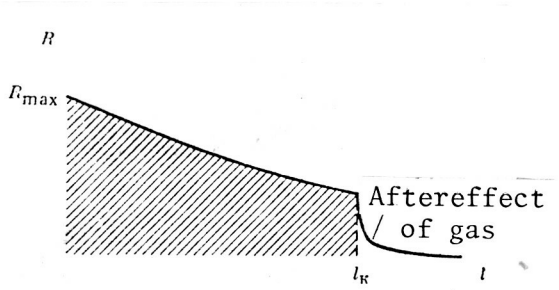

Figure 106. Change in Force Acting on Piston as a Function of its Stroke (l_k Corresponds to the Moment when the Piston Leaves the Tube)

tests on Earth, all of the work body and formula (3.20) becomes

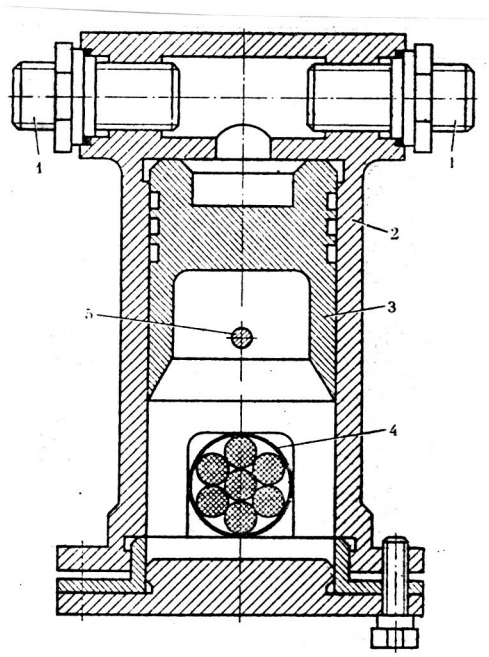

Figure 107. Explosive Knife. 1, Explosive Charge; 2, Breech Tube; 3, Piston with Blade; 4, Cable; 5, Pin

With central separation of two bodies, the work of the pusher will be equal to the kinetic energy of the separated bodies

(3.20)

We can determine velocities V_1 and V_2 by using the equation for the conservation of momentum

$$m_1V_1 = m_2V_2. \qquad (3.21)$$

If the second body is immobile, which may occur during is expended in accelerating one

$$A = \frac{m_1V_1^2}{2}. \qquad (3.22)$$

We should note that the actual work of an explosive pusher will be less than that calculated by formula (3.19) due to losses expended in heating the explosive pusher and its supporting elements. The thermal losses will vary, depending on the design of the pusher. Therefore, for each new design the work performed by the pusher must be determined experimentally.

Explosive plugs and explosive knives for cable cutting are used to break electrical and high-frequency connections. An explosive plug connection is made so that one end is connected to the station, the other end to the base spacecraft. When the station is separated, the plugs are unplugged. This method of breaking of connections has the shortcoming

that the force required to break the plug connection varies quite widely due to variations in the force of friction between plugs and jacks. This results in considerable perturbation of the station as it separates. This problem can be eliminated by the use of explosive knives which cut the cables before separation. /183

An explosive knife (Figure 107), like a pusher, is a tube with a chamber into which the explosive cartridges are screwed; a piston with a knife at its end moves within the tube. When the explosive cartridges are ignited, the knife pushes against the cable and cuts it.

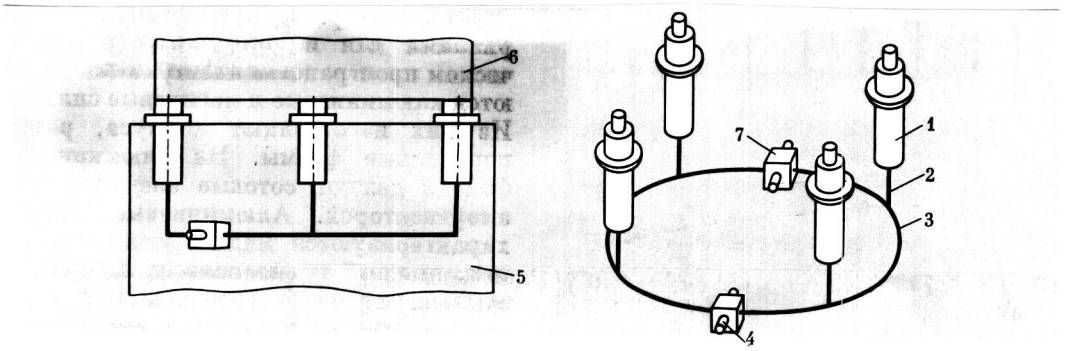

Figure 108. Installation of Peripheral Pushers. 1, Explosive Clamp with Pusher; 2, Feeder Tube; 3, Collector; 4, Explosive Cartridge; 5, Base Spacecraft; 6, Station; 7, Receiver

We have just studied the design of explosive clamps, pushers and knives. In some cases, in order to save weight and space, an explosive clamp and pusher, and sometimes knife as well, are combined into a single unit. The separation is then performed in the following sequence: 1) cutting of cable; 2) releasing of clamp; 3) ejection of the station from the base spacecraft.

The explosive pusher should be placed so that its longitudinal axis passes through the center of mass of the station and the base spacecraft. In this case, no angular perturbation will be imparted to the station or spacecraft upon separation, eliminating the possibility of a collision between them after separation. Design limitations sometimes make it impossible to use a single central pusher; in this case, several peripheral explosive clamps and pushers are installed. In order to decrease the perturbations, the explosive pushers are installed symmetrically around the center of mass and connected by a common collector and receivers (Figure 108) into which the explosive cartridges are screwed. The collector assures simultaneous operation of all pushers.

Peripheral explosive clamps may be installed without a common collector, with explosive cartridges on each clamp, but in this

case, the electrical circuit must assure that voltage is fed to all explosive clamps simultaneously. All wires carrying current tothe explosive clamps must be shielded to protect against random induction; a two-wire electrical circuit is used. After the cartridges are screwed into the system, the continuity of the ignition caps in the explosive cartridges is tested by passing a weak current through them, insufficient to ignite the caps.

12.7. Materials

In selecting a material for the structure, one should consider its mechanical and physical properties, its resistance to the conditions of space and the conditions on the surface of the planet, as well as its workability. However, the main requirement is that the material provide the minimum structural weight while assuring the required strength and rigidity. The main criteria for acceptability of materials are: specific strength (ratio of rupture strength to specific gravity σ_b/γ) and specific rigidity (ratio of modulus of elasticity to specific gravity E/γ). Figures 109 and 110 show the ratios σ_b/γ and E/γ as functions of temperature for several materials [1]. /184

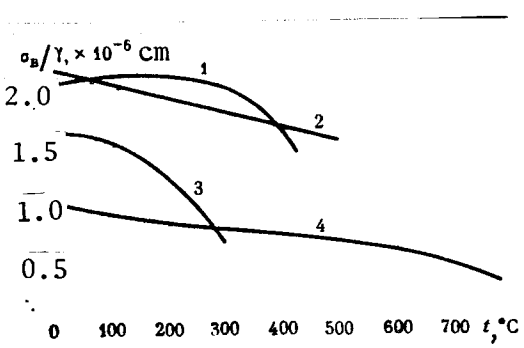

Figure 109. Ratio σ_b/γ as a Function of Temperature: 1, High Strength Alloy Steel; 2, Titanium Alloy; 3, Aluminum Alloy; 4, Stainless Steel

The most common materials for structures used in space are aluminum and magnesium alloys. They are used for bodies, frames and cross bridges. Aluminum foil is used to make honeycomb elements for shock absorbers. Aluminum alloys have low specific weight, high technological ductility, good corrosion resistance, high heat and electrical conductivity and are easily worked by cutting. Magnesium alloys have low specific gravity, relatively high mechanical properties, good ability to withstand impact loading and vibration oscillations, chemical resistance to alkalis, kerosene, gasoline and certain oils and are workable by cutting. However, magnesium alloys are inferior to aluminum alloys as to corrosion resistance in the atmosphere, since the MgO film formed on their surfaces (in contrast to the Al_2O_3 film, is loose, porous and weak, and therefor protects the base metal from further oxidation poorly. Parts and products of magnesium alloy are protected from corrosion by oxidation and application of paint and varnish coatings. With this protection, they can operate for extended periods of time under atmospheric conditions.

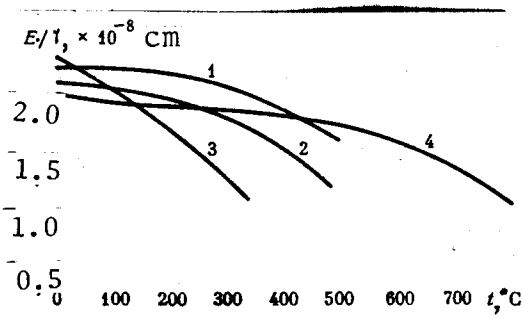

Figure 110. Ratio E/γ as a Function of Temperature (Symbols Same as Figure 109)

The workable aluminum alloys AMg3, AMg6, D16 and V95 and the workable magnesium alloys MA2 and MA2-1 are most frequently used. Aluminum alloys AMg3, AMg6, based on the Al-Mg system, have good corrosion resistance, high ductility, and are easily stamped and welded. AMg6 alloy is significantly better than the other alloys in this system as to strength, a result of its high content of magnesium and the presence of titanium. The alloy is suitable for cutting and welding by argon-arc and contact welding methods. The strength of joints made by argon-arc welding is 90-97% of the strength of the base metal. AMg3 alloy can be welded by all types of welding and can be cut satisfactorily. AMg3 and AMg6 alloys are used annealed and cold hardened without hardening heat treatment for moderately loaded structures. /185

The aluminum alloys D16 and V95, hardened by heat treatment, have high strength and good workability by cutting, but low corrosion resistance. These alloys can be spot welded but are unsuitable for gas welding. V95 alloy has high notch sensitivity. D16 and V95 alloys are used in high strength structures, for the manufacture of skins, stringers, ribs, riveted load-bearing frames and girders. For heavily loaded parts, V95 alloy is preferable to D16.

Magnesium alloy MA2 has high ductility, satisfactory corrosion resistance and weldability. It is not hardened by heat treatment. MA2 alloy is used for the manufacture of moderately loaded forged and stamped parts of complex shape which must operate for extended periods of time at up to 150° C.

MA2-1 alloy has great strength and ductility at 20° C, a result of its higher content of aluminum and zinc than the other magnesium alloys in the Mg-Al-Zn system. In contrast to the other alloys of this system, MA2-1 has good welding properties; the strength of joints made by argon-arc welding is 98-100% of the strength of the base metal. Its corrosion resistance when painted is quite satisfactory. MA2-1 alloy is not hardened by heat treatment, and is delivered in the annealed and hot-rolled state in all types of semifinished goods. MA2-1 alloy is used for welded structures which must operate for extended periods of time at up to 150° C.

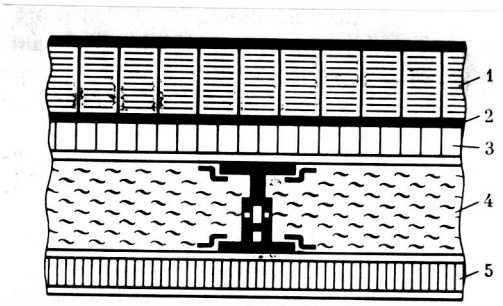

Figure 111. Design of Thermal Protection of Crew Section of Apollo Spacecraft. 1, Heat Protective Ablation Material; 2, Transition Layer; 3, Outer Shell of Stainless Steel Honeycomb Material; 4, Glass Fiber Insulation; 5, Inner Aluminum Alloy Honeycomb Structure

When parts made of magnesium alloys are joined to parts of other materials, the high coefficient of thermal expansion of magnesium alloys must be considered, as well as the possibility of contact corrosion and the corrosiveness of nonmetallic materials to magnesium. Parts of magnesium alloy must be protected during storage and transportation from corrosion by oxidation or lubrication. Work is currently being performed on the creation of new aluminum and magnesium alloys with high strength and thermal stability.

Parts operating under high loads over a broad temperature range are made using titanium alloys. Titanium alloys are used /186 for explosive clamps, explosive pushers, connecting beams, gas storage tanks and honeycomb elements for shock absorbers.

Of the titanium alloys, the most commonly used are OT4, VT4, VT5 and VT14. They have corrosion resistance, are easily stamped hot and satisfactorily worked by cutting. All of these alloys can be satisfactorily welded by argon-arc welding; the strength of welded joints is about 90% of the strength of the base metal. Titanium alloys have high thermal resistance; therefore, they are frequently used to make parts which act simultaneously as load-bearing elements and thermal bridges in the structure.

Alloy steels are used primarily for the manufacture of springs, fasteners, strip antennas, clamps, etc. Cases are known of the manufacture of load-bearing beams of steel.

Nonmetallic materials are widely used in space technology. Antennas and thermal insulation are made of plastic foam, textolite, asbotextolite and glass fabric.

As we have noted, spacecraft are covered with screen-vacuum insulation consisting of a number of screens made of metallized polyethylene teraphthalate film or aluminum foil, in order to maintain the required thermal mode. Glass wool or glass fiber is placed between the screens.

AG-4, a strong pressed material, is widely used for the manufacture of parts.

Structural glass-reinforced plastics with ultimate strengths σ_b = 70-90 kg/cm^2 have been developed. Glass-reinforced plastics combine high specific strength and low heat conductivity and therefore can act as structural and heat insulating materials simultaneously. Over a short period of time (up to 60 seconds), they operate satisfactorily at temperatures of the flow of 1300-1700° C.

Phenol-formaldehyde adhesives and epoxy-based adhesives are used to bond plastics to each other and to metals.

Optical materials used include quartz and optical glass types K8, K19, BK10, LF5, BF7, etc. In order to increase light transmission and contrast of the image, optical parts are clarified by application of single or multiple-layer coatings. Mirrors and mirror-lens systems utilize reflecting coatings, the reflection factor of which depends on the wavelength of the incident radiation. Such coatings include silver coatings protected by aluminum oxide, silver protected by copper and varnish, aluminum protected by silicon monoxide, etc.

Ablation materials are used for thermal protection of the station as it descends through the atmosphere. These materials sublimate as they are heated by the onrushing stream, thus carrying heat away from the station during the descent.

As an example, let us study the design of the thermal protection of the crew compartment of the Apollo spacecraft (Figure 111) [11]. The crew compartment consists of two individual structural shells. The shell of the sealed container serving as the crew space is a honeycomb structure of aluminum alloy. It is contained in an outer shell of honeycomb design made of stainless steel. This shell is the load-bearing element of the thermal protection system. The outer shell is attached to the inner shell by means of stringers of glass-reinforced plastic, which also provide thermal insulation for the inner structure. Additional insulation is provided by a layer of glass fiber between the shells. The outer surface of the stainless steel shell is covered by a heat-protective ablation material of low density, phenol-epoxy novolak resin. The resin is poured into the honeycomb structure of phenol nylon, which is open on one side; this structure is attached to the stainless steel shell by means of a high-temperature phenol binder. /187

12.8. Testing of Structures

Tests are an important stage in the preparation of an APS for operation. During testing, the parameters of the structure are

refined, and weak points and errors in planning and manufacture are found. Experimental investigation of a structure is performed both in the stage of planning and during the period of manufacture, and sometimes during flight testing as well.

During testing of spacecraft, the external conditions acting on it during use should be reproduced as precisely as possible. All parts and working substances used in the mechanisms and apparatus should correspond precisely to the drawings and arbitrary changes during the testing stage are not permitted.

Stations are tested: for reliability of operation of individual mechanisms and aggregates; for strength of the load-bearing structure; for strength and efficiency of the landing devices; for tightness of seal; for heat and cold.

All mechanisms and aggregates are subjected to refinement testing, during which the reliability of operation is checked after exposure to vibration, under conditions of vacuum and throughout the design temperature range. Mechanisms whose manufacture involves complex technology are subjected to refinement testing plus selection testing.

In order to save time and money, the testing of the load-bearing structure for strength, testing to check the operation of separation systems and landing devices as well as thermal testing are performed on models, generally made in 1:1 scale.

Strength testing is performed in order to determine the actual strength and rigidity of the structural elements and includes static and dynamic strength testing. The primary difficulty in these tests consists in the necessity of sufficiently precise imitation of the actual loading plan and the actual conditions of operation of the structure.

During testing of landing devices, the stability of the station during landing, the efficiency of the shock-absorbing devices and strength of the structure are tested and the accelerations acting on the station during landing in three mutually perpendicular directions are determined. During these tests, the surface area on which the landing is to be performed must be imitated.

Thermal testing is performed in order to check the design thermal mode. The thermal model includes the body of the station with the instruments or their thermal equivalents and thermal regulation elements (radiators, flaps, etc.) in place. The entire model is placed in the heat and pressure chamber, in which the conditions of heat exchange in space and on the surface of the planet are imitated.

Experimental models are made from the drawings from the flying model. Mechanically and electrically, they are identical to the

flying model, but they are tested under greater modes and to their full strength reserve, and are therefore not suitable for use in flight after testing. The test models must imitate all operation of the station under conditions as close as possible to flying conditions.

CHAPTER 13

DESIGN OF RADIO ELECTRONIC EQUIPMENT OF AUTOMATIC PLANETARY STATIONS

13.1. Placement of Radio Electronic Equipment and Some Problems of its Design

/188

The design of radio electronic apparatus (REA) depends on the purpose of the APS, its volume, shape and the method of its delivery to the region of operations. In addition to this, the design of REA depends on the complexity of the system, i.e., the number of stages and elements, operating principle, range of frequencies, transmitter power, antennas and methods of performance of the scientific experiments. The design of the REA in turn influences the shape of the compartment, supporting frame and individual units of the APS. Presently, combined planning of spacecraft + REA is widely used, allowing the optimal version of the APS to be selected.

The placement of the REA in the spacecraft is an independent area of design. The correctness of placement of instruments and units within the volume set aside will go far toward determining the qualitative indicators of the operation of the electronic system and of the station as a whole.

During the placement of the instruments, the following problems must be solved:

-- provision of the proper thermal modes of the instruments, units and individual elements;
-- accuracy of installation of instruments;
-- consideration of electromagnetic compatibility;
-- protection from the influence of radiation;
-- selection of connecting lines, i.e., lengths of cables and wires;
-- protection from vibration and impact loading.

To assure convenience of installation of instruments or individual units during placement, good access to each instrument must be provided. One important requirement placed on the arrangement of REA is the proper position of the center of gravity and assurance of high reliability. The position of the center of gravity influences the stability of the station during operation of course correction and braking engines, stabilization during descent through the atmosphere, stability of the station upon landing, as well as its orientation on the surface.

For orientation sensors and optical instruments, in addition to the problems listed, the necessary field of vision must be provided -- the structural elements cannot block the field of vision (unless specially called for).

The scientific apparatus may be placed inside or outside the sealed compartment. The proper microclimate is created in the sealed compartment: the required pressure, gas composition and temperature range must be maintained. The sealed compartment is usually made in the form of two half shells with flanges. A sealing rubber gasket is placed between the flanges (Figure 112). The two half shells are tightened around the flanges with bolts. The sealed high-frequency and low-frequency leads are attached to the half shells. The instruments within the sealed compartment are carried on a frame which is mounted on the flange of one of the half shells. Some instruments may be installed directly on the half shells, for which purpose special lugs and flanges are welded to the shells. /189

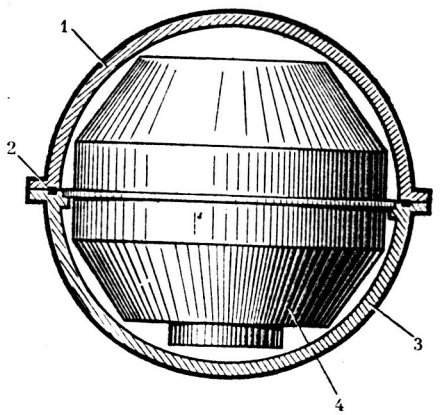

Figure 112. Schematic Diagram of Sealed Compartment: 1, Upper Half Shell; 2, Gasket; 3, Lower Half Shell; 4, Apparatus

Sealing under deep vacuum conditions is a difficult technical problem. The optimal arrangement of the instruments within the sealed compartment is difficult.

Elements, units and apparatus capable of operating in the vacuum of space are available now, but the temperature range over which the can operate is limited. If the instrument compartment is not sealed, the devices which liberate the most heat must be placed around the periphery of the section. In this case, one of the walls directed away from the station should be made to act as a radiator to carry away the heat.

In order to eliminate the influence of the heat liberation of one instrument on the others, the remaining walls of the instrument should be covered with screen-vacuum insulation. Unsealed structures are easier to manufacture and allow better versions of placement of electronic apparatus and sensors to be selected. Unsealed sections allow the dimensions and weight of the APS to be reduced. Therefore, the advantages fall on the side of unsealed compartments, although a number of problems related to the provision of the operation of certain electronic

elements, units and instruments in deep vacuum or in an unusual medium such as the atmosphere of Venus remain to be solved.

In developing APS, as we have noted, one of the most difficult problems is the provision of normal thermal modes of the apparatus. For example, when apparatus is located on the surface of the moon where there is no atmosphere, the convective component of heat exchange is totally absent. Consequently, in this case heat exchange between elements of instruments and the body of the station is by heat conductivity and radiation, requiring that structural materials with good heat conductivity be used and that the corresponding optical coefficients of the surfaces be selected. Evaporation of materials in a vacuum is a less difficult problem, since most materials are used at temperatures significantly lower than those at which noticeable evaporation occurs.

The significant portion of the volume and weight of the APS apparatus consists of power supplies. Therefore, in selecting the circuits and devices for the electronic system, an attempt must be made to increase the power efficiency of instruments and decrease the consumption of electric power by all supplementary systems. Placement of the REA in the volume of the sealed compartment set aside may be according to a single-layer or a multilayer plan (Figure 113 and 114). /190

For convenience of access to the instruments, a single-layer arrangement is preferable, although for practical reasons this is very difficult to achieve in the volume and shape provided (generally a sphere, cylinder or cone).

At the present time, there is no well developed method for arrangement of equipment in compartments considering the multiplicity of factors such as thermal and electromagnetic compatibility, mechanical rigidity, strength, impact resistance and vibration resistance, convenience of access to any instrument in a complex multilayer arrangement. These problems are generally solved intuitively rather than by the use of any well founded method of design.

The modern requirements for combined planned of REA + spacecraft make it necessary to select definite criteria for optimization.

The difficulties involved in selecting criteria for optimization are related to the variety of type of APS, technical, production as well as economic factors.

Investigations in the are of optimization of the design of REA and its arrangement should be directed toward consideration of the variety of these factors.

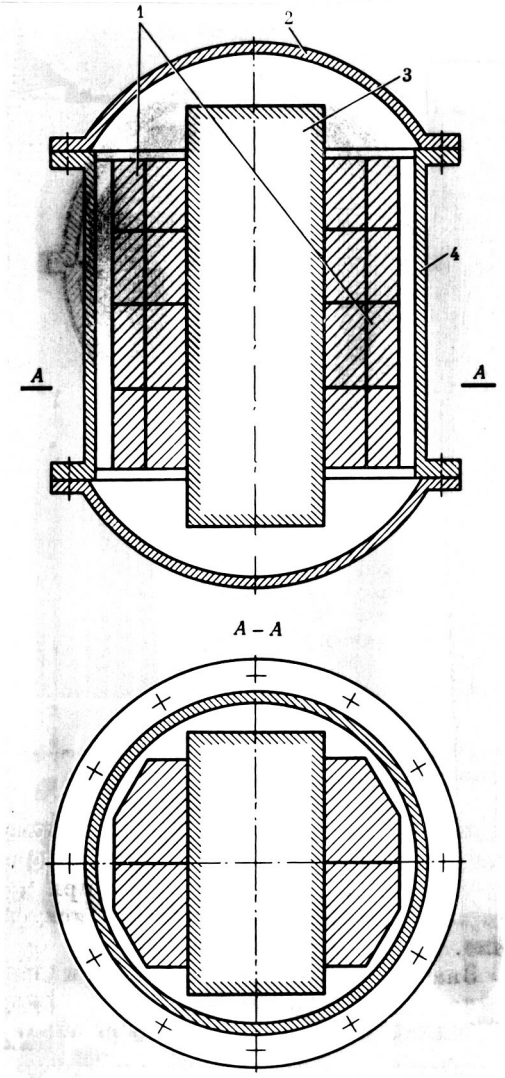

Figure 113. Single-Layer Arrangement of Electronic Apparatus in Compartment: 1, Electronic Apparatus; 2, Cover; 3, Power Supply; 4, Body

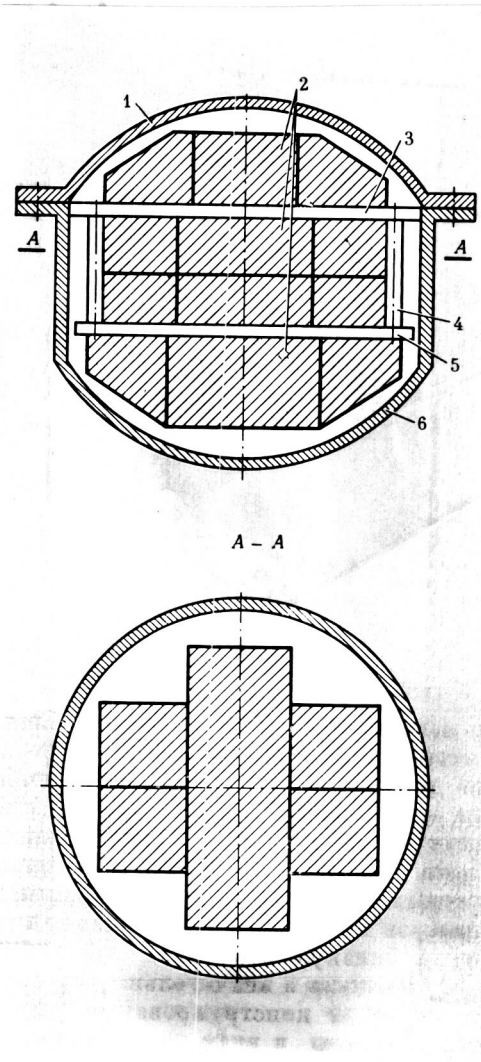

Figure 114. Multilayer Arrangement of Electronic Apparatus in Compartment: 1, Cover; 2, Electronic Apparatus; 3 and 5, Bases; 4, Support; 6, Body

Due to the complexity of the prediction of the reliability of instruments, the design of any REA instrument should allow the location and cause of any defect to be established as rapidly as possible. In order for this requirement to be met, convenient access to it in the element or module must be provided. Therefore, the designer's skill will determine the convenience of access to any unit even with a complex arrangement.

The use of modules in the design of instruments best solves the problem of provision of access and repairability of equipment. All electric circuits should have easy access for testing and

measuring instruments and adjusting tools. The laying of cables and conductors should allow easy removal of individual units, parts and boards, and if hinged, tilting structures are used, cable placement should allow the hinges to rotate freely. The use of easily removed units and modules in instruments causes some increase in volume and weight; therefore, while considering easy access to instruments, one must also consider other factors influencing the selection of the optimal version of design.

Figure 114 shows a centralized multi-layer arrangement of REA instruments. All instruments are placed on a frame which is a three-dimensional closed beam, the upper portion of which is attached to the load-bearing flange. The instruments, oriented with their plug panels and controlling elements on top, are attached to the horizontal bases. This assures easy access to the contacts of any instrument. The horizontal load-bearing bases are connected by vertical supports, the design of which assures the necessary frame strength.

In most cases, the instruments are made in the form of parallelepipeds with holes for mounting in one of the planes.

The plus connections should be made on one of the side walls, and only in certain individual cases on two opposite walls, for example in high-frequency amplifiers, where parasitic coupling between stages is great. Therefore, the supporting bars carrying the stages of these amplifiers are designed so that a signal at one frequency, amplified as to level, is geometrically displaced in one direction, far from the input (Figure 115). Failure to observe this requirement may cause undesirable influence of the output signals on the input of the device.

In designing REA, attempts are made to decrease weight and volume of the apparatus and increase its operational reliability -- /192
a task of prime importance. Significant success in this direction has been achieved by designing instruments to use printed circuits, by the modular method of design and particularly by the introduction of integrated and hybrid circuits.

The modular design method is based on the division of a circuit into individual functional units, made considering this division. The best version of a functional unit is that which combines the advantages of functional and structural divisions. Therefore, the attempts must be made to see that a unit includes a functionally distinct portion of the circuit and has a final structure which satisfies the mechanical and operational requirements.

The use of integrated and hybrid circuits significantly changes the design of instruments, greatly reducing their volume and weight, as well as their power consumption. The attempts to

create small apparatus with optimal characteristics have led to the development of widely varied types of instruments of widely varied size, making selection of an effective design of a single unit in the section of an APS more difficult. The shape of the units and instruments must be selected so that as the REA is arranged in the compartment, the filling factor reaches its maximum.

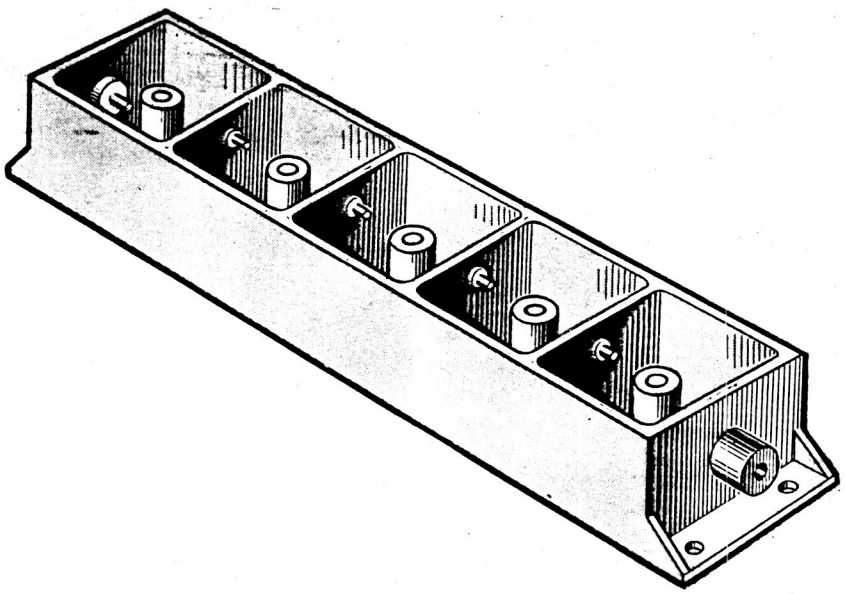

Figure 115. Schematic Diagram of High-Frequency Amplifier

This is partially achieved by the use of even-multiple dimensions of instruments and mounts, allowing hear-optimal arrangement in the section and significantly simplifying subsequent design of the instruments. Instruments in the form of rectangular parallelepipeds can be placed with a given filling factor in compartments of /193
any shape, although when the instruments must be placed in sections of cylindrical or spherical shape a segmented or prismatic shape of instruments may be more efficient. The use of instruments of a definite shape allows standardization of apparatus, load-bearing frames and APS sealed compartments. Problems of heat exchange are most effectively solved where the designs of frames and compartments are standardized, since the heat conductors (air paths) and radiators can be placed in the frame in directions corresponding to the design heat flow directions. Knowing the boundary conditions and geometric dimensions of a compartment, it is easy to calculate the quantity of heat which can be transmitted through the heat conductors or air paths from the instruments to the body of the compartment. The results of calculation can be used for

optimal arrangement of REA, and also for analysis and calculation of the thermal modes of the apparatus. In selecting the arrangement of the instruments, one must consider the ease of manufacture of the instrument frame and, therefore, its economy of production.

The instrument frame is a complex shape; therefore, the sequence of its manufacture must provide effective distribution of various types of technological processes and the greatest utilization factor of the material, i.e., the ratio of the mass of the finished product to the total mass of raw material expended.

Frames may be case, welded frame structures or welded frameless structures of rolled sheet material. In order to improve the weight characteristics, they are made of aluminum or magnesium alloys. In studying the advantages of one technological version or another, it can be concluded that welded frame and frameless structures are most economically suitable. They are more resistant to impact loads than are cast structures. The weights of such frames amount to 8 or 10% of the weight of the instruments. The labor consumption involved in the manufacture of a cast frame is 40 to 50% greater than for a welded frame; consequently, the cost of cast frames is also higher.

In order to meet the requirements for easy access to plugs and points of attachment of instruments by means of standard tools, the instrument frame can be made using telescopic guides, hinged loops, extending and overlapping bodies. When such complex frames are used, one must recall the strength properties and design frames for mechanical strength considering the linear and impact loads expected, as well as vibration effects.

In selecting the arrangement of REA, one must know how external factors influence the equipment and what protective measures must be taken. Thus, in the development of instruments resistant to the effects of ionizing radiation, one must know how the radiation imfluences the materials and elements of the circuit and what technical steps can be taken to prevent the harmful influence of radiation.

After determining the mechanical effects on the apparatus of the APS, one must determine whether it should be shock isolated from perturbing forces. The ability to analyze and calculate electromagnetic compatibility and temperature fields allows highly reliable apparatus to be created.

13.2. Electromagnetic Compatibility of Electronic Apparatus

The sense of compatibility consists in that any electronic or electrical device must not create impermissible interference /194
for the normal operation of other devices, and must operate normally within its surroundings. The REA should operate according

to its purpose under conditions of internal and external electromagnetic fields. The electromagnetic fields include all radiation from external sources which act to any extent on the APS apparatus, internal fields include the noise induced by the REA itself which is located in the compartment.

With the limited volume of APS, great quantities of apparatus must be placed with high installation density. Therefore, when apparatus is placed in the APS compartment, full analysis of the electromagnetic conditions must be made and their influence on the REA predicted, in order to consider and eliminate or minimize the effects of these influences. During analysis, one considers the source of noise, time of its action, frequency and power of the transmitter, gain and orientation of antennas, selectivity of the receiver in the pass band of the frequencies, mutual placement of electric and magnetic circuits. Considering the effects of external and internal noise, one must find sources of radio interference in preliminary calculation, then change the placement of instruments or introduce shieldings so as to eliminate the undesirable signal. The development of REA considering electromagnetic compatibility requires precise analysis of REA circuits and designs as concerns their susceptibility to noise and their analysis as sources of noise. The analysis can be divided into the following stages:

-- determination of noise sources;
-- determination of apparatus sensitive to noise;
-- determination of REA characteristics;
-- determination of requirements for insulation, shielding, selection of high frequency cables and connecting conductors;
-- selection of the method of grounding (at many points or at one point);
-- selection of methods of suppression of noise within apparatus and selection of devices for suppression (decoupling of circuits, insulation of circuits or individual stages, filtration, etc.).

The REA of an APS generally includes transmitters which radiate energy in a fixed frequency band and transmit a fixed signal. In practice, in addition to signals at the fixed frequency, transmitters create radiation at undesirable frequencies.

The reasons for radiation of side signals in radio communications and telemetry transmitters are:

-- parasitic oscillation;
-- nonlinear distortions caused by overloading of amplifiers;
-- mutual modulation occurring in a nonlinear element;
-- excess expansion of side bands, i.e., appearance of radiation outside the band of frequencies set aside for the transmitter.

In developing receiving apparatus with low-noise parametric amplifiers and tunnel diodes, in addition to the production of high sensitivity, considerable attention must be given to the

investigation of filters and other selective devices designed to eliminate or attenuate interfering signals consisting of the side band radiation, various parasitic signals, cross and internal modulation, etc.

Thus, in solving problems of electromagnetic compatibility of REA, the primary difficulty consists in the insufficient spatial and frequency separation of radio equipment, the output signals of which act on each other. Determination of sources of noise and additional (parasitic) electrical coupling is a difficult task, and the elimination of undesirable signals may require great changes in the design of equipment, or sometimes even complete restructuring. Therefore, careful analysis of all sources and receivers of undesirable signals must be taken as a basis in design. /195

Sources and paths of induction of undesirable signals may be both due to direct electrical contact between individual elements in the structure and due to the influence of electrical, magnetic and electromagnetic fields. This problem is discussed in detail in [12].

Undesirable signals are transmitted over the following paths:

-- coupling through a common resistance, including through power supplies;

-- inductive coupling;

-- capacitive and inductive coupling involving secondary conductors;

-- coupling through an eleetromagnetic field.

Two means can be used to suppress or reduce noise. One involves attempting to prevent or limit the interfering radiation and its propagation, the other involves attempting to create REA which is less sensitive to noise. The following methods are used to suppress noise where it develops: improvement of the characteristics of devices radiating noise; attenuation of noise in places near the source where it develops. At points where noise is received, filters, shields and special circuits can be used. Noise is attenuated by shielding of the source of receiver of the noise, which in some cases is the primary method of noise control.

If it is difficult to achieve shielding due to poor seams, barriers, ventilation apertures, loose fitting of covers, bases, etc., then special design measures must be used, i.e., metal or metallized shields must be added.

Thus, metal barriers and foil-covered plates which must have good direct electrical contact with the body (base) of the instrument or section, can be used to reduce undesirable coupling through an electric field. The use of connecting wires between the shield and body significantly worsens the shielding effect

by increasing the inductive reactance at high frequencies.

High frequency amplifiers are frequently made in the form of a line of several sections (cells) shielded from each other by barriers and covered with a common cover which makes good contact around the perimeter at several points.

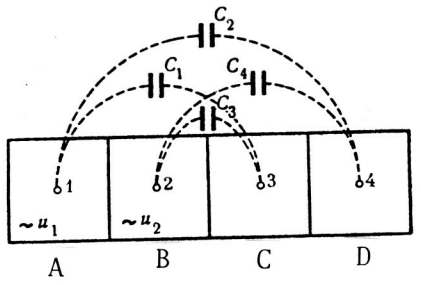

Figure 116. Parasitic Coupling in a High-Frequency Amplifier without a Cover

Let us study an example of induction of undesirable coupling taken from [12]. The design consists of sections A, B, C and D (Figure 116). Suppose in sections A and B at points 1 and 2 sources of undesirable induction u_1 and u_2 are found. Sections C and D contain elements in which undesirable signals are induced (points 3 and 4). With the cover removed, the coupling between sources and receivers of induction in through the parasitic capacitances C_1 and C_2, C_3 and C_4. With the cover closed (Figure 117), capacitances C_1' and C_2' are formed in sections A and B between points 1 and 1', 2 and 2' and in sections C and D -- C_3' and C_4' between points 3 and 3', 4 and 4'. /196

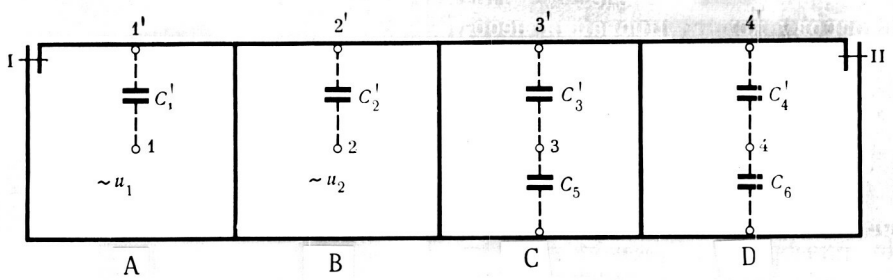

Figure 117. Parasitic Coupling Through a Common Cover

At low frequencies, where the influence of the inductive reactance of the cover is not felt and the contact resistance between cover and body at points I and II is not great, these capacitances are connected to the body and the presence of the cover almost completely eliminates the undesirable inductance. The picture is different at high frequencies. Points 1, 2 and 3, 4 are coupled through the same capacitance C_1' and C_2', C_3' and C_4' and the inductive divider which is formed by several sections of

the shielding cover. Figure 118 shows the equivalent circuit which transmits the undesirable (parasitic) signal through the cover. Transmission of an undesirable signal from a source of inductance u_1 to the receiving point 4 occurs through the first divider, consisting of capacitance C_1' and inductance $L_{1'I}$ in cover sector 1'-I, the second divider consisting of $L_{1'4'}$ and $L_{4'II}$ in cover sectors 1'-4' and 4'-II, and a third divider consisting of capacitances C_4, and C_6.

/197

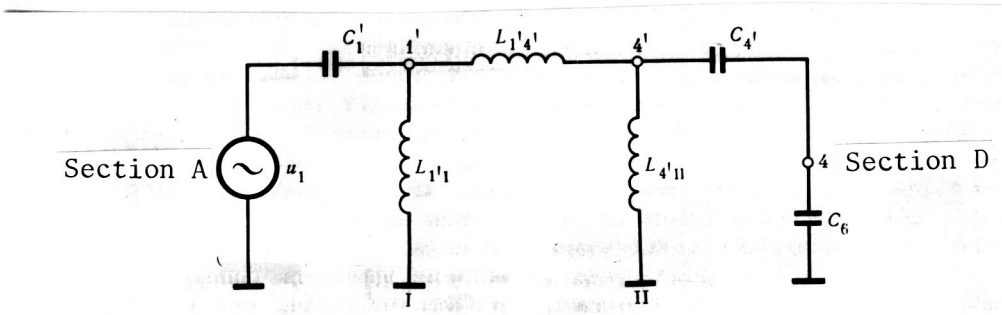

Figure 118. Equivalent Circuit

Capacitances C_1', C_2', C_3' and C_4' (see Figure 117) are significantly greater than capacitances C_1, C_2, C_3 and C_4 (see Figure 116); therefore, we may find that when the high frequency line is covered by a common cover, undesirable coupling increases. Consequently, to assure effective shielding each section should be covered with a separate cover (which is quite difficult without increasing the dimensions of the instrument) or, after determining the sections in which sources are present, these can be covered with a single cover, while the sections in which receivers are present is covered with another cover.

Undesirable inductance is located during operations with the equipment. The process of determination of a source of inductance is cumbersome and requires a great deal of time; therefore, during planning and design work it is necessary to analyze carefully possible mutual interference.

Effective installation and design of individual instruments and proper arrangement of the REA are both important for reliable operation of the electronic system of an APS.

13.3. Influence of Ionizing Radiation on the Operation of Electronic Equipment.

Considerable attention is currently being given to the study of the influence of ionizing radiation on REA, its elements and materials. To design apparatus which is resistant to the influence of ionizing radiation, one must know what forms of radiation and levels of radiation will act upon it. A knowledge of the influence of radiation on materials and elements of circuits from the standpoint of ionizing damage allows the designer to select properly the circuit to be used in an instrument, the elements which make it up, the structural materials which are used, to arrange them effecientlv and select the location of the apparatus in the APS compartment, and if necessary to use protective measures for the instrument or some of its individual elements.

Depending on the specific purpose of the APS and the planet to which it is sent to perform its scientific studies, the REA may be acted upon by radiation from natural or artificial sources. The most intensive radiation strikes REA in the radiation belts of the Earth, on spacecraft with nuclear power sources, or in the zone of action of nuclear or thermonuclear explosions and during solar flares. The greatest danger to the REA of APS comes from: primary cosmic radiation and solar cosmic radiation, arising during intensive chromosphere flares on the sun. During flights from Earth to the planets the apparatus of a spacecraft moving through its trajectory may be acted upon by proton and electron radiation in the inner radiation belt around the Earth and electron radiation from the artificial radiation belts around the Earth.

Ionizing radiation is divided into corpuscular and quantum radiation. Corpuscular radiation includes streams of elementary particles (neutrons, protons, beta particles, etc.). Quantum radiation consists of electromagnetic ionizing radiation -- gamma particles and x-rays. All materials used for the manufacture of REA and its elements, from the standpoint of ionizing damage, can be divided into metals, inorganic and organic materials and semiconductors. Let us study the defects arising in these types of materials under the influence of radiation.

Quantum and corpuscular radiation, passing through a substance, interacts either with the nuclei of the atoms or with the electrons, altering the properties of the substance. This process has two stages -- the primary and secondary stages. The primary stage involves interaction of the particles of ionizing radiation with particles of the matter, excitation of electrons, atoms and molecules, displacement of atoms from their positions in the lattice and nuclear conversion. The secondary stage involves subsequent excitation of atoms and ions ejected (displaced) as a result of the primary processes. Defects arising as a result of ionizing radiation include vacancies (vacant

lattice positions), impurity atoms, collisions during substitution, thermal peaks, displacement peaks and ionization effects.

When high energy particles collide with atoms of a solid, /198
vacant nodes may be formed, i.e., an atom or ion is knocked out of its position in the crystal. If this process occurs with high energy, further displacement of the atoms is possible (secondary stage). If the displaced atoms do not recombine with neighboring vacant locations, but rather are decelerated in the intervals between they are called interstitial atoms, occupying unstable positions.

Neutron bombardment resulting from nuclear reaction forms atoms of various impurities. The atomic decay products produced as a result of the nuclear reaction, entering the lattide of the irradiated substance, may significantly change its properties. If the energy of a particle is insufficient to knock an atom from its position in the lattice, but rather increases the amplitude of its oscillations about its position, intensive oscillations of the atoms may arise along the path of the particle, the energy of the oscillations then being converted to heat. This process is called a thermal peak.

In addition to its action on atoms of matter, all ionizing radiation causes excitation and ionization of electrons. Ionization refers to the process of formation of electron-hole pairs, free electrons and ions in the substance by breaking the interatomic bonds and displacement of the electrons from their orbits. With the beginning of ionization, the process of recombination of ions also begins, forming a neutral atom from a positive ion and an electron. During ionization, chemical reactions, luminescence and photoconductivity may arise, as well as increases in temperature and other changes in the properties of the matter.

REA designed for spacecraft makes wide use of aluminum, copper, magnesium and titanium alloys. Let us study the influence and types of radiation damage of some of these.

We have established that the primary changes in the properties of metals result from displacement of atoms from the nodes of the crystalline lattice. Among the materials used in REA, metals are least sensitive to radiation, since they have a high concentration of free carriers and, furthermore, the properties of metals depend little on the presence of lattice defects. The change in the properties of metals, like other materials, depends on the energy and density of ionizing radiation. Studies have shown that when aluminum alloys are bombarded by an integral flux of $9.84 \cdot 10^{20}$ neutrons/cm^2 at 49° C, the yield point increases from 18.3 to 38.3 kg/mm^2. Magnesium alloys, when exposed to the same flux, change their yield point from 31.9 to 46.5 kg/mm^2, the tensile strength from 50.3 to 59.7-kg/mm^2, the relative elongation from 26 to 24%. Copper, when bombarded

by an integral flux of $9.5 \cdot 10^{17}$ to $1.07 \cdot 10^{20}$ neutrons/cm^2 at 20° C, increases its yield point from 4.9 to 21.8 kg/mm^2, its strength from 22.5 to 27.4 kg/mm^2. When absorbed, the energy of ionizing radiation is converted to thermal energy, which is particularly true of metals and heavy materials.

If we know the particle flux density of ionizing radiation, we can determine the quantity of thermal energy induced in the product. During short-term bombardment, the quantity of heat is determined by the expression [13]

$$Q = \varphi \sum_{i=1}^{n} k_i v = \varphi \sum_{i=1}^{n} k_i \frac{m_i}{\rho_i}, \tag{3.23}$$

where Q is the quantity of thermal energy liberated, w; ϕ is the density of the flux of particles (quanta) of ionizing radiation, particles/(m^2·sec); m_i and ρ_i are the mass and density of the material respectively; k_i is the heat liberation factor of the material, w·sec/(m·particle); n is the quantity of material included in the product. /199

For long-term irradiation of a product under conditions of a vacuum, the quantity of thermal energy remaining in the product is determined by the formula

$$q = Q - \varepsilon_1 \sigma T_1^4 - \varepsilon_2 \sigma T_2^4 = \varphi \sum_{i=1}^{n} k_i \frac{m_i}{\rho_i} - \varepsilon_1 \sigma T_1^4 - \varepsilon_2 \sigma T_2^4, \tag{3.24}$$

where ε_1 and ε_2 are the radiation factors of the outer and inner surfaces of the product; T_1 and T_2 are the temperatures of the outer and inner surfaces of the product;

$$\sigma = 5{,}78 \cdot 10^{-8} \text{ w/(m}^2 \cdot \text{hr} \cdot \text{K)}.$$

The radiation energy, when converted to thermal energy, may heat elements of the structure and elements of circuits to very high temperatures (on the order of 200°); great heating is observed when massive products are irradiated.

In addition to the changes in mechanical properties, ionizing radiation can also change the physical properties of metals. Table 10 [14] shows the change in resistivity of certain metals.

TABLE 10

Metal	Temperature of Irradiation, ° C	Integral Flux, $x10^{19}$ neutrons/cm^2	Change in Resistivity, %
Tungsten	30	1 (thermal)	+10
Molybdenum	30	1 (thermal)	-7
Platinum	30	0.5 (thermal)	+1
Copper	-150	1.1	+20
Aluminum	-150	1.1	+33
Annealed Copper	90	20-70 (thermal)	+8.0

In studies of radiation damage, resistivity can be used as a good parameter for telemetry, since it is easily measured.

Inorganic materials (ceramics, glass, quartz, etc.), like metals, have high radiation resistance. Ionizing radiation causes changes in the electrical conductivity, dielectric permeability and loss angle tangent in inorganic materials. In addition to these changes, in ceramics we find displacement of atoms in the crystalline lattice where particle energies are over 25 eV. The injection of interstitial atoms causes swelling, which can rupture the material if sufficiently developed.

Organic materials are most sensitive to the effects of radiation. In products of organic materials, all types of radiation cause chemical reactions, breaking existing bonds and forming new bonds. The reactions which occur in irradiated organic materials can be looked upon as cross-linking or destruction.

With destruction, the primary bonds of the polymer molecules are broken. Destruction results in softening, decreased tensile strength, increase relative elongation at rupture, decreased shear strength and decreased melting point. During cross linking we observe increases in hardness, brittleness and melting point, decreases in solubility and increases in density.

Let us study the influence of irradiation on some materials widely used in REA.

Thermosetting materials. Phenol resins without fillers swell after irradiation, become brittle, are easily broken, break down in water, i.e., have low radiation resistance. For example, with a dose of $3 \cdot 10^{10}$ erg/g, the tensile strength and impact strength are decreased by 50%. The use of mineral /200

fillers increases the service life and bending strength.

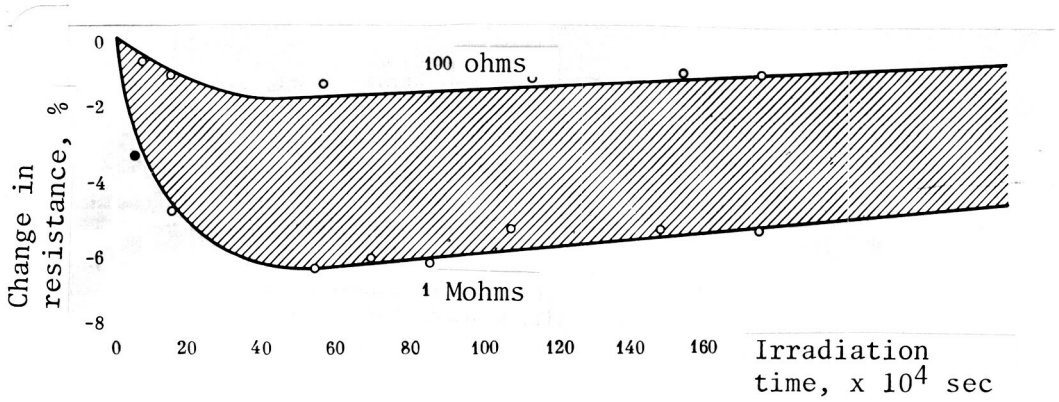

Figure 119. Change in Resistance of Carbon Resistors as a Function of Irradiation Time. Irradiation Conditions: Thermal Neutron Flux $1.37 \cdot 10^{12}$ neutrons$\cdot$cm$^{-2}\cdot$sec^{-1}; Fast Neutrons $2.3 \cdot 10^{9}$ neutrons$\cdot$cm$^{-2}\cdot$sec^{-1}; Gamma Radiation Dose Intensity $3.9 \cdot 10^{4}$ erg$\cdot$g$^{-1}\cdot$sec^{-1}

Epoxy resins can withstand a radiation dose of up to $9.5 \cdot 10^{10}$ erg/g without deterioration of properties, i.e., they have moderate radiation resistance.

Polyurethane foam. Irradiation of specimens with a dose of $1 \cdot 10^{11}$ erg/g, no deterioration of mechanical properties was observed.

Polyester resins have low radiation resistance. When irradiated they become hard and crack. The tensile strength and impact toughness drop.

The introduction of mineral fillers increases the radiation resistance by approximately 100 times. For example, multilayer polyester plastics with glass fiber filler following irradiation with a dose of $2.4 \cdot 10^{9}$ erg/g showed no significant changes in physical properties.

Organosilicon resins show no significant changes following an irradiation dose of 10^{10} erg/g, and with fillers withstands a dose of 10^{11} erg/g with some changes in dielectric properties. Consequently, glass-reinforced plastics based on organosilicon resins can operate normally at 20° C with an irradiation dose of 10^{11} erg/g.

Aminoplastics. Urea-formaldehyde resins have moderate radiation resistance and do not change their properties with radiation doses of up to $8.3 \cdot 10^{8}$ erg/g. Melamine-formaldehyde plastics have better resistance than urea-formaldehyde resin, while aniline-formaldehyde resins are still more resistant to radiation.

Thermoplastic materials. Polystyrene is most resistant to radiation in comparison to other high polymer materials and can withstand a radiation dose of 10^{10} erg/g, but 25% damage occurs with a dose of 10^{12} erg/g. 25% damage means that one (not necessarily all) of the numerical values of characteristics of the material changes by this amount. Ionizing radiation has less influence on the optical properties of polystyrene than on those of plexiglass or glass.

Polyethylene withstands a dose of up to $1.9 \cdot 10^9$ erg/g without significant changes in properties. With a dose of $9.3 \cdot 10^9$ erg/g, 25% damage occurs. Polymers containing fluorine (for example teflon, which can be used under high temperature conditions), has low radiation resistance. For example, the damage threshold is observed with irradiation with a dose of $1.7 \cdot 10^6$ erg/g, while 25% damage occurs at a dose of $3.4 \cdot 10^6$ erg/g. /201

Electronic circuit elements. Resistors. Wire-wound resistors are considered more radiation resistant than carbon or film resistors. For example, when bombarded with an integral fast neutron flux of $1.8 \cdot 10^{18}$ neutrons/cm^2, the maximum change in resistance was 0.8%. No residual changes were observed.

Solid carbon resistors change their resistance upon bombardment as a function of the integral neutron flux and the nominal resistance. Figure 119 shows that for a 100 ohm resistor, the deviation was approximately 1.7%, while a nominal 1 megohm resistor changed by 6.8%. The figures for resistors with nominal values in the range from 100 ohm to 1 megohm fall within the shaded area. The results of irradiation of film carbon resistors are shown in Figure 120.

The change in resistance of metallized film resistors during irradiation is shown in Figure 121. The data for resistors with intermediate values of nominal resistance fall in the shaded area.

Condensors. The selection of radiation-resistance condensors is a very important factor in the design of electronic systems to operate under conditions of irradiation. The primary reason for the change in capacitance is an increase or decrease in the distance between plates under the influence of irradiation.

Ionization of air has an important influence on the insulating materials used in condensers. Figure 122 shows the influence of fast-neutron irradiation on changes in the capacitance of various types of condensers.

Multilayer foil-coated plastics or printed circuit plates. At the present time, foil plastics are widely used in electronic circuits. However, foil-coated teflon plates break when irradiated. The damage, in the form of swelling and warping with the

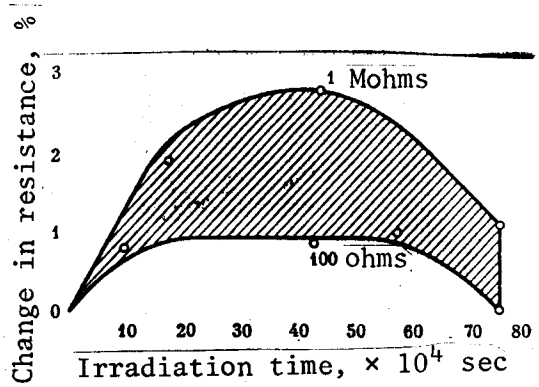

Figure 120. Change in Resistance of Film Carbon Resistors as a Function of Irradiation Time. Irradiation Conditions: Thermal Neutron Flux $1.25 \cdot 10^{12}$ neutrons$\cdot$cm$^{-2}\cdot$sec^{-2}; Fast Neutrons $2.4 \cdot 10^{9}$ neutrons$\cdot$cm$^{-2}\cdot$sec^{-1}; Gamma Radiation Dose $4 \cdot 10^{4}$ erg$\cdot$g$^{-1}\cdot$sec^{-1}

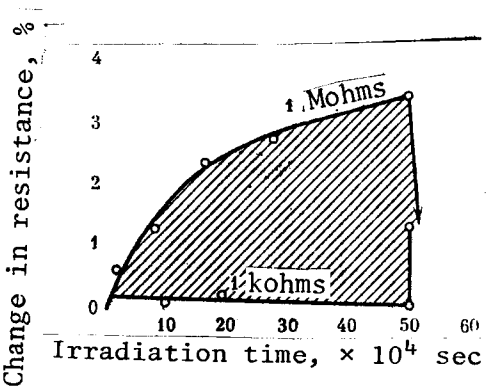

Figure 121. Change in Resistance of Metallized Film Resistors as a Function of Irradiation Time. Irradiation Conditions: Thermal Neutron Flux $4 \cdot 10^{12}$ neutrons$\cdot$cm$^{-2}\cdot$sec^{-1}; Fast Neutron Flux $2.5 \cdot 10^{8}$ neutrons$\cdot$cm$^{-2}\cdot$sec^{-1}; Superthermal Neutron Flux $39 \cdot 10^{9}$ neutrons$\cdot$cm$^{-2}\cdot$sec^{-1}; Gamma Radiation Dose $2.7 \cdot 10^{4}$ erg$\cdot$g$^{-1}\cdot$sec^{-1}

appearance of metal oxide on the copper foil without coating is characteristic for all materials. Improvement of the electrical characteristics of foil-covered plates can be achieved by the use of coatings. Silicone varnish, nitrocellulose varnish, epoxy-polyamide and polyester coatings improve the radiation resistance of foil-covered plastics. /202

The results of investigation of the influence of ionizing radiation on materials and electronic elements as a function of dose are presented in Figures 123 and 124 [13]. As we can see from these figures, the radiation stability of electronic elements varies widely. Therefore, in developing circuits and designs of instruments with increased radiation stability, one must select elements carefully. Semiconductor devices and certain types of resistors and condensers have the lowest radiation stability.

The planning of a circuit resistant to the effects of radiation begins with an analysis of the characteristics of the ionizing radiation, i.e., the type of radiation which will act on the apparatus and the level of radiation expected must be known.

After determining the degree of shielding of the station itself, we must determine wheter additional shielding of individual electronic circuits and units is required. The use of additional shielding is reasonable for slow electrons and protons. Fast streams cause secondary ionizing radiation to be formed in the shield material. Any passive shield increases the weight of the station, and therefore the shield should be combined

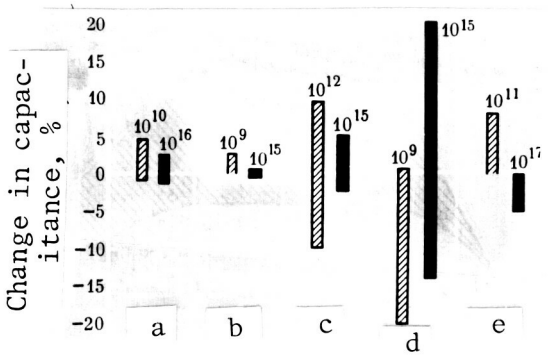

Figure 122. Influence of Fast-Neutron Bombardment on Changes in the Capacitance of Glass-Enamel (a), Glass (b), Mica (c), Ceramic (d) and Electrolytical Tantalum (e) Condensers. Values of Fast Neutron Fluxes [neutrons/(cm^2·sec)] Given for Reversible Changes (Shaded Areas), Values of Integral Fluxes of Fast Neutrons [neutrons/cm^2] Given for Irreversible Changes (Black Areas)

with the load-bearing structure. Electrostatic or magnetic methods /203
of shielding from charged particles are worth considering.
If the radiation resistance of the instruments is below the level of ionizing radiation, the following methods are recommended to reduce the influence of the radiation:

-- use of elements and materials which are less sensitive to ionizing radiation;

-- creation of circuits resistant to the effects of radiation, i.e., circuits in which the changes in parameters of individual elements have little influence on the characteristics of the entire circuit;

-- decreasing the sensitivity of switching circuits to changes in input signals, power supply and bias voltages;

-- use of blocking, compensating circuits and devices allowing circuits to be disconnected for the time of exposure to impulse radiation;

-- increasing the distance between elements under electric voltage by placing the elements /204
on plates;

-- use of circuits with low operating voltages;

-- use of special shields protecting the apparatus from the direct influence of ionizing radiation.

13.4. Mechanical Effects on Electronic Apparatus

The REA used in APS is subjected to external mechanical influences -- vibrations and shock. The influence of these actions causes the breakage of elements, parts and units of the structure. For example, vibration involves motion in alternating directions, caused by periodic forces. Vibration is characterized by its acceleration, amplitude of movement and oscillating frequency.

Apparatus is exposed to vibration during the powered section of flight, to shock loads during staging and also during the landing on the surface of the planet. REA is also exposed to dynamic effects during transportation.

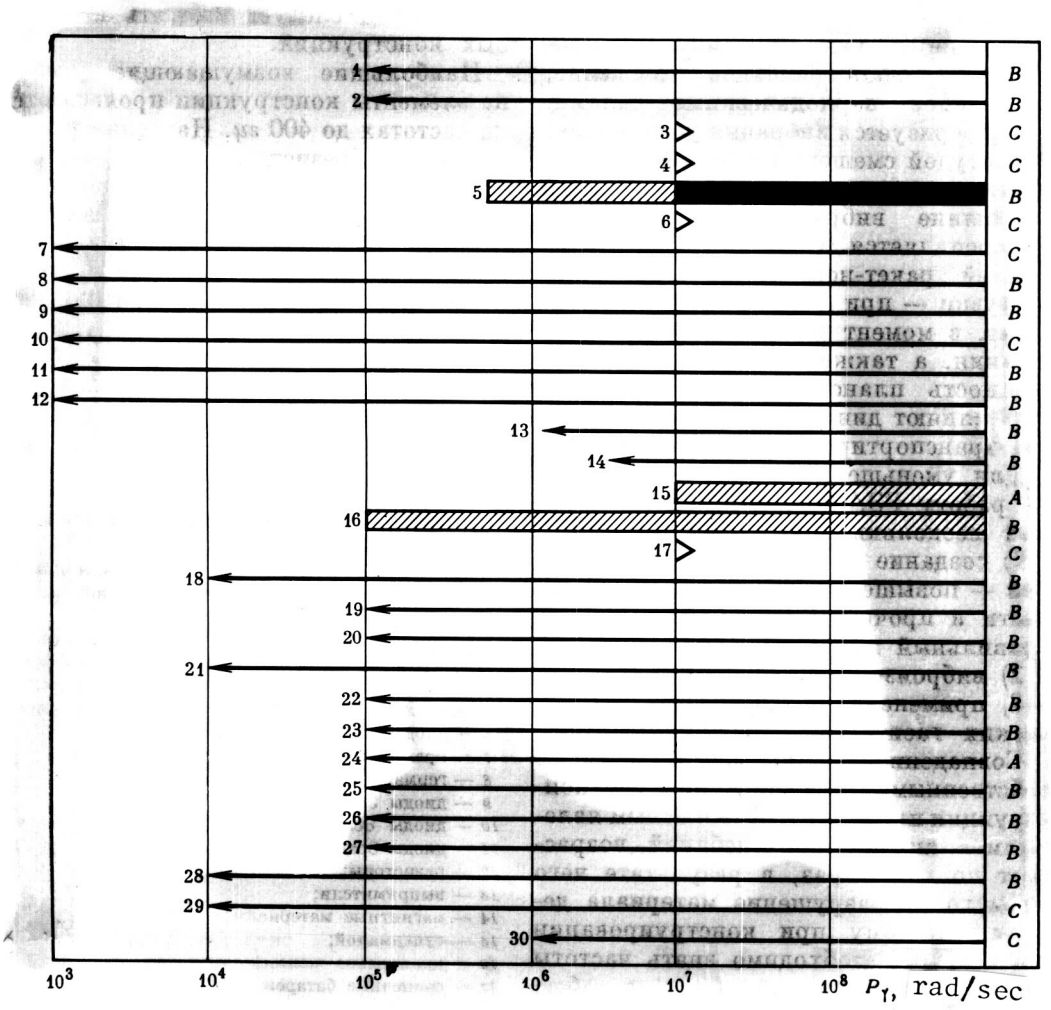

Figure 123. Influence of Radiation Exposure for Gamma Radiation (Carbon) on Materials and Electronic Elements. The arrow shows the beginning of reversible changes; the black bar shows where elements fail; the shaded bar indicates that elements can still operate; the > means that a change in parameters occurs for a dose of over 10^7 rad/sec; the letters represent the degree of reliability; A, Good; B, Incomplete; C, Insufficient; 1, Transistors; 2, Common Diodes; 3, Zener Diodes; 4, Esaki Diodes; 5, Rectifiers; 6, Magnetic Material; 7, Solar Batteries; 8, Phosphorus; 9, Optical Instruments; 10, Optical Glass; 11, IR Elements; 12, Photoelectric Elements; 13, Resistors; 14, Electron Tubes; 15, Thyratrons; 16, Spark Discharge Units; 17, Batteries; 18, Dielectric Materials; 19, Organic Materials; 20, Ceramic Materials; 21, Air; 22, Ceramic Condensers; 23, Aluminum Electrolytic Condensers; 24, Tantalum Condensers; 25, Polyethylene Teraphthalate Condensers; 26, Mica Condensers; 27, Paper Condensers; 28, Microcircuits; 29, Semiconductors; 30, TMM Integrated Circuits

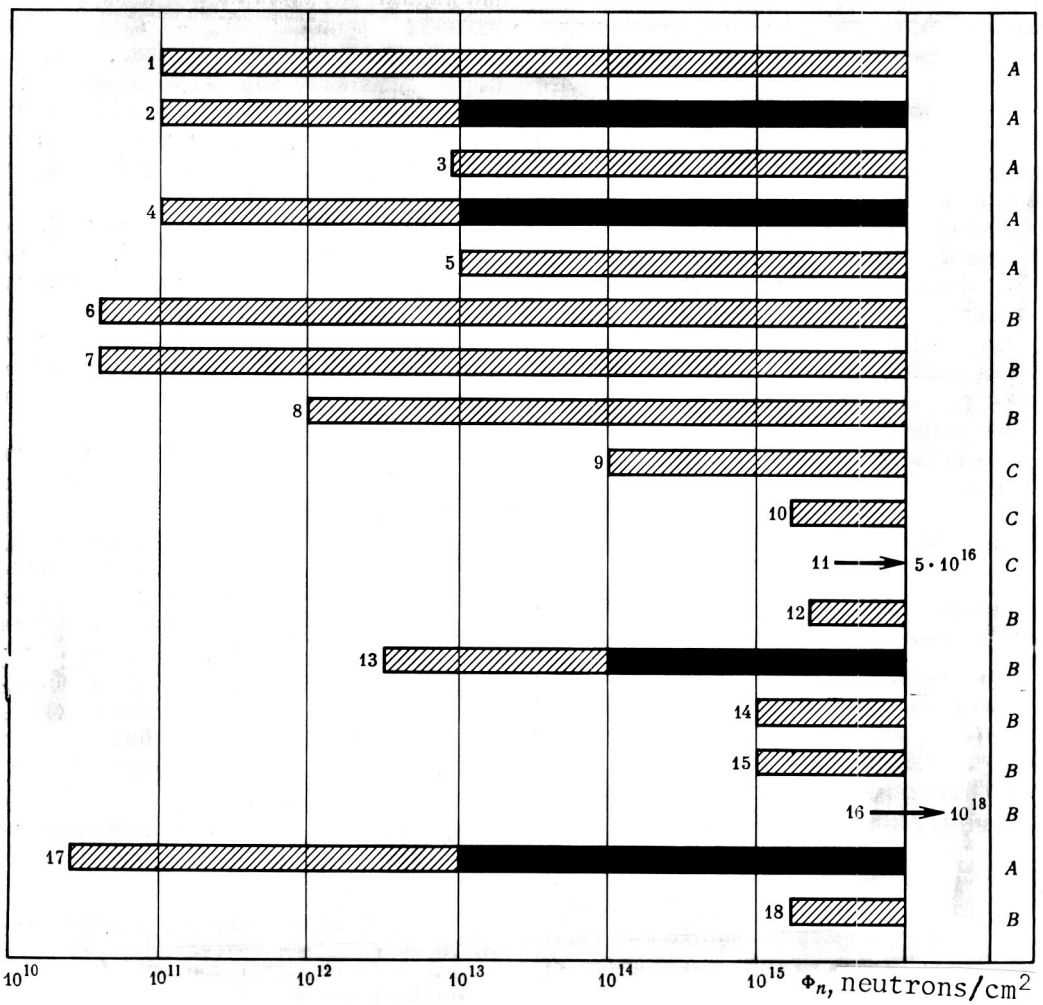

Figure 124. Influence of a Stream of Neutrons on Materials and Electronic Elements. Symbols same as on Figure 123; arrow shows the change arises at the flux indicated: 1, Transistors; 2, Low-Frequency Germanium Transistors; 3, High-Frequency Germanium Transistors; 4, Low-Frequency Silicon Transistors; 5, High-Frequency Silicon Transistors; 6, Diodes; 7, General Purpose Silicon Diodes; 8, General Purpose Germanium Diodes; 9, Zener Diodes; 10, Esaki Silicon Diodes; 11, Esake Germanium Diodes; 12, Resistors; 13, Rectifiers; 14, Magnetic Materials; 15, Supermalloy; 16, Silicon Iron; 17, Solar Batteries; 18, Electron Tubes (Glass)

The designer has several means to decrease the influence of vibration on the operation of REA:

1) creation of an efficient design to increase mechanical rigidity and strength of parts and units and selection of effective means of attachment;

2) vibration insulation;

3) the use of dynamic oscillation dampers.

If the perturbing frequencies correspond to the natural frequencies of parts of the structure, resonance phenomena occur -- the amplitude of oscillation increases greatly, causing damage to the material of the parts. Therefore, in designing apparatus one must know the frequency of the perturbing forces, as well as the natural oscillating frequency of the elements, parts and units of the instruments being designed. Analytic determination of natural frequencies of the parts of an instrument is rather difficult; therefore, the experimental method of determination of natural oscillating frequencies on vibration test stands with variable oscillating frequency is widely used. Resonant frequencies can be changed by changing the rigidity of parts or units or by using stronger materials.

To increase the natural oscillating frequency, one must analyze the attachment of parts, units and of the instrument, always avoiding cantilever designs.

The maximum perturbing forces on structural elements occur at frequencies up to 400 Hz. Suspended elements (resistors, condensers, etc.) must be mounted on leads of minimum possible length, thus increasing the natural frequencies. Elements with great mass must be attached to the mounting plate by other means in addition to their leads.

Studies have shown that the natural oscillating frequencies of resistors and condensers with this type of mounting lie above 600 Hz.

If the analysis performed shows that the methods used to create an effecient structure have not yielded positive results, shock-absorbing mounting must be used. Individual instruments or an entire package of instruments may be shock mounted. Vibration insulation is the most effective method of protection of REA from the influence of vibration. Shock absorbing structures should be selected or designed so as to eliminate the possibility of resonance.

Analysis of the shock mounting system is quite complex; therefore, certain simplifications are accepted in order to produce the initial data. In place of the 6° of freedom which an instrument on its shock mounts actually has, a linear oscillating system with 1° of freedom is studied, with the perturbing force assumed to be applied in the direction of the axis of the shock-absorbing mount under consideration.

In evaluating vibration protection, one must consider damping in the shock absorbing devices themselves. Two main types of damping are distinguished: with viscous resistance and due to the internal absorption of energy in the material of the shock absorber. If the vibration insulation protects the base from oscillations arising in the instrument it is called active. Protection of instruments from oscillations arising in the base is called passive vibration insulation. /206

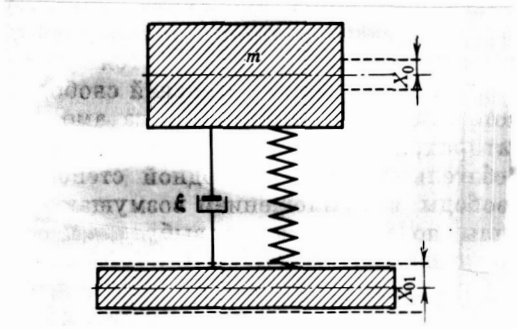

Figure 125. System with One Mass

To determine the effects of vibration insulation, one must know the exciting force P_e and force P_{tr}, transmit through the vibration insulator. The ratio P_{tr} to P_e is called the vibration insulation factor:

$$K_i = \frac{P_{tr}}{P_e} << 1.$$

Good protection from vibration is achieved where $K_i \leq 1/5\text{-}1/8$.

With passive vibration insulation, it is more convenient to use terms of displacements; for example, vibration insulation should reduce the amplitude of oscillations of the protected body in comparison to the amplitude of the base:

$$K_i = \frac{X_0}{X_{01}} << 1,$$

where X_0 is the amplitude of the motions of the instrument; X_{01} is the amplitude of the motions of the base.

For a given vibration insulating device we can write

$$K_i = \frac{P_{tr}}{P_e} = \frac{X_0}{X_{01}}. \qquad (3.25)$$

The vibration insulation factor, considering damping, for th system shown in Figure 125 is determined as follows:

$$K_i = \frac{X_0}{X_{01}} = \frac{P_{tr}}{P_e} = \frac{\sqrt{1 + 4D^2\lambda^2}}{\sqrt{(1 - \lambda^2)^2 + 4D^2\lambda^2}} \qquad (3.26)$$

where $D = \xi/\xi_{cr}$ is the oscillation damping factor; ξ is the viscous friction factor; ξ_{cr} is the critical viscous friction factor, for which the motion does not become oscillating motion; $\lambda = \omega/\omega_c$ is the ratio of the excitation frequency to the natural oscillating frequency of a system (tuning of the system).

Figure 126 shows graphs constructed from equation (3.26). Analyzing these graphs, we can draw the following conclusions.

1. Where $\lambda \leq 0.5$, when the excitation frequency ω is significantly less than frequency ω_c of natural oscillations of the instrument being protected, the shock absorbers yield no insulating effect, since the vibration insulation factor is not over 1.5.

2. As $\lambda \to 1$, when the excitation frequency is near the frequency of natural oscillations, the vibration insulation factor with slight damping increases sharply (resonance). If in designing and instrument it is difficult to avoid matching of natural and forced frequencies, dampers must be selected which eliminate the possibility of resonance.

3. Where $\lambda = \sqrt{2}$, the vibration insulating factor is equal to 1 with any damping. Further increases in λ improve the insulating effect. Damping due to internal absorption of energy in the material of the shock absorbers in the area $\lambda > \sqrt{2}$ is slight and need not be considered in calculations. /208

The phase shift angle ϕ between the forced oscillating frequency and the frequency of natural oscillations of the instrument insulated is determined by the expression

$$\tan \phi = \frac{2D\lambda^3}{1 - \lambda^2 + 4D^2\lambda^2}. \qquad (3.27)$$

Frequently, the vibration accelerations are fixed rather than their amplitude, and then

$$k_i = \frac{j_2}{j_1},$$

where j_1 is the vibration acceleration of the plate (base); j_2 is the vibration acceleration of the instrument.

Detailed analysis and a method of calculation of protection of apparatus from dynamic effects are presented in [15].

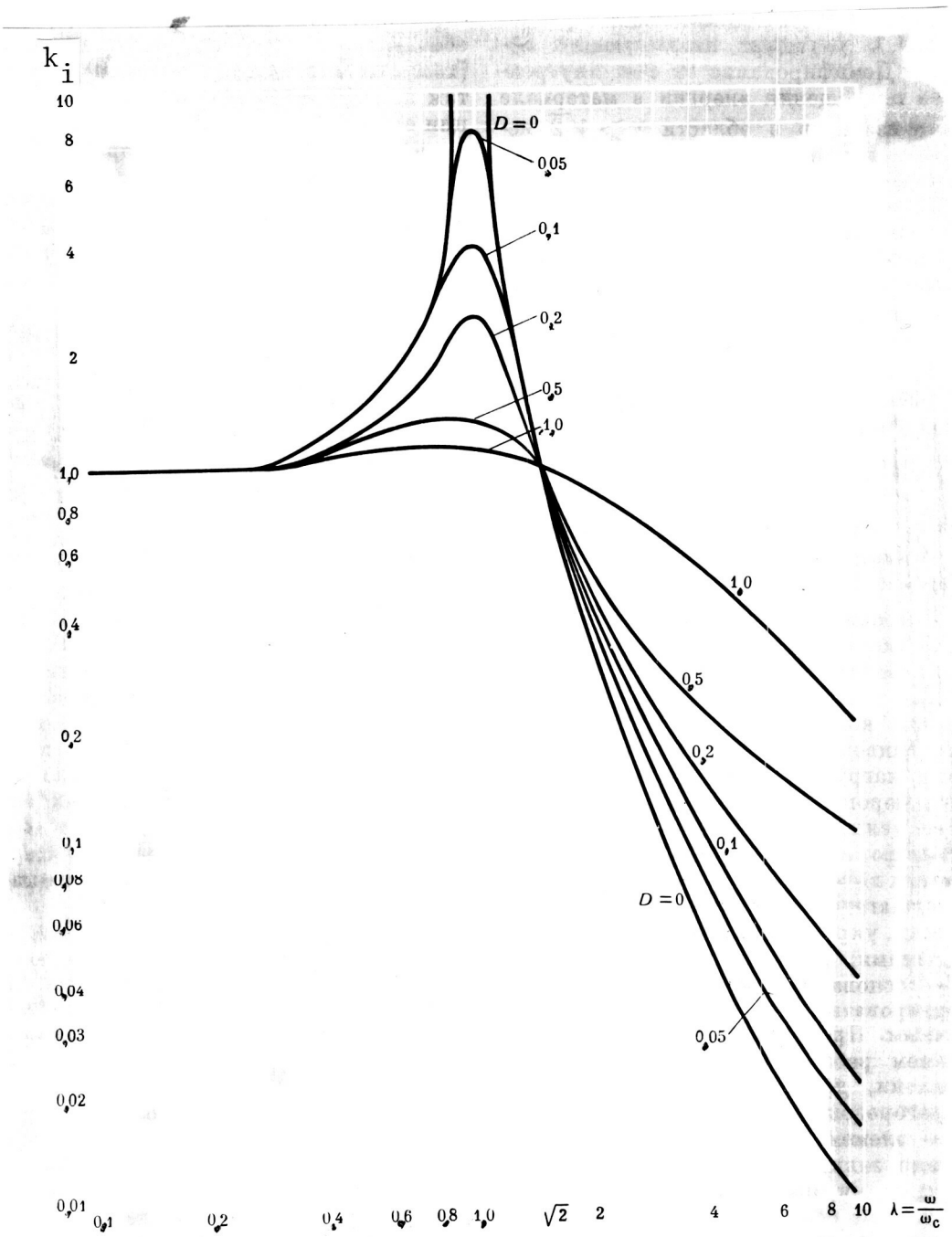

Figure 126. Vibration Insulation Factor as a Function of Ratio of Excitation Frequency to Frequency of Natural Oscillations of the System for Various Values of the Oscillating Damping Factor

In designing apparatus resistant to the effects of mechanical loads, we must consider a number of measures:

-- units with high mass (transformers, chokes, relays, high-frequency amplifiers, etc.) must be placed on the base of the instrument at points supported by ribs or brackets;

-- the base of the chassis must be strong, light and easy to manufacture. Strength is achieved by the use of rigidity ribs, flanges, depressions, additional edge plates and walls;

-- REA elements with low mass can be surrounded with compounds or plastic foam, after which the apparatus can withstand accelerations of over 100 g without damage, although heat liberation from the elements and repairability of the apparatus deteriorates;

-- installation conductors should be combined into groups and attached by brackets (clamps) or adhesive to rigid structural elements. When using structures with bodies which swing open, one must recall that it is better to deform cables by twisting than by bending;

-- printed circuits should be used to increase the reliability of apparatus. Printed circuit plates can be increased in rigidity by means of additional mountings, or by covering the plates with plastic foam or compound.

13.5. The Thermal Mode of Electronic Apparatus

The thermal mode of REA elements is one of the most important factors determining the reliability of their operation. Therefore, in designing instrument and placing REA in the APS compartment, one must take measures to minimize the heating of elements and parts of the apparatus.

Whereas in ordinary apparatus, thermal modes are maintained by such measures as increasing the heat transfer surface, special painting, forced cooling (air or liquid), in microminiaturized apparatus, widely used in space electronics, the problem of the thermal mode is more difficult to solve.

One important factor for conservation of the efficiency of microcircuits is evenness of the distribution of heat sources, since this decreases the likelihood of formation of hot spots, leading to local overheating.

APS must operate under complex temperature conditions; therefore, in planning REA one must simultaneously analyze the problem of decreasing the harmful effects of temperature on the apparatus. This can be done by decreasing the range of change of temperature in the APS compartment or by using elements and parts with broad operating temperature ranges. In designing electronic systems, /209
the discrete or digital principle of operation of the apparatus should be used, minimizing the influence of instability of parameters on output characteristics.

In sealed compartments with maintenance of microclimate, where thermal regulation systems are used, the temperature range of the surrounding medium can be reduced, although this is a difficult problem. Elimination of local overheating resulting from the liberation of heat by individual elements of the apparatus is no easy task. The use of individual means of cooling, fans, thermoelectric coolers, etc. is cumbersome and uneconomical, since these devices have low efficiencies.

Local overheating can be controlled by selecting circuits with high efficiency and by intelligent design decisions. Transistors, diodes and modules allow the efficiency to be increased significantly while decreasing power consumption. The heating of units, parts and elements will be less for the same dissipated power in those instruments which have better heat exchange with the surrounding medium. In planning REA, one must recall that overheating and cooling can change the characteristics of elements excessively, causing reversible or irreversible damage to materials, parts and structural units.

The following methods are used to assure optimal design of instruments: determination of the class of the instrument on the basis of its structural characteristics, design and creation of a thermal model, testing of the model, refinement of the calculations, development of the structure and its testing under operating conditions.

Thermal calculation does not yield high accuracy, since the fundamental theory of heat transfer by convection, conduction and radiation cannot be applied unaltered to thermal calculation of REA. REA elements, parts, units and instruments have limited and complex geometric shapes; therefore, additional coefficients must be introduced to the formulas and a number of assumptions made, since the design of REA rarely corresponds to the geometric shapes for which the thermal calculation formulas are written. However, in spite of the approximate nature of the calculation formulas, they must be used, since this allows more correct estimation of the thermal modes of the apparatus during the planning stage.

The REA designer must turn great attention to thermal processes and be able to estimate thermal modes by calculation methods. Problems of temperature stability can be rather easily solved where heat resistant elements and materials are available, but we must recall that some elements do not have good temperature characteristics. The temperature fields of REA are described by complex dependences, and there are always hotter spots, from which the heat must be carried away.

Before beginning the calculation of the temperature fields of apparatus, we must know:

-- the duty cycle of the apparatus;

-- the power consumption and effeciency of the elements and devices;
-- the environmental conditions (medium, pressure, temperature);
-- the thermal characteristics of the elements used.

The APS compartment containing the REA can be considered a system of many bodies with a large number of concentrated sources of energy. Analysis of the temperature fields of such a system is a difficult task, which is solved by approximate methods.

The theoretical principles of the methods of calculation of certain classes of REA which can be used for the design of apparatus used in APS can serve as a basis for the creation of new methods of calculation considering the specifics of the apparatus used are given in [16]. /210

As a rule, APS operate periodically; therefore, as we analyze the thermal modes of apparatus we must consider the unstable thermal processes (for example, the time required to establish a stable mode may be significantly greater than the operating time of the apparatus).

The design of REA, based on improved methods of calculation of thermal modes of the apparatus, allows optimal versions of designs to be selected. The heat exchange processes in sealed compartments are based on the heat conductivity of the structural elements and layers of air between them, radiation between the shell around an instrument and the walls of the compartment, as well as forced or natural convection. The thermal mode of the REA in a compartment depends on the energy dissipated by the elements and instruments as they operate, the temperature of the surrounding medium, the heat conducting devices used and the geometric dimensions of the compartment.

The overall energy balance for such a compartment can be expressed by the equation

$$Q_{sum} = Q_t + Q_c + Q_r, \qquad (3.28)$$

where $Q_{sum} = \sum_{j+1}^{n} Q_i$ is the summary power liberated by the instrument; Q_t is the thermal flux applied to the shell by conductivity; Q_c is the heat flux carried away by convection; Q_r is the flux carried away by radiation.

Let us determine the influence of each component of the flux on the thermal mode of the compartment. When the station operates under weightless conditions, the convective component is minimized

without forced convection and a greater portion of the heat flux is carried by conductivity. Under these conditions, structural materials must be used with high heat conductivity, large cross-sectional area and short length. The flux carried away by radiation will amount to only a few % (6-8%) of Q_t. Forced ventilation with good aerodynamic characteristics allows the heat carried away from the instruments to be increased significantly.

Depending on the thermal energy liberated by the instruments, a system of thermal mode support (TMSS) is selected sufficient to maintain the required temperature range within the sealed compartment. Analysis and design of TMSS were studied in detail in Part 2. Apparatus in which electrical energy is converted to thermal energy is the source of heat, the body of the compartment and radiators of the TMSS are heat sinks, and the frame, structural elements and surrounding medium act as heat transmitting devices.

The propagation of heat by conductivity follows Fourier's rule and is expressed by the formula

$$Q_t = \frac{\lambda}{b} S (t_i - t_j), \qquad (3.29)$$

where Q_t is the quantity of heat transmitted per unit time through a section of material; λ is the heat conductivity factor, characterizing the properties of the material; b is the thickness of the material; S is the cross-sectional area; $(t_i - t_j)$ is the temperature difference between isothermal surfaces i and j.

Heat transmitting devices consist of rods, flat ordinary and multilayered walls, pipes, etc., for which we can use expression (3.29) to determine the quantity of heat transmitted in the stable mode. The heat conductivity factors of metals is approximately 400 w/(m·deg), of nonmetallic materials $5 \cdot 10^{-2}$-$8 \cdot 10^{-1}$ w/(m·deg), of liquids $9 \cdot 10^{-2}$-$5 \cdot 10^{-1}$ w/(m·deg), while the heat conductivity of gasses amounts to approximately 1/10th of the heat conductivity factor of liquids. /211

Analysis of thermal processes involves drawing an analogy between the processes of heat transfer and electricity. The temperature difference $(t_i - t_j)$ is similar to the difference in electric potentials $(E_1 - E_2)$, the quantity of heat Q -- to the current I, the quantity $b/\lambda S$ -- to resistance R. The theraml resistance

$$R_{ij} = \frac{b}{\lambda S} \tag{3.30}$$

similar to the electrical resistance $R = \rho (\ell/S)$; the inverse quantity $1/R_{ij} = \sigma ij$ is called the thermal conductivity.

Expression (3.29) can be written as

$$Q_t = \frac{t_i - t_j}{R_{ij}}. \tag{3.31}$$

The quantity of heat transferred per unit time from a solid to the air medium or from the air medium to a solid is determined by the Newton-Richtman formula

$$Q_c = \alpha_c (t_i - t_j) S_i, \tag{3.32}$$

where Q_c is the quantity of heat transmitted from the surface of the solid to the medium; α_c is the convective heat exchange factor between the surface of the body and of the medium; t_i, t_j or the temperatures of the surface of the body and the medium; S_i is the area of the heat exchange surface.

The convective heat exchange factor is a complex function of a large number of components. Determination of the value of α_k by calculation is a very difficult task. Therefore, experimental data produced under certain conditions are frequently used, with corrections for the boundary conditions which actually apply. Determination of α_c by calculation is outlined in detail in monograph [16].

The thermal resistance and thermal conductivity for convective heat transfer follow these dependences:

$$R_{ij} = 1/\alpha_c S_i \text{ and } \sigma_{ij} = \alpha_c S_i. \tag{3.33}$$

The transmission of thermal energy by radiation is achieved by means of electromagnetic waves in the range of 0.3 to 10 μ and follows the Stefan-Boltzmann law, which is described by the equation

$$Q_r = \varepsilon_{cij}\left[\left(\frac{T_i}{100}\right)^4 - \left(\frac{T_j}{100}\right)^4\right]S_i\phi_{ij}, \qquad (3.34)$$

where

$$\varepsilon_{cij} = \frac{1}{\frac{1}{\varepsilon_i} + \frac{1}{\varepsilon_j} - 1} \qquad (3.35)$$

is the corrected degree of blackness of bodies i and j; C_0 is the radiation factor of an absolutely black body; T_i, T_j are the absolute temperatures of bodies i and j; S_i is the surface area of the body; ϕ_{ij} is the irradiance factor of the ith body by the jth body.

The thermal resistance and thermal conductivity for heat exchange by radiation are determined by the following expressions:

$$R_{ij} = \frac{1}{\alpha_r S_i}, \quad \sigma_{ij} = \alpha_r S_i, \qquad (3.36)$$

where

$$\alpha_r = \varepsilon_{cij}\phi_{ij}f(t_i, t_j),$$

$$f(t_i, t_j) = 5.67\cdot 10^{-8}\frac{(t_i + 273.2)^4 - (t_j + 273.2)^4}{t_i - t_j} \qquad (3.37)$$

The transmission of heat by radiation is more effective at high temperatures (over 100° C), and also when the radiating surface S and its degree of blackness ε increase.

REA can be classified according to structural characteristics as:

-- monoblock apparatus in dustproof, sealed, perforated covers;
-- with high, medium or low mounting density;
-- cassette-type;
-- with various degrees of heat liberation, etc.

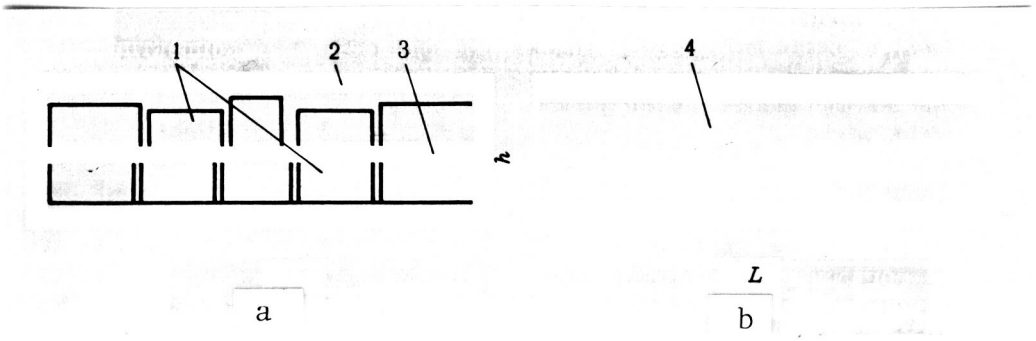

Figure 127. Schematic (a) and Arbitrary (b) Representations of Instruments (h represents height of arbitrary heated zone): 1, Elements of Instrument; 2, Cover; 3, Base (Chassis); 4, Arbitrary Heated Zone

Apparatus of any class, when used in APS, is characterized by its component density. The small distances between elements, parts and units create areas of stagnant air within the apparatus, i.e., convective motion of the gas is nil and heat exchange is only by conduction through the structural elements and the gas intervals and partially by radiation. Only those elements near the cover and chassis participate in radiation, the radiation of thermal energy from elements located in the internal portion of the apparatus being shielded by neighboring elements. Consequently, the apparatus of APS in weightlessness and on the surface of planets can be looked upon as a body surrounded by a closed shell without any convective component.

The thermal characteristics of apparatus are determined by the method of successive approximations, since the dependence of heat transfer factor on temperature is nonlinear in nature. In the method developed [16], the electronic apparatus is looked upon as a system of bodies consisting of a cover (shell), a heated zone which includes the elements which liberate heat at known power and the medium filling the free volume of the apparatus.

Figure 127 schematically and arbitrarily shows a monoblock electronic apparatus, the calculation of the thermal mode of which with known geometric dimensions of the apparatus, fixed values of temperature of the surrounding medium t_c and dissipated power Q is achieved in two stages.

First, the temperature of the cover t_k is determined by expression [16]

$$t_k = t_c + Q(1/\sigma_{kc}), \qquad (3.38)$$

where σ_{kc} is the heat conductivity from the cover to the medium. Then, the temperature of the arbitrary heated zone is determined

$$t_{hz} = t_k + Q(1/\sigma_{hzk}), \qquad (3.39)$$

where σ_{hzk} is the heat conductivity from the arbitrary heated zone to the cover.

Analyzing expressions (3.38) and (3.39), we see that the heat conductivity is a function of the design of the apparatus, i.e., the placement of heat liberating and structural elements, the quality of the "heat bridges" between the heated zone and the cover (or chassis), the heat conductivity of the materials and of the geometric dimensions of the electronic apparatus. /213

The excess temperature of the cover $\Delta t = t_k - t_c$ is a function of the following parameters:

$$\Delta t = \Delta t(Q, L, h, t_c, \varepsilon, H),$$

where L, h are the geometric dimensions of the apparatus and the heated zone, H is the pressure of the gas medium.

The results of calculation used to construct graphs (Figure 128)

$$f_1(Q) = t_k - t_c, \qquad (3.40)$$

$$f_2(Q) = t_{hz} - t_c. \qquad (3.41)$$

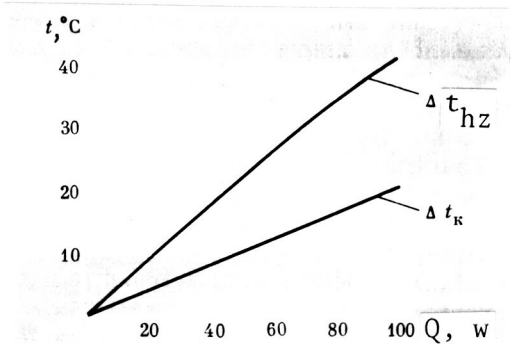

Figure 128. Thermal Characteristics of Cover and Heated Zone

Based on these graphs, we can draw the following conclusions:

1) in designing REA, one must attempt to decrease the temperature drop between t_k and t_{hz};

2) the thermal characteristics can be used to determine the temperature of the cover t_k and the temperature of the arbitrary heated zone t_{hz} with a fixed power Q and temperature of the surrounding medium t_c.

The fixed excess temperatures Δt_{hz} and Δt_k can also be used to determine the maximum power dissipated by the elements.

Efficient structural and technological methods of manufacture of apparatus can significantly improve the thermal modes of REA. For example, covering of parts and the cover with paints with degree of blackness $\varepsilon = 0.9$ can decrease the temperature of the cover in comparison to unpainted surfaces by 20-30%, the temperature of the heated zone by 12-18%.

The use of "heat bridges" made of materials with high heat conductivity factors can reduce the temperature by 30-40%. To improve thermal modes, all cooling methods must be combined.

When the REA is placed in an unsealed APS compartment, the designers of the apparatus have additional problems, one of which is the provision of a normal thermal mode.

As we have shown, the role of the convective component during heat exchange in a sealed APS compartment is minimized, and the gas layers between elements and the cover present high thermal resistance, i.e., a limited quantity of heat is transmitted through them. The absence of these gas layers in a vacuum has little influence on the process of heat exchange in the apparatus. That portion of the heat which was transmitted through the gas layers from heat liberating elements to the cover can be transmitted in a vacuum by means of good heat bridges. The main portion of the heat in a vacuum will be transmitted by heat conductivity and radiation. Therefore, in the design of apparatus particular attention must be given to structural and technological problems.

In the arrangement of circuit elements (if the electrical connections permit), one should attempt to connect the most heat liberating elements with the body (chassis) or cover by heat bridges of highly heat-conductive materials, and to decrease shielding to allow better transmission of heat to neighboring elements. Also, coatings with the necessary degree of blackness ε should be carefully selected, keeping in mind that under deep vacuum conditions some coatings might evaporate and change the value of ε. /214

Contacting surfaces in the apparatus and frame of an unsealed compartment should be quite flat and smooth in order to reduce thermal resistance. The thermal resistance of a contact decreases with increasing load on the contacting surfaces, but is little dependent on load if the contacting surfaces are very smooth.

The following methods can be used to decrease thermal resistance:

-- highly heat conductive and highly plastic metals can be

applied to contacting surfaces by evaporation or galvanic coating;
-- highly heat conductive interlayers of soft metals can be used;
-- powdered substances can be introduced to the contact zone;
-- soldering or welding can be used;
-- adhesive compounds with highly heat conductive fillers can be used.

If REA with high heat liberation is developed for a sealed compartment using forced gas cooling, when this apparatus is placed in an unsealed compartment careful analysis must be made of the thermal model, the temperature fields must be calculated and the apparatus tested. In order to assure normal thermal modes in the apparatus, surfaces with a high degree of blackness must be developed, heat sources spread throughout the volume of the apparatus evenly and structural materials with high heat conductivity used.

Another important problem is evaporation or sublimation of materials. The rate of sublimation increases with increasing temperature. Most metals which are widely used in REA, such as aluminum, copper and titanium alloys, as well as germanium and silicon semiconductors, have slight losses at moderate temperatures. Cadmium and zinc, used as metal coatings, have the highest evaporation rate.

In inorganic compounds, losses may occur due to sublimation of molecules of the compound or decomposition of the compound into its elements or simpler compounds; some of these compounds may be volatile. Organic materials used in REA are polymer compounds, the losses of which in a vacuum occur not due to sublimation, but rather due to conversion of the compounds into simpler and more volatile fractions.

When there is a temperature gradient between the surfaces of elements, metal may sublimate from the heated surface and condense on the cold surface, forming a thin film which may cause a short circuit. The decomposition products of organic and inorganic materials may precipitate in the form of an insulating layer and disrupt normal operation of circuit elements.

One method of preventing sublimation is the use of protective surface coatings on materials, as well as the creation of the minimum thermal gradient between structural elements.

If the REA is used in a vacuum on the order of 10^{-10}-10^{-12} mm hg, the pressure within the apparatus will be greater, since the materials used liberate gasses. The quantity of gas and, consequently, the pressure in the internal portion of the apparatus can be regulated by changing the dimensions of slits in

the cover, and also by the use of special gas-liberating substances.

The gas pressure within the apparatus may reach 10^{-3}-10^{0} mm hg. Low gas pressure is most dangerous for electrical breakdown. As we know, the electrical breakdown voltage of a gas space is a function of the product of gas pressure p times the distance between electrodes d (Paschin's rule): /215

$$u_b = f(pd).$$

Analysis of Paschin's curve shows that a pressure of 1-0.1 mm hg is most dangerous, but that at a voltage of less than 200 v there is little danger of air gap breakdown.

At voltages of over 200 v, additional insulation must be used or the distance between dangerous electrodes increased. The dielectric permeability of air changes at low pressure, which may change the frequency of a stable circuit. When designing apparatus in which the frequencies of the circuits must be stable, the method of testing in air and in a vacuum must be carefully developed or partial sealing must be used.

REFERENCES

1. Afonin, P. M., et al., Bespilotnyye Letatel'nyye Apparaty [Unmanned Flight Vehicles], Moscow, Mashinostroyeniye Press, 1967.
2. Kroshkin, M. G., Fiziko-Tekhnicheskiye Osnovy Kosmicheskikh Issledovaniy [Physical and Technical Principles of Space Research], Moscow, Mashinostroyeniye Press, 1969.
3. Ginzburg, Ye. G., Volnovyye Zubchatyye Peredachi [Wave-type Transmissions], Leningrad, Mashinostroyeniye Press, 1969.
4. Olsen, "Planning of Electronic Apparatus Considering the Effects of Radiation, Part 2," Elektronika, 1965, Vol. 38, No. 1.
5. Jaffe, Rittenhaus, "The Behavior of Materials under Space Conditions," Raketnaya Tekhnika, 1962, No. 3.
6. Wilkinson, "Criteria for Penetration of Two-Layer Structures Upon Meteorite Collision," Raketnaya Tekhnika i Kosmonavtika, 1969, No. 10.
7. Leont'yev, L. V., A. V. Tarasov, I. A. Tereshkin, "Some Peculiarities of the Shapes of Craters Formed by High-Speed Particles in a Semi-Infinite Barrier," Kosmicheskiye Issledovaniya, 1971, Vol. 9, No. 5.
8. Perser, P. Ye., et al., Pilotiruyemyye Kosmicheskiye Korabli [Manned Spacecraft], Moscow, Mashinostroyeniye Press, 1968.
9. Worth, "System for Descent and Landing of Unmanned Spacecraft on Mars," Raketnaya Tekhnika i Kosmonavtika, 1967, Vol. 5, No. 1.
10. Katys, G. P., et al., Informatsionnyye Roboty i Manipulyatory [Information Robots and Manipulators], Moscow, Energiya Press, 1968.
11. Strukhal, Carri, Jenni, "Thermal Protection of the Crew Compartment of the Apollo Spacecraft," Voprosy Raketnoy Tekhniki, 1967, No. 4.
12. Volin, M. L., Parazitnyye Svyazi i Navodki [Parasitic Coupling and Inductance], Moscow, Sovetskoye Radio Press, 1965.
13. Shirshev, L. G., Ioniziruyushchiye Izlucheniya i Elektronika [Ionizing Radiation and Electronics], Moscow, Sovetskoye Radio Press, 1969.
14. Vliyaniye Oblucheniya na Materialy i Elementy Elektronnykh Skhem. [Influence of Radiation on Materials and Elements of Electronic Circuits], Translated from the English, Edited by S. P. Solov'yeva and V. N. Bykov, Moscow, Atomizdat Press, 1967.
15. Il'inskiy, V. S., Zashchita Apparatov ot Dinamicheskikh Vozdeystviy [Protection of Apparatus from Dynamic Effects], Moscow, Energiya Press, 1970.
16. Dul'nev, G. N., E. M. Semyashkin, Teploobmen v Radioelektronnykh Apparatakh [Heat Exchange in Electronic Apparatus], Moscow, Energiya Press, 1968.

PART 4

METHODS FOR COLLECTION AND TRANSMISSION OF INFORMATION AND POWER SUPPLY SYSTEMS

The importance of the problem of transmission of information /216
in space studies is tremendous. The practical value of any experiment is determined greatly by the method used to transmit information from the spacecraft. The rate and accuracy of processing of information on board the spacecraft determine the reliability of the information when restored at the reception point. In any analysis of the reliability of information, it is also important to know how it was transmitted from the APS to Earth, i.e., the reliability of the transmitted information or its interference stability.

One interesting problem in the transmission of information is its information effectiveness. This term refers to the economy and efficiency with which we load the radio transmission line with information. These two parameters -- interference stability and information effectivenss -- are the most important of all parameters determining the effectiveness of the radio communications line as a whole. Therefore, in planning space radio communications lines, maximum attention is given to problems of interference stable coding, restoration of data, reduction of redundancy and selection of message models. In order to illustrate the material, we present data on the capabilities of a radio link for transmission of information from spacecraft with low power capacities.

Further mastery of space is impossible without reliable sources of power, capable of operating for extended periods of time under the unfavorable conditions of interplanetary space and providing continuous power to the scientific and telemetry equipment on board the APS. At the present time, the ratio of the weight of the on board power equipment to the total weight of the spacecraft averages 25%. The lack of reliable, long-lived power supplies may prove to be a bottleneck in future space studies.

CHAPTER 14

THE COMMUNICATIONS SYSTEM OF AN AUTOMATIC PLANETARY STATION

14.1. Characteristics of Information Sources

During telemetry measurements, the physical quantity to be determined is converted by sensors to an electrical voltage, which modulates the signal of the radio link. The main types of sensors fall into two groups -- analog and digital. /217

Analog sensors include tensometric, inductive, potentiometric sensors and voltage sensors, the amplitude of which varies within limits established by the standard. This voltage must be proportional to the variable physical quantity. The initial coding is designed to convert the message so that its value corresponds to the established standard.

Digital sensors perform the same conversion, the difference being that the output of these devices carries not a voltage, but rather a sequence of pulses, chaotically distributed along the time axis. Various types of accumulators are used for their further conversion and transmission. Usually, the accumulators are counters which receive a sequence of randomly placed pulses from the sensor during a fixed time interval. At the end of this period, the information contained in the counter is read out by the coding device. Modern measurement equipment uses large number of digital sensors in combination with accumulators. They also include digital sensors with logarithmic counters, digital sensor pulse amplitude analyzers, etc.

Let us study the signals taken from analog and digital sensors. In order to describe the processes taken from analog sensors, we can use such known characteristics of random processes as the distribution density with fixed time, mathematical expectation, dispersion, correlation function or instantaneous spectral density of power. The properties of the process taken from a digital sensor are described by the characteristics of a stream of random events or quantities.

Usually, all random processes are divided into stationary and nonstationary types. For stationary processes, various parameters (moments, distribution functions, etc.) are independent of time. The class of nonstationary processes includes processes for which the corresponding parameters depend in some way on the beginning of the reading (or on time).

The signals from sensors are processes which are described by the partial indicators u(t) where t is time. Consequently, the processes taken from sensors (both analog and digital) can be considered nonstationary. Analysis of such processes in general form is difficult; therefore, the concept of the quasistable process is used, encompassing a large group of nonstationary signals, analyzed in communications theory. /218

Let us study some of the properties of processes taken from analog sensors. Quasistable process u(t) in this case is characterized by an exponential or exponential-cosinusoidal correlation function $R(\tau)$ over the interval of stability [1, 2]. This means that the spectral density of the process is a rational function. If the actual correlation function is not exponential, where $R|\tau| \to 0$ as $\tau \to \infty$ it can be approximated by the method of least squares by a linear combination of exponents [1]:

$$R(\tau) = e^{-\alpha|\tau|}(1 + \alpha|\tau|). \tag{4.1}$$

For a quasistable process, one necessary condition is fulfillment of the inequality $T_{stat} >> T_{trans}$, where T_{trans} is the time of the transient process as the characteristics of random function u(t) change, while T_{stat} is the time of the stationary process. Frequently, the requirement of mean-square differentiability is placed on the signal, which under actual conditions means filtration of the signal through linear devices. This means that random process u(t) is produced by passing normal white noise through a low-frequency filter, the passband of which $\Delta\omega$ changes smoothly during time T_{trans} at interval T_{stat}, with the condition expressed in the inequality above.

The width of the spectrum of a quasistable process has a Rayleigh distribution, since the spectrum spends the greatest portion of time in the low-frequency area. One of the characteristics of this process is the spectral density in the interval T_{stat}. We know from the theory of continuous Markov processes that if random process u(t) is a result of passage of normal white noise $\xi(t)$ with spectral density $G_0/2$ through a linear device with frequency characteristic $K(j\omega)$, the spectral density of process u(t) will be rational and is determined by the expression [3].

$$S_u(\omega) = \frac{G_0}{2}[K(j\omega)]^2, \tag{4.2}$$

where

$$[K(j\omega)]^2 = \frac{4\alpha^3}{(\alpha^2+\omega^2)^2}, \quad \alpha = \frac{I}{RC}. \tag{4.3}$$

Here α is a random quantity with Rayleigh distribution:

$$\tag{4.4}$$

Expression (4.2) can be represented in a different form:

$$S_u(\omega) = \frac{\sigma^2}{\pi}\frac{4\alpha^3}{(\alpha^2+\omega^2)^2}, \tag{4.5}$$

where σ^2 is the dispersion of process u(t). Here, the maximum specific content of the signal or the maximum rate of information transmission is equal to

$$I_c = \Delta F_c \log_2 (1 + \frac{P_c}{P_n}) \tag{4.6}$$

where ΔF_c is the width of the spectrum of the signal, equal to $S_u(\omega)$.

For a quasistable process, formula (4.6) can be converted:

$$I_c(\Delta t_i) = S[\omega(\Delta t_i)] \log_2 [1 + \frac{P_c(\Delta t_i)}{P_n}]. \tag{4.7}$$

Thus, the source of the quasistable signal can be looked upon as a certain information generator, the productivity of which changes suddenly upon transition from the ith time interval to the (i + 1)th time interval.

If the characteristics of the information transmission channel do not depend on the signal transmitted (as is the case in most modern communciations systems), the throughput capacity of the communications channel I_c must be calculated for the worst signal, i.e., for the maximum value of $I_s(\Delta t_i)$ where

/219

$S[\omega(\Delta t_i)] \to S_{max}[\omega(\Delta t_i)]$. Therefore, when information with low error probability is transmitted, the following condition is usually observed:

$$I_c = I_{smax}\Delta F_{cmax} \log_2 \left(1 + \frac{P_{cmax}}{P_n}\right). \qquad (4.8)$$

For practically all signals, the value of ΔF_{cmax} is realized comparatively rarely (due to the Rayleigh distribution), and therefore most of the time the communications system operates ineffectively.

Let us study a model of a signal taken from a digital sensor. Digital sensors usually output a binary signal similar to a random telegraph signal. The information is contained at the moments of transition of the signal through 0. We can analyze the model either by methods of queueing theory [4, 5] or by the method of discrete Markov chains [6-8].

As a model of the signal in the first approximation we can use a Poisson stream characterized by instantaneous density $\lambda(t)$ [5, 9]. The rule of distribution of time between two neighboring changes in polarity (points) is determined by the expression [4, 5, 9]

$$W_{t_0}(t) = \lambda(t_0 + t)\exp\left\{\int_{t_0}^{t_0+t} \lambda(t)\,dt\right\}, \qquad (4.9)$$

where t_0 is the beginning of the reading, corresponding to the first of the two neighboring changes of sign.

Let us study an unstable Poisson stream of points. For this process, it is expedient to use the model of a homogeneous Markov source [7, 8]. Then the problem of the mean time between neighboring changes in polarity will be similar to the problem of a random walk of a particle with two states.

Let us introduce some symbols: E is an event equivalent to a change of sign; $\bar{E}$ is the opposite event; α is the probability that event E will occur at moment $t = (k + 1)\,T_0$, if at moment kT_0 event E occurred; β is the probability that event E will occur at moment $t = (k + 1)\,T_0$ if event $\bar{E}$ occurred at moment kT_0; P_I is the probability of appearance of event E in the first cycle; q_I is the probability of appearance of $\bar{E}$ in the first cycle; $q_I = 1 - P_1$.

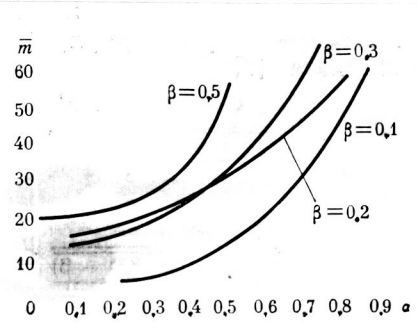

Figure 129. Dependence of $\bar{m}$ on α for Various Values of β

A simple Markov chain can be defined using the transition matrix

$$\pi = \begin{Vmatrix} \alpha & 1-\alpha \\ \beta & 1-\beta \end{Vmatrix}. \tag{4.10}$$

To determine the mean interval between changes of sign, we must know the probability of m-times appearance of event E in n cycles (in time nT_0). Let us represent the probability of appearance of this event by $P_n(m)$. Then the mean number of changes of sign in time nT_0 is determined by the expression

$$\bar{m} = \sum_{m=0}^{n} m P_n(m). \tag{4.11}$$

To calculate $P_n(m)$, we can use the asymptotic de Moivre-Lanyaas formula [7] /220

$$P_n(m) = \frac{1}{\sqrt{2\pi n P q \dfrac{1+\alpha-\beta}{1-\alpha+\beta}}} e^{-\frac{z^2}{2}}, \tag{4.12}$$

where

$$z = \frac{m(1-P)}{\sqrt{\dfrac{m\alpha(1-\alpha)+(n+m)\beta(1-\beta)}{(1-\alpha+\beta)^2}}}. \tag{4.13}$$

The dependences of $\bar{m}$ on α for various values of β are presented in Figure 129.

14.2. Selection of a Coding Method

In order to transmit information on the characteristics of a state or behavior of a set of scientific devices over some distance or record the information, a set of messages is formed at the transmitting end. Having or receiving the messages, after certain operations performed on the messages, we can extract the information of interest to us. There are many methods of formation of messages (voltages from sensors) with various physical information carriers. The mathematical description of messages is referred to as their representation. The set of representations is generally written in the form of a matrix

$$V(t)=\left\|\begin{matrix} v_1(t) \\ \vdots \\ v_n(t) \end{matrix}\right\|, \tag{4.14}$$

i.e., the message is represented by a random vector function V(t), described by a set of random functions $V_1(t)$, $V_2(t)$,..., $V_n(t)$.

The message carriers in the communications channel are electric and radio signals. The transmission of information on the behavior of an object in this case can be represented as a sequence of transforms

$$U(t)\rightarrow V(t)\rightarrow S(t)\rightarrow X(t)\rightarrow \\ \rightarrow V_B(t)\rightarrow U_B(t),$$

where U(t) is the set of a finite number of partial indicators of the object tested; S(t) is the set of useful signals formed on the transmitting end to transmit messages V(t); X(t) are the signals received at the receiving end, differing from S(t) due to distortions.

The difference X(t) and S(t) results from the fact that the restored messages $V_B(t)$ and the behavior characteristics of the object $U_B(t)$ differ from the true values of V(t) and U(t).

From the set of possible representations, we must select the best one, based on the requirements of [10] that the representation satisfy the following conditions:

1) allow the possibility of restoration of the characteristics of the state and behavior of the object with the required

probability, using communications channels with the minimum actual throughput capacity C_c;

2) be usable in apparatus of acceptable complexity with sufficiently high operational reliability;

3) facilitate the performance of the task of practically simultaneous transmission of information concerning a large group of particular indicators and characteristics, i.e., facilitate the construction of multichannel communications links.

All of these requirements are equally obligatory for both analog and digital communications systems.

One peculiarity of analog communications systems is the fact that representation $V^{(i)}$ is fixed by the set of realizations $v^{(i)}$, while the equivalent peculiarity of digial systems is that representation $V^{(i)}$ is fixed by the finite denumerable set $v_1^{(i)}, \ldots, v_n^{(i)}$.

Digital systems have a number of significant advantages over analog systems and have therefore been given ever increasing attention in recent times. The primary advantages of digital systems are as follows [10]:

1) possibility of transmission of the results of measurement with significantly lower errors introduced by the system; /221

2) the slight errors which are introduced are not accumulated during repeated relays;

3) while providing high transmission accuracy of the results of measurements and good power indicators, these systems may occupy a smaller band of frequencies than analog systems.

Digital methods of transmission of information can be subdivided into pulse-amplitude, pulse-time, pulse-width and pulse-code modulation (PCM) methods. PCM is most interference resistant.

Let us study the coding of information in general form. We know that coding means the representation of messages by symbols or groups of symbols according to certain rules and that a particular case is the representation of the information of interest to us, when the set of realizations is finite and denumerable. Codes are characterized by an alphabet and by the number of symbols in the alphabet. The number of different symbols in the alphabet is the code base. A signal formed by combining several symbols is called a word or a code combination. The number of code combinations is defined by the expression

$$M = a^k, \qquad (4.15)$$

where a is the base of the code; k is the length of the code, i.e., the number of symbols in a word.

Recently, pulse code modulation has come to be the primary communications system used. PCM includes various modifications of codes. The most important properties of this type of code are studied below [11].

The bandwidth

$$W_{PCM} = 2mW_0, \tag{4.16}$$

where m is the number of symbols in a code group; W_0 is the width of the spectrum of the signal of a sensor.

The band of frequencies necessary for PCM in the ideal case is m times greater than that required for direct transmission of the signal W_0.

The threshold power with equal probability of all levels is

$$P_s = K^2 N_0 \frac{a^2 - 1}{12}, \tag{4.17}$$

where K is a coefficient ($K \simeq 10$); N is the power of noise in band W; a is the base of the code.

The throughput capacity of a communications system is expressed by the equation

$$C_{c_2} = W \log_2 \left(1 + \frac{P_c}{N_0}\right), \tag{4.18}$$

where P_c is the mean power of the signal; N_0 is the spectral power of the noise, or

$$C_{c_2} = W \log_2 \left(1 + \frac{12P_s}{K^2 N_0}\right). \tag{4.19}$$

Where $P_s = K^2 P_c/12$, equations (4.18) and (4.19) coincide. Thus, PCM requires $K^2/12 \simeq 8$ times more power than that theoretically necessary to maintain a channel with the fixed throughput capacity for the given bandwidth.

The interference stability of PCM is determined by the value of the signal/noise ratio (P_c/P_n) in the band $2mW_0$ necessary for proper reproduction of the code on the receiving end. For APC with low power capacity, the problem of interference stability, i.e., minimization of the ratio P_c/P_n per binary digit, is of great significance, since this ratio determines whether it is necessary to decrease or increase the power of the transmitter.

The probability of error in a code symbol can be calculated by the formula

$$P_{er} = F\left(\sqrt{\frac{2E_b}{N_0}}\right) = F\left(\sqrt{\frac{2P_c}{RN0}}\right),$$

where /222

$$F(x) = \frac{1}{2}\left[1 - \operatorname{erf}\left(\frac{x}{\sqrt{2}}\right)\right] \qquad (4.21)$$

is the probability integral; E_b is the energy expended per bit.

We know that the probability of error of a word is [12]

$$P_{erw} = 1 - (1 - P)^k = 1 - (1 - P_{er})^{RT}, \qquad (4.22)$$

where k is the length of the word (1, 2, 3,...K); R is the rate of the source of messages, bits per second; T is the length of the message, sec.

According to relationships (4.20) and (4.22), with any fixed R and P_c the probability of an error approaches 1 as the length of message T increases and, consequently, K increases. With fixed T and N_0, the probability can be decreased only by increasing the power expended per bit which, in turn, is achieved only by increasing the mean power P_c, or by decreasing the rate R. In [12], the value of the mean probability of error of a code word is presented, suitable for any type of code:

$$\overline{P}_{erw} < 2^z[R_0 - R_N], \qquad (4.23)$$

where z is the length of a code word;

$$R_0 = 1 - \log_2 \{1 + \exp [-\frac{E_b RT}{N_o z}]\}; \quad (4.24)$$

$$R_N = \frac{R}{D} = \frac{\text{bits/sec}}{\text{measurements/sec}} \quad (4.25)$$

Based on relationship (4.23), the mean probability of an error and, consequently, the probability of an error in at least one code in a set can be made arbitrarily small by selecting sufficiently great z, if R_N is a quantity less than the power of the exponential estimate of R_0. As $E_b \to \infty$, $R_0 \to 1$. It can be suggested as a result that in planning a transmission system in which P_{er} decreases exponentially with increasing z, we can select z so great that the numbers $10 P_{er}$ and $100 P_{er}$ will be quite small.

We must establish whether there is a practically realizable code for which the probability of error satisfies the upper estimate produced from formula (4.23). In order for the probability of error to satisfy the boundary of random coding with parameter R, the signals must be statistically independent (in pairs) [12]. These signals include codes with parity checking. For these codes, the words are statistically independent in pairs and each code in a set can be constructed by a device, the complexity of which increases with increasing length of the code limitations Z:

$$Z = RT \quad (4.26)$$

Recently, a number of studies have been performed of coding devices with parity checking, and catalogues of optimal binary codes, i.e., codes having the minimum error P_{er} have been composed for cases when Z and Z - k are both small [12, 13]. The existing methods of determination of optimal codes essentially consists only of methods of trial and error and testing. These methods usually cannot be used if Z (or Z - k) is great. No general algorithm is known for construction of a specific code for which it can be proven that the error probability is estimated at its greatest by (4.23).

Another class of codes is also used, related to them by correlation processing. The problem of coding in this case consists in determining signals with the minimum correlation with each other. This class of codes includes primarily orthogonal sequences. /223 The term "orthogonality" means noncorrelation of signals, i.e., maximum dissimilarity. There are several modifications of orthogonal codes, including biorthogonal codes.

Orthogonal codes satisfy the requirements [12]

$$\rho(V_i, V_j) = 0, \quad i \neq j, \tag{4.27}$$

where $\rho(x)$ is the correlation function; V_i, V_j are orthogonal codes.

For these codes, the condition M = k should be satisfied, since the number of orthogonal vectors in a M-dimensional space is equal to M.

Biorthogonal codes are formed of vectors or orthogonal codes and their negatives. A negative is a code produced from an initial code by replacement of 1 by -1 and vice versa. For these codes, the following condition should be fulfilled:

$$2k = M. \tag{4.28}$$

Let us study orthogonal and biorthogonal codes from the standpoint of their interference stability. The probability of proper reception of an orthogonal signal is expressed by the fromula [14]

$$P_c = \int_{-\infty}^{+\infty} \frac{\exp[-v_1^2/2]}{\sqrt{2\pi}} \times \left[\operatorname{erf}\left(v_1 + \sqrt{2PT/N_0}\right)\right]^{M-1} dv_1, \tag{4.29}$$

where v_1 is the integration variable.

Where $M \to \infty$

$$\lim P_{er} = \begin{cases} 1 & \text{where } \beta < \ln 2, \\ 0 & \text{where } \beta > \ln 2, \end{cases} \tag{4.30}$$

where $\beta = P_c T_b / N_0$.

The orthogonal signals as $M \to \infty$ can be error-free transmission at the rate

$$R = \frac{1}{T_b} < \frac{P}{\ln 2 N_0} = \lim_{W \to \infty} C_p.$$

Thus, if the band of frequencies is not limited, while the length of the signal may increase without limit, orthogonal codes have the best characteristics where $M \to \infty$ and the transmission rate approaches the limiting rate, i.e., bandwidth is exchanged for input power of the signal.

For a biorthogonal code, the expression for the error of reception is similar to the expression for an orthogonal code, but the probability of error is somewhat less. Table 11 presents data on the interference stability P_{er} of ordinary PCM, orthogonal and biorthogonal codes where k = 5, indicating that the radio communications system becomes more interference stable when the biorthogonal code is used.

TABLE 11

P_c/P_n	P_{er}		
	Uncoated PCM	Orthogonal Code	Biorthogonal Code
2	$8 \cdot 10^{-1}$	$8 \cdot 10^{-2}$	$8 \cdot 10^{-2}$
3.5	$2 \cdot 10^{-1}$	$9 \cdot 10^{-3}$	$2 \cdot 10^{-3}$
6	$2 \cdot 10^{-2}$	$\to 0$	$\to 0$
10	$1 \cdot 10^{-3}$	$\to 0$	$\to 0$

For an orthogonal code, the ratio of the bandwidth of the low frequency filter W_{1f} to the productivity of the information source R is [14]

$$\frac{W_{1f}}{R} = \frac{M}{2 \log_2 M} = \frac{2^{k-1}}{k}, \qquad (4.31)$$

where $M = 2^k$, while for a biorthogonal code

$$\frac{W_{1f}}{R} = \frac{M/2}{2 \log_2 M} = \frac{2^{k-2}}{k}. \qquad (4.32)$$

Comparison of formulas (4.31) and (4.32) indicates that the ratio W_{1f}/R for a system with biorthogonal codes is half that of a system with orthogonal codes. Furthermore, in a system using biorthogonal signals reception requires only M/2 different correlators or matched filters, since the other M/2 signals have the same form but the opposite sign. This allows significant simplification of the communications system. Therefore, biorthogonal

/224

codes have already been used in space communications system [15].

For comparison let us note that with element-by-element reception of uncoded PCM (by signal envelope) in order to maximize P_c/P_n it is necessary $W_{1f}/R \approx 1.5$ [16]. Thus, when simple uncoded PCM is used, in order to achieve an acceptable error probability per symbol of the code $R_{er} \approx 10^{-3}$, the signal/noise ratio must be over 10. For correcting codes, there is a threshold power with $P_c/P_n \approx 4$; above this power, correcting codes are quite effective. These codes require a large number of test symbols to approach the upper estimate of P_{er}. Correcting codes are more interference stable than simple codes, but do not fully solve the problem of interference stability of a communications system. More hopeful results are yielded by orthogonal codes [$R_0 > 1$] [see formula (4.23)]. When these codes are used, the limiting value of throughput capacity of the communications channel can be approached.

One significant shortcoming of orthogonal codes is the need to expand the communications bandwidth, which is equivalent to increasing the transmission rate R with the previous rate of interrogation of sensors. On the receiving end in this case there must be M or M/2 correlation receivers, which greatly increases the cost of the communications system. Consequently, a compromise must be sought among all codes so that the codes might have comparatively high interference stability and at the same time the band which they occupy might be comparable to the bandwidth of uncoded PCM. We shall study below a code which meets these requirements to some extent.

In this code, not all of the words are replaced by absolutely new combinations of characters (as is the case for recoding by orthogonal codes), but rather a priori known combinations of binary characters in thh ordinary code are replaced by new characters, but with certain correlation properties. Since biorthogonal codes require less bandwidth than orthogonal codes, the new combinations must be given preference. The rule for the recoding is formulated as follows: for recoding of a message it is necessary that, first of all, the number of code symbols in the primary word be even and, secondly, each primary code combination must be divided into k/2 groups and each pair of symbols (groups) in the word must be coded in a certain order only by a biorthogonal three-digit code which belongs to it. The number of symbols in this code is equal to 4 [see formula (4.28)].

Let us explain this by an example. Suppose there is an eight-digit code (primary information). Let us divide it into k/2 groups, i.e., into four groups of two symbols per group. We know that in two-digit coding, the combinations can be as follows: 00, 11, 01, 10. The next stage is recoding of each combination

with a new three-digit biorthogonal code, i.e., a code containing four symbols per word. A diode matrix outputs the instruction to use one or another biorthogonal code according to the incoming two-digit combination, and the new rate (R', bits per second) is twice the rate of the initial code. The three-digit biorthogonal code is selected because with this structure of the new code, the ratio of bandwidths of ordinary PCM and biorthogonal code is practically identical, while the power necessary for proper reproduction of the information differs. This means that whereas for reception of a symbol of a code combination in uncoded PCM bandwidth $W_{1f} = 1.5\ k_1/T$ (where k_1 is the length of the code, T is the length of a word), for the biorthogonal code suggested $W_{1f} = 2^{k_2-2}K_1/2T$ (where k_2 is the length of the biorthogonal code). The signal/noise ratio also changes [see formulas (4.20) and (4.29).

/225

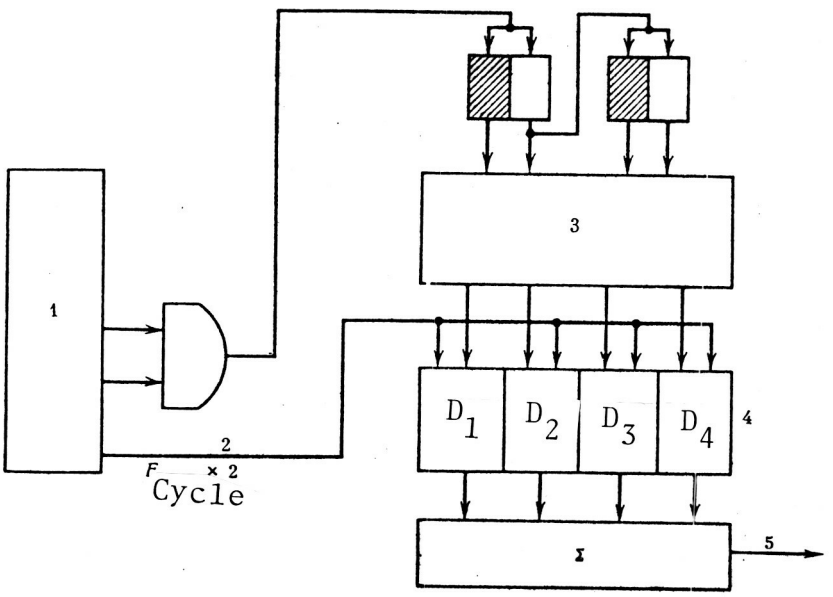

Figure 130. Block Diagram of Recoding Device. 1, Coding Device; 2, Synchronization Signal; 3, Diode Matric; 4, Code Generators; 5, Deterministic Code

A block diagram of the coding device is presented in Figure 130, its time diagrams in Figure 131.

The effectiveness of the communications system (β) when this code is used, which we will refer to as a deterministic code, is improved in comparison to ordinary uncoded binary code (Table 12; values of R taken arbitrarily).

The use of the deterministic code for low-power spacecraft can yield a definite gain in the power characteristics of the radio link. Reception of the deterministic code on Earth will be much more complex than simple element-by-element reception, since four correlation receivers (differentiator), a threshold device and a shaper device are required after the detector. If the peak of the autocorrelation function at the output of the threshold device exceeds the threshold, the shaper must formulate a code combination corresponding to the given channel, but the form of the code must be the initial form (i.e., a combination not of four symbols, but of two). Figure 132 presents a block diagram of the receiver. /226

TABLE 12

Parameters	Uncoded PCM	Deterministic Code
Productivity of information source R, bits per second	1700	3400
Bandwidth of low frequency filters W_{1f}, Hz	2600	2600
Probability of error P_{er} per word where $k_i = 6$	$1.5 \cdot 10^{-3}$	$1.5 \cdot 10^{-3}$
Signal/noise ratio after low-frequency filter $(P_c/P_n)\ W_{1f}$	12.2	4.0
Transmitter power P, arbitrary units	1	0.3
Effectiveness of Communications system β	0.055	0.33

Since the deterministic signals have known code combinations, they can be entered into computer memory, thus simplifying the process of decoding of the signals. In this case, the computer acts as a correlator. In accordance with the program, the computer outputs finished results, divided into channels in real time.

14.3. Rate of Interrogation of Sensors and Number of Quantization Levels of Analog Signal

One of the requirements placed on telemetry devices is effective utilization of the channel width of available.

We have just studied a model of a signal taken from a sensor. This model represents a quasistable process, and in spectral form is similar to a compressing and expanding spring. With ordinary coding, signal readings are taken at intervals of $1/(2\ W_{0max})$, in spite of the fact that the maximum spectral density

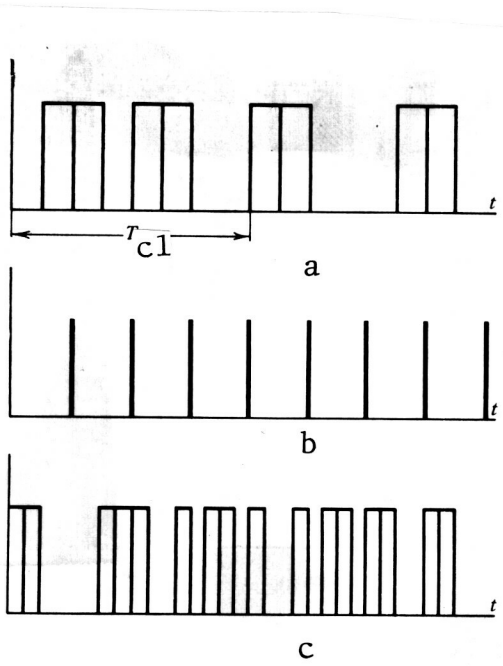

Figure 131. Time Diagram of Recoding Device. a, Output telemetry signal; b, Synchronization signal with $F_c = 2F_{cycle}$; c, Signal from recoding device with $F_{code} = 2F_{cycle}$

of the signal is grouped in the lower-frequency area (Rayleigh distribution).

Let us study the discretization of the rate of interrogation of sensors. This discretization can improve the utilization of the channel width and increase the effectiveness of the communications link. We will need the following symbols: μ is the frequency of replacement of microprocesses in a quasistable signal; m_n is the number of discrete rates. If $W(\Delta_{\omega in})$ is the differential distribution function of the width of the input signal spectrum, then as a result of discretization of the rate of interrogation $W(\Delta_{\omega in})$ is converted to a discrete function [2] /227

$$W_d(\Delta\omega_{in}) = \sum_{i=1}^{m_n} \delta(\Delta\omega_{in} - \Delta\omega_{ini}) x \int_{\Delta\omega_{ini-1}}^{\Delta\omega_{ini}} W(\Delta\omega_{in}) \alpha \Delta\omega_{in}, \quad (4.33)$$

where $i = 1, 2, \ldots, m_n$.

We present below the first order moments of the initial distribution function and discrete function respectively:

$$\overline{\Delta\omega}_{in} = \int_0^{\infty} \Delta\omega_{in} W(\Delta\omega_{in}) \alpha \Delta\omega_{in}, \quad (4.34)$$

$$\overline{\Delta\omega}_{ind} = \sum_{i=1}^{m_n} \Delta\omega_{ini} \int_{\Delta\omega_{ini-1}}^{\Delta\omega_{ini}} W(\Delta\omega_{in}) \alpha \Delta\omega_{in}. \quad (4.35)$$

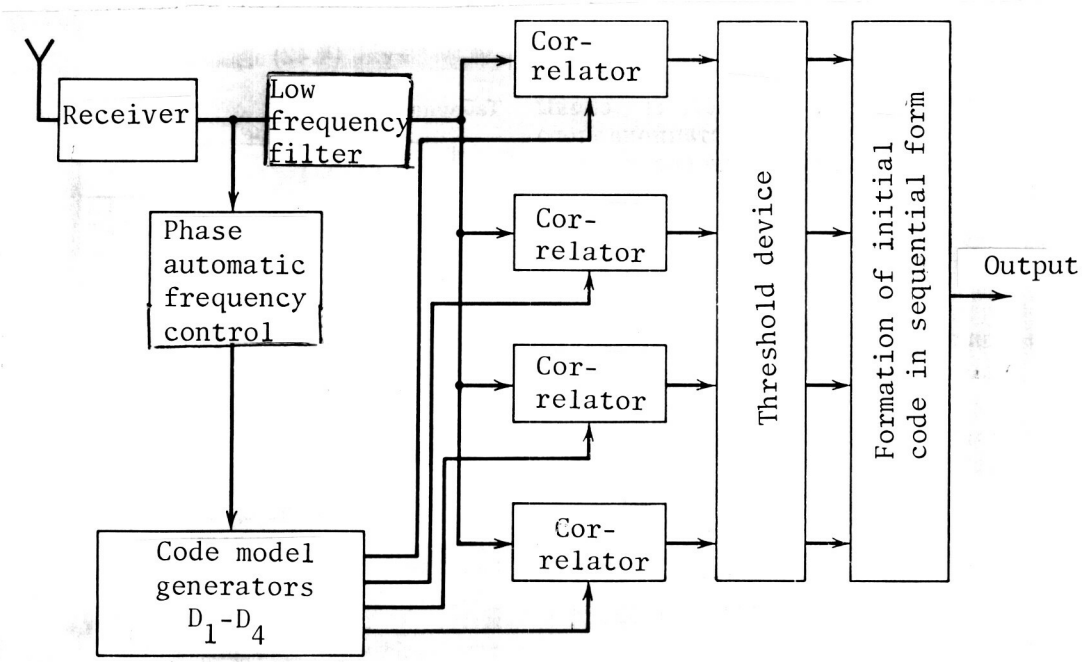

Figure 132. Block Diagram of Deterministic Code Receiver

Let us represent $\Delta_{\omega in}/\Delta_{\omega ind} = \eta_d$, where η_d is the actual compression of the spectrum considering discretization of the rate of interrogation of the sensors. With identical intervals between discrete values $\Delta_{\omega ini}$

$$\Delta\omega_{in} = \Delta\omega_{ind} = \frac{\omega_{in\ max}}{2m_n}, \tag{4.36}$$

where $\omega_{in\ max}/2m_n$ is the quantization step of the effective input signal spectral width.

For large values of m_n and even quantization of the spectral width, we have

$$\eta_d = \frac{\Delta\omega_{in\ max}}{\Delta\omega_{in}\frac{\Delta\omega_{in\ max}}{2m_n}}. \tag{4.37}$$

The rate of transmission of useful information C in a system with averaging is

$$C = 2\overline{\Delta\omega}\ \log_2 M, \qquad (4.38)$$

where M is the necessary number of gradations of amplitude of the transmitted message. /228

The effectiveness η_T of a system which averages the rate of transmission of information can be determined considering discretization of the rate of interrogation of the sensors and losses for transmission of supplementary service information concerning the changes in rate by formula [2]

$$\eta_T = \nu\frac{C}{dC + C_{cl}} = \frac{\log_2 M}{[1/\eta + 1/(2m_n)][\log_2 M + \nu/(2\log_2 m_n)]}, \qquad (4.39)$$

where ν is the ratio of the frequency of changes of microprocesses inthe quasistable signal to the mean width of the signal spectrum:

$$\nu = \frac{\nu_{max}(m_n - 1)}{m_n}, \quad \nu_{max} = \frac{\mu_{max}}{\overline{\Delta\omega}_{in}},$$

for a quasistable signal $0.1 \geq \nu_{max} \geq 0{,}001$, while $\eta = \Delta\omega_{in\ max}/\Delta\omega_{in}$.

In order to determine the optimal number of discrete values of transmission rate, we must differentiate expression (4.39) with respect to m_n and set it equal to 0. Let us introduce the symbol noted above for ν into (4.39); then

$$\eta_T = \frac{\log_2 M}{f(m_n)} = \log_2 M \left\{[1/\eta + 1/(2m_n)] \times \times \left[\log_2 M + \frac{\nu_{max}(m_n - 1)}{2}\log_2 m_n\right]\right\}^{-1}. \qquad (4.40)$$

The derivative of expression (4.40) is

$$\frac{d\eta_T}{dm_n} = \frac{\nu_{max}}{\eta}\left(\log_2 m_n + \frac{m_n - 1}{\ln 2}\right) - \log_2 M + \frac{\nu_{max}}{2} \times \times \left(\frac{2 - m_n}{m_n}\log_2 m_n + \frac{m_n - 1}{m_n \ln 2}\right) = 0. \qquad (4.41)$$

Solution of equation (4.41) yi

$$m_n \approx \frac{\eta}{\nu_{max}} \ln 2 \left[\log_2 M + \nu_{max} \times \left(\frac{1}{2} - \frac{1}{\eta}\right) \log_2 \frac{1}{\nu_{max}}\right] + 1 - \eta/2. \quad (4.42)$$

Equation (4.42) al.. ..s us to find the approximate value of the optimal number of discrete rates as a function of the parameters of the quasistable process η, ν_{max} and the necessary accuracy of transmission of messages. Table 13 as an example shows the results of certain calculations performed using formula (4.42) where $\eta = 5$.

TABLE 13

M	ν_{max}	m_{opt}	η_T	η_T		
				$m_n = 3$	$m_n = 5$	$m_n = 10$
2	0,1	39	3,74	2,59	3,05	3,48
2	1,0	4	4,79	1,78	1,73	1,60
20	0,1	156	4,54	2,69	3,26	3,87
20	1,0	16	3,01	2,43	2,74	2,97
100	0,1	237	4,67	2,70	3,30	4,0

Evaluating the results presented in Table 13, we can note that in the overwhelming majority of cases the value of m_n clearly goes beyond the reasonable capabilities of contemporary equipment. Therefore, if $m_n > 4$-5, the technical capabilities available should be used to select the number of discrete levels. Thus, by discretization of the rate of interrogation of the sensors we can achieve more complete loading of the communications channel. It has been assumed that the changes in spectrum of the signals of the sensors follow the Rayleigh distribution; therefore, the use of discretization in the lower frequency end of the spectrum can improve the effectiveness of the communications link.

Let us study quantization of a continuous quantity characterized by a Rayleigh probability density. First of all, let us define the estimate of the message following decoding [17]: /229

$$S^*(x_1^k) = \frac{1}{P_{pr}(x^k)} \int_{\eta(k-1)}^{\eta(k)} \int_{-\infty}^{+\infty} SW(S, S_1) dS dS_1, \qquad (4.43)$$

where $\eta(k)$ are the quantization thresholds; $P_{pr}(x^k)$ is the a priori probability of the signal x_1^k;

$$P_{pr}(x^k) = \int_{\eta(k-1)}^{\eta(k)} W(s_1)\, dS_1;$$

$W(S, S_1)$ is the two-dimensional Rayleigh densith represented as a series with respect to orthogonal Laguerre polynomials:

$$W(S, S_1) = \frac{SS_1}{\sigma_\psi^4} \exp\left[-\frac{S^2 + S_1^2}{2\sigma_\psi^2}\right] \times \times \sum_{n=0}^{\infty} L_n\left(\frac{S^2}{2\sigma_\psi^2}\right) L\left(\frac{S_1^2}{2\sigma_\psi^2}\right) \frac{\sigma_\psi^2}{(n!)^2}. \qquad (4.44)$$

Here σ_ψ^2 is the dispersion of the normal quasiharmonic process $\psi(t)$, the envelope of which is the Rayleigh process $S(t)$, while $L_n(z)$ are the Laguerre polynomials satisfying the relationship

$$L_n(z) = e^z \frac{d^n}{dz^n}(z^n e^{-z}). \qquad (4.45)$$

The mean value, dispersion and correlation factor of the Rayleigh process are respectively [17]

$$m_S = \sigma_\psi \sqrt{\pi/2}, \quad \sigma_S^2 = (2 - \pi/2)\sigma_\psi^2, \quad R_S(\tau) \approx R_\psi^2(t). \qquad (4.46)$$

Substituting (4.44) into (4.43), we have

$$S^*(x^k) = \frac{1}{P_{pr}(x^k)} \sum_{n=0}^{\infty} \frac{1}{\sigma_\psi^2 (n!)^2} A_n B_n, \qquad (4.47)$$

where

$$A_n = \sigma_\psi^3 \frac{\Gamma(n-0,5)}{\sqrt{2}\,(n!)}, \tag{4.48}$$

$$B_n = \sigma_\psi^4 \int_{z(k-1)}^{z(k)} e^{-z_1} L_n(z_1)\, dz_1, \tag{4.49}$$

$$z_1 = S_1^2/2\sigma_\psi^2, \quad z(k) = [h^k]^2/2\sigma_\psi^2,$$
$$z(k-1) = [h^{k-1}]^2/2\sigma_\psi^2. \tag{4.50}$$

Using these formulas and equation (4.47), we can calculate the optimal values of estimates corresponding to various signals x (k = = 1, 2, 3,...). This requires that we know the dispersion of the message σ_S^2, the correlation factor $R_S(\tau)$ and the quantization thresholds. The correlation factor and dispersion can be calculated by formula (4.1), while the quantization thresholds h^k can be calculated by the method described below.

Let us introduce the function [17]

$$f(h^{(k)}) = \frac{1}{W[S_1 = h^{(k)}]} \int_0^\infty SW(S, S_1) = h^{(k)} dS. \tag{4.51}$$

Substituting expressions (4.44) and (4.47) here, we produce

$$f(h^{(k)}) = \frac{\sigma_\psi}{\sqrt{2}} \sum_{n=0}^{\infty} L_n\left\{\frac{(h^{(k)})^2}{2\sigma_\psi^2}\right\} \times$$
$$\times \frac{1}{(n!)^3}\Gamma(n-0,5) \tag{4.52}$$

or

$$f(h^{(k)}) = \frac{1}{2}\{S^*(x_1^k) + S^*(x^{k+1})\}. \tag{4.53}$$

The formulas produced, using the method of successive approximations, allow us to perform numerical calculation of the optimal quantization thresholds and levels of estimate $S^*(x^k)$. The procedure for determination of these values is as follows. First of all, using formula (4.52), we must construct a graph of function $f(h^{(k)})$ with the required accuracy. Beginning our calculations, we should assign arbitrary values to the levels of estimate $S(x^k)$ where k = 1, 2,..., M. After this, using formula (4.53), we calculate the corresponding values of function $f(h^{(k)})$ where k = 1, 2,..., M - 1. Further, using the graph of function $f(h^{(k)})$, we define the values of the quantization thresholds $h^{(k)}$.

With a limitation on the transmission rate, the quantization of the message as to time and number of levels follows the equation /230

$$T = \frac{\log_2 M}{R}. \qquad (4.54)$$

We see from (4.54) that with a fixed rate of transmission of pulses, as the number of levels increases, the accuracy of the system increases. Due to the reduction in quantization error as to level, the quantization step as to time increases and, consequently, the discretization error increases. In these cases, the selection of the optimal relationship between system parameters T and M is not obvious.

The formula for calculation of the mean square error [17]

$$\varepsilon^2 = \sigma_S^2\left[1 - (1 - \varepsilon_0^2)\frac{1}{T}\int_0^T R_S^2(\tau)\,d\tau\right] \qquad (4.55)$$

does not include the number of levels, which determines only the tabular value of ε_0^2, which is also the mean square error, but normalized relative to the dispersion of the message σ_S^2; therefore, it is impossible to produce an analytic expression for calculation of the optimal parameters.

The optimal parameters can be determined by calculating the mean square error for various numbers of quantization levels with fixed pulse transmission rate through the channel and selection of the M for which the error is minimal.

Let us study as an example a binary channel with a pulse transmission rate of R [bits/sec]. There is no noise in the channel. Let us take a one-dimension Markov process described by the correlation function

(4.56)

$$R_S(\tau) = \exp[-\Delta\omega_{max}/\tau].$$

Let us multiply the right and left portions of equation (4.55) by $\Delta\omega_{max}$, substituting the expressions produced into (4.56) and integrating. We produce

$$\varepsilon^2 = \sigma_S^2\left[1-(1-\varepsilon_0^2)\frac{1-e^{-2\frac{\Delta\omega}{R}\log_2 M}}{2\log_2 M}\frac{R}{\Delta\omega}\right]. \tag{4.57}$$

The results of calculation of the mean square error based on this formula are presented in Table 14.

TABLE 14

$R/\Delta\omega$	$M=2$	4	8	16	32
10^{-1}	1	1	1	1	1
1	0,8	0,8	0,8	0,8	0,8
10	0,5	0,5	0,5	0,5	0,5
10^2	0,5	0,2	$8\cdot10^{-2}$	$7\cdot10^{-2}$	$7\cdot10^{-2}$
10^3	0,5	0,2	$6\cdot10^{-2}$	$2\cdot10^{-2}$	$8\cdot10^{-3}$

When there is noise in the channel, the task of selection of optimal parameters of the communications system is more complex.

During the development of a communications system as a whole, signals at the input of the receiver (P_c) and spectral noise density (N_0) may be fixed. Let us assume that the duration of binary signals $\tau_i = 1/R$. As transmission rate R is increased, on the one hand, the descretization error of the message will be decreased, while on the other hand, due to the reduced energy of the signals, the number of errors caused by the influence of noise in the communications channel will increase.

Let us study the method of calculation of the mean square errors in a channel with noise. We assume that the values of P_c, N_0 and ΔW_{max} are fixed. The mean square error for the entire system with optimal coding is [17]

(4.58)

where ε_1^2 is the mean square quantization error, determined by formula (4.57); ε_2^2 is the mean square decoding error. The value of ε_2^2 is determined by the formula

$$\varepsilon^2 = \varepsilon_1^2 + \varepsilon_2^2,$$

$$\varepsilon_2^2 = \sigma_S^2 a_L P_{er} \tag{4.59}$$

where a_L is a coefficient which depends on the message, type of code and length (a_L = 6.1 where M = 8, a_L = 7.6 where M = 16, a_L = 9.5 where M = 32). /231

Let us define ε_2^2, using formulas (4.55) and (4.59)

$$\varepsilon_2^2 = \sigma_S a_L P_{er} \frac{1 - e^{-2\frac{\Delta\omega}{R}\log_2 M}}{2\log_2 M} \frac{R}{\Delta\omega}, \tag{4.60}$$

where P_{er} is the probability of an error in reception of one element of code. Usually the calculation of P_{er} includes the signal/noise ratio, which can be written as follows:

$$\frac{2E}{N_0 \Delta\omega_{max}} = \left(\frac{2P_c}{N_0\Delta\omega}\right)\left(\frac{\Delta\omega}{R}\right). \tag{4.61}$$

The first cofactor in the right portion of equation (4.61) is assigned, while the second is an independent variable. By changing $R/\Delta\omega$ and M, we can calculate the corresponding values of mean square error. In table 15, for example, we present the results of calculation of mean square error as a function of M and $R/\Delta\omega$ where $P_c/N_0\Delta\omega$ = 500.

TABLE 15

$R/\Delta\omega$	$M=2$	4	8	16	32
1	0,8	0,8	0,8	0,8	0,8
10	0,6	0,5	0,5	0,5	0,5
100	0,5	0,2	$8\cdot10^{-2}$	$6\cdot10^{-2}$	$7\cdot10^{-2}$
1000	0,8	0,8	0,9	0,9	0,9

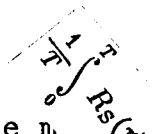

The data in the table show that the most accurate communications system is that with quantization in levels and transmission rate $R = 100\ \Delta\omega$.

Thus, in order to assure optimal operation of a communications system it is necessary that the throughput capacity of the communications channel be effectively used, i.e., that the sensor interrogation rate be discretized. The number of levels of quantization should not be excessive, due to the minimum increase in accuracy thus achieved. The number of quantization levels must be selected in accordance with the parameters of the radio link.

14.4. Storage and Reproduction of Information

Memory devices are used to store long-term information between communications sessions, to compress the spectrum of the signal, to record test values in devices for elimination of redundancy, etc. Their use does increase the complexity of the communications system apparatus somewhat. However, in many cases the use of memory devices is necessary, since the physical processes occurring in space cannot always be recorded and transmitted immediately [18]. In [19], the dependence of the activity of channels (N) on periodicity of interrogation (T) is presented. For example, with periodicity T = 7 sec, the number of active sensors is not over 10-15% of the entire number of sensors (measurement accuracy parameters about 3%).

With a periodicity of direct transmission sessions of about 20 hours, a great quantity of useful information will not be recorded. Let us assume that an APS is resting on the lunar surface. However, since the moon cannot be seen from the Earth at all times of day, we must use information on the duration of radio visibility of the moon, published each year in the astronomical calender. The radio visibility of the moon varies from $T_{min} \approx 3$ hours to $T_{max} \approx 9$ hours. If we use T_{min} as a basis of the most probable quantity, the pause between communications sessions is approximately 20 hours. Consequently, in this case the communications system will not be very informative unless memory devices are used.

They are particularly necessary when APS operate on the surfaces of the planets: in these cases, this necessity is dictated not only by the brevity of radio visibility, but also by the energetics of the radio link. /232

When memory devices are introduced as a part of the APS, yet another important problem is solved -- compression of the signal spectrum. Whereas direct recording from the sensors is sometimes slow, sometimes fast, during reproduction of the indications of the sensors the information can be transmitted at a single speed, selected to provide best reception accuracy on Earth.

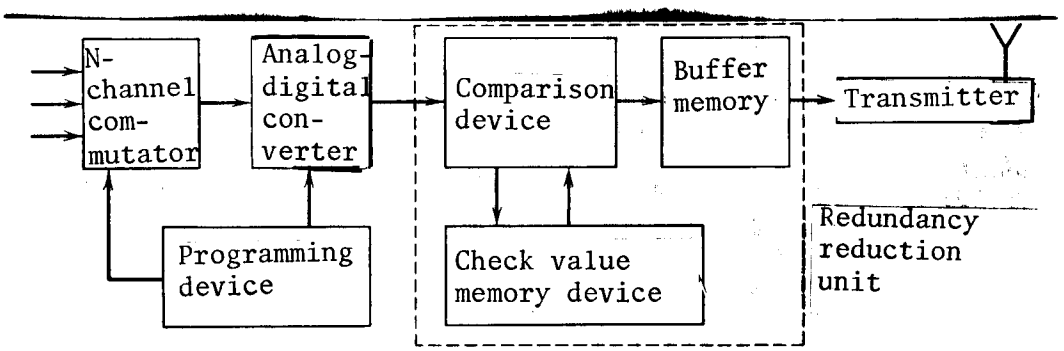

Figure 133. Example Block Diagram of System for Reduction of Redundancy

In order to encompass a large number of active sensors, a certain periodicity of interrogation is usually established (based on a priori known data); therefore, start-stop memory devices have been given preference recently. Their operating principle is that the memory is turned on at the moment when the coding device begins to operate, then recording is stopped at the end of a frame. When the frames are reproduced, they follow one another without interruption.

Let us study the application of a memory device to a PCM system with reduction of redundancy. The principle of construction of the redundancy reduction unit is shown in Figure 133.

The comparison device in an arithmetic unit capable of identifying and excluding redundant data.

The check value memory device is used to store constants (tolerances, priorities, algorithms, etc.), instructions and variables. since these check values may vary for the different channels, the capacity of the memory device must be proportional to the number of channels of data. The number of bits required for each check value depends on the type of special instructions used, the flexibility of the system and the concepts upon which the system is based.

The buffer memory device is the element of the system required to actually achieve the possibilities of data reduction which appear. The buffer stage has finite capacity, so that there is a certain probability of loss of data if it is overloaded. The capacity of the buffer stage is limited by considerations of weight and size. At the output of the buffer memory, control signals are created, corresponding to the various degrees of buffer loading, and these signals are used to regulate the mean rate of data input.

In a PCM system, as the redundancy decreases the role of the main memory device in performed by the buffer memory. The degree of utilization of the memory device in this system is highest, and only that information carried by the most significant data is recorded. /233

Thus, considering the long time which the APS spends on a planet and the variety of the physical phenomena measured by the telemetry device, the inclusion of a memory device in the APS apparatus is quite necessary.

14.5. Effectiveness of the Communications System

Let us study means for increasing the information effectiveness of a communications system, generally expressed by the relationship

$$H/H_0 = h, \tag{4.62}$$

where h is the relative entropy, while

$$H = -\sum_{i=1}^{M} P_i \log_2 P_i, \tag{4.63}$$

$$H_0 = \log_2 M. \tag{4.64}$$

The redundancy of the information

$$\gamma = 1 - H/H_0. \tag{4.65}$$

Maximization of h is achieved where $H = H_0$. According to the theorem of Shannon [20], in order for entropy H to be maximal, it is necessary that a message have maximum uncertainty.

It was shown in [19] that with a single cycle of interrogation, the number of active channels, i.e., the number of channels carrying nonredundant information, is about 6-8% of the total number of channels. Consequently, the spacecraft transmits a great deal of redundant information, and the effectiveness of the communications system is very low. This parameter of the communications link must be improved in order to save power, reduce the capacity of the on-board memory device, reduce the information processing time at

the receiving end and for other reasons which interact with these.

Let us study some methods of increasing the information effectiveness by decreasing the natural redundancy of messages. In contrast to known methods of reduction [22], we suggest a device consisting of a polynomial predictor, the operating mode of which is determined by aperture algorithms, and a decorrelation unit, the operating mode of which is determined by a Fourier transform or Walsh transform algorithm. A block diagram of a telemetry device including these units is presented in Figure 134.

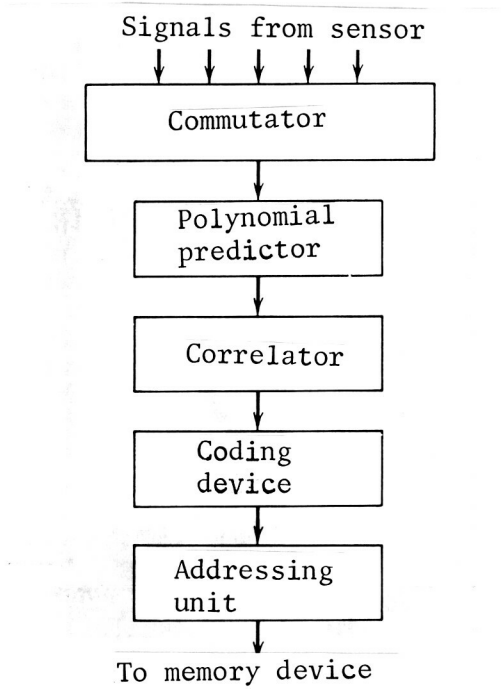

Figure 134. Block Diagram of Redundancy Reduction Device

Let us begin our analysis of the device with the polynomial predictor. Suppose mean square error ξ^2 is assigned with even discretization, and suppose we can ignore high-frequency components with $\omega_{hf} = \Delta\omega > \Delta\omega_{max}$, the probability of appearance of which is $P = 10^{-6}\text{-}10^{-9}$. Then, the discretization interval is determined by the assigned ξ^2 and P. /234

Assuming relative errors upon quantization of samples to be slight, we can ignore them and consider the signal sent to the compression unit to be continuous. Under these conditions, the reduction factor is calculated by the formula

$$K_{rd} = \int_0^{\Delta\omega_{max}} K_{st}(\Delta\omega) W(\Delta\omega) d(\Delta\omega), \qquad (4.66)$$

where K_{st} is the reduction factor with a stationary input signal to the redundancy elimination unit, and integration with weight $W(\Delta\omega)$ considers the instability of process $\xi(t)$.

In order to produce the mean square error with adaptive discretization, as with even discretization, $\Delta t_A \to 0$, which leads to continuous reading at the limit, since otherwise the error will result not only from the method of compression but also from the finite value of $\Delta t_A << \Delta t$. Under these assumptions, random process $\xi(t)$ can be considered a component of a multidimensional Markov process [3].

We present below a calculation of the effectiveness of algorithms for zero order prediction (ZOP) and first order prediction (FOP) [21]. We select these algorithms because they are widely used and easily technically realized methods of reduction of natural redundancy in analog messages [22]. As a model of our message, we take a differentiable normal stable process with zero mean and correlation function

$$R(\tau)=\sigma^2 e^{-\alpha|\tau|}\left(\cos\beta\tau+\frac{\alpha}{\beta}\sin\beta|\tau|\right).$$

Since usually the frequency of reading of the process is significantly greater than the width of its spectrum Δf, we will assume the reading to be continuous. Process U(t) with fixed correlation function can be looked upon as a stable solution of the equation [3]

$$\frac{d^2U}{dt^2}+2\alpha\frac{dU}{dt}+\gamma^2U=2\sigma\sqrt{\alpha\gamma^2}\,\xi(t), \tag{4.67}$$

where $\xi(t)$ is white noise, $\gamma^2 = \alpha^2 + \beta^2$.

Determination of the effectiveness of ZOP and FOP algorithms is reduced to determination of the distribution of time θ between nonredundant readings [22]. This can be found as an integral with respect to the assigned tolerance area D of the solution of the two-dimensional second equation of Kolmogorov [3], corresponding to equation (4.67):

$$\frac{dW}{dt}+\frac{d}{dy_1}(y_2W)-\frac{d}{dy_2}[(\gamma^2y_1+2\alpha y_2)W]-2\sigma^2\alpha\gamma^2\frac{dW^2}{dy_2^2}=0 \tag{4.68}$$

with the initial condition

$$\tau=t=0,\quad W=\delta(y_1-x_1)\,\delta(y_2-x_2) \tag{4.69}$$

and the boundary condition $\tau > t$, $y_1 \to K_1$, $y_1 \to K_2$, $y_2 < K_1'$, $y_2 > K_2'$.

The boundaries of the tolerance area $K_1(t) = 1t + x_1 - \Delta x$ and $K_2(t) = 1t + x_1 + \Delta x$ ($2\Delta x$ is the width of the aperture), where for ZOP the slope $1 = 0$ and for FOP $1 = x_2$ (tolerance band directed along the derivative, which differentiates this method of FOP from that studied in [23].

The solution of equation (4.68) under condition (4.69) is difficult to find, so let us study an approximate solution with zero boundary conditions:

(4.70)

where $W = W(t; y_1; y_2; 0; x_1; x_2)$.

In this case for constant boundaries K_1 and K_2 (for ZOP) we can use the method of supplementary sources [24]. Here, the solution of equation (4.68) can be represented as a linear combination /235 of the fundamental solutions

$$W_0(t; \bar{y}; 0; \bar{x}):$$
$$W(t; \bar{y}; 0; x) \approx W_0(t; \bar{y}; 0; x) - \\ - \gamma_1 W_0(\bar{y}; 0; \bar{x}_1) - \gamma_2 W_0(t; \bar{y}; 0; \bar{x}_2), \tag{4.71}$$

where $\bar{x}_1 = (x_{11}; x_{22})$ and $\bar{x}_2 = (x_{12}; x_{21})$ are the coordinates of the supplementary sources, symmetrically placed relative to point $\bar{x} = (x_1; x_2)$, i.e., $x_{11} = x_1 - 2\Delta x$, $x_{12} = -x_2$, $x_{21} = x_1 - 2\Delta x$, $x_{22} = -x_2$.

The fundamental solution is a two-dimensional normal rule [3]

$$W_0(t; \bar{y}; 0; x) = \frac{1}{2\pi \sqrt{K_{11}K_{22} - K_{12}^2}} \times \\ \times \exp\left\{ - \frac{1}{[2(K_{11}K_{22} - K_{12}^2)]^2} [K_{11}(y_1 - \bar{y}_1)^2 - \right. \\ \left. - 2K_{12}(y_1 - \bar{y}_1)(y_2 - \bar{y}_2) + K_{22}(y_2 - \bar{y}_2)] \right\}^2, \tag{4.72}$$

where $\bar{y}_1$, $\bar{y}_2$, K_{11}, K_{12}, K_{22} are defined by the expressions

$$\bar{y}_1 = e^{-\alpha\tau}\left[x_1\cos\beta\tau + \frac{1}{\beta}(x_2+\alpha x_1)\sin\beta\tau\right],$$

$$\bar{y}_2 = e^{-\alpha\tau}\left[x_2\cos\beta\tau - \right.$$

$$\left. -\left(\frac{\gamma^2}{\beta^2}x_1 + \frac{\alpha}{\beta}x_2\right)\sin\beta\tau\right],$$

$$K_{11} = \sigma^2\left\{1 - 2e^{-\alpha\tau}\left[\frac{\gamma^2}{\beta^2} - \frac{\alpha^2}{\beta^2}\cos 2\beta\tau + \right.\right.$$

$$\left.\left. + \frac{\alpha}{\beta}\sin 2\beta\tau\right]\right\},$$

$$K_{12} = \frac{\sigma^2\alpha\gamma^2}{\beta^2}e^{-2\alpha\tau}(1-\cos 2\beta\tau),$$

$$K_{22} = \gamma^2\sigma^2\left\{1 - \frac{\gamma^2}{\beta^2}e^{-2\alpha\tau}\left[1 - \frac{\alpha^2}{\gamma^2}\cos 2\beta\tau - \right.\right.$$

$$\left.\left. - \frac{\alpha\beta}{\gamma^2}\sin 2\beta\tau\right]\right\}. \qquad (4.73)$$

In the general case, we cannot find constant intensity factors γ_1 and γ_2 of the supplementary sources which satisfy the conditions of continuity of probability density $W(t; \bar{y}; 0; \bar{x})$ [24]. Therefore we select γ_1 and γ_2 from the condition of equality of the probability density at the boundaries of tolerance band D to zero on the average over the observation time t_H. Here, the desired coefficients can be found from the system of algebraic equations

$$\lim_{y_1\to K_1} W = \lim_{y_2\to K_2} W = 0,$$

$$\int_0^{t_H} W_0(K_1; t; \bar{x})\,dt = \gamma_1\int_0^{t_H} W_0(K_1; t; x_1)\,dt + $$

$$+ \gamma_2\int_0^{t_H} W_0(K_1; t; x_2)\,dt,$$

$$\int_0^{t_H} W_0(K_2; t; \bar{x})\,dt = \gamma_1\int_0^{t_H} W_0(K_2; t; x_1)\,dt + $$

$$+ \gamma_2\int_0^{t_H} W_0(K_2; t; x_2)\,dt, \qquad (4.74)$$

where $W_0(K; t; x)$ are the one-dimensional probability densities. The solution of this system is studied in [24].

For our case, we must take t_H equal to the correlation time τ_k of process u(t).

The probability that process u(t) will be in the tolerance area D [3]

$$P_{ZOP} = \int_{-\infty}^{+\infty} \int_{K_1}^{K_2} W(\tau; \bar{\xi}; 0; \bar{x})\, dy_1 dy_2, \qquad (4.75)$$

which is related to the desired distribution of time θ by relationship [3]

$$W(\theta) = \frac{dP(\tau)}{d\tau}\Big|_{\tau=\theta}. \qquad (4.76)$$

In order to determine the effectiveness of FOP, let us study process $V(t) = u(t) + m(t)$, where $m(t) = -1t$. Trajectories ω of processes $u(t)$ and $V(t)$, studied in the corresponding tolerance areas D_0 and D_ℓ, continue the probability measures P_0 and P_m, where P_m is absolutely continuous relative to P_0 [25]. According to the Radon-Nicodim theorem, there is a funtional $f(\omega) = dP_m/dP_0$ /236 such that

$$P_m = \int_{\omega \in D_0} f(\omega)\, dP. \qquad (4.77)$$

It is proven in [25] that the following relationship exists between the probability measures P_0 and P_m, induced in the sampling functions of process $u(t)$ with fixed correlation function and mean value $0 - m$

$$f(u, m) = \exp\left\{(u, m)_R - \frac{1}{2}(m, m)_R\right\}, \qquad (4.78)$$

where $(h, g)_R$ is the scalar product of the two functions in Hilbert space H with reproducing kernel R. The latter is determined for the fixed correlation function by the relationship

$$(h, g)_R = (4\sigma^2\alpha\gamma^2)^{-1}\left\{\int_0^t (h'' + 2\alpha h + \gamma^2 h) \times \right.$$
$$\times (g'' + 2\alpha g + \gamma^2 g)\, dt + 4\alpha\gamma^2 h(0) +$$
$$\left. + 4\alpha h'(0) g'(0)\right\}. \qquad (4.79)$$

For most telemetered processes we can consider $\beta = 0$. Then, considering (4.79), functional (4.78), omitting cumbersome calculations, can be represented as

$$f(u, m) = \exp\left\{-(4\sigma^2\alpha^3)^{-1}\left[3\alpha^2 l(u(t) - u(0)) + 2\alpha^3 l t u(t) + \alpha^4 l \int_0^{t_н} u(t)\,t\,dt + 2lu'(t)(2+\alpha t) + 2\alpha l u'(0) + \frac{2l^2}{\sigma} \times (2+\alpha t)^3 + \frac{5}{3}\alpha l^2\right]\right\}. \tag{4.80}$$

For small apertures ($\Delta x << \sigma$) we can assume for ZOP $u(t) = u(0) = x_1$. Then, considering (4.77)-(4.79) for FOP we produce the expression of the probability that process u(t) will be in the tolerance area D_ℓ ($\ell = x_2$):

$$P_{FOP}(t) \approx \int_{-\infty}^{\infty}\left\{\exp\left[-(4\sigma^2\alpha^3)^{-1}\right] \times \left[\alpha^3 l t x_1 (2 + t/2) + 2\alpha l x_2 + \frac{\alpha l^2}{6} \times (2+\alpha t)^3 + \frac{5\alpha l^2}{3} + \alpha l (2+\alpha t) y_2\right] \times \int_{x_1-\Delta x}^{x_1+\Delta x} W(t; x_1; x_2 0; y_1; y_2)\,dy_1\right\} dy_2, \tag{4.81}$$

where $y_2 = u'(t)$, $x_2 = u'(0)$.

Expression (4.81) can be reduced to a simpler form by direct integration:

$$P(t) \approx \exp\left[-B(t) + A^2(t)\frac{K_{11}}{2}\right] \times \left\{\exp\left[-A(t)y_2\right]\left[\Phi(x_1; \bar{y}; \Delta x) - \Phi(x_1; \bar{y}_1; -\Delta x)\right] - \gamma_1 \times \exp\left[-A(t)\bar{y}_{22}\right]\left[\Phi(x_1; \bar{y}_{21}; \Delta x) - \Phi(x_1; \bar{y}_{21}; -\Delta x)\right] - \gamma_2 \times \exp\left[-A(t)\bar{y}_{12}\right]\left[\Phi(x_1; \bar{y}_{11}; \Delta x) - \Phi(x_1; \bar{y}_{11}; -\Delta x)\right]\right\}, \tag{4.82}$$

using the symbols

$$A(t) = [4\sigma^2\alpha^3]^{-1}\alpha l(2+\alpha t),$$
$$B(t) = [4\sigma^2\alpha^3]^{-1}[\alpha^3 l t x_1(2+t/2)+$$
$$+\alpha l x_2 + \frac{\alpha l^2}{6}(2+\alpha t)^3 + \frac{5}{3}\alpha l,$$

$\Phi(z)$ is the probability integral.

Formula (4.82) is common: where $\ell = 0$, we produce $P(t) = P_{ZOP}$ and where $\ell \neq 0$, $P(t) = P_{FOP}(t)$.

The mean value of time between nonredundant readings is found the expression [3]

$$\bar{\theta} = \int_0^\infty P(t)\,dt. \qquad (4.83)$$

The results of the solution for ZOP and FOP are presented in Table 16 according to formulas (4.81) and (4.82). /237

Analysis of these results leads to the following conclusions:
-- the FOP method has higher effectiveness with small apertures;
-- the model of the "smooth" process yields much higher values than the model of the "undifferentiable" process.

Using the data produced on $\bar{\theta}$, we can calculate the reduction factor

$$K_{rd}K_{rd} = 1 + \bar{\theta}\frac{\tau_0}{\tau},$$

where τ_0 is the interval of correlation of the signal, τ is the interval of its discretization (Figure 135).

In addition to the generally accepted method of elimination of redundancy using polymonial predictors, another, decorrelator unit is suggested. Its primary purpose is elimination of correlated or interrelated readings from the group of sensors selected.

TABLE 16

x_1	x_2	ZOP			FOP		
		$\Delta x = 0{,}01$	$\Delta x = 0{,}05$	$\Delta x = 0{,}10$	$\Delta x = 0{,}01$	$\Delta x = 0{,}05$	$\Delta x = 0{,}10$
0	0	0,07	0,21	0,51	0,07	0,21	0,51
	0,01	0,06	0,16	0,52	0,05	0,13	0,47
	0,025	0,04	0,15	0,54	0,03	0,09	0,41
	0,5	0,02	0,12	0,42	0,01	0,05	0,30
1	0	0,06	0,17	0,50	0,06	0,17	0,50
	0,01	0,05	0,19	0,52	0,10	0,22	0,49
	0,025	0,04	0,21	0,52	0,09	0,19	0,45
	0,5	0,02	0,13	0,51	0,05	0,10	0,31
	—0,01	0,04	0,16	0,47	0,18	0,28	0,59
	—0,025	0,03	0,12	0,41	0,21	0,34	0,63
	—0,5	0,01	0,09	0,33	0,25	0,28	0,64
2	0	0,06	0,16	0,47	0,06	0,16	0,47
	0,01	0,07	0,17	0,48	0,09	0,25	0,45
	0,025	0,08	0,19	0,52	0,07	0,19	0,41
	0,5	0,10	0,16	0,53	0,05	0,15	0,36
	1	0,08	0,12	0,49	0,03	0,10	0,27
	—0,01	0,05	0,11	0,45	0,12	0,26	0,57
	—0,025	0,04	0,10	0,39	0,32	0,37	0,63
	—0,5	0,03	0,08	0,33	0,37	0,31	0,69
	—1	0,02	0,05	0,29	0,29	0,25	0,68
	$\bar{\theta}$	0,048	0,14	0,46	0,125	0,205	0,49

Grouping of sensors means combination of certain scientific measurements during their telemetry processing about one "priority" phenomenon, which is related to the remaining group of phenomena. For example, an increase in cosmic ray energy causes magnetic storms and polar auroras on Earth, while an increase in solar short-wave radiation causes changes of pressure, temperature and density in the Earth's atmosphere. /238
The interrelationship of magnetic or electric field energy with electron concentration is particularly clearly expressed.

Figure 136 shows the time diagrams of magnetic field intensity and electron concentration, measured near the surface of Venus by the Soviet Venera-3 spacecraft.

Figure 137 shows the approximate mutual correlation function (MCF) of two processes -- magnetic field intensity and electron concentration -- and the autocorrelation function (ACF) of the magnetic field. The diagrams show the characteristic peculiarities of these phenomena: exponential drop of the function and periodic component with frequency equal to β.

Both of these functions can be described by the same expression:

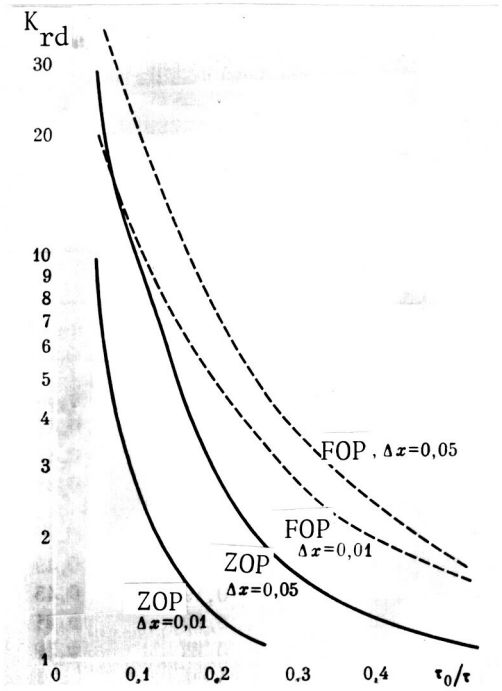

Figure 135. K_{rd} as a Function of Type of Predictor and τ/τ_0 Ratio

$$R(\tau) \approx e^{-\alpha\tau}\left(\cos\beta\tau + \frac{\alpha}{\beta}\sin\beta|\tau|\right).$$

The mutual correlation function of magnetic field intensity and electron concentration is equal to approximately 0.7.

Since most processes in space are related either to the magnetic field or to streams of charged particles, detailed statistical analysis of these phenomena is desirable.

These premises are correct as a foundation for the application of the method of decorrelation of a group signal, since we know that when interrelated signals are decorrelated, some of them become rather small, achieving an additional reduction in natural redundancy of the initial information by decreasing the number of signals in the group.

The algorithm for conversion of the time readings into decorrelated signals is as follows:

$$N\bar{x} = W\bar{x},$$

where $N\bar{x} = x_1, x_2, \ldots, x_n$ are the initial readings of the signal; $\bar{x} = x_1, x_2, \ldots, x_n$ are the decorrelated signals -- the Fourier, Walsh and other coefficients; W is the transformation matrix.

For the case of transformation by the Fourier method, we must multiply the initial readings (f_k) by the orthogonal functions $\cos\omega_{kt}$ or $\sin\omega_{kt}$ as add them. As a result of this operation, the Fourier coefficients ($A_0, A_., B_., \ldots, A_n$) are produced. In the case of a Fourier-Walsh method transform, similar operations are required, but they are somewhat different in their technical realization.

Let us explain the principle of a Fourier-Walsh transform. Suppose we are given a random function $\{f_k(t)\}$, discrete as to time /239

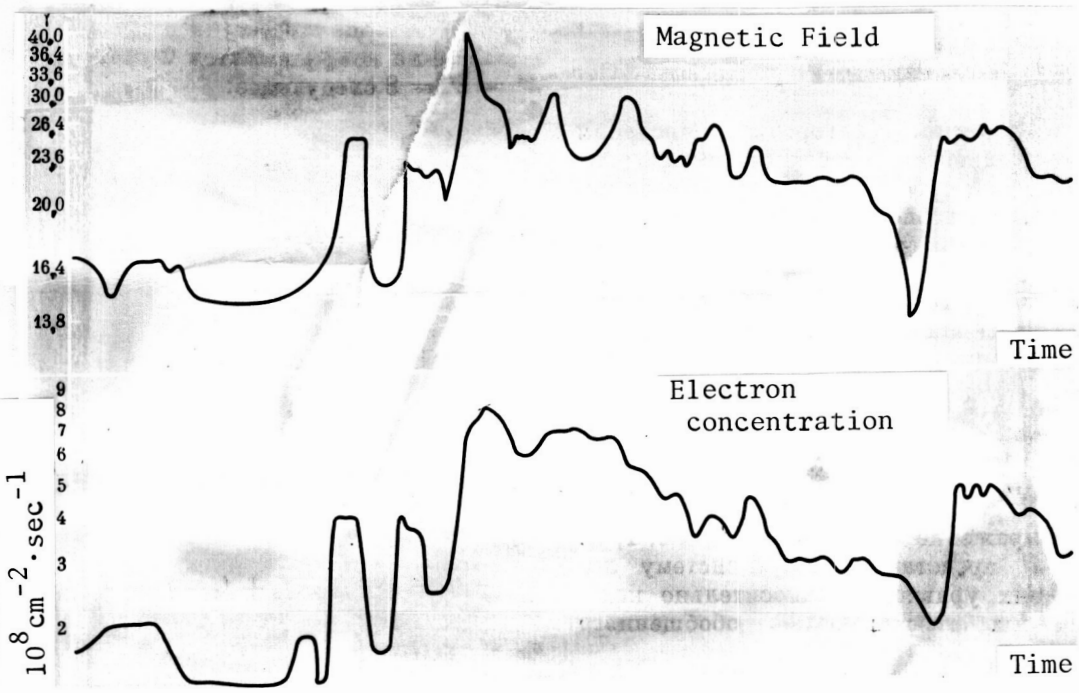

Figure 136. Time Diagrams of Magnetic Field Intensity and Electron Concentration

and level in interval (0, 1). The number of discrete time intervals is 2^n, where n is an integer; the number of discrete levels is equal to m. The number of possible discrete realizations of function $\{f_k(t)\}$ in interval (0, 1) is equal to m^{2n}.

Let us represent a specific realization of random function $\{f_k(t)\}$ $f_k(t)$ in interval (0, 1) as a generalized Fourier series with respect to the system of Walsh functions, orthonormalized in the same time interval:

$$f_k(t) = \sum_{i=0}^{N} a_{ki} W_i(t), \quad 0 \leqslant t \leqslant 1, \tag{4.84}$$

where a_{ki} is the ith Fourier coefficient of function $f_k(t)$, $W_i(t)$ is the ith Walsh function.

For the fixed set of functions $\{f_k(t)\}$ and known discretization interval for time $1/2^n$, number N in (4.84) is the number of Walsh functions in the generalized Fourier series, where $N = 2^n$ with numbering from i = 0 to $i = N' = 2^n - 1$. The number of possible sums (4.84) is equal to the number of possible discrete functions $\{f_k(t)\} = m^{2n}$, if we assume that each Walsh function can take on n possible values as to level.

The algorithm for calculation of the generalized Fourier coefficients generates a functional operation such as

$$a_{ki} = \int_0^1 f_k(t)\, W_i(t)\, dt. \tag{4.85}$$

In order to calculate the 2^n coefficients of the generalized Fourier series of function $f_k(t)$ according to formula (4.85), we must perform 2^n multiplication operations and 2^n integration operations.

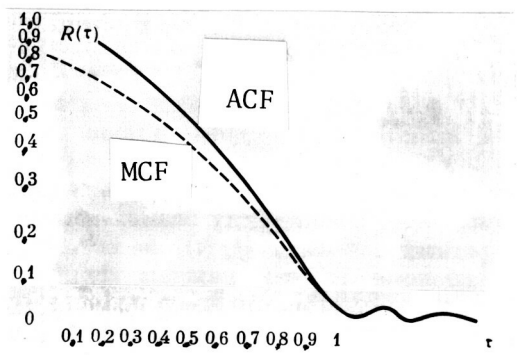

Figure 137. Autocorrelation Function of Magnetic Field and Mutual Correlation Function of Magnetic Field and Electron Concentration

Let us study the algorithm for calculation of the coefficients of the generalized Fourier series, realized without using the operation of multiplication. /240

Discrete function $f_k(t)$ is fed to the discrete adder, the output of which carries the following numbers at discrete moments in time Δt_ℓ (discretization interval):

$$\sum_{i=0}^{N} a_{ki} \sum_{l=0}^{N'} W_i(\Delta t) = \sum_{l=0}^{N'} f_k(\Delta t) = f_{N'}, \tag{4.86}$$

where N' = 0, 1, 2,..., N.

Expression (4.86) where N' = 0, 1,..., N is a system of linear equations relative to the unknown coefficients of the generalized Fourier series a_{ki} (i = 0, 1, 2,..., N) with known coefficients $\Sigma W_i(\Delta t)$ and right parts of the equations $\sum_{l=0}^{N'} f_k(\Delta t)$.

The system of linear equations (4.86) can be solved by means of a matrix of resistors. The block diagram for calculation of the generalized Fourier coefficients of function $\{f_k(t)\}$ by means of the orthonormalized system of Walsh functions is presented in Figure 138.

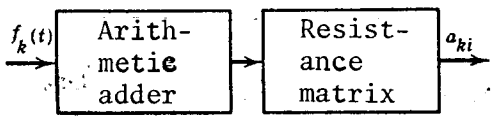

Figure 138. Block Diagram for Calculation of Generalzied Fourier Coefficients

Compression algorithms were analyzed by computer. The calculations utilized the Fourier transform. Using the transformation algorithm for $N\bar{x} = Y$ groups of random numbers x with normal distribution were discretely multiplied by the correlation matrices, the values of which were selected in the range from 0.1 to 0.95.

The values of Fourier coefficients for $2^n = 2^3 = 8$ are as follows:

$$a_{k_0} = \frac{1}{8}\sum_1^N f_k = \frac{1}{8} f_8,$$

$$a_{k_1} = \frac{1}{4}[f_4 - 0{,}5f_8],$$

$$a_{k_2} = \frac{1}{4}[f_2 - f_6 - 0{,}5f_8],$$

$$a_{k_3} = \frac{1}{4}[f_2 - f_4 - f_6 + 0{,}5f_8],$$

$$a_{k_4} = \frac{1}{4}[f_1 - f_3 - f_5 - f_7 + 0{,}5f_8],$$

$$a_{k_5} = \frac{1}{4}[f_1 - f_3 - f_4 - f_5 + f_7 - 0{,}5f_8],$$

$$a_{k_6} = \frac{1}{4}\left[f_1 - f_2 + f_3 + f_5 + f_6 - f_7 + \frac{3}{2} f_8\right],$$

$$a_{k_7} = \frac{1}{4}\left[f_1 - f_2 + f_3 - f_4 + f_5 - f_6 + f_7 - \frac{3}{2} f_8\right]. \quad (4.87)$$

The new numbers Y_k produced were transformed by algorithms (4.85) and (4.88) /241

$$A_m = \frac{2}{N}\sum_{k=1}^{N,2} Y_k \cos mk\frac{2\pi}{N},$$

$$B_m = \frac{2}{N}\sum_{k=1}^{N,2-1} Y_k \sin mk\frac{2\pi}{N}. \quad (4.88)$$

The Fourier coefficients were calculated using algorithms (4.85) and the Fourier-Walsh algorithm (4.88). The program for investigation of algorithms (4.83), (4.85) and (4.88) is presented in Figure 139.

The results of calculation of the reduction factors as functions of correlation coefficient between sensors in a group are presented in Table 17. The number of sensors in the group N = 8.

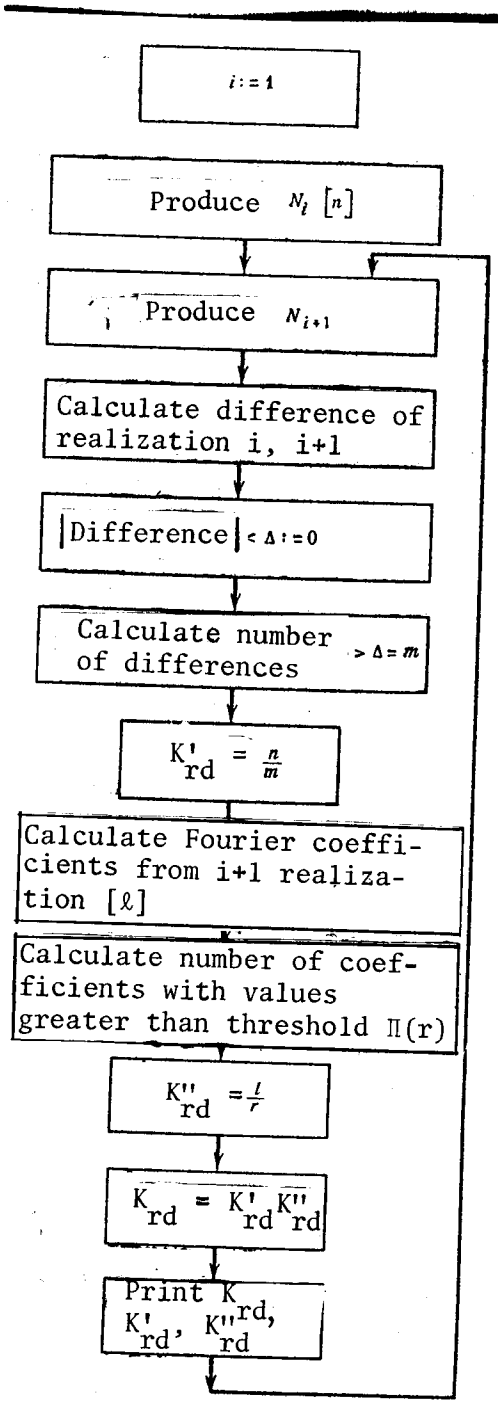

Figure 139. Flow Chart of Program for Calculation of K_{rd}

It was found that when a signal was processed by the decorrelation unit, the reduction factor, even with weak correlation, was equivalent in effectiveness to polynomial predictors. Similar data was produced for the Fourier-Walsh method.

Thus, when two units are used, a polynomial predictor and a decorrelator, the reduction factor depends on the correlation coefficient between the sources, the discretization interval and the permissible mean square error. Figure 140 shows a final diagram of the values of reduction factors when the method of ZOP and decorrelation is used with a mean square error of 1%.

Digital sensors in the data transmission system output a binary signal similar to a random telegraph signal, the information being contained in the moments of transition through zero. Consequently, the signal need by transmitted only at moments in time when the polarity of the bindary signal changes. These moments in time can be determined by the primary reduction unit with the ZOP algorithm, i.e., by transition to trinary code. This recoding of the signal can also be performed more simply: after each binary sensor a differentiating circuit and shaper are installed. This achieves a savings of memory capacity in the main unit. /242

TABLE 17

Correlation Coefficient	0,1	0,3	0,4	0,5	0,6	0,7	0,8	0,9	0,95
	Reduction factor K_{rd}								
$\Delta x = 0,01$	1,11	1,15	1,2	1,27	1,37	1,5	1,65	1,9	2,3
$\Delta x = 0,05$	1,17	1,22	1,35	1,52	1,61	1,8	2,15	3,1	4,0

If we are not concerned with interference stability, the signal can be recoded again into binary code using a λ_Δ transform [10], but transmission of the trinary signal allows an additional check of the transmitted polarity, preventing accumulation of errors upon δ modulation.

To determine the effectiveness of recoding of digital sensor signals, we must calculate the reduction factor and, therefore, determine the statistical characteristics of the time intervals between changes in polarity. This can be done by methods of queueing theory [4, 5].

As a mathematical model of the signal, in the first approximation we can select a Poisson stream, characterized by instantaneous density λ(t) [5, 9]. The rule of distribution of time between two neighboring changes in polarity (points) is defined by the expression [4]

$$\omega_{t_0}(t) = \lambda(t_0 + t)\exp\left[\int_{t_0}^{t_0+t} \lambda(t)\, dt\right], \quad t > 0, \tag{4.89}$$

where t_0 is the beginning of the time reading, corresponding to the first of two neighboring changes in sign.

Let us study stable and unstable Poisson streams of points, if the points can appear only at discrete moment in time $t = t_k = kT$, whre $k = 0, 1, 2...$ This model of the signal is similar to a random telegraph signal with transmission of information by even code [16]. For it, the function

$$\Lambda(t_0, t) = \int_{t_0}^{t} \lambda(z)\, dz \tag{4.90}$$

is discontinuous. This stream is called singular [4].

For the first case, we can assume that $\lambda(t) = \lambda_0 = \text{const}$. In this case, we ignore the discrete nature of the time intervals between changes in polarity in certain digital signals with sufficiently low values of discretization, i.e., the time of transitions through 0 is considered continuous. We can then use the exponential distribution of time intervals between the derivatives of two neighboring changes in polarity:

(4.91)

where λ is a parameter characterizing the number of transitions through 0 per unit time.

The interrogation interval Δt is selected from the condition that the probability of transition through 0 in time $t < \Delta t$ is less than $P = 10^{-3}$-10^{-6}. From this, it is easy to see that /243

$$\Delta t = -\ln(\lambda - P)/\lambda. \tag{4.92}$$

The mean value of Δt_A and its dispersion of distribution are [26]

$$\overline{\Delta t_A} = \frac{1}{\lambda}, \quad \sigma^2 = \frac{1}{\lambda^2}. \tag{4.93}$$

Then the reduction factor, ignoring address information,

$$K_{rd} = \frac{\overline{\Delta t_A}}{\Delta t} = -\frac{1}{\ln(1-P)}. \tag{4.94}$$

Consideration of the additional number of bits used in the address is similar to the case of reduction of continuous information. Here, however, we are transmitting not the amplitude value but only the address. We then have

$$K_{rd} = -\frac{1}{\log_2 A \ln(1-P)}. \tag{4.95}$$

We can expect that with the number of sensors N = 50 and probability $P = 10^{-3}$-10^{-6}, the value of the reduction factor $K_{rd} = 10^2$-10^5. Such high values of K_{rd} result from the assumption

of continuity of the time through which the stream of random changes in sign flows.

In the second case, calculation of K_{rd} is based on the assumption that the stream of points is r[illegible] 0, r, while probability P_3 of a change in sign at moments [illegible] $t > k/T$ does not change. Then, under the condition that the [illegible] $W(t) = \lambda e^{-\lambda t}$, no change in sign at time $(k - 1)T_0$, the probabilit[illegible] sign change at moments kT_0 is:

$$P(t) \triangleq P(kT_0) = P_3^k. \tag{4.96}$$

from this, we can easily calculate the mean time interval between neighboring points

$$\overline{\Delta t} = kT_0 = \sum_{k=1}^{\infty} kP_3^k = 2T_0, \quad P_3 = 0{,}5. \tag{4.97}$$

Obviously, considering the transmission of the address, there will be no time compression. However, we can assume that consideration of the aftereffect and instability of the probability of a change in sign $P_3 = P_3(t)$ will yield a value of $K_{rd} > 1$. The data presented allow us, in the first approximation, to give a positive answer to the question of the need to use reduction algorithms for digital sensor signals.

One interesting peculiarity appears in a communications system when a data reduction device is used in it. As we know, the energetic effectiveness of a communications system depends on a number of factors. These factors include the information transmission rate (R), overall gain of the communications system (B), bandwidth of the receiver before the detector (W_{hf}) and necessary ratio of probabilities P_c/P_n following the low-frequency filter (W_{lf}).

The formula for calculation of the effectiveness of a communications system is written as [27] /244

$$\beta = \frac{RB}{W_{hf}(P_c/P_n)W_{lf}}. \tag{4.98}$$

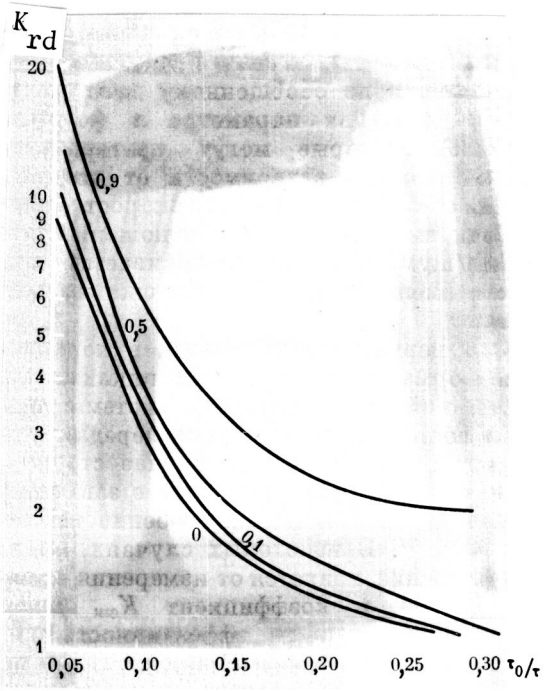

Figure 140. Final Diagram of K_{rd} for Various Values of Correlation Coefficient

In this formula, the values of B and W_{1f} should not change whether a reduction system is used or not. This affirmation is based on the fact that if two systems are compared, one with elimination of redundancy, the other without, both of these systems must be placed under identical conditions as to transmission rate in bits per second, bandwidth and overall gain. Two parameters remain in formula (4.98) which can be changed as a function of the structure of the communications system: the information transmission rate R and the signal/noise ratio, which increase as the entropy of the reduced data increases.

In the first case, when no changes are made during transmission of information, the effectiveness of the communications system is constant throughout the entire time of transmission of information. In the second case, the structure of the signal will change as a function of the statistical peculiarities of the messages. In some cases, when the message changes from measurement to measurement and factor K_{rd} is approximately equal to 1, the effectiveness of communications may be determined completely by formula (4.98).

In most cases, redundancy is always present in the messages. When a reduction system is used, it is as if all information were transmitted, no matter what its type, and therefore the information transmission rate, whereas it formally remains as before, actually increases in proportion to K_{rd}. This statement is based primarily on the fact that no matter how the information is reduced, when it is received and processed it must be restored to its real time scale and the gaps representing rejected channels must be refilled with prior transmitted information.

Let us introduce the term conditional effectiveness of the communications system, which shows the number of times by which the effectiveness of the communications system is increased when we consider the statistical properties of the messages restored upon reception at the transmission rate. Formula (4.98), in its new form, will be

$$\beta' = \frac{RK_{rd}B}{W_{hf}(P_c/P_n)'W_{1f}}. \qquad (4.99)$$

At first glance, it might seem that if the reduction factor is high enough, the effectiveness might reach its limiting value, but in practice it is usually found that K_{rd} is somewhere between 10 and 15 [19]. Thus, the system of redundancy reduction improves the power effectiveness, but cannot completely solve the problem.

The solution of the problem of β effectiveness lies in combined improvement of the information effectiveness and interference stability of codes. However, the redundancy of information cannot be decreased without limit, since the accuracy characteristics of the initial message may be lost upon its restoration. There are certain requirements during reception of information for error probability P_{er} per bit, and for the ratio of the information transmission rate R to the maximum message frequency (α) [17]. Thus, when the mean square error criterion ε^2 is used, rigid requirements are placed on P_{er} and R/α, expressed by the formula [17] for a one-dimensional Markov model of the message

$$\varepsilon^2 = \alpha_L P_{er} \frac{1 - e^{(2\alpha/R)\log_2 L}}{2\log_2 L} R/\alpha, \qquad (4.100)$$

where $R = 2\alpha_{max} \log_2 LN$, α_{max} is the maximum frequency of the message taken from the sensor; L is the number of levels of readings; N is the number of sensors.

Calculation using formula (4.100) shows that the minimum mean square error is reached with a ratio $R/\alpha = 100$. Considering this formula, the optimum reduction factor can be expressed as: /245

$$K_{rd} = \frac{R}{100\alpha(t)}, \qquad (4.101)$$

where $\alpha(t)$ is the random value of message frequency, following the Rayleigh distribution rule

$$W(\alpha) = \frac{\alpha}{\sigma_\alpha^2} e^{-\frac{\alpha^2}{2\sigma_\alpha}}, \qquad (4.102)$$

where σ_α^2 is the dispersion.

As an example, let us study a telemetry device with the following data: L = 16, N = 16, α_{max} = 100 Hz, $P_{er} = 10^{-3}$, α_L = 7 (coefficient dependent on type of code selected), number of discrete values $\alpha(t)$ = 30. Using (4.101) with the minimum value $\alpha(t)$ = 3 Hz, K_{rd} = 40, with the maximum value $\alpha(t)$ = 100 Hz, K_{rd} = 1.3. The mean square decoding error is 3% in this case. Thus, in the reduction system we must not only consider the information content of the message, but also the capability for error-free restoration of information. In the USA, reduction systems were used in testing the Polaris and Agena rockets.

With an error tolerance (aperture) of about 2 and 1%, the application of a ZOP yielded reduction factors K_{rd} of 30 and 12 respectively, the use of a 0 order interpolator yielded factors of 40 and 22, while a first order interpolator yielded factors of 80 and 36. Processing of television information from the Tyros satellite by means of a first order interpolator with a tolerance of 3% yielded K_{rd} = 10 [18].

14.6. Radio Link Parameters

The main task of an APS is transmission of information on the physical and chemical phenomena occurring on the planets.

Let us study problems related to the passage of the signal from an automatic station to Earth. The basic parameter in the signal/noise ratio, since it determines the accuracy of the information received.

The coupling equation, in the case of active transmission, is written as follows [27]

$$P_t = S_b k(T_0 + T_{ex}) W \frac{16R^2 r_1 r_2 N_1}{G_1 D_2^2 \eta}. \tag{4.103}$$

where P_t is the required radiated power of the on-board transmitter; S_b is the signal/noise ratio at the input of the detector; k is Boltzmann's constant; T_0 is the equivalent temperature of internal noise in the receiver; T_{ex} is the equivalent temperature of external noise; W is the transmission bandwidth of the receiver before the detector; R is the distance from the receiving point to the APS; r_1, r_2 are the radio wave absorption factors in the

atomsphere of the Earth and in the atmosphere of the planet, respectively; N_1 is the reserve factor, considering the polarization losses, losses in the antenna-feeder system, losses due to unevenness of the radiation pattern and losses due to inaccuracy of aiming of the Earth antenna toward the APS; G_1 is the gain of the APS antenna; D_2 is the diameter of the Earth antenna; η is the antenna area utilization factor.

Let us study formula (4.103).

One of the limiting factors in radio communications is the noise in the radio receiving device -- the equipment noise T_0 and external noises T_{ex}. The total noise temperature is

$$T_\Sigma = T_0 + T_{ex}.$$

At today's level of development of radio physics, T_0 can be decreased to a few degrees. T_{ex} is a quantity several tens or hundreds of times greater than T_0.

Sources of external noise include galactic noise and the noise of the planet from which the message is transmitted. The effective noise temperature in the antenna, resulting from galactic noise, when the receiving antenna is directed toward the center of the galaxy is [27] $T_{agal} \approx \lambda^{2.4}469$ K, where λ is the wavelength, m. /246

The effective noise temperature in the antena resulting from planetary noise (the temperature of the surface of the planet $T = T_{pl}$) is [3]

$$T_{apl} = \left(\frac{Q_1}{Q_2}\right)^2 T_{pl}, \quad Q_1 \leq Q_2. \tag{4.104}$$

where Q_1 is the angular size of the planet as observed from the Earth, equal to the ratio of the diameter of the planet D_1 to the range R; $Q_2 = \lambda/D_2$ is the width of the reception pattern of the receiving antenna.

Considering what we have said, equation (4.103) can be written as

$$P_t = S_b k \left[T_0 + \lambda^{2.4}469 + \frac{Q_1^2 D_2^2}{\lambda^2} T_{pl}\right] \times \times W \frac{16R^2}{G_1 D_2^2 \eta}. \tag{4.105}$$

A no less serious factor limiting communications is the available antenna system. The expediency of using narrowly directed or omnidirectional antennas in communicatins systems with APS depends on the method of delivery of the station to the surface of the planet, as well as the orientation of the antennas toward Earth.

If the APS is to be shot out of a landing capsule to one side and no antenna aiming system is provided in the capsule, the antenna must be omnidirectional. If the APS carries an astronaut, he can aim his antenna toward Earth using sensors, and in this case the antenna can be directional. The antenna can also be directional if the APS is shot off to one side but the station includes an antenna aiming system. The following two cases can be studied for directional antennas [3].

1. Strong signal

$$S_m \frac{2W_m}{W} > 1, \tag{4.106}$$

where S_m is the signal/noise ratio after the low-frequency filter; W_m is the passband of the low frequency filter; W is the passband of the receiver at the radio frequency.

With limited radiated power of the on-board transmitter, relationship (4.106) is realized for the case of almost complete compensation of the frequency shift due to the Doppler effect and various instabilities. Due to the low effectiveness of APS antennas, there is good reason to consider transmission of information (PCM) at low rates.

If we know the operating frequency of the radio link f_0, we can find the required accuracy of compensation for frequency shift $\nu_{unst} + \nu_d$. Under condition (4.106), the signal/noise ratio at the input of the detector will be determined by the expression

$$S_0 \simeq S_m \frac{2W_m}{W}, \tag{4.107}$$

and the coupling equation is written as

$$P_t = 2S_m W_m \left[T_0 + \lambda^{2,4} 469 \frac{Q_1^2 D_2^2}{\lambda^2} T_{pl}\right] \times \times \frac{16R^2}{D_2^2 \eta}. \tag{4.108}$$

Differentiating P_t with respect to λ, we produce the equation for determination of the optimal wavelength

$$4.4(\log \lambda_{opt}) = \log \left(\frac{Q_1^2 D_2^2 T_{pl}}{565}\right). \quad (4.109)$$

In (4.109), the antenna diameter D_2 is a quantity which can be increased in order to decrease the energy expenditures of the radio link. However, the antenna diameter cannot be increased without limit, since this decreases the efficiency of the antenna and increases the level of the side lobes. The critical wavelength for a given diameter D_2 is determined by the condition

$$\lambda_2^* = 16\sigma D_2, \quad (4.110)$$

where $\sigma = \lambda/16D_2$ is the relative accuracy of manufacture of the the surface of the antenna. /247

2. Weak signal

$$S_m = \frac{2W_m}{W} << 1. \quad (4.111)$$

This case is most frequently encountered in space communications practice. With a low signal/noise ratio, it is expedient to use a square-law detector, and

$$S_b \approx 1{,}27\sqrt{\frac{4}{3}S_m\frac{W}{\Delta t = -\ln(\lambda - P)/\lambda}}. \quad (4.112)$$

The coupling equation becomes

$$P_t = 1{,}27\sqrt{\frac{4}{3}S_m W_m W} \times \times k\left[T_0 + \lambda^{2,4}469 + \frac{Q_1^2 D_2^2 T_{pl}}{\lambda}\right]\frac{16R^2}{D_2^2\eta}, \quad (4.113)$$

where $W = 3f_0\ (\nu_{unst} + \nu_d)$.

With a fixed diameter of the Earth antenna D_2, the optimal operating wavelength from the standpoint of power consumption is found from the condition of the minimum of (4.113):

$$\lambda_{opt}^{2.4} 1780 = T_0 + \frac{5Q_1^2 D_2^2 T_{p1}}{\lambda_2}, \tag{4.114}$$

The maximum gain of the transmitting directional APS antenna is limited by the angle of view of the Earth's surface from the planet. In the case of operations from the moon, the width of the main lobe of the antenna radiation pattern $Q_2 = 2\alpha + \gamma \approx 12°$ (where α is the angle of view of the moon, γ is the libration angle). The width of the pattern for operation from the planets may be still less:

$$\alpha = \arcsin \frac{R_0}{R_0 + h} = 1\text{-}3°,$$

where R_0 is the radius of the Earth; h is the range.

Considering the radiation pattern, the gain of the antenna

$$G_1 = \frac{\pi^2 D_1^2 h}{\lambda^2} = \frac{1}{1 - \cos \frac{Q}{2}}. \tag{4.115}$$

Substituting the value of G_1 into the coupling equation, we produce

$$P_t = S_0 k \left[T_0 + \lambda^{2,4} 469 + \frac{Q_1^2 D_2^2 T_{p1}}{\lambda^2} \right] \times \times W \frac{16 R^2 \lambda^2}{\pi^2 D_1^2 D_2^2 \eta^2}. \tag{4.116}$$

The optimal wavelength λ from the standpoint of power consumption is $\lambda_{opt} = \lambda_2^*$, where $\lambda_2^* = 16\sigma D_2$.

The passband of the receiver before the detector is also one of the most important factors in radio communications. The passband is selected considering the signal spectrum, frequency instability and Doppler frequency shift.

Let us study the influence of the Doppler effect in the case when the APS is on the surface of the planet:

$$\Delta f_d \simeq v_1 \frac{f_0}{c}, \qquad (4.117)$$

where v_1 is the velocity of motion of the planet relative to the Earth; f_0 is the carrier frequency; c is the speed of light.

Considering the angular velocities of the planet and Earth and the difference between the corresponding points

$$\Delta f_{max} = \frac{f_0}{c}[\Omega R_i + R_{oi}\omega_i + R_0\omega_3], \qquad (4.118)$$

where $\Omega = \omega_1 - \omega_2$ is the difference between the angular velocities of the planet and Earth; R_i is the radius of the Earth's orbit; R_{0i} is the radius of the planet; R_0 is the radius of the Earth; ω_1 is the angular velocity of rotation of the planet; ω_3 is the angular velocity of the Earth.

A frequency shift also results from the instability of the carrier frequency source in the transmitter. When an LC oscillator is used, $\nu_{unst} \simeq 10^{-3}$, while when the oscillations are stabilized by a quartz crystal $\nu_{unst} = 10^{-7}$-10^{-5}, the value of 10^{-5} being produced without thermostatic crystal oscillator, the value of 10^{-7} being produced by thermostating the oscillator. In spacecraft located on remote planets, due to the low signal/noise ratio, it is desirable to have a narrower band W, requiring highly stable oscillators with $\nu_{unst} = 10^{-7}$. If APS utilize transmitter frequencies in the range from 100 MHz to 10 GHz, their attenuation in the atmopsheres of Earth and the planets can be ignored. /248

Table 18 presents results of calculation of the parameters of a radio link, based on the following data:

-- information transmission rate 40 bits/sec in ordinary telemetry;

-- probability of error per word with $k_1 = 6$ equal to $1.5 \cdot 10^{-3}$;

-- information transmission rate with deterministic code 80 bits/sec (considering memory device on board APS and data reduction system);

-- Earth antenna diameter 25 m;

-- T_{n0} of receiving apparatus 50 K;

-- instability of transmitter carrier oscillator 10^{-7};

-- phase modulation, $\phi = 120°$.

The table leads to the following conclusions:

1) when a narrow band telemetry signal is transmitted from the surface of the moon, an isotropic omnidirectional antenna can be used; for transmission from the planets, a directional antenna should be used;

2) the use of a deterministic code and its decoding not only increases the effectiveness of the communications system, but also helps to decrease the APS transmitter power.

TABLE 18

Parameter	Moon		Mars		Venus	
	Deterministic code	PCM	Deterministic code	PCM	Deterministic code	PCM
	Omnidirectional antenna					
λ_{opt}, m	0,23	0,23	0,56	0,56	0,16	0,16
W_{hf}, Hz	$2 \cdot 10^3$	$2 \cdot 10^3$	$1,2 \cdot 10^4$	$1,2 \cdot 10^4$	$3,2 \cdot 10^4$	$2 \cdot 10^4$
T_0, K	50	50	50	50	50	50
T_{ex}, K	200	200	1	1	1	1
T_Σ, K	250	250	51	51	51	51
P_t, Hz	0,2	0,6	104	3104	$1,5 \cdot 10^3$	$4,5 \cdot 10^3$
S_m	4	12,2	4	12,2	4	12,2
W_m, w	60	60	60	60	60	60
S_b	0,16	0,366	0,16	0,366	0,16	0,366
G_1	1	1	1	1	1	1
	Directional antenna					
λ_{opt}, m	0,23	0,23	0,06	0,06	0,08	0,08
W_{hf}, Hz	$1,2 \cdot 10^3$	$1,2 \cdot 10^3$	$1,2 \cdot 10^4$	$1,2 \cdot 10^4$	$3,2 \cdot 10^4$	$3,2 \cdot 10^4$
T_0, K	50	50	50	50	50	50
T_{ex}, K	200	200	1	1	1	1
T_Σ, K	250	250	51	51	51	51
P_t, w	0,017	0,051	0,36	1,44	0,1	0,3
S_m	4	12,2	4	12,2	4	12,2
W_m, Hz	60	60	60	60	60	60
S_b	0,16	0,36	0,16	0,36	0,16	0,36
G_1	23	23	$5,5 \cdot 10^3$	$5,5 \cdot 10^3$	$3 \cdot 10^3$	$3 \cdot 10^3$

CHAPTER 15

PECULIARITIES OF THE APPARATUS OF AUTOMATIC PLANETARY STATIONS

In order to allow transmission of information only during periods of radio visibility of the planet, the equipment of an APS must include a device fixing the time intervals for operation and for pauses. This device might be either an automatic device with a fixed program of operation, or a command device controlled from Earth. The use of either type is dictated by the power characteristics of the APS. /249

The duration of a communication session depends on the quantity of information accumulated, the transmission rate, the power of the radio transmitter, the power capacity of the APS and the operating life of the station. To allow more complete study of the physical and chemical characteristics of the planet, it is desirable that the station spend a long time on the planet; in this case, the signals transmitted must carry the maximum possible information.

Let us recall some measures which help to minimize the volume and rate of transmission and the power of a radio transmitter. These include the use of a redundancy-reduction system, a deterministic code and sharply directional antennas. The service functions of collection and transmission of information are performed by various APS devices: the transmitter, time programming device or, and receiver, telemetry device with redundancy-reduction system, antenna orientation system, recoding device and certain other supplementary devices. Figure 141 shows a block diagram of the information collection and transmission system. Let us study the interaction of the devices shown.

When the APS arrives on the surface of the planet, an automatic device should operate, starting the time-programming device; after a certain time, it sends out the command to open the antennas and turn on the telemetry. After the first interrogation of sensors, the redundancy-reduction system (in the constant storage unit) collects the first measurements, which are also immediately transmitted to buffer memory. During the second interrogation of sensors, the excess information is eliminated, and the nonredundant information is sent to the buffer memory. This continues until it is filled. When a certain period of time has passed, the command receiver or programmed timer outputs the instruction to transmit the information to the receiver. At this point, the telemetry device stops operating. Before the radio transmitter is turned on, the orientation system checks to see that the antenna is aimed

properly toward Earth. The telemetry information from buffer memory is then sent to the input of the modulator of the radio transmitter through a coding device. After all information stored in buffer memory has been transmitted, the apparatus returns to its initial state.

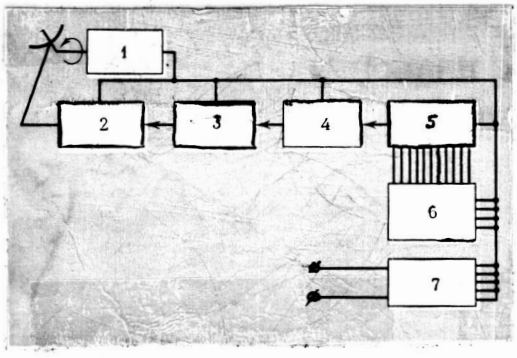

Figure 141. Block Diagram of Information Collection and Transmission System: 1, antenna orientation system; 2, transmitter; 3, recoding device; 4, redundancy-reduction system; 5, telemetry device; 6, sensors and scientific apparatus; 7, programmed timer.

Let us study some of the devices in the information collection and transmission apparatus of an APS. /250

Radio transmitter. The radio transmitter is one of the most important instruments of any spacecraft. Regardless of the functions which it performs, the transmitter must satisfy one main requirement -- have maximum efficiency, thus minimizing its power consumption. The power actually radiated by the transmitting antenna is always less than the power at the output of the transmitter (due to the efficiency of the antenna and losses in the feeder). Electron tubes produce higher power at many frequencies than semiconductor devices, but semiconductors are more frequently used due to their low weight, low power consumption and high reliability.

Semiconductor transmitters use transistor amplifiers and multipliers, as well as veractor frequency multipliers, particularly in those cases when the spacecraft must carry a stable-frequency superhigh frequency medium-power oscillator. Multipliers which use gallium arsenide diodes can generate power in the range of tens of watts with a conversion efficiency of 80% in the meter and decimeter wave range and hundreds of milliwatts in the centimeter wave band [28].

Veractors can be connected in parallel to achieve greater output power. When veractor multiplier circuits are excited by a transistorized crystal oscillator, a power level of a few watts can be achieved. A transistorized self-oscillator must operate at a frequency assuring high efficiency. The greatest efficiency and highest output power can be achieved by placing transistor amplifiers between multiplier stages.

In the last chapter we noted the frequencies of APS radio transmitters at the boundary between the decimeter and centimeter

wave bands. The principle of design of radio transmitters described above is quite suitable for APS transmitters. Considering the use of a deterministic code and the radiation frequencies noted, the output power will amount to some tenths of a watt, allowing semiconductor elements to be used.

Let us study one more feature of the radio transmitter -- its heat output. It is not desirable to use forced liquid or air cooling of transmitters on APS. Proper arrangement of energy dissipating elements can assure the maximum liberation and radiation of heat. Therefore, proper placement of transmitter parts near panels with large surface areas to dissipate the heat and the use of copper buses for connections with neighboring structural elements create paths for heat liberation and heat radiation and decrease the thermal resistance between heat sources and sinks. /251
The cooling of elements which radiate energy under space conditions can be achieved only by thermal conductivity to a heat absorber (radiator), which radiates the heat into space.

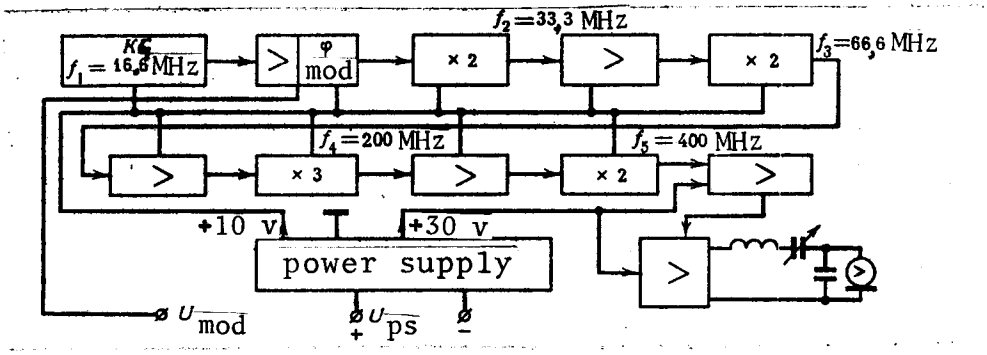

Figure 142. Block Diagram of Transmitter with R_{out} ≥ 4 w at f_5 = 400 MHz, efficiency ≈ 20-30%.

The problem of miniaturization of transmitters can be solved by the use of SHF modules. Each SHF stage is looked upon as a single element consisting of a transistor or veractor with built-in resonators.

Thus, combined solution of the problem of reduction of weight, increasing efficiency and improvement of heat transfer will help to improve the usage properties of the radio transmitter (Figure 142).

The telemetry device and redundancy-reduction system. This device usually consists of three parts: the channel switch, analog-digital converter and telemetry control unit. The interaction and operation of each unit have been described in detail in [29, 30]. Figure 143 shows a block diagram of such a device. We shall

study only the portion of the device which is basically new -- the redundancy-reduction system. It is considered in combination with the scientific instruments and switching unit.

The basic idea of the design of a telemetry system in which systematization and analysis of the indications of the sensors are used to minimize the redundancy of the information transmitted is as follows [31, 32]. The sensors, the indications of which reflect the various physical processes, are divided into subsets -- groups of sensors similar in nature of change of the physical quantities measured with time. Within each group, a priority sensor is selected if possible, the indications of which, due to their correlation with the indications of the sensors in the group, determine the value of the information of the entire group. The sensors whose indications are, due to the physical nature of the quantities measured, not correlated, and digital sensors (interrogation) is performed at a constant rate.

The procedure for reduction of the redundancy of the indications of the sensors consists of several stages. During the first stage, the indications of the priority sensors are analyzed and those groups of sensors in which no significant change has occurred in the indications of the priority sensor for various time intervals are eliminated from the data stream.

The redundance of noncorrelated sensors is reduced similarly. In this case, the indications of each noncorrelated sensor are studied separately and a decision is made concerning the value of /252
the information. The redundance of the indications of digital sensors is reduced by application of difference methods. During the second stage, the group of indications of similar correlated sensors is studied by means of a discrete Fourier transform for linear independence, after which linearly dependent readings are eliminated from the data stream.

The even sequence of readings of the indications of the sensors making up the telemetry information for a time interval equal to the time required to interrogate all sensors is converted by the redundancy-reduction procedure to an uneven sequence of readings.

The uneven sequence of readings of the indications of the sensors has a real time scale fixed by the duration and known sequence of the readings of the sensors, allowing addresses to be assigned to the nonredundant readings of the sensors.

The nonredundant readings are addressed by means of an address generator, which assigns a code mark to the signal from each sensor, utilizing the idea of code division of signals. The beginning and end of an uneven sequence of readings (or the time of

a single interrogation of all sensors of the system) are fixed by two synchronization signals. All of these addressing operations are performed in real time.

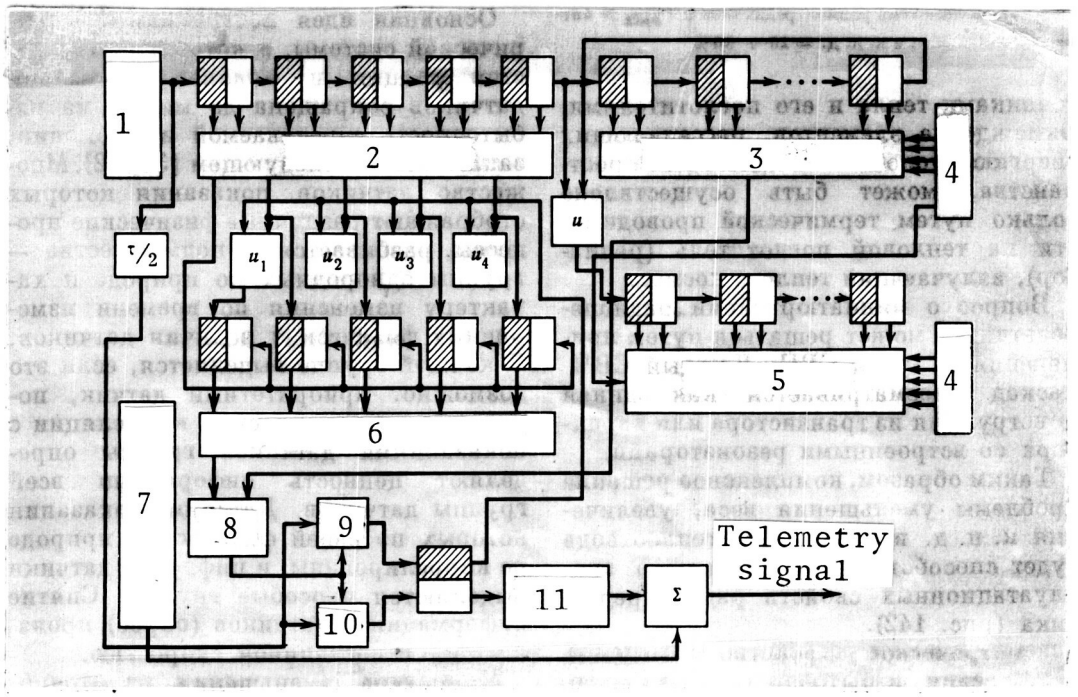

Figure 143. Block Diagram of Telemetry Device with Parity Checking System: 1, cycle pulse generator; 2, diode matrix; 3, main commutator; 4, sensors; 5, subcommutator; 6, resistance matrix; 7, m-sequence generator; 8, null organ; 9, NOT; 10, AND; 11, parity check.

Time compression of the telemetry information is performed in the memory unit, utilizing the time formerly occupied by the redundant readings eliminated from the data stream. Figures 144 and 145 show a functional diagram of the reduction in redundancy of telemetry information. /253

Let us study the construction of a telemetry system designed to process scientific information. We assume that the system has N sensors with analog and digital output voltages. The nature and characteristic peculiarities of the physical processes measured, as indicated by the sensors, are known, as are the maximum possible dynamic range and the maximum spectral width of the signals of the sensors.

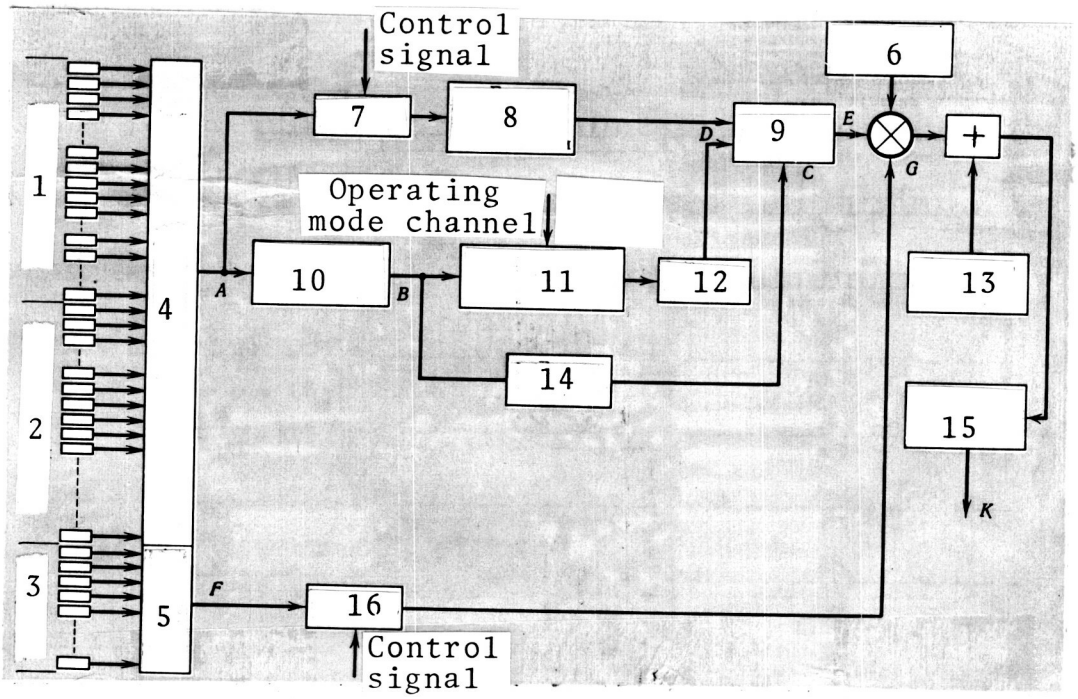

Figure 144. Functional Diagram of Telemetry Information Redundancy-Reduction System: 1, correlated sensors; 2, noncorrelated sensors; 3, digital sensors; 4, commutator; 5, recoding device; 6, system address generator; 7, switch no. 1; 8, group redundancy-reduction unit; 9, main switch; 10, analog-digital converter; 11, main redundancy-reduction unit; 12, delay unit; 13, synch signal generator; 14, delay unit; 15, memory unit; 16, switch no. 2.

The time of interrogation of all sensors (length of one frame) for this system is fixed and equal to NT, where $T \geq 1/2F_{max}N$ is the time interval between neighboring readings of the indications of the various sensors in a frame. The processing of information in the telemetry system in question is explained by the functional diagram (see Figure 144) and the diagram of the signal at various points in the functional diagram presented in Figure 145.

An arbitrary realization of the indications of the analog sensors of the system at the output of the commutator for a length of time equal to three frames is shown in Figure 145. The neighboring frames are shifted in time by ΔT of the synchronization signal, the duration of the synchronizing words which will later be necessary to assign the address to each frame, which arbitrarily shown in Figure 145 A by the vertical dividing lines between frames.

The structure of each frame is as follows. Time interval ΔT_{corr} at the beginning of each frame is occupied by readings of the correlated groups of sensors, time interval ΔT_{ncorr} -- by the readings of noncorrelated sensors, time interval ΔT_{dig} -- by the indications of the digital sensors. /254

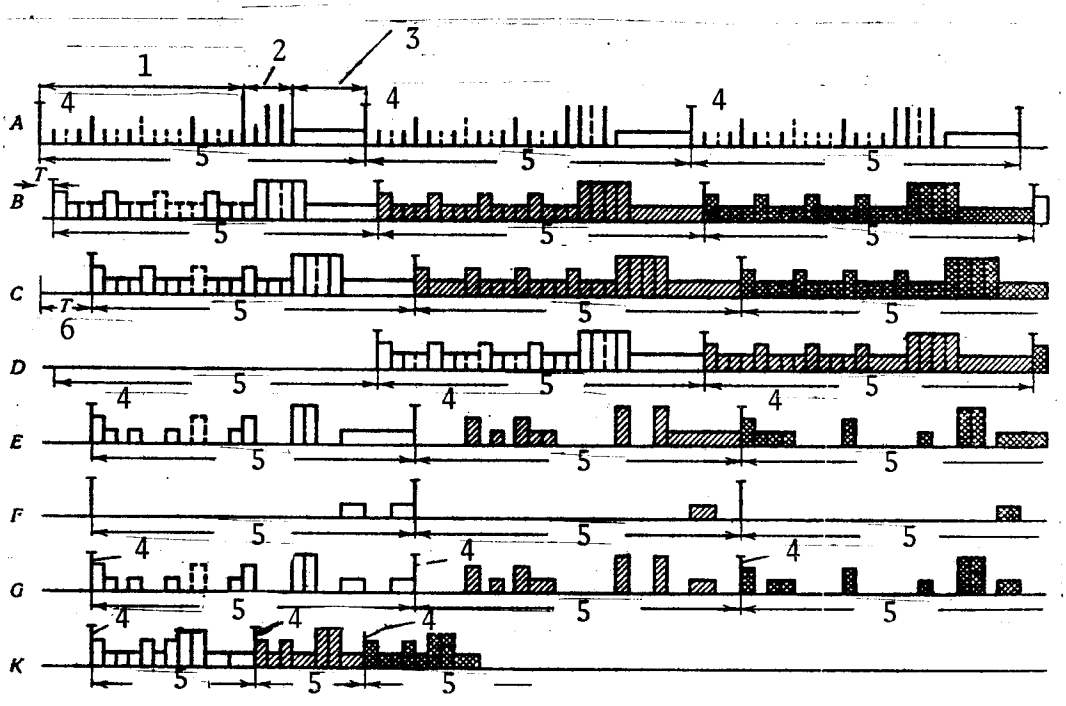

Figure 145. Time Diagrams of Telemetry Information Redundancy-Reduction System: 1, correlated sensors; 2, noncorrelated sensors; 3, digital sensor interrogation time; 4, synchronization signal; 5, frame; 6, group.

The signal from the output of the commutator goes to the input of an analog-digital converter and through switch no. 1 to the input of the group redundancy-reduction unit. The signal at the output of the analog-digital converter is shown in coded form in Figure 145 B. This converter delays the information as it operates by time T -- the time interval between neighboring readings of sensors in a frame. The digital signal from the output of the analog-digital converter is sent to the main redundancy-reduction unit and through a delay unit to the main switch at point C (see Figure 144). The signal at point C is shown in Figure 145 C.

The group redundancy-reduction unit, the output of which receives only the indications of correlated sensors through switch

no. 1, uses a discrete Fourier transform to analyze the indications of the sensors to determine linearly dependent (redundant) readings [1, 2]. When there are redundant readings in the group, this unit outputs a "block" instruction, which goes to the main switch, causing code combinations corresponding to redundant readings of the group of sensors to be eliminated from the overall digital information stream (point E in Figure 144). The signal at point E is arbitrarily shown in Figure 145 E. The main data reduction unit compares the indications of the priority sensors for a time interval equal to the length of two frames.

Signal B (see Fibure 145) is delayed in the main unit by a time of one frame, after which the indications of the priority sensors are compared in digital form. If the change in the indications of a priority sensor from one frame to the next is not greater than the permissible value, the unit outputs a "block" instruction for the entire group of indications of sensors including the priority sensor in question. The quote "block" instruction from the main redundancy-reduction unit goes to the main switch, at the output of which the redundant groups of indications of sensors are eliminated from the data stream (signal E in Figure 145). /255

The signals of digital sensors are processed in the recoding device (see Figure 144). In this device, the parallel code (parallel outputs of sensors) is converted to a sequential code, with the simultaneous operation of reduction of redundancy of the digital sensor indications.

The reduction of redundancy of the digital sensor indications is based on the application of different methods of information coding [13]. When difference methods of information coding are used, it is not the absolute values of the indications of the sensors which are transmitted, but rather arbitrary signals of changes in polarity in the indications of the sensors; if the indications of a sensor are unchanged for various interrogation intervals, the null signal or pause is tranmitted. Elimination of pauses from the signal representing the indications of the digital sensors allows the signal to be compressed in time, i. e. the redundancy of the digital signal is reduced.

The signal of the output of the recoding device is arbitrarily shown in Figure 145 F. As we can see by comparison of Figures 145 E and 145 F, the coded signals of the analog sensors and the signals of the digital sensors do not overlap in time (which is assured by switch no. 2, see Figure 144), have real time scale and a certain order of sequence of the numbers of analog and digital sensors.

Based on these structural properties of the signals, the coded readings of the indications of analog and digital sensors can be addressed. Addressing of the indications of the sensors is

performed by the system address generator (see Figure 144) by addition of code marks to the signals from the various sensors [22]. Functionally, this operation is reduced to multiplication of the signals shown in Figure 145 E and 145 F by a special address generator signal.

The signal at the output of the multiplier (see Figure 123) is shown in arbitrary form in Figure 145 G. This signal then goes further to an adder, where the synchronization signals are added, noting the beginning and end of each frame. The signal thus formed is then sent to the memory unit, where the signal is time compressed. The memory unit performs start-stop recording of signals at its input (Figure 145 K). The siganl from the output memory unit goes to the transmitting stages of the system. The signal at the receiving end of the telemetry system can be restored using the principles of code separation of signals [22].

CHAPTER 16

POWER SUPPLY SYSTEMS

The first Soviet and American lunar landers (Luna-9, Luna-13 and Surveyor) carried electrochemical power supplies (batteries) and photoelectric solar energy converters (solar batteries), allowing these automatic stations to operate for several months. However, the short service lives of the batteries and the dependence of the solar batteries on sunlight, make it impossible for these systems to be used for extended operation where there is no sunlight, or on the surfaces of planets with dense atmospheres or planets far from the sun. /256

The development of radioactive isotope fuel supplies and fuel cells allowed the problem of comparatively long-term power supply of APS to be solved to some extent. Thermoelectric generators utilizing isotopes and fuel cells have been successfully used to supply the equipment of the Surveyor and Apollo spacecraft.

Unfortunately, the high cost of radioactive isotopes and the requirements of reliable shielding of scientific and service equipment from penetrating radiation produced by certain types of isotopes limit their use somewhat. Also, the problem of regeneration of the substances used in fuel cells must be solved in order to allow them to be used over long periods of time.

Thus, one of the main tasks involved in the creation of small APS is the development of a small, reliable power plant, satisfying such requirements as: 1) reliability; 2) long service life; 3) high specific power output; 4) small size and weight; 5) radiation stability. We must note that each individual case of application of a power supply must be studied in detail.

Let us briefly study the most important currently available and prospective power supply systems, describing their operating principle and analyzing them from the standpoint of their use in small APS.

16.1. Chemical Sources of Current

Chemical sources of energy (galvanic elements, cells and batteries) were the primary power supplies used in the first space objects, since due to their reliability, convenience of use and high specific power they could provide the power needs of the spacecraft apparatus for short periods of time. Now, since the

problems of flight to the planets and creation of automatic stations for use on the surfaces of the planets can be solved, chemical sources of current are being gradually replaced with improved /257
power systems (solar batteries, thermoelectric converters using isotopes and fuel cells, etc.). However, chemical batteries and cells are quite convenient for use as power supplies for spacecraft during the launch, flights in "shadow" orbits, and also for comparatively long-term operation in combination with other power sources, when the use of the other sources becomes either impossible (solar batteries in the shade) or too expensive (radio isotope generators). Therefore, extensive studies continue on the creation of spacecraft chemical sources of current which can satisfy the requirements for high power capacity, durability and usability over a broad range of temperatures, high specific power output and operating convenience.

We will not discuss the analysis of oxidation-reduction processes occurring on the electrodes of chemical elements in detail, since this question has been widely discussed in the literature.

As to the nature of their operation, chemical sources of power can be divided into the following two groups:

1) primary sources of power -- galvanic cells and batteries, allowing one-time use of the active materials which they contain;

2) secondary sources -- electrical batteries which can be recharged by means of a second electric power supply.

Primary chemical sources of current. The primary sources of current include manganese-zinc cells and batteries, which are widely produced by industry (Krona, Polet, KBS and other batteries). In spite of the simplicity of their production technology and other advantages, manganese-zinc drycells have great shortcomings, preventing their use on spacecraft: 1) low specific power; 2) rapidly dropping discharge voltage; 3) narrow range of operating temperatures (-30 to +60° C); 4) insufficient vibration resistance.

The first artificial Earth satellites widely used mercury batteries, which do not have many of the shortcomings of manganese-zinc batteries. The primary advantage of these batteries is their stable and constant emf produced over a long period of time, particularly when discharged slowly. Furthermore, these batteries have high vibration resistance (up to 200 g) and a broad range of /258
operating temperatures (+40 to -30° C). We should note that the efficiency of a mercury cell can be restored after exposure to low temperatures by simply heating. Recently, some spacecraft with short operating lives have been powered by mercury-zinc batteries. The characteristics of some mercury batteries are presented in Table 19.

TABLE 19.

Type of battery	Capacity, a·hr	Operating temperature, deg	Storage life, months	Dimensions Diam., mm	Dimensions Length mm	Weight, g
OR-3	1.8	-5 to +70	18	25.7	13.5	30.0
OR-4	2.8	-5 to +70	18	30.1	14.1	40.0
OR-4K	1.6	-5 to +70	12	30.1	9.4	28.0
RTs 83-X	1.5	-30 to +50	12	30.1	9.4	28.2
RTs 84	2.5	0 to +50	28	30.1	14.0	45.0
RTs 85	2.5	0 to +50	28	30.1	14.0	39.5
RTs 85-X	2.5	-30 to +50	18	30.1	14.0	39.5
RTs 93	13.0	0 to +50	6	31.0	60.0	170.0

All mercury batteris have high specific power capacity (80-100 w·hr/kg).

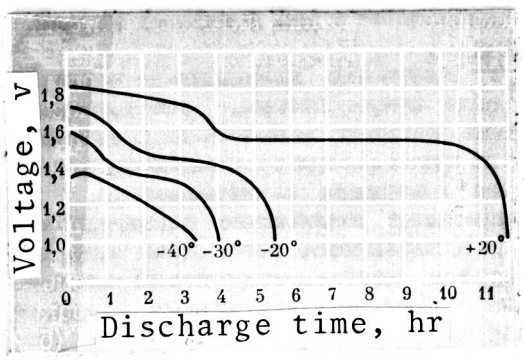

Figure 146. Discharge Curves of Silver-Zinc Batteries with 20 a·hr Capacity (discharge by 2 a current following 2-hour holding in a cold chamber).

In spite of the many positive qualities of mercury batteries, primary current sources are not desirable for use in APS, due to their low power capacity and the impossibility of recharging these batteries.

Secondary chemical sources of current. The main advantage of secondary sources of current (storage batteries) is the possibility of their repeated use by recharging with other sources of electric power. For this reason, storage batteries are widely used in all spacecraft. Among these batteries, the most widely used types in space technology are the cadmium-nickel, silver-cadmium, silver-zinc and nickel-zinc batteries. All of these batteries have high specific power capacity, are reliable, and have a broad range of operating temperatures. However, we must note one important shortcoming of alkali cadmium-nickel batteries: they liberate gaseous oxygen at the positive electrode, making it difficult to seal these batteries.

Silver-zinc and silver-cadmium batteries do not have this shortcoming. Furthermore, another significant advantage of these batteries over the other types is the high permissible current den-

sity (up to 0.5 a/cm^2) and low internal resistance. This makes it possible to use these batteries effectively with impulse loading. The normal operating temperature range of silver-zinc batteries is -30 to +70° C. The dependence of discharge voltage of these batteries on temperature is shown in Figure 146. Comparative characteristics of several types of batteries are presented in Table 20.

New developments in battery technology are intended to increase specific power and reliability, expand the operating temperature range, reduce cost and increase the number of charge-discharge cycles.

We note in conclusion that in combination with other sources of electric power, batteries can be considered among the most important types of power supplies for automatic planetary stations.

16.2. Photoelectric Solar Energy Converters.

Solar batteries using the photoelectric effect of direct conversion of solar radiation to electric power currently represent one of the main sources of electric power supply for spacecraft. /259

Although the power capacity of the first solar batteries was not over a few tens of watts, which indicated that their use might be quite limited, recent studies in this area have revealed the possibility of producing powers on the order of several tens of kilowatts by this method. At the present time, the best substance for use in solar photocells is monocrystalline tetravalent silicon of high purity, doped by thermal diffusion with pentavalent phosphorous and trivalent boron.

When a photocell absorbs a flux of photons from solar radiation, the following phenomenon occurs. If the energy of a photon exceeds the so-called activation energy of the atoms of silicon, when the photon is absorbed a pair of excess charge carriers (electron plus hole) arises. Intensive irradiation of the solar cell causes positive and negative charges to accumulate, resulting in the development of an emf, reaching several tens of volts.

We should note that the losses to reflection in silicon cells amount to 30% of the incident solar radiation. Furthermore, the absorption of the solar energy is not total, which reduces the overall efficiency of a solar cell. The portion of the solar energy which under ideal conditions might be converted to electric power is shown in Figure 147 (by the shaded area).

TABLE 20.

Type of batteries	Specific power		Operating temperature, degrees	Operating voltage, v	Service life		Loss of capacity in 3 months, %
	w·hr/kg	w·hr/l			Cycles	Months	
Nickel-cadmium	24	70	+5 to +30	1.45	300	20-30	up to 30
Silver-zinc	130	200	-40 to +70	1.5	100	15-18	5-10
Silver-cadmium	70	130	-30 to +30	1.15	300	15-18	0-5
Nickel-zinc	65	110	-30 to +40	1.65	100	15-18	up to 20

Silicon elements can utilize photons with wave length not over 1.15 μ, since their energy is greater than the activation energy of 1.07 eV. Photons with wave length less than 1.15 μ give up their excess energy to the crystalline lattice, which is thermally excited.

In the range of wave lengths below 0.4 μ and over 1.15 μ, the sensitivy of silicon solar elements, from the standpoint of conversion of solar energy to electrical energy, is significantly less than within this range. Therefore, ultraviolet and infrared coatings can be used to decrease the absorption of solar radiation in this area and thereby lower the working temperature, since the voltage drop in a silicon solar cell is 0.5% per degree of temperature rise.

A schematic diagram of a typical silicon solar battery cell is shown in Figure 148.

The effectiveness of solar cells depends to a great extent on the operating temperature, which should not be over 100° C (Figure 149 [33]). /260

For these reasons, the efficiency of modern solar converters is not over 11-14%. Presently, the most promising semiconductor is gallium arsenide, the theoretical efficiency of which reaches 25%. The graph presented below (Figure 150) can allow us to judge the effectiveness of materials used in solar converters [33]. However, we should note that the efficiency of other devices involving direct conversion of solar energy to electrical energy, for example photogalvanic cells, is 1% and less.

Recently, various methods have been developed to increase the effectiveness of solar cells, consisting mainly in application of transparent and protective coatings, decreasing the number of contact points between elements by increasing the size of a cell, the

use of special coatings in the infrared and ultraviolet areas of the spectrum, etc.

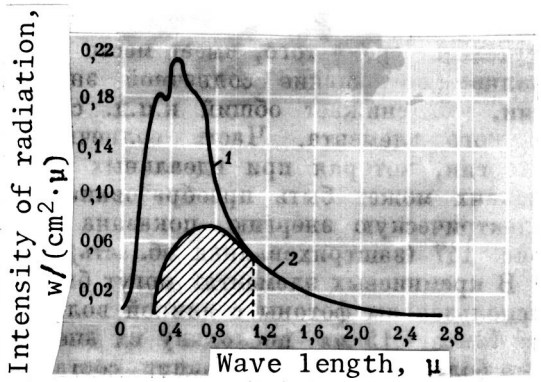

Figure 147. Spectrum of Solar Radiation and Its Utilization in Silicon Solar Batteries: 1, solar spectrum; 2, light sensitivity of silicon cells.

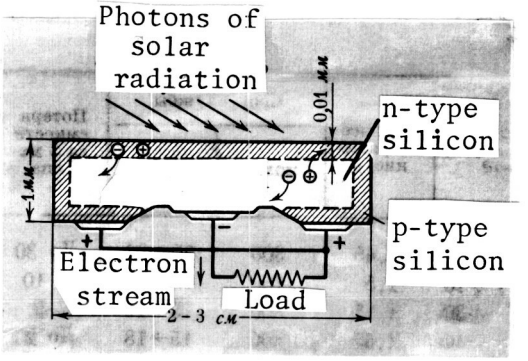

Figure 148. Diagram of a Typical Silicon Cell.

The work on the use of photoconverters with solar radiation concentrators, allowing the number of cells to be decreased with the same output power by increasing the intensity of the incident radiation, is very interesting. It has been established that the degree of concentration should not exceed 2.5 in order to avoid significant overheating of the solar cells.

Figure 151 shows a V-shaped concentrator, the most suitable for use in space, the degree of concentration of which is not over 1.9.

In order to produce greater power capacities, extensive studies have been performed in recent years on the manufacture of silicon solar cells of dendritic strips, as well as the creation of thin-film elements based on such semiconductor compounds as CdS, GaAs, CdTe and GaP. One of the advantages of the use of dendritic strips is the possiblity of producing large-area elements, decreasing the number of contacts as they are switched (by 15 times in comparison to elements measuring 1×2 cm). At the present time, dendritic strips are used for the manufacture of elements measuring 30×1×0.05 cm, with an efficiency of 8%.

Solar batteries can be made of monocrystalline elements, dendritic strips and thin-film elements. Solar batteries of the first type are most widely used at present.

There are many methods of installation of solar cells. The panels of solar batteries may be attached directly to the body of the spacecraft, or to extended, nonoriented panels, or to extended panels oriented perpendicular to the direction to the sun. This last method is most effective, but requires an additional drive unit to orient the panels. Modern solar batteries can produce 100 w per square meter of surface when directly illuminated by the sun. /261

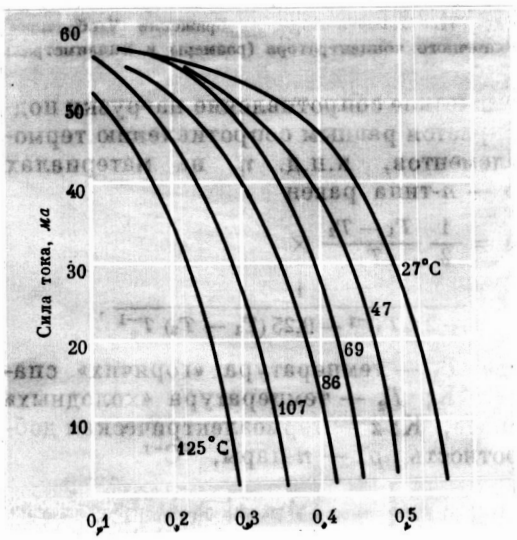

Figure 149. Current of a Silicon Cell as a Function of Voltage for Various Val ues of Working Temperatures.

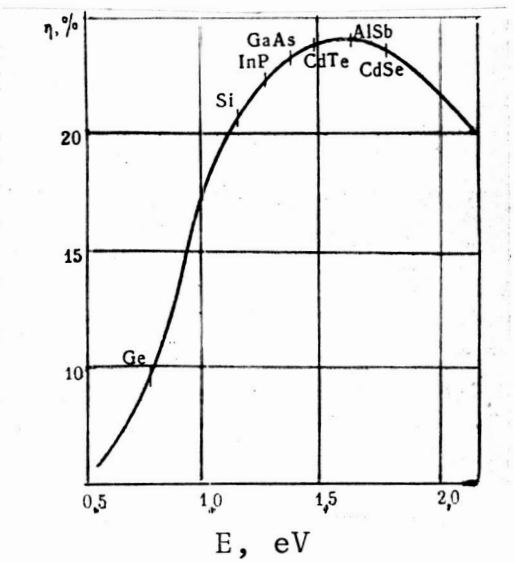

Figure 150. Theoretical Effectiveness of Materials Used in Solar Converters.

In conclusion, we should note that due to the high effectiveness resulting from the direct conversion of solar energy to electrical energy, solar photoelectric converters are without peer when the solar radiation is intense.

Unfortunately, the use of solar batteries alone to supply the power for small automatic stations on the surface of planets with nontransparent atmosphere (Venus) or where the intensity of the solar radiation is low (Mars), or where the solar radiation is intermittent (moon) is quite impossible or requires great size and weight in order to achieve sufficient power.

16.3. Thermoelectric Generators.

The operating principle of a thermoelectric generator is based on the Seebeck effect [34], the essence of which is that a

thermo-emf arises in a closed electrical circuit consisting of dissimilar materials if the points of contact are maintained at different temperatures. The magnitude of the current depends primarily on the nature of the metals and alloys which make up the circuit, and on the temperature difference between the "hot" and "cold" junctions.

At the present time, highly alloyed semiconductor compounds and alloys are broadly used as the materials in the thermoelectric elements. The selection of the materials for an element is a determining factor in the planning of a thermoelectric generator, since its efficiency depends primarily on the thermoelectric quality of the material z.

In the maximum output power mode, which is achieved when the load resistance is equal to the resistance of the thermoelectric cells, the efficiency η with p-n-type materials is /262

$$\eta = \frac{1}{2}\frac{T_1 - T_2}{T_1}\frac{1}{1 + 2(zT_1)^{-1} - 0.25(T_1 - T_2)T_1^{-1}},$$

where T_1 is the temperature of the hot junction, K; T_2 is the temperature of the cold junction, K; z is the thermoelectric quality of the p-n pair, decree C^{-1}.

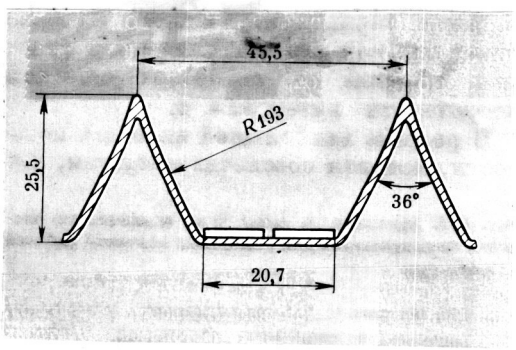

Figure 151. Schematic Diagram of V-Shaped Solar Concentrator (dimensions in millimeters).

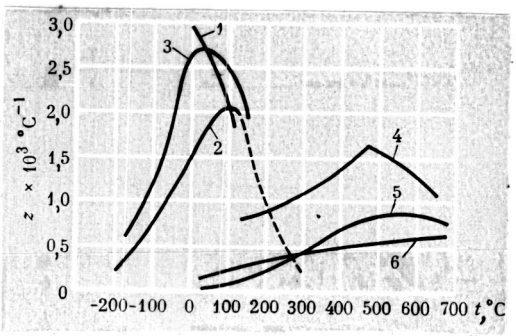

Figure 152. Thermoelectric Quality of Certain p-Type Materials as a Function of Temperature: 1, Bi_2SbTe_3 + 0.56% Se; 2, Bi_2SbTe_3 + 0.28% Ag + 0.5% Se; 3, $(BiSb)_2Te_3$; 4, $(GeTe)_{0.95}(BiTe_3)_{0.051}$; 5, GeTe; 6, P $Si_{0.7}Ge_{0.3}$.

The graphs (Figures 152 and 153) show the dependence of thermoelectric quality of certain p-n-type materials on temperature.

Depending on the primary source of heat, thermoelectric generators are divided into radio isotope and solar types.

Radio isotope thermoelectric generators. One method of maintaining a high temperature on the hot junctions of thermoelectric generators is to use the thermal energy formed upon decay of radioactive isotopes. This combination of a thermoelectric generator with radio isotopes, due to its high effectiveness and reliability, has become widely used in spacecraft for the study both of interplanetary space and of the surface of the moon and the planets. Radio isotope energy sources are particularly convenient for extended work on the surface of the planets which have dense, nontransparent atmospheres, when other sources of energy are either unsuitable (solar batteries) or cannot continue operating for long enough (chemical batteries, fuel cells).

Thus, the basic advantages of radio isotope thermoelectric generators are:

1) long service life (even when there is no solar radiation);
2) high reliability and specific power;
3) simplicity of regulation;
4) possiblity of operation under conditions of high radiation.

The fuel for thermoelectric generators may be various radioactive isotopes; the characteristics of some of these are presented in Table 21 [35].

Radio isotopes are a unique fuel source, providing high energy density. However, radio isotopes have certain disadvantages as well. The most important of these, in addition to high cost, is radioactive radiation. /264

There are four main types of nuclear radiation dangerous for man and destructive to equipment:

1) high energy γ-quanta, i. e. X-rays arising in the process of decomposition of isotopes;
2) neutrons, produced upon spontaneous fission of heavy elements;
3) β-particles arising as a result of nuclear decay;
4) α-particles.

Of these types of radiation, only γ-quanta and β-particles cause the most serious damage. Without considering the influence of these types of radiation on servicing personnel, we should note that intense γ- and β-radiation cause ionization and excitation of atoms of materials, which is particularly dangerous for the equipment of a spacecraft. At the present time, the weight of the

shielding elements of radio isotope thermoelectric generators amounts to up to 80% of the total weight of the generator.

TABLE 21. /263

Isotopes	Type of radiation	Half-life	Fuel	Specific gravity of fuel $g \cdot cm^{-3}$	Heat of decay	Melting point, deg	Area of application
Po^{210}	α	138 days	Po	9.3	141	154	Station with short service life
Cm^{242}	α; (γ)	163 days	Cm_2O_3	10.7	110	1500	same
Cm^{244}	α; (γ)	18 days	--	--	2.8	--	Very promising for long-lived APS
Pu^{238}	α; (γ)	86.4 years	PuC	13.6	0.52	1650	Long-lived stations
Ce^{144}	Hard γ-radiation β	285 days	CeO_2	7.12	21	2600	Stations with short servive life
Pm^{147}	β	2.6 years	Pm_2O_3	6.6	0.31	1500	Long-lived stations
Cs^{137}	β	33 years	CsCl	3.97	0.22	646	same
Sr^{90}	β; (γ)	27.7 years	$SrTiO_3$	4.0	0.25	1600	Preferable in terrestrial installations

Note. Polonium-210, curium-242 and curium-244 require light shielding, while plutonium-238 requires moderate shielding and cerium-144, promethium-147, cezium-137 and strontium-90 require heavy shielding.

Figures 154 and 155 show the dependences of the thickness of shielding of certain α- and β-radiators on thermal power rating [36].

Figures 156 and 157 show typical diagrams of space thermoelectric generators, while Table 22 presents the basic data on radio isotope thermoelectric generators made in the USA. /265

The Snap-27 50-watt generator was developed at the request of NASA to power the equipment left on the surface of the moon as a part of the Apollo program. The instruments in the container are to collect and transmit information to Earth for 6-12 months after

the departure of the astronauts. The maximum temperature of the hot junctions is 549° C, of the cold junctions 273° C; the design efficiency is 4%.

TABLE 22.

Generator	Snap-38	Snap-9A	Snap-11	Snap-17	Snap-19	Snap-27
Operating life, years	5	6	0,25	5(3)	3	1
Power at end of operation, w	2,7	25,0	18,6—25	25—30	22—30	50
Fuel	Pu-238	Pu-238	Cm-242	Sr-90	Pu-238	Pu-238
Characteristics at end of operation						
Voltage, v	2,7	6,4	3,0	6,6	4,75	14
Current, a	1,0	4,6	8,33	3,8	4,65	4
Load, ohm	3,0	2,0	0,42	1,75	1,02	3,5
Dimensions						
Length, cm	13,97	24,13	27,94	31,75	24,74	45,97
Diameter, cm	12,19	50,80	45,72	16,76	13,56	39,88
Weight, kg	2,1	12,3	13,6	11,4	9,6	16,5
Installed in	Transit-4	Transit-5	Surveyor	Communi-cations satellies	Nimbus	Apollo program

It can be expected that space systems in the near future will use low-power radio isotope thermoelectric generators (25-50 w), utilizing the energy of decay of radioactive isotopes plutonium-238 (for stations with service lives over 1 year) and polonium-210 (for stations with service lives of 1-2 months). Due to the limited production capacity for these isotopes, they will be used for one-time important jobs, which cannot be performed using chemical sources of current or solar batteries, for example for operation where there is no sunlight.

Solar thermoelectric generators. These are generators in which the energy of solar radiation is used to heat the hot junctions and which are very promising, due to their potential advantages over solar batteries. Solar thermoelectric generators are most promising for spacecraft which fly to the sun or the planets /266
near the sun, when the operating temperature will reach several hundreds of degrees. For example, whereas the thermal flux of solar energy at the surface of the Earth is 1370 w/m^2, on Mercury and Venus it is 9290 and 2700 w/m^2 respectively. Furthermore, when a thermal battery is used, solar thermoelectric generators can provide power for the spacecraft as it flies through the shadow side of its orbit.

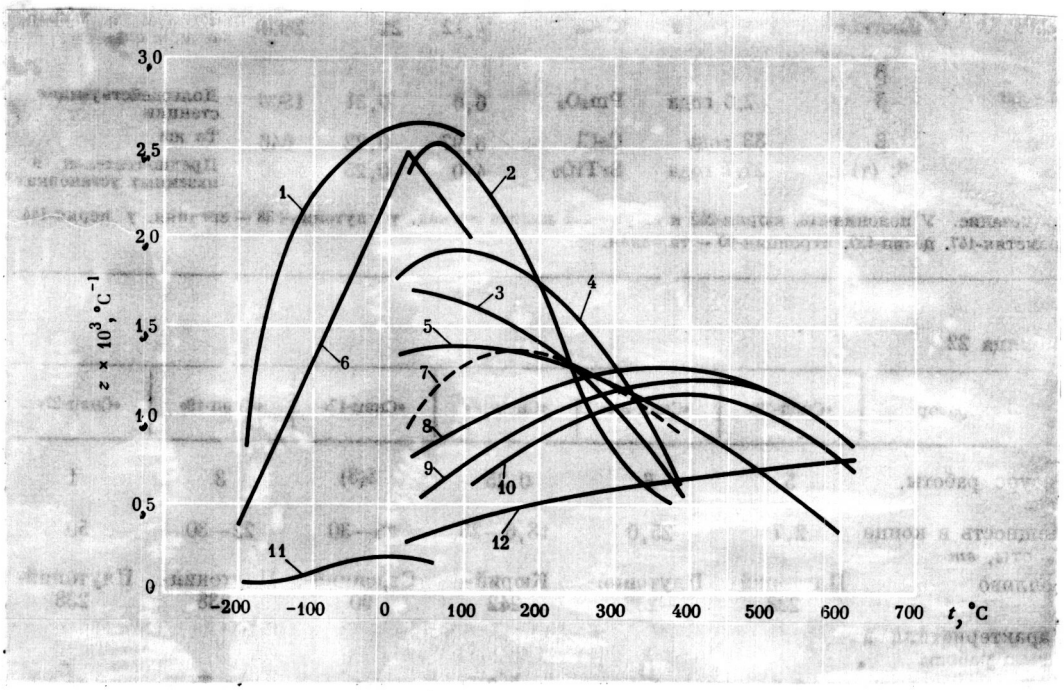

Figure 153. Thermoelectric Quality of Certain n-Type Materials as a Function of Temperature: 1, $20Bi_2Te_3$ + Bi_2Se_3 + 0.5% CuBr; 2, $Bi_2Te_{2.4}Se_{0.6}$ + 0.05% CuBr; 3, $Bi_2Te_{2.4}Se_{0.6}$ + 0.10% CuBr; 4, Bi_2Te_2Se + 0.05% CuBr; 5, PbTe + 0.04% Bi; 6, Bi_2Te_3 + 0.085% CuBr; 7, Bi_2Te_3Se + 0.10% CuBr; 8, PbTe + 0.10% Bi; 9, PbTe + 0.15% Bi; 10, PbTe + 0.07% Bi; 11, Bi_2Te_2Se; 12, n $Si_{0.7}Ge_{0.3}$.

At the present time, such generators have been developed in the shape of flat panels (without concentrators) and with solar concentrators. One advantage of flat solar thermoelectric generators is the comparatively low requirement for accuracy of orientation toward the sun. The primary shortcoming is their low efficiency.

The concentration of solar energy allows very high temperatures of the hot junctions of the thermal cells to be achieved, significantly increasing efficiency. At the present time, several types of concentrators are under development and study: Fresnel concentrators, inflated concentrators, one-piece concentrators, lobe concentrators, umbrella concentrators and other types (Figure 158). From the standpoint of temperature, the one-piece concentrator is the most attractive, as it allows temperatures of around 1900° C to be reached.

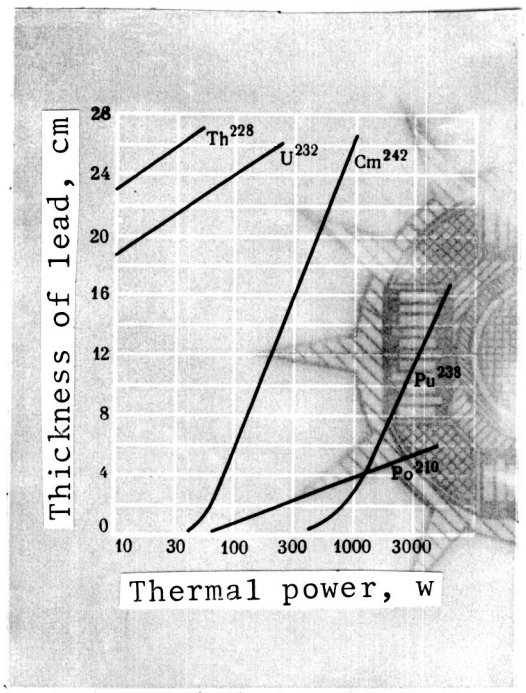

Figure 154. Thickness of Shielding of α-Radiator as a Function of Thermal Power.

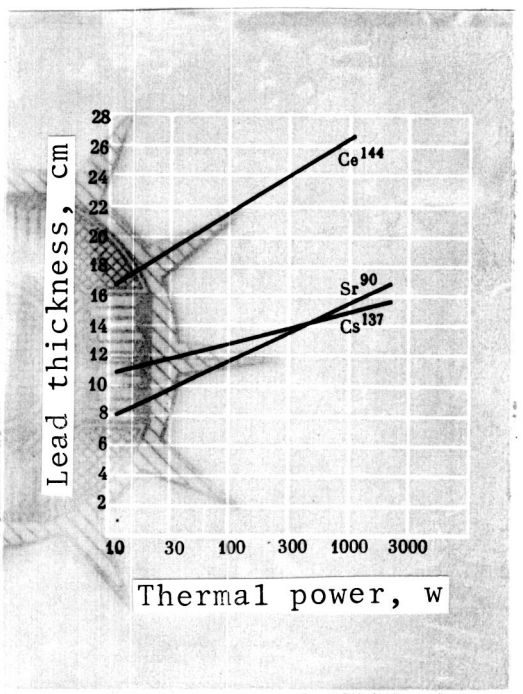

Figure 155. Thickness of Shielding of β-Radiators as a Function of Thermal Power.

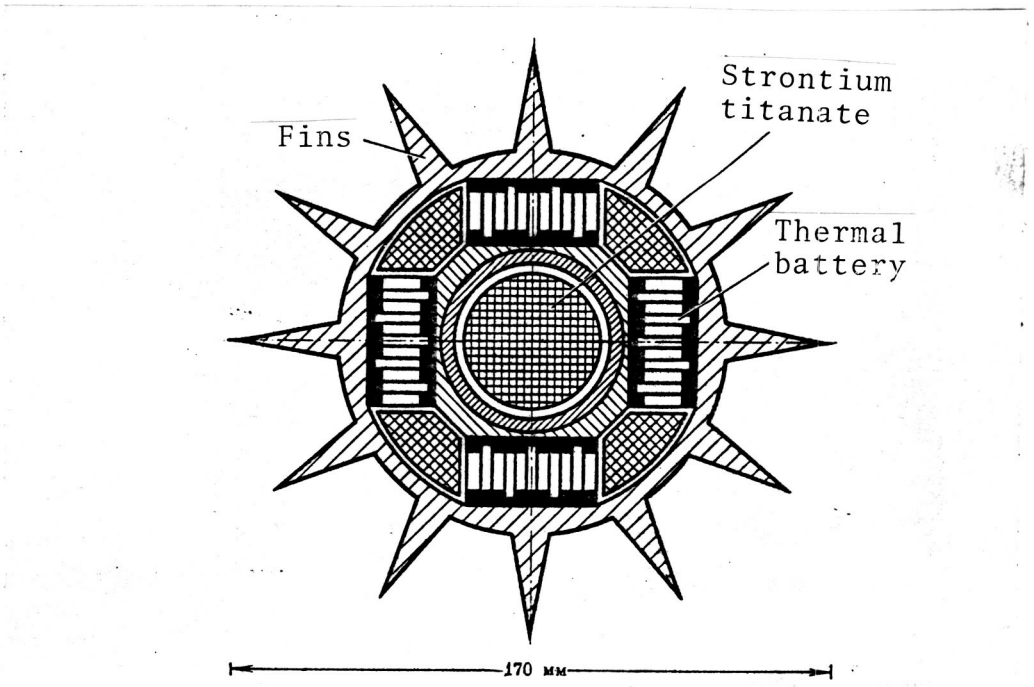

Figure 156. Diagram of a Strontium-Powered Thermoelectric Generator.

The basic characteristics of several concentrators are presented in Table 23 [37].

There is great interest in the combination of a solar thermoelectric generator and a thermal battery. In this case, a substance with a high melting point is placed at the focal point of solar concentrator on the hot junction of the solar thermoelectric generator. The solar energy causes the substance of the thermal battery to melt, maintaining the hot junction of the thermal cell at constant temperature. During flight through the shadow portion of an orbit, the melted substance of the thermal accumulator solidifies, giving up its stored heat to the energy converter. Consequently, the thermal battery causes the solar thermoelectric generator to keep operating in the shade for a length of time comparable to the time of illumination. /267

The best thermal battery materials are lithium hydride and fluoride (LiH, LiF), with melting points of 673 and 845° C respectively (the heat of melting is ~650 and 325 $kcal \cdot kg^{-1} \cdot hr^{-1}$).

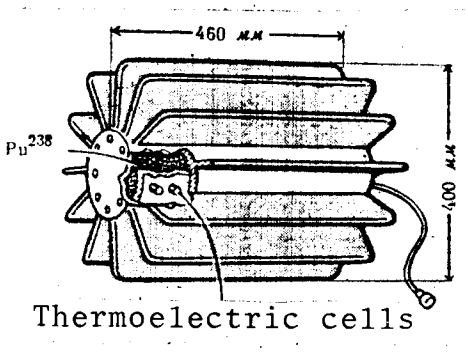

Figure 157. Thermoelectric Generator Developed for Apollo Program.

One possible design of a solar thermoelectric generator with thermal accumulator is shown in Figure 159.

In spite of a number of positive qualities of solar thermoelectric generators, we should also note some shortcomings which hinder their broad application in space: the difficulty of creation of concentrators with high optical characteristics and the need for precise orientation toward the sun within limits of ±0.5° in order to produce sufficiently high efficiency. Therefore, solar thermoelectric generators are not currently competitive with solar batteries and radio isotope thermoelectric generators.

16.4. Fuel Cells (Electrochemical Generators).

The principle of operation of fuel cells is similar to the principle of operation of ordinary chemical sources of current (dry cells, storage batteries). In these cells, electric power is consumed in the form of a discharge, the quantity of active material of the electrodes (anode and cathode) being decreased. When the chemical energy is fully consumed, the discharge of the cell stops.

However, if the substances acting as anode and cathode are continually replenished, the discharge of the cell will continue. /268

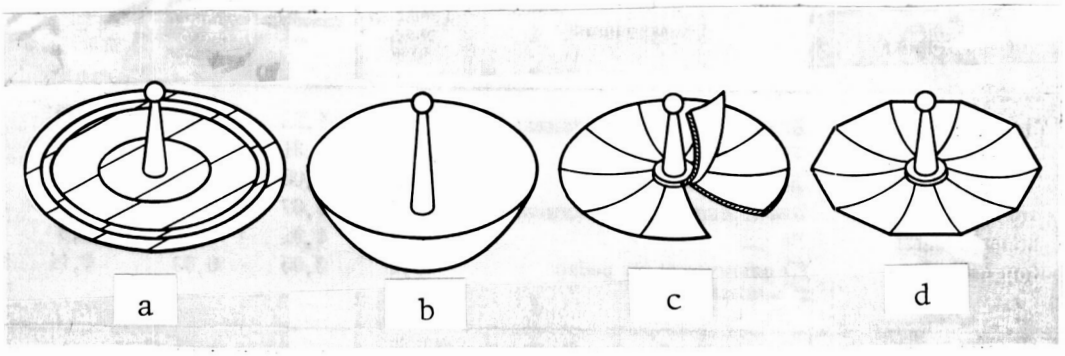

Figure 158. Types of Solar Energy Concentrators: a, Fresnel; b, one-piece; c, lobe; d, umbrella.

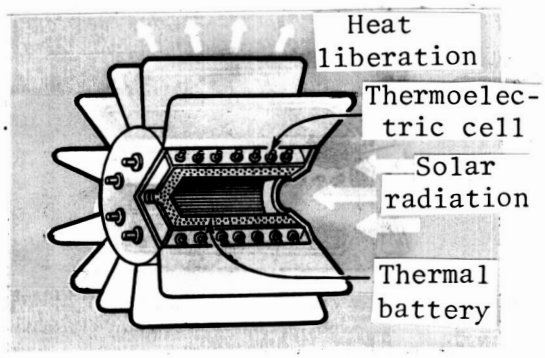

Figure 159. Possible design of a Solar Thermoelectric Generator with Thermal Battery.

Devices which allow electric power to be produced for a long time in this manner are called fuel cells or electrochemical generators.

Thus, the difference between fuel cells and chemical sources of current is the placement of the active substances. Whereas in chemical sources of current they are structurally connected to the electrodes and their entire reserve lies within the source of current, in fuel cells the active substances are stored separately and are constantly fed into the zone of the electrochemical reaction.

The electrodes of fuel cells, which act as catalysts and current leads, are not consumed during the operation of the cell and could operate for an unlimited period of time but for certain factors which limit their service lives.

The active substance of the negative electrode in fuel cells is either some natural fuel (for example natural gas, containing hydrocarbons) or a substance which can easily be produced from natural fuel (hydrogen, carbon monoxide, water gas, etc). The active substance of the positive electrode is most frequently oxygen in the air or pure oxygen.

As we have noted, the active substances are stored separately from the fuel cell and fed into it as consumed.

TABLE 23.

Type of concentrator	Structural material	Solid angle, deg	Diameter, m	Reflectivity	Specific weight, lbs/foot^3
Fresnel	Electrolyzed nickel	40.0	1.22	0.85	0.46
Inflated	Stretched mylar	53.1	1.31	--	0.03
Inflated	Lobes of mylar	60.0	3.05	--	3.82
One-piece	Electrolyzed nickel	61.5	1.67	0.89-0.9	0.96
Lobe	same	53.1	1.31	--	0.3
Umbrella	60 aluminum ribs and mylar	90.0	3.05	0.83	0.11

In this respect, the fuel cell is similar to thermal machines, but one significant difference between fuel cells and thermal machines is the mechanism of conversion of energy. Furthermore, the most important advantage of fuel cells over thermal machines is that they can in principle have much higher efficiency. Actually, according to the second law of thermodynamics, the efficiency of /269 any thermal machine cannot exceed

$$\eta_{max} = 1 - \frac{T_1}{T_2},$$

where T_1 and T_2 are the minimum and maximum absolute temperatures of the thermal cycle respectively.

Practically, the efficiency of various thermal machines does not exceed 30-40% for turbine installations and 25-30% for internal combustion engines.

With direct conversion of chemical energy to electric power, the maximum efficiency is not limited by this equation and can be

(depending on the sign of the thermal effect of the current-forming reaction) less than, greater than or equal to 100%. The maximum efficiency of conversion of chemical energy to electric power is expressed by the equation

$$\eta_{max} = 1 + \frac{T\Delta S}{Q},$$

where T is the absolute temperature; ΔS is the entropy increment; Q is the thermal effect of the current-forming reaction.

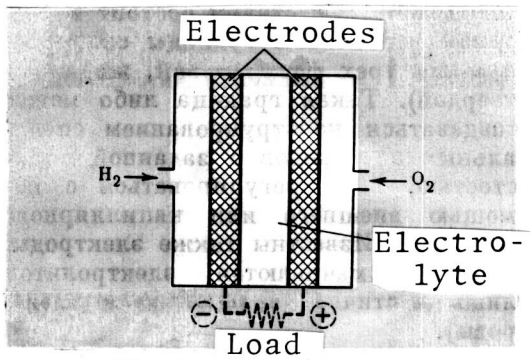

Figure 160. Diagram of Hydrogen-Oxygen Fuel Cell.

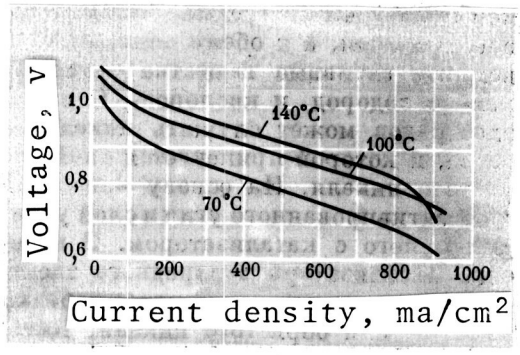

Figure 161. Volt-Ampere Characteristics of H_2-O_2 Fuel Cell.

When the efficiency exceeds 100%, this means that the current-forming reaction involves absorption of heat. In modern fuel cells, the efficiency reaches 55-60%, or with low-current discharge even 60-70%.

In addition to their high efficiency, fuel cells have a number of other advantages, the most important of which are the high specific power, the absence of moving parts, vibration, noise, etc. There is presently a great variety of types of fuel cells, differing in type of fuel, oxidizer and composition of electrolyte, operating conditions (temperature, pressure), types of electrodes, etc.

In addition to hydrogen, various types of alcohols, liquid and gaseous hydrocarbons, hydrozine, ammonia and carbon monoxide are used as fuels. The oxidizers include oxygen, halides (chlorine, bromine), hydrogen peroxide and nitric acid. The electrolyte may be an alkali or an acid.

Let us study the prinicple of operation of an electrochemical generator on the example of the most common low-temperature hydrogen-oxygen fuel cell (Figure 160). Two electrodes, plates of materials with electron conductivity, divide the volume of a chamber

into three parts; the middle portion is filled with the electrolyte, while the active substances -- gaseous hydrogen and oxygen -- are fed to the two side parts. The electrodes might consist of a nickel screen, to which a layer of porous nickel is attached. A layer of activated carbon and a layer of carbon mixed with a catalyst are placed on this base. The catalyst on the hydrogen electrode might be a very slight quantity of platinum or nickel boride. The catalyst on the oxygen electrode might be silver, osmium or cobalt oxide. The electrolyte might be an acid or alkali solution. /270

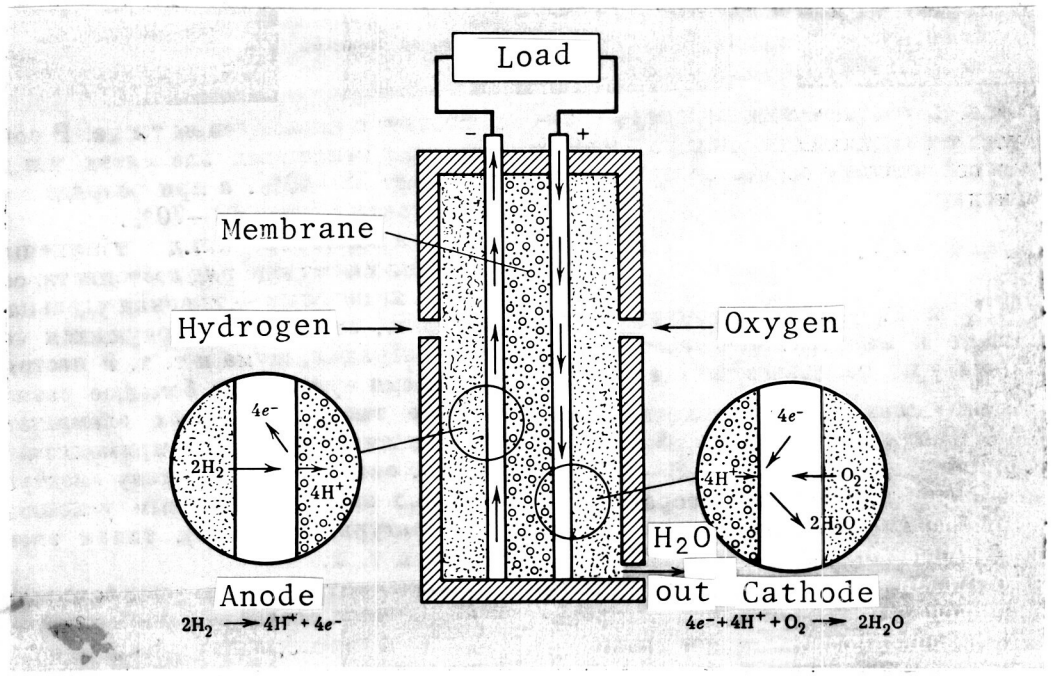

Figure 162. Schematic Diagram of Operation of Fuel Cell with Ion-Exchange Membrane.

The active hydrogen and oxygen propagate within the plate, contacting the penetrating electrode. The main difficulty in the development of fuel cells with gaseous active substances consists in the creation of a stable contact boundary of the three phases (gas, liquid and solid). Such a boundary can either be created by construction of special electrodes with the required porosity, or may be regulated by external or capillary pressure. Electrodes are also known which are wet only partially with the electrolyte (rotating electrodes).

The electrodes, when saturated with the active substances and electrolyte, are brought up to the working condition and are called

gas electrodes. When the gas electrodes are connected through an external circuit and when the hydrogen and oxygen are activated the oxidation-reduction reaction occurs, and energy is produced. There are two methods of activation: by means of catalysts and by temperature.

In 1965, fuel cells were produced with a current density of /271
200 ma/cm^2 and an emf of ∿0.8 v. As the current density is increased, the temperature rises rapidly (especially on the anode), requiring forced cooling of the fuel cell.

Modern electrochemical generators, depending on the operating temperature, can be roughly classified into low-temperature ($t_p \leq$ 250° C) and high-temperature ($t_p \geq 250°$ C) types. For low-temperature fuel cells, the primary difficulty is in electrocatalysis, i. e. increasing the current density by means of the electrode materials. For high-temperature fuel cells, the problem of stability of materials with the strongly corrosive effect of the electrolytes arises.

Figure 161 shows typical volt-ampere curves of H_2-O_2 fuel cells. The electrolyte is a KOH solution.

The high characteristics of H_2-O_2 fuel cells with liquid electrolyte have allowed them to be used in orbital flights and in studies of the moon as a part of the Apollo program. A battery of fuel cells with a total power capacity of 2 kw (following extended operation the power is reduced to 1 kw) and a voltage of 29 v was used. Total weight of the battery was 810 kg. The operating temperature was ∿82° C.

In 1958, Grubb [38] suggested an interesting H_2-O_2 fuel cell in which the electrolyte consists of ion-exchange membranes. The operating principle of a fuel cell with ion-exchange membrane is explained by Figure 162. The ion exchange membrane is placed between the two electrodes, which in this case consist of a thin wire screen of titanium-palladium alloy set in a thin layer of platinum black. During the process of operation, the hydrogen and oxygen enter the side chambers, where they are activated. The electrons of the hydrogen atoms are directed to the external circuit, forming an electric current. The hydrogen ions pass through the membrane and, together with the ionized oxygen, form water on the oxygen electrode.

Extensive studies are currently being conducted of various types of fuel cells with metal-ceramic electrodes, plastic-based electrodes, capillary membranes, soluble liquid fuel, hydrozine, etc. There is particular interest in the possibility of creating fuel cells based on rocket fuel with long storage life, which is particularly important for long flights. We should note that the

cryogenic storage of hydrogen and oxygen is rather difficult, while the storage of hydrogen in the compressed state (up to 200 atm) causes the weight of cylinders to increase by 100 and more times in comparison to the weight of the hydrogen itself)

The first results produced in studies of asymmetrical dimethylhydrozine and nitrogen dioxide as fuel and oxidizer [39] indicate the promise of the use of these substances in fuel cells. The reaction which occurs in this case

$$(CH_3)_2N - NH_2 + 4H_2O \rightarrow 2CO_2 + H_2 + 16H^+ + 16e^- \qquad /272$$

yields high output power.

So-called regenerative fuel cells in which the products produced in the electrochemical reaction are restored to the initial active substances and returned to the fuel cell (Figure 163) are quite promising, particularly for provision of electric power for space stations with long service lives.

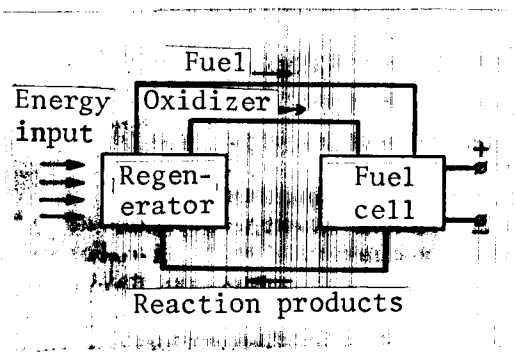

Figure 163. Schematic Diagram of Operation of Regenerative Fuel Cell.

Depending on the method of regeneration, we distinguish between regenerative fuel cells with thermal, chemical, photochemical and radiochemical reactions. An example of a fuel cell with a thermal reaction is the system with lithium hydride (LiH). A schematic diagram of such an installation is shown in Figure 164.

The electrolyte is an LiH utectic. Fuel cell operates at 450° C. The reaction products dissociate in the regenerator at t = 850° C. The open-circuit voltage of this system is U_{oc} = 0.6 v. When loaded by a current with a density of 160 ma/cm^2, the voltage drops to 0.3 v. This system requires further study and improvement, but in combination with any source of thermal energy (particularly a solar concentrator) it seems quite interesting.

16.5. Thermal Emission Converters.

A diode electron tube is an elementary prototype of a thermal emission converter. It has been discovered that the current in a radio tube does not vanish when the external load applied to it is equal to zero. Consequently, a radio tube with a hot cathode can be used to generate electric power.

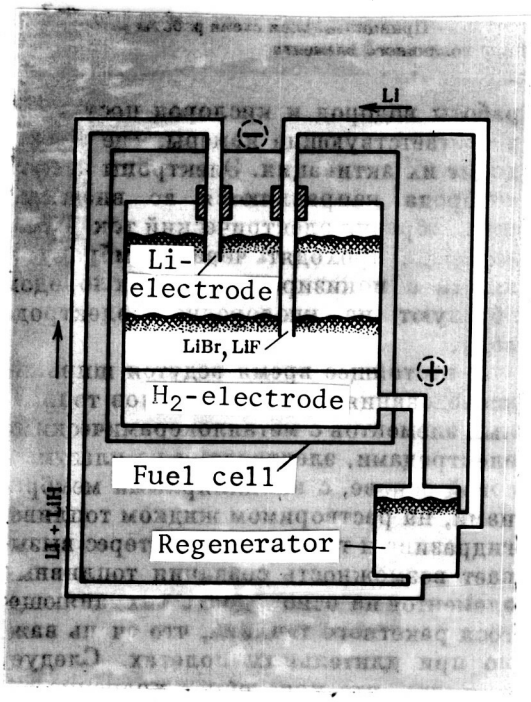

Figure 164. Schematic Diagram of the Operation of a Regenerative Fuel Cell with a Thermal Reaction.

The operation of a thermal emission converter, on the example of a diode, can be imagined as follows. The heat applied to the cathode imparts energy to the electrons of the cathode, which exceeds the work function for removal of the electrons from the material of the cathode. The electron gas, crossing the interelectrode gap, is abosrbed by the anode, and gives up a portion of its energy, equal to the work function from the anode. The energy absorbed by the electrons upon emission from the cathode at high temperature is liberated upon absorption on the cold anode. As a result, the electron gas at the anode has excess energy which can be used to move it from the anode to the cathode through an external circuit (through a load). This process is effective only if the electron emission is rather great, which is possible only if the hot cathode temperature is 1200-2200 K. /273

In 1959, academician A. F. Ioffe suggested a vacuum converter consisting of a hot cathode with a high work function and a cold anode with a low work function. In this case the voltage taken from the converter was approximately equal to the difference in work functions of cathode and anode.

The primary shortcoming of this converter was the very slight distance between electrodes (10^{-3}-10^{-4} cm). As the gap was increased, the current taken from the converter dropped sharply.

In 1929, Langmuir [40] showed that a neutral atom, striking the surface with high work function, could give up an electron and bounce off as an ion. The probability of this process is great if the work function of the cathode surface is higher than the ionization potential of the neutral atom. Consequently, injection into the interelectrode space of atoms of an element with low ionization potential results in the formation of a plasma.

Cesium is used as such an element with low ionization potential. The injunction of cesium into the interelectrode space allows, with comparatively high interelectrode distances, an increase in the pressure within the thermal emission converter from 10^{-4}-10^{-3} to 1-10 mm hg.

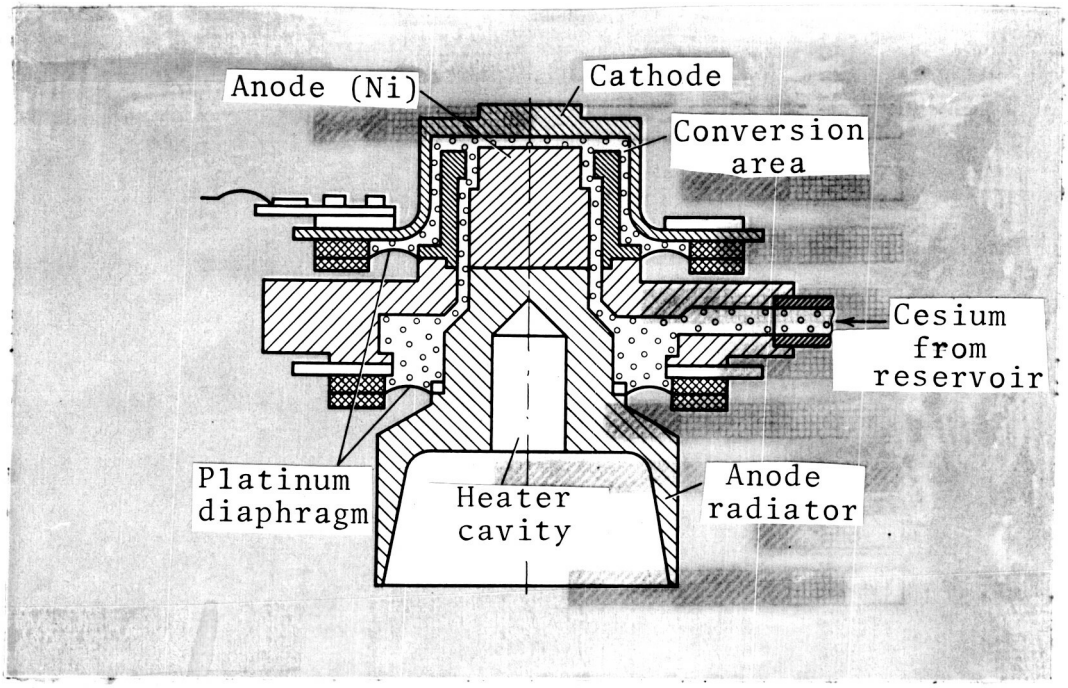

Figure 165. Possible Design of Thermal Emission Converter.

In the early 1960's, it became clear that the creation of a thermal emission converter was a definite possiblity. The main advantages of such a converter are the lack of moving parts, plus the fact that they require no strong magnetic fields and have high conversion efficiency.

The first thermal emission converters in which the cesium vapor pressure was 0.1 mm hg, yielded 10 w/cm^2 with an efficiency of 10%, cathode temperature up to 2300 K and distance between electrodes up to 1 mm. High-pressure converters (1-10 mm hg) produced powers of up to 40 w/cm^2 at a cathode temperature of $\sim$2200 K and distance between electrodes 100 μ. Efficiencies of $\sim$20% were achieved. Figure 165 shows a cross section of a laboratory thermal emission converter. /274

We should note that, in spite of the high efficiency of conversion and comparative simplicity of design, work in the area of creation of thermal emission converters is still in the stage of laboratory models with limited service life. The main means for increasing effectiveness consist in increasing the temperature of the cathode to the technologically determined limit and the use of alkali-Earth metals such as barium rather than cesium in order to reduce the cathode work function. All of this gives some hope that in the near future thermal emission converters, together with radio

isotope heat sources, can be used to supply power for small planetary stations.

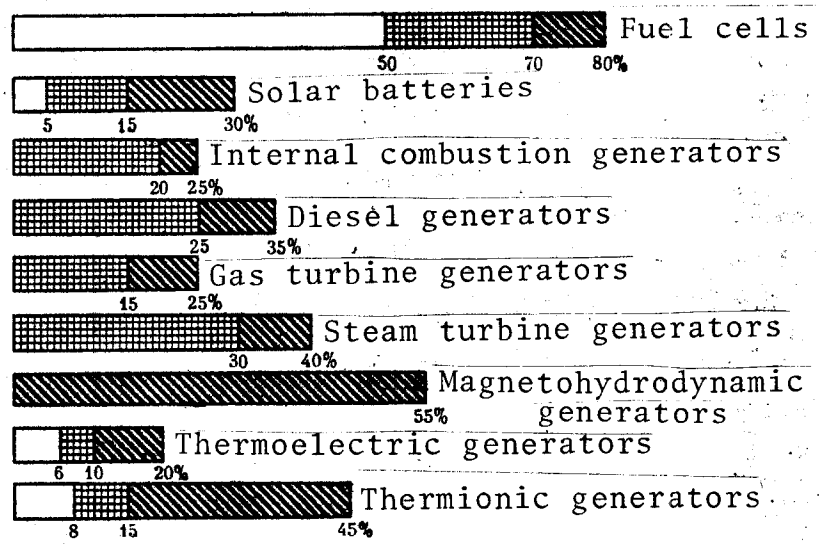

Figure 166. Efficiency of Existing (checkerboard) and Prospective (stripes) Power Systems.

In this chapter, we have studied only a few of the best-known power supply systems. We could also mention nuclear batteries, directly converting the energy of radioactive decay to electric energy, but operating at very low power levels (less than 1 μw), the Brighton and Rankin thermal cycles, fuel cells with thermal regeneration using radio isotopes, etc. However, most of these /275
systems are still not perfected, are in the developmental stage and cannot be used to supply power to planetary spacecraft.

Figure 166 shows the efficiencies of existing and prospective power systems. Obviously, solar batteries and solar thermoelectric generators are effective only with good illumination. Chemical sources of current and fuel cells are quite convenient for comparatively short-term use.

In the general case, the problem of long-term power supply of planetary stations can be solved only by a combination of several different power systems (solar batteries plus electric storage batteries, solar batteries plus fuel cells, electric storage batteries plus thermoelectric generators using isotopes or solar thermoelectric generators, etc.)

However, the most convenient power supply system, satisfying most requirments for the provision of electric power to small planetary stations for long periods of time under extremely unfavorable conditions is the thermoelectric generator with radio isotope heat source, using radio isotopes with predominantly α-radiation (polonium-210, plutonium-238, curium-242). These generators can supply both electric and thermal power for spacecraft, to avoid excessive cooling of the apparatus. Furthermore, we can hope that in the near future great successes will be achieved in the area of development of thermal emission converters and particularly regenerative fuel cells, which might become the basic sources of electric power.

We should emphasize once more that the problem of provision of power to small APS for extended periods of time is very complex and requires an individual approach to each specific case, considering all the peculiarities of the situation.

18. Vozdushno-Kosmicheskaya Telemetriya [Air-Space Telemetry], collection of translations edited by K. N. Trofimov, Moscow, Voyenizdat Press, 1968.
19. Khodarev, Yu. K., V. P. Yevdokimov, V. M. Pokrass,"Statistical Analysis of Data Produced by Remote Spacecraft," Apparatura Ispol'zuemaya v Kosmicheskikh Issledovaniyakh [Equipment Used in Space Studies, Collection of Works], Moscow, Nauka Press, 1972.
20. Shannon, C.,"Communications in the Presence of Noise," Raboty po Teorii Informatsii i Kibernetike [Works on Information Theory and Cybernetics], Moscow, Foreign Literature Press, 1963.
21. Sviridenko, V. A., V. I. Berezin, "Effectiveness of Polynomial Methods of Reduction of Redundancy in Analog Messages," Tezisy Dokl. na II Nauch.-Tekhn. Konf. po Kosmicheskoy Radiosvyazi [Abstracts of Reports of Second Scientific-Technical Conference on Space Radio Communications](Moscow, 1971), 1971.
22. Erman, A.,"Analysis of Certain Methods of Reduction of the Frequency Band by Elimination of Redundancy," TIIER, 1967, 1, No. 3.
23. Medlin, I. E., Sampled-Data Prediction for Telemetry Band-Width Compression, IEEE Trans., V-set-11. March 1965.
24. Obrezkov, G. V., "Probability of Reaching the Boundary in Nonlinear Self-Regulation Systems," Izv. AN SSSR Tekhnicheskaya Kibernetika, 1968, No. 3.
25. Parzen, E., Regression Analysis of Continuous Parameter Time Series, Proc. 4th Sympos. Barkley, 1960, Vol. I.
26. Zayezdnyy, A. M., OznovyRachetov po Satisticheskoy Radiotekhnike [Principles of Calculations in Statistical Radio Engineering], Moscow, Svyaz' Press, 1965.
27. Petrovich, N. T., Ye. F. Kamenev, Voprosy Kosmicheskoy Radiosvyazi [Problems of Space Radio Communications], Moscow, Sovetskoye Radio Press, 1965.
28. Crassner, G. N., J. V. Michaels, Vvedeniye v Sistemy Kosmicheskoy Svyazi [Introduction to Space Communications Systems], Moscow, Svyaz' Press, 1967.
29. Teplyakov, I. M., Radiotelemetriya [Radiotelemetry], Moscow, Sovetskoye Radio Press, 1966.
30. Smolov, V. B. et al, Poluprovodnikovyye Kodiruyushchiye i Dekodiruyushchiye Preobrazovateli Napryazheniya [Semiconductor Coding and Decoding Voltage Converters], Moscow, Energiya Press, 1967.
31. Berezin, V. I., M. V. Nazarov, "Grouping Method in Information Compression System," Report at National Telemetry Conference (USA, 1971), preprint, Moscow, IKA AN SSSR, 1971.
32. Nazarov, M. V., V. I. Berezin, V. A. Sviridenko et al,"System for Transmission of Telemetry Messages with Increased Information Content," Tezisy Dokladov na II Nauch.-Tekhn. Konf. po Kosmicheskoy Radiosvyazi [Abstracts of Reports of Second Scientific-Technical Conference on Space Radio Communications], (Moscow, 1971), 1971.

33. Pryamoye Preobrazovaniye Energii [Direct Conversion of Energy], collection of articles translated from the English, Moscow, Mir Press, 1969.
34. Seebek, T., Uber den Magnetismus der Galvansichen, Kette, 1821.
35. Zills, E., Kernenergie als Energielieferant fur Raumstationen, Luftfahrt-Zubehor, 1967, N. 11/12.
36. Korliss, U., D. Harvey, Istochniki Energii na Radioaktivnykh Izotopakh [Radioactive Isotope Power Sources], Moscow, Mir Press, 1967.
37. Szego, G. C.,"Space Power Systems,State of the Art," J. Spacecraft and Rockets, 1965, 2. No. 5.
38. Grubb, W. T., "Comparison of Platinum and Its Group VIII Nearest Neightbors as Anode Electrocatalysts in Propane-Phosphoric Acid Fuel Cells," J. Electrochem. Soc., 1966, 113. No. 2.
39. Boies, D. B., L. G. Forgala, "Storable Propellant Fuel Cells," Electrochem. Technol., 1967, No. 5, pp. 7-8.
40. Langmiur, J., "The Interaction of Electrons and Positive Ion Space Charges in Cathode Sheaths," Phys. Rev., 1929, 33.